Optimising Non-destructive Examination of newbuilding ship hull structures by developing a data-centric risk and reliability framework based on fracture mechanics

A thesis presented in fulfilment of the requirements for the degree of

Doctor of Philosophy

University of Strathclyde

Department of Naval Architecture, Ocean and Marine Engineering

Peyman Amirafshari

May 2019

Declaration of Authenticity and Author's Rights

This thesis is the result of the author's original research. It has been composed by the author and has not been previously submitted for examination, which has led to the award of a degree.

Signed: Peyman Amirafshari 24 May 2019

To my sister Negar

The quotes below express lessons learnt through this trip to knowledge.

Hoping to motivate.

"ذرّه را تا نبود همت عالی حافظ طالب چشمه ی خورشید درخشان نشود"

"One who is not filled with great fortitude will never dream of seeking light"

(Hafez, Persian poet)

"There is nothing either good or bad, but thinking makes it so."

(William Shakespeare, Hamlet)

"Obvious is the most dangerous word in mathematics"

(Eric Temple Bell, Mathematician)

"As far as the laws of mathematics refer to reality, they are not certain; and as far as they are certain, they do not refer to reality"

(Albert Einstein)

ACKNOWLEDGMENTS

I like to thank my family for their endless and unconditional love throughout this journey. My sister Negar, who has been my greatest supporter, my best friend and my mentor in life. My mother Farangis, my father Nader, and my brother Sasan, whose prayers were always with me.

I would like to express my gratitude to my fantastic supervisor team for their continuous support:

My academic supervisor Professor Nigel Barltrop, who supported me from the very beginning of my research career, and has been immensely generous with his time and knowledge and partly funded my PhD from his account. It was an honour and privilege to work with him. Without his wisdom and his directions, the goals of this research would have not been achieved. I could not have wished for a better supervisor.

Many thanks to my industrial supervisor from TWI Dr Ujjwal Bharadwaj, for his professional guidance, his support and mentorship during my time in TWI.

I am deeply thankful to my industrial supervisor from Lloyds Register Group Mr Martyn Wright, a true friend and a brilliant mentor, who also made the acquisition of data possible and created opportunities for me to experience a number of invaluable industrial visits.

I like to thank my second academic supervisor Dr Selda Oterkus, for her encouragements and positive ideas.

I am deeply thankful to Mr Andrew MacdDonald global head of materials welding & NDE at Lloyds Register for his great support during this research.

I also like to thank Dr Jan Przydatek and Professor Richard Clegg from Lloyds Register Foundation for their continuous support throughout and to the end of this research.

My sincere gratitude to Dr Isabel Hadley, for her insightful inputs regarding BS7910 standard, and Dr David Howse, for sharing his knowledge about welding engineering.

Many thanks to Mr Alessio Cendron, for sharing his valuable experience, Mr Mario Croce, and Mr Philip Lesworth, from Lloyds Register office in Italy for their kind hospitality.

I am also thankful to Mr Philip Leaver and Mr Stephen Smith for sharing their knowledge and experiences about ship inspection which were significantly valuable and insightful.

Many thanks to Mr Juan Manuel Gonzalez, Mr Hernan Gonzalez and Mr Carlos Lamas from Lloyds Register office in Cadiz for sharing their experiences and their hospitality.

I also like to thank Mr Clive Arnold for assisting me with fracture toughness data.

Moreover, I would like to thank the people in the office, Stefanie, Paco, Renaud, Yao, Abbas, Hadi, Martin, Payam, Amr, Kamran and Shervin who made working there fun and joyful for me.

I am thankful to my friend, Mohammad Kianifar, for his regular encouragements. I also like to thank my friends Mojtaba and Ariyan, as well.

Many thanks to the NAOME Postgraduate Research Administrators Thelma Will and Susan Pawson, to the TWI operations team Caroline Knight and Alison Dodd, and to the fantastic library staff at TWI: Paul, Joanne, Catherin and Sue.

Last but certainly not least, I would like to thank the funding bodies:

This PhD was made possible by the sponsorship and support of Lloyd's Register Foundation. Lloyd's Register Foundation helps to protect life and property by supporting engineering-related education, public engagement and the application of research. The work was enabled through, and undertaken at, the National Structural Integrity Research Centre (NSIRC), a postgraduate engineering facility for industry-led research into structural integrity. NSIRC was established and is managed by TWI through a network of both national and international Universities and industry. For the purpose of this research, the University of Strathclyde, Lloyd's Register Foundation and TWI Ltd collaborated under the auspices of NSIRC.

TABLE OF CONTENTS

ACKNOWLEDGMENTS III
TABLE OF CONTENTS V
LIST OF FIGURES XIV
LIST OF TABLES XXII
ABBREVIATIONS XXVI
NOMENCLATURE XXIX
ABSTRACT XXXI
1 Chapter 1: Introduction 1
1.1 Non-destructive Examination of newbuilding ship hull structures 1
1.1.1 Challenges: Background, scale and Impacts 2
1.1.2 The Approach: Risk-Based Inspection 8
1.1.3 Case-study: Cruise ship deck structure 10
1.2 Aims & Objectives 12
1.3 Structure of the Thesis 13
2 Chapter 2: Background & Literature review 16
2.1 Chapter Outline 16
2.2 Ship Fabrication Process 16
2.3 Weld 23
2.4 Welding process 23
2.4.1 Shielded Metal Arc Welding (SMAW) 23
2.4.2 Submerged arc welding (SAW) 24
2.4.3 Gas Metal Arc Welding (GMAW) 25
2.4.4 Flux Cord Arc Welding (FCAW) 26
2.4.5 Hybrid Laser Arc Welding (HLAW) 26

2.4.6 Common Welding Processes in ship production 27
2.5 Weld Defects 29
2.5.1 Porosity 30
2.5.2 Solid inclusion 30
2.5.3 Lack of Fusion (LOF) 31
2.5.4 Lack of Penetration 31
2.5.5 Cracks 31
2.6 Significance of weld defects 35
2.6.1 Static Ultimate Strength 35
2.6.2 Effect on fatigue performance 35
2.6.3 Treatment of defects in this research 38
2.7 Non-Destructive Examination of Welds 39
2.7.1 Visual Testing (VT) 39
2.7.2 Ultrasonic Testing (UT) 39
2.7.3 Advanced Ultrasonic Testing 40
2.7.4 Radiography Testing (RT) 42
2.7.5 Penetrant Testing (PT) 43
2.7.6 Magnetic Particle Inspection (MPI) 45
2.7.7 Eddy Current Testing (EC) 47
2.8 Review of NDE approaches by classification societies 47
2.8.1 NDE from a quality-assurance perspective 48
2.8.2 NDE from structural criticality perspective 50
2.8.3 Weld Type as a factor for selection of NDE technique 52
2.8.4 NDE technique 53
2.8.5 Welding Process 53
2.8.6 Weld repair 54
2.8.7 Additional inspections 54
2.8.8 Acceptance criteria 57

2.8.9 Scope for potential improvement 58
2.8.10 Concluding remarks on review of classification societies approaches 60
2.9 NDE inspection in non-marine industries 61
2.9.1 Automotive 61
2.9.2 Aerospace 66
2.9.3 Civil engineering 66
2.9.4 Petroleum Industry 67
2.9.5 Amusement devices 68
2.10 Chapter conclusion 68
3 Chapter 3: Risk and Reliability 71
3.1 Outline 71
3.2 Defect assessment using Fracture Mechanics 71
3.3 Determinist vs Probabilistic Fracture Mechanics 73
3.4 Uncertainty and reliability 75
3.5 Reliability and codes 80
3.6 Levels of Reliability Analysis 81
3.7 Risk Assessment 86
3.8 Proposed Risk and reliability framework of weld defects in ship hulls 88
3.9 System definition and consequence of failure 90
3.9.1 Failure Mode and Effect Analysis (FMEA) 91
3.9.2 Event Tree Analysis (ETA) 91
3.9.3 Fault Tree Analysis (FTA) 92
3.9.4 Specifying consequence of failure classes 92
3.10 Target reliability 97
3.10.1 Target reliabilities for ship hull structures 100
3.11 Chapter summary and conclusions 101
4 Chapter 4: Defect Size and Frequency Statistics 103
4.1 Chapter outline: 103

4.2 Significance of weld defect statistics 103
4.3 Influencing variables 104
4.3.1 Joint Type 105
4.3.2 Thickness: 106
4.3.3 NDE Type: 106
4.4 Flaw frequency analysis 107
4.5 Detection probability 111
4.5.1 Published work on the modelling of POD 114
4.5.2 Detection probability-Bayesian theorem 120
4.6 Defect rates 123
4.7 Defect size 127
4.7.1 Defect height/depth 129
4.7.2 Defect length 131
4.7.3 Defect aspect ratio 135
4.7.4 Initial Defect Length 136
4.7.5 Summary and discussion of defect size distributions 136
4.8 Chapter summary and conclusions 137
5 Chapter 5: Probabilistic analysis of fracture toughness 141
5.1 Chapter outline 141
5.2 Fracture 141
5.3 Fracture toughness 142
5.4 Parameters affecting fracture toughness 142
5.4.1 Temperature 143
5.4.2 Loading rate 144
5.4.3 Constraint 146
5.4.4 Plate rolling direction 148
5.5 Measures of fracture toughness 149
5.5.1 The stress intensity factor (K) 149

5.5.2 CTOD (δ) 150
5.5.3 J-integral 150
5.6 Fracture toughness testing 151
5.7 Statistical treatment of fracture toughness data 152
5.7.1 Master curve 153
5.7.2 MC with censored data 155
5.7.3 Bi-modal MC 155
5.7.4 MC with random inhomogeneities 156
5.7.5 Choice of statistical method 156
5.8 The Charpy impact testing 157
5.9 Analysis of Charpy data 158
5.9.1 Indirect estimation of toughness from the Charpy energies 159
5.9.2 Correlation equations 160
5.10 Fracture toughness data set used in this research 164
5.11 Analyses of scatter 165
5.11.1 Scatter of toughness among manufacturers 165
5.11.2 Scatter across steel batches 167
5.11.3 The conclusion from analyses of fracture toughness scatter 172
5.12 Fracture toughness 173
5.13 Fracture toughness and steel quality 174
5.14 Chapter summary and conclusion 175
6 Chapter 6: Reliability Calculation 179
6.1 Chapter Outline 179
6.2 Limit state function 180
6.3 Reliability analysis based on S-N curve 181
6.4 Fracture Mechanics 183
6.4.1 FAD 186
6.5 Methods of reliability analysis 189

6.5.1 The Monte Carlo simulation code 190
6.5.2 The Convolution Integral Code 191
6.6 The reliability framework and uncertain variables 195
6.6.1 Stress calculation 195
6.6.2 Residual stress 199
6.6.3 Stress Intensity Factor (SIF) in Stiffened plates 201
6.6.4 Crack growth parameters 205
6.6.5 Choice of crack growth parameters 211
6.6.6 FAD uncertainty 212
6.7 Fracture Mechanics case studies 217
6.7.1 Assessment of the stiffener fillet weld 217
6.7.2 Assessment of the butt weld of a grand block joint 221
6.8 Chapter summary 227
7 Chapter 7: Statistical sampling and process control 230
7.1 Chapter outline 230
7.2 Type of errors and their detection schemes 231
7.3 Sample size and statistical confidence 232
7.3.1 Point Estimate of distribution 233
7.3.2 Interval estimate of the distribution parameters 234
7.4 Effect of extent of inspection on statistical confidence 236
7.5 Effect of confidence on reliability 242
7.6 Effect of extent of inspection on the reliability 244
7.7 Point estimate of defect rate 245
7.7.1 The epistemic uncertainty of defect rate model 250
7.8 Determining sample size from the confidence interval 251
7.9 Bayesian Inference 253
7.9.1 Bayesian estimate of defect size 256
7.9.2 Bayesian estimate of defect rate 261

7.9.3 Bayesian estimate of Fracture toughness....262
7.10 Statistical Process control....263
7.11 Control Charts....265
7.11.1 Control charts based on exact probability limits....267
7.11.2 c-chart:....269
7.11.3 p-chart....270
7.12 Chapter summary and conclusions....270
8 Chapter 8: The proposed method for improved inspection....273
8.1 Chapter outline....273
8.2 Overview of the method....273
8.3 Data acquisition and data statistical inference....277
8.4 Risk and Reliability....279
8.5 Statistical Sampling....280
8.6 Quality control....281
8.7 Process control....282
8.8 Quality Improvement....283
8.9 Application to the case study structure....286
8.9.1 Description of the case study deck....286
8.9.2 Stage 1 and 2: Data collection and data processing....288
8.9.3 Stage 3: Risk and reliability analysis....289
8.9.4 Stage 4: Calculation of checkpoints....290
8.9.5 Stage 5: Inspection....293
8.9.6 Stage 6: Quality control and process control....294
8.9.7 Bayesian updating....296
8.9.8 Remarks on the application of the proposed framework to the case study structure....299
8.10 Chapter summary....300
9 Chapter 9: Concluding remarks....301

9.1 Novelty of present research 301
9.1.1 Gaps 301
9.1.2 Approach 301
9.1.3 Contribution to knowledge 302
9.1.4 Key findings and review of the thesis 302
9.2 Recommendations for future works 303
9.2.1 Methodology 303
9.2.2 Case study 304
9.2.3 Transferability 304
9.3 Contribution 305
9.3.1 Lloyds Register sponsoring 305
9.3.2 TWI sponsoring 306
9.3.3 Ship manufacturing stakeholders 306
9.3.4 Academic impact 307
9.3.5 Final thoughts 307
REFERENCES 308
A. Appendix A 322
B. Appendix B 324
Tanker Ship 324
Bulk Carrier 325
Container ship 326
C. Appendix C 327
Maximum likelihood estimate 327
Statistical distributions 327
Normal distribution 327
Lognormal distribution 327
Exponential distribution 328
Weibull distribution 328

D. Appendix D 329
Fracture toughness.....329
Normal Grade steels 329
High strength steel grades 331
E. Appendix E.....333
NDE inspection plan 334
Structural data 337
NDE inspection raw data 344
F. Appendix F.....362
G. Appendix G 366
Peer reviewed publications 366
Conferences and oral presentations 366

LIST OF FIGURES

Figure 1-1 Example of NDE inspection plan for part a ship side shell (Bow-Starboard)..... 2
Figure 1-2 International seaborne trade, selected years, Millions of tons loaded, (Asariotis et al., 2018). 3
Figure 1-3 Goods loaded worldwide (UNCTAD, 2017) 3
Figure 1-4 (Cruise-Market-Watch, 2018) 4
Figure 1-5 Distribution of casualty events with a ship from 2011 to 2017 (EMSA, 2018) 5
Figure 1-6 Welding work break down of a 15 deck cruise ship 11
Figure 1-7 Overview of the inspection framework..... 15
Figure 2-1 Block weight depends on the crane capacity available 16
Figure 2-2 Part 1: Panel line and sub-assembly 17
Figure 2-3 Assembly of pre-assembled parts in blocks 18
Figure 2-4 Grand blocks at a shipyard (Passenger ship) 19
Figure 2-5 Empty dry dock (right). A ship at outfitting stage (left). 20
Figure 2-6 Block erection in dry dock 20
Figure 2-7 Sub-assembly and Block assembly and Grand Block assembly process .. 21
Figure 2-8 Hull Erection..... 22
Figure 2-9 MMA/ SMAW process diagram (Wikimedia, 1993)..... 24
Figure 2-10 Submerged Arc Welding (SAW): Principle (Left), Process in practice (TWI, 2018 a)..... 24
Figure 2-11 Gas Metal Arc Welding (GMAW) diagram (Wikimedia, 2012) 25
Figure 2-12 Flux Cord Arc Welding (FCAW) diagram (Journal, 2009)..... 26
Figure 2-13 Hybrid Laser Arc Welding (HLAW) (TWI, 2018 b)..... 27
Figure 2-14 Typical weld types application in shipbuilding (Boekholt, 1996), (Kobelco, 2011). 28
Figure 2-15 Common Weld imperfections..... 29
Figure 2-16 Three modes of Lack of Penetration 31
Figure 2-17 Weld Crakes diagram..... 32
Figure 2-18 Solidification Cracking diagram..... 32
Figure 2-19 Solidification Crack (TWI, 2016 a) 32

Figure 2-20 Difference between residual stresses causing Transverse crack and HAZ crack. Picture adapted from (Milella, 2012) 35
Figure 2-21 Effect of porosity (Jonsson et al., 2013) 38
Figure 2-22 Effect of Inclusion (Jonsson et al., 2013) 38
Figure 2-23 Ultrasonic Testing (UT) principle (Wikimedia, 2006 a) 40
Figure 2-24 Ultrasonic Testing (UT) equipment (TWI.Ltd, 2018d) 40
Figure 2-25 Phased Array Ultrasonic Testing (PAUT) (Wikimedia, 2006 b), PAUT display (TWI, 2013) 41
Figure 2-26 Principle of Time of Flight Diffraction (TOFD) examination (Wikimedia, 2011) 41
Figure 2-27 Radiography Examination diagram (TWI, 2018 c)..... 42
Figure 2-28 Defects as appear on radiograph and their diagram 43
Figure 2-29 Stages of Colour-contrast Penetrant testing 44
Figure 2-30 Colour-contrast penetrant testing after bleeding (TWI, 2018 d) 44
Figure 2-31 Fluorescent penetrant testing (Wikimedia, 2014) 45
Figure 2-32 Principle of MPI (TWI, 2018 d) 46
Figure 2-33 MPI using AC yoke (TWI, 2018 d) 46
Figure 2-34 Principle of Eddy Current testing (i.Stack, 2018) 47
Figure 2-35 single sample plan for the Normal inspection (ISO-28590, 2017) 65
Figure 3-1 Fracture mechanics Framework, adapted from (Zerbst et al., 2015) 73
Figure 3-2 Types of uncertainties in engineering design 77
Figure 3-3 Schematic of key uncertain variables and their relationship to the reliability framework..... 80
Figure 3-4 Representation of a level I reliability 82
Figure 3-5 Illustration of Reliability index (β) method..... 82
Figure 3-6 Comparison between FORM and SORM (Du, 2005) 83
Figure 3-7 Joint probability distribution of load and resistance 84
Figure 3-8 Example of a Monte Carlo simulation method..... 85
Figure 3-9 Load and resistance distributions for Convolution integral 86
Figure 3-10 A typical Risk matrix diagram..... 87
Figure 3-11 ALARP Carrot diagram based on (HSE, 2001 b) 88
Figure 3-12 Proposed Risk and reliability framework of weld defects in ship hulls . 89
Figure 3-13 Photo of Castor tanker failure (E-bookshelf.de, 2000) 90
Figure 3-14 Example of an Event Tree Analysis (ETA) for a weld defect 91
Figure 3-15 Combined criticality (ABS, 2012)..... 94

Figure 3-16 Fault tree model of hull girder failure concerning weld defect..... 96
Figure 3-17 Developed consequence model for a passenger ship..... 97
Figure 4-1 Welding break down with respect to procces from ship #1 108
Figure 4-2 NDE break down with respect to process from ship #2.....108
Figure 4-3 Welding break down with respect to hull area, Level of Automation and process from ship #1. 109
Figure 4-4 Welding processes Defect rate with Binary Method 110
Figure 4-5 Welding processes Defect rate with (Length-by-Length Method) 110
Figure 4-6 Defect percentage break down for ship #2 111
Figure 4-7 Schematic POD curve of defect 112
Figure 4-8 Schematic representation of detecting a defect of size ɑ with probability of detection of %60.....112
Figure 4-9 Relationship between crack size distribution, Probability of detection and detected crack size distribution 113
Figure 4-10 DNV POD for visual inspection. Replotted from (DNV, 2015) 115
Figure 4-11 DNV POD for surface NDE. Replotted from (DNV, 2015) 115
Figure 4-12 POD curve for Ultrasonic Inspection. Replotted from (DNV, 2015) 116
Figure 4-13 HSE POD curves reproduced from NTIAC report with of longitudinal Cracks for RT (Georgiou, 2006). 117
Figure 4-14 Postulated PODs by Dufresne (Dufresne, 1981).....117
Figure 4-15 Nordtest POD curves for RT (Sensitivity level R4) for different defect types. Figures extracted from (Visser, 2002) 118
Figure 4-16 Nordtest POD versus defect height for planar weld defects using UT and RT. Figures extracted (Visser, 2002) 118
Figure 4-17 Schematic description of defect size distributions 122
Figure 4-18 Probabaility of detection curves for shipyard data.....123
Figure 4-19 Defect rate breakdown based on welding process for ship #2 127
Figure 4-20 Dimensions of an idealised embedded defect 128
Figure 4-21 Crack height density distribution from (Kountouris and Baker, 1989 c) and (Kountouris and Baker, 1989 a) 131
Figure 4-22 Weibull and Lognormal fits to crack length data from ship #2 133
Figure 4-23 Crack length cumulative distribution from ((Kountouris and Baker, 1989 a) and this work 135
Figure 4-24 Initial defect length density functions for shipyard data 136
Figure 5-1 Schematic transition curve 143

Figure 5-2 Merchant ship operating temperature (Hodgson and Boyd, 1958) 144
Figure 5-3 Schematic illustration of the effect of loading rate on fracture toughness 145
Figure 5-4 effect of loading rate ($\boldsymbol{MPa\sqrt{m}s}$) on a typical AH36 grade steel 146
Figure 5-5 Effect of constraint on fracture toughness (Moon et al., 2017) 147
Figure 5-6 Effect of specimen thickness on fracture toughness (TWI, 2015 b) 147
Figure 5-7 Charpy absorbed energies for Z-quality AH36 steel in (L-T) and (T-L) directions 148
Figure 5-8 Plate rolling direction relative to ship orientation and test specimens ..149
Figure 5-9 the hinge model for estimating CTOD from three-point bend test 150
Figure 5-10 Schematic illustration of δ and J 151
Figure 5-11 The Charpy test set up diagram (Left), fractured specimens (Right) 157
Figure 5-12 Possible fitting algorithms for CVN data (Wallin, 2011) 159
Figure 5-13 The effect of main differences between the Charpy test and fracture toughness 159
Figure 5-14 Transition curve for z-quality steel 170
Figure 5-15 transition curve of manufacturer #3 and different batches 171
Figure 5-16 Transition curves of manufacturer #4 batches (90% prediction bounds) 172
Figure 5-17 Steel toughness distribution for manufacturer # 5 at (0°C) 174
Figure 5-18 Trend of fracture toughness versus year of manufacture 175
Figure 6-1 Schematic illustration of the S-N curve 181
Figure 6-2 Relationship between Fatigue design safety factor and Failure probability (DNV, 2010) 183
Figure 6-3 Schematic of crack propagation curve according to Paris-Erdogan law .184
Figure 6-4 Failure Assessment Diagram (FAD) 189
Figure 6-5 Illustration of calculating failure probability using Monte Carlo Simulation for FAD 190
Figure 6-6 Time-dependent (Fatigue and Fracture) reliability calculation algorithm 191
Figure 6-7 schematic principle of the convolution integral method 192
Figure 6-8 Algorithm of time-dependent reliability for Convolution Integral code .194
Figure 6-9 Framework for fatigue and fracture reliability analysis 195
Figure 6-10 Longitudinal strength global loads, adapted from (Wikimedia, 2006 c) 196

Figure 6-11 Left: Transverse stress during rolling (Wikimedia, 2009), Right: Local load effect (Okumoto et al., 2009) 197
Figure 6-12 Global FEA of case study ship for Deck 16 Still water+ Hogging, σxx stress (Fr: Frame Number) 198
Figure 6-13 Global FEA of case study ship for Deck 16 Still water+ Sagging, σxx stress 198
Figure 6-14 Transverse and longitudinal residual stresses in butt welds adapted from (Milella, 2012) 200
Figure 6-15 Effect of tensile residual stress on cyclic stress range 200
Figure 6-16 Schematic Stiffened plate in ship bottom and deck 202
Figure 6-17 K solution for a panel with integral stiffeners proposed by (Poe, 1971) 203
Figure 6-18 Residual stress measurement of the stiffened plate by (Mahmoud and Dexter, 2005). 204
Figure 6-19 Effect of residual stress and constraint on the crack growth rate of stiffened plates (Mahmoud and Dexter, 2005). 205
Figure 6-20 Schematic of crack growth models by Paris law 207
Figure 6-21 Comparison of correlation relationship equations 209
Figure 6-22 Comparison between equation from (Cortie and Garrett, 1988) and (Baker and Stanley, 2008) 209
Figure 6-23 Effect of choice of crack propagation parameters.....210
Figure 6-24 Comparison between crack growth curves of various C values 212
Figure 6-25 Wide plate failure results from (Muhammed et al., 2000 a).....213
Figure 6-26 Diagram of uncertainty in the (FAD), (Muhammed et al., 2000 a) 213
Figure 6-27 Uncertainty modelling in the Fracture dominant zone.....215
Figure 6-28 FAL uncertainty (Left: Assessment points. Middle: Simulated FADs with Normal dist., Right: Simulated FADs with Weibull distribution) 216
Figure 6-29 Monte Carlo reliability method sensitivity to the number of simulations 216
Figure 6-30 Studied stiffened panel detail 217
Figure 6-31 Fracture Mechanics results for crack growth in the plate with residual stress 219
Figure 6-32 Fracture Mechanics results for crack growth in the stiffener 221
Figure 6-33 Time-dependent probability calculations (No Inspection).....223
Figure 6-34 Time-dependent probability calculations (Visual Inspection) 223

Figure 6-35 Effect of visual inspection on failure probability 224
Figure 6-36 Effect of choice of NDT technique 225
Figure 6-37 Effect of defect rate on failure probability 226
Figure 6-38 Effect of in-service visual inspection on through-life reliability 227
Figure 7-1 Common causes vs assignable causes (Oakland, 2008) 231
Figure 7-2 Population and sample distributions 233
Figure 7-3 Schematics of the sample mean and standard deviation parameter uncertainty distributions 234
Figure 7-4 Confidence interval and significance level 236
Figure 7-5 Samples mean ln drawn from the dataset 237
Figure 7-6 Mean of defect length ln values against sample size ratio 238
Figure 7-7 Standard deviation of defect length ln values against sample size ratios 239
Figure 7-8 Upper bound crack length cumulative lognormal distributions.....239
Figure 7-9 Effect of number of the defects on confidence 241
Figure 7-10 Final year failure probability of the case study joint for different sample sizes 242
Figure 7-11 Through life failure probability of the case study joint for different sample sizes 243
Figure 7-12 Rate of change in final year failure probability of the case study joint with respect to sample size 243
Figure 7-13 Effect of extent of the inspection on the number of remaining defects after the inspection (for inspection with 100% POD) 245
Figure 7-14 Poisson and binomial distribution of defect rate in a structure comprising 60 checkpoints 246
Figure 7-15 Binomial distributions of different sample sizes for a joint comprising 60 possible checkpoints 247
Figure 7-16 Probability of exceedance 248
Figure 7-17 Probability of exceedance for 8.74/60 defect rate (p) 248
Figure 7-18 Illustration of Probability of Inclusion (POI) for three different defect rates 249
Figure 7-19 Beta density function for the binomial distribution Parameter 250
Figure 7-20 Sample error and confidence level diagram 251
Figure 7-21 Example of Bayesian inference model: material Yield strength, N=3 ..255

Figure 7-22 Example of Bayesian inference model: material Yield strength (N=30) 255
Figure 7-23 Bayesian inference Normal distributions of defect length with N=2 ...257
Figure 7-24 Bayesian inference lognormal distributions of defect length with N=2 257
Figure 7-25 Bayesian inference Normal distributions of defect length with N=10..258
Figure 7-26 Bayesian inference lognormal distributions of defect length with N=10 258
Figure 7-27 Recursive Bayesian updating 260
Figure 7-28 Non-Bayesian randomly drawn samples 261
Figure 7-29 Mean defect rate (p) estimation using Bayesian method 262
Figure 7-30 Defect rate (defect per 60 checkpoints) estimation using the Bayesian method 262
Figure 7-31 Bayesian estimation distributions for the toughness example 263
Figure 7-32 Illustration of Statistical Process Control (Montgomery, 2009). 264
Figure 7-33 Illustration of a traditional control chart 266
Figure 7-34 UCL limits for various samples sizes of the case study joint 269
Figure 7-35 c-chat UCL values for different sample sizes 270
Figure 8-1 Big picture of the proposed inspection scheme 274
Figure 8-2 Overview of the inspection framework.....276
Figure 8-3 Data acquisition and statistical inference flow diagram 278
Figure 8-4 Risk and reliability flow diagram 279
Figure 8-5 Flow diagram for calculating the required number of checkpoints 280
Figure 8-6 Quality control flow diagram 282
Figure 8-7 Process control flow diagram 283
Figure 8-8 Pareto diagram of planar defects in ship #3.....284
Figure 8-9 Root cause analysis of weld cracking using the Ishikawa diagram 285
Figure 8-10 Diagram of deck 16.....287
Figure 8-11 Stress due to global bending (Hogging) at around frame 200 291
Figure 8-12 Probability of exceedance for various samples assuming the defect rate of 0.1447 (per checkpoint) 295
Figure 8-13 Defect length distribution Bayesian updating of detected defects for deck 16 297
Figure 8-14 Probability distribution of initial defects length using Bayesian updating for deck 16.....298

Figure 8-15 Probability distribution of defect rate using Bayesian updating for deck 16 298
Figure 8-16 Updated probability of failure for joint No 200.....299
Figure B-1 Criticality Class model for Tanker ships proposed by (ABS, 2012) 324
Figure B-2 Criticality Class model for Bulk Carrier ships proposed by (ABS, 2012)..325
Figure B-3 Criticality Class model for Container ships proposed by (ABS, 2012).....326
Figure D-1 Normal Cumulative density function of grade A steel.....329
Figure D-2 Normal Cumulative density function of grade D steel 330
Figure D-3 Normal Cumulative density function of grade D steel 330
Figure D-4 Normal Cumulative density function of grade AH32 steel 331
Figure D-5 Normal Cumulative density function of grade A36 steel.....331
Figure D-6 Normal Cumulative density function of grade DH36 steel 332
Figure E-1 Existing inspection plan for deck 16 (Stern) 334
Figure E-2 Existing inspection plan for deck 16 (mid ship) 335
Figure E-3 Existing inspection plan for deck 16 (Bow).....336
Figure E-4 FEA counter plot for deck 16 (Still water +Wave Hogging) 337
Figure E-5 FEA counter plot for deck 16 (Still water +Wave Sagging) 338
Figure E-6 Global bending moment diagrams for ship (Wave hogging).....339
Figure E-7 Global bending moment diagrams for ship (Wave sagging) 340
Figure E-8 Ship Global bending moment and shear force table (Wave Hogging)....341
Figure E-9 Ship Global bending moment and shear force table (Wave sagging)....342
Figure E-10 Ship Global bending moment and shear force table 343
Figure F-1 Time variant probabilities of failure for frame 34, 56, 76, 98, 348, and 364 in deck 16 362
Figure F-2 Time variant probabilities of failure for frame 116, 136, and 326 in deck 16 362
Figure F-3 Time variant probabilities of failure for frame 156, and 304 in deck 16 363
Figure F-4 Time variant probabilities of failure for frame 176, 196, 260, 272, 276, and 282 in deck 16.....363
Figure F-5 Time variant probabilities of failure for centre part of frame 220 in deck 16 364
Figure F-6 Time variant probabilities of failure for frame 240 in deck 16.....364
Figure F-7 Time variant probabilities of failure for frame 380, and 392 in deck 16 365

LIST OF TABLES

Table 1-1 Newbuild cargo carrier ships cost estimate..... 6
Table 1-2 Examples of newbuild cruise ship costs (Ship-Order-Book, 2019) 7
Table 2-1 Advantages and disadvantages of MMA process (TWI, 2015 a) 24
Table 2-2 Advantages and disadvantages of the GMAW process (TWI, 2015 a)..... 26
Table 2-3 Typical weld types and processes in shipbuilding ((Boekholt, 1996), (Kobelco, 2011))..... 28
Table 2-4 Porosity causes and remedies (TWI, 2015 a), and (Timings, 2008) 30
Table 2-5 Solid inclusion causes and remedies (TWI, 2015 a), and (Timings, 2008). 30
Table 2-6 Lack of fusion causes and remedies (TWI, 2015 a) and (Timings, 2008)... 31
Table 2-7 Classification of weld cracking and their causes..... 32
Table 2-8 Centreline cracks causes and their preventive measures (TWI, 2015 a), and (Timings, 2008) 33
Table 2-9 HAZ cracking preventive measures (TWI, 2015 a), and (Timings, 2008)... 34
Table 2-10 Acceptance levels for weld toe undercut in steel (Jonsson et al., 2013)and (BSI, 2017)..... 36
Table 2-11 Acceptance levels for porosity and inclusions in welds in steel (Jonsson et al., 2013) and (BSI, 2017) 38
Table 2-12 Weld imperfections categories 39
Table 2-13 Advantages and disadvantages of Ultrasonic Examination (TWI.Ltd, 2015) 40
Table 2-14 Advantages and disadvantages of Radiography Examination (TWI, 2015 a) 43
Table 2-15 advantages and disadvantages of penetrant testing 45
Table 2-16 Advantages and disadvantages of MPI testing 46
Table 2-17 Advantages and disadvantages of Eddy Current testing 47
Table 2-18 Requirements of classification societies for NDE method 53
Table 2-19 Requirements of classification societies for automatic welding 54
Table 2-20 Requirements of classification societies for additional inspection..... 56
Table 2-21 Sample size code letters ISO 2859 (ISO-28590, 2017) 63
Table 2-22 Extent of NDT based on execution class specified in Eurocode 67
Table 3-1 Identified uncertain variables in reliability assessment of fabrication defects..... 79

Table 3-2 Relationship between reliability index ($\beta 0$) and failure probability 83
Table 3-3 Definition of Criticality Class (ABS, 2012) 93
Table 3-4 Typical descriptions of the Criticality Class (ABS, 2012) 94
Table 3-5 Recommendations for repairs based on the criticality class of a fracture (ABS, 2012) 94
Table 3-6 Recommendations for additional inspection based on the criticality class of a fracture for newbuilds 95
Table 3-7 Examples of target reliabilities specified by codes and standards 99
Table 3-8 Target reliability indexes proposed by (Mansour, 1996) 100
Table 3-9 Description of Categories given Table 3-8 101
Table 3-10 Target Reliabilities used in this work 101
Table 4-1 Common conventional NDE methods 106
Table 4-2 Comparison between basic characteristics of ship#1 and Ship #2 107
Table 4-3 importance of defect types based on ship #2 data, based on Figure 4-6 111
Table 4-4 DNV Parameters for POD curves (DNV, 2015) 115
Table 4-5 Some of detection probabilities from NTIAC report (Georgiou, 2006). ...116
Table 4-6 50% detection probabilities for R4 testing of Nordtest programme 118
Table 4-7 Representative detection probabilities for R4 testing of Nordtest programme 119
Table 4-8 Representative Planar weld defects detection probabilities for RT and UT testing of Nordtest programme 119
Table 4-9 (BS7910, 2015 a) Example of inspection capabilities for sub-surface flaws 119
Table 4-10 summary of reviewed literature and their relevance to this work 120
Table 4-11 Summary of distribution parameter estimation of shipyard data 122
Table 4-12 Defect rates from literature 125
Table 4-13 Defect rates from shipyards 125
Table 4-14 corrected defect rates 126
Table 4-15 Defect rates from shipyards 127
Table 4-16 Defect height distribution parameters from literature 130
Table 4-17 Planar defect length distributions from shipyards with 0.975 and 0.025 confidence values. 132
Table 4-18 Defect distributions distribution parameters from literature 134
Table 4-19 Defect aspect ratio distribution parameters from (Kountouris and Baker, 1989 a) 135

Table 5-1 Methods of describing toughness scatter 157
Table 5-2 Charpy impact test temperature and acceptance criteria (Lloyd's-Register, 2015) 158
Table 5-3 Key differences between toughness test and the Charpy test.....159
Table 5-4 List of manufacturers codes, origin and the year of steel productions ...164
Table 5-5 Details of the data set.....165
Table 5-6 Fracture toughness Statistics from various manufacturers 166
Table 5-7 Statistics of fracture toughness for AH 36, A and Welds (Calculations based on mean values from each manufacturer) 167
Table 5-8 steel batches variation of toughness (average of three tests data) 168
Table 5-9 T27 Variation of steel batches for manufacturer #5 (Transition curve analysis).....171
Table 5-10 Variation of T27 across steel batches for manufacturer # 4 (Transition curve analysis) 172
Table 5-11 Fracture toughness of analysed data 173
Table 6-1 m and c values for the single slope crack growth model 207
Table 6-2 Two slope crack growth model (King, 1998) and (BS7910, 2015 a) (Annex K) 208
Table 6-3 (Chatzidouros et al., 2015).....208
Table 6-4 Comparison of correlation relationship equations 208
Table 6-5 Results of statistical analysis of model uncertainty in terms of R-r from (Muhammed et al., 2000 a).....214
Table 6-6 Failure probabilities.....215
Table 6-7 Assessment inputs for crack growth in the plate.....218
Table 6-8 Fracture Mechanics results for crack growth in the plate.....219
Table 6-9 Assessment inputs for crack growth in the Stiffener 220
Table 6-10 Fracture Mechanics results for crack growth in the stiffener 220
Table 6-11 parameters used in the reliability analysis of the grand block butt weld 222
Table 7-1 Summary of the randomly taken samples.....237
Table 7-2 Mean and standard deviation and of ln values and their upper bound limits at each sample size ratio 238
Table 7-3 Final year failure probability of the case study joint for different sample sizes.....242

Table 7-4 Minimum Sample size for the grand block joint in deck 16 midship area 252
Table 7-5 Common conjugate priors (Hamada et al., 2008).....254
Table 7-6 Prior, Likelihood and the resulting Posterior parameter derived from Bayesian inference, N=2.....257
Table 7-7 Prior, Likelihood and the resulting Posterior parameter derived from Bayesian inference, N=10.....258
Table 7-8 Summary of the input assumption in Recursive Bayesian example 259
Table 7-9 Summary of Bayesian estimation for the toughness example 263
Table 7-10 UCL limits for various samples size of the case study joint 268
Table 8-1 Material properties of the case study structure 288
Table 8-2 Defect size data for case study ship based on table 4-13 289
Table 8-3 Defect rate data for case study ship based on table 4-15.....289
Table 8-4 NDT reliability characteristics assumptions based on section 4.5 289
Table 8-5 Final year failure probabilities at any location along the joint due to the presence of a planar defect.....290
Table 8-6 Calculation of required number of checkpoints based on reliability analysis 291
Table 8-7 Calculation of required number of checkpoints based on statistical process control limits.....292
Table 8-8 Proposed inspection plan based on the unified approach.....293
Table 8-9 The results of defected checkpoints containing planer defects 294
Table 8-10 limits for unacceptable checkpoints per joint 295
Table 8-11 Identifying joints which require further inspection 296
Table 8-12 Parameter estimate using Bayesian updating of detected defects for deck 16 297
Table 8-13 Parameter estimate using Bayesian updating of initial defects length and POD for RT in deck 16.....297
Table 8-14 Parameter estimate of defect rate distribution using Bayesian updating in deck 16 298
Table D-1 Descriptive statistics of the raw data.....329

ABBREVIATIONS

ABS	American Bureau of Shipping
ACI	American Concrete Institute
AI	Artificial Intelligence
AISC	American Institute of Steel Construction
ALARP	as low as reasonably practicable
AM	Asset Management
API	American Petroleum Institute
AQL	Acceptance Quality Limit
CCA	Cause Consequence Analysis
CCT	centre-cracked tension
COV	Coeficient of variation
CR	Computed Radiography
CT	Computed Tomography
CT	Compact Tension
CTOD	crack-tip opening displacement
CVN	Charo V-notch
DFF	design fatigue factor
DNV	DNV GL.
DPI	Dye Penetrant inspection
DPT	Dye Penetrant testing
DR	Digital Radiography
DT	Digital Twin
EC	Eddy Current testing
EPFM	elastic-plastic fracture mechanics
ETA	Event tree
EXC	execution classes
FAD	failure assessment diagram
FAL	failure assessment line
FATT	fracture appearance transition temperature

FCAW	Flux Cord Arc Welding
FM	Fracture mechanics
FMEA	Failure Mode and Effect Analysis
FORM	First Order Reliability Method
FTA	Fault Tress Analysis
GMAW	Gas Metal Arc Welding
HAZ	Heat Affected Zone
HAZOP	Hazard and Operability analysis
HLAW	Hybrid Laser Arc Welding
IACS	International Association of Classification Societies
ICAO	International Civil Aviation Organization
IoT	Internet of the Thing
KR	Korean Classification Society
LCL	lower control limit
LEFM	linear elastic fracture mechanics
LOF	Lack of Fusion
LOP	Lack of Penetration
LR	Lloyds Register
LRFD	Load and Resistance Factor Design
LRG	Lloyds Register Group
LSM	least square method
MC	Master curve
MLE	maximum likelihood estimate
MMA	Manual metal arc welding
MPI	Magnetic Particle Inspection
MVFOSM	mean value first order second moment
NDE	Non Destructive Examination
NDT	Non Destructive Testing
NK	Nippon Kaiji Kyokai
PAUT	Phased Array Ultrasonic Testing
POD	probability of detection

PT	Penetrant testing
PWHT	post weld heat treated
QA	Quality Assurance
QC	Quality Control
RBI	Risk-based inspection
RINA	Registro Italiano Navale
RT	Radiography testing
RTR	Real-Time Radiography
SAW	Submerged Arc Welding
SD	Standard deviation
SENB	single-edge notch bend test
SMAW	Shielded metal arc welding
SORM	Second Order Reliability Method
SPC	statistical process control
SSC	Ship Structure Committee
Std.	Standard deviation
TOFD	Time of Flight Diffraction
UCL	upper control limit
UT	Ultrasonic testing
VT	Visual Testing

NOMENCLATURE

a	Notch depth
a_0	Initial crack size
a_f	Final crack size
b_0	Initial ligament size
C_{Vmin}	Minimum Charpy energy
C_{V-US}	Upper shelf Charpy energy
C, m	Material constants in Paris equation
D_{total}	Total accumulated fatigue damage
$\dot{\varepsilon}$	Strain rate
$\Delta\sigma$	Stress range
$\Delta\sigma_{eq}$	Equivalent constant stress range
ΔK_{th}	Threshold stress intensity facture
ΔT_0	Temperature shift in transition temperature
$\frac{da}{dN}$	Rate of crack growth in Paris equation
δ	Crack tip displacement
δ_{el}	Elastic Crack tip displacement
δ_{pl}	Plastic Crack tip displacement
E	Elastic modulus
J	J-integral
J_{1mm}	J-integral value at 1 mm crack growth
J_{el}	Elastic J-integral
J_{pl}	Plastic J-integral
K	Stress intensity factor
K_0	Master curve Scale parameter Fracture for toughness
K_{IC}	Plane strain fracture toughness
K_{ID}	Dynamic fracture toughness
K_{JC}	Elastic-plastic
K_{mat}	Material fracture toughness
K_{min}	Minimum fracture toughness
K_r	Normalised crack driving force
$\dot{K}$	Rate of increase of the linear elastic stress intensity factor

L_r	Ratio between applied load and yield load
ν	Material's Poisson ratio
P_f	Probability of failure
r_p	Rotational factor
σ_c	Compressive stress
σ_l	Longitudinal stress
σ_{res}	Residual stress
σ_t	Transverse stress, or tensile stress
σ_U	Ultimate Tensile strength
σ_Y	Yield stress
σ_{ys}	Tensile strength at static loading rate
T_0	Transition temperature
T_0^{stat}	Transition temperature
t_{ref}	Reference thickness
t_p	Plate thickness
Y	Geometry function

ABSTRACT

Ship structures are made of steel members that are joined with welds. Welded connections may contain various imperfections. These imperfections are inherent to this joining technology. Design rules and standards are based on the assumption that welds are made to good a workmanship level. Hence, a ship is inspected during construction to make sure it is reasonably defect-free. However, since 100% inspection coverage is not feasible, only partial inspection has been required by classification societies. Classification societies have developed rules, standards, and guidelines specifying the extent to which inspection should be performed.

In this research, a review of rules and standards from classification bodies showed some limitations in current practices. One key limitation is that the rules favour a "one-size-fits-all" approach. In addition to that, a significant discrepancy exists between rules of different classification societies.

In this thesis, an innovative framework is proposed, which combines a risk and reliability approach with a statistical sampling scheme achieving targeted and cost-effective inspections. The developed reliability model predicts the failure probability of the structure based on probabilistic fracture mechanics. Various uncertain variables influencing the predictive reliability model are identified, and their effects are considered. The data for two key variables, namely, defect statistics and material toughness are gathered and analysed using appropriate statistical analysis methods. A reliability code is developed based Convolution Integral (CI), which estimates the predictive reliability using the analysed data. Statistical sampling principles are then used to specify the number required NDT checkpoints to achieve a certain statistical confidence about the reliability of structure and the limits set by statistical process control (SPC). The framework allows for updating the predictive reliability estimation of the structure using the inspection findings by employing a Bayesian updating method.

The applicability of the framework is clearly demonstrated in a case study structure.

Chapter 1

Introduction

1.1 Non-destructive Examination of newbuilding ship hull structures

Ship structures are joined with hundreds of kilometres of weld lines. The presence of weld in a structure potentially reduces the structure's fatigue life by introducing a discontinuity into the completed weld/parent material joint; this could be further amplified by the presence of defects which is inherent to the welding process. Rules, standards, and guidelines may require manufacturers to carry out certain procedures for enhancing weld's reliability, such as weld toe grinding to enhance weld profile geometry (and hence fatigue improvement), heat treatment to improve welded joint's toughness, and Non-destructive examination (NDE) to detect weld defects. Performing NDE for finished welds is the best way to find possible defects, and relevant rules for classification of ships require manufacturers to do so.

Since welds are designed assuming a good execution, the rules set flaw size acceptance criteria up to a point, which aims to verify the good workmanship/quality levels. Ship structures contain a large number of welded joints, and apart from visual inspection, it is not feasible to perform 100% NDE. Hence, only a number of checkpoints are selected on a sampling basis and subject to NDE (Amirafshari et al., 2018). Figure 1-1 depicts an example of NDE inspection plan for part of a ship side shell (Bow end). The checkpoints are marked with green colour in this figure. In merchant ships, the total number of checkpoints for the whole ship starts at around 500 checkpoints and can be as many as 10000, depending on the ship type, size, and the classification society to whose rules the ship is built.

The checkpoints assess the general quality of welding as well as ensuring that the critical structural elements are free from major defects (Amirafshari et al., 2018). This is aimed to be achieved through prescribing tables, formulas, and clauses defining the minimum number or length of inspection in various parts of the ship.

Prescribed tables and equations have evolved based on engineering judgement and historical experiences of cracks (Amirafshari et al., 2018).

As one of the funding partners of this research was Lloyds Register Foundation, the research proposal was put together in collaboration with Lloyds Register Group. Lloyds Register Group (LRG) is a maritime classification society and member of the International Association of Classification Societies (IACS). LRG was interested in assessing the adequacy of its rules and rules from other major classification societies against a robust engineering approach such as risk and reliability based inspection.

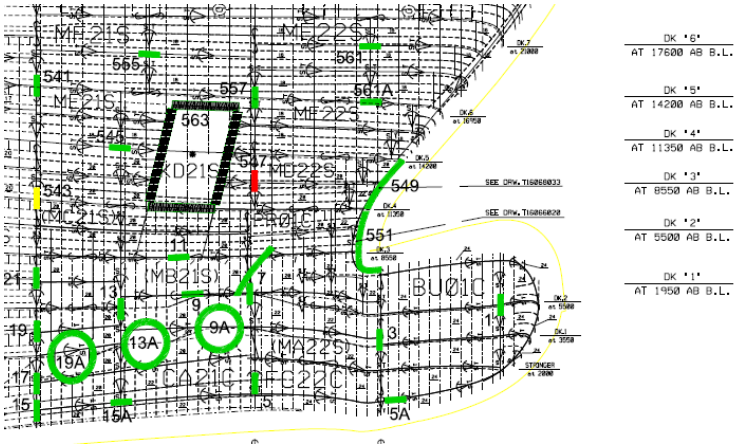

Colour key:
Black= Radiography tested
Green= Magnetic Particle Inspection/ Dye Penetrant Inspection
Yellow= Checkpoint failed NDT inspection in the first inspection
Red= Checkpoint failed the second NDT inspection after repair

Figure 1-1 Example of NDE inspection plan for part a ship side shell (Bow- Starboard)

1.1.1 Challenges: Background, scale and Impacts

Shipping is the pillar of the global economy. Approximately 80% of world trade by volume and 76% by value is transported by over 50,000 merchant ships trading internationally (UNCTAD, 2015). Ships are sophisticated, high-value assets and the operation and maintenance of merchant ships produce estimated annual revenue of over half a trillion US Dollars in freight rates.

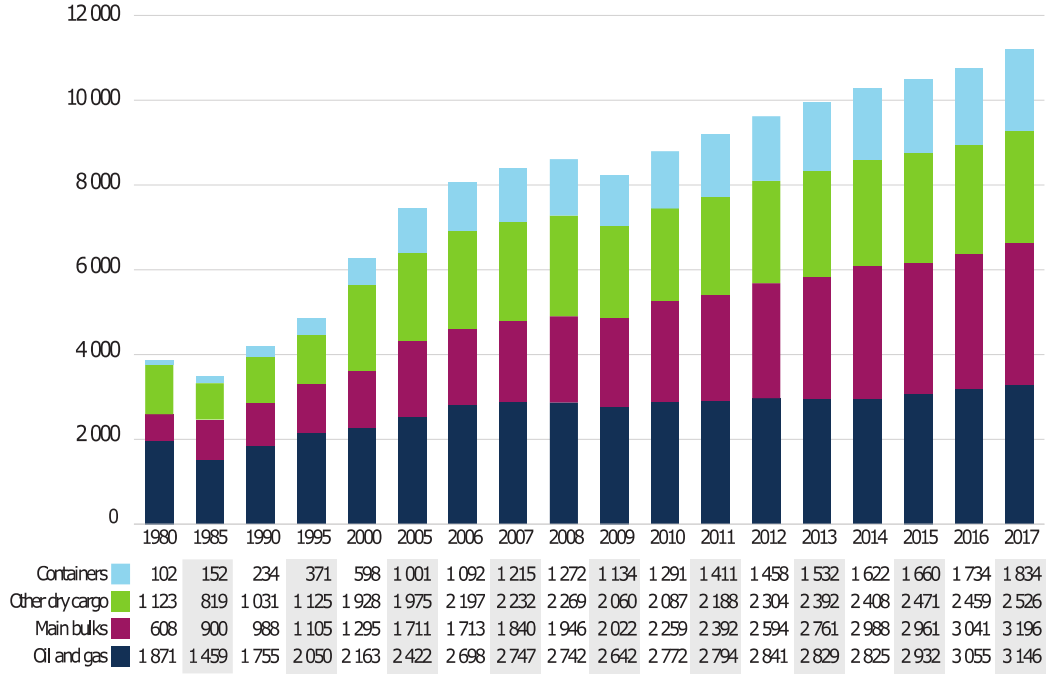

Figure 1-2 International seaborne trade, selected years, Millions of tons loaded, (Asariotis et al., 2018).

Seaborne trade continues to grow through its competitive shipping costs. Thanks to its improving efficiency, the prospects for the industry for further growth continue to be strong Figure 1-2 and Figure 1-3.

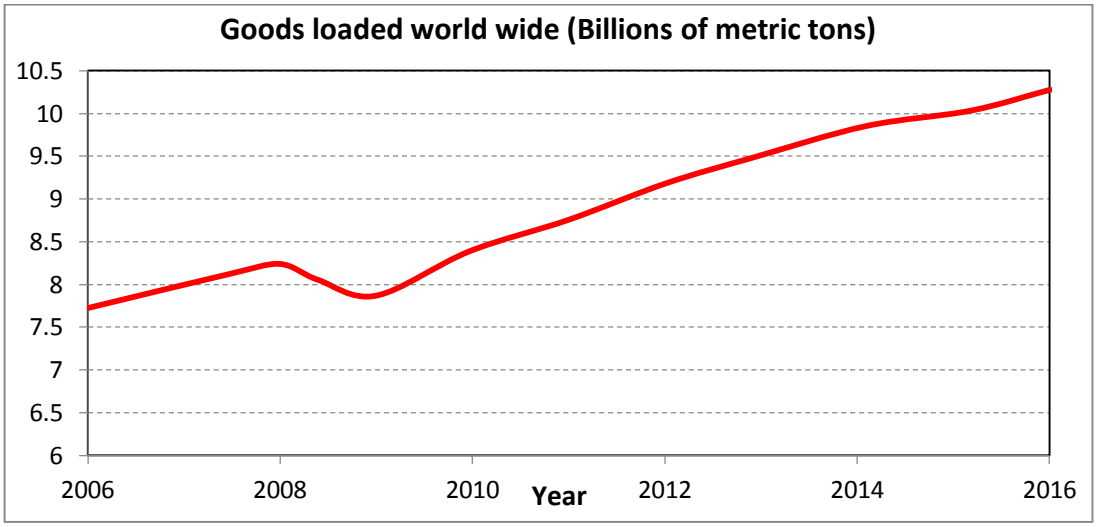

Figure 1-3 Goods loaded worldwide (UNCTAD, 2017)

In addition to seaborne trades provided by cargo carrier ships, the cruise industry produces substantial revenue worldwide with 386 ships. The 2018 total worldwide cruise industry is estimated at $40 billion with 26.7 million annualized passengers carried (Figure 1-4). The revenue is estimated based on the average revenue generated by each passenger for the major cruise companies over the past year,

which is $1500 per cruise. The market capacity is expected to increase to 36.9 million passengers by 2023 and to 39.57 million passengers by 2027 (Cruise-Industry-News, 2018). The cruise industry is the fastest-growing class in the leisure travel market. Since the early 1980s, the industry has seen an average passenger growth rate of nearly 7% per annum (f-cca.com, 2019).

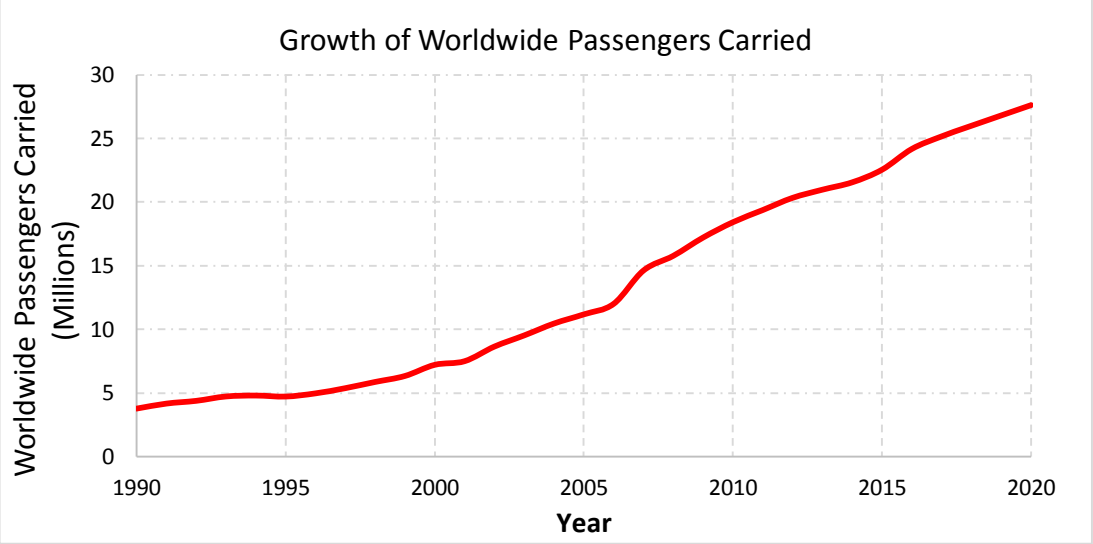

Figure 1-4 (Cruise-Market-Watch, 2018)

The growth in seaborne trade and cruise industry and retirement of old ships means constant demand for newbuilding ship production to meet market demands.

A total of 1.3 million gross tons and over 35,000 berths was estimated to have entered the market between April and December 2018. This represents approximately a seven per cent increase both in worldwide tonnage and overall berths (Jordan, 2018).

Two critical challenges in maritime industry related to this work are:

1. Improving ship safety,
2. Reducing construction, operation and maintenance costs.

1.1.1.1 Safety

Safety is possibly the most crucial parameter in ship management. A common way to quantify the safety of ships and investigate the causes are by measuring the statistic of ship accidents. Figure 1-5 shows Major Seaborne incidents and casualties' occurrences and their causes for 3647 ships from 2011 to 2017. Such information is used to optimise the areas of focus in ship safety improvement. For example, the

combination of collision (23.2%) contact (16.3%), and grounding/stranding (16.6%) shows the navigational casualties represent 53.1% of all casualties with ships. They also represent 37.8% of all occurrences. This suggests potential benefits of investing in navigational improvements. On the other hand casualties related to hull failure (a failure affecting general strength of the ship) were the least among all causes suggesting more economically optimised structural design and construction may be allowed.

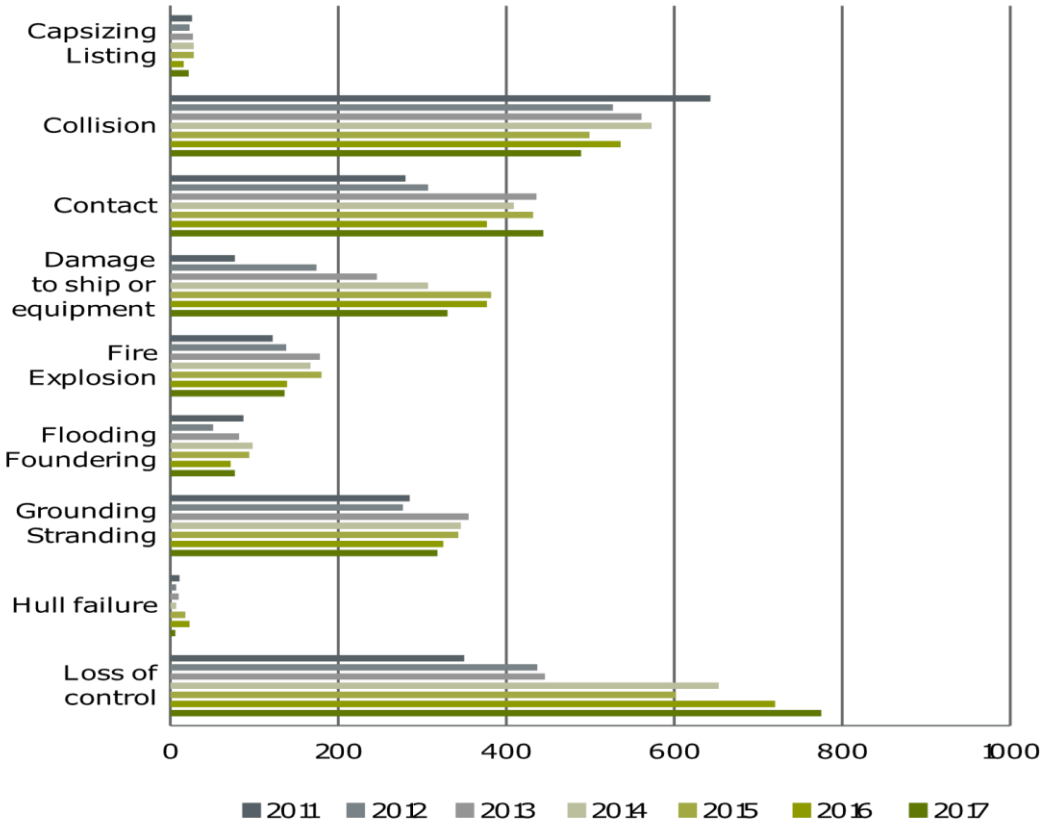

Figure 1-5 Distribution of casualty events with a ship from 2011 to 2017 (EMSA, 2018)

The maritime industry has been continuously investing in enhancing safety through R&D, employing existing and new technologies, training and automation of processes, autonomous shipping and developing risk-based approaches in design and Asset Management (AM).

Furthermore, emerging technologies such as Big data, blockchain technologies, Internet of the Thing (IoT), Artificial Intelligence (AI) and digital twin are perceived to have high potentials to address current safety issues (IUMI, 2018). Risk-based approaches, in particular, have shown to be very effective to reduce the risk of an accident through modelling risk scenarios, quantifying uncertainties of influencing

variables and forming risk barriers. The approach may be further enhanced through integration with emerging technologies such as big data, IoT, AI and Digital Twin (DT).

1.1.1.2 Costs

Life-cycle costs are also important. Any adjustment to the status quo should be financially beneficial to the stakeholders to meet the competitive market demands. Non-destructive examination of newbuilding ships has a direct impact on construction costs and an indirect impact on in-service inspection and maintenance costs.

Construction costs depend on the ship type and size. As presented in Table 1-1 for cargo carrier ships, the costs vary between $26 Million to $109 Million.

Ship type	Size Class		Cost (USD)
Bulk Carrier (BRSBrokers, 2018)	Handymax	Prices at the end of 2017 in China, South Korea and Japan	$23M to $24M
	Panamax		$26.5M to $28.5M
	Capesize		$46M to $48M
Tanker (BRSBrokers, 2018)	Suezmax		$53M to $58M
	Aframax		$46M to $52M
	VLCC		$78M to $83M
Container (Clarkson, 2017)	Feeder, 1000 TEUs, End of 2016		$16.3M
	Intermediate, 6 600 TEUs, End of 2016		$60M
	Neo-Panamax, 13 000 TEUs, End of 2016		$109M

Table 1-1 Newbuild cargo carrier ships cost estimate

Contrary to the cargo carrier ships which usually have one strength deck, the cruise ships typically have 10 to 18 passenger decks making them heavier in terms of steel and in turn more expensive. Cruise ships have much higher construction cost due to expensive outfitting and equipment; they are essentially floating hotels with cinemas, swimming pools, shopping centres, casinos, etc. Therefore, the cost is directly related to the passenger capacity. Currently, a typical cruise ship has around 3500 passenger capacity with a construction cost of around $400 Million. The largest cruise ships have around 6500 passenger capacity with a total cost of $1.4 Billion. Some examples of cruise ships construction costs are given in Table 1-2.

Ship	Year of Construction	Dimensions (m) LXBXD	Passenger capacity	Decks	Cost
MV Britannia	2013-2015	330X44X70.7	3647	16	£473 Million
MV Viking Sky	2012-2016	227X27 (D unknown)	930	14	$400 Million
Oasis of the Seas	2007-2009	361X47X60	6296	17	$1.4 Billion
Symphony of the Seas	2015-2018	361X47X72	6680	18	$1.35 Billion

Table 1-2 Examples of newbuild cruise ship costs (Ship-Order-Book, 2019)

Furthermore, the new cruise ships should make companies more profitable as passengers are willing to pay more to cruise on the newest vessels, which in turn tend to offer more spending opportunities on-board, while also being more cost effective to build and more efficient to operate (Cruise-Industry-News, 2018).

1.1.1.3 Stakeholders interests

For any inspection regime, it is crucial to outline inspection objectives according to the goals of the stakeholders that are involved in the process. There are three key stakeholders in ship construction;

1. Ship owner,
2. Manufacturer, and
3. Classification society.

A Ship owner's aim is to ensure that the structure is made to the highest quality possible so that the in-service maintenance costs are minimised. The fewer defects a ship contains before entering service, the more reliably it operates, and the less the long-term maintenance and through-life repair costs will be.

Ship manufacturers can reduce construction expenditure by reducing the number of NDE checkpoints, which subsequently decreases remedial actions and speeds up construction. It is common that Ship owners order ships which are classed under different classification societies, and one of their question is that why some classification societies have less demand for NDE checkpoints than others. Classification societies that permit reduced inspection (other things being equal)

argue that their rules are sufficient, and hence, there is no need for more extensive inspection. Some manufacturers, on the other hand, would claim that their general workmanship quality is good, and thus, more inspection is considered “redundant” (or no value added). They feel that some rules are overly conservative and do not take into account the welding quality achieved. This means that they are required to do the same extent of inspection as a manufacturer with a reputation for less emphasis on welding quality. Classification societies strive to rationalise their rules and achieve a more robust philosophy for their NDE checkpoint regimes. International Association of Classification Societies (IACS) members, in particular, try to establish, review, promote, and develop minimum satisfactory technical requirements in relation to design, construction, and survey of ships, and other marine units as part of their commitments to IACS directions.

1.1.2 The Approach: Risk-Based Inspection

Risk-based inspection (RBI) and maintenance have been used in a variety of industry sectors. There are specific standards for adopting RBI methods for plant and process equipment (API, 2009), and (API, 2008). In the offshore sector, such approaches have been used particularly for jacket structures, semisubmersibles, and FPSOs integrity management by, (DNV, 1996), (DNV, 2000) and (DNV, 2015). In the shipping sector, periodic inspections have traditionally been carried out. However, recently there has been increasing interest in RBIs (Bharadwaj and Wintle, 2011), (Barltrop, 2011 a), (Amirafshari, 2017), (Mansour, 1994), (Shinozuka, 1990), (Moan and Ayala-Uraga, 2008), (Mansour and Hovem, 1994), (Ayala-Uraga, 2009), (ABS, 2012) , (Moan, 2005), and (Ayyub et al., 2002), and classification societies are developing frameworks (LR, 2017) to enable such approaches to be used, often complementing the traditional time-based approach, but sometimes justifying changes to periodic inspections. Recent and ongoing developments in shipbuilding technologies and competitive market demand have pushed shipbuilders to building bigger and more complex ships. It is a challenge for the stakeholders to ensure the safety and reliability of vessels cost-effectively. Application of established risk-based approaches could allow shipbuilders to implement new complexity and innovations, which cannot be justified through current prescriptive rules due to their limitations (Papanikolaou, 2009).

1.1.2.1 Risk model

Risk-based approaches require an accurate, efficient and bespoke risk and reliability framework to be developed. The risk in this context is the combination of the

likelihood of an undesirable event and the consequence of such an event. Once the risk, i.e. associated with components or system is estimated, one can take action toward the improvement of that component or system. The improvement can be in design, or optimising maintenance inspection interval or extent. Risk assessment can be qualitative, which normally involves extensive use of engineering judgement, or quantitative, which requires a significant amount of data and numerical estimation of failure probability of the structure. A third approach is semi-quantitative where the attributes are those of both quantitative and qualitative approaches. The choice of the assessment depends on the availability of the data and assessment tools.

Here, the risk model needs to consider failure scenarios that can occur due to the presence of fabrication weld defects which remain in the structure after partial inspection, and to quantify the failure probabilities and the subsequent consequences.

1.1.2.2 Uncertainty

Risk-based methods are useful in the assessment of systems with significant uncertainty; particularly in degrading structures. Degrading mechanisms are usually governed by variables which pose a great deal of uncertainty; in these cases, the assessors have two options: 1) To deal with the problem by reasonably presuming the worst case scenario and design or inspect the structure accordingly, which is not always feasible. 2) To collect as much information as possible to reduce the uncertainty in order to predict the degradation of the system more accurately and also to assess the consequence of the degradation. The latter approach is the essence of risk-based methods. Model and variable uncertainties will result in an uncertainty in the occurrence of failure, or in other words probability of failure (1- Reliability).

1.1.2.3 Consequence

In addition to failure probabilities, consequence of failure is the other pillar of the risk assessment. With respect to failures caused by fabrication defects in ship hull structures a number of consequences are possible: failures of local, secondary and primary structure or hull girder which in turn can cause loss of service, repair costs, cargo and water leak, loss of reputation etc.

The tolerances against different consequences can considerably vary across ship types. It was pointed out to the author by one cruise ship owner that for example, a 20 cm crack at a cabin door frame will probably not endanger structural integrity of

the structure and the repair cost is relatively cheap, but it will damage the company's reputation in the eyes of the passengers and public. He said, "*The last thing I want is that a passenger takes a photo from that crack and posts it into social media or worse: pass it to a news corporate*". Such damage to reputation may have higher financial consequences for bigger companies. Companies such as Virgin Voyages have businesses in other sectors such as air travel, and one ship incident can jeopardise their entire corporate business. Thus, they may tolerate less risk levels or ask for higher target reliabilities.

One benefit of consequence modelling in the context of risk is that it allows for acceptable levels of risk to be chosen in a more systematic and rational way.

1.1.2.4 Relationship to the inspection

As outlined previously, Risk-based inspections have been found to be very effective in inspection planning by targeting areas with a higher risk profile. Additionally, inspection finding can be used to update the predictive reliability model by reducing uncertainty in variables related to defect statistics. In this research, one key aim is to use this capability of risk and reliability approaches to determine the required extent of inspection so that a certain confidence level on predictive structural reliability is achieved. Finally, it is aimed to quantify the effect of various levels of partial inspections on improving the actual reliability of the structure.

1.1.3 Case-study: Cruise ship deck structure

Among available ship types, a cruise ship was selected as the case study vessel. Contrary to the cargo carrier ships which have only one strength deck, cruise ships do not have a clear strength deck but instead are comprised of multi decks (including supperstucture) which contribute to the global strength of the structure (Shi and Gao, 2018). Modern cruise ships commonly have 10 to 16 decks. Thus, the majority of welding work is concentrated in this area of the hull. Figure 1-6 presents total welding work breakdown of a cruise ship with the main particulars of 306.02 X 37.2 X 8.20 (m) and 15 decks. Deck structure makes up 85% of the total welding of the structure. The data for this vessel was obtained by the author and from a cruise ship manufacturer.

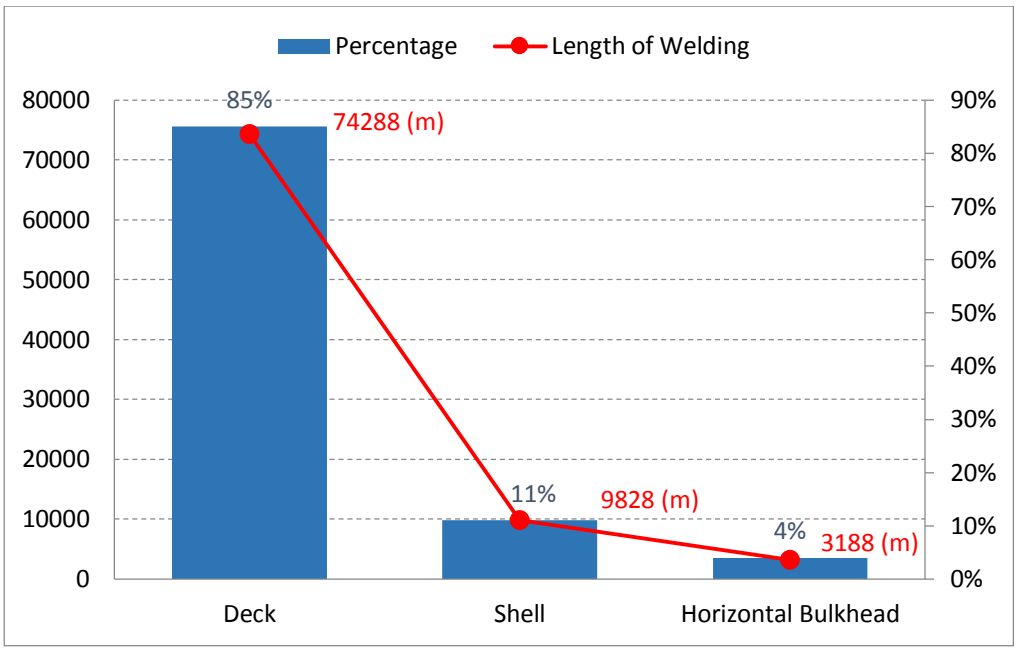

Figure 1-6 Welding work break down of a 15 deck cruise ship

From the stakeholders' points of view, the deck area in cruise ships is a subject of a serious debate:

Manufactures often argue that possible fabrication defects will not cause an in-service failure with a considerable consequence referring to the multi-deck nature of the structure.

On the other hand, the shipowner is concern about his investment ($400 Million to $1.4 Billion) and requires as many NDE as possible.

From a structural integrity point of view, one cannot be confident about the fitness of the structure for the intended propose until fracture mechanics proves it so. The acceptability of the structure under the presence of the weld fabrication defects will depend on the defect size and type, material toughness, stresses and the stress intensity solution. To the best of the author's knowledge, such a study for deck structure of a cruise ship has not been carried out before. Consequently, one of the objectives of this research is to conduct such a study.

From structural point of view, cruise ships can be much more complex than cargo carrying ships, particularly recently constructed cruise ship are designed to contain big opening within decks to accommodate leisure facilities such theatres, waterparks, etc. This creates unusual stress distributions within the deck structure which makes

basing decisions on engineering judgment or past experiences insufficient and further emphasises the need for a robust defect assessment study.

From a through-life inspection perspective, unlike cargo ships, the passenger decks in cruise ships will be covered by outfitting after structural construction and in-service inspection will be difficult and is left only to the special circumstances. Therefore, inspection during construction is probably the last time the joints are inspected before a failure occurs. This requires careful assessment of structural integrity of the decks and the effects the NDE extent may have on the through life structural reliability.

In this research, the focus will be on the deck structure of a cruise ship with the particulars of 330 X 44 X 70 (m) comprising 18 decks. More detail information about the ship is provided in Appendix E.

1.2 Aims & Objectives

The aim of the work presented in this thesis was to optimise the NDE inspection of Newbuilding ship hull structures by developing a Risk and Reliability Framework. In order to achieve this aim a number of objectives had to be met:

1. To clarify the context of the problem including clarification of the type of structure and structural components. And to The current and desired state had to be understood by conducting a gap analysis considering, business demands, stakeholders' interests, state-of-the-art and limitations which illuminated the areas the framework had to focus on.
2. To develop a risk model which represents risks associated with the presence of weld defects in ship hull structures, Key input variables and resulting target reliabilities.
3. To develop a bespoke reliability model and computer code (software) based on fracture mechanics to predict time-dependant reliability of the stiffened panel hull structures was developed.
4. To develop and method to calculate the required number of checkpoints which links target and predictive reliabilities to statistical confidence. The method uses Point estimate and Bayesian updating methods. In this

approach, acceptable defect rates are obtained based on target reliability and in conjunction with limits set by statistical process control (SPC).

5. Finally, a framework for optimised NDE inspection was proposed which combines the developed work from objectives three to seven and its applicability was demonstrated on the case study structure.

1.3 Structure of the Thesis

This thesis comprises the following chapters: An introduction to the topic, the problem, business demands and stakeholder's interests have been presented in this chapter (Chapter 1). This is followed by detail background information about shipbuilding process, weld defects, non-destructive testing and a review of the literature in Chapter 2, which is focussed on methodologies and approaches that have been applied in shipbuilding and other relevant industries. Then, relevant approaches are highlighted, as well as gaps and limitations in existing work. The methodology is described in Chapter 3. It focuses on developing a risk model and identifying key random variables, consequences of failure and target levels of reliabilities. Predictive reliability models and the respective results are discussed in detail in Chapter 6. In general terms, risk can be seen as the product of the probability of failure (1-Reliability) and the consequence of failure. A major task in this work was to develop a predictive reliability model which accurately predicts time-dependent reliability of the structure with a relationship to the information obtained from NDE inspection. The volume of the final work showed that this required an independent chapter. Since uncertainty assessment of defect data and fracture toughness has a significant impact on the predictive reliability results, they are presented in Chapter 4 and Chapter 5, respectively and prior to the reliability chapter (Chapter 6). Chapter 7 studies the effect of statistical confidence on the predictive reliability and specifies the required number of NDE checkpoints by treating them as samples that are representative of the entire weld joint and all other similar joint with the corresponding statistical confidence level. Bayesian statistics tools are developed to update initial assumptions about input variables, particularly defect statistics, which can be used to update predictive reliabilities as well as deciding about increasing or reducing future inspections. Reflections on the learning outcomes from the development of the methodology and its application to the case study are discussed separately in each chapter wherever it is relevant. A proposed framework for

optimised inspection and its application to the case study structure is presented in Chapter 8. The overview of the framework is shown in Figure 1-7. Concluding remarks together with potential transferability to other problems are provided in Chapter 9.

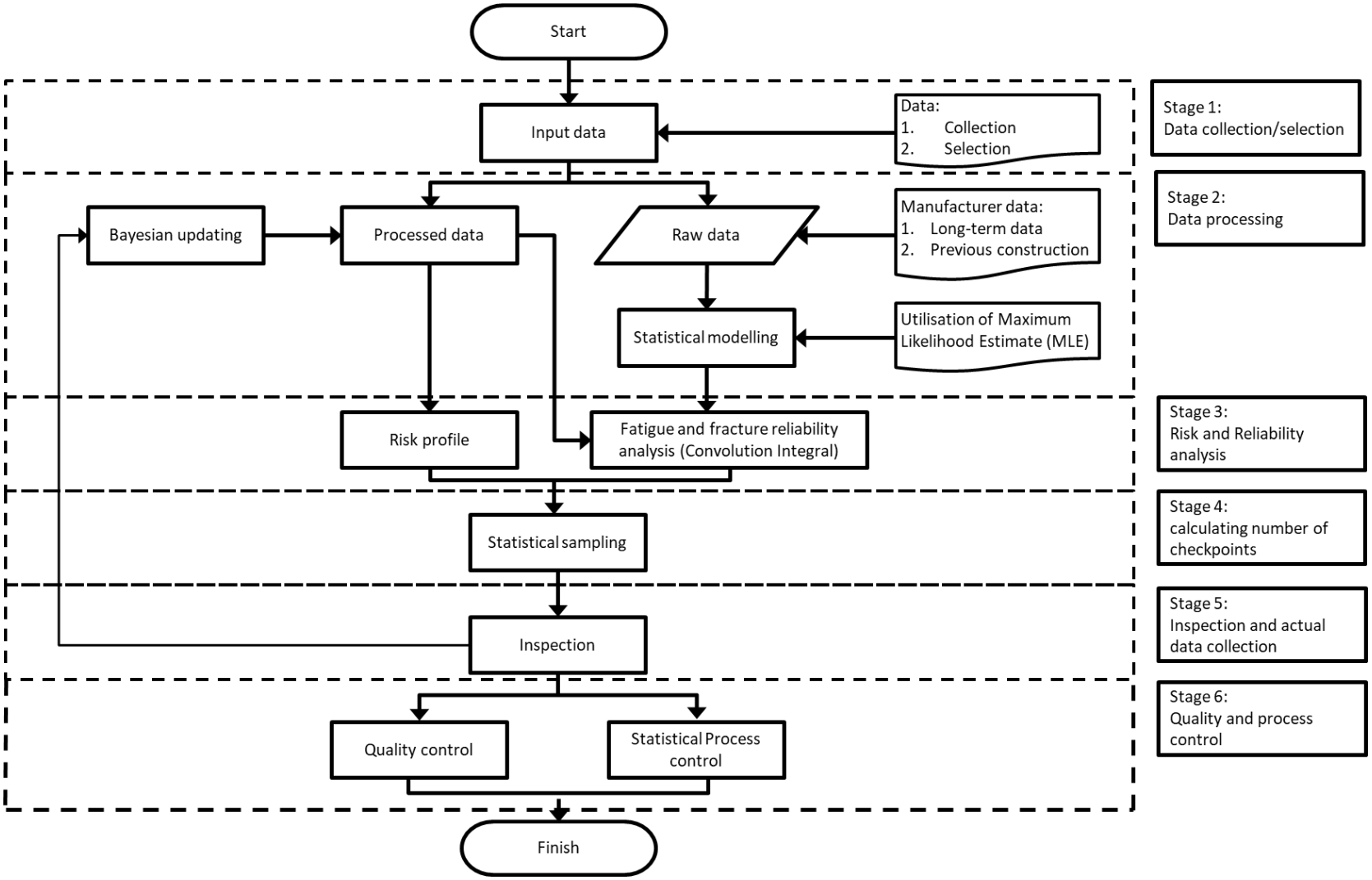

Figure 1-7 Overview of the inspection framework

Chapter 2

Background & Literature review

2.1 Chapter Outline

Ship hull structures are built from steel plates and components that are joined together using welding. Formation of defects is inherent to this joining technique. Non-destructive Examination (NDE) is used to detect these defects in the finished welds. This chapter provides background information about shipbuilding process, welding defects and their significance, welding processes, NDE techniques and a critical review of current approaches in NDE inspection of newbuilding ship hull structures. Additionally, The NDE inspection strategies of newly finished welds in other industries are reviewed.

2.2 Ship Fabrication Process

The block assembly production method is the most common method of shipbuilding. The blocks are constructed in the covered workshops and then transported to building docks. The pre-erected fabrication block weight depends on the crane capacity available. Figure 2-1 shows a shipyard crane transporting a block.

Figure 2-1 Block weight depends on the crane capacity available

Generally, the following production phases are standard procedures in manufacturing and assembling which may be categorised into three phases:

Phase 1 (Panel line):

- Steel storage
- Part fabrication which is about 15% of the block workload and includes manufacturing of bending models, plate marking and cutting, profile making and cutting, forming of plates, and forming of profiles.
- Part assembly which includes preliminary assembly, related part fabrication of brackets, floors and keel plates and bulkheads.
- Sub-block assembly in panel line which includes joining plates using butt welding and installation of stiffeners on the plates (see Figure 2-2 and Figure 2-7).

Plates are cut and the stiffeners are attached using an automated welding process

Figure 2-2 Part 1: Panel line and sub-assembly

Figure 2-3 Assembly of pre-assembled parts in blocks

Phase 2 (Block Assembly):

- Assembly of pre-assembled parts in blocks (Figure 2-3 and Figure 2-7);
- Assembly of blocks in grand-blocks or sections-blocks (Figure 2-4 and Figure 2-7)

Grand-blocks are:

- Ship parts composed of the shell structure, bilge/wing tanks
- Multilayer part of superstructure
- Larger part of ship's stern or bow

Section blocks are slices of ship including the whole cross-section and usually require special transmission equipment.

Despite the above distinction "Grand-block" and "Section-block" notations are often used interchangeably.

Figure 2-4 Grand blocks at a shipyard (Passenger ship)

Part 3, Hull erection in the building dock or spillway:

Grand blocks and section blocks are transferred to the dry dock for the final stage of hull assembly (Figure 2-6 and Figure 2-8). This is the last stage of structural assembly, and once this stage is completed, the dry dock is filled with water and the vessel may be transferred to the adjacent dock for the outfitting stage (Figure 2-5).

Figure 2-5 Empty dry dock (right). A ship at outfitting stage (left).

Figure 2-6 Block erection in dry dock

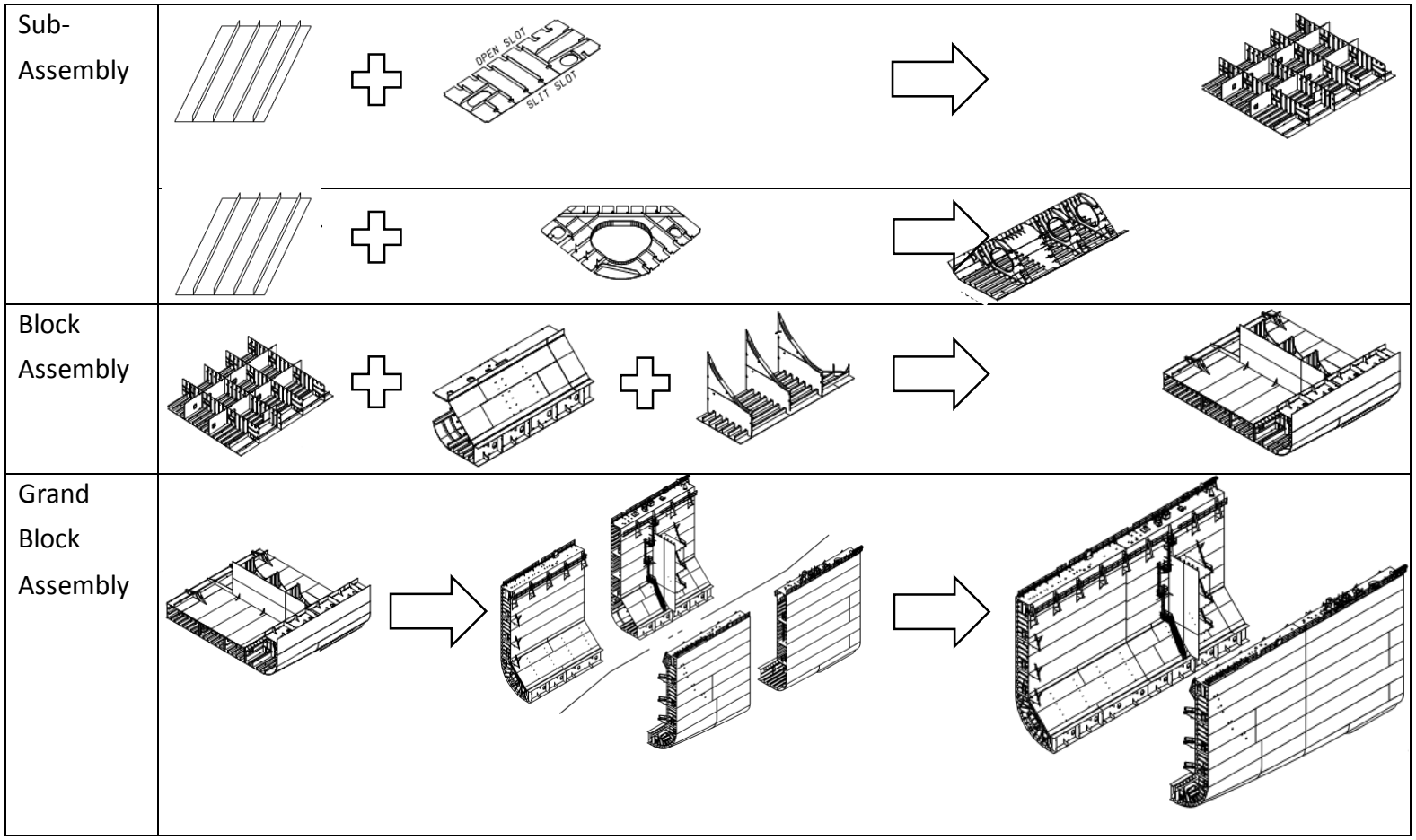

Figure 2-7 Sub-assembly and Block assembly and Grand Block assembly process

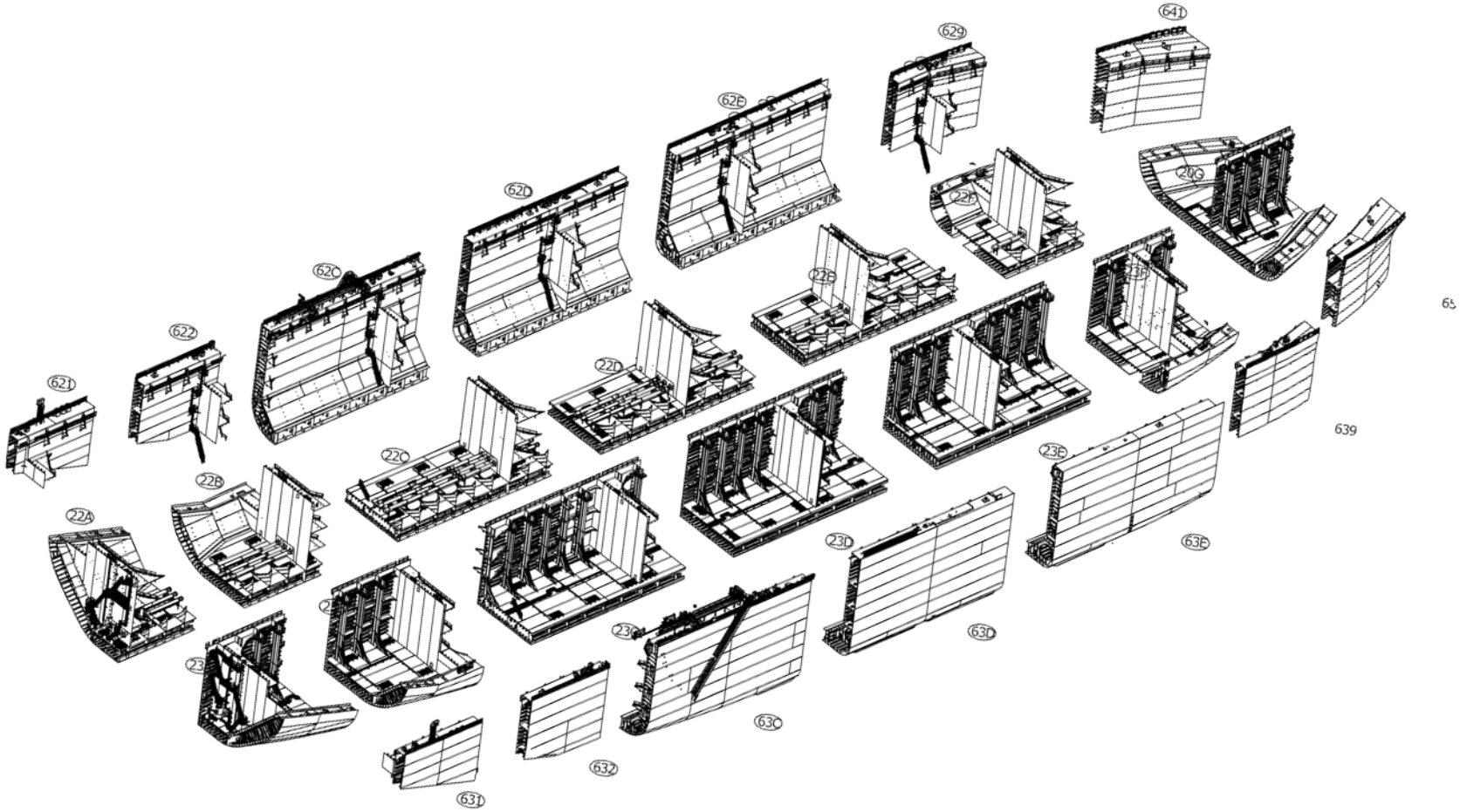

Figure 2-8 Hull Erection

2.3 Weld

Welding is joining materials by fusing them using high heat input, usually with the addition of more molten material, and letting them cool down together to form a unified part, contrary to brazing and soldering in which the parent material is not melted. There are several broad welding process categories including Arc welding, Gas welding, Resistance welding, Energy beam welding and Solid-state welding. Ship hull structures are predominantly joined using arc processes due to their costs and efficiency. Hence, only the arc process and the Hybrid Laser Arc Welding process are discussed here.

2.4 Welding process

2.4.1 Shielded Metal Arc Welding (SMAW)

Shielded metal arc welding (SMAW) or Manual Metal Arc Welding (MMA) was invented in Russia in 1888. It involved a bare metal rod with no flux coating to give a protective gas shield. The development of coated electrodes did not occur until the early 1900s when the Kjellberg process was invented in Sweden, and the quasi-arc method was introduced in the UK (TWI, 2015 a).

The MMA process is the most versatile of the welding processes and is suitable for most ferrous and non-ferrous metals, over a wide range of thicknesses. It can be used in all positions, with reasonable ease of use and is relatively inexpensive. The final quality is primarily dependent on the skill of the welder (TWI, 2015 a).

When an arc is struck between the coated electrode and workpiece, both the electrode and workpiece surface melt to form a weld pool. The average temperature of the arc is approximately 6000 °C, which is sufficient to simultaneously melt the parent metal, consumable core wire and flux coating, see Figure 2-9. The flux forms gas and slag, which protect the weld pool from oxygen and nitrogen of the surrounding atmosphere. The molten slag solidifies and cools and must be removed from the weld bead once the weld run is complete (or before the next weld pass is deposited). The process allows only short lengths of weld to be produced before a new electrode needs to be inserted in the holder.

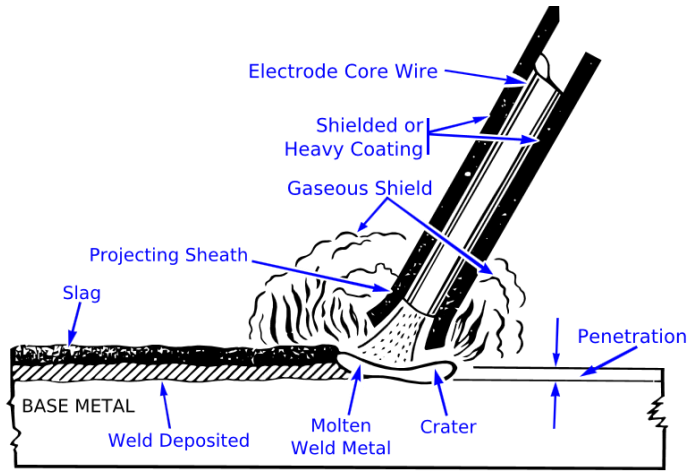

Figure 2-9 MMA/ SMAW process diagram (Wikimedia, 1993)

The advantages and disadvantages of the MMA process are:

Advantages	Disadvantages
• Can be used in field and shop • A wide range of consumables • All positional • Simple and portable equipment	• High welder skill is required • Arc strike and slag inclusion are common • High level of fumes (Health and Safety) • Hydrogen control

Table 2-1 Advantages and disadvantages of MMA process (TWI, 2015 a)

2.4.2 Submerged arc welding (SAW)

Submerged arc welding (SAW), is a welding process in which an arc is struck between a continuous wire and the parent metal. The arc, electrode tip and molten pool are submerged in a flux, which changes into gas and slag in its lower layers when subjected to the arc heat, protecting the weld from impurities. The wire electrode is fed uninterruptedly. The flux is fed from a hopper attached to the welding head, and a tube from hopper spreads the flux in a constant elongated embankment in front of the arc along the intended weld line, the weld is shielded from the atmosphere (TWI, 2015 a), see Figure 2-10. Unmelted flux is recovered for use.

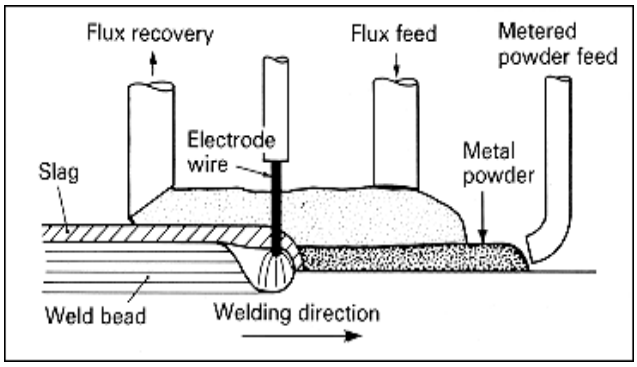

Figure 2-10 Submerged Arc Welding (SAW): Principle (Left), Process in practice (TWI, 2018 a)

The notable advantage of SAW is its ability to employ high currents due to the properties of the flux. Such currents provide deep penetration and high deposition rates (TWI, 2015 a). SAW is widely used in the fabrication of ships, pressure vessels, pipelines and railway carriages and anywhere where long welds are required. It can be used to weld thicknesses from 1.5 mm upwards. The use of powdered flux limits the process to the flat and horizontal-vertical welding positions.

2.4.3 Gas Metal Arc Welding (GMAW)

Known in the USA as gas metal arc welding (GMAW), the metal inert gas (MIG) or metal active gas (MAG) welding process is a flexible welding process suitable for both thin and thick section components in most metallic materials. An arc is hit between the tip of a wire electrode and workpiece, melting both to form a weld pool, and serves as the source of heat (via the arc at the wire end) and filler metal for the joint, see Figure 2-11. The wire is fed via a copper contact duct which conveys electric current into the wire. The weld pool is shielded from the air by a shielding gas fed through a nozzle surrounding the wire. The wire is fed from a spool by a motor drive, and the welder or machine moves the welding gun or torch along the joint line. The process offers high productivity and is economical since the consumable wire is continuously fed (TWI, 2015 a).

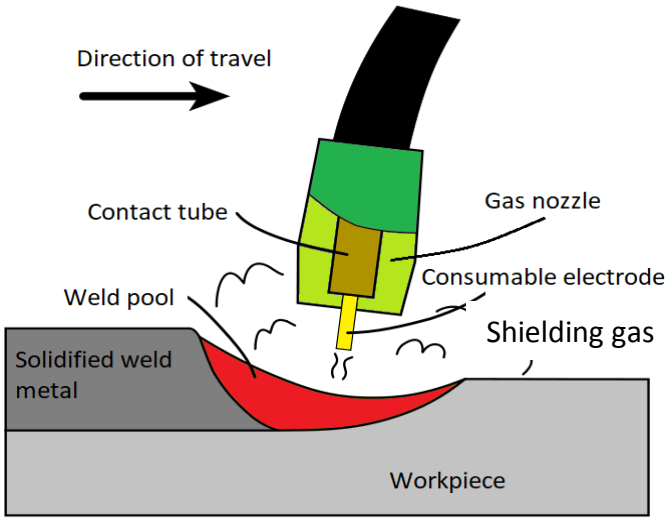

Figure 2-11 Gas Metal Arc Welding (GMAW) diagram (Wikimedia, 2012)

The process uses semi-automatic, mechanised or automatic equipment. In semi-automatic equipment welding, the wire feed rate and arc length are controlled automatically, but the wire position and travel speed are under manual control. In mechanised welding, all parameters are under automatic control, but they can be

varied manually during welding, e.g. steering of the welding head and adjustment of wire feed speed and arc voltage. With the automatic kit, there is no manual involvement during welding. The advantages and disadvantages of the process are:

Advantages	Disadvantages
• High productivity • Easily automated • All positional (di, pulse and FCAW) • Material thickness range	• Lack of fusion (dip transfer) is common • Limited range of consumables • Protection for site working • Complex equipment • High ozone levels

Table 2-2 Advantages and disadvantages of the GMAW process (TWI, 2015 a)

2.4.4 Flux Cord Arc Welding (FCAW)

The development of self- and gas-shielded FCAW in the mid-1980s was a major innovation in the successful application of on-site semi-automatic welding and has also enabled a much wider range of materials to be welded. The cored wire consists of a metal covering holding a granular flux. This flux can contain components that would usually be used in MMA electrodes, so the process has a broad range of applications (TWI, 2015 a).

Additionally, the flux can be enhanced by the addition of gas-creating compounds so the process can be free of separate gas shield, which limits the use of conventional GMAW welding in many circumstances. See Figure 2-12.

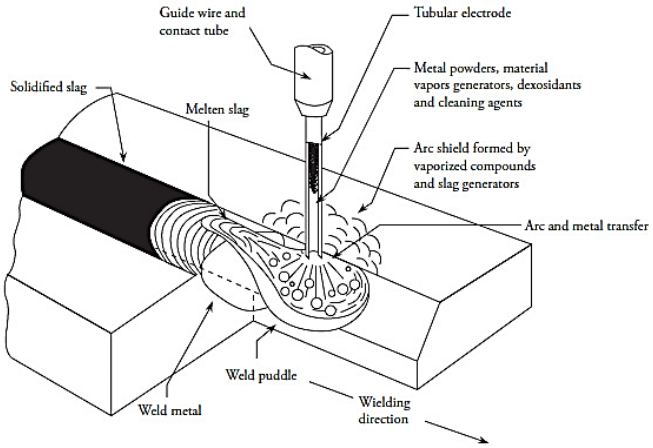

Figure 2-12 Flux Cord Arc Welding (FCAW) diagram (Journal, 2009)

2.4.5 Hybrid Laser Arc Welding (HLAW)

Laser beam welding (WBE) is a joining process using laser beam. The focussed heat generated by the laser beam is used to create a narrow and deep weld. The process is also very efficient owing to its high deposition rate (Webster et al., 2008). Hybrid

laser-arc welding (HLAW) combines laser with an arc process in the same melted pool resulting in a process which has the benefits of both processes, see Figure 2-13. Deep pentation hybrid welds made by this process are comparable to those achieved by laser welds and also having weld cap profile similar to arc welds. HLAW may be further improved by adding a gas-blend containing consumables, resulting in more enhanced weld quality than laser welds (Gerritsen and Howarth, 2005).

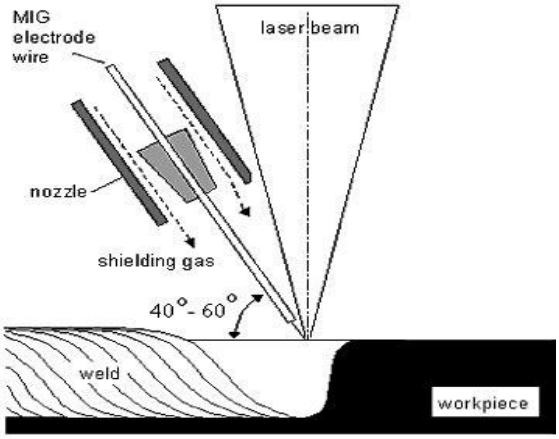

Figure 2-13 Hybrid Laser Arc Welding (HLAW) (TWI, 2018 b)

HLAW has been increasingly used in shipbuilding due to its merits over the arc welding: Higher welding speed and penetration, compared with arc welding alternatives such as GMAW welding or SAW, are significant: the net heat input can be reduced, resulting in lower distortion, making the process an efficient choice for the welding of long seam welds joining plates or sections, etc. The costs related to distortion correction and rectification is also reduced, subsequently (Olsen, 2009).

2.4.6 Common Welding Processes in ship production

A number of welding processes are used in ship production. Detailed reporting on the choice of the welding process is not the intention of this research. A comprehensive study as a joint industrial project was conducted and reported on welding mechanisation, and automation worldwide in 1996 and referenced are made to (Boekholt, 1996). Commonly used welding processes and weld types in ship hull fabrication are given in Table 2-3 and Figure 2-14.

No.	Component	Weld type	Process	Remarks
1	Panel plate to panel plate	Horizontal Butt (Seam)	One-sided SAW	Automatic
2	Longitudinal member to panel plate	Fillet	FCAW, HLAW	Automatic
3	Double bottom inside	Fillet	FCAW	Semi-automatic
4	Side shell(Section weld)	Transverse Butt (Butt)	FCAW	Semi-automatic
5	Longitudinal member to Longitudinal member	Transverse Butt (Butt)	One-sided FCAW	Semi-automatic
6	Tank top plate to Hopper tank plate and bulkhead	Fillet	FCAW	Semi-automatic
7	Tank top plate to tank top plate	Horizontal Butt (Seam)	One-sided SAW	Automatic
			One-sided GMAW	Automatic GMAW

Table 2-3 Typical weld types and processes in shipbuilding ((Boekholt, 1996), (Kobelco, 2011))

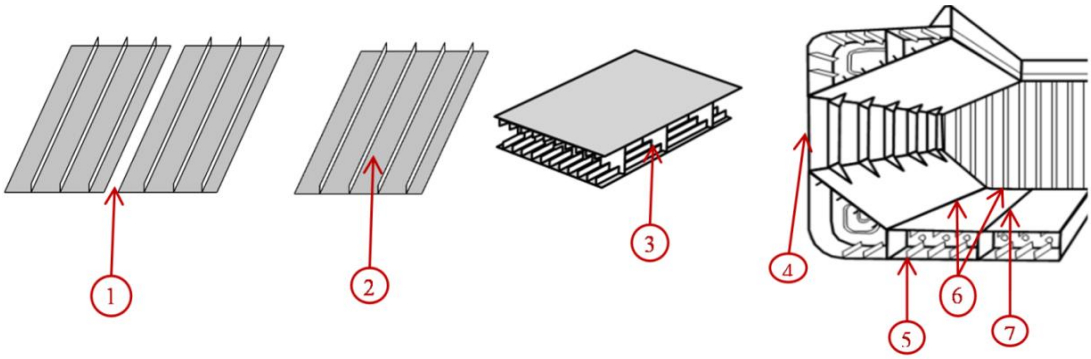

Figure 2-14 Typical weld types application in shipbuilding (Boekholt, 1996), (Kobelco, 2011).

Most commonly used welding processes in the shipbuilding industry are flux-cored arc welding (FCAWs), submerged arc welding (SAW), double-sided and one-sided, automatic, portable welder, line welder, semiautomatic, and robotic (Table 2-3). FCAWs are popular, as they offer higher deposition rates over other types of filler metals, thus improving welding efficiency. FCAWs are also capable of high usability in all positions, which is suitable for ship hull construction as hulls comprise large components with flat, vertical, overhead, and curved welding lines (Kobelco, 2011).

Since hull structures have many confined areas that are difficult to access, one-sided welding by FCAW is common. SAW process is particularly used for one-sided welding of butt joints of large shell plates (Kobelco, 2011).

2.5 Weld Defects

Figure 2-15 illustrates common weld defect types. (ISO, 2007) provides a detail description of flaw and defect types. The standard recognises 26 different types of weld imperfections. This standard is adopted by many ship classification societies. It should be noted that there is a distinction between flaw and defect in (ISO, 2007): A flaw is considered as any weld imperfection, but a defect is an unacceptable flaw.

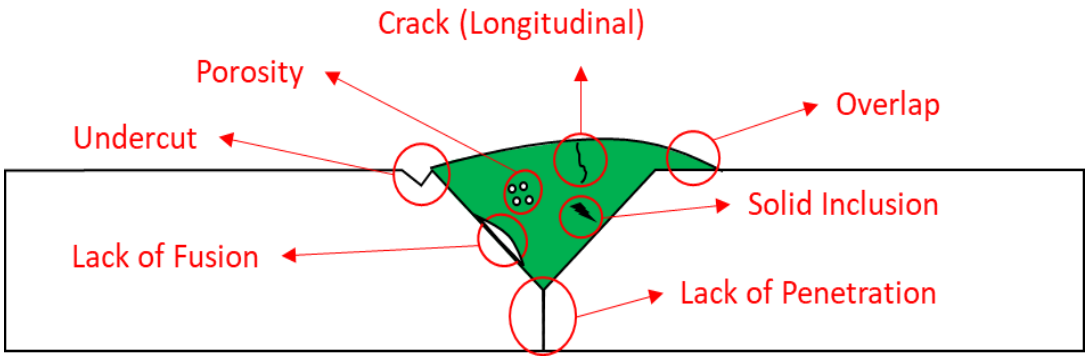

Figure 2-15 Common Weld imperfections

Severe flaws such as crack-like defects are always unacceptable, so can either be regarded as flaws or defects. Fracture mechanics assessment may be used to show acceptability of certain planar flaws. Currently, a well-established acceptability assessment of non-planar flaws using fracture mechanics is not available. Such defects are commonly assessed using a quality category approach. In this approach, the weld joint needs to be qualified for a certain quality level. In practice, stress at weld joint is calculated, and the required fatigue class is specified based on the related design S-N curve. The lower the stress, the lower fatigue class is allowed. A lower quality level requires less strict acceptance criteria. This is explained in more details in section "2.6 Significance of weld defects".

Stress Corrosion Cracking (SCC) is a generic term to describe any behaviour in which combination of a static load and an aggressive environment results in progressive propagation of a corrosion crack (Milella, 2012). The effect of defects on structural integrity in corrosive environment will be more adverse due to increased rate of crack growth. When thikness loss due to corrosion is considered, incearesed levels of local stresses need to be considered, as well. In this research, since the case study structure is in deck area corrosion effects are not considered. Crack growth rates in corrosive environment can be found in one of the available crack assessment standards such as (BS7910, 2015 a). Furthur information about stress corrosion cracking can be found in (Milella, 2012).

2.5.1 Porosity

Porosity is the formation of voids in the weld metal as a result of entrapment of gas released from the weld pool when it solidifies. Porosity can be in the form of single, clustered or distributed pores and could be embedded or surface breaking. Common causes and possible preventive measures of the Porosity are listed in Table 2-4.

Cause	Prevention
Rust, oil, paint, or moisture on the joint fusion faces and high sulphur content of the base metal	Cleaning the joint fusion faces
Moisture in coatings (SMAW), flux (SAW), or shielding gases (GMAW)	Drying coatings (SMAW) and fluxes (SAW) and use suitable shielding gases (GMAW)
Too little shielding gas (GMAW) or flux-burden height (SAW)	Use a proper amount of shielding gas (GMAW) and flux-burden height (SAW)
Strong wind (SMAW, GMAW)	Use a wind screen (SMAW, GMAW)
Too high welding amperage, arc length, or arc voltages	Use appropriate parameter

Table 2-4 Porosity causes and remedies (TWI, 2015 a), and (Timings, 2008)

2.5.2 Solid inclusion

Solid inclusion is the presence of external solid substances in the weld metal entrapped in the weld pool during solidifications. Solid inclusion can be: slag inclusion caused by entrapment of weld slag in the molten weld pool, flux inclusion which is only found in flux related welding processes (i.e. MMA, SAW and FCAW), Oxide inclusion or Tungsten inclusion (only in tungsten inert gas (TIG) process) (TWI, 2015 a) and (Lincoln, 2015). Common causes and possible preventive measures are listed in Table 2-5.

Cause	Prevention
Low heat input	Increase current input and,or arc voltage;
Incomplete slag removal from the surface of below weld pass in the multi-pass weld	Remove slag of the preceding layer completely
Slag flooding ahead of the arc	Position work to gain control of slag
Incompletely melted flux becomes trapped in the weld	Change the flux/wire. Adjust welding parametric, i.e. current, voltage etc. to produce satisfactory welding conditions.

Table 2-5 Solid inclusion causes and remedies (TWI, 2015 a), and (Timings, 2008)

2.5.3 Lack of Fusion (LOF)

Lack of fusion or cold lapping, occurs when there is an insufficient fusion between the weld metal and the base plate. Lack of fusion is commonly caused by poor welding technic and is related to the welder's skill (TWI, 2015 a) and (Lincoln, 2015). Common causes and possible preventive measures are given in Table 2-6.

Causes	Prevention
Low heat input to the weld	Increase welding current
Inappropriate weld parameters controlled by the welder, Large MMA electrodes, Large root face, Small root gap, and incorrect electrode angle	Use appropriate welding parameters technique

Table 2-6 Lack of fusion causes and remedies (TWI, 2015 a) and (Timings, 2008)

2.5.4 Lack of Penetration

Lack of Penetration occurs when the weld metal fails to penetrate the entire thickness of the plate, two opposing weld beads do not interpenetrate, or the weld bead fails to penetrate the toe of a fillet weld but only links across it. This is illustrated in Figure 2-16.

Similar to lack of fusion, lack of penetration is commonly caused by low heat input or too low welding speed and can be avoided by increasing welding current (TWI, 2015 a) and (Lincoln, 2015).

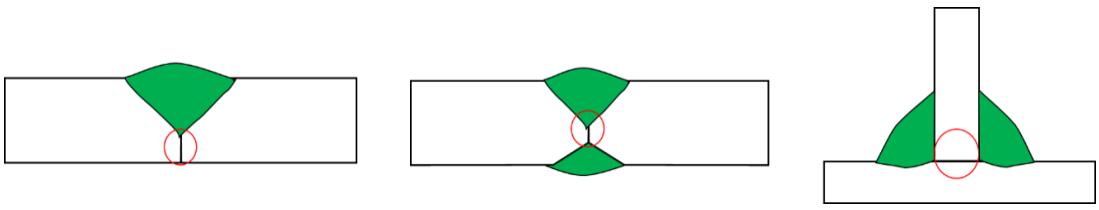

Figure 2-16 Three modes of Lack of Penetration

2.5.5 Cracks

Cracking is an imperfection produced by a local rupture in the solid state weld, which may be caused by cooling or stresses. As shown in Figure 2-17, cracks formed parallel to weld direction are called longitudinal cracks, and those approximately perpendicular to the joints direction are called transverse cracks. Longitudinal cracks can be centreline cracks which are normally induced by unfavourable segregation, bead shape, or surface profile. Longitudinal cracks occur at the Heat Affected Zone (HAZ) and are normally hydrogen induced by nature. Transverse cracks are also usually hydrogen assisted or caused by overmatching. The classification weld cracking is summarised in Table 2-7.

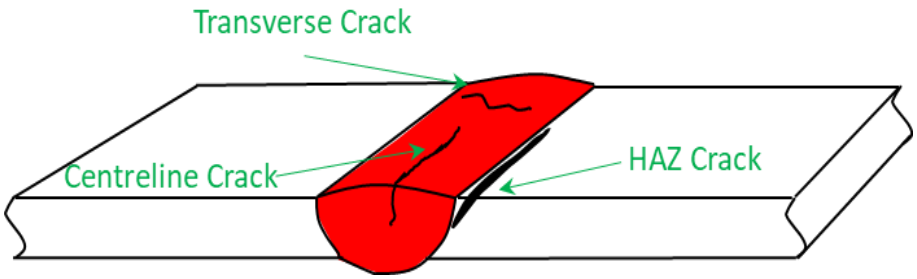

Figure 2-17 Weld Crakes diagram

Longitudinal Cracks		Transverse Cracks
Centreline Cracks	HAZ Cracks	• Overmatching • Hydrogen assisted
• Segregation Induced Cracking • Bead Shape Induced Cracking • Surface Profile Induced Cracking	Hydrogen Induced Cracks	

Table 2-7 Classification of weld cracking and their causes

2.5.5.1 Longitudinal Cracks

Weld fabrication cracking occurs as a result of weld shrinkage stress, solidification and cooling during the weld formation process. The development of this type of weld cracking is not a result of service loads. Weld fabrication cracking can be categorised into hot cracking and cold cracking. Hot cracking occurs at elevated temperature and is normally related to the solidification process. Cold cracking happens after the weld cooling process completed and is usually hydrogen-related.

Shrinkage strain that occurs during weld metal cooling is the main cause of most weld cracking, as illustrated in Figure 2-18. If the contraction is restricted, the shrinkage strains generate residual stresses which may lead to crack formation. The shrinkage stresses are resisted by the joint boundary loads. Larger weld sizes and deeper penetration procedures are more likely to cause such cracking. Higher weld yield strength (Overmatching), also, produces higher residual stresses and in turn more susceptibility to cracking (Lincoln, 2015).

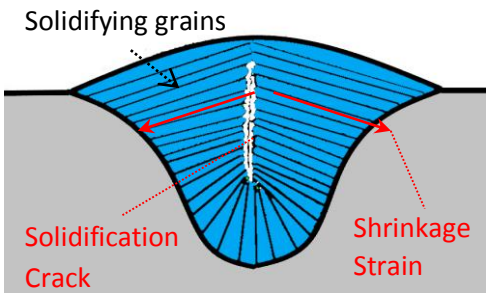

Figure 2-18 Solidification Cracking diagram

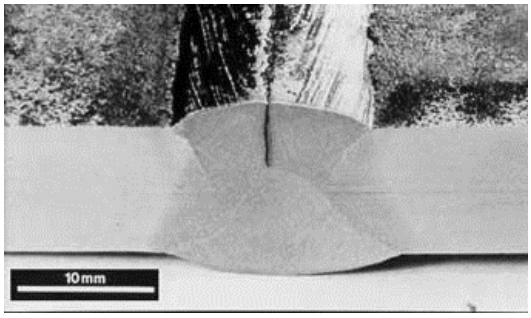

Figure 2-19 Solidification Crack (TWI, 2016 a)

2.5.5.1.1 Centreline Cracks

If a longitudinal crack happens to be at the centre of the weld bead, it is referred to as a centreline crack (Figure 2-19). In the case of single pass welds, the crack is always in the centreline of the joint, but in multi-pass cracks, the crack may not occur in the geometric centre of the joint. As explained in the previous section, Centreline cracks can be caused by segregation which occurs when elements of the weld pool such as copper, zinc, phosphorus and sulphur compounds move to the centre of the weld due to their low melting point. The weld tends to detach as the solidified mixture contracts away from the centre region which is still liquid. When a weld cross-section has more depth than the gap width, the solidifying grains forming perpendicular to the surface, Figure 2-18, do not bind across the joint and a crack induced by weld bead shape occurs (Lincoln, 2015). The final mechanism of Centreline cracks formation is surface profile conditions, and it is when internal shrinkage stresses create tension stress on the weld surface as a result of a concave weld profile. Causes and the preventive measures for these three mechanisms are given in Table 2-8.

Mechanism of crack formation	Cause	Prevention
Segregation	Contaminant pick up	• Limit penetration • Use buttering technique • Use filler with magnesium to avoid the formation of low melting point sulphide irons (for steels with high sulphur content)
Bead shape	Deep penetrating processes (e.g. SAW and CO2 shielded FCAW)	• Increase width to depth ratio by reducing current density
Surface profile	• High voltage • High-speed welding • Vertical-down position	• Decrease voltage • Reduce welding speed • Use vertical-up position

Table 2-8 Centreline cracks causes and their preventive measures (TWI, 2015 a), and (Timings, 2008)

2.5.5.1.2 Heat Affected Zone (HAZ) Cracks

HAZ cracking is primarily induced by hydrogen and occurs in the grain-coarsened section of the HAZ and is also known as cold, delayed, underbead or toe cracking. Underbead cracking lies parallel to the fusion boundary, and its path is usually a combination of intergranular cracking. The principal residual tensile stress can cause the crack path to grow away from the fusion boundary towards an area in HAZ of

lower sensitivity to hydrogen cracking. When this happens, the crack growth rate decreases and eventually arrests. For hydrogen cracking to occur three factors need to be present simultaneously:

- Hydrogen level > 15 ml/100g of weld metal deposited.
- Stress >0.5 of the yield stress.
- Susceptible microstructure > 400 Hv hardness.

If any of above factors is not satisfied, cracking is prevented. Therefore, cracking can be avoided by controlling of one or more of these factors (TWI, 2015 a). Commonly practised preventive measures to restrict HAZ cracking are listed in Table 2-9.

Cause	Prevention
Hydrogen Level	• Post heat on completion • Improving the welding process (e.g. using covered electrodes) • Use temper bead or hot pass technique • Use dry shielding gases • Clean rust from joint
Stress	• Post Weld Heat Treatment (PWHT) • Weld profile blending (reduce stress concentration)
Susceptible microstructure formation	• Apply preheat • Maintain interpass temperature • PWHT • Use multi-run weld instead of single run • Use temper bead or hot pass technique • Use austenitic or nickel filler

Table 2-9 HAZ cracking preventive measures (TWI, 2015 a), and (Timings, 2008)

2.5.5.2 Transverse Cracks

Transverse cracking is less frequent than longitudinal cracking and is commonly induced by weld metal overmatching. Similar to HAZ cracks this type of cracking can be assisted by hydrogen, residual stress and sensitive microstructure. The key difference between Transverse cracking and HAZ cracking is that transverse cracks are induced by longitudinal residual stresses as opposed to transverse residual stresses in HAZ cracks (Lincoln, 2015). This is illustrated in Figure 2-20.

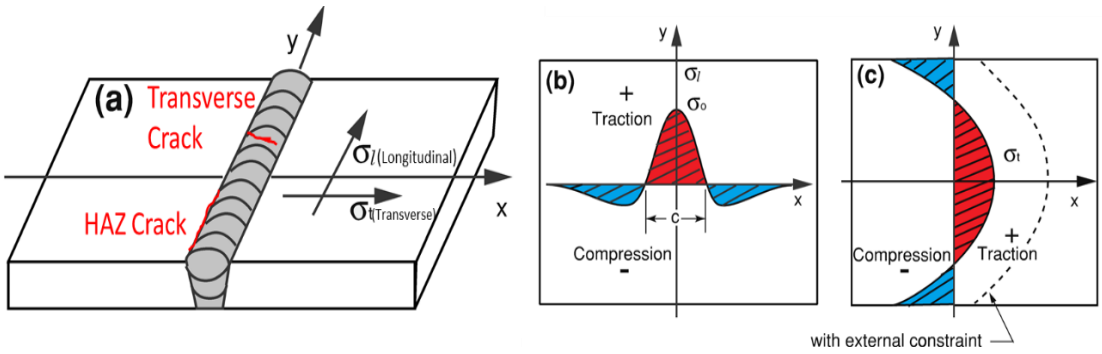

Figure 2-20 Difference between residual stresses causing Transverse crack and HAZ crack. Picture adapted from (Milella, 2012)

2.6 Significance of weld defects

The significance of weld defects is considered in relation to the static ultimate strength of structure and fatigue performance of the joint.

2.6.1 Static Ultimate Strength

The resistence of a butt welding joint is adequate for static loads. That is since the ultimate strength of deposited metal is said to be more than that of the base metal, and weld metal normally has reinforcement. Hence, small welding defects will have little effects on static strength (Mandal, 2017).

2.6.2 Effect on fatigue performance

A great deal of effort has been made to study the effect of various types of weld imperfections on fatigue performance of common welded joint types. The body of knowledge has been built into "IIW Guidance on Weld Quality in Relationship to Fatigue Strength" (Jonsson et al., 2013) and "ISO 20273 Guidance on Weld Quality in Relationship to Fatigue Strength" (BSI, 2017). Fatigue performance of welded joints is conventionally assessed using S-N curves (see chapter 6). Common welded joints are classified in tables which are available in the relevant standards. Fatigue resistance of such details are established using comprehensive test programs. The main cause of fatigue failure for such details is found to be cracks initiating at structural discontinuities introduced by weld geometry shape (e.g. weld toe). However, weld fabrication defects can affect the fatigue resistance. Above guidelines provide provisions for assessment of such defects with a particular focus on nonplanar defects. Planar defects are assessed using Fracture Mechanics (see chapter 6) and references are made to standards such as (BS7910, 2015 a).

The effects of weld defects on fatigue performance of welded joints can be:

Increase of general stress level

This is the effect of all types of misalignment by introducing a secondary bending. The effect can be considered using a magnification factor. The fatigue life of the structure considering the misalignment will be reduced by division of this factor (Hobbacher, 2008).

Additive notch effect

If the weld defect is located at the location of structural discontinuity (e.g. weld toe), the fatigue resistance is decreased by the additive notch effect (Hobbacher, 2008).

Competitive notch effect

If the defect is not located at the structural discontinuity, the notches are in competiton. Both notches need to be considered separately. The joint fatigue life is considered to be governed by the notch giving the lowest fatigue (Hobbacher, 2008).

2.6.2.1 Crack like defects

Crack like defects are the most sever types of defects, and are never permitted by standards for quality control of welds (Amirafshari et al., 2018). They are required to be repaired if found during NDT inspection of newly fabricated welds. Assessment of crack-like flaws and their effect on fatigue life can be assessed using Fracture Mechanics (BS7910, 2015 a).

2.6.2.2 Undercuts

The effect of undercut can be assessed directly using the effective notch stress or, similar to cracks using fracture mechanics method. IIW Guidelines on weld quality in relationship to fatigue strength (Jonsson et al., 2013) provides a simplified method as given in Table 2-10. Where, u is the depth of undercut and t is the joint thickness.

Fatigue Class	Allowable undercut u/t	
	Butt Welds	Fillet Welds
100	0.025	Not Applicable
90	0.05	Not Applicable
80	0.075	0.05
71	0.10	0.075
63	0.10	0.10
56 or lower	0.10	0.10
Notes: (a) Undercuts deeper than 1mm assessed like a crack (b) The table is valid for plate thicknesses from 10 to 20 mm		

Table 2-10 Acceptance levels for weld toe undercut in steel (Jonsson et al., 2013)and (BSI, 2017)

2.6.2.3 Lack of Penetration (LOP) and Lack of Fusion

Lack of Penetration (LOP) and Lack of Fusion (LOF) are severe weld defect and are considered as planar defects (Hobbacher, 2008).

(Tobe and Lawrence Jr, 1977) tested 56 double-V butt welds of ASTM A514 steel plate, 20 mm thickness including 13 sound welds and 43 test specimens containing LOP defects tested at stress ratios equal to R=0 and R=-1. They showed that LOP defects as small as 0.5 mm wide reduced the fatigue life below the normal expectancy for sound welds; however, LOP defects as large as 1 mm may be tolerated if the lower confidence limit (below 97.5% confidence interval) for sound weld data is adopted as a criterion. The influence of full-length LOP defects -longer than 2 mm with a width ranging from 1 to 8 mm- life is a very strong function of the width of the defect. (Tobe and Lawrence Jr, 1977) suggests that the short lives resulted from these defects is because the initiation portion of life is decreased to negligible values as a result of the high-stress concentration at the tip of the defect. Therefore, for specimens loaded exceeding the threshold value of stress intensity factor K_{th} (see Chapter 6), the majority of life is spent in propagation phase, which can be described by Paris law (see Chapter 6). Even the smallest defect considered—0.5 mm wide, 6 mm long (a less-than-full-length LOP) —resulted in a life shorter than the average for sound butt welds.

LOP and LOF defects are therefore assessed like crack type defects using fracture mechanics (BS7910, 2015 a), (Hobbacher, 2008) and (Naess, 1985).

2.6.2.4 Porosity and inclusion

Embedded volumetric defects, such as inclusions and porosity (see Figure 2-21 and Figure 2-22)are treated as competitive weld defects and can be unconventional sites of crack initiation in contrast to those covered by classified fatigue resistance details available in standards (Jonsson et al., 2013).

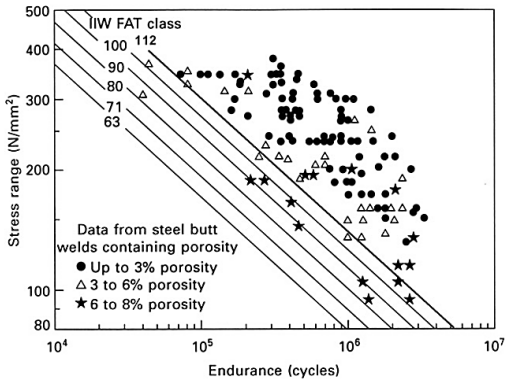

Figure 2-21 Effect of porosity (Jonsson et al., 2013)

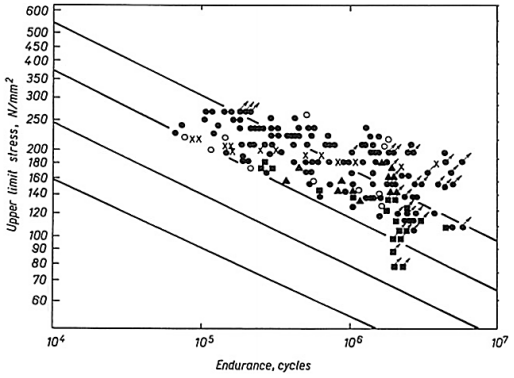

Figure 2-22 Effect of Inclusion (Jonsson et al., 2013)

Suggested limitations are given in Table 2-12 with relation to IIW fatigue classes (Hobbacher, 2008). The assumption here is that the detected porosities and inclusion are embedded defects found using a volumetric NDT method. It is assumed that surface-breaking pores and blow holes are detected using visual inspection and repaired subsequently. It should be noted that the prerequisite to fatigue assessment of joints containing porosity or inclusion using Table 2-12 is to ensure that the conditions apply for competitive imperfection, i.e., there is no interaction between various defects believed to be present at the joint.

Fatigue Class	Maximum length of inclusion in mm		Limits of Porosity in % of area[a,b]
	As-welded	Stress relieved[c]	
112	-	-	3
100	1.5	7.5	3
90	2.5	19	3
80	4	58	3
71	10	No limit	5
63	35	No limit	5
56 or lower	No limit	No limit	5
Notes: (a) Area of radiograph (b) Max pore diameter or width of inclusion < than 1/4 thickness or 6 mm (c) Stress relieved by post-weld heat treatment			

Table 2-11 Acceptance levels for porosity and inclusions in welds in steel (Jonsson et al., 2013) and (BSI, 2017)

2.6.3 Treatment of defects in this research

In this research, the focus is on planar defects (cracks, lack of fusion, lack of penetration and crack like defects) due to their higher criticality from the crack growth point of view. Nonplanar defects may be assessed for acceptability using Table 2-11. However, the probabilistic assessment of nonplanar defects is not possible in this research since currently, a well-established acceptability assessment

of non-planar flaws using fracture mechanics is not available and it is an area requiring future research. Misalignments are also excluded from this research; they are not the target defects in the NDE methods in this study and are checked during fabrication using special gauges. Table 2-12 describes the weld defects, their effects on structural integrity and the appropriate assessment methods.

Effect of imperfection		Type of imperfection	Assessment
Rise of general stress level		Misalignment	Formulae for effective stress concentration, refer to (Jonsson et al., 2013)
Local notch effect	Additive	Weld shape imperfections, undercuts	*Table 2-10
	Competitive	Porosity and solid inclusions not near the surface (Volumetric flaw)	*Table 2-11
Crack-like imperfection		Planar flaws: Cracks, lack of fusion, and lack penetration	Fracture Mechanics

Table 2-12 Weld imperfections categories

2.7 Non-Destructive Examination of Welds

Non-destructive Examination (NDE) is a wide range of methods to examine the characteristics of materials including presence of defects without permanently altering the material under examination. The terms Non-destructive Testing (NDT), Non-destructive Inspection (NDI), and Non-destructive Evaluation (NDE) are also used to refer to this technology. The six most commonly used techniques are Visual Testing (VT), Ultrasonic Testing (UT), Radiography Testing (RT), Penetrant Testing (PT), Magnetic Particle Inspection (MPI) and Eddy Current Testing (EC).

2.7.1 Visual Testing (VT)

Visual testing is the most basic form of NDE and is examination of the welds using human eye. The method is capable of detecting only relatively large surface imperfections.

2.7.2 Ultrasonic Testing (UT)

Ultrasonic testing involves sending a beam of high-frequency sound into material and registering and evaluating any echoes that are sent back. Ultrasonic testing procedures are now widely used for flaw detection in welds, forgings, castings, plate and pipe, thickness measurement, lamination checks and corrosion monitoring (TWI, 2015 a).

In UT a sound pulse is sent into a solid object and an echo returns from any flaws in that object or from the other side of the object (a reflector). An echo is returned from a solid-air interface or any solid-non-solid interface in the object being examined. We can send ultrasonic pulses into material by making a piezo-electric crystal vibrate in a probe. The pulses can travel in compression, shear or transverse mode. This is the basis of ultrasonic testing. To present information from the returning echoes for interpretation the UT set, or flaw detector is used. (Hellier and Shakinovsky, 2001).

In the majority of UT sets the information is presented on the screen in a display called the A-Scan, see Figure 2-24. The bottom of the display as a vertical signal; the height is known as the amplitude and represents the amount of sound returning to the probe. By seeing how far the signal appears along the time-based we can, if the time is calibrated, determine the distance to the reflector, see Figure 2-23.

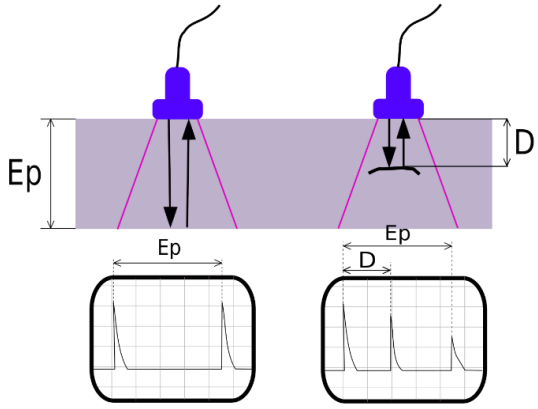

Figure 2-23 Ultrasonic Testing (UT) principle (Wikimedia, 2006 a)

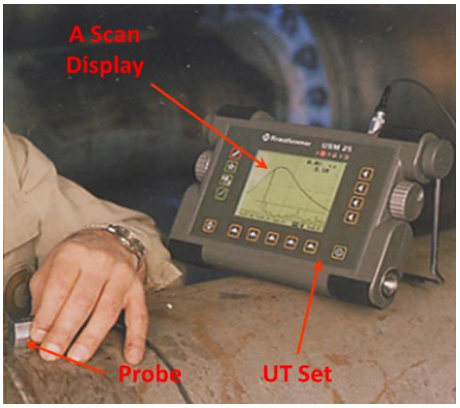

Figure 2-24 Ultrasonic Testing (UT) equipment (TWI.Ltd, 2018d)

Advantages	Disadvantages
• Sensitive to cracks at various orientations • Portability • Safety • Ability to penetrate thick sections • Measures through-wall extent	• No permanent record, unless automated • Difficult to apply to complex geometries and rough surfaces • Reliant on defect orientation • Unsuited for thin sections (<8mm)

Table 2-13 Advantages and disadvantages of Ultrasonic Examination (TWI.Ltd, 2015)

2.7.3 Advanced Ultrasonic Testing

The major limitation of basic UT is that it is reliant on the defect orientation and operator's skill (TWI, 2015 a). Two more advanced ultrasonic testing methods which

show substantially improved capabilities considering such limitations are the Phased Array Ultrasonic Testing and the Time of Flight Diffraction method.

2.7.3.1 Phased Array Ultrasonic Testing (PAUT)

In PAUT technique the probe consists of a number of transducers sending an array of pulses with changing relative time delays (Phased). This allows the beam to scan the area of interest and to construct a visual image of the cross-section of the area of interest (Figure 2-25). Contrasting the basic UT, the method has the benefit of providing a visual image of the flaw, capability of permanent data storage, ability to focus and steer the beam onto the area of interest without the need to move the probe (TWI, 2015 a).

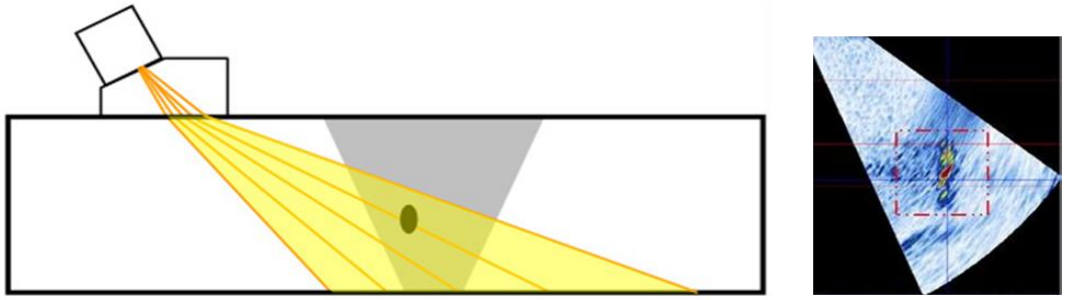

Figure 2-25 Phased Array Ultrasonic Testing (PAUT) (Wikimedia, 2006 b), PAUT display (TWI, 2013)

2.7.3.2 Time of Flight Diffraction (TOFD)

TOFD is a form of UT but uses a pair of probes on each side of the area of interest (Figure 2-26). The pair is normally mounted on a scanning device to maintain a constant distance during scanning. One transducer sends the ultrasonic beam into the material, and the other receives reflected and diffracted ultrasound from discontinuities and geometric reflectors (TWI, 2015 a).

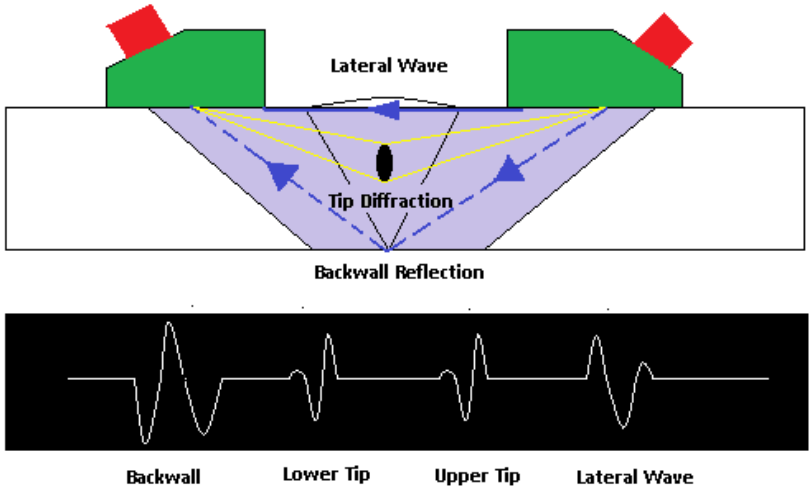

Figure 2-26 Principle of Time of Flight Diffraction (TOFD) examination (Wikimedia, 2011)

The method is an accurate and reliable flaw detection and sizing, and is relatively indifferent to flaw orientation to the initial beam direction since it is based on diffraction. The set up and testing procedure is faster than basic UT, as a single beam offers a large area of coverage. TOFD equipment is more economical than the Phased Array since it utilises conventional UT probes (TWI, 2015 a).

2.7.4 Radiography Testing (RT)

Radiography examination is based on the variation in capabilities of different materials to absorb a radiographic beam. In this technique, as illustrated in Figure 2-27, the target test object is placed between the radiation source and the detector. The object will attenuate the radiation. The differences in absorption, which depends on material density and thickness difference, are captured on the detector (i.e. film or an electronic means). There are several imaging methods available to display the image: Film Radiography, Real-Time Radiography (RTR), Digital Radiography (DR), Computed Radiography (CR) and Computed Tomography (CT) (Hellier and Shakinovsky, 2001). Among them the Film Radiography is the most commonly used method in ship fabrication (Amirafshari et al., 2018).

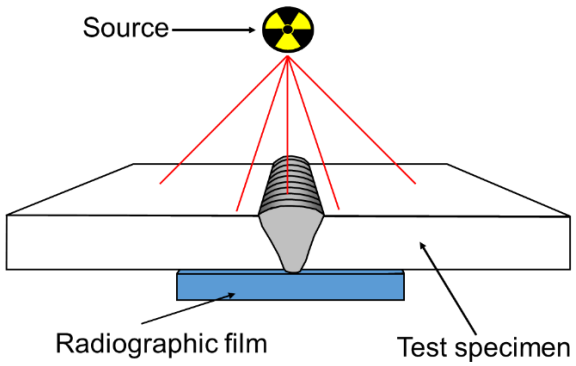

Figure 2-27 Radiography Examination diagram (TWI, 2018 c)

Weld metal has a higher density than parent metal and absorbs more radiation and appears brighter on the film. If the weld contains imperfections, they appear darker on the film. Figure 2-28 shows typical weld defects as they appear on the radiograph. Advantages and disadvantages of the Radiography Examination are listed in Table 2-14.

Advantages	Disadvantages
• Permanent record (the radiograph) • Detects internal flaws • Good detection of volumetric flaws • Can be used on most materials • Provides a direct image of flaws (although fine planar defects are not reliably detected)	• Unreliable for detection of fine planar flaws • Health and safety hazard due to radiation • Requires access to both sides of the object • Dependent on the interpretation of the examiner • A relatively slow method of NDT • High capital and running costs

Table 2-14 Advantages and disadvantages of Radiography Examination (TWI, 2015 a)

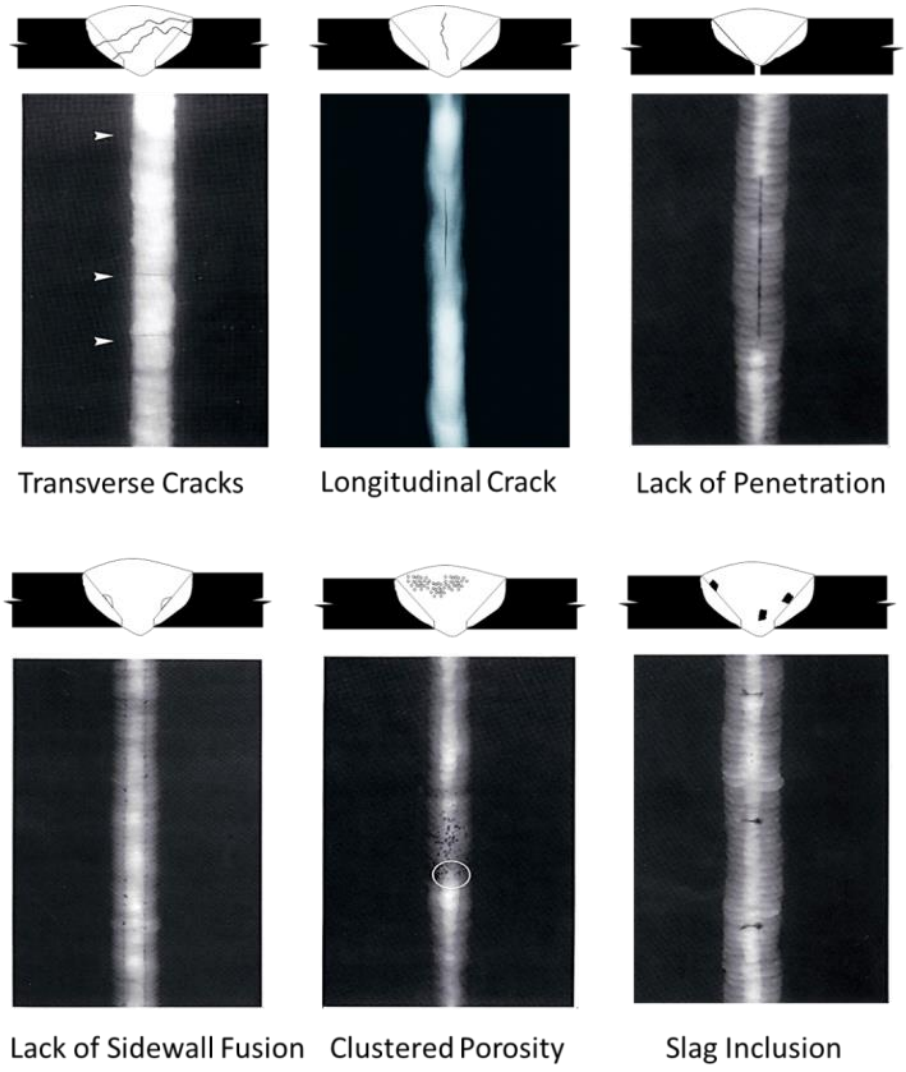

Figure 2-28 Defects as appear on radiograph and their diagram

2.7.5 Penetrant Testing (PT)

Penetrant testing was introduced in the USA during the Second World War; low viscosity hydrocarbons with fluorescent dyes were used to find flaws in aero engines.

Colour contrast systems were developed in the UK in the immediate post-war years (Tracy and Moore, 2003).

Penetration inspection (colour contrast) comprises a number of set stages:

- Pre-cleaning the component so that no grease, paint or dirt fills surface-breaking flaws.
- Application of the penetrant by spraying, brushing or dipping.
- Removal of surface penetrant without washing penetrant from potential flaws and Development with an absorbent coating.
- Inspection after development time of at least ten minutes using natural light or ultraviolet radiation.
- Post-cleaning and protection.

Figure 2-28 shows the diagram of the first four stages of the colour-contrast method. Detected defects appear as colour bleeding similar to Figure 2-30.

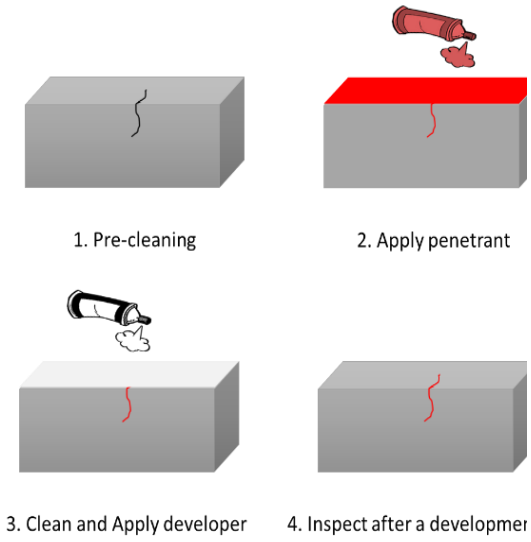

Figure 2-29 Stages of Colour-contrast Penetrant testing

Figure 2-30 Colour-contrast penetrant testing after bleeding (TWI, 2018 d)

Another method of penetrant testing is the Fluorescent penetrants method which uses the ability of certain materials to absorb electromagnetic energy of a certain wavelength and in response produce light at a different wavelength. Molecules within fluorescent penetrants absorb ultraviolet light, become excited and then shed some of their energy by releasing yellow-green visible light (Tracy and Moore, 2003).

Indications are viewed under darkened conditions with the operator thus viewing bright indications against a dark background. They are mainly used in factories, on castings, forgings, precision parts, aluminium alloy and stainless steels and so on. Fluorescent penetrants are more sensitive than colour contrast as the indications produced are 10 times more visible (Tracy and Moore, 2003). Figure 2-31 shows a surface crack detected by Fluorescent penetrant testing.

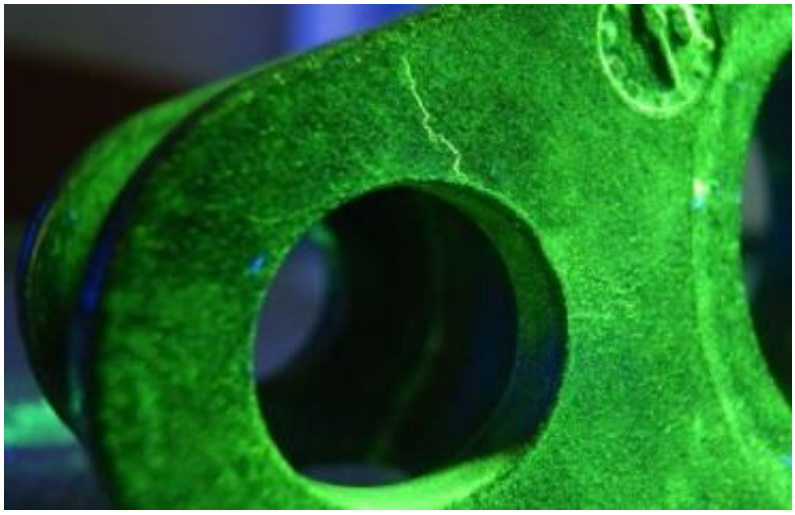

Figure 2-31 Fluorescent penetrant testing (Wikimedia, 2014)

The advantages and disadvantages of penetrant testing are listed in the table below:

Advantages	Disadvantages
• Applicable to non-ferromagnetic • Ability to test great elements with a portable kit • Batch testing is possible • Applicable to small parts with complex geometry • Simple, inexpensive and easy to interpret • Good sensitivity to surface breaking defects	• Only detects surface breaking flaws • Rigorous surface preparation is required • Temperature dependent • Cannot retest indefinitely

Table 2-15 advantages and disadvantages of penetrant testing

2.7.6 Magnetic Particle Inspection (MPI)

Magnetic Particle Inspection (MPI) is a method to detect surface-breaking and shallow subsurface flaws in ferromagnetic materials- ferritic (Not austenitic) steels. The general principle of the method is that the test object is subjected under a magnetic field and flux is generated in the object, as shown in Figure 2-32 below.

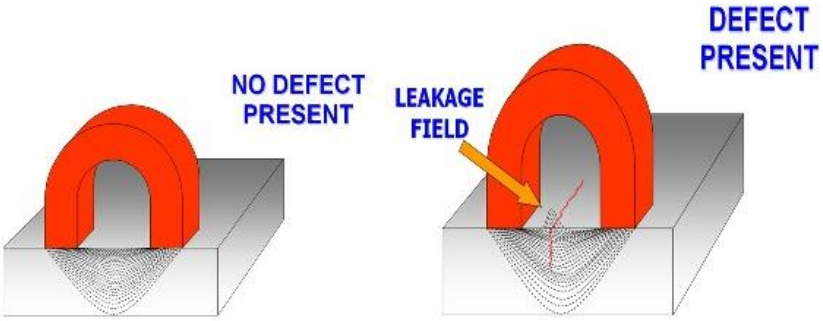

Figure 2-32 Principle of MPI (TWI, 2018 d)

A commonly used MPI equipment, the electromagnets (yoke), is made from soft iron laminates to reduce eddy current losses. The yoke laminates are encased in multi-turn coil usually powered by means of electricity. The legs of the equipment are normally articulated to access uneven surfaces. Diagram of an electromagnet is shown in Figure 2-33 below.

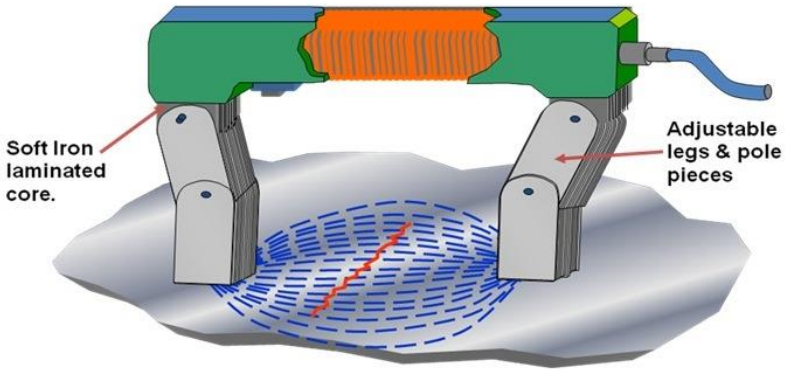

Figure 2-33 MPI using AC yoke (TWI, 2018 d)

Electromagnets produce a longitudinal field, as shown in Figure 2-33. Optimum defect detectability is 90˚ to the poles (legs). Rectified AC current or DC current from a battery may be used. AC current magnetising method achieves better flux levels and is hence the preferred method. Advantages and disadvantages of the MPI method are listed in Table 2-16 .

Advantages	Disadvantaged
• Capable of detecting some sub-surface defects • Rapid and simple to understand • Pre-cleaning not as critical as DPI • Will work through thin coatings • Inexpensive equipment • Direct test method	• Ferromagnetic materials only • Required to be test in two directions • Demagnetisation may be required • Complexly shaped joints difficult to test • Not suited to batch testing • Can damage the component under test

Table 2-16 Advantages and disadvantages of MPI testing

2.7.7 Eddy Current Testing (EC)

EC technique is based on the principle of electromagnetism. The name “Eddi” comes from the “eddies” that are formed when a fluid flows in a circular path around objects under certain conditions. When alternating current flows in a conductor (i.e. coil), a magnetic field is generated in and around the conductor. If a conductive material approaches the primary magnetic field an electrical current is induced in the conductive material. The induced electrical fields that follow a circular pattern are called Eddy currents. Presence of defect causes a change in the eddy current and in turn changes the phase and amplitude of the secondary magnetic field that can be detected by measuring impedance change in the coil.

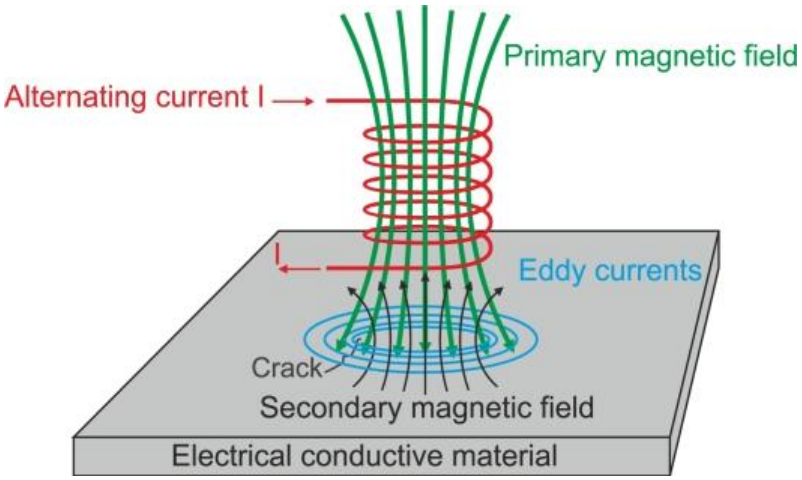

Figure 2-34 Principle of Eddy Current testing (i.Stack, 2018)

Advantages and disadvantages of the Eddy Current method are listed in Table 2-17.

Advantages	Disadvantages
• Suitable for surface defects • Can detect through several layers • Can detect through surface coating • Accurate conductivity measurements • Can be automated • Little pre-cleaning required • Portability	• Susceptible to permeability changes • Only on conductive materials • Will not detect defects parallel to surface • Not suitable for large or complex geometries • Signal interpretation is required • No permanent record (unless automated)

Table 2-17 Advantages and disadvantages of Eddy Current testing

2.8 Review of NDE approaches by classification societies

Newbuilding ship structures are required to be built in accordance with rules of a chosen classification society in order to be certified under that classification society.

Here, rules and guidelines from mainstream members of International Association of Classification Societies (IACS) are studied. The study was also published in "Journal of ship production and design". The overall philosophy of studied documents seems to aim at focusing on three aspects:

1. General welding quality of the hull structure
2. Increased attention to critical structural members
3. Find and resolve any disproportionate variation in defect rates

Additionally, provision with respect to NDT technique, Weld process, additional inspections, and etc. are given, as well. In following sections these provisions are discussed. In general two approaches are adopted:

1. NDE from quality assurance perspective
2. NDE from structural criticality point of view

The first approach aims to define a base number for checkpoints to represent weld quality and the second's objective is to target joints where occurrence of structural failure is deemed more likely or the consequence of failure is expected to be higher. Some classification societies adopt a mixture of both approaches. . As it will become apparent in coming sections, implementation these approaches in the relevant standards are very crude.

2.8.1 NDE from a quality-assurance perspective

The extent of NDE in terms of the minimum number of check- points or percentage of welded lines is specified by rules and guidelines. A number of classification societies define the number for whole structure using an equation which is function of dimensions of ship or its members. Some classification societies use tables defining the percentage or number of checkpoints for structural members and the rest use a combination of the equation and tables.

2.8.1.1 American Bureau of Shipping (ABS)

ABS defines a minimum number of required checkpoints within 0.6L around amidships, using equation (2-1):

$$N = \frac{L * (D + B)}{46.5} \tag{2-1}$$

where L is the length of the vessel between perpendiculars, in meters, B is greatest molded breadth, in meters, and D = molded depth at the side, in meters, measured at L/2. ABS clearly states that spot check of butt joints should be carried out to assess the quality of workmanship (ABS, 2014).

2.8.1.2 Registro Italiano Navale (RINA)

RINA also adopts equation (2-1) for 0.6L amidship areas and spot examination for areas outside 0.6L area and sensitive locations (RINA, 2007).

2.8.1.3 Korean Classification Society (KR)

KR, distinguishes between shell plating joints and internal joints of members and uses equation (2-1) to estimate the minimum number of checkpoints at deck and shell plating in 0.6L amidship areas. This number is reduced to N/10 outside of 0.6L amidship. KR prescribes the required number of checkpoints in Table 5 of KR (KR, 2015), depending on whether they are inside or outside 0.6L amidship, and general location of members, in terms of fractions of ship's length L/40, L/8, and L/16, respectively. This results in higher number of checkpoints compared to ABS and RINA as far as minimum number of checkpoints is concerned. KR also recommends additional examinations for the sake of workmanship control in locations such as parts of start, interrupted and end points of automatically welded joints, hatch corner welds, and other high critical areas (KR, 2015).

2.8.1.4 Nippon Kaiji Kyokai (NK)

NK, defines the number of checkpoints in terms of portion of ship length, individually for each structural member; however, as opposed to KR which employs this method only for internal members, NK applies this method to both internal members and shell plating. Depending on the type, the location of the member and whether it is a butt joint or fillet weld, the number of checkpoints differs. Strength deck, side shell plating, bottom shell plating, and hatch side coaming will have 8 to 12 times more checkpoints than other members. Butt joints in 0.6L have three times more checkpoints than those are outside 0.6L area. The number of seam joint checkpoints in plates remains constant across dimensions of the structure (NK, 2015). In ship construction, it is common to call butt welds in the longitudinal direction along the length of the ship "seam welds," and refer to butt welds in the transverse direction as "butt welds."

2.8.1.5 DNV GL. (DNV)

DNV, on the other hand, does not specify a minimum number of checkpoints and instead requires a minimum % of weld seam needed to be examined. Critical areas receive the most attention (20% of the weldment needs inspection) followed by deck/bottom plating within 0.4L amidship (5% of the weldment needs inspection), the lowest extent of examination is prescribed for general areas (2% of weld seam length) (DNV.GL, 2015).

2.8.1.6 Lloyds Register (LR)

LR does not specify a minimum number checkpoints for the whole ship and instead recommends the extent of inspection be defined based on type and location of structural members. Structural members with higher susceptibility to crack initiation receive significantly greater examination extent, either 50% or 100% examinations. More attention is paid to the intersection of butt and seams of fabrication and section welds where 50% examination is required, and if these are located at a highly stressed area, 100% is required, instead. Bilge keel butt welds within 0.4L amidship also must be inspected 100% and 33% outside 0.4L amidship. Other items require less examination (1–5%) (LR, 2015).

2.8.2 NDE from structural criticality perspective

When a structure is not 100% examined, members that are considered to be more critical receive more attention. Classification societies' rules more or less reflect this principle in their specifications. As 0.4L–0.6L amidship area of vessels goes under the higher global bending moment, classification societies require more inspection within this area. Additionally, locations that receive higher stress levels are also required to receive more attention. These locations are normally regarded as critical locations. The extent of NDE concerning critical locations, from different classification societies' perspective, is reviewed as follows:

2.8.2.1 American Bureau of Shipping (ABS)

ABS recommends that when it comes to the selection of checkpoints, more attention should be paid to welds in highly stressed areas, and members that are considered as important structural members by ABS Engineering/Materials/Survey department but does not specify a quantified measure or specify any particular members (ABS, 2014).

2.8.2.2 Registro Italiano Navale (RINA)

RINA, on the other hand, lists members and the areas that should be examined. Some of these require a specific number of checkpoints to be inspected and some are just indicated that they should be a target for inspection (RINA, 2007).

2.8.2.3 Korean Classification Society (KR)

KR requires selection of checkpoints at 0.6L amidship, i.e., 10 times more than outside of this region. When it comes to an internal member, the difference between the number of checkpoints in a member within 0.6L amidship and outside is 2.5 and 5 times, respectively, depending on structural hierarchy and crack susceptibility. For internal members within 0.6L amidship area, weld joints located at the strength deck needs to have twice as many checkpoints as other parts due to their higher contribution to the load resistance (KR, 2015).

2.8.2.4 Nippon Kaiji Kyokai (NK)

NK prescribes more inspection checkpoints for butt welds within 0.6L amidship than outside of this zone, but the difference is three times (NK, 2015).

2.8.2.5 DNV GL. (DNV)

DNV divides the ship into three areas: 1) critical areas—defined as areas in the way of critical load transfer points and large stress concentrations where a failure will endanger the safety of the vessel, 2) deck/bottom plating within 0.4L amidship, and 3) general areas—deck/bottom plating within 0.4L amidship to be inspected moderately more (5% of their weld seam length) than general areas (2% of their weld seam length).

There is a significant rise in percentage of inspection for critical areas to 20%. The same percentage of the weld seam of fillet welds in critical areas is also required to be examined for surface cracks using either magnetic particle inspection (MPI) or dye penetrant inspection (DPI). Examination of fillet welds in general and deck/ bottom plating within 0.4L amidship is not required. DNV states that for vessels with no clearly defined strength deck, e.g., cruise ships, the decks which contribute most to hull strength should be regarded as strength deck (DNV.GL, 2015).

2.8.2.6 Lloyds Register (LR)

LR, as opposed to DNV, requires 100% inspection of all critical areas as identified through LR's ShipRight Structural Design Assessment procedure and ShipRight

Fatigue Design Assessment procedure (LR, 2015). Also, intersections of butts and seams of fabrication and section welds at highly stressed areas, and hatchways coaming to deck at hatchway ends within 0.4L amidships, and bilge keel butt welds within 0.4L amidship are required to be examined 100%. Bilge keel butt welds outside 0.4L are required to be examined 1 in 3 [(33%)% of length].

2.8.3 Weld Type as a factor for selection of NDE technique

Welded joints can be made from butt welds or fillet welds. Butt welds can be longitudinally loaded (also known as seam welds in some standards) or transversely loaded, and made fully or partially penetrated welds. Figure 2-14 and Table 2-3 illustrate some typical applications of weld type in shipbuilding. Butt weld connections have higher static strength compared to parent materials because, the ultimate strength of deposited metal is more than that of the base metal (Okumoto et al., 2009).

Butt welds generally possess higher fatigue strength as opposed to connections made with fillet welds. A study by TWI Ltd (Marcello Consonni, 2012) based on a questionnaire answered by professionals from companies within TWI industrial membership suggests that joint type is the third most important contributing factor in defect repair rate; it has 15% influence on defect repair rate. The same study also suggests that 90% of weld defects are found in fillet welds and 10% in butt welds (Marcello Consonni, 2012).

ABS does not specify any special requirement or limits the NDE to particular weld joints (ABS, 2014). RINA, on the other hand, limits radiography and ultrasonic examination to butt welds, leaving the application of MPI and DPI to surveyors' decision to complement visual inspection (RINA, 2007). KR allows application of VT, MPI, DPI (Visual Testing), MPI, DPI, and UT (ultrasonic testing) for butt welds, tee joints, corner joints, and cruciform joints with both full and partial penetration and RT only for butt welds with full penetration, however KR states the distribution of checkpoints only for butt welds (KR, 2015). NK and LR specify the extent and distribution of NDE checkpoints for butt welds (NK, 2015). DNV requires MPI/DPI of butt T-joints in all areas and fillet welds in critical areas. DNV requires a volumetric examination of butt welds and T-joints with full penetration while limiting volumetric examination of T-joints to UT (DNV.GL, 2015). LR emphasises the use of MPI for ends

of fillet welds, T-joints, or crossings in main structural members at stern frame connections (LR, 2015).

2.8.4 NDE technique

The choice of method in ship construction depends on the limitations of the test object. Generally, UT cannot be applied for plate thicknesses below 8 mm, where radiography must be chosen. Radiography requires access to both sides of the test object and is not applicable to connections with complex geometries such as T-joints, cruciform joints, and fillet welds. Table 2-18 summarizes the classification societies' rules regarding the application of NDE techniques on finished welds.

Class	NDE method
ABS	• MPI and DPI defined by the manufacturer and approved by surveyors • Volumetric examination checkpoints defined as described • No preference between UT and RT; left to surveyors decision based on shipyards capabilities
RINA	• MPI/ DPI to complement VT • RT is preferred over UT
KC	• MPI is preferred over DPI • Extent of MP is not defined • RT is preferred over UT for thicknesses above 30 mm UT is to be used
NK	• RT is preferred over UT
DNV	• 2% of MPI or DPI in general areas • 5% of MPI or DPI for locations within 0.4L amidship • 20% of MPI or DPI in critical locations
LR	• Radiography for plates below 8 mm • UT for of full penetration tee, butt or cruciform joints or similar configuration • Advanced UT techniques, such as PAUT, may be used as a volumetric testing in lieu of radiography or manual ultrasonic testing • Attention to defect rates of butt welds in longitudinals. If defects are found in more than 10% of these welds additional inspection needs to be performed.

Table 2-18 Requirements of classification societies for NDE method

2.8.5 Welding Process

The welding process could be automated, semi-automated, or manual. Automated welding is more consistent, but if defective, it is more likely that defects have occurred more extensively. The influence of the welder on the weld parameters is, in most cases, limited to pressing start and stop. Therefore, the most important variable in automated weld processes is the operator. The rules implement special

requirements for automated welded connection, particularly at start/stop points (Table 2-18).

Class	Automatic welding provisions
ABS	Can reduce the frequency of inspection if Quality-Assurance techniques indicate consistent satisfactory quality, but does not specify the amount of the reduction
KC	• All start/stop points of automatic welding processes to be examined using RT or UT except for internal members where the extent of testing should be agreed. • Allows reduction of checkpoints if automatic welding has been carried out and the results of the survey verify that the quality of welding procedure is consistent satisfactory quality • If a weld that needs to be repaired is found in an automatically welded joint whose inspections have been reduced, additional radiographs negating the reduction are required until an appropriate period has elapsed and the quality is verified to be stable and satisfactory
NK	1) If defects are found in automatic welding, additional NDT is to be extended to all lengths of the welded joints 2) In (1), the faulty welds to be repaired 3) Apart from (2), all lengths or all joints may be repaired 4) Faulty welds found in preceding (2), are to be repaired. 5) Notwithstanding preceding (1) to (4), repair process and additional NDE in other welded joints are to be carried out according to the surveyors' direction
RINA, DNV & LR	Not Applicable

Table 2-19 Requirements of classification societies for automatic welding

2.8.6 Weld repair

When defects are found there is general agreement between different rules that the full extent of any defect must be completely removed and, where necessary, re-welded and examined. If the original welds were subjected to post weld heat treatment (PWHT), this need to be repeated after completion of repaired welds. Normally, where NDE reveals that the original defect has not been successfully removed, one more attempt may be performed. In practice, the aim is not to repeat the repair more than two times.

2.8.7 Additional inspections

Since the inspection is performed partially, it is crucial to interpret the NDE results and to decide if any additional inspection is needed. This is to:

1) Make sure the presence of defects is not systematic and if so, such defects are found and rectified, and;
2) Ensure that welding quality is of good workmanship level.

Apart from RINA which has no specific requirement for additional NDT, the requirements from other classification societies are summarised in Table 2-20.

Register	ABS	KC	NK	DNV	LR
Additional NDT if one defect found	Additional UT to determine the extent of non-conformity	N/A	(1) Additional NDT for other two parts within welds lines if the defect is found in plates members and girders (2) In (1), NDT is to be extended to all length of the welded joints (3) Notwithstanding the requirements specified in (2), all length or all number of welded joints may be repaired (4) Faulty welds found in (2), are to be repaired. (5) Notwithstanding (1) to (4), repair and additional NDT in other joints are to be performed	For each section of the weld to be repaired two more of the same length shall be tested	
Additional NDT if defect rate exceeds a certain value	If a high ratio of checkpoints (i.e. 90% ,95%) are defect free, NDT length can be reduced from 1250 mm to 750 mm	If repair exceeds 20% of the total number of checkpoints, survey should be increased to a minimum of 40%.	If faulty welds are more than 10% of the of inspected, requires investigation of cause and improving quality	N/A	If it is beyond Normal limits necessary corrective actions, need to be taken
Remarks	(1) Additional inspection is required if the pattern of defect suggests that defects exists for an extended distance. (2) When defect is at the end of a checkpoint, extra UT is required to define extent of the defected part.	N/A	N/A	(1) If systematically repeated defects are revealed, the extent of the testing shall be increased where similar defects may be expected (2) If defects are found to occur regularly, the reason shall be investigated. The Welding Procedure Specification (WPS) shall be reassessed before the continuation of welding	(1) When alerted by previous results, the extent increase (2) When continuous or semi-continuous defects are found an additional length of welds adjacent to and on both sides of the defective length are to be subject to further volumetric examination

Table 2-20 Requirements of classification societies for additional inspection

2.8.8 Acceptance criteria

For any weld imperfection, there are two approaches for defining acceptance criteria: the first approach is based on good workmanship level and is generally independent of nature the structure, loading, and in-service environment. The second approach is based on fitness for service (FFS), which takes into account stresses that the imperfection may experience during service and the environment in which the structure will operate. FFS is commonly practised as an assessment tool rather than a design scheme due to the complexity of its inputs and higher computation power that is required comapred to the S-N curve approch. However, for design philosophies that are based on inspactability of the structures a fracture mechanics approch is a more effective design approch (Chapter 3 section 3.2).A review of classification societies' rules and standards shows that acceptance criteria for weld inspection in the shipbuilding industry are based on good workmanship level and not FFS. This is because FFS involves detailed fracture mechanics assessment requiring specific inputs that are not commonly available given the current practice in the ship industry. Apart from ABS and DNV, all other classification societies apply the same acceptance criteria for all locations and weld types of a vessel. As per ABS, the areas to be inspected are categorised in two classes: Class A and Class B. Inspection of full penetration welds for all surface vessels 150 m (500 ft) long and over in 0.6L of amidship is to meet the requirements of Class A. Class A may also be specified and applied to surface vessels less than 150 m (500 ft) long when special hull material or hull design justifies this severity level. Full-penetration welds in way of integral or independent tanks, except membrane tanks, of all vessels intended to carry liquefied natural gas or liquefied petroleum gas cargo are to meet the requirements of Class A. Inspection of full penetration welds for surface vessels under 150 m (500 ft), and for welds located outside 0.6L of amidship, regardless of the size of the vessels, is to meet the requirements of Class B, provided that Class A has not been specified in accordance with the special conditions noted in the Class A criteria above. Areas that are classified as Class A generally have more stringent acceptance criteria (ABS, 2014). DNV adopts ISO 23278 standards acceptance criteria for magnetic particle testing (BSI, 2015 a), ISO 23277 for penetrant testing (BSI, 2015 b), ISO 10675 for radiographic testing (BSI, 2013), and ISO 11666 for ultrasonic testing (BSI, 2011 a). Depending on the location of the checkpoint, level 1–3 (in decreasing order of rigour

of inspection), an acceptance criterion is assigned. Generally, areas within 0.4L amidships for container ships have a higher level of acceptance criteria for volumetric inspection (DNV.GL, 2015).

2.8.9 Scope for potential improvement

2.8.9.1 Limitations of current approaches

Current approaches are "one-size-fits-all," in that they generally do not depend on the ship type nor allow for a reduction in NDE effort even when there may be clear evidence of good workmanship. In such cases, the question that arises is what rationale should be applied for determining a reduced NDE regime.

Current inspection planning methods focus on critical structural members; however, such approaches account only for stress distribution among structural members. An improved method should take into account defect frequency and size distribution as well as member's stress.

Current methods do not strictly differentiate between structural members in terms of the consequence of their failure. Hence, e.g. failure of a welded connection in the shell plate, which can result in water or cargo leakage, has the same severity as a crack failure in a deck plate of a multi-deck passenger ship.

Formation and characteristics of weld defects are a function of welding variables such as welding process, positions, and consumables. Apart from checking start/stop of auto- mated welding, prescribed by KR, NK, and ABS, current approaches do not fully take into account these variables.

Although the defect rate is recorded by shipyard and surveyors, there is no clear explanation how to interpret this rate: some shipyards adopt a binary method by dividing the number of failed checkpoints by the total number of checkpoints. Other shipyards use a length by length method by dividing the total length of defects found by the total length of measured welds. This results in significant discrepancy between recorded defect rates. It is also not clear how this number represents the welding quality or how it affects the structural integrity of the ship. Should there be a benchmark average defect rate? How should this benchmark be defined? And last but not least, how should this affect the remaining and additional inspections?

The number and extent of the inspection checkpoints should include an appropriate sample of all weldments. The sample should correspond to the desired confidence level and take into account weld-related variables, structural criticality, as well as the fabrication stage at which the defect is found. Current rules do not seem to have a robust and/ or consistent method to define the number and the location of inspection checkpoints from the sampling perspective.

2.8.9.2 Risk-based inspection (RBI)

Risk-based inspection (RBI) and maintenance have been used in a variety of industry sectors. There are specific standards for adopting RBI methods for plant and process equipment (API, 2009), and (API, 2008) and there are many software packages supporting operators in implementing such approaches, e.g., RiskWISE® (TWI, 2016 b). In the offshore sector, such approaches have been used particularly for jacket structures, semisubmersibles, and FPSOs integrity management by, (DNV, 1996), (DNV, 2000) and (DNV, 2015). In the shipping sector, periodic inspections have traditionally been carried out. However, recently there has been increasing interest in RBIs (Bharadwaj and Wintle, 2011), (Barltrop, 2011 a), (Amirafshari, 2017), (Mansour, 1994), (Shinozuka, 1990), (Moan and Ayala-Uraga, 2008), (Mansour and Hovem, 1994), (Ayala-Uraga, 2009), (ABS, 2012) , (Moan, 2005), and (Ayyub et al., 2002), and classification societies are developing frameworks (LR, 2017) to enable such approaches to be used, often complementing the traditional time-based approach, but some- times justifying changes to periodic inspections. Recent and ongoing developments in shipbuilding technologies and competitive market demand have pushed shipbuilders to building bigger and more complex ships. It is a challenge for the stakeholders to ensure the safety and reliability of vessels cost-effectively. Application of established risk-based approaches could allow shipbuilders to implement new complexity and innovations, which cannot be justified through current prescriptive rules due to their limitations (Papanikolaou, 2009).

2.8.9.3 A Risk-based approach in conjunction with sampling theory for quality assurance

Risk-based approaches support decision makers to optimise their inspection by making targeted inspections such that the asset system remains within tolerable levels of risk. In certain cases, time-based regimes are informed by risk-based assessments to justify reduced or increased inspection (both in terms of inspection frequency and extent).

To address the “one-size-fits-all” NDE inspection regime, in which regardless of evidence of good workmanship in a particular shipyard, the same rigorous regime is advocated, experience from quality assurance as used in other industry sectors can be transferred. One could have two levels of inspection, with the first level aimed at assessing the quality of workmanship from an appropriate sample (so that desired confidence is achieved), and depending on the result of the first level, determine a more detailed level (with a bigger sample of inspection checkpoints) that is required.

2.8.10 Concluding remarks on review of classification societies approaches

Classification societies have developed rules, standards, and guidelines specifying the extent to which inspection should be performed, which intends to:

- Verify welding execution quality level.
- Ensure that areas and members with higher susceptibility to defects receive sufficient attention.
- Find and rectify any excessive variation in defect rates.

A review of rules and standards from classification bodies that are members of IACS shows some limitations in current practices. One key limitation is that the rules favour a “one-size-fits-all” approach. In addition to that, a significant discrepancy exists between rules of different classification societies. Inspection regimes need to be adjusted taking cognizance of the perspectives of key stakeholders involved in shipbuilding—specifically, ship owners, manufacturers, and classification societies. Factors that interest these stakeholders include assurance of intended safety and structural reliability of the vessel, saving time and the costs associated with NDE and subsequent remedial action, and incorporating manufacturing quality.

A promising way to achieve targeted and cost-effective inspections is to take a Risk-based approach to inspection. The RBI process helps to identify the potential hazard and failure scenarios, their likelihood, and the corresponding consequences, which in turn enables decision makers to optimise inspection. Current rules, standards, and guidelines, in essence, have some level of qualitative risk assessment built into them. However, this assessment has evolved over time and is substantially based on expert opinion and engineering judgement. A more systematic and quantitative (analyses based) approach is therefore needed.

For the purpose of inspection during manufacturing (QC inspection), the risk-based approach needs to be further complemented by statistical methods to allow incorporating data and experiences from a manufacturer's quality-assurance program so that the amount of inspection may be adjusted based on the expected level of quality.

2.9 NDE inspection in non-marine industries

There are generally two approaches for inspection of items for nonconformities:

The first approach is a "Testing-based" or "Empirical" in which components/devices are tested, and the numbers of failed components are recorded. Many identically manufactured systems are tested similarly, and the expected nonconforming items in samples of different sizes and the whole population are estimated using classical statistics. This approach is useful in the manufacturing of industries in which many identical components are produced. The manufacturer or the costumer set an acceptable level of nonconformities based on the financial risk they are ready to take and statistical approaches are employed to achieve that level. For example, in manufacturing electrical devices the manufacturer provides a return warranty for the faulty devices. The aim is to make sure that the sum of incurred costs which is related to the total number of returned items do not exceed a certain amount.

The second approach is "Physics-based" or "computational" estimation and is useful when dealing with large systems such as bridges, ships, space vehicles, etc., where it is impossible to build several identical units for testing. The aim, in this approach, is to predict items/components where the occurrence of nonconformities are more likely or have a higher consequence of failure. The challenge in this approach is the model accuracy and its sensitivity to errors and it is therefore normally complemented by engineering judgments and elicitations.

In the following sections, NDT inspection approaches in industries that welded connections play a key role in final products are reviewed.

2.9.1 Automotive

In the Automotive industry, manufacturing is of a mass production nature. Manufacturing lines constantly produce batches of identical items. For assemblies, components and connections NDT inspection are, mostly, applied offline and rely on visual inspections and operator interpretation. If a serious defect is found, the whole

batch may be rejected because the manufacturing conditions that lead to defects will have been applied to the whole batch. Use of a statistical sampling approach has traditionally been popular in manufacturing including the automotive industry (Smith, 2017). Many tests are destructive; hence 100% inspections are not possible. The general approach is that a number of samples from product lots (batches) are tested. The sample is considered to be representative of the lot therefore, depending on the required statistical confidence and the risk, accepted by the manufacturer, a minimum sample size and an Acceptance Quality Level (AQL) are specified, respectively. The numbers of non-conformances in samples are compared against the AQL; exceeding AQL levels will result in the whole lot being rejected. The method is also widely adopted in many other industries including, electronic equipment, medical devices, food industry, and etc. ISO/DIS 28590 series on "Sampling procedures for inspection by attributes" (ISO-28590, 2017) is the commonly adopted standard for such purposes. The standard prescribes three inspection schemes:

1. Normal inspection
2. Tightened inspection
3. Reduced inspection

The inspection starts with the Normal scheme and is switched to tighten inspection if 2 out of 5 consecutive lots are rejected. The Normal inspection shall be re-instated when five consecutive lots have been considered acceptable on original inspection. Normal inspection may be switched to reduced inspection if production is at a stable rate; and reduced inspection is considered appropriate by the accountable authority.

The Inspection plan also consists of inspection levels. The inspection level defines the relative severity of examination. Three examination levels, I, II and III are specified and are given in Table 2-21 for general use. Unless otherwise indicated, level II shall be used. Level I may be used when less acumen is needed or level III when greater acumen is required. Four additional special levels, S-1, S-2, S-3 and S-4 are also given in Table 2-21 and may be used where small sample sizes are required and greater sampling risks can be borne.

Lot size		Special Inspection levels				General Inspection levels		
		S-1	S-2	S-3	S-4	I	II	III
2 to	8	A	A	A	A	A	A	B
9 to	15	A	A	A	A	A	B	C
16 to	25	A	A	B	B	B	C	D
26 to	50	A	B	B	C	C	D	E
51 to	90	B	B	C	C	C	E	F
91 to	150	B	B	C	D	D	F	G
151 to	280	B	C	D	E	E	G	H
281 to	500	B	C	D	E	F	H	J
501 to	1200	C	C	E	F	G	J	K
1201 to	3200	C	D	E	G	H	K	L
3201 to	10000	C	D	F	G	J	L	M
10001 to	35000	C	D	F	H	K	M	N
35001 to	150000	D	E	G	J	L	N	P
150001 to	500000	D	E	G	J	M	P	Q
500001	and over	D	E	G	K	N	Q	R

Table 2-21 Sample size code letters ISO 2859 (ISO-28590, 2017)

The inspection level required shall be specified by the accountable authority. This allows the authority to require greater refinement for some purposes and less for others.

At each inspection level, the switching rules require normal, tightened and reduced inspection, as specified before. The choice of inspection level is independent from these three severities. Thus, the specified inspection level should be maintained when switching between normal, tightened and reduced inspection.

The Inspection plan may also be a single sampling, double sampling or multiple sampling. In single sampling, if the number of nonconformities is equal or above the rejection number the sample is rejected. In double sampling, if the number of nonconformities is between the rejection number and acceptance number, a second sample is drawn. The test results from second sample are then added to the first sample, and the accumulated nonconformities are compared against corresponding limits. In multiple sampling, the approach is similar two double sampling, but multiple samples are drawn instead of two.

Once the sample code is specified using Table 2-21, the corresponding sample size, acceptance number and rejection number are determined based the Acceptance Quality Limit (AQL) for a chosen inspection plan using relevant tables given in the standard. For example Figure 2-35 shows Table 2-A from the standard document specifying provisions of single sample plan for the Normal inspection.

As an example, if we were to examine stiffened panels produced on the panel line in one day production assuming that the total production of the day is 500 panels, and the acceptable limits for the welding process is 6.5%. Starting with Table 2-21 and assuming default inspection level as general level II, the sample code is determined as H. Going to Figure 2-35 the sample size should be 50. For 6.5% AQL the acceptable and unacceptable number of nonconformities are 7 and 8, respectively. If 8 or more nonconformities are found total day production will be rejected and a higher sample size may be adopted to validate the lot.

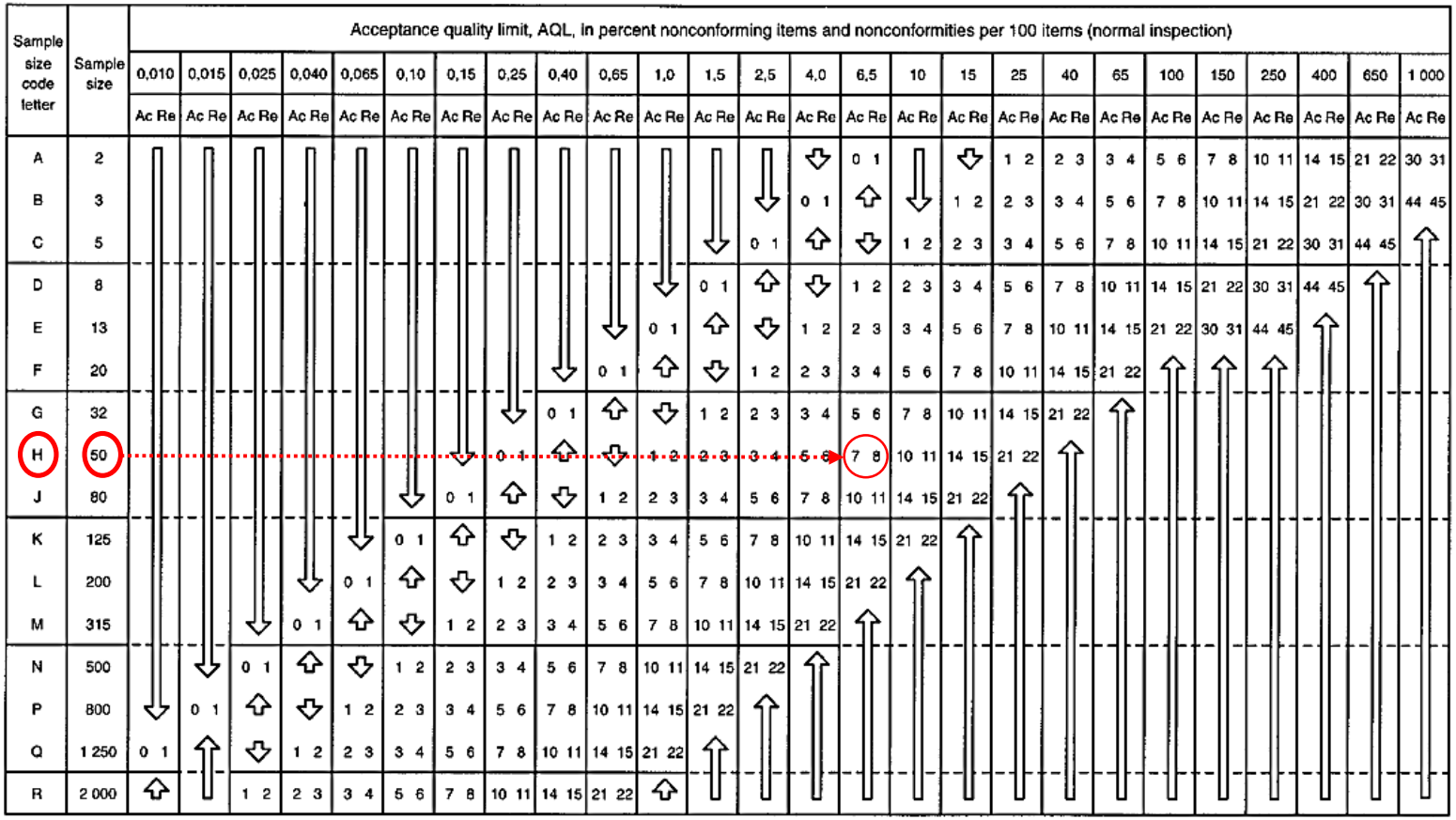

⇩ = Use the first sampling plan below the arrow. If sample size equals, or exceeds, lot size, carry out 100 % inspection.

⇧ = Use the first sampling plan above the arrow.

Ac = Acceptance number

Re = Rejection number

Figure 2-35 single sample plan for the Normal inspection (ISO-28590, 2017)

In the automotive industry and many mass production manufacturing industries, the acceptance limits are establish based on the risk that the product supplier affords to take. The approach essentially ensures that the amount of nonconformist products, supplied to the customers, is kept below a certain value. The acceptable limits are calculated based on the costs for the manufacture to fulfil the warranties.

The efficiency of the method to meet customer satisfaction has allowed the manufacturers to adopt the approach in some cases where Non-destructive inspection is used, as well.

The current trend in automotive industry is to develop and implement cost-effective automated NDT techniques that can provide 100% NDT of joints (Pires et al., 2006).

2.9.2 Aerospace

NDT inspection in Aerospace industry is to some extent similar to the automotive industry: the production is a mass production manufacturing and all aircraft of the same model need to have identical parts, joints and joining process. The fitness of the aeroplane for flight (airworthiness) needs to be ensured by the manufacturer and through regulations of the International Civil Aviation Organization (ICAO) (De Florio, 2016). High quality welding techniques are developed to produce close to perfection connections (Chaturvedi, 2011). The level of NDT for fatigue prone joints in the aerospace industry is almost 100% (Jenkinson et al., 1999).

2.9.3 Civil engineering

AWS D.15, Bridge Welding Code, (AWS, 2015) adopts AWS D1.1.2000, Structural Welding Code-Steel, (AWS, 1999), and specifies that the provisions of NDT inspections should be agreed between the owner and the contractor. Additionally, for Tubular Connection for complete joint penetration groove butt welds welded from one side without backing, the entire length of all completed tubular production welds shall be examined by either radiographic or ultrasonic testing.

Eurocode 3, Design of steel structures — Part 2: Steel bridges, (Eurocode-3, 2006) adopts EN 1090, Execution of steel structures and aluminium structures, (BSI, 2011 b), in which four execution classes (EXC) are defined. Welded joints required to have partial NDT length depending on the type of the joint (Butt welds, T-Joint, Transversely loaded, longitudinally loaded, etc.) and the execution class is designated by the designer and may be 0%, 5%, 10%, or 20%, as specified in Table 2-22.

Type of weld	Shop and site welds		
	EXC1	EXC2	EXC3[a]
Transverse butt welds and partial penetration welds in butt joints	0%[b]	10%	20%
Transverse butt welds and partial penetration welds in: • Cruciform joints • T-joints	 0%[b] 0%	 10% 5%	 20% 10%
Transverse fillet welds[C] : With a>12mm or t> 30 mm With a≤ 12 mm or t≤ 30 mm	 0% 0%	 5% 0%	 10% 5%
Full penetration longitudinal welds between web and top flange of crane girders	0%	10%	20%
Other longitudinal welds[d] , welds to stiffeners and welds[d] specified in the execution specification as being in compression	0%	0%	5%
a For EXC4 the percentage extent shall be at least that given for EXC3 b 10% for such welds executed in steel ≥S420 c Terms a and t refers respectively to throat thickness and the thickest material being joined d Longitudinal welds are those made parallel to the component axis. All others are considered as transverse.			

Table 2-22 Extent of NDT based on execution class specified in Eurocode

Additionally, Eurocode 3, Design of steel structures — Part 2: Steel bridges, (Eurocode-3, 2006) require supplementary NDT inspection specific to bridge structures in Table C.4 of the standard. The choice of the NDT method and the extent of the inspection are dependent on the welded joint (filet, butt, etc.) and structural function (deck plate, stiffener, etc.). The prescribed method is Visual Inspection and in some cases supplemented by UT or RT. The extent of the inspection varies from 0% to 100%. In most of the cases, 100% visual inspection is the only requirement.

2.9.4 Petroleum Industry

In the petroleum industry the approach is the 100% inspection of structural welds since the structures of interest are generally non-redundant; failure of the joint tends to result in temporary or permanent failure of the system (i.e. pipeline or storage tank). API 650, “Welded Steel Tanks for Oil storage” (API, 1998), require inspection of all butt welds with full penetration using preferably Radiography testing or ultrasonic testing if agreed between the owner and the manufacturer. For fillet welds only visual

inspection is required. API 1104, “Welding of Pipelines and related facilities (API, 1999)”, states that the company should have the right to inspect all welds using non-destructive testing. The company in the standard is defined as the owner company or the engineering company in charge of the construction.

2.9.5 Amusement devices

ISO 17842, “Safety of amusement rides and amusement devices (BSI, 2015 c)” adopts the provisions of ISO 17635 (ISO, 2016). All welds of dynamic loaded parts shall meet the requirements of ISO 5817, “Quality levels for imperfections” (ISO, 2014), quality level B and all welds of static loaded parts and subordinate components shall meet the requirements of quality level C. In ISO 5817 three levels of weld qualities are given. They are designated by symbols B, C and D. Quality level B corresponds to highest requirement on the finished weld. The quality refers to production and good workmanship. The quality levels are based on “IIW Guidance on Weld Quality in Relationship to Fatigue Strength” (Jonsson et al., 2013), which was explained in 2.6.3.

2.10 Chapter conclusion

Ship hull structures are built from steel plates and components that are joined together using welding. Formation of defects is inherent to this joining technique. Non-destructive Examination (NDE) is used to detect these defects in the finished welds. Understanding the characteristics, requirements and boundaries of the NDE inspection of newbuilding ship hull structures was a crucial step in this research. The challenge here was that this research focuses on an area which involves a number of technologies namely ship production, welding, non-destructive testing and manufacturing quality control. Any attempt to improve the status quo without a full understanding of the above technologies, their capabilities, limitations and their relevance to ship manufacturing would have been ill-functioned and possibly inaccurate. The understanding of welding processes and NDE techniques was obtained through training courses provided by TWI Ltd (Formerly The Welding Institute). Appreciation of ship NDE inspection of newbuilding ships and those in-service was achieved through a number of industrial visits including six days at two shipyards and one day on board of a passenger ship witnessing in-service inspections. During the shipyard visits the author accompanied surveyors of the classification society during their day to day inspection duties comprising visual inspection of various parts of the structure (stiffened panels, blocks, grand blocks, confined spaces with a low level of access, etc.) interpreting RT radiographs and conduction of DPT

and UT inspections. The author also spent three days at the design approval office learning and discussing the process and the details of preparing NDE inspection plans with the staff in-charge. The industrial visits helped the author to gain a holistic and detailed real-life understanding of the NDE inspection of newbuilding ship hull structures. Data was obtained which provided a useful and necessary background about shipbuilding process, welding defects, NDE techniques, and welding processes which were outlined in this chapter. Further information about collecting experts' opinions data can be found in Appendix A. A critical review of rules for NDE inspection of newbuilding ship hull structures undergoing classification society survey was conducted by studying relevant sections of the rules of mainstream International Classification Societies (IACS) members. The study allowed the author to capture various aspects of the rules and identify areas for improvement.

One key limitation is that the rules favour a "one-size-fits- all" approach. In addition to that, a significant discrepancy exists between rules of different classification societies. Inspection regimes need to be adjusted taking cognizance of the perspectives of key stakeholders involved in shipbuilding—specifically, ship owners, manufacturers, and classification societies. Factors that interest these stakeholders include assurance of intended safety and structural reliability of the vessel, saving time and the costs associated with NDE and subsequent remedial action, and incorporating manufacturing quality.

The findings of this study was also published in an article in Journal of Ship Production and Design (JSPD).

Additionally, the NDE inspection strategies of newly finished welds in other industries are reviewed; there are generally two approaches for inspection of items for nonconformities:

The first approach is "testing-based" and uses classical statistics. This approach is useful in the manufacturing of industries in which many identical components are produced.

The second approach is "physics-based" estimation complemented by engineering judgment and is useful when dealing with large systems such as bridges, ships, space vehicles, etc., where it is impossible to build several identical units for testing.

A promising way to achieve targeted and cost-effective inspections is to combine quality control with a risk-based approach to inspection. The RBI process helps to identify the potential hazard and failure scenarios, their likelihood, and the corresponding consequences, whilst the quality control determines that sufficient inspection has been done to ensure the quality of the welding and to improve it if necessary. These in turn enable decision makers to optimise inspection.

Chapter 3

Risk and Reliability

3.1 Outline

This chapter aims to develop a risk model for integrity assessment of welded joints of ship hull structures containing planar weld defects.

In this chapter:

- Deterministic fracture mechanics is presented as a tool for durability assessment and inspection planning of structures containing defects. The capabilities and limitations of the method are discussed. Probabilistic fracture mechanics, or reliability analysis, as an improved substitute to deterministic fracture mechanics is introduced, and different approaches of reliability assessment are briefly explained.
- Risk-based analysis as a branch of the reliability method is described, and subsequently, the developed risk-based framework for reliability assessment of ship hull structures containing weld defects is outlined.
- A model for the assessment of failure consequences in ship hull structures is developed, and the target reliabilities corresponding to the specified consequence classes are determined.

3.2 Defect assessment using Fracture Mechanics

Defect assessment is a branch of engineering science that employs a set of theoretical approaches, validated by test programs, to assess the safety of structures containing defects. Procedures such R6, and BS7910 are well-established and have been widely used for such purpose since the development of R6 in 1976. Flaw assessment has been initially aimed at nuclear pressure vessels and piping (Dowling et al., 2005) but has been gradually adopted in other industries, e.g. aerospace, offshore, construction. Now BS7910 is applicable to any metallic structure.

Any assessment or design approach is applied within the boundaries of the chosen design philosophy.

Safe-life design philosophy: This design philosophy is based on the assumption that the structure is initially free from imperfections that could cause failure and no regular monitoring in service is specified.

Fail-safe design philosophy: In this approach, the aim is to design a structure that even if a crack in a component part of becomes unstable and suddenly propagates, the failure of that component does not lead to the catastrophic failure of the structure. This is best achieved in hyper-static (overdetermined) or redundant structures with alternative load paths. For example in ship structure tougher steel 'arrestor strakes' are used at shear strakes to attempt to prevent a crack running from deck to side shell or vice versa. If they work they effectively convert the single hull girder into several parallel girders. In-service monitoring may also be provided but the monitoring can have a moderate probability of missing a defect that will become unstable, providing the crack that has run and been arrested has a very high probability of being found quickly during the everyday operation of the structure.

Damage-tolerant design philosophy: In this approach, the structure can carry on its safe operation even when the damages are present, and it will not suffer from catastrophic failure before the next scheduled inspection. For ship structure, the damage tolerant strategy is more applicable given the high redundancy of the structure and mandatory inspection programmes (Béghin et al., 2010)and (Papanikolaou, 2009). It should be noted that a damage tolerant structure is a design goal, and is only achieved with suitable design, inspection and appropriate fabrication quality.

Fracture mechanics approaches are usefully applied within the framework of design damage-tolerant philosophy. Here, fracture mechanics is used to determining the residual life of the structure given an initial crack is present. The objective is to determine an inspection interval so that the crack is found before it can cause a failure. The NDT should be capable of reliable detection of the predicated crack size at the time of inspection (Zerbst et al., 2015). Figure 3-1 demonstrates a typical framework of defect assessment using a fracture mechanics approach (Zerbst et al., 2015).

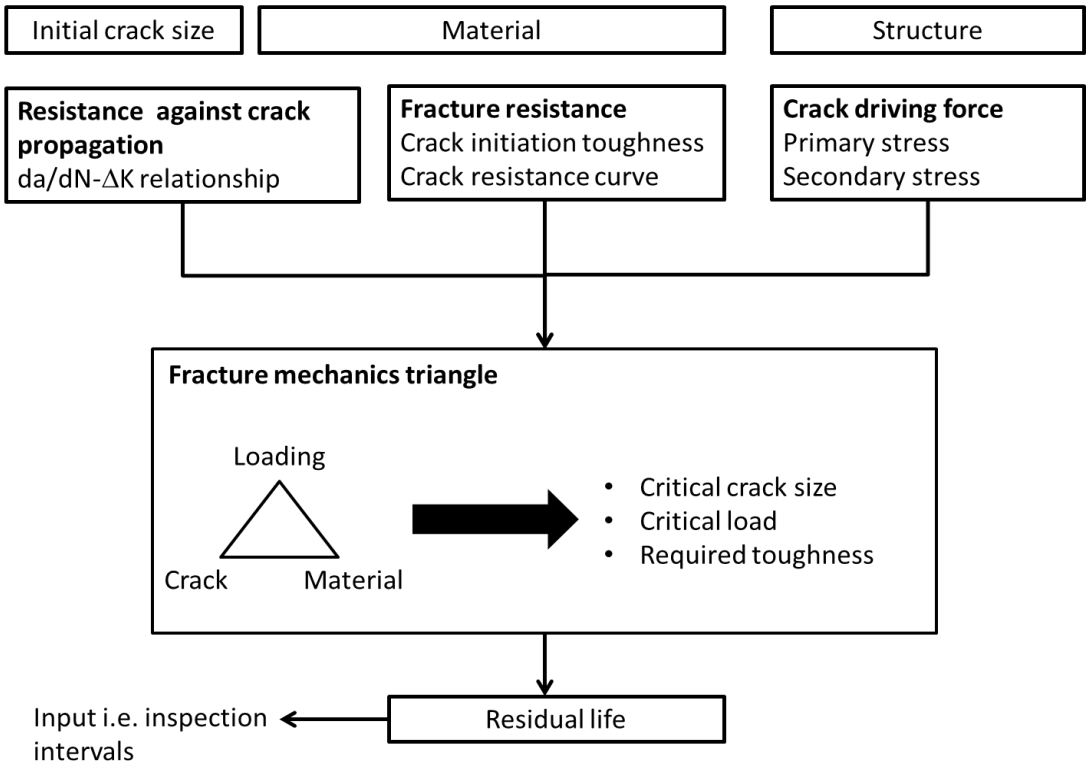

Figure 3-1 Fracture mechanics Framework, adapted from (Zerbst et al., 2015)

Fracture mechanics uses defect dimensions, material properties and the stress field at the defect to assess the possibility of structural failure. These three key inputs are commonly referred to as the fracture mechanics triangle in the literature (Figure 3-1). Time-dependent fracture mechanics analysis is also possible by prediction of crack propagation using Paris-Erdogan which relates rate crack propagation (da/dN) to change of stress intensity factor ΔK. Further details about fracture mechanics theory are given in chapter 4 of this thesis.

3.3 Determinist vs Probabilistic Fracture Mechanics

Fracture mechanics approaches used in the procedures such as R6 and BS7910 are deterministic and generally have a hierarchical nature, i.e. the analyst may progressively reduce conservative assumptions by increasing the complexity level of the analysis and consequently the precision of results until the operation of the structure is found to be fit for service. Otherwise, the structure will require a repair, a reduction of service (for example lowering primary stress) or resistance improvements (i.e. reduction of secondary stresses by stress relief techniques). This type of approach is particularly useful in the assessment of safety cases where the aim is to demonstrate that the structure is safe given conservative assumption of input variables. If the analysis fails to prove the safety of structure the variables may

be refined: detection size may be estimated by a more precise method (for example PAUT instead of conventional UT), crack driving force could be calculated using Finite Element Analysis (FEA) of the cracked body rather than using a standard K-solution, the residual stress field at the crack tip may be calculated and/or measured, or crack tip constraint may be analysed in more details.

Since these procedures are primarily meant to ensure the safety of nuclear systems, the level of conservatism built into them is believed to be very high. For instance, determination of fracture toughness is almost always based on the assumption that the plain strain conditions are dominant. This is a reasonable assumption for thick-walled pressure vessels (around 50 mm). In structures such as ship hull structures where average thickness is around 15 mm, the plain stress conditions, associated with higher toughness, are more applicable.

In deterministic analyses uncertainty in variables are dealt with by taking upper bound and lower bound of those variables- upper bound values of applied variables such as stress and flaw size, with lower bound values of resistance variables such as fracture toughness. In reality, the probability of all unfavourable conditions occurring at the same time is very low and often too conservative. As an example, lower bound fracture toughness is commonly determined as the 5th percentile of a model based on a weakest link approach, secondary stress due to weld residual stress in the as-welded condition (standard practice in shipbuilding) is conservatively assumed to be equal to material yield stress. Now, assuming a conservative 90 percentile initial crack length would result in a very early failure prediction of the structure, even a median crack size will show a very short fatigue life, as well. This is obviously not the case in real life and the fracture failures appearing in ship structures occur with bigger defects or less frequently than this method predicts. An alternative approach is a probabilistic analysis, in which, uncertain variables are treated stochastically and as random variables. In this approach possible combinations of input variables leading to failure are compared against total possible combinations, and a probability of failure is estimated instead of a definite fail or not- fail evaluation. Probabilistic analysis is also in-line with the damage tolerant strategy where the structure can deal with some levels of damage, and regular inspection is provided to find the cracks before they lead to catastrophic failure. In real life, cracks are continuously found and repaired during ship operation and at scheduled surveys. The general methodology is to calculate the through-life probability of failure and compare it with an

established target probability of failure (target reliability). The time at which that the structure is likely to exceed the acceptable target failure probability is calculated, as well. The inspection is then scheduled to be prior-to but close to that time. An expected critical size at the time of inspection is calculated so that an appropriate NDT method capable of finding that size is chosen.

One limitation of deterministic fracture mechanics is that conservative prediction of critical defect size and the time to the failure may reduce inspection efficiency by targeting wrong defect sizes and at a wrong time in service, whereas probabilistic assessment will provide a more efficient result (Lotsberg et al., 2016). Probabilistic failure assessment of the structures is also known as Reliability analysis. These two terminologies are often used interchangeably in the literature, but they have an identical meaning in this thesis.

3.4 Uncertainty and reliability

There is a close connection between calculated reliability and the uncertainties. Reliability analysis is in essence, assessment of uncertainties. If the exact quantity of all variables were known (i.e. certain) and the assessment model was precise, the reliability analysis would have resulted in either 100% or 0% reliability (Safe or Fail). However, in practice, there is uncertainty in both loading and resistance, which leads to a calculated reliability between 100% and 0%. Often in reliability analysis, the calculated reliability is compared against a target level of reliability and if the calculated reliability is below the target reliability corrective measures need to be taken to improve the reliability. One way that may improve the predicted reliability is to refine the predictive reliability by making a better estimate of stochastic variables, i.e. reducing uncertainty. Here, we are not improving the actual reliability of the structure but our estimate of the reliability (calculated reliability).

Epistemic uncertainties (from the Greek word *episteme* meaning knowledge) are a function of understanding and knowledge. They influence the confidence in the evaluated failure probability. A problem with low epistemic uncertainty leads to a failure probability with a high degree of confidence that tends towards the 'true' failure probability (HSE, 2001 a). The particular interest of this research is the uncertainties associated with weld defect statistics which have a direct relation with the extent and efficiency of NDE inspection. Additionally, better estimates of other stochastic variables (i.e. fracture toughness, stresses, etc.) and chosen model could

potentially increase or decrease calculated reliability and in turn, may allow a reduction or require an increase in NDE checkpoints to ensure that the target reliability is achieved. Thus understanding the nature of uncertainties and the means to quantify them is a crucial step.

As shown in Figure 3-2, uncertainties associated with an engineering problem may be grouped as follows:

- Physical uncertainty (intrinsic or inherent uncertainty) is the natural randomness of a quantity (DNV, 1996). This could be inherent or intrinsic uncertainty in time, i.e. variables that change with time and are often referred to as stochastic processes or stochastic variables. Examples include the wind velocity, corrosion rate and wave height. The inherent uncertainty could also be in space. Examples include the natural variations of the strength of materials from one specimen to another and the uncertainty in the fracture toughness of the steel as caused by the randomness of carbide sites distributed within the component.
- Measurement uncertainty is uncertainty caused by imperfect instruments and sample disturbance when observing a quantity due to limited information such as a limited number of observation of a quantity (DNV, 1996), for instance uncertainty in the probability of detection (POD) curves.
- Statistical uncertainty can be due to uncertainty in the distribution parameter and occurs when the parameters of a distribution are determined from a limited set of data (DNV, 1996). The smaller the data set, the larger the parameter uncertainty. Statistical uncertainty can also be the result of uncertainty in the choice of statistical distribution. It is a particular problem when deriving extreme value distributions. Often it is difficult to differentiate between the two types of statistical uncertainty, since with limited data both the parameters and distribution type may be uncertain. Statistical uncertainty can also be categorised into statistical uncertainty due to variations in space and time.
- Model uncertainty is uncertainty due to imperfections and idealisations made in physical model formulations of limit state (DNV, 1996), such as idealising the stress intensity factor of a stiffened plate with that for an unstiffened plate.

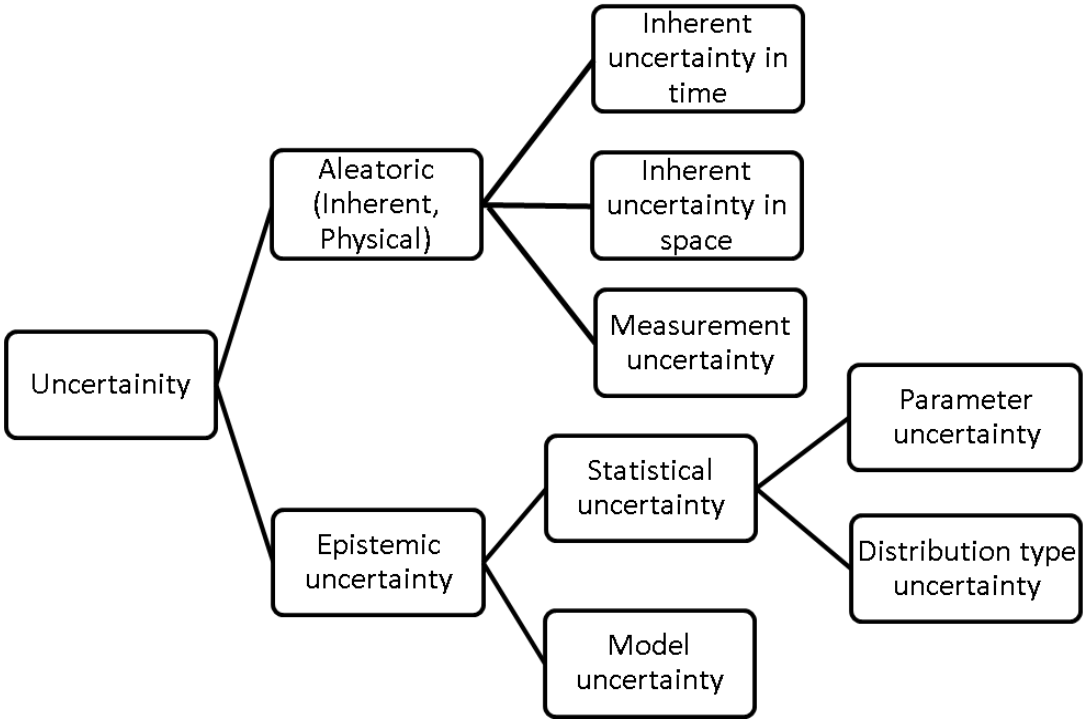

Figure 3-2 Types of uncertainties in engineering design

Statistical uncertainty associated with variations of variables in time can be reduced by sampling the occurrences for a longer period (DNV, 1996), i.e. in significant wave height data analysis. Statistical uncertainty associated with the variations in space can be reduced by carrying out further tests, i.e. taking more NDE checkpoints increases confidence in the distribution parameter estimate.

In this research, a probabilistic model which best describes structural failure due to the presence of a weld defect is formulated, and stochastic variables are defined. The source of uncertainty for each variable is identified and wherever possible efforts are made to quantify and reduce these uncertainties by collecting data, using improved statistical methods to quantify the data, and developing better models or using state-of-the-art literature.

Identified uncertain variables in reliability assessment of fabrication defects, the corresponding type and sources of the uncertainties, and the chosen strategy to reduce them are given in Table 3-1.

Figure 3-3 shows a schematic of key uncertain variables and their connection to the fatigue and fracture mechanics reliability framework adopted in this work.

Defect statistic, material toughness and their influencing variables have the greatest impact on the through-life reliability of the structure. They are both representatives of manufacturing quality and may vary from one shipyard to another. Thus, a great effort in this work has been made to study their variation and to quantify them and their influencing parameters. The results are presented in chapter four and five of this thesis.

Stress variability is to some extent accounted for by modelling the long-term distribution of stress for the ship. However, due to the unknown journeys the vessel will experience in its life, the design assumptions are adopted to predict stress cycles. A classic long-term stress analysis recommended by the International Association of Classification Societies is used.

It should be noted that there is always a trade-off between more refined but complex models and computational efficiency. Therefore the sensitivity of the calculated reliability to the modelled variables needs to be considered to develop a framework that is optimised as a whole.

Uncertain Variable	Type of uncertainty	Source of uncertainty	Uncertainty reduction strategy
Fracture toughness (steel grade)	The inherent uncertainty in space	The randomness of carbide inclusions in the material	Study the variables: Temperature, etc.
	Statistical uncertainty in space	Different manufacturers, Steel batches	Study influence of variables, take more samples
NDT reliability	The inherent uncertainty in space	Human errors, skills	Allow for human error, take mitigation actions
	Measurement uncertainty	NDT method limitations	Use a better method
Defect size and defect rate	Statistical Uncertainty; variation in time	Out of process causes, extreme events	Observe samples in the longer time span. Stabilise process
	Statistical Uncertainty; variation in space	Natural variability, Welder skills, plate thickness (different ship types)	More samples
	The inherent uncertainty in space	Weld process, restraint, thickness	Refined interpretation (planar / non-planar), Sufficient sample size
FAD uncertainty	Model uncertainty	Scatter of test results used to describe FAD locus	Quantify uncertainty with test results
Crack growth parameters	The inherent uncertainty in space	Material type (Weld, Parent material), Stress ratio	Gather more information about the structure
	Model uncertainty	Correlation between parameters	Develop a correlation relationship
Residual stress	Model uncertainty	Complex configurations	Develop better models
	Inherent uncertainty	Weld parameters Service load history (Shakedown)	Probabilistic analysis of residual stress (not addressed in this research)

Table 3-1 Identified uncertain variables in reliability assessment of fabrication defects

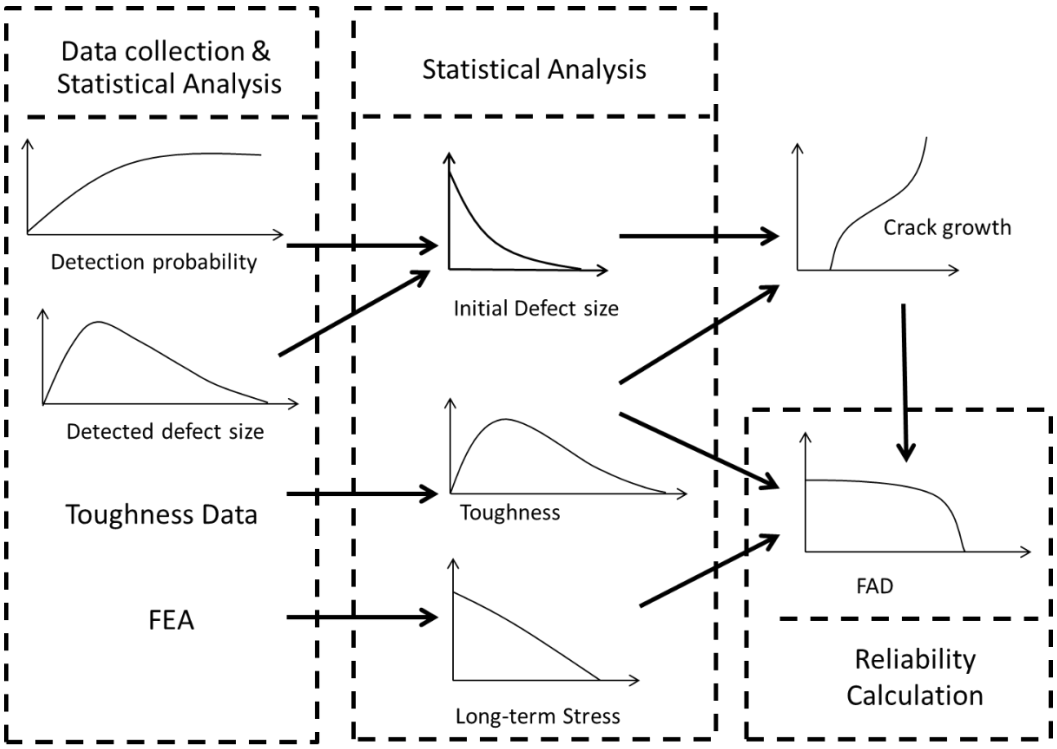

Figure 3-3 Schematic of key uncertain variables and their relationship to the reliability framework

3.5 Reliability and codes

The American Concrete Institute (ACI) and American Institute of Steel Construction (AISC) were the first institutes to develop a Reliability-based design codes. ACI used a mean value first order second moment (MVFOSM) method. (ACI, 1999), and AISC used a method based on lognormal format to calibrate a Load and Resistance Factor Design methodology (LRFD),(ANSI/AISC, 1999).

In ship hull design structural scateling is based on both method. According to common structural Rules (CSR) from International Association of Classification Societies (IACS), *in general, the Working Stress Design (WSD) method is applied in the requirements, except for the hull girder ultimate strength criteria where the Partial safety Factor (PF) method is applied. The partial safety factor format is applied for this highly critical failure mode to better account for uncertainties related to static loads, dynamic loads and capacity formulations* (IACS, 2012).

In the offshore industry, there has been a strong inclination towards developing reliability-based procedures due to the uncertain nature of degrading mechanisms which affect the integrity of the offshore structures and the financial benefits gained from the undisrupted supply of energy produced by offshore structures. Thus, the American Petroleum Institute (API) calibrated its recommended practice for use in

fixed offshore platforms (API, 1993) using LRFD method to provide a more uniform reliability than in previous codes.

Many current codes also allow for the direct use of reliability methods in design. The DNV (Det Norske Veritas) Rules for the design of fixed offshore structures have for many years allowed three alternative design approaches: allowable stress, partial coefficient, and reliability design (DNV-GL, 2017). In 2015 DNV published a recommended practice on Probabilistic methods for the planning of inspection for fatigue cracks in offshore structures (DNV, 2015). DNV also have a useful Classification Note for the practical use of structural reliability (DNV, 1992). Lloyds Register has recently published a guideline on risk-based inspection of hull structures (LR, 2017). Since 1998 there has also been an ISO standard covering the general principles for the use of structural reliability (ISO 2394, 2015).

The British Standard "Guide to methods for assessing the acceptability of flaws in metallic structures" (BS7910, 2015 a) recognises fatigue and fracture mechanics reliability assessment and provides an informative annexe (Annexe K) which describes methods of probabilistic defect assessment.

3.6 Levels of Reliability Analysis

According to (DNV, 1992), structural reliability analyses are commonly classified concerning level, moment and order. Level refers to the approximation in solving the structural reliability problem. Moment refers to the order of statistical moment used to describe uncertain variable and its probability distribution, Mean is the first statistical moment, and the standard deviation is the second moment. Order refers to the order of polynomial applied to approximate limit state surface. For example, First Order Reliability Method (FORM) uses a first-order polynomial function (a plane) to approximate failure function and Second Order Reliability Method (SORM) uses a second-order polynomial function to approximate failure function (Figure 3-6).

Level I methods, such as partial safety factor method, are deterministic reliability methods that use a characteristic or nominal value in conjunction with a safety factor to describe the uncertain variable (Figure 3-4). Level 1 design is acceptable providing: (Characteristic strength/partial strength factor) ≥ (Characteristic load x partial load factor). Ideal design would have the quantities equal. The safety factors are usually determined using a higher level of reliability analysis to account for the scatter in the limit function and the consequence of exceeding the safety margin.

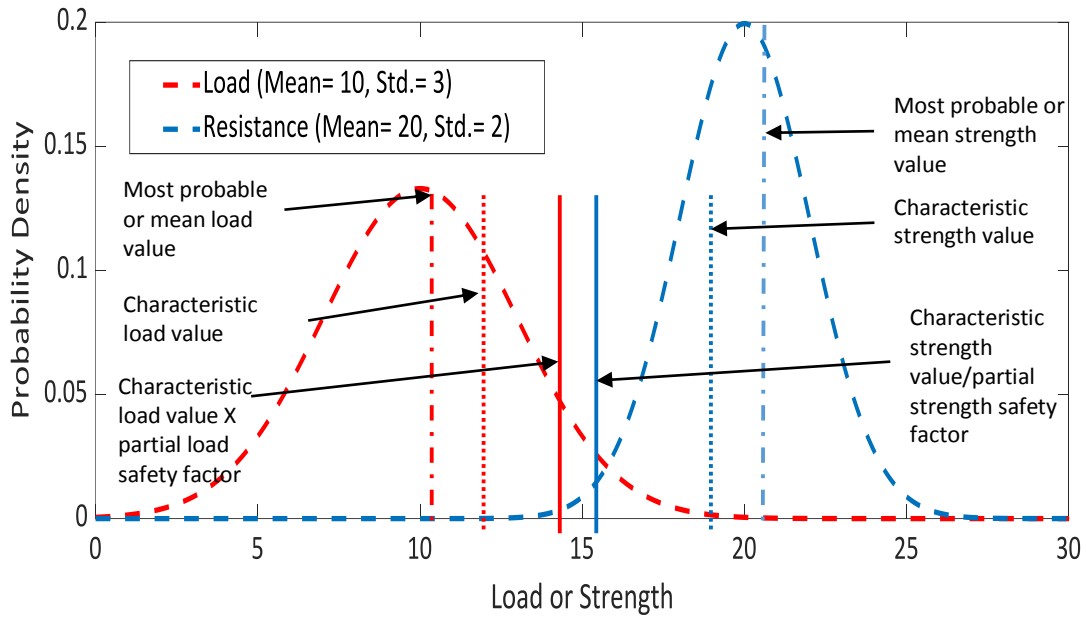

Figure 3-4 Representation of a level I reliability

Level II methods use two parameters to describe variable uncertainty, i.e. a mean value and standard deviation. Where two variables are correlated, a parameter to measure their correlation degree is needed, too. Among the level II methods the FORM and SORM methods, which produce a reliability index (β) are the most frequently used methods (Figure 3-5). Level II methods are based on the use of the normal distribution (Melchers, 1999).

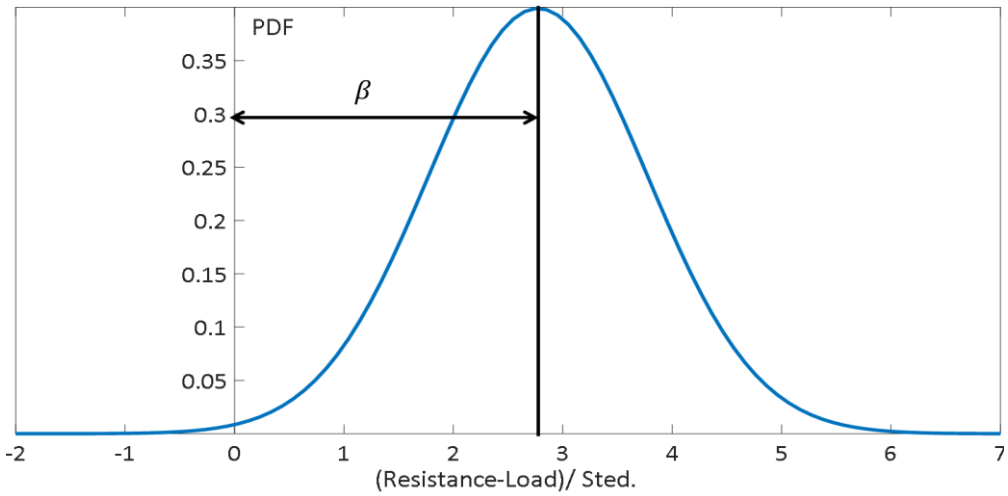

Figure 3-5 Illustration of Reliability index (β) method

This concept was initially introduced by Freudenthal (Freudenthal et al., 1964) and subsequently, Cornell (Cornell, 1969) defined a reliability safety index as:

$$\beta = \frac{E(M)}{\sigma(M)} \tag{3-1}$$

where M is the margin of safety. $E(M)$, the mean value of safety margin is $E(Resistance) - E(Load)$, and $\sigma(M) = \sqrt{\sigma(Resistance)^2 + \sigma(Load)^2}$.

$$\beta = -\Phi^{-1}(P_f) \tag{3-2}$$

where, $\Phi^{-1}(.)$ is the inverse of standard Normal probability distribution function. Thus the probability of failure (P_f) is equal to cumulative standard normal distribution of ($-\beta$). Table **3-2** shows the relationship between some typical reliability index values and their corresponding failure probabilities.

Reliability Index (β_0)	2	2.5	3	3.5	4	4.5	5
Probability of failure (Pf)	2.28E-02	6.21E-03	1.35E-03	2.33E-04	3.17E-05	3.40E-06	2.87E-07

Table 3-2 Relationship between reliability index (β_0) and failure probability

The limitation of the Cornell safety index is that it is not an invariant safety index but depends on how the limit state function is defined: if the safety function is defined by a non-linear relationship between the various loading and strength variables the safety index based on the mean values of the variables will not be correct. In linearized form, this was corrected by Hasofer and Lind (Hasofer and Lind, 1974) but is not discussed here, also see (Béghin et al., 2010) for further details. Further improvements to the method allow for a second order approximation to the failure surface. Common approximative analytical methods are first order and second order reliability methods (i.e. FORM and SORM). The difference between FORM and SORM is depicted in Figure 3-6.

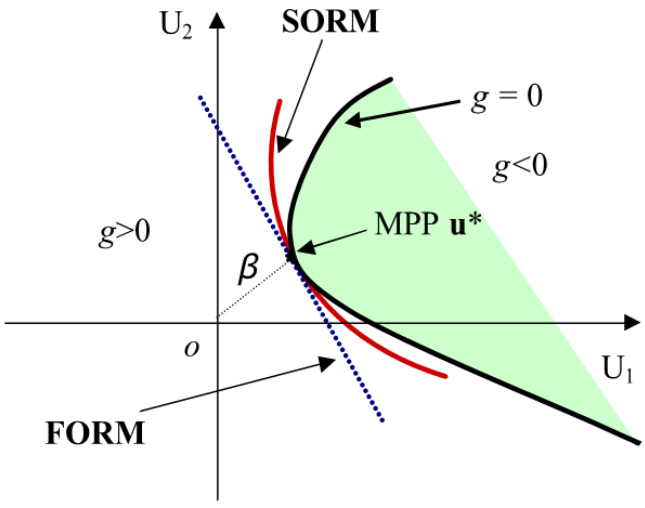

Figure 3-6 Comparison between FORM and SORM (Du, 2005)

Level III methods are fully probabilistic methods and use joint probability distribution of all relevant uncertain variables to describe these variables (Figure 3-7). Examples of Level III methods include numerical integration, i.e. convolution integral, and simulation methods, i.e. Monte Carlo simulation, which though approximate, converge towards exact solutions (DNV, 1992).

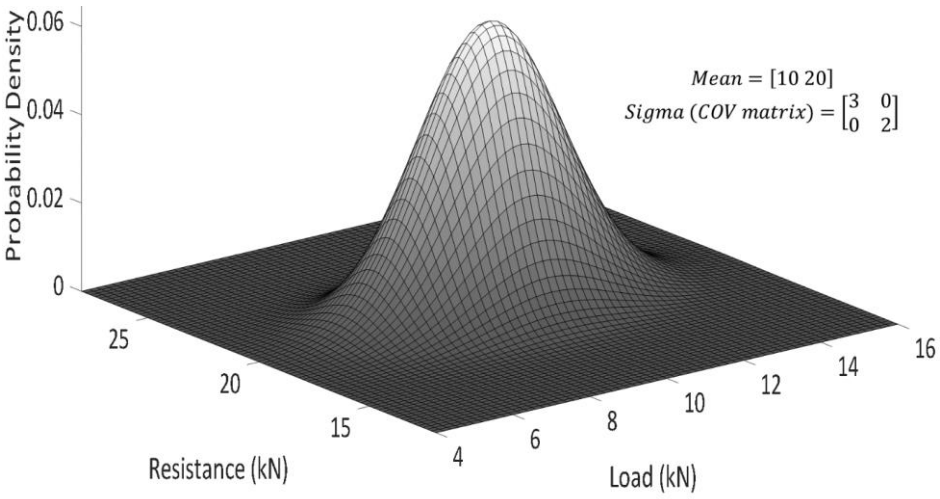

Figure 3-7 Joint probability distribution of load and resistance

First order reliability methods (FORM) and second order reliability methods (SORM) has traditionally been prevalent compared with level III methods, such as Monte Carlo method, because they require lower computer resources. Generally, among the three methods, Monte Carlo method is more precise if sufficient numbers of samples are provided.

When the failure probability is large, or the limit state function is highly nonlinear, analytical methods may lead to inaccurate results. In these cases, Monte Carlo simulations are more effective (Béghin et al., 2010). A random sampling is considered to simulate calculation. For each simulation cycle, the limit state is calculated and compared to failure, and calculations are repeated until convergence is achieved. The probability of failure is the number of simulations that yielded failure divided by the total number of simulations. $P_f = \frac{N_f}{N}$. Figure 3-8 shows Example of a Monte Carlo simulation method for Fracture mechanics analysis based on failure assessment diagram (FAD) failure criteria. For small failure probabilities, the method can be improved by 'importance sampling' where, as failures are identified, more samples are taken in that region so that, after correcting for the biased sampling, the failure probability, may be estimated with a smaller number of samples.

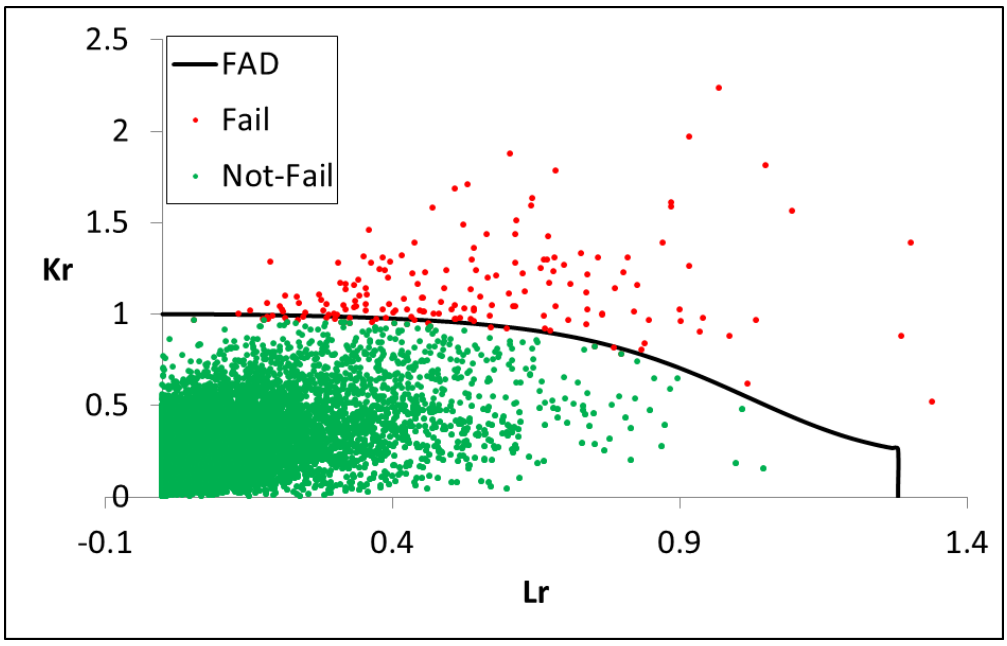

Figure 3-8 Example of a Monte Carlo simulation method

Convolution integral is a numerical method and is illustrated in Figure 3-9, for a given load and resistance distribution. The method performs the integration in equation (3-3).

$$P_f = \int_0^{\infty} PDF_{load} * CDF_{resistance} dload \qquad (3\text{-}3)$$

At any Load level, the probability of the Resistance being less than the Load is simply the cumulative value of the Resistance at that Load level. This calculation is repeated for all possible load levels. Then the results are multiplied by the probability of that load level, to obtain the probability of failure at that load level. The probabilities for all load levels are added together to obtain the overall failure probability (Barltrop, 2011 b).

Alternately, it is possible to integrate resistance over the probability density of all resistance values times the probability that the load exceeds that resistance value; the calculated failure probability will be the same.

The method can be used for simple failure criteria (Loading exceeds Resistance) but, unlike the First or second order second-moment methods (FORM/SORM) it can cope easily with any form of distribution, including distributions with multiple peaks corresponding to multiple failure modes (Barltrop, 2011 b). However, the solution of the reliability problem using convolution integral becomes computationally

inefficient as the number of stochastistic variables increses. As explained in Chapter 6, the solution of the reliability problem for three stochastic variables is very fast.

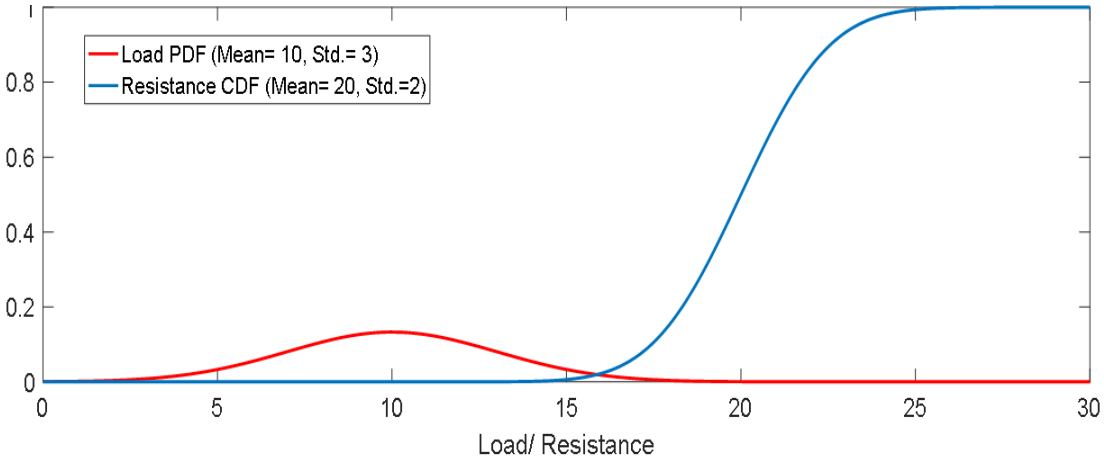

Figure 3-9 Load and resistance distributions for Convolution integral

In the recent years, due to the considerable advancement in computation power, Monte Carlo methods have become increasingly popular. In this research two methods, one based on the Monte Carlo method and a faster numerical integration method based on the Convolution Integral have been developed and are discussed later in chapter 6.

Level IV methods combine both probabilities of failure and the consequence of failure, costs and benefits and costs of construction, monitoring, maintenance, and repair. These methods can be used to determine target reliabilities to be used as acceptance criteria for lower levels of reliability analysis. Level IV reliability methods are referred to as Risk-based methods. The risk is defined as the product of the probability of failure and the consequence of that failure.

$$Risk = (Probability\ of\ failure * Consequence\ of\ failure) \qquad (3\text{-}4)$$

3.7 Risk Assessment

The purpose of risk analysis is to comprehend the nature of risk and its characteristics including, where appropriate, the level of risk. Risk analysis involves a detailed consideration of uncertainties, risk sources, consequences, likelihood, events, scenarios, controls and their effectiveness. An event can have multiple causes and consequences and can affect multiple objectives (ISO-31000, 2018). Risk remaining after protective measures are taken is called residual risk (ISO-14971, 2012). The purpose of risk evaluation is to support decisions. Risk evaluation involves comparing

the results of the risk analysis with the established risk criteria to determine where additional action is required (ISO-31000, 2018). The overall procedure for risk analysis and risk evaluation is a risk assessment (ISO-31000, 2018).

A commonly used method of risk evaluation is the so-called Risk Matrix model in which the failure probability is shown in one axis and the consequence of failure on the on the other. The failure probability and consequence failure maybe specified quantitatively, qualitatively, or semi-quantitatively, depending on the complexity of the model and the availability of data. Each combination of failure probability and consequence of failure will then be assigned a corresponding risk level. It is useful to show these levels in specific colour coding convention. One such convention is an adapted traffic light convention in which low-risk levels are shown in green, extreme risks in red and medium risk levels are coloured in yellow. It is also possible to refine this colour coding further, for example, light yellow and dark yellow, to allow for more risk levels. An example Risk Matrix is shown in Figure 3-10.

Probability of failure	5. Frequent	HIGH	HIGH	EXTREME	EXTREME	EXTREME
	4. Likely	MEDIUM	HIGH	HIGH	EXTREME	EXTREME
	3. Possible	MEDIUM	MEDIUM	HIGH	HIGH	EXTREME
	2. Unlikely	LOW	MEDIUM	MEDIUM	HIGH	HIGH
	1. Rare	LOW	LOW	MEDIUM	HIGH	HIGH
		1. Negligible	2. Minor	3. Moderate	4. Major	5. Catastrophic
		Consequence of failure				

Figure 3-10 A typical Risk matrix diagram

In order to assign an appropriate risk level (i.e. colour in the risk matrix) it is necessary to establish risk acceptance levels. If a system has a risk value above the accepted levels, actions should be taken to improve the safety through risk reduction measures. One challenge in this practice is defining acceptable safety levels for activities, industries, structures, etc. Since the acceptance of risk depends upon society perceptions, the acceptance criteria do not depend on the risk value alone (Ayyub et al., 2002). As an example, the author came across a case where a multinational venture capital conglomerate decided to expand its business in sea cruise market by starting a cruise line. The company demanded extra safety measures in design and construction of their ships, referring to the fact that a safety incident could jeopardise business of the whole conglomerate.

Another common risk evaluation method is the ALARP, which stands for "as low as reasonably practicable", or ALARA (as low as reasonably achievable) (HSE, 2001 b). The ALARP basis is that tolerable residual risk is reduced as far as reasonably practicable. For a risk to be ALARP, the cost in reducing the risk further would be grossly disproportionate to the benefit gained. The basis of ALARP is illustrated by the so-called carrot diagram in Figure 3-11.

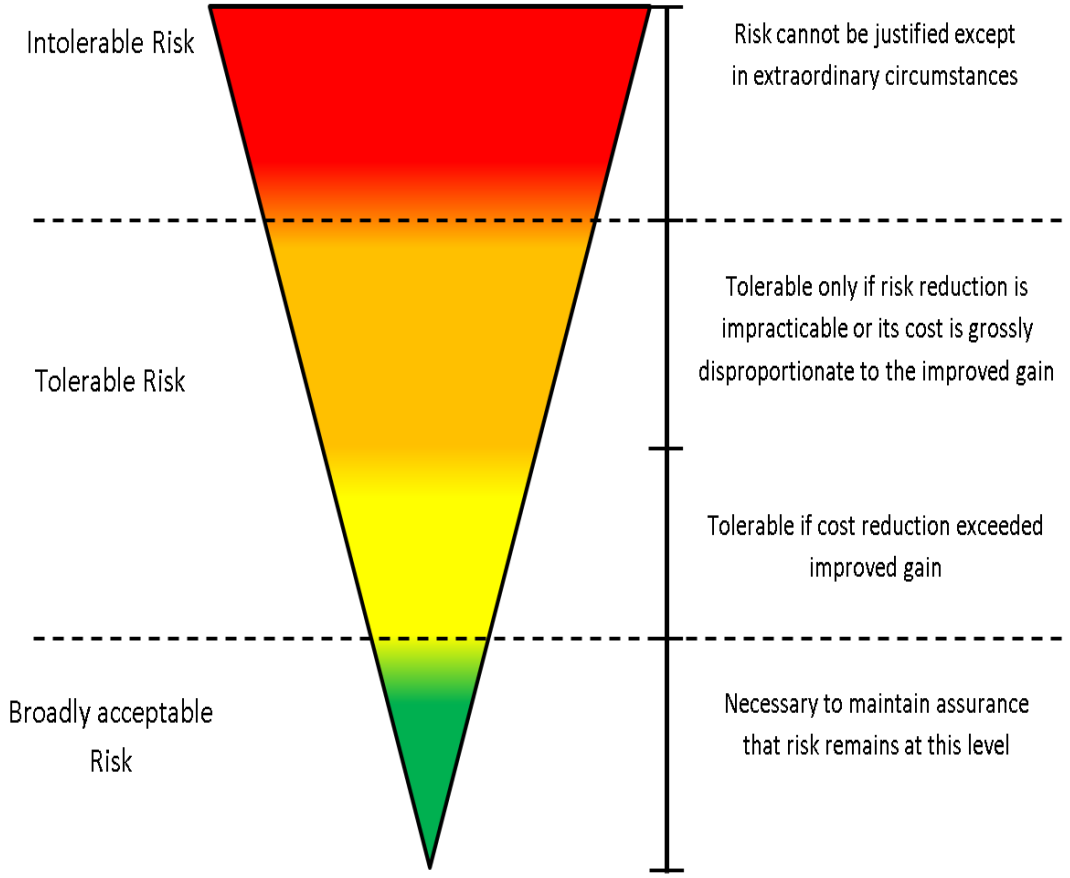

Figure 3-11 ALARP Carrot diagram based on (HSE, 2001 b)

3.8 Proposed Risk and reliability framework of weld defects in ship hulls

In this research, risk assessment of welded joints in newbuilding ship hull structures aims at ensuring the intended reliability of the joints by following the six steps given in Figure 3-12:

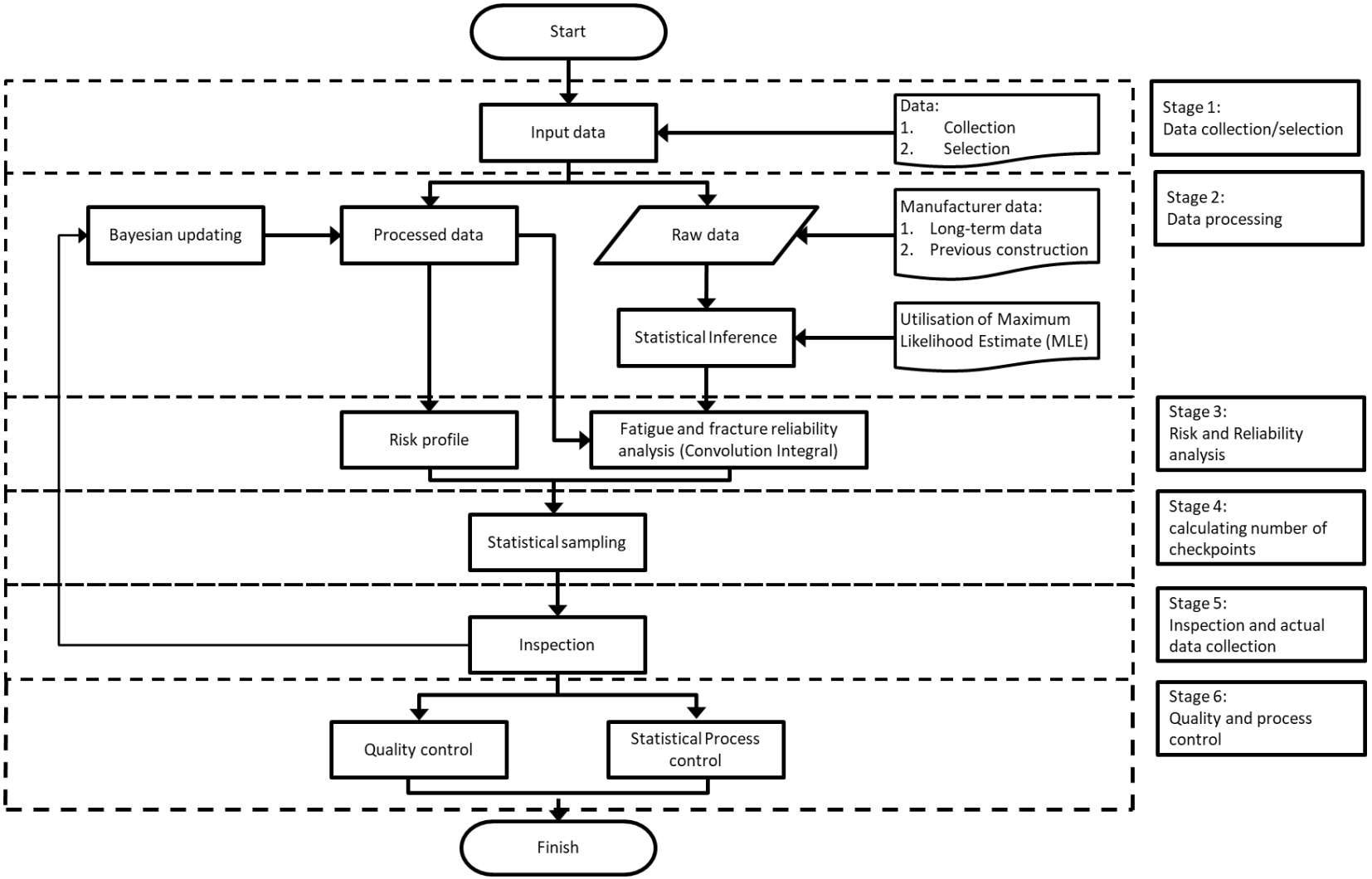

Figure 3-12 Proposed Risk and reliability framework of weld defects in ship hulls

3.9 System definition and consequence of failure

The consequence of a fracture, in many occasions, are only a small repair cost but if it is left untreated and extends to a larger length and in combination with other unfavourable conditions such as heavy seas, low temperature and poor toughness it can lead to more severe consequences such as:

- loss of the ship or part of the ship (Kurdistan Tanker incident), Loss of service (Castor Tanker (Figure 3-13)),
- Environmental consequence (e.g. Prestige Tanker failure),
- Or, cause danger to the people on-board.

In all cases, it would have financial consequences.

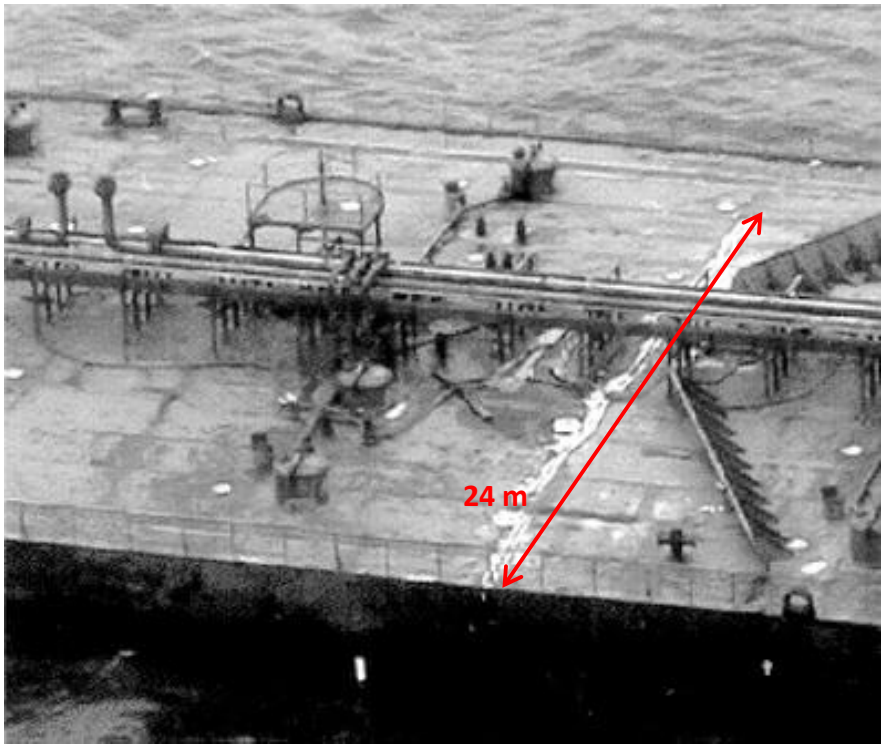

Figure 3-13 Photo of Castor tanker failure (E-bookshelf.de, 2000)

Consequence analysis of ship fracture would require the application of one of hazard identification and incident scenarios techniques such as Failure Mode and Effect Analysis (FMEA), event tree Analysis (ETA), or Fault Tress Analysis (FTA). Other more complex methods include Cause Consequence Analysis (CCA), and Hazard and Operability analysis (HAZOP) that are more applicable to process engineering where systems are defined more rigorously.

3.9.1 Failure Mode and Effect Analysis (FMEA)

FMEA uses a 'bottom-up' approach (as opposed to the 'top-down' approach). The method starts at the lowest level by assuming a failure mode or mechanism for each component and then studies the consequences for the larger system (BS-31010, 2010).

3.9.2 Event Tree Analysis (ETA)

ETA is another bottom-up method similar to FMEA and is a graphical logic method for identifying the various possible consequences of a given event, known as an initiating event. The impact on the system from the incident of the initiating event until its ultimate consequences is determined by the service or failure of different components. Event trees help to identify those events which are most critical and have the greatest impact on system failure (BS-31010, 2010). Figure 3-14 shows an example of an Event Tree Analysis (ETA) for a weld defect located in the plating of the deck structure stiffened panel. It shows, for example, that low toughness in deck material can cause the local fracture which may be found during service and can be repaired, but it may also propagate further to cause deck failure with higher consequence of failure such as loss of service as happened in the case of Castor Tanker (Figure 3-13) or propagate to side shell and cause higher consequence of failure such as the hull failure. Here, a possible risk mitigation action is increasing toughness in the vicinity of the interface between the deck and the side shell to provide a crack arrest mechanism.

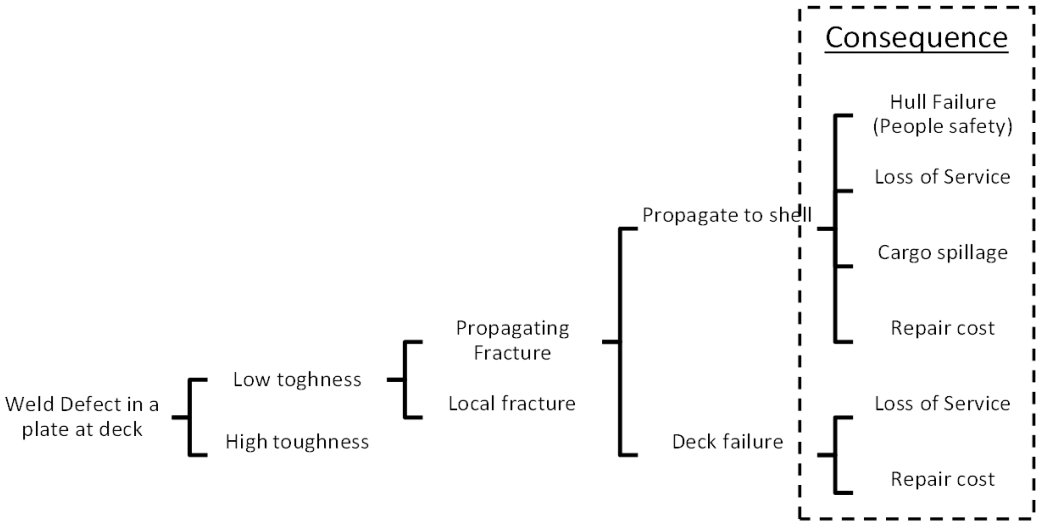

Figure 3-14 Example of an Event Tree Analysis (ETA) for a weld defect

3.9.3 Fault Tree Analysis (FTA)

A fault tree is based on the opposite procedure to an event tree; starting from some failure event, it is analysed how this may have been caused (BS-31010, 2010). Fault trees are constructed in a sequence of logic gates descending through subsidiary events resulting from basic events at the bottom of the tree. In drawing up a fault tree, symbols such as AND gates and OR gates are used. The AND gate corresponds to a parallel arrangement and the OR gate to a series arrangement. Main limitations of FTA are that it is narrow-focus (single failure), requires significant process information, and it can be time-consuming. Similar to the ETA example, Figure 3-16 illustrates the Fault Tree Analysis (FTA) for a weld defect located at the plating of the deck structure stiffened panel. Unlike the ETA case, here, the focus is to prevent hull girder failure and a weld defect is one of the risk drivers for this event.

Although it is possible to perform a detail Hazard incident scenario analysis accompanied by the corresponding detail consequence assessment (cost-benefit, oil leakage, .etc.), it is felt that such a model will be prone to inaccuracy due to its complexity, added entities of uncertainty and its sensitivities to additional inputs. The problem becomes more apparent when considering that other measures of risk managements that are present on a ship (lifeboats, the efficiency of the evacuation plan, variation in the cost of repair, the dependency of social consequences on the size of the owner's business, etc.) are varied considerably. A better strategy will be to employ a systematic, simple but conservative approach to evaluate relevant risks associated with the fracture in structural components.

3.9.4 Specifying consequence of failure classes

In order to evaluate criticality (a consequence of failure) of different members in a hull structural system, a model developed by Ship Structure Committee (SSC) based on an earlier recommended model by (IACS, 2006) has been adapted for passenger ships. The method uses an event tree analysis (ETA) type approach in which criticality is defined based on the possible consequence of failure and also the relationship of the member with other components of the structural system and relative to their rank in the structural hierarchy. The model was developed as follows:

IACS Common Structural Rules for Double Hull Oil Tankers (IACS, 2006) presents a schematic diagram of the "criticality class" for structural components in the cargo region. This classification facilitated the selection of acceptance criteria and capacity

models such that the more critical components have stricter requirements and hence require a lower probability of failure (IACS, 2006).
The preceding approach was adopted and modified by ABS (ABS, 2012) who were commissioned by the Ship Structure Committee (SSC) to conduct a study to review industry experience of fractures and fracture repairs, and to develop a comprehensive and usable steel hull fracture repair guide. The project focused on the marine industry practice of repairing fractures and evaluating the effect of a fracture on the structural integrity of the vessel. It should be noted that here fracture is defined as "Propagation of a crack through the thickness of a material" (IACS, 2003).

The criticality of each structural component was evaluated based on loss of intended function (containment or providing strength) upon failure concerning consequences to People (P), Environment (E) and Serviceability (S). The consequence categories are defined as:

- People (P): Potential for human injury and fatality
- Environment (E): Potential for release/ leakage leading to environmental pollution
- Serviceability (S): Potential for structural failure leading to structural damage and subsequent impairment of ship serviceability.

Each of the consequence categories (People, Environment and Serviceability) are affected differently by the structural failure mechanisms. Therefore, for each structural component, the consequence of failure needs to be assessed for each of these categories. Criticality Class value was classified into one of the three categories: High, Medium and Low as defined in Table 3-3.

Criticality Class	Description
High	For structural components where failure may imply high potential for fatality or human injury, significant environmental pollution or ship going out of service
Medium	When failure may imply medium potential for human injury, medium environmental pollution or impairment of ship serviceability
Low	When failure may imply the low potential for human injury, minor environmental or impairment of ship serviceability

Table 3-3 Definition of Criticality Class (ABS, 2012)

Descriptions of the High, Medium and Low categories for People, Environment and Serviceability used in the assessment are presented in Table 3-4.

Consequences	Criticality Class		
	Low	**Medium**	**High**
People (P)	Injuries: Few Fatalities: None	Injuries: Many Fatalities: None	Injuries: Many Fatalities: 1 or more
Environment (E)	No or Negligible release of pollutant	Minor release of a pollutant	A major release of a pollutant
Serviceability (S)	No impairment of service (No effect on normal operation)	May lead to limited impairment of service (Restricted operation)	May lead to a ship going out of service

Table 3-4 Typical descriptions of the Criticality Class (ABS, 2012)

(ABS, 2012) also provides a recommendation of repair for corresponding critical class and is given in Table 3-5.

Combined Criticality	Recommendation of Repair
High	Initiate immediate corrective action
Medium	Evaluate necessity for corrective action when failure is found. Conduct temporary repair and monitor the vessel's condition until a permanent repair is carried out
Low	No immediate corrective action required. Needs to be monitored and re-examined at next scheduled inspection

Table 3-5 Recommendations for repairs based on the criticality class of a fracture (ABS, 2012)

The assessment can be simplified by establishing a single combined criticality class for each structural component. As shown in Figure 3-15, the combined criticality class of the structural component is determined by the highest criticality class assigned to its consequence categories (P, E and S).

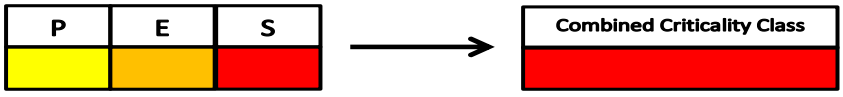

Figure 3-15 Combined criticality (ABS, 2012)

A major difference in the proposed model for a passenger ship and the merchant ship model is that since the passenger ship has no clear strength deck and instead all the decks contribute to longitudinal strength of the structure, the consequence of deck fracture failure in passenger ships are considered lower and are taken as equal to the criticality class of a secondary deck of a container ship. Criticality class models for Tankers, Bulk carriers and container ships are adopted exactly from (ABS, 2012) and are given in the Appendix B.

By adopting (ABS, 2012) methodology and using an event tree analysis approach the criticality class for the passenger ship was developed and is illustrated in Figure 3-17.

As an example, if a crack in one of the deck longitudinals is not extended to plate it will remain a local level problem with medium criticality, but if it is extended or likely to be extended to the plate (crack at fillet weld connection between stiffener and the plate) then it will be a panel issue at primary structure level and consequently will have a medium criticality class.

Although repair recommendations given in Table 3-5 are for fracture failures found in-service, a similar approach can be adapted for newbuilding hulls. For example, recommendations given in Table 3-6 can be suggested for treating NDT checkpoints containing defects. Recommendations are based on expert opinions of experienced NDT technicians and shipyard surveyors gathered by the author. Summary of the gathered data from expert opinion survey is given in Appendix A.

Combined Criticality	Recommendation of Repair
High	Extend inspection to the full length of weld line performed with the same parameters (same joint, same welder, date, workshop, weld robot, etc.)
Medium	Extend the inspection to double the length of the initial checkpoint and in each direction (4 times initial checkpoint length).
Low	No further inspection is required

Table 3-6 Recommendations for additional inspection based on the criticality class of a fracture for newbuilds

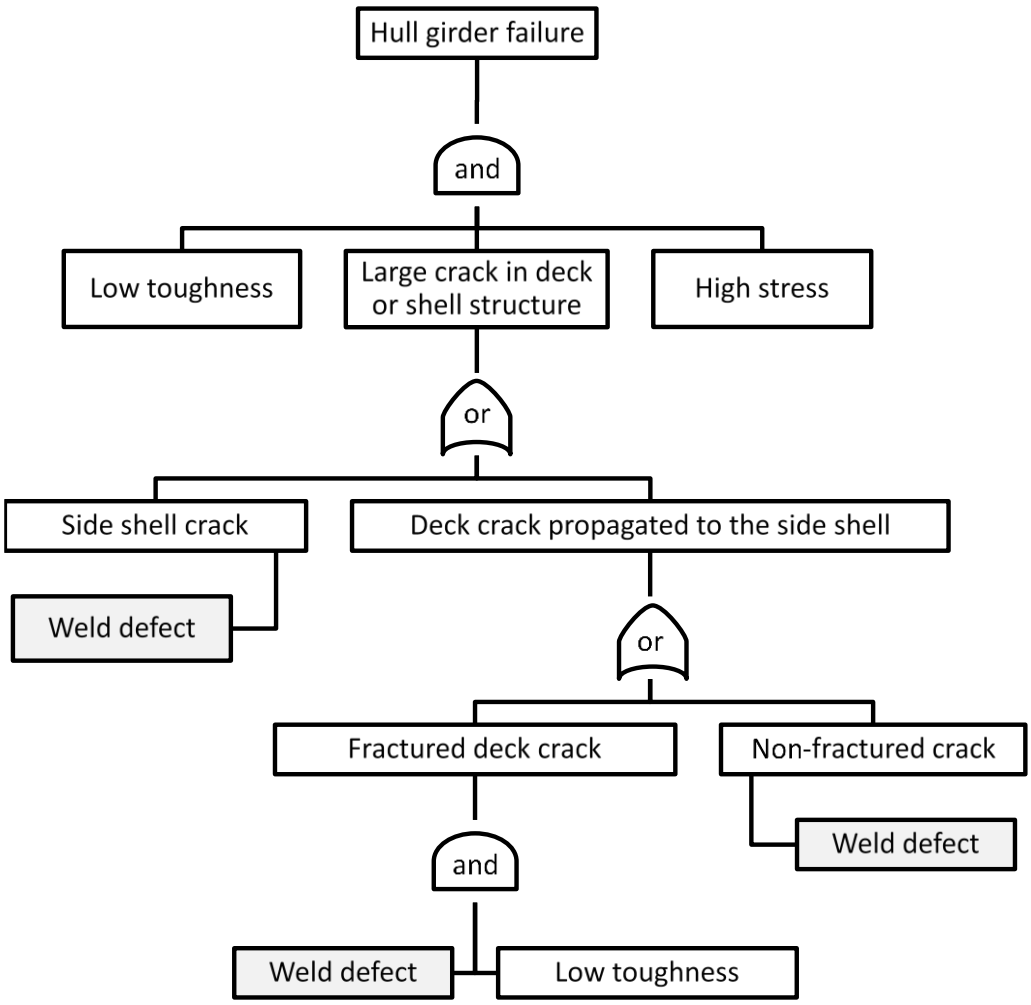

Figure 3-16 Fault tree model of hull girder failure concerning weld defect

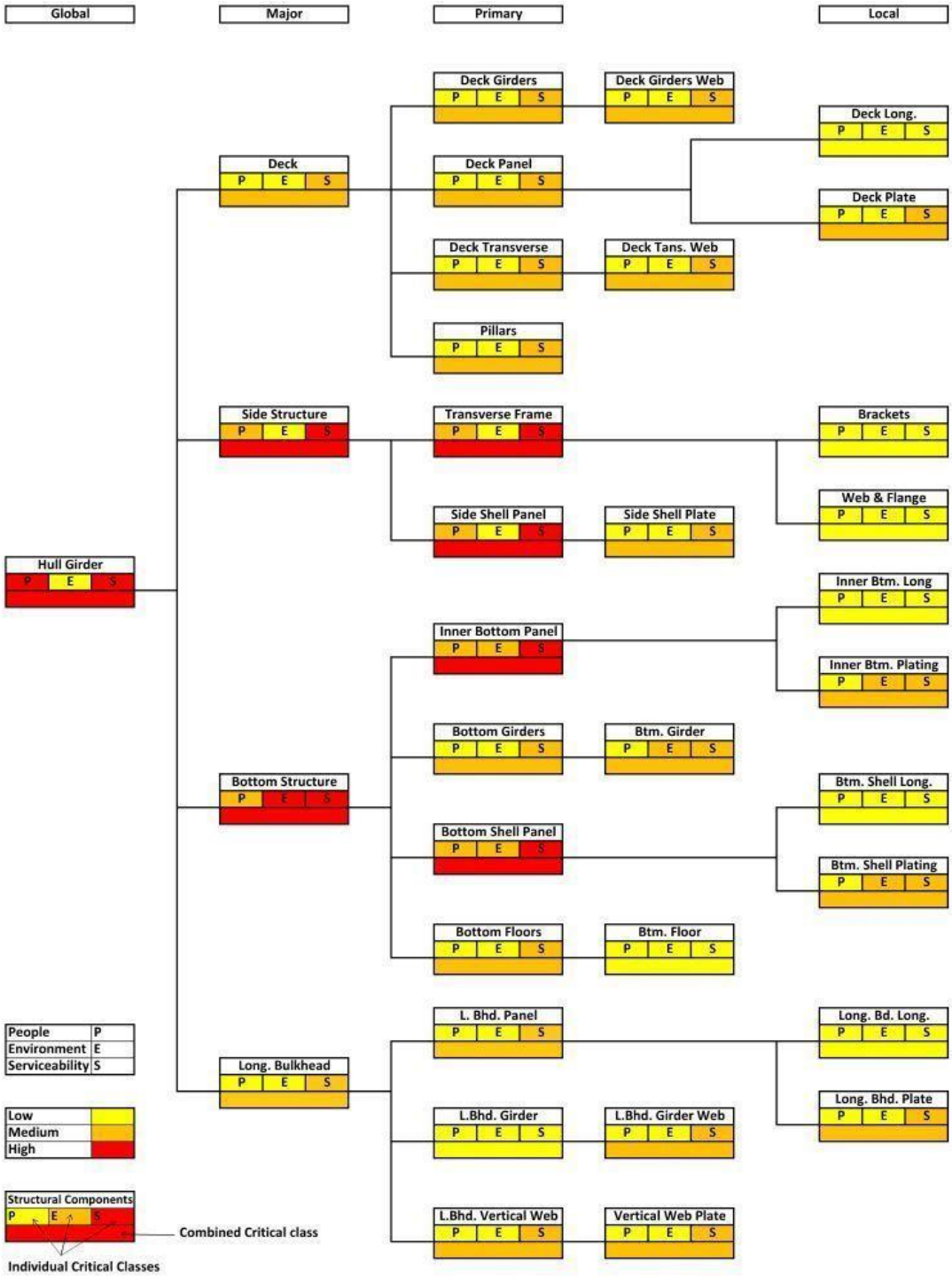

Figure 3-17 Developed consequence model for a passenger ship

3.10 Target reliability

Target reliability values may be employed to ensure that a required level of safety is achieved. The target reliability measures depend on the failure consequence as well as the cost and effort to reduce the risk of failure. The consequence of failure can be the risk of human injury and fatality, economic consequence, and social impacts. The

target reliability should always correspond to a reference period, e.g. annual or service life probability of failure. If the relevant consequence is the risk of human life, annual failure probabilities are preferred to ensure a consistent level of tolerable risks at any time. Target reliabilities maybe defined four different ways:

1. The standard developers recommend a reasonable value. This method is used for novel structures.
2. Reliability implied by standards. The level of risk is estimated for a design standard that is considered to be satisfactory. This method has been commonly used for standard revisions, particularly where the intention has been to provide a more uniform safety level for different structural types and loading types. By carrying out a reliability analysis of the structure satisfying a specific code using a given probabilistic model, the implicit required level in this code will be obtained, which may be applied as the target reliability level. The advantage with this approach compared to applying a predefined reliability level is that the same probabilistic approach is applied in the definition of the inherent reliability of the code specified structure and the considered structure, reducing the influence of the applied uncertainty modelling in the determination of the target reliability level.
3. The target level for risk assessment based on failure experiences. This method is particularly useful when the functional reliability of the system is more important than the reliability of individual components. In the automotive industry or electronic components manufacturing component reliability is determined by failure rate data of real components. The failure rate data is then used in system reliability calculation (Bertsche, 2008).
4. Economic value analysis (cost-benefit analysis). Target reliabilities are chosen to minimise total expected costs over the service life of the structure. In theory, this would be the preferred method, but it is often impractical because of the data requirements for the model.

Examples of target reliabilities prescribed by codes and standards are listed in Table 3-7. For the relationship between reliability index and failure, probabilities see Table **3-2**. For further information abaot available models for developing target reliability levels for novel structures reference is made to (Bhattacharya et al., 2001).

Source	Scope	Limit state function	Minimum Reliability index
Eurocode: The basis of structural design (BSI, 2005)	Buildings and civil engineering works	Ultimate limit states	3.3 to 4.3 for 50 years reference period and 4.2 to 5.2 for annual
	Residential and office buildings, public buildings where consequences of failure are medium (e.g. an office building)	Fatigue limit state	1.5 to 3.8[1)] for 50 years reference period (Table C2)
DNV (DNV, 1992)	Marine structures		3.09 to 4.75
1) Depends on degree of inspectability, reparability and damage tolerance.			

Table 3-7 Examples of target reliabilities specified by codes and standards

When calculated reliability is compared against target reliabilities driven from standards or real life frequentist reliabilities, special attentions should be paid to the close relation between uncertainty modelling and the target reliability level, as the calculated reliability in a reliability analysis is dependent on the chosen uncertainty modelling.

Achieving target reliabilities can be used to ensure a certain safety level. A reliability analysis can be used to verify that such target reliability is achieved. The challenge in this context is that the uncertainties included in a structural reliability analysis will differ from real life reliabilities due to the deviation of calculated reliabilities from gross errors which occur in real life. Moreover, the reliability analysis includes 'epistemic uncertainty': statistical uncertainty and model uncertainty in addition to the 'aleatory uncertainty': physical variability which is present in real life. Hence, reliability analysis determines a nominal value, dependent on the analysis model, rather than a real reliability value.

The output of this research is construction guidance, which by its nature needs to be conservative (safe) and therefore the uncertain variables and failure function are estimated with conservatism. For example, it will be seen in chapter 6 that stiffened panels are idealised by plain plates without considering the restraint effect caused by the stiffeners and the compressive residual stress induced in the plate. Both effects retard crack propagation.

3.10.1 Target reliabilities for ship hull structures

For ship hull structure the most comprehensive work has been done by (Mansour, 1996). Mansour's work is based on several preceding research projects looking at fatigue and fracture in ships and reliability assessment of aged tankers and cruisers (cruise ships) published by the Ship Structures Committee (SSC). (Béghin et al., 2010) also recommends values proposed by (Mansour, 1996). (Mansour, 1996) have recommended safety levels for fatigue by:

(1) reliability analysis of existing ship structure
(2) prior reliability analysis of ship structure and structural components
(3) use of target values in related applications
(4) the application of professional judgment

Detailed background to (Mansour, 1996) work on establishing the target reliabilities is available in Appendix B of "PROBABILITY-BASED SHIP DESIGN: IMPLEMENTATION OF DESIGN GUIDELINES (Mansour, 1996)". These values, which are presented in Table 3-8, are lifetime values.

Ultimate Limit State	Tanker, β_0	Cruiser, β_0
Hull girder collapse	4	5
Hull girder initial yield	4.5	5.5
Unstiffened panel	3	3.5
Stiffened panel	3.5	4
Fatigue Limit state	Tanker, β_0	Cruiser, β_0
Category 1 (Not Serious)	2	2.5
Category 2 (Serious)	2.5	3
Category 3 (Very Serious)	3	3.5

Table 3-8 Target reliability indexes proposed by (Mansour, 1996)

(Mansour, 1996)'s description of category classes is given in Table 3-9. The description is compatible with the definition criticality classes defined in Table 3-4 of "System definition and consequence of failure" section.

Category 1	A significant fatigue crack that is not considered to be dangerous to the crew, will not compromise the integrity of the ship structure, will not result in pollution; repairs should be relatively inexpensive
Category 2	A significant fatigue crack that is not considered to be immediately dangerous to the crew, will not immediately compromise the integrity of the ship, and will not result in pollution; repairs will be relatively expensive
Category 3	A significant fatigue crack that is considered to compromise the integrity of the ship and put the crew at risk and/or will result in pollution. Severe economic and political consequences will result from significant growth of the crack

Table 3-9 Description of Categories given Table 3-8

In this research target reliability indices proposed by (Mansour, 1996) have been adopted as target reliability values. The target reliabilities are assigned to criticality classes defined in Table 3-4 of the "System definition and consequence of failure" section. Table 3-10 presents the target reliabilities in this work. The assignment has been made by mapping the consequences of failure defined by (Mansour, 1996) and the consequences of the failure for criticality classes defined by (ABS, 2012).

Criticality Class	**Target Reliability**	
	β_0	P_f
High	4	3.17E-05
Medium	3.5	2.33E-04
Low	3	1.35E-03

Table 3-10 Target Reliabilities used in this work

3.11 Chapter summary and conclusions

In this chapter, fracture mechanics as a means of defect assessment was explained and its applications to the safety assessment of newbuilding ship hull were described.

Ship hull structures are damage tolerant structures with the capability of continuing with their normal operation even if they experience some level of local fracture. The damage tolerant capabilities of ships depend on variables such as material toughness, initial defect size and frequency of occurrence, etc., which are uncertain. Deterministic fracture mechanics analysis of ship hull structure can lead to very conservative and inaccurate results due to its sensitivity to uncertain variables. Probabilistic Fracture Mechanics as a division of reliability analysis can evaluate the safety levels of the structure accounting for those uncertainties.

Various types of uncertainties and their relevance to the defect assessment of ship hulls and the strategies to reduce and quantify them were outlined.

Principles of reliability analysis, the levels and methods of reliability analysis were briefly introduced.

In this research, two independent algorithms and their respective computer programmes, one based Monte Carlo simulation, and the other based on convolution integral are developed to perform fracture mechanics based reliability analysis. These two programmes are explained in chapter 6.

Risk analysis as a level IV reliability process was explained, and its connection to risk matrix and ALARP method was described. Additionally, a proposed risk and reliability framework of weld defects for ship hulls was outlined.

The structural system for the risk and reliability analyses was defined, and a proposed framework of assigning consequence of failure of the structural system was developed based on a criticality class framework recommended by (IACS, 2006) and (ABS, 2012).

Target reliabilities were specified based on recommended values by (Mansour, 1996).

The challenge in reliability analysis is to quantify uncertainties in the reliability analysis which are specific to the particular problem under investigation. Chapter 4, 5 and 6 will study these uncertainties. The reliability calculation is studied in chapter 6.

Chapter 4

Defect Size and Frequency Statistics

4.1 Chapter outline:

As explained in chapter 3, data on flaw frequency and size distribution is a crucial input for risk and reliability assessment of new fabrications. In flaw assessment, it is vital to differentiate between various defect types since their criticality differs. Defect probability of occurrence (defect rate) is an important variable and has a direct relation with failure probability. Other key variables are defect size statistics which considerably affect calculated failure probability of a defected joint. Last but not least is the reliability of NDE methods. NDE methods have different capabilities with respect to defect type and size, which influences the recorded information in flaw datasets. Therefore, the reliability of the NDE method needs to be accurately quantified and considered in the probabilistic fatigue and fracture mechanics assessment.

In this chapter, to begin with, variables that have a bearing in defect statistical analysis are explained, then defect type frequency statistics from a shipyard is presented. Moreover, a review of literature is given on detection probabilities of conventional NDE methods, then a detection probability calculation using Bayesian-Inference method is explained and the relevant PODs of conventional NDEs are estimated. Additionally, defect probabilities of occurrence (defect rates) are calculated accounting for PODs. Furthermore, defect size statistics from the literature and the shipyards are discussed. Finally, defect size statistics used in reliability analysis of this thesis are derived.

4.2 Significance of weld defect statistics

In inspection of newly finished joint for ship, butt welds are subject to radiographic inspection at a selected sample of locations. Other parts will receive visual inspection. This thesis investigates possible benefits of the NDE and looks into to optimise them; clearly the purpose is to obtain a ship that is safe i.e. has, when properly maintained through its life, a sufficiently low through-life probability of failure. To some extent the inspection is intended for quality control; only a sample of the welds is thoroughly

inspected, thus the NDE inspection is not performed on the the entire structure, however a general walk around with visual inspection may pick up serious welding defects that were not at the detailed inspection locations. The flaw frequency may be a good indicator of general welding quality but is insufficient on its own as a measure of the reliability. Defect size information is also required for estimation of reliability. For surface breaking and embedded flaws, normally the height and length are important but radiographic inspection may only provide the length of the defect. One possibility is to consider the measured statistical distribution of flaw length and a correlation between height and length. For a through thickness flaw only flaw length is required as the flaw height is equal to the plate thickness.

4.3 Influencing variables

A crucial step is to assess the flaw frequency and size data according to the influencing variables. It is important that attention is paid to variables that have more effect on the reliability of the structure. A report by Marcello Consonni (2012) based on a questionnaire, asked from experts, suggests that welder's skill is responsible for 27% of all repair rates across all industries followed by welding position (e.g. position, accessibility) 16%, thickness/number of runs 6% and welding process 6%. This paper also reports that, in terms of joint type, 10% of defects are found among butt welds and 90% among fillet welds. In terms of specific weld runs, 75% occurs in root runs and 25% in fill or cap. Not all these variables are individually controllable/assessable within inspection planning. For example, welder's skill is very difficult to quantify and is normally verified through an approval of competency procedure. A reasonable way to deal with the assessment of these variables is to assess those that are quantifiable.

An industrial report by TWI (Wintle, 2002) based on expert elicitation (asking experts' opinion at a meeting) suggests six key factors as influencing the frequency of flaws during the welding of reactor components. Each factor can have a range of states (indicated in brackets):

1. Welding process.
2. Restraint (high, medium, low).
3. Material (C/C-Mn steel, low alloy steel, austenitic stainless steels).
4. Welding location (workshop, site weld).
5. Welding position
6. Access (good, average, restricted).

Type, frequency, and size of fabrication flaws are dependent on a number of variables such as joint type, welding process, welding position (PA-PG), welding procedure, restraint, material, welding location (workshop, site weld) and access. (Zhao and Stacey, 2002), (Wintle, 2002) and (Marcello Consonni, 2012). Kountouris and Baker (1989 a) analysed defect data in relation to below parameters;

1. Welding process.
2. Type of weld joints.
3. Defect type.
4. Welding procedure
5. Defect location.

In reality, there is a correlation between these variables. For example, submerged arc welding is limited to the flat position with good access, or MMA process is only performed where access is restricted. Choice of these variables in a shipyard is governed by welding productivity; welding processes with higher deposition rate and less cost are preferred. Some of the variables such as welder's skill and weld variables (heat input, electrode type, welding speed and etc.) are hard to quantify at a large scale, thus, they are not considered here. Instead, if defective welding is causing problems, it may be investigated through a root cause analysis to improve the quality of ongoing and future welding. Backgrounds about welding process, NDE methods and defect types are given in chapter 2 here a brief explanation about joint type, and material thickness is presented.

Furthermore, defect occurrence and size variation along the weld line could be an important variable to consider. This may, particularly, help to trigger additional inspection after finding defects. In this research, expert elicitation suggested that when a defect is found, there is a good chance that it has occurred in other locations along the weld-line as the weld parameters are likely to remain constant.

The analysed dataset did not include sufficient information with regard to the weld parameters, hence, such correlation study was not possible. But this could be an area of future research.

4.3.1 Joint Type

There are four common welded joint types in ship production: Butt joints, Fillet joints, T-joints and Cruciform joints. It appears that the practice of the case study shipyard

is to focus on NDE of straight butt welds only. The justification seems to be the fact that volumetric examination interpretation is more reliable for butt welds than fillet welds and the understanding of the manufacturer from rules philosophy is to assess the general quality of ship welding. Also butt welds are perceived as more critical than fillet welds (although that may not always be the case as cracks at stiffener connections and ratholes may grow and threaten the whole structure). The datasets of studied ships do not specify weld joint types, but, it is believed to be mostly butt weld. As a result, it was not possible to investigate the effect of joint type.

4.3.2 Thickness:

Plate thickness is believed to be a contributing factor in defect formation owing to their physical formation process, particularly, defects such as lack of fusion and lack of penetration. The two key variables causing the defects are heat input and too great a heat sink. It is widely believed that magnitude of the heat sink is a function of plate thickness (Townend, 1980). In this work, almost no correlation was found between material thickness and defect type, frequency or defect size. However thicker plates may also be more sensitive to the occurrence of defects.

4.3.3 NDE Type:

Common conventional NDE methods used in ship production are listed in Table 4-1. NDE methods can be categorised into; surface examinations, which are suitable for detection of surface breaking flaws and volumetric examinations which can detect embedded flaws as well as surface breaking flaws. Some classification societies emphasise on volumetric NDE as all welds are required to be inspected by 100% visual inspection, and volumetric NDE is used to complement visual inspection (Amirafshari et al., 2018). Other more sophisticated NDE methods such as time of flight diffraction (TOFD) and phased array ultrasonic testing (PAUT) are permitted by rules but not commonly used at present (2018). Choice of NDE method affects the detection probability and in turn actual flaw statistics. As an example, ultrasonic testing (UT) exhibits better probability of detection and detects smaller defects than radiography testing (RT). This is discussed in more details in “Detection probability” section.

Volumetric Examination	Ultrasonic Testing (UT)
	Radiography Testing (RT)
Surface Examination	Visual Testing (VT)
	Magnetic Particle Testing (MPT)
	Dye Penetrant Testing (DPT)

Table 4-1 Common conventional NDE methods

4.4 Flaw frequency analysis

In this section the frequency of various defect types in different welding processes is investigated. Within the studied ships, three welding processes are used: Submerged Arc Welding process (SAW), Hybrid Laser Arc Welding (HLAW) and Flux Cored Arc Welding (FCAW). From the ship #2 and ship #3 datasets, the breakdown of executed welding processes is not available; however, such data is available from ship #1 which was built in the same ship yard and with comparatively similar basic dimensions (Table 4-2).

Figure 4-3 shows the breakdown of welding processes within the hull areas.

Characteristic	Welding data ship #1	NDE Data ship #2
Length	305.60 m	330 m
Beam	37.2 m	44 m
Height	-	70.67 m
Number of Decks	15	15
Draught	8.20 m	8.30 m

Table 4-2 Comparison between basic characteristics of ship#1 and Ship #2

As Figure 4-1 shows over 60% of weldments are made with Hybrid Laser Arc Welding (HLAW). However, as it is shown in Figure 4-2, only 7% of the checkpoints are selected from HLAW weldments. Weldments joining stiffeners to underlying plates is not the focus of Lloyds Register rules, based on which this ship was manufactured (Amirafshari et al., 2018). Only 5% of welds are made with SAW process. 2% of NDE checkpoints are from joints made with SAW. The FCAW makes up about 30% of welds, but, comprise majority of NDE checkpoints possessing 91% total checkpoints (Figure 4-2). FCAW process is used in joints where SAW and HLAW cannot be used due to access restrictions such as the connection between grand blocks.

These joints are believed to be more prone to defect formation, particularly, crack type defects as a result of higher joint restraint and welding condition (outdoor workshop).

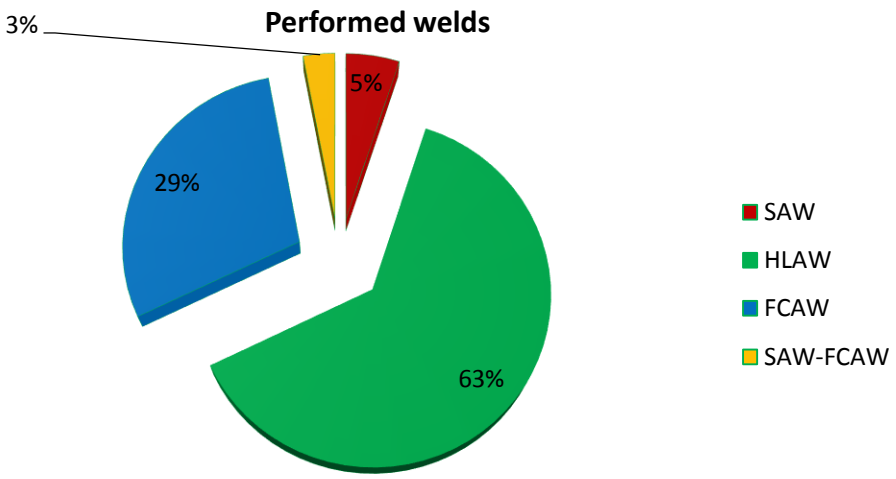

Figure 4-1 Welding break down with respect to procces from ship #1

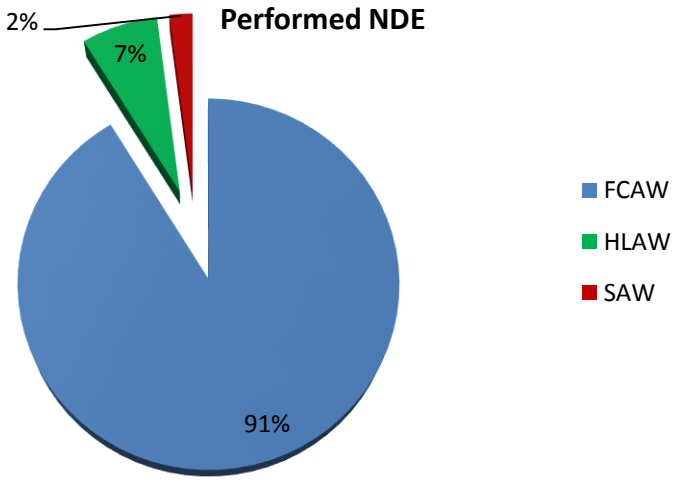

Figure 4-2 NDE break down with respect to process from ship #2

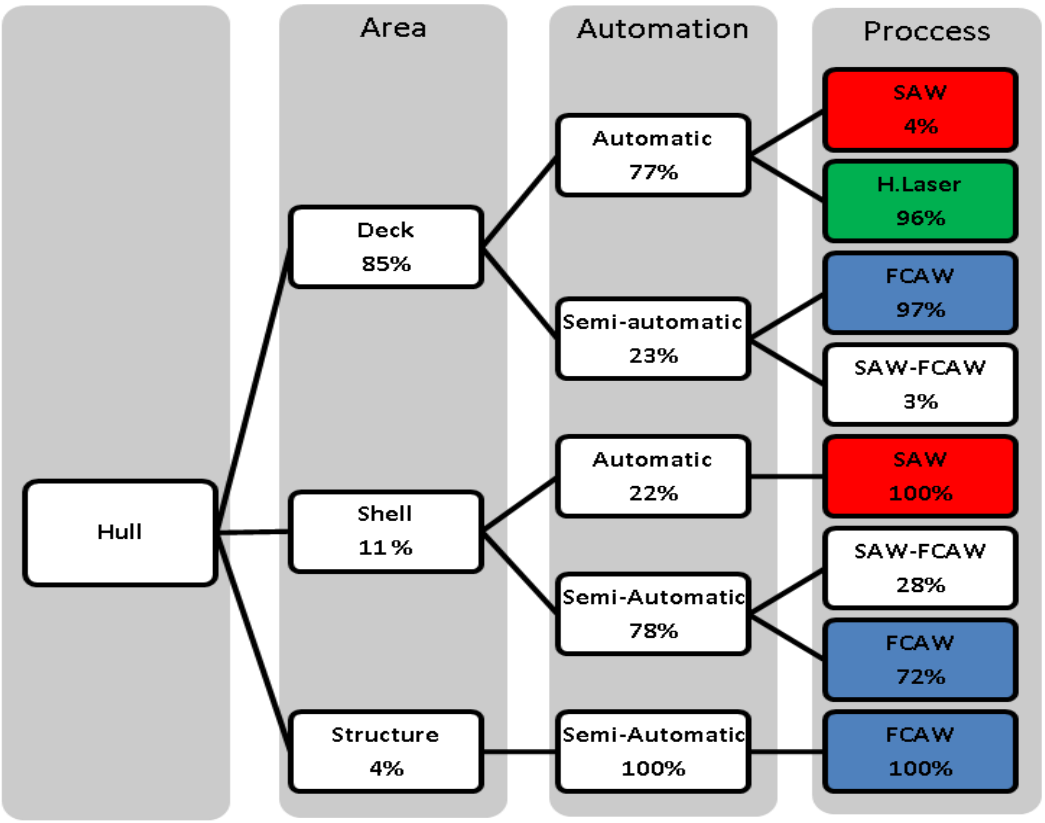

Figure 4-3 Welding break down with respect to hull area, Level of Automation and process from ship #1.

Figure 4-4 and Figure 4-5 show defect rates from the three welding processes. HLAW process creates significantly lower defect rates at around three times lower than other two welding process. This can mean that less inspection may be allowed. From the quality control point of view, there are two methods practiced in the shipyards for estimating defect rates: one method is the binary method which divides the number of failed checkpoints by total number of checkpoints. Figure 4-4 shows defect rates calculated using the binary method. The second method divides total length of defects by the total length of examined welds. Figure 4-5 shows defect rates of ship #2 using length/length method. From the reliability perspective, a defect rate indicating the number of planar defects per joint is more meaningful as it gives the probability of a defect being present at the joint. This is discussed in more details in section “Defect rates”.

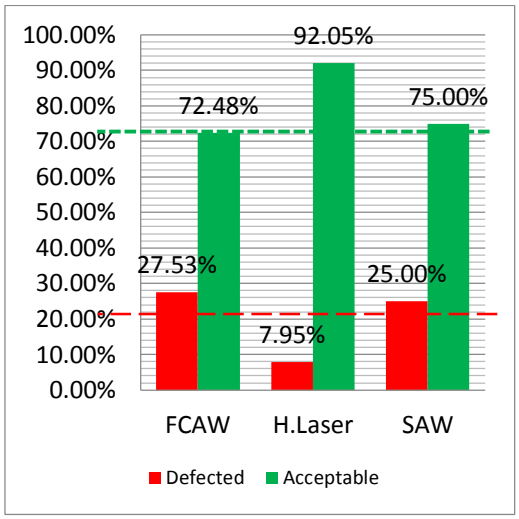

Figure 4-4 Welding processes Defect rate with Binary Method

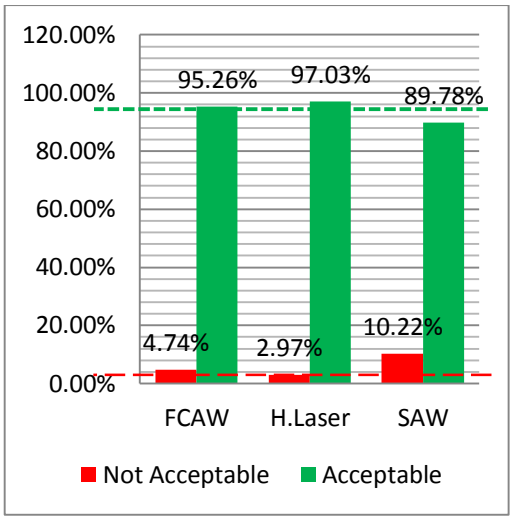

Figure 4-5 Welding processes Defect rate with (Length-by-Length Method)

Figure 4-6 shows defect percentage breakdown for ship #2. Cavities are the most commonly imperfections found in SAW process with over 30% of all defects being cavities. Cavities are not generally considered very harmful unless they are extensive with relation to weld cross-section. Cracks are not common, in this particular SAW process dataset, and only one crack was found. However, it should be pointed out that since SAW is an automatic process, if there is a systemic problem in the process, significant number of crcaks can be created. Lack of fusion and lack of penetration are of particular interest as they are both common and can considerably reduce the fatigue life of the joints. Similar to the SAW process, cavities are the most common imperfections in FCAW weld. Contrary to the SAW process, solid inclusions are more common than lack of fusion/penetration in FCAW process. Frequency percentages of HLAW weld defects are similar to SAW and FCAW processes. In HLAW only 6% of defects are solid inclusions but this value is considerably higher in FCAW with 34% and SAW with 25%.

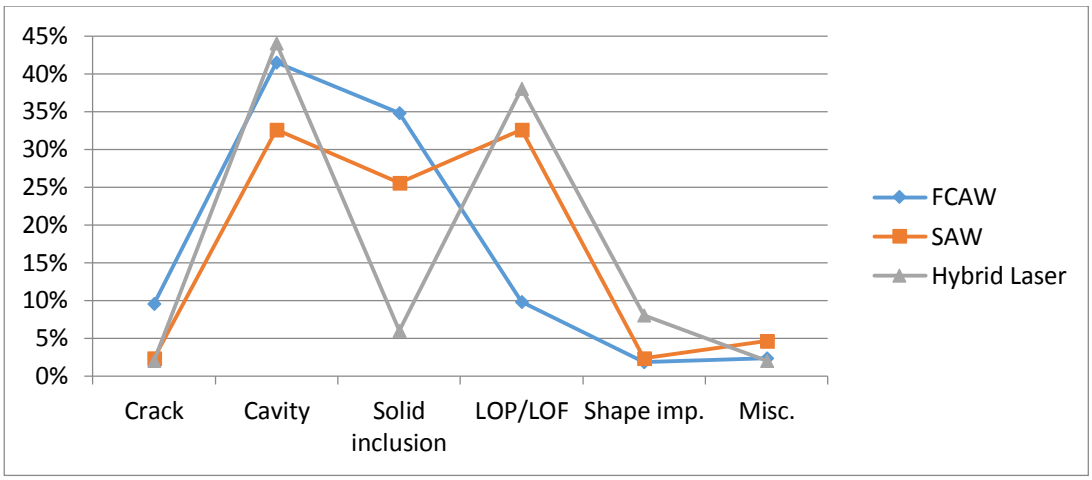

Figure 4-6 Defect percentage break down for ship #2

Table 4-3 shows a relative importance of major defect types in ship #2 based on their criticality and their frequency ranking. Cracks are considered the most critical defect type as they have sharp tips. Lack of fusion and lack of penetration defects are commonly categorised as planar defects and considered the second most critical ones here. The cavity and solid inclusion defects are judged to be the least critical defects among the four defect types. Frequency ranking number refers to the relative frequency of defect types within weld process category. 1 being the most frequent and 4 being the least frequent. Table 4-3 suggests that lack of fusion/penetration defects could be the primary initiation site of propagating cracks since they are both highly critical and highly frequent.

Defect	Criticality	Frequency rank in the dataset		
		FCAW	SAW	HLAW
Crack	Very High	4	4	4
Lack of Fusion/ Penetration	High	3	1	2
Cavity (Porosity)	Moderate	1	1	1
Solid inclusion	Low	2	3	3

Table 4-3 importance of defect types based on ship #2 data, based on Figure 4-6

4.5 Detection probability

NDE methods can only detect a limited number of defects of a certain size. For instance, an NDE method with 50% probability of detection for a certain size, misses 50% of the defects of that size, in other words, the real number of the defects with that size is likely to be 100% more than detected, see Figure 4-8. In structural integrity assessment, it is often convenient to plot detection probability against defect, size which constructs the so-called probability of detection curve: Figure 4-7. Detection

capabilities of non-destructive examination methods depend on sizing of flaws (BS7910, 2015 a), (Zhao and Stacey, 2002), (Georgiou, 2006), (Partner, 1999), (Kountouris and Baker, 1989 b), (Becher and Hansen, 1974), and (DNV, 2015). The bigger the flaw sizes the more likely that they are detected. Hence, it is necessary to consider the probability of detection for employed NDE methods and estimate the real frequency and size distribution of defects. Figure 4-9 shows the relationship between detected defect size distribution, the probability of detection of defect sizes and the actual defect size distribution.

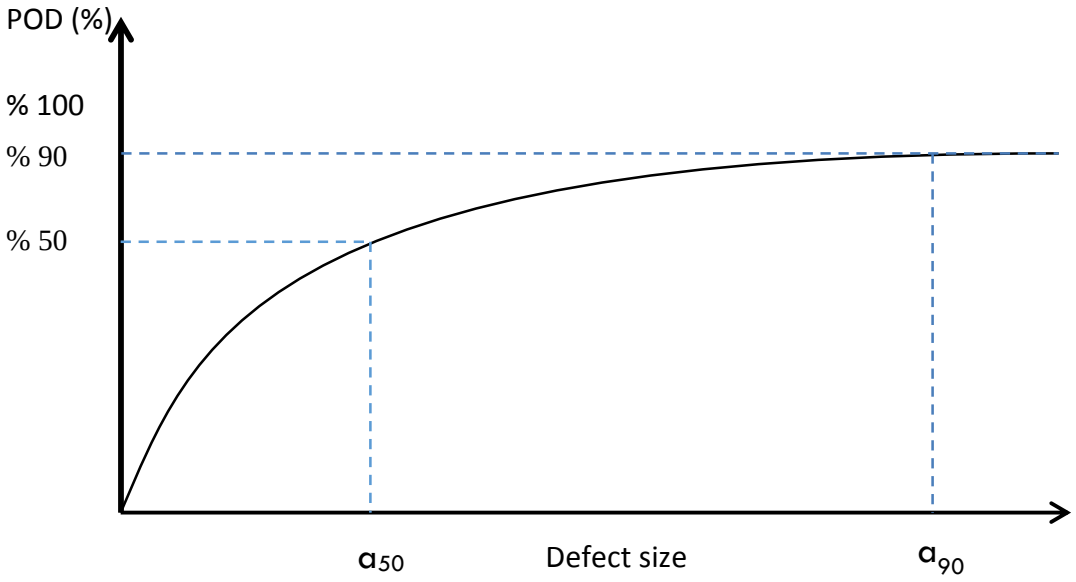

Figure 4-7 Schematic POD curve of defect

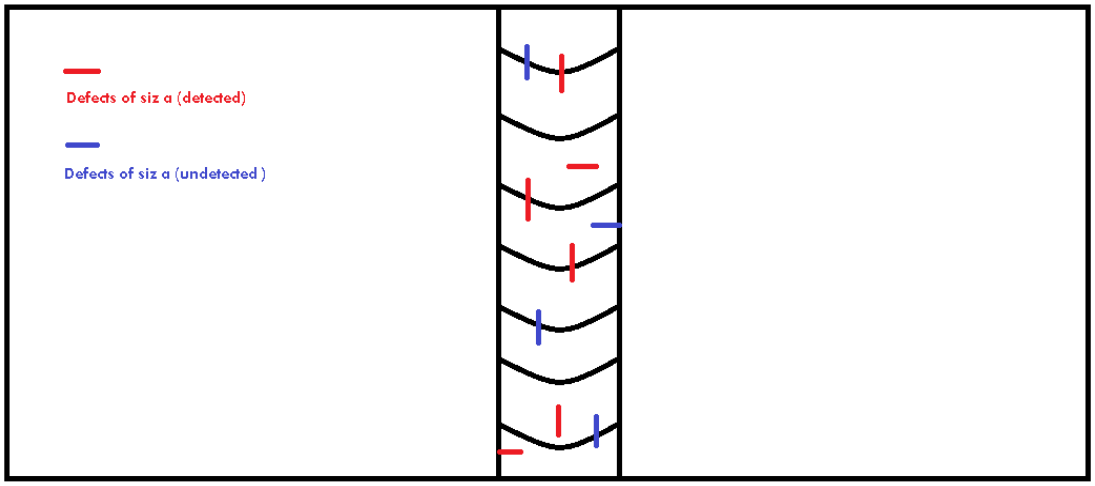

Figure 4-8 Schematic representation of detecting a defect of size a with probability of detection of %60

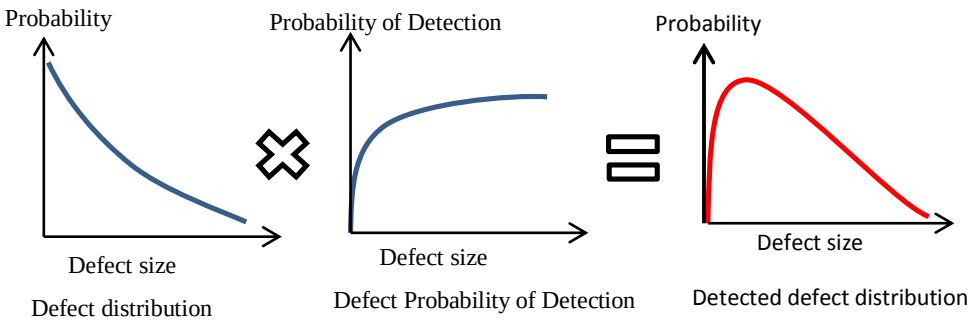

Figure 4-9 Relationship between crack size distribution, Probability of detection and detected crack size distribution

There are two related probabilistic methods for producing POD curves as function of the flaw size. Originally, NDE results were only recorded in terms of whether the defect was detected or not. This type of data is called 'hit/miss' data and it is discrete data.

In some NDE systems there is more information in the NDE response (e.g. peak voltage in eddy current NDE, the signal amplitude in ultrasonic NDE, the light intensity in fluorescent penetrant NDE). Since the NDE signal response can be interpreted as the perceived flaw size, the data is sometimes called $\hat{a}$ data (i.e. 'a hat data') or 'signal response' data and it is continuous data.

Each type of data (i.e. hit/miss or signal response) is usually analysed using a different probabilistic method to produce a POD(a) function. The detail of the complete theoretical analysis is beyond the scope of this research. More information can be found in well-referenced publications (Georgiou, 2006) and (Matzkanin and Yolken, 2001). For hit/miss data a number of different statistical distributions are considered for the best fit among which log-logistic, lognormal, and exponential distributions are the most accepted models (Zhao and Stacey, 2002).

For signal response data, much more information is supplied in the signal for analysis than in the hit/miss data. It has been observed in a number of studies that an approximate linear relationship exists between $ln(\hat{a})$ and $ln(a)$.

$$ln(\hat{a}) = \alpha_1 + \beta_1 ln(a) + \gamma$$

Where, γ is an error term and is normally distributed with zero mean and constant standard deviation σ_γ.In signal response data, a flaw is regarded as 'detected' if $\hat{a}$ exceeds some predefined threshold $\hat{a}_{th}$. The POD(a) function for signal response data(i.e. $ln(\hat{a})$) can be expressed as:

$$POD(a) = Probability\ (ln(\hat{a}) > ln(\hat{a}_{th}))$$

NDE inspection of ship hull structures is done within welding quality control scope by using conventional NDE methods and the data is usually available in the form of hit/miss data, hence only 'hit/miss' data analysis is covered in this research.

The probability of detection depends on a number of factors: inspection technology, environmental condition, the existence of multiple cracking or defect, human factors, mathematical uncertainties from the resultant crack PDF after detection or inspection, other geometric factors, e.g. plate thickness, crack orientation, etc. In general, the probability of detection POD curve follows a monotonic incremental distribution function and is affected by many variables. The simplistic exponential function still represents an adequate form. However, considerations should be given to inspection quality, human errors and multiple probabilistic events. (Zhao and Stacey, 2002).

4.5.1 Published work on the modelling of POD

A number of published works on POD curves have been studied and are reviewed as follows.

(DNV, 2015) introduces a series of POD curves for Visual inspection, Surface NDE, and Ultrasonic. The curves provide lower bound values and are conservative. The equation for the curves are as follows:

$$P(x, X_0, b) = 1 - \frac{1}{1 + \left(\frac{x}{X_0}\right)^b} \tag{4-1}$$

Where $X_0$and b depend on the inspection scenario with recommended values given in Table 4-4.

Visual inspection PODs are given with relation to defect length, as the human eye can only detect the length of a surface breaking defect. X_0, and b of visual inspection depend on three different access conditions; Easy, Moderate and difficult access. These curves are plotted in Figure 4-10. POD curves are particularly important as all welds are inspected visually. Visual examination of welds with easy access for inspection has 50% detection probability for defects of 16 mm length and 90% detection probability of 121 mm long defects.

Description		X0	b	50% POD (mm)	90% POD (mm)
Surface NDE	Ground welds or similar good conditions above water	0.4	1.43	0.4	1.9
	Normal working conditions above water	0.45	0.9	0.45	5.17
	Below water or less good working conditions above water	1.16	0.9	1.16	13.3
Visual NDE	Easy access	15.8	1.08	16	121
	Moderate access	37.2	0.95	37	375
	Difficult access	83.0	1.08	83	636
UT		0.41	0.62	0.41	14.2

Table 4-4 DNV Parameters for POD curves (DNV, 2015)

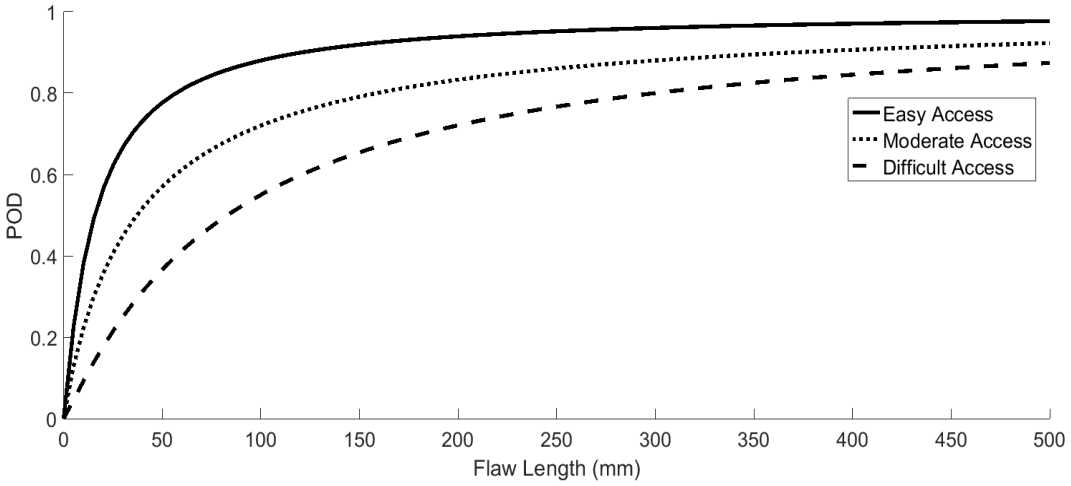

Figure 4-10 DNV POD for visual inspection. Replotted from (DNV, 2015)

As it is given in Table 4-4, for surface NDE, POD parameters depend on conditions of weld joints. These POD curves are shown in Figure 4-11 as a function of flaw height and condition parameters.

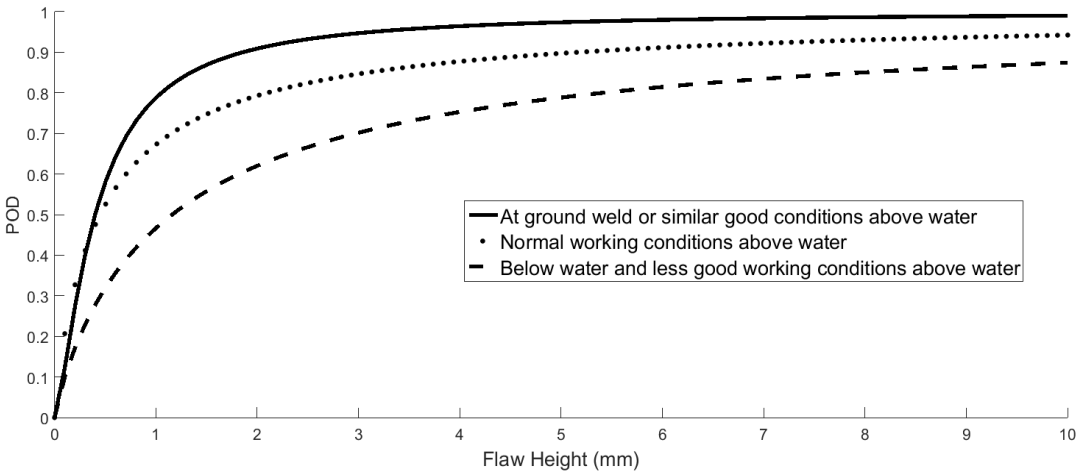

Figure 4-11 DNV POD for surface NDE. Replotted from (DNV, 2015)

(DNV, 2015) proposes below POD curve for UT inspection, shown in Figure 4-12. The POD curve is given with relation to flaw height. 50% detection probability is achieved by flaw depth (height) of 0.8 mm, and 90% probability of detection is achieved by flaw depth (height) of 10 mm.

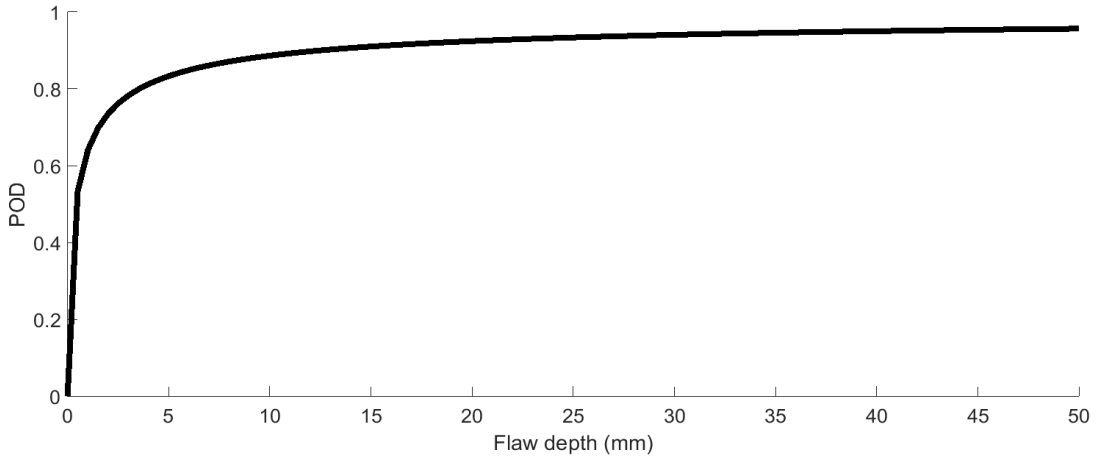

Figure 4-12 POD curve for Ultrasonic Inspection. Replotted from (DNV, 2015)

(Georgiou, 2006) reported probability of detection curves based on a number of independent research projects. Figure 4-13 shows log-odds model POD curve of Radiography examination of weld joints. The graph is reproduced from NTIAC report (Georgiou, 2006). As summarised in Table 4-5, for welds with crowns, 50% detection probability length is reported to be 5.6 mm, where this POD for weld ground flushed is 4.83 mm. In both cases, 90% detection probability was not achieved in the test programme.

	50% POD	90% POD
X-Ray Welds Ground Flushed	4.83 mm	Not Achieved in the test programme
X-Ray Welds with Crowns	5.6 mm	Not Achieved in the test programme

Table 4-5 Some of detection probabilities from NTIAC report (Georgiou, 2006).

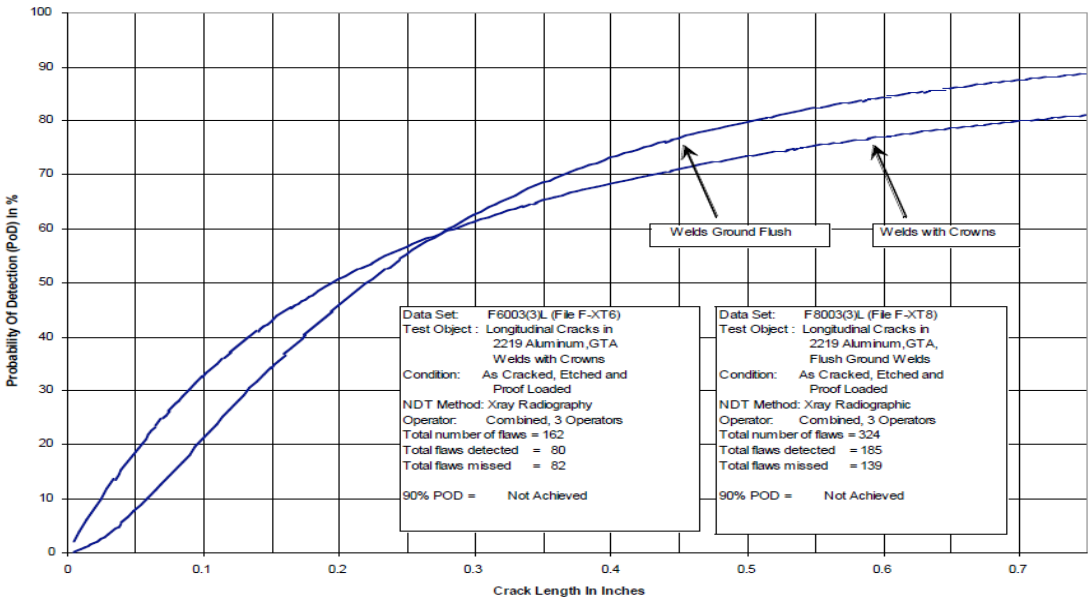

Figure 4-13 HSE POD curves reproduced from NTIAC report with of longitudinal Cracks for RT (Georgiou, 2006).

(Dufresne, 1981) proposes postulated POD curves, primarily applicable to thick section pressure vessels, as a function of defect length for different ranges of defect width and is given in Figure 4-14. The probability of detection curves are believed to be assumed by author of the paper and not based on experimental data but illustrates an insightful relationship between the combined effect of flaw height and flaw length and detection probability.

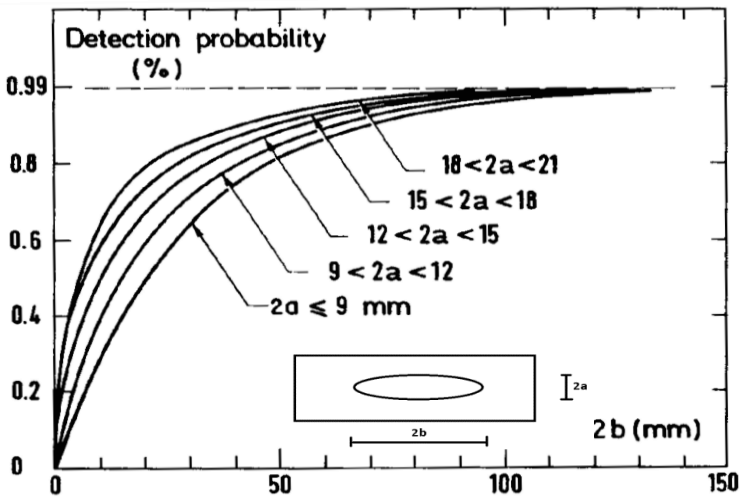

Figure 4-14 Postulated PODs by Dufresne (Dufresne, 1981)

(Visser, 2002) reports a summary of selective parts of the Nordtest NDE programme. The programme took place from 1984 - 1990 in four Scandinavian countries. 730 embedded weld defects and 635 surface defects are reported. The results are based on 3400 RT, 4600 UT, 9000 MPI and 9000 penetrant observations. Figure 4-15 shows

POD curves for radiography testing (R) and ultrasonic testing (U) for planar weld defects, the numbers next to R correspond to sensitivity levels defined by the test programme. Table 4-6, Table 4-7 and Table 4-8 provide some representative POD values extracted from Figure 4-15. Figure 4-16 shows POD curves of radiography testing (R4) for weld defects, porosity (A), slag inclusion (B), incomplete penetration (C), lack of fusion (D), cracks (E). Table 4-6 and Table 4-7 provide some representative POD values extracted from Figure 4-16. It can be seen that for 10mm defects, 50% detection probability of cracks is not achieved with this radiography testing, suggesting unreliability of the method for crack detection. In contrast, 90% detection probability for slag inclusion and porosity defects are achieved showing the efficiency of the method for these defect types. Curves from Figure 4-16 are particularly useful to measure relative detection probability of different weld defects and are used to calculate actual defect type proportions in the "Flaw frequency analysis" section.

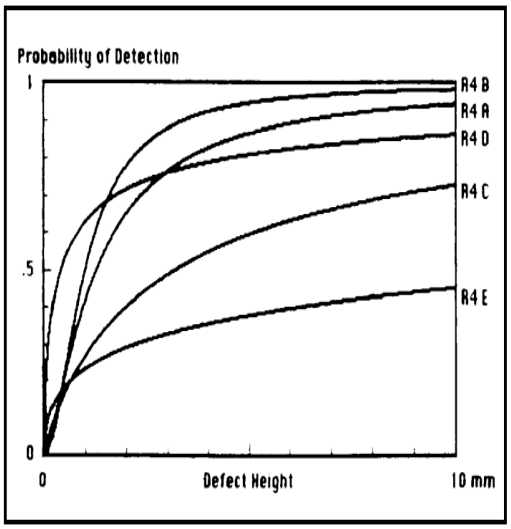

Figure 4-15 Nordtest POD curves for RT (Sensitivity level R4) for different defect types. Figures extracted from (Visser, 2002)

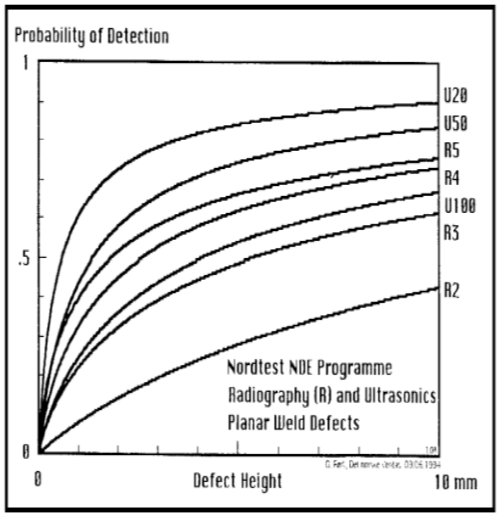

Figure 4-16 Nordtest POD versus defect height for planar weld defects using UT and RT. Figures extracted (Visser, 2002)

R4	Porosity	Slag Inclusion	Incomplete penetration	lack of fusion	cracks
50% POD	1.3	1.01	3.27	0.44	Not Achieved

Table 4-6 50% detection probabilities for R4 testing of Nordtest programme

R4	Porosity	Slag Inclusion	Incomplete penetration	lack of fusion	cracks
Probability at 10 mm	0.94	0.97	0.72	0.86	0.44
Probability at 2.5 mm	0.71	0.84	0.45	0.74	0.32

Table 4-7 Representative detection probabilities for R4 testing of Nordtest programme

	RT	UT
POD at 10 mm	67%	90%
POD at 2.5 mm (Assumed mean defect height)	50%	76%

Table 4-8 Representative Planar weld defects detection probabilities for RT and UT testing of Nordtest programme

Annex T of (BS7910, 2015 a) provides information on the reliability of NDE methods in terms of deterministic values for the minimum size that can be reliably detected and sized, and sizing errors. Some example values are given in Table 4-9. (BS7910, 2015 a) recommends that Radiography testing is not a reliable method for detection of planar defects but is very reliable in detecting porosity type defects. This is consistent with Nordtest results, however, (BS7910, 2015 a) philosophy is highly conservative and is generally the subject of short cracks. In reality as proposed by (Dufresne, 1981) detection probability using radiography testing increases as the defect length increases which is relevant to long cracks that are tolerable by hull structures.

	UT	RT
Minimum size that can be reliably detected, 2a × 2c	3X15 mm	1.2 ϕ pore
Minimum size that can be reliably sized, 2a × 2c	3X7 mm	NA
Length sizing accuracy, Δ2c	±10 mm	±2
Through-thickness sizing accuracy, Δ2a	4 mm undersize 1 mm oversizing	NA
Ligament sizing accuracy Δp	±3	NA

Table 4-9 (BS7910, 2015 a) Example of inspection capabilities for sub-surface flaws

In this section POD curves from five published documents have been reviewed. A summary of key features of each document and their relevant application to this research is given in Table 4-10 below.

Source	Key features	Application to this work
DNV	Lower bound POD curves for VT and surface testing	POD are used In the assessment of the welds outside checkpoints
NTIAC programme	POD for RT with respect to defect length	Estimation of defect distribution of collected data and validation of detection probability using Bayesian Inference (next section)
(Dufresne, 1981)	Relates POD curves to both defect length and height	Provides insight about POD curves
Nordtest programme	PODs of different defect types for RT	Effectiveness of RT for different defects
BS7910	Sizing error	Crack assessment

Table 4-10 summary of reviewed literature and their relevance to this work

4.5.2 Detection probability-Bayesian theorem

In probabilistic flaw assessment, initial flaw size distribution is more relevant than detected flaw distribution as it accounts for detected and undetected flaws. The reliability of the structure depends on both detected and undetected defects. In practice, first, flaw size information is recorded, then using one of the distribution fitting methods a probability density function, which suitably fits to the data, is estimated, then detection probability of corresponding NDE method is used to calculate initial flaw size distribution. The limitation of this procedure is that detection probability depends on and is very sensitive to variables such as human reliability, test environment (shop, laboratory) specimens geometry, flaw characteristics and material properties (Georgiou, 2006)(Zhao and Stacey, 2002). This would require the acquisition of detection probabilities specific to performed NDE. Such data is not normally available with good confidence. An alternative approach is to drive detected flaw distribution in terms probability of detection and initial flaw distribution by means of the Bayesian theorem (below equation) and estimating their parameters by fitting the collected data to detected flaw distribution.

$$P(A|B) = \frac{P(B|A) * P(A)}{P(B)} \tag{4-2}$$

Where, $P(A|B)$is a conditional probability and is the likelihood of event *A* occurring given *B* is true. In this case, it is the probability of a flaw size *A* given a flaw is detected.

$P(B|A)$ is a conditional probability and is the likelihood of event *A* occurring given *B* is true. Here, it is the probability of detecting a flaw given a flaw of size *A* is present.

$P(A)$ and $P(B)$ the probability of observing *A* and *B* independently. Here $P(A)$ is the occurrence probability of flaw size *A*. $P(B)$ is the probability of detecting a flaw of any size.

A convenient choice of distribution is the exponential distribution which is only defined by one parameter making parameter estimation using regression analysis more consistent. The likely population of manufacturing defects in a weld fabrication can be represented by a curve where representing large number of small defects and a much lower number of larger defects. The exponential probability function is an appropriate choice to represent initial flaw size distribution with mean flaw size λ_0.

$$f_{A0}(a) = \frac{1}{\lambda_0} e^{-a/\lambda_0} \quad (4\text{-}3)$$

The POD curve is approximated by cumulative exponential function with crack size parameterλ. (Moan et al., 1997).

$$POD(a) = 1 - e^{-a/\lambda} \quad (4\text{-}4)$$

The probability of detecting a flaw of any size can then be calculated as follows:

$$P_D = \int_0^\infty POD(a)\, f_{A0}(a) da \quad (4\text{-}5)$$

The probability density of detected flaws of size *a* is:

$$f_{A,D}(a) = \frac{P_D(a) f_{A0}(a)}{P_D} \quad (4\text{-}6)$$

Note: the division by the integral term ensures that the area under the probability density curve = 1. This is used in conjunction with P_D to allow for defects not being present at every location.

The probability density of defects, at inspection locations, that are not detected is:

$$f_{A,ND}(a) = f_A(a)(1 - P_D(a)) \Big/ \left(\int_0^\infty f_{A0}(a)(1 - P_D(a)) da\right) \quad (4\text{-}7)$$

where, $\int_0^\infty f_{A0}(a)(1 - P_D(a)) da$ is the probability of an undiscovered defect at an inspected location.

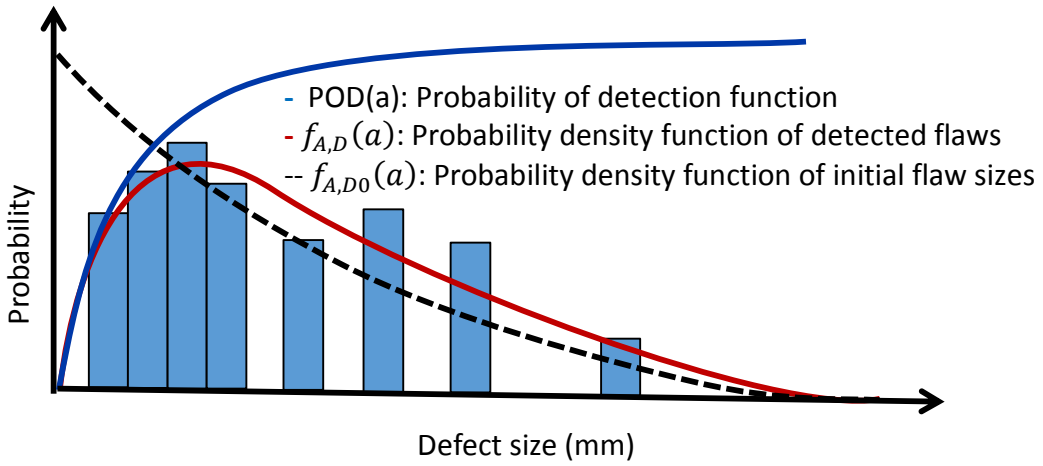

Figure 4-17 Schematic description of defect size distributions

Distribution fitting of detected crack size is discused in Defect size section of this chapter. Planar defect length data were fit to $f_{A,D}(a)$, using nonlinear least square method (LSM) $and\ \lambda_0$ and λ values were calculated. The summary parameter estimation and the 50% POD is given in Table 4-11.

Case	Defect Type	λ_0	λ	50% POD
Ship#2	Crack	30	13.5	9.35
	Crack+LOP+LOF	72.4	4.6	3.1
Ship#3	Crack	20.81	9.6	6.65
	Crack+LOP+LOF	41.15	3.1	2.14

Table 4-11 Summary of distribution parameter estimation of shipyard data

It can be observed that crack type defects show a significantly lower probability of detection than combined planar defects (cracks+LOP+LOF). This is consistent with Figure 4-15 and Table 4-7 extracted from the Nordtest programme (Visser, 2002). 50% probability of detection values are also reasonably consistent with Table 4-5 from the NTIAC test programme (Georgiou, 2006), considering test condition (Laboratory / shipyard), parent material (Aluminium / ship steel) and natural variability of results; notice that detection probability of shipyard #3 is higher than shipyard #2. The probabaility of detection curves are shown in Figure 4-18.

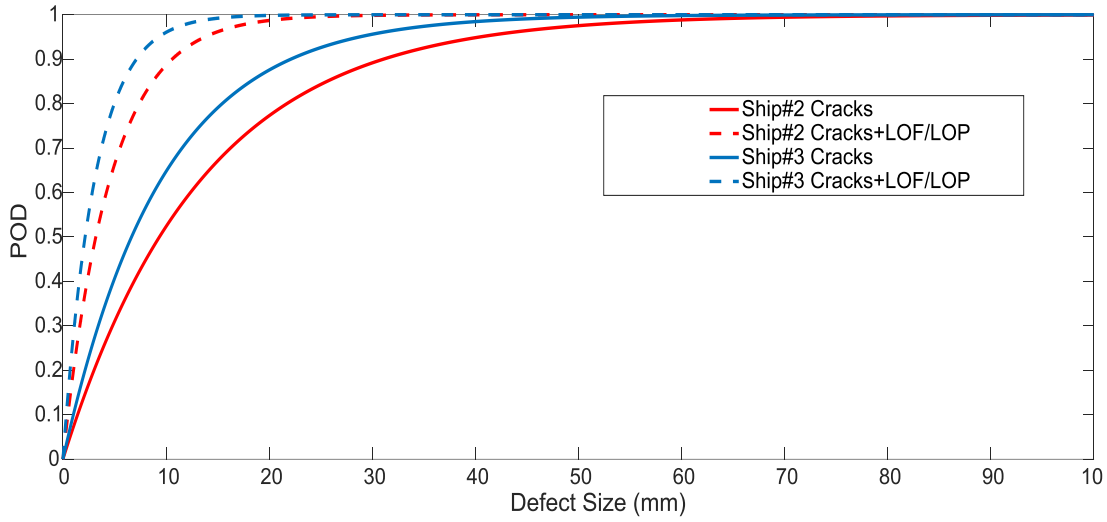

Figure 4-18 Probabaility of detection curves for shipyard data

4.6 Defect rates

Defect rate is a crucial factor in the calculation of total reliability of a structure (Zhao and Stacey, 2002). In a reliability assessment based on fracture mechanics, a defect size probability distribution is used to calculate the (conditional) probability of failure due to the presence of a defect. Based on the Kolmogorov definition of conditional probability (Kolmogorov and others, 1950), this value, however, needs to be multiplied by the probability of the structure being defective (defect occurrence probability), and using below equation:

$$P(A|B) = \frac{P(A \cap B)}{P(B)} \qquad (4\text{-}8)$$

Here, $P(B)$ is Probability of a joint being defective. $P(A|B)$ is the probability of detection given the joint is defective, where the size of the defect is uncertain. $P(A \cap B)$, the joint probability of *A* and *B*, and is the total failure probability of the joint.

(Harris, 1995) assumed that the number of cracks in a body of volume V is a Poisson distribution with a mean of $10^{-4}/in^3$. The probability of n defects occurring in a weld under a Poisson model is:

$$P(X = n) = e^{-\lambda} * \lambda^n / n! \qquad (4\text{-}9)$$

Where, λ is the mean rate of occurrence of all defect sizes.

The defect rate is subject to great uncertainty. QA/QC departments of manufacturers tend to work with repair rates. Repair rates are generally defined as percentages value. The method used to calculate such values may vary. Commonly, these are

calculated as the fraction of the length of repair versus the total weld length, whereas some departments define this as the number of repaired welds versus the total number of welds. The former provides lower repair rate and may be preferred by manufacturer.

A study by (Marcello Consonni, 2012) based on a questionnaire gathered from TWI Ltd's industrial members reports that average repair rates range from 0.5 to 10% depending on the industry sector. For offshore structures the reported value is 2%. (Baker et al., 1988) found that defect rate as a ratio of defect length to total length of weld, lies in the range 0.010 to 0.014. They also found that defect rates for different yards are found to be radically different. (Marshall, 1982) reports that there are 3.65 microscopic surface breaking defects of all sizes per pressure vessel. (Bokalrud and Karlsen, 1982) found the defect rate to be 16 defects per metre, including rather small cracks. (Rogerson and Wong, 1982) reported the defect rate of 0.7 per meter in a North Sea structure. Data from (Moan et al., 1997) suggests a defect rate of 0.075 considering defect rate as mean number of defects per inspection for surface breaking cracks. Summary of reviewed defect rates from literature are given in Table 4-12.

It is apparent from comparison of the defect rates that the values vary significantly across the data sources. One reason is the way the defect rate is specified i.e.; number of defects versus weld length, number of defects versus number of joints, or total defect length versus total inspected length. The second reason is the target defect type: if the data is acquired from a manufacturing quality control process, commonly all the defect types are treated the same way whereas if the inspection is part of an integrity assessment typically planar defects are of interest. The third key factor is reliability of the NDE method: some NDE methods are less effective than others for certain defect types and sizes. For instance, MPI and EC are more reliable for detection of surface breaking flaws than UT but cannot detect embedded flaws. They are also capable of detecting smaller defect sizes than UT. RT is not generally reliable for detection of planar defects but exhibit good efficiency for detection of pore cavities (BS7910, 2015 a).

Therefore, when comparing defect rates from deferent sources it is vital to account for the above factors to avoid misinterpretation of defect rates. For similar reasons, mention above (e.g. ambiguity in defining deftc rates), judging possible

improvements in consistency of the weld quality in not possible using studied data sets.

Investigator	Joint	Defect type	NDE method	Sample	Defect rate
(Moan et al., 1997)	23 jacket structures	Fabrication Cracks	MPI	2386	0.09 (crack per inspection)
(Marcello Consonni, 2012)	Offshore structures	Defects	Expert elicitation	N/A	0.02 repair length versus length of inspection
(Bokalrud and Karlsen, 1982)				827 joints 3200 m	16/m (microscopic cracks)
(Moan et al., 2001)		Cracks	MPI and EC underwater	4000 inspection	1/3 per joint
Baker (Baker et al., 1988)	Lower hull of Conoco TLP	Defects	MPI and UT	27000 m	0.01 to 0.014 defect length/ total weld length
(Harris, 1995)					10^{-4}/ in^3 per volume
(Marshall, 1982)	Pressure vessel				3.65 microscopic per pressure vessel
(Rogerson and Wong, 1982)	North sea structure, splash zone	Embedded defects	MPI and UT	1000 m welds; 18 joints	0.7/m

Table 4-12 Defect rates from literature

In this research defect rates data from three cruise ships are investigated. The availability of details varies among data sets. Data from Ship #1 only includes repair lengths, inspected lengths and the relevant NDE method, however, no information is available with regard to defect types and sizes. Ship #2 data is the most comprehensive dataset and includes type, location, welding process, NDE method, and length of detected defects. Data from ship #3 contains almost the same level of detail information, however, the number of the checkpoints are less than 50% of ship #2. Defect rates of these three vessels, the sample sizes and the NDE methods are given in Table 4-13.

Data set	NDT Type	Sample size	Defect rate:	
Ship #1	RT 22% and UT 78%	7200 (m)	0.13	Repair Length / inspection length
Ship #2	RT 95%, UT 2%, MT 2.5%, PT 0.1%	3408 (m)	0.075	Repair Length / inspection length
			0.047	Defect length / inspection length
Ship #3	RT 92%, UT 8%	1441 (m)	0.03	Defect length /inspection length

Table 4-13 Defect rates from shipyards

It can be seen from comparison of defect rates given in Table 4-13 that ship #1 has 70% higher defect rate than ship #2 and more than 4 times higher than ship #3, while

the sample size for ship #1 is twice that for ship #2 and five times that for ship #3. However, the majority of inspection in ship #1 is performed by ultrasonic testing and generally possess better probability of detection versus radiography testing which in ship #2 and ship #3 dominates the dataset.

In order to investigate the effect of NDE method on recorded defect rates, recorded defect rates have been divided by probability detection using the procedure give in the "Detection probability-Bayesian theorem" section. The results are presented in Table 4-14 below. The results show that corrected defect rates from ship #1 and ship #2 are really close which suggests that the difference between the detected defect rates are due to the reliability of chosen NDE methods and the sample size is insignificant. These two vessels have very similar structural dimensions and were built and inspected by the same workshops, further suggesting that the only affecting factor is NDE method. The corrected defect rates also have good agreement with defect rate reported by (Moan et al., 1997).

Ship #3, however, has significantly lower defect rates. This is primarily because repair rate is higher than rate of crack length; when repair is executed in the workshop an extra length of weld in addition to defect length is grinded and rewelded. Notice the difference between repair rate and Length/Length defect rate for ship #2 in Table 4-13 (0.047 vs. 0.075). This is, also, partially due to either statistical uncertainty of defect rates being significantly influenced by sample size as the number of samples increase from 3037 samples to 7099 samples or the effect of better welding quality of ship #3 compared to ship #1 and ship #2.

In the case of better weld quality, it results in an increase in the structural reliability, so, fewer NDE checkpoints may be allowed. Effect of statistical confidence on defect rates due to sample size is investigated in chapter 6.

Data set	NDT Type	Defect rates	
		Detected	Corrected
Ship #1	RT 22% and UT 78%	0.13	0.24
Ship #2	RT 95%, UT 2%, MT 2.5%, PT 0.1%	0.075	0.224
(Moan et al., 1997)	MPI	0.09	0.27

Table 4-14 corrected defect rates

Defect rates when used in reliability calculation based on fracture mechanics should be treated with care; fracture mechanics is only applicable for planar flaws, hence, only planar defects rate should be used. Defect rates for cracks, lack of penetration /

lack of fusion and combined planar defects are given in Table 4-15. Although the rate of crack type defects is significantly lower than rate of all defect types given in Table 4-14, combined crack and LOP/LOF defect rates are close to total defect rates of Table 4-14. In fracture mechanics assessment all planar defects are treated as crack type defects.

Data set	Sample size	Planar Defect	Defect rate	
			Defect number vs. number of inspections(n/N)	Number of defects per meter (n/m)
Ship #2	7099 checkpoints; 3444.9 (m)	Crack	0.033	0.069
		LOP/LOF	0.038	0.079
		Cracks+ LOP/LOF	0.071	0.148
Ship #3	3039 checkpoints; 1441.2 (m)	Crack	0.021	0.045
		LOP/LOF	0.013	0.027
		Cracks+ LOP/LOF	0.034	0.072

Table 4-15 Defect rates from shipyards

Planar defect rates for different weld process have also been studied and are shown in Figure 4-19. It can be seen from the figure that crack rate in FCAW process is five times higher than SAW process and 17 times higher than Hybrid Laser process. This is believed to be due to higher restraint in grand block assembly joints which increases secondary stress at welded connections and consequently increases the probability of solidification crack formation (Gurney, 1979) , and (Mandal, 2017).

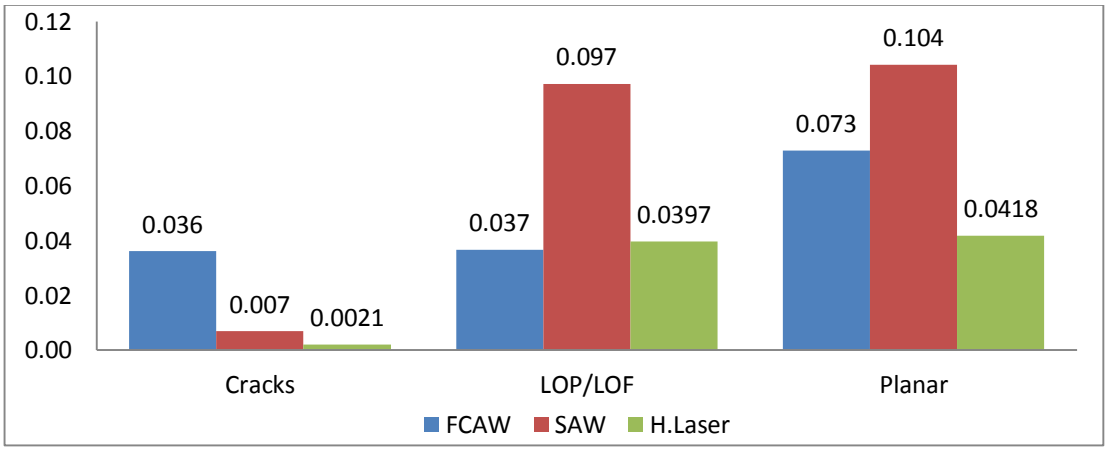

Figure 4-19 Defect rate breakdown based on welding process for ship #2

4.7 Defect size

Defect size distribution is one of three key input variables to probabilistic fracture mechanics assessment along with stress and material fracture toughness. These three inputs are known as fracture mechanics triangle (Amirafshari, 2017) and

(Wallin, 2011). In engineering critical assessment, when reliable data over the whole range of possible values are not available, it is common to treat one or all of these parameters deterministically by assuming (an) upper/lower bound value(s). In this research, however, the aim is to optimise NDE inspection and since the main purpose of NDE is to detect the defects, it is apparent that efforts should be made to obtain accurate and realistic defect size distributions.

A wide-ranging review of literature is carried out and the reported defect distributions are summarised in this section. Additionally, two defect size dataset from shipbuilding manufacturers were collected and size data were fitted into candidate distributions using maximum likelihood estimate (MLE). This method is explained in Appendix C. The choice of distribution type depends on two factors: 1. the nature of physical phenomena modelled and 2: the goodness of fit of the data to distribution.

A structure is likely to contain a large number of small defects and a much lower number of larger defects. When detected by NDE, a lower number of very small defects are found due to the poorer probability of detection for these defects; the probability of detection reduces as the sizes get smaller. Thus Lognormal and Weibull functions show suitable fits and are commonly used in the literature. When the effect of probability of detection is taken into account exponential distribution may be used. The Kolmogorov-Smirnov test was used to validate goodness of fit for studied distributions.

The defect characteristics which have been included in the statistical analysis shown in Figure 4-20 are as follows:

- Defect height (2a) also called defect depth for surface-breaking defect (a).
- Defect length (2c)
- Defect aspect ratio (taken as Length/Height)

In this research, the Lognormal and Weibull distributions have been fitted to the data. Greater emphasis has been given to lognormal distribution for which there is some theoretical justification for its use; (Kountouris and Baker, 1989 b).

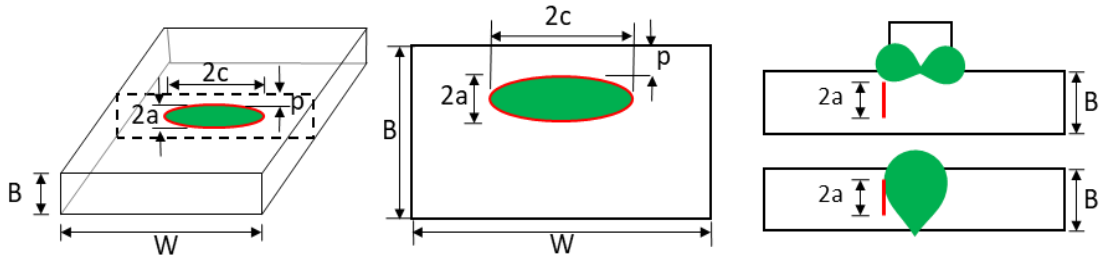

Figure 4-20 Dimensions of an idealised embedded defect

4.7.1 Defect height/depth

In many structures defect height/depth is the important dimension of the assumed flaw. For example, in a pressure vessel containing pressurized and possibly toxic or flammable substances, this can lead to severe consequences or an undercut surface crack in a bracing of an offshore jacket can lead into the failure of the member (Naess, 1985). In ship structures, an embedded or surface crack can grow into a through thickness crack and further grow into a very long crack before causing a severe fracture (Lassen and Recho, 2013), (Glenn, 1999), (Bäckström and Kivimaa, 2009), however occasionally a small crack can become unstable, as with the Kurdistan (Garwood, 2001), and ("KurdistanTWI," n.d.).

Fabrication defect height data is not always available from NDE inspection of newbuilding ship hull structures for two main reasons. Firstly, traditionally NDE inspection has been practised as part of shipyards quality control scheme and not for fitness for service assessment. Defect height data is not commonly used after inspection. Defect length is used by quality control departments to calculate defect rate which is a measure of shipyard's quality. Secondly, some widely practised NDE methods such as Radiography Examination and Dye Penetrant examination will only provide the length of the defect. In this research, datasets gathered from the shipyards only includes defect length data. An extensive review of literature was carried out and the summary of distribution parameters is given in Table 4-16 below. (Townend, 1980) fitted a Weibull distribution to lack of fusion and lack of penetration of welds from 1980 metres of node welds fabricated by manual metal arc welding in offshore structures. (Rogerson and Wong, 1982) presented results on embedded defect height from a study of 1000 metres weld length in vertical and horizontal nodes of an offshore structure. Comparisons between the models for the two investigations show that cumulative probabilities fall reasonably in the same range for depths up to 15mm but there are marked variations for defects of depth larger than 15mm.

(Kountouris and Baker, 1989 a) fitted Weibull and Lognormal functions to height and length of embedded defects resulting from Ultrasonic testing of the lower hull of Conoco TLP. Selective parameters for planar defects in cruciforms and tee butts and plate butts extracted from (Kountouris and Baker, 1989 c) are shown in Table 4-16. They found that the welding process did not have a significant influence on embedded defects, however, the planar defect depths were found to be noticeably different for the two types of the joints.

Turning now to surface-breaking defects, these tend to be more important from the fracture point of view because they tend to associate with a larger stress intensity factor. (Becher and Hansen, 1974) presented data from PWR vessels of defect length for slag inclusion and surface cracks. The 233 surface cracks were not weld defects but were due to some kind of stress corrosion. They were detected by MPI and the crack dimension was measured as the depth of grinding.(Moan et al., 1997) presented data from 23 jacket offshore structures of surface breaking cracks. Similar to (Becher and Hansen, 1974), they were detected by MPI and the crack dimension was measured as the depth of grinding.

Investigator	NDT	Joint Type	Welding Process	Flaw Type	Lognormal		Weibull		
					μ	σ	Shape	Scale	Median (mm)
(Kountouris and Baker, 1989 a)	UT	Butt	SMAW	LOF	1.22	0.48	1.64	4.4	3.52
				Crack	1.93	0.64	1.56	9.57	7.57
			GMAW	LOF	1.14	0.47	1.66	4.05	3.25
		Cruciform	SMAW	LOF	1.52	0.65	1.39	6.46	4.96
				Crack	2.17	0.67	1.67	12.2	9.80
			GMAW	LOF	1.45	0.64	1.38	6.04	4.63
				Crack	2.11	0.70	1.57	11.67	9.24
	MPI	Butt and Fillet	SMAW	Centre crack	1.76	0.6	1.67	7.92	6.36
			GMAW	Centre crack	2.015	0.73	1.6	10.66	8.48
			Merged	Toe Crack	0.346	0.15	1.31	1.62	1.22
(Becher and Hansen, 1974)	MPI	Butt	MMA	Surface Crack	0.16	1.15	2.06	0.95	1.4
(Rogerson and Wong, 1982)	MPI and UT			Embedded Planar	1.28	0.83	5.33	1.43	4.12
(Burdekin and Towned, 1981)	UT	Butt	MMA	LOF	1.68	0.58	7.0	2.18	2.07
				LOP	1.9	0.46	8.13	2.76	2.64
(Townend, 1980)	UT	Butt	MMA	Merged data	1.76	0.49	7.2	2.43	6.19
(Moan et al., 1997)	MPI			Surface crack	0.35	0.73	2.05	1.41	1.18

Table 4-16 Defect height distribution parameters from literature

(Kountouris and Baker, 1989 c) fitted Weibull and Lognormal functions to depth and length of surface-breaking defects resulting from MPI testing of weld length in the order of 50km in an offshore structure. They have shown a strong dependence of distribution parameters on the weld type, welding process and defect location within the joint. Selective parameters for planar defects in cruciform and tee butts, and plate butts extracted from (Kountouris and Baker, 1989 c) are shown in Table 4-16.

Among all the reviewed published work, defect size analyses reports from (Kountouris and Baker, 1989 c) and (Kountouris and Baker, 1989 a) are the most

comprehensive. The reports include information about joint type, defect type, defect location welding process and NDE method thus the extraction of defect size statistics are accurate and more reliable. Surface-breaking cracks reported by (Becher and Hansen, 1974) and (Moan et al., 1997) are reasonably in the same size range but significantly different from (Kountouris and Baker, 1989 c) surface breaking cracks in weld centre. Toe cracks from (Kountouris and Baker, 1989 c) are consistent with (Becher and Hansen, 1974) and (Moan et al., 1997). This suggests that surface breaking cracks at the centre of weld metal are bigger in height than the surface breaking cracks at the toe of the joint.

In the absence of information about the location of the defect, it may be prudent to assume a centre crack. However, the notch stress at weld toe is higher than the weld centre line due to weld profile angle. When a weld is ground flush this stress concentration is reduced but then again the depth of a centre line crack will be reduced as well, therefore it is not possible to make an accurate comparison of the severity of these two types of cracks at this stage and further crack growth analysis is required. Figure 4-21 shows a crack height probability density function from (Kountouris and Baker, 1989 c) and (Kountouris and Baker, 1989 a). Apart from surface breaking cracks from SMAW process, there is a reasonable agreement among fitted functions.

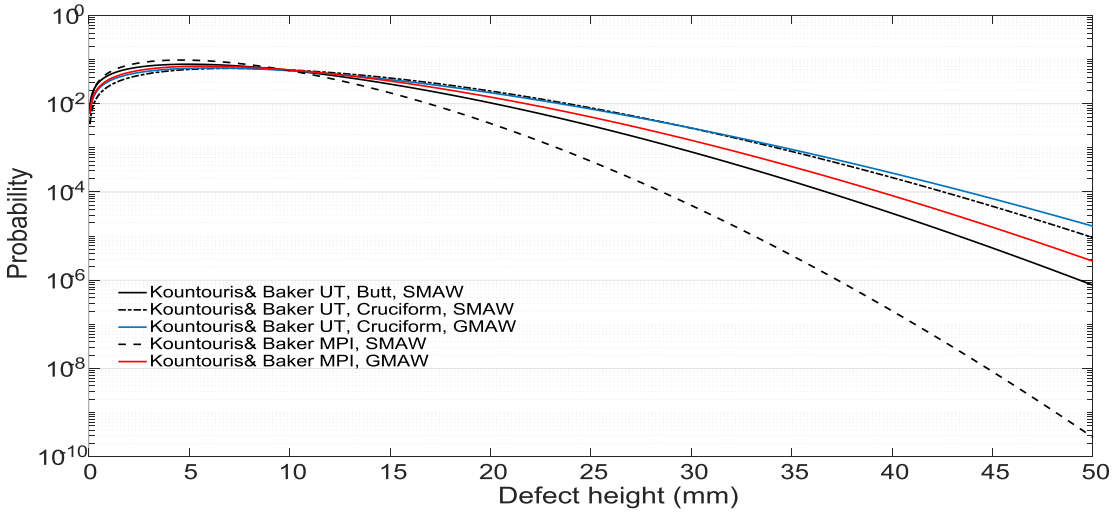

Figure 4-21 Crack height density distribution from (Kountouris and Baker, 1989 c) and (Kountouris and Baker, 1989 a)

4.7.2 Defect length

Defect length information is the most important defect size data in crack growth assessment of ship hull structures as these structures can resist relatively long through thickness cracks before failure. Defect length information is used in terms of

a probability density function in reliability analysis. Here, data gathered from two shipyards are presented. Only planar defects can be used in fracture mechanics reliability analysis, therefore, crack-like defects and cracks combined with lack of fusion and lack of penetration defects have been fitted to Lognormal and Weibull distributions and distribution parameters are presented in Table 4-17 in conjunction with sample size, welding processes and confidence bounds. Additionally, median defect length of lognormal distribution is given to provide a better feel for differences between distributions. Kolmogorov-Smirnov test showed that lognormal distribution is a better fit to the data. To a degree, this can also be observed visually in Figure 4-22.

Possible outliers in the dataset were assessed by considering the data points that were visually far from the best fit curves. Then the values were presented to a welding engineering expert and the decisions were made on a case-by-case basis by the author and the expert. Furthermore, wherever there ware both planar and nonplanar defect reported for single size data points but only one combined defect size was recorded, that data point was removed from the dataset.

Defect	Data Set	Fit bounds	Weibull		Lognormal			Sample	Process
			Scale	Shape	Mu	Sigma	Median		
Cracks	Ship#2	Best	50.85	1.02	3.49	0.81	33	154	FCAW
		Upper	59.99	1.13	3.62	0.92	38		
		Lower	43.1	0.92	3.37	0.73	29		
	Ship#3	Best	35.28	0.97	3.12	0.80	23	56	FCAW
		Upper	47.06	1.15	3.34	1.00	28		
		Lower	26.46	0.82	2.91	0.68	18		
Planar	Ship#2	Best	101.3	0.78	3.98	1.21	53	168	FCAW
		Upper	124.3	0.88	4.16	1.36	64		
		Lower	82.49	0.70	3.79	1.09	44		
	Ship#3	Best	57.02	0.83	3.46	1.09	32	95	FCAW
		Upper	73.91	0.95	3.69	1.28	40		
		Lower	43.99	0.72	3.24	0.96	26		
		Upper	100.4	1.11	4.08	1.16	59		
		Lower	68.34	0.86	3.71	0.9	41		

Table 4-17 Planar defect length distributions from shipyards with 0.975 and 0.025 confidence values.

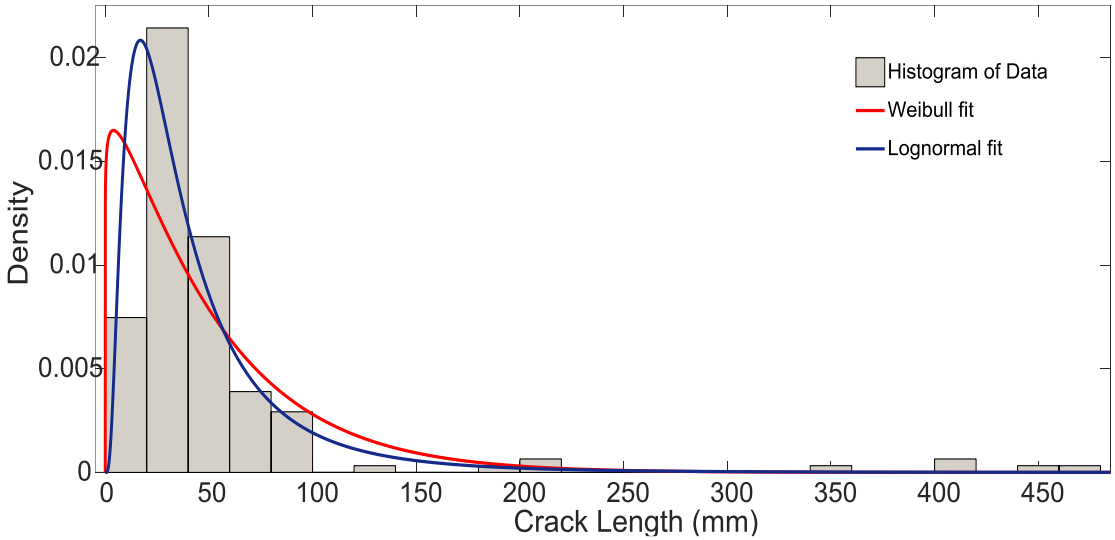

Figure 4-22 Weibull and Lognormal fits to crack length data from ship #2

Moreover, a number of published fabrication defect lengths are reviewed and the summary of distribution parameters is presented in Table 4-18. (Kountouris and Baker, 1989 a) show that incomplete penetration and crack-like defects typically have the highest mean lengths. Mean values for the latter range from 260- 414 mm.

Surface-breaking cracks are found to have significantly smaller length than embedded defects. One explanation could be that surface breaking cracks larger than a certain length have a very high probability of being detected by visual inspection. i.e. median crack heights are 30-37 mm, according to Figure 4-10 the probability of detection with visual inspection of this range of crack length for easy access condition is 70-80 % . 90% probability of detection is achieved for cracks length above 160 mm.

(Burdekin and Towned, 1981) reported distribution of lack of fusion and lack of penetration in tube to tube joints produced by manual metal arc welding of BS4360 50D steel and reported median defect length ranging between 280-330 mm.

(Becher and Hansen, 1974) reported solid inclusion length of ship steel grades produced by manual metal arc welding from radiography examination and suggest median defect length of 8 mm.(Kihara et al., 1971) fitted crack length data of shell plates to the Weibull distribution which gave the median value of 19.5 mm.

Investigator	NDT	Joint Type	Process	Flaw Type	Lognormal		Weibull		
					μ	σ	Scale	Shape	Median (mm)
(Kountouris and Baker, 1989 a)	UT	Butt	SMAW	LOF	4.5	1.24	164.7	0.93	111.05
				Crack	5.08	1.17	270.8	1.12	195.22
				Slag inc.	4.63	1.14	179.17	0.97	122.79
			GMAW	Slag inc.	3.77	1.72	163.4	0.94	110.64
				LOF	1.66	2.01	233.9	0.84	151.19
		Cruciform	SMAW	LOF	5.04	1.09	265.3	0.87	174.09
				Crack	5.06	1.11	272.31	0.98	187.34
				Slag inc.	4.63	1.14	223.45	0.97	153.14
				Porosity	5.04	1.18	275.16	0.93	185.54
			GMAW	LOF	4.98	1.27	276.12	0.80	174.63
				Crack	1.57	3.42	334.2	0.75	205
				Slag inc.	5.02	1.77	280.6	0.82	179.46
				Porosity	1.33	2.66	174.8	0.93	117.87
(Kountouris and Baker, 1989 c)	MPI	Butt and Fillet	SMAW	Centre crack	3.49	0.95	52.18	1.04	36.68
			GMAW	Centre crack	3.31	0.65	36.5	2.1	30.65
(Burdekin and Towned, 1981)	UT	Butt	MMA	LOF	0.94	0.61	341	2.14	287.32
				LOP	1.11	0.36	361	3.65	326.51
(Becher and Hansen, 1974)	RT	Butt	MMA	Slag inc.	1.97	0.81	10.87	1.2	8.01
(Kihara et al., 1971)		Shell plates		Crack	2.97	0.06	20.25	10.1	19.5

Table 4-18 Defect distributions distribution parameters from literature

Cumulative crack length distribution of ship #2 and ship #3 (this research) and those from (Kountouris and Baker, 1989 a) are shown in Figure 4-23. It can be seen that data collected from the shipyards show shorter cracks in length than those from (Kountouris and Baker, 1989 a) collected from an offshore platform. This could mean better welding quality of the studied shipyard or effect of welding process; the shipyards use FCAW, SAW, and HLAW process, whereas, the platform was built using SMAW and GMAW. Another possible reason could be the effect of thickness; studied ships are made of very thin plates ranging from 5-10 mm in deck area and 16-22 mm in side-shell and bottom area. The offshore platform from (Kountouris and Baker, 1989 a) is believed to be fabricated from considerably thicker sections. The thicker the parent material the more weld passes the joint needs. Every weld pass introduces more heat input to the joint and consequently, more residual stress is formed. Weld residual stress is a key cause of the formation of weld pool cracks.

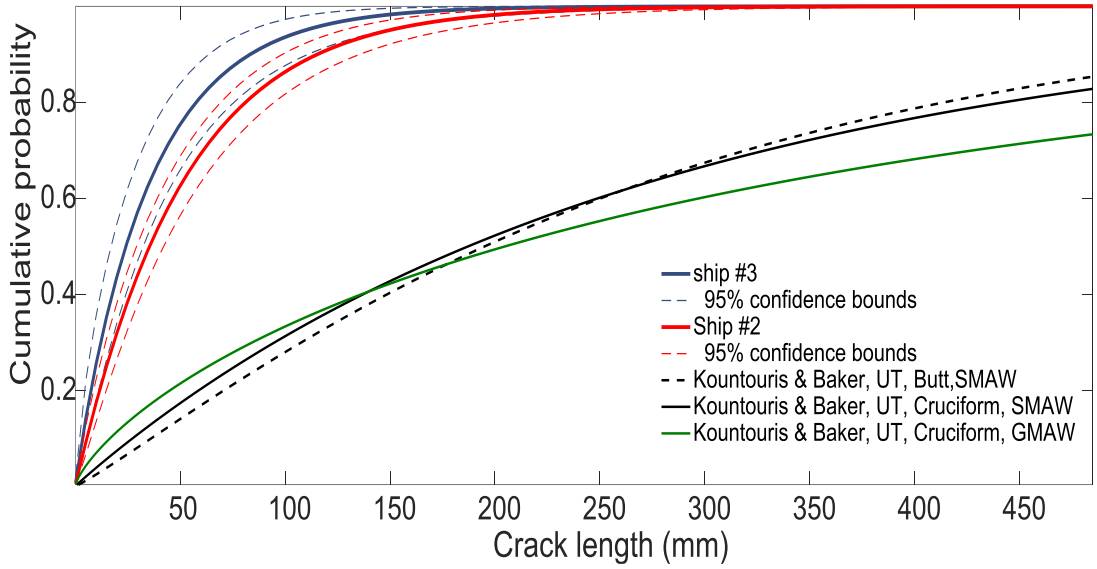

Figure 4-23 Crack length cumulative distribution from ((Kountouris and Baker, 1989 a) and this work

4.7.3 Defect aspect ratio

Reliable data on the aspect ratio defined as the ratio of defect length to defect depth are virtually non-existent. (Kountouris and Baker, 1989 c) have fitted Lognormal and Weibull distributions to surface-breaking defects and embedded defects in an offshore structure. They showed that the distribution parameters are highly dependent on defect type, weld type, welding process and defect location within the joint. Table 4-19 shows the lognormal and Weibull parameters, obtained for a sample of cases in cruciform and tee butt welds.

Investigator	NDT	Joint	Process	Flaw Type	Lognormal		Weibull		
					μ	σ	Scale	Shape	Median
(Kountouris and Baker, 1989 a)	UT	Butt	SMAW	LOF	3.29	1.28	49.55	0.90	33.03
				Crack	3.15	1.26	42.97	0.88	28.33
				Slag inc.	3.67	1.20	70.92	0.89	46.98
			GMAW	Slag inc.	3.58	1.21	65.27	0.87	42.83
				LOF	3.65	1.41	77.70	0.77	48.27
		Cruciform	SMAW	LOF	3.28	1.28	61.40	0.81	39.05
				Crack	3.15	1.26	32.40	0.87	21.26
				Slag inc.	3.66	1.20	84.00	0.96	57.34
			GMAW	LOF	3.53	1.39	68.57	0.72	41.22
				Crack	3.02	1.35	40.00	0.76	24.70
				Slag inc.	4.07	1.24	109.7	0.82	70.16
				Porosity	2.98	1.14	34.70	0.89	22.99
	MPI	Butt and Fillet	SMAW	Centre crack	1.92	1.06	11.61	0.87	7.62
			GMAW	Centre crack	2.06	0.92	11.95	1.30	9.01

Table 4-19 Defect aspect ratio distribution parameters from (Kountouris and Baker, 1989 a)

4.7.4 Initial Defect Length

As explained in Detection probability-Bayesian theorem section, initial defect size can be derived from the detected defect size distribution and respective POD function using Bayesian-Inference principles. Distribution fitting of detected crack size is discussed in section 4.7. of this chapter. Planar defect length data were fit to $f_{A,D}(a)$, using the nonlinear least square method (LSM), and λ_0 and λ values were calculated. The summary parameter estimation and the 50% POD is given in Table 4-11. Figure 4-24 shows Initial defect length density functions for shipyard data. These distributions are directly used in probabilistic fatigue and fracture mechanics assessment of this research.

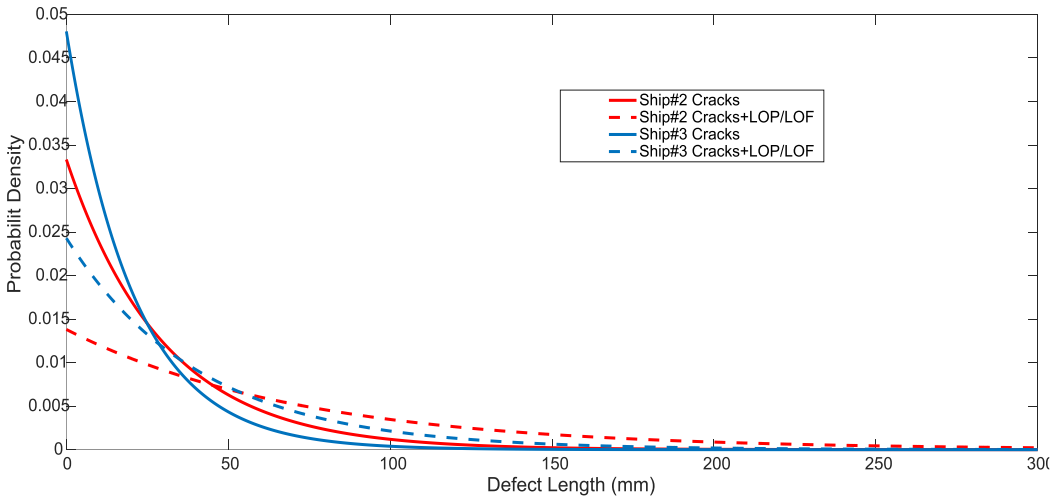

Figure 4-24 Initial defect length density functions for shipyard data

4.7.5 Summary and discussion of defect size distributions

Quantifying defect size is a crucial part of reliability assessment. A defect size is mostly defined by its length and height. Another useful term in the analysis is the aspect ratio that is the ratio between length and height of the defect which can be used to estimate one dimension of the defect from the other dimension.

Defect length is useful in defect assessment of ship hull structures where long through-thickness cracks are common. In structures where a through thickness flaw may lead into leakage of substances for instance in oil tankers the defect height may be the most important parameter. In structures containing pressurised containments such as pressure vessels in which a non-through thickness crack may lead to structural failure, the defect height and length may both be significant from the fracture point of view.

In this research defect length data from two shipyards, detected mainly by Radiography Testing (RT), have been analysed and it was found that median crack length ranged from 18 mm to 38 mm. A broad review of published work on fabrication defect size was carried out and Lognormal and Weibull fit of defect length, height and aspect ratios were presented. It is concluded that the planer defect lengths of studied shipyards are significantly smaller than those from the literature indicating a possible better quality of welding.

Defect size is highly dependent on the type of the defect (planar/ nonplanar, crack like/lack of fusion-penetration) and defect location (weld toe, weld metal) but less dependent on welding process. When used in reliability analysis and fracture mechanics it is crucial that, wherever possible, a distribution is used that adequately represents the detail under study; similar defect type and location. Otherwise conservative assumptions should be made.

The initial defect length density functions were estimated using Bayesian-Inference principles. These functions are directly used as inputs in reliability analysis of this research.

4.8 Chapter summary and conclusions

In this chapter, the frequency of occurrence of major weld defect types, the possible influencing variables, common Non-destructive examination methods to detect them and the reliability of the methods, and statistics of the defect sizes have been investigated using data from three case study ships and published work from the literature.

Welding process, choice of the NDE method, joint type, weld variables (weld bead size, heat input, etc.), weld procedure parameters (welding position, access, restraint, etc.), and human factors have bearings on the frequency of occurrence and sizes of the weld defects. Data on weld process, the NDE method, the joint type, and the parent material thickness is normally available from NDE report. Other variables cannot be reliably evaluated at a large scale manufacturing development like a shipyard with current data recording capabilities.

Defect type frequency statistics from a shipyard were presented, detection probabilities of conventional NDE methods based on “hit-and-miss” data from literature were reviewed. Detection probability calculation using Bayesian-Inference

method was explained and subsequently, POD curves of Radiography Testing (RT) from two shipyards were estimated. Additionally, defect probabilities of occurrence (defect rates) are calculated accounting for detection probabilities. Moreover, defect size statistics from the literature were reviewed. Defect length data gathered from two shipyards were fitted to candidate probability distribution functions (PDFs) using the maximum likelihood estimate method. Lognormal and Weibull distributions were found to be the best distribution fits. Finally, fitted detected crack length distributions and estimated probability of detection were used to estimate initial defect length distribution by means of the Least Square Method (LSM).

In this chapter, it was found that:

- Hybrid Laser Arc Welding (HLAW) process shows a better quality in terms of defect occurrence than the other two process with binary defect rate of 8% compared to 25% for Submerged Arc Welding (SAW) and 27.5% for Flux Cored Arc Welding (FCAW) . When length of defect vs. length of inspected method of defect rate calculation was used, HLAW had 3% defect rate compared to 10% SAW and 4.7% FCAW.
- All three weld process show similar relative distribution of defects types by producing a reasonably low amount of cracks (2%-10%) and high amount of cavities (32%-40%). The HLAW process produces considerably lower solid inclusions of 6% compared to 25% in SAW and 40% in FCAW. FCAW creates significantly lower LOF/LOP compared to the other two methods which can mean that it is a safer process as far as type of defect is concerned since; LOF/LOP defects are planar defects and are more likely to propagate under cyclic loading.
- It was not possible to investigate the effect of joint type using the data from shipyards due to lack of information in the datasets, however, studies from literature suggest that defects in fillet welds are more common than in the butt welds (Marcello Consonni (2012)).
- Studied data from the shipyards showed that within the range of thinness of 5.5mm-22 mm no connection was found between plate thickness and defect frequency, or defect length.
- Choice of NDE method found to be affecting defect rate, defect size distribution and frequency of detected defect types significantly; Radiography testing is less efficient in finding planar defects than Ultrasonic testing.

Detected defect rates from shipyard #1 were almost twice as high as from shipyard #2 (13% for shipyard #1 and 7.5% shipyard #2). When reliability of NDE methods were accounted, actual defect rates become very close (24% for ship #1 and 22.4 for ship #2). This suggests that Ultrasonic Testing should be preferred over Radiography testing where possible. Firstly, defect rates should only be compared with each other if the effect of their NDE method reliability is accounted for. Secondly, If UT cannot be used due to thickness limitations (UT cannot be used for thicknesses below 8 mm), Radiography Testing should be used in conjunction with a surface inspection method such as MPI or DPT

- POD functions are normally given as a function of defect height. In cruise ship fabrication with thin deck plating where cracks are usually through thickness it is useful to quantify POD curves as a function of defect length. Using the Bayesian-Inference method POD curves where estimated and mean detection length of 9.35 mm for cracks and 3.1mm for combined crack and LOP/LOF were estimated for shipyard #1. Mean detection length of 6.55mm for cracks and 2.14mm for combined Crack and LOP/LOF were estimated for shipyard #2.
- There is significant variation in planar defect height reported in literature. Reported median height varies between 1.2 mm to 9.8 mm. The variation is due to dependency of defect height on type of the planar defect type (crack or incomplete fusion/penetration) and defect location (weld toe or weld metal). Cracks are typically 2-3 times bigger in height than incomplete fusion/ penetration defects. Longitudinal cracks at the centre of weld metal are 3-4 times bigger in height than those at the joint toe.
- Published data on planar defect length shows that embedded defects are 4-6 times longer than surface breaking defects (Kountouris and Baker, 1989 a), (Kountouris and Baker, 1989 c).
- Planar defect length distributions from two studied cruise ships constructed in 2012 are 3-7 times smaller than the offshore constructions from literature based on fabrication in the 1980's.
- Exponential distribution is assumed to best represent initial defect length distribution of fabrication planar defects with mean crack size of 20.81 mm for ship #3 and 30 mm for ship #2. Mean defect sizes of pooled planar defects are 72 mm for ship #2 and 41 mm for ship #3.

As highlighted in chapter 2 and (Amirafshari et al., 2018), rules of classification of ships from different classification societies suffer from a considerable discrepancy in a number of themes. In this chapter it was made possible to make relevant suggestions:

- Choice of volumetric examination: Ultrasonic testing should be the preferred method and when due to thickness limitations Radiography testing is used it is suggested that it is accompanied by a surface NDE.
- Defect type: Cracks and other planar defects are more critical than nonplanar defects from the structural integrity and fatigue life points of view and should receive more attention.
- Defect rates: In the calculation of defect rates, it is suggested that the detection probability of the adopted NDE method is accounted for. Also, the defect rate of planar defects and nonplanar defects are recommended to be dealt with separately.
- Joint type: joints with higher restraint such as butt welds connecting grand-blocks are more likely to be the site of cracks and are recommended to receive more attention.
- Welding process: Those processes likely to create more cracks, such as FCAW, or planar defects, such as SAW, should receive more attention

Chapter 5

Probabilistic analysis of fracture toughness

5.1 Chapter outline

As explained in chapter three, fracture toughness is one of the three critical inputs in reliability analysis and fracture mechanics. Acceptability of a given flaw is very sensitive to fracture toughness of the material. Hence, accurate evaluation of this variable is a task of great importance.

In this chapter, first fracture failure and fracture toughness are briefly introduced, and variables that affect them and their relevance to ship hull structures are explained, the methods of measuring fracture toughness and interpreting the test data are discussed. Finally, the probabilistic analyses of the collected toughness test data are discussed.

It is concluded that fracture toughness of shipbuilding steel has significant scatter due to the inherent randomness of the toughness for any piece of steel, the variation of toughness among different batches of steel and the deviation of toughness quality between different steel manufacturers. The steel fracture toughness improved from 1947 to 2000 (Kent and Sumpter, 2007), and the results from this work show that it has continued to improve in the recent years with a consistent trend, suggesting that recently built ships are expected to be more damage tolerant than older ships, and a less extensive NDT inspection may be appropriate.

5.2 Fracture

In a brittle material, fracture occurs by cleavage or intergranular fracture. The two modes of fracture are similar at a macroscopic scale, with the fracture path dictated by the weakest link mechanism.

Cleavage-type crack propagation typically initiates several microns ahead of the crack tip, at small carbide inclusions in steel. Very little plastic work is associated with the propagation of cracks by cleavage or intergranular fracture, and so limited

permanent deformation occurs. Ferritic steels with high ductile to brittle temperatures relative to the operating temperature (e.g. poor quality steel or steel at low temperatures) are prone to brittle fracture by this mechanism. Susceptibility to cleavage fracture is enhanced by any factor that increases the yield strength such as Low temperature, tri-axial stress state, high strain rate (Wallin, 2011), and (Rolfe and Barsom, 1977).

If a crack in a ductile material is subjected to a stress, the crack will initially blunt, and then if the loading is increased a ductile tear will initiate and propagate by microvoid coalescence. If the stress is increased further, then unstable conditions may be reached, and rapid ductile fracture will occur.

Ductile fracture is characteristic of ferritic steels at upper-shelf temperatures. Here, considerable local plastic strains are associated with crack propagation. Although plastic deformation occurs near the crack, the global deformation may be small, and on a macroscopic scale, the fracture may become unstable and propagate rapidly (although ductile cracks propagate at a slower speed than cleavage-type cracks).

5.3 Fracture toughness

The resistance of a material to fracture is known as its fracture toughness. Fracture toughness is a crucial variable in fracture mechanics based reliability analysis. Fracture toughness generally depends on temperature, environment, strain rate, the composition of the material and its microstructure, together with geometric effects (constraint). The factors are of particular importance for welded joints, where the metallurgical and geometric effects are complex.

5.4 Parameters affecting fracture toughness

Fracture toughness is not a constant quantity and is affected by conditions of the structure. The fundamental conditions that have a significant effect on the toughness are temperature, constraint and loading rate. Thus, before the engineer can use fracture-toughness values in design, fracture control, failure analysis, or fitness for service, the critical fracture toughness value for the particular service temperature, loading rate and constraint level must be known. In this section, we shall describe the general effects of these three variables on the fracture toughness of shipbuilding steels.

5.4.1 Temperature

At lower temperatures, ferritic materials fractures in cleavage fracture mode and fracture face shows little to no shear deformation but 100% crystallinity. The fracture toughness is almost unaffected by temperature change in this region. This behaviour is called lower shelf behaviour. At high temperatures failure is associated with high shear deformation; the fracture face shows zero cleavage and is 100% fibrous. Similar to lower shelf region fracture toughness it is almost unaffected by temperature change. Between lower shelf and upper shelf regions, a transition in behaviour occurs from ductile upper-shelf behaviour (high fracture toughness) to brittle lower-shelf behaviour (low fracture toughness). The behaviour of ferritic materials with respect to temperature is schematised in Figure 5-1. Scatter of fracture toughness test data is relatively low and narrow banded in lower shelf and upper shelf regions. Conversely, in the transitional region, the scatter is high. This is due to a statistical sampling effect. On initial loading in the upper transition region, cleavage does not occur, as there are no critical particles near the crack tip, as the crack grows by ductile tearing, however, more material is sampled. Eventually, the growing crack samples a critical particle and the cleavage occurs. Since the fracture toughness in the transition region is governed by the statistical sampling effects; the data tend to be highly scattered (Anderson, 2005).

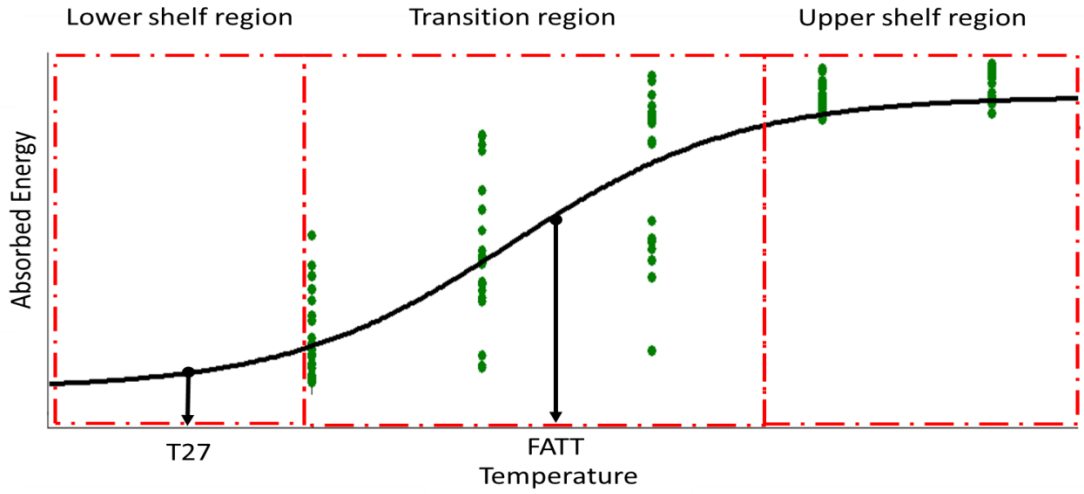

Figure 5-1 Schematic transition curve

Temperature is such an important variable that fracture toughness is often characterised by the temperatures corresponding to defined conditions. One such transition temperature is *T27J* or *T28J* temperatures which are widely used as specified minimums for fracture quality of ferritic material. Another temperature is

fracture appearance transition temperature (FATT) that corresponds to 50% crystallinity. These temperatures are shown schematically in Figure 5-1. When a structure is assessed using fracture mechanics one prerequisite is to determine its operating temperature so that the fracture toughness is estimated correctly. Normal ship hull structures are intended to safely operate down to -20 ˚C. Ships that have a normal operating temperature below -20 ˚C are regarded as ice-class vessels and have more stringent material requirements. (Hodgson and Boyd, 1958) reports that the operating temperature of merchant ships follow a normal distribution with mean value of 17.5 ˚C and standard deviation of 8.3 ˚C. The probability density function is depicted in Figure 5-2. Probabilities of the temperature being below 0, -10, and -20 ˚C are 1.75 * 10^{-2}, 4.6 * 10^{-4}, and 3.12 * 10^{-6}, respectively. Fracture mechanics assessment of ship plates are commonly studied at waterline where the temperature is conservatively taken as 0 ˚C temperature and under slam loading rate which is considered to be the critical condition under which cleavage fracture happens. Temperatures below 0 ˚C might occur at the deck but loading rate will be lower, as well (Sumpter and Caudrey, 1995). The effect of loading rate on fracture toughness is explained in the next section.

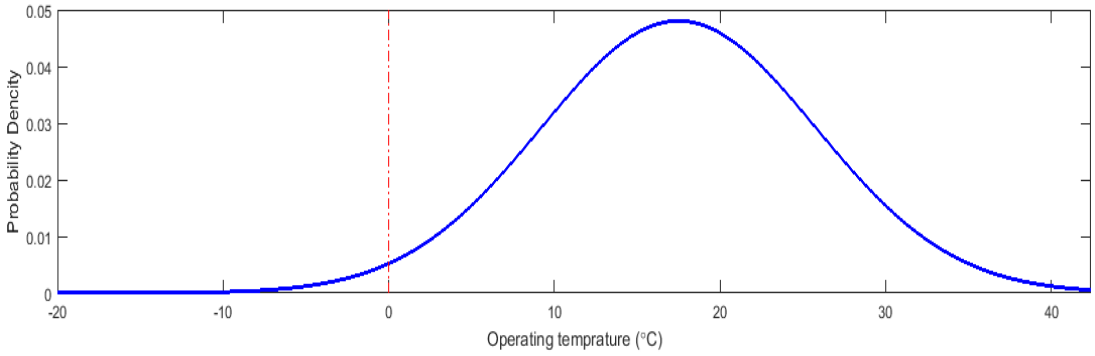

Figure 5-2 Merchant ship operating temperature (Hodgson and Boyd, 1958)

5.4.2 Loading rate

Strain rate at the crack tip affects fracture toughness significantly (Rolfe and Barsom, 1977). Generally, an increase in strain rate results in a reduction of fracture toughness for ferritic materials, this is shown, schematically, in Figure 5-3. Loading rate may be expressed in term of strain rate, $\dot{\varepsilon}$, or the rate of increase of the linear elastic stress intensity factor $\dot{K}$. The latter parameter is a more appropriate measure for loading rates in fracture mechanics specimens and flawed structures as it includes the relevant geometries and flaw dimensions. BS7448-1 fracture toughness testing procedures covers loading rates of 2.5 $MPa\sqrt{m}/s$ to 3 $MPa\sqrt{m}/s$ for quasi-static

loading and BS7448-3 covers test procedure for higher loading rates up dynamic loading of $3000\ MP\sqrt{m}/s$.

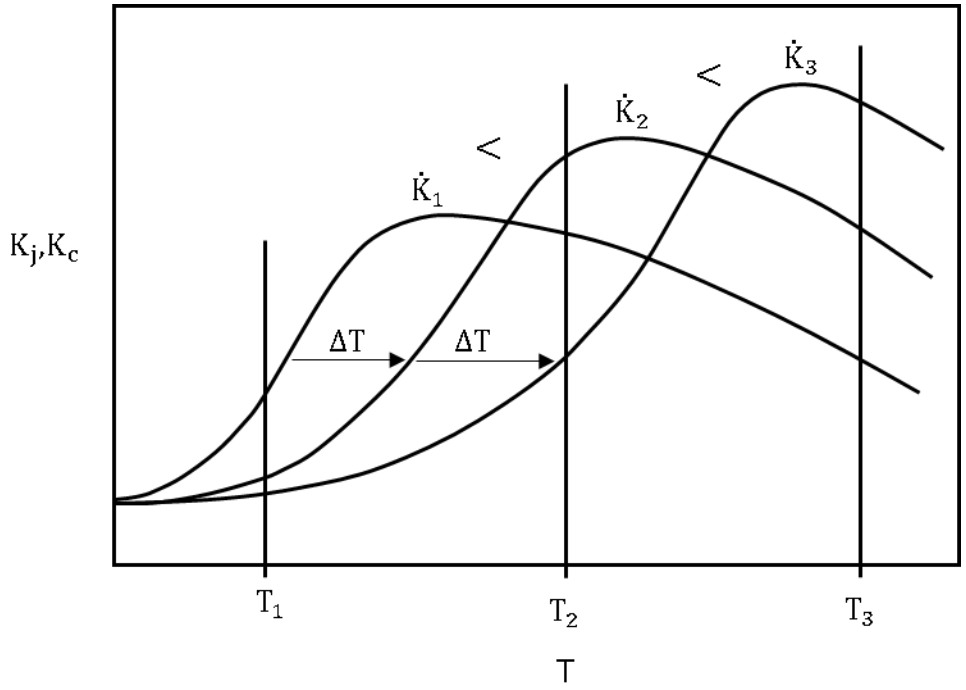

Figure 5-3 Schematic illustration of the effect of loading rate on fracture toughness

The effect of increasing loading rate could be taken into account as temperature shift, ΔT_0 in transition curve. (Wiesner and MacGillivray, 1999) propose below equations to calculate the temperature shift term ΔT0:

$$\Delta T_0 = \frac{T_0^{stat} ln(\dot{K})}{\Gamma - ln(\dot{K})} \qquad (5\text{-}1)$$

with:

$$\Gamma = 9.9\ exp\left[(T_0^{stat}/190)^{1.66} + \left(\sigma_{ys}/722\right)^{1.09}\right] \qquad (5\text{-}2)$$

Where T_0^{stat} and $\sigma_{ys}$are transition temperature and tensile strength at static loading rate, respectively. For ship hull structures the critical loading rate which may cause cleavage fracture is considered to be slamming condition. (Kent and Sumpter, 2007) argue that although for a long time it was believed that the loading rate of $1 - 3 * 10^4\ MPa\sqrt{m}/s$ in the keel of the ship was believed to be a suitable critical loading rate for fracture mechanics assessment of ships, this rate will almost never

exceed 300 $MPa\sqrt{m}/s$ even at deck over severe storm representing slam. Later, (Sumpter and Kent, 2004) suggested that the 250 $MPa\sqrt{m}/s$ loading rate for 1 meter long crack in the deck is a suitable conservative upper bound value. The effect of loading rate on fracture toughness of a typical AH36 steel is shown in Figure 5-4, assuming yield strength equal to 256 MPa (Lloyds Register minimum requirement), and $T_{27} = -44$ (manufacturer #3 in Table 5-11).

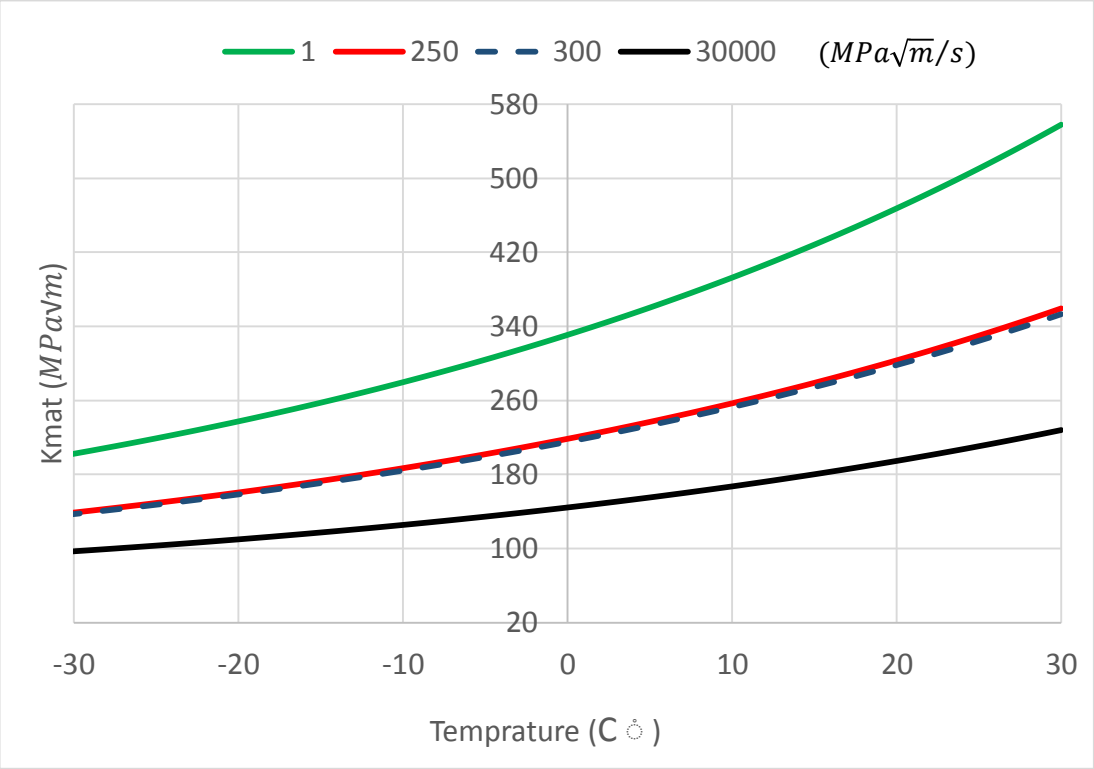

Figure 5-4 effect of loading rate ($\frac{MPa\sqrt{m}}{s}$) on a typical AH36 grade steel

5.4.3 Constraint

Stress and geometry-related factors that influence stress tri-axiality (and level of plasticity) near the crack tip are generally called constraint effects. Thick sections and complex joints generally result in higher levels of constraint, reduced levels of plasticity, and lower levels of fracture toughness. This means that fracture toughness is a property of material and geometry. Even standard test specimens have different constraint level and consequently different fracture toughness (Figure 5-5). These differences need to be accounted for when fracture toughness is derived from the test specimens.

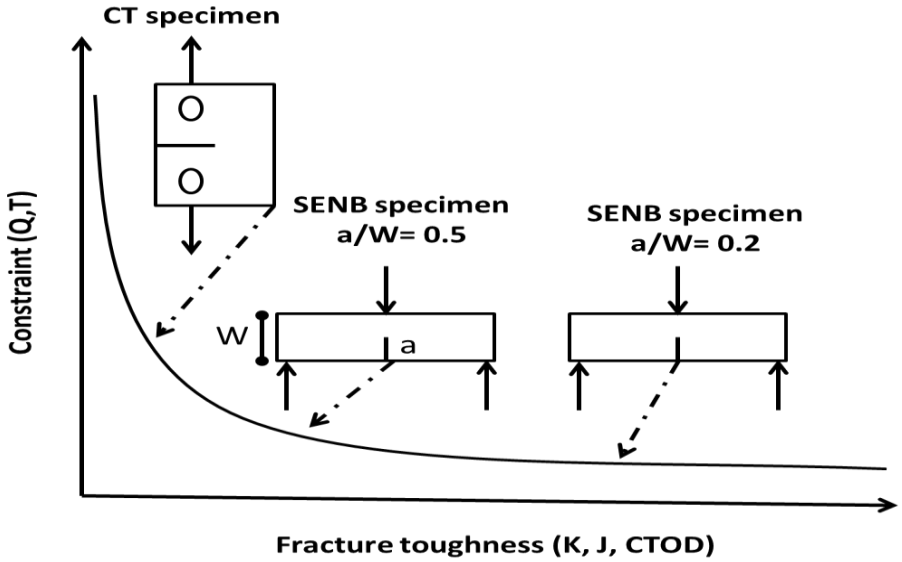

Figure 5-5 Effect of constraint on fracture toughness (Moon et al., 2017)

Near the surface, plane stress (low constraint) conditions are approached, as material near the surface is free to deform in the through-thickness direction. For very thick sections, these surface effects are small, and fracture toughness does not depend on geometry (i.e. the plane strain fracture toughness, K_{IC} is a material property). For thin sections, plane stress conditions occur throughout the section, associated with increased levels of plasticity and higher values of toughness. For very thin materials, other stress modes dominate and fracture toughness decrease. Figure 5-6 schematises the effect of section thickness on fracture toughness. For fully ductile material or upper shelf behaviour, the thickness effect may be reversed (Wallin, 2011).

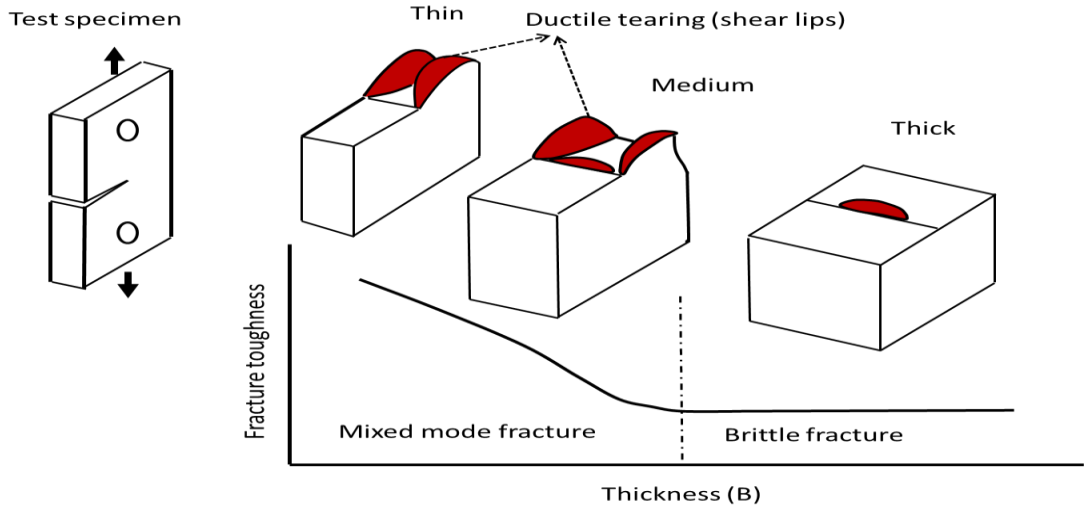

Figure 5-6 Effect of specimen thickness on fracture toughness (TWI, 2015 b)

Ship plates range between 5-30 mm and are considered to be thin sections with low constraint (Kent and Sumpter, 2007).

5.4.4 Plate rolling direction

Fracture toughness of steel is higher in longitudinal (rolling) (L-T) direction (Figure 5-8) compared to the transverse direction (T-L). The grains of steel are formed parallel to the rolling direction during steel manufacturing which makes the material stronger in this direction in terms of tensile strength and toughness capacity. As it can be understood from Table 5-2, required impact energy in the transverse direction is on average 30% lower than in the longitudinal direction. In the dataset of this work, only one manufacturer provided test results in both directions. This is shown in Figure 5-7. The variation in the lower transition zone is 27% comparable with the corresponding variation of 29% from Table 5-2. Note that the upper shelf variation is much larger.

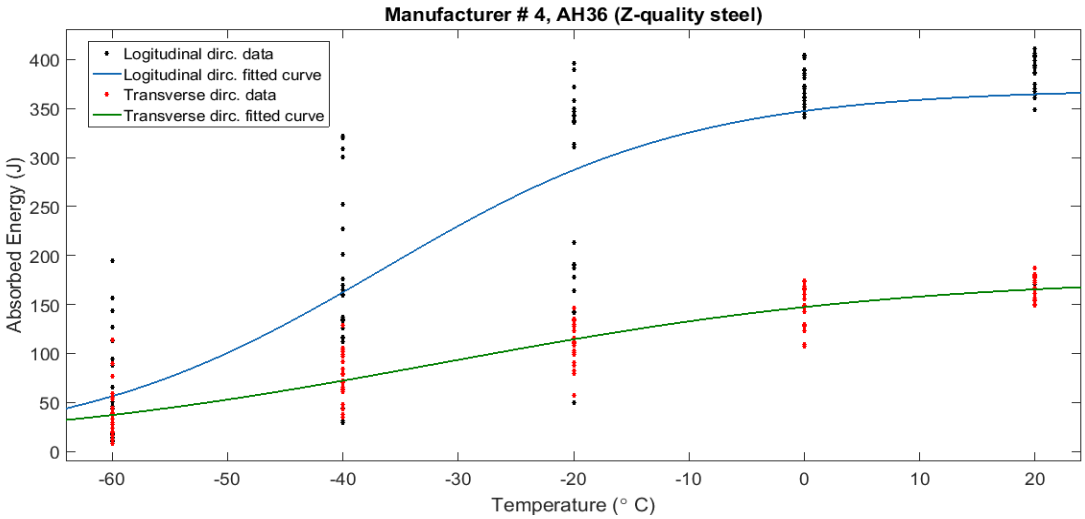

Figure 5-7 Charpy absorbed energies for Z-quality AH36 steel in (L-T) and (T-L) directions

The rule in ship construction is to lay the plates from their length (Figure 5-8) along the ship longitudinal axis to resist σ_{xx}, induced by the vessel's global bending load. This is favorable to fracture resistance, as well. The cracks are likely to grow along the transverse direction (L-T) as a result of σ_{xx}. In the perpendicular direction, acting stresses on a possible fabrication defect, present in deck plates and side shells, are σ_{yy}, and σ_{zz}, respectively. The stresses are small and will not usually cause overall hull girder fracture but may contribute to a local, e.g. sideshell, failure following fatigue cracking.

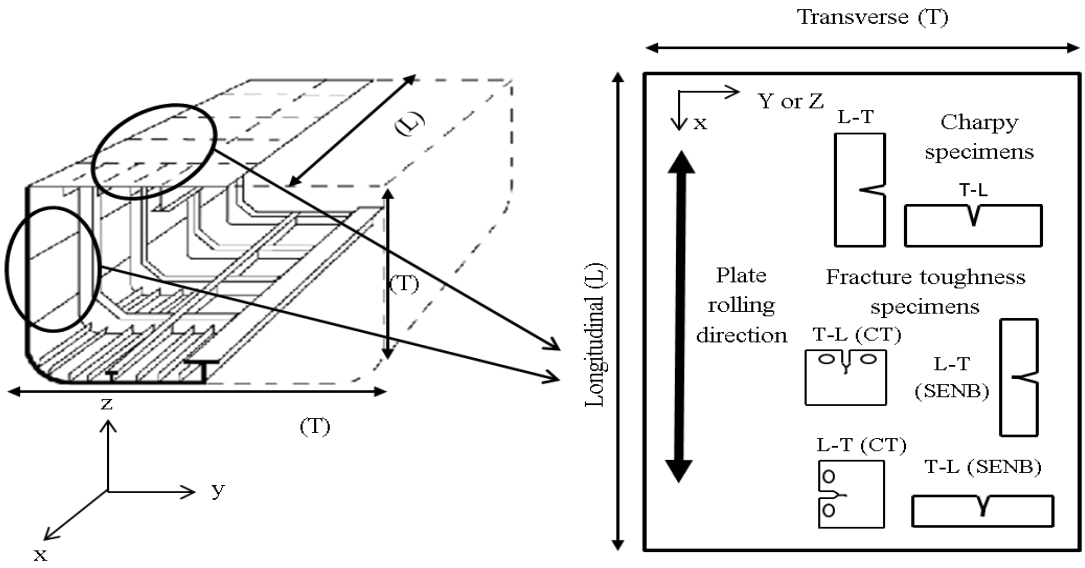

Figure 5-8 Plate rolling direction relative to ship orientation and test specimens

5.5 Measures of fracture toughness

Fracture toughness may be characterised by three different measures depending on the mode of fracture. The three primary measures of fracture toughness are:

5.5.1 The stress intensity factor (K)

K is a stress-based measure, applicable to fracture in brittle materials. When K is estimated from tests, it is derived from a function which depends on the load (stress) at failure (or at the point where the test is stopped, at a significant pop-in (a reduction in the resisting load during the test), or the maximum load). K also depends on geometry (the flaw depth, together with a geometric function).

$$K = Y\sigma\sqrt{(\pi a)} \qquad (5\text{-}3)$$

Stress intensity factor (*K*), was initially defined by Irwin. The derivation of *K* is based on the assumption that the material behaves in a linear elastic fashion (i.e. linear elastic fracture mechanics: LEFM). For most structural material, plasticity plays an important role, and the original theory of Irwin has been subsequently modified to account for plasticity effects.

The primary limitation of linear elastic fracture mechanics (i.e. K-based LEFM) for fracture assessment is that it is only valid for materials which are relatively brittle, or where joints are highly constrained (i.e. where plastic zone sizes are small in comparison with section dimensions). For ductile materials, plasticity correction must be included. This limitation is less restrictive for fatigue assessments. Under

fluctuating loading, the cyclic plastic zone at the crack tip depends on twice the yield strength (due to reversed plasticity) and is therefore only one quarter the size of the static plastic zone. As a result, ΔK is still a useful parameter for characterising fatigue crack growth (plane strain or plane stress), even under high stress/low cycle fatigue conditions (Anderson, 2005).

5.5.2 CTOD (δ)

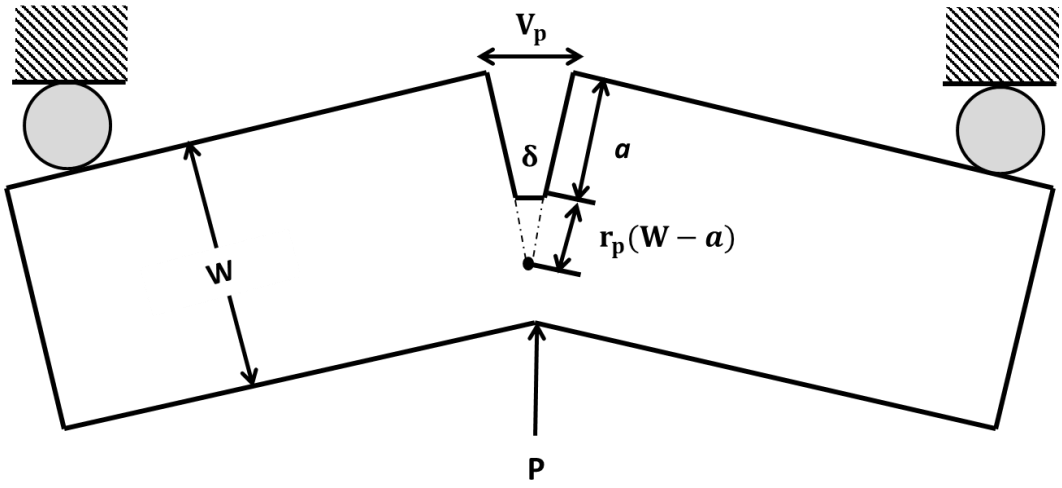

Figure 5-9 the hinge model for estimating CTOD from three-point bend test

CTOD (δ), the crack-tip opening displacement, represents the physical opening of the crack near the tip (measured in mm). See Figure 5-9 and Figure 5-10. δ is thus a strain-based parameter and applies to fracture in the ductile material. δ is separated unto elastic and plastic components. When measured from tests, the elastic part of δ is derived from the stress intensity factor, k (based on LEFM). The plastic part is derived from the crack mouth opening displacement (Anderson, 2005).

$$\delta = \delta_{el} + \delta_{pl} = \frac{K^2(1-\nu^2)}{(2\sigma_Y E)} + \frac{[r_p(W-a)V_p]}{[r_p(W-a)+a]} \qquad (5\text{-}4)$$

Where E is elastic modulus, ν is material's Poisson ratio, W is section width, a is notch depth, $r_p$is the rotational factor , a costant approximately 0.44 for typical materials and test specimens (Anderson, 2005). $V_p$is displacement.

5.5.3 J-integral

J, or the J-integral is an energy-based parameter, is applicable to ductile materials. The SI units for J are kJ/m^2 or N/mm. The J-integral which is based on robust

mathematical methods is derived by integrating the change in energy associated with crack advance, within a region near the crack tip. Experimentally, J is derived by measuring the mechanical work done while loading the fracture toughness specimen. The elastic component is based on K, while the plastic component is derived from the plastic area under the load-displacement curve (Anderson, 2005).

$$J = J_{el} + J_{pl} = \frac{K^2(1-\nu^2)}{E} + \frac{\eta U_p}{B b_0} \qquad (5\text{-}5)$$

Where, η is a dimensionless constant, $U_p$is the strain energy stored in in body, B is section thickness and b_0 is the initial ligament length in the specimen ((W-a) in Figure 5-9). For linear elastic materials, J can be converted into K, although the conversion to CTOD is less certain (depending on constraint factor, m).

$$J = \frac{K^2}{\acute{E}} = m\sigma_Y \delta \qquad (5\text{-}6)$$

Where $\acute{E} = E$ for plane stress and $\acute{E} = \frac{E}{(1-\nu^2)}$ for the plain strain.

Generally, linear elastic fracture mechanics (LEFM) is applicable only to the lower shelf or very thick sections (K measure). For transition and upper shelf temperatures, where plasticity is significant, elastic-plastic fracture mechanics (EPFM) must be used. For this regime, CTOD or J must be used.

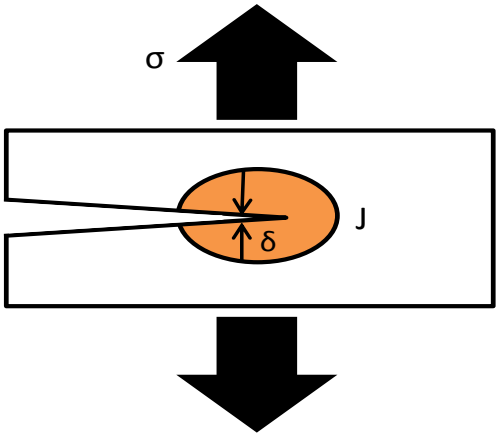

Figure 5-10 Schematic illustration of δ and J

5.6 Fracture toughness testing

Various toughness tests exist, including, the widely used impact energy test. While it is possible to correlate Charpy energy with fracture toughness, it is preferable to measure fracture toughness more rigorously, in terms of K (stress intensity factor),

CTOD (crack tip opening displacement), or *J* (the J integral). Most common specimen configurations are the single-edge notch bend test SENB specimen and compact tension (CT) specimen (Figure 5-5). The CT specimen has the advantage that it requires less materials, but is more expensive to machine and more complicated to test compared to the SENB specimen. A sharp fatigue notch is placed in the specimen and loaded to failure. The crack driving force is calculated for the failure condition, giving the fracture toughness. Other specimen configurations include centre-cracked tension (CCT) panels, single notch tension (SENT) specimens, shallow-crack tests. These specific tests have lower levels of constraint and can be more structurally representative than SENB or CT specimens, although they are not usually used for flaw assessment procedures. For some applications large-scale fracture mechanics testing is required, such as wide-plate or burst tests.

The position and orientation of the specimen are important. Specifically, the location and orientation of the notch is critical, especially for welded joints. Usually, the notch (fatigue pre-crack) is positioned such that a particular microstructure is sampled. The orientation of the notch is defined with relation to either the weld axis for welded joints, or the rolling direction or forging axis for other components. Ideally the component should be tested in several orientations; or the low toughness orientation. To assess specific conditions the orientation that matches the flaw being assessed should be selected (TWI, 2015 b).

For fracture toughness testing, it is vital that temperature effects be taken into account. Typically fracture toughness tests are performed at a temperature equal to the service temperature. For ferritic steel, this is normally equal to minimum design temperature or service temperature.

5.7 Statistical treatment of fracture toughness data

A number of methods are commonly used to take into account uncertainty in fracture toughness test results. All of these methods are based on the 'master curve' approach. The original master curve (MC) approach was developed by (Wallin, 2011) and is adopted by fracture testing and assessment standards (ASTM, 2016) and (BS7910, 2015 a). These methods are based on the weakest link failure assumption applicable to a cleavage mechanism.

The basic master curve approach uses a three-parameter Weibull distribution to quantify scatter in fracture toughness for a given temperature and a mean line to estimate fracture toughness in other temperatures in the lower shelf and transition region. Other notable methods based on the master curve approach are: MC with censored data (BS7910, 2015 a), Bi modal MC (Wallin et al., 2004), Engineering lower bound (Zerbst et al., 1998), Bimodal MC with adjusted lower bound (Sumpter and Kent, 2004), and MC with random inhomogeneities (SINTAP, 1999).

For assessment of toughness test data from test specimens other than standard 25 mm test specimens, the test results need to be adjusted to reference test specimen thickness using the below equation:

$$K_{mat(25mm)} = K_{min} + (K_{mat} - K_{min})\left(\frac{B}{25}\right)^{1/4} \quad (5\text{-}7)$$

Where, $K_{min}$is the minimum fracture tougness value and is equal to 20 $(MPa\sqrt{m})$ (BS7910, 2015 a).

(ASTM, 2016), and (BS7910, 2015 a) impose a validity limit for toughness data given by the below equation:

$$K_{mat} = \sqrt{\frac{b_0 \sigma_y E}{M(1-\nu^2)}} \quad (5\text{-}8)$$

Where, *M* is a constant and is taken as 30. Fracture toughness values above this limit should be censored when using methods based on the master curve approach. This is because the conditions of plane stress are not met at the specimen crack tip. The master curve analysis is typically used to extrapolate to thicker specimens used in the nuclear industry. However, for ship applications, the condition of plane stress may be more applicable (Kent and Sumpter, 2007). Hence, this limit is disregarded.

5.7.1 Master curve

Cleavage fracture happens at carbides or non-metallic inclusions that are distributed throughout the component. Variability of fracture toughness is due to the random location of these sites. (ASTM, 2016). As the crack propagates, there is a respective probability of sampling a weak link which leads to cleavage failure. In the master curve approach, the fracture toughness of a material is described by a three-parameter Weibull distribution where the shape parameter is assumed to have a

constant value of 4 (Wallin, 1984). The scale parameter is defined by K_0, fracture toughness value corresponding to 63.2% cumulative probability at a given temperature. The location parameter $K_{min}$is a lower bound value for fracture toughness. (Wallin, 2011) recommends a fixed value of 20 $MPa\sqrt{m}$ based on experimental results, however (Zerbst et al., 1998) argues that this is a mathematical limit instead of an experimental value. Shape parameter of 4 is defined theoretically and based on "weak link" nature of failure (Wallin, 2011). Scale parameter of any Weibull distribution corresponds to 63.2 percentile of the distribution, and so doesK_0.

The master curve for a single temperature can be written as:

$$P_f(K_{mat}) = 1 - exp\left[-(\frac{K_{mat} - K_{min}}{K_0 - K_{min}})^4\right] \quad (5\text{-}9)$$

The equation below describes the trend of fracture toughness as a function of temperature:

$$K_{mat} = 20 + (11 + 70exp[0.019(T - T_0)])\left(\frac{25}{B}\right)^{0.25}\left(-ln(1 - P_f)\right)^{0.25} \quad (5\text{-}10)$$

Where, T_0 isthe transition temperature for a median fracture toughness (50 th percentile) of 100 $MPa\sqrt{m}$ normalised to a 25mm thick specimen. If $P_f = 0.632, K_{mat} = K_{0.}$ If $P_f = 0.5, K_{mat} = K_{median.}$ T_0 characterizes the fracture toughness of ferritic steels that experience onset of cleavage cracking at elastic, or elastic-plastic $\mathrm{K_{jc}}$ instabilities, or both (ASTM, 2016). In this method first K_0 at the test temperature (T) is estimated by maximum likelihood estimate (MLE) of equation (5-9). Then using equation (5-10), T_0 is estimated. Equation (5-10) then can be used to estimate fracture toughness at any temperature in transition region.

When tests are performed at different temperatures the MML equation below may be used to estimateT_0.

$$\sum_{i=1}^{n} \frac{\exp[0.019(T_i - T_0)]}{11 + 77\exp[0.019(T_i - T_0)]} - \sum_{i=1}^{n} \frac{(K_i - 20)^4 \exp[0.019(T_i - T_0)]}{\{11 + 77\exp[0.019(T_i - T_0)]\}^5} = 0 \quad (5\text{-}11)$$

5.7.2 MC with censored data

For macroscopically homogeneous ferritic steels such as parent material or post weld heat treated (PWHT) welds the master curve approach is sufficient. For inhomogeneous materials such as welds in the as-welded condition, the data set will possess significant scatter. A common procedure in any engineering assessment is to consider conservative situations. (BS7910, 2015 a) adopts the FITNET lower tail MML procedure which is based on censoring higher fracture toughness values in the upper tail region of distribution. In this approach first T_0 is estimated using the original MC procedure, and then upper tail fracture toughness values higher than median fracture toughness values are censored. Using censored values a new T_0 is calculated. If the new T_0 is higher than previous T_0 the censoring is repeated using new toughness values as bench mark. The iteration process is repeated until a constant T_0 is achieved. This method provides a conservative estimate of fracture toughness values of inhomogeneous datasets and is suitable for deterministic analysis. For probabilistic analysis, the bi-modal MC approach or the MC with random inhomogenities are more applicable.

5.7.3 Bi-modal MC

When the fracture toughness test dataset contains small inhomogeneity, a bi-modal master curve may be used to describe fracture toughness distributions (Wallin et al., 2004). The equation for such distribution is as follows:

$$P_f(K_{mat}) = 1 - P_a * exp\left[-\left(\frac{K_{mat} - K_{min}}{K_{01} - K_{min}}\right)^4\right] - (1 - P_a) * exp\left[-\left(\frac{K_{mat} - K_{min}}{K_{02} - K_{min}}\right)^4\right] \quad (5\text{-}12)$$

Where $P_a$is the probability of the toughness belonging to the first distribution and $K_{01}$and $K_{02}$are characteristic toughness values for two parameters. P_a, $K_{01}$and K_{02} are estimated using MML. If the method is applied to a dataset which fits well to the basic MC distribution $P_a$will be close to 1. In this research one set of data that belong

to Z-quality steel in its upper transitional are shown to have two peaks which could be modelled with this method (Figure 5-14).

5.7.4 MC with random inhomogeneities

The bi-modal master curve is intended for datasets, where inhomogeneity is small. Where inhomogeneity increases, K_0 and T_0 become random variables. i.e. when the dataset is pooled from several different materials. K_0 will have a mean value of $\mu_{K_0}$and $\sigma_{K_0}$and can be described by a normal distribution (Kent and Sumpter, 2007):

$$P(K_0) = \frac{1}{\sigma_{K_0}\sqrt{2\mu}} exp\left[-\frac{\left(K_0 - \mu_{K_0}\right)^2}{2{\sigma_{K_0}}^2}\right] \quad (5\text{-}13)$$

The probability density function toughness is described by:

$$p(K_{mat}) = 4\frac{(K_{mat} - K_{min})^3}{(K_0 - K_{min})^4} exp\left[-\left(\frac{K_{mat} - K_{min}}{K_0 - K_{min}}\right)^4\right] \quad (5\text{-}14)$$

The maximum likelihood estimate is given by:

$$lnL = \sum_{i=1}^{N} ln\left[\int_{-\infty}^{\infty} p(K_{mat})P(K_0)\, dK_0\right] \quad (5\text{-}15)$$

Maximising the above equation gives $\mu_{K_0}$and σ_{K_0}.

5.7.5 Choice of statistical method

When toughness data is homogeneous, i.e. parent material of one ferritic material or PWHT weld, the basic master curve is a suitable choice (Sumpter and Kent, 2004). For inhomogenous test data, FITNET MC with censored values may be used for deterministic assessments. When toughness data has small inhomogeneity, i.e. parent material of low-quality production or as-welded weld metal and HAZ Bi-modal MC can be used to describe scatter of toughness (Sumpter and Kent, 2004). For random inhomogeneous material consisting of mixed data, MC with random inhomogeneities may be used to perform probabilistic fracture mechanics analysis (Sumpter and Kent, 2004). Summary of the methods are given in Table 5-1 below:

Method	Intended for	limitations
Basic MC	Macroscopic inhomogeneity, PWHT welds	Inhomogeneities
MC with censored	High homogeneity, lower bound estimate	Probabilistic assessment
Bimodal MC	Small inhomogeneities, HAZ, as welded weld	High inhomogeneity
MC with random inhomogeneities	High inhomogeneity, Mixed datasets	Complicated calculation

Table 5-1 Methods of describing toughness scatter

5.8 The Charpy impact testing

Estimation of Fracture toughness for fitness-for-service assessment is best done by the relevant fracture toughness testing, i.e. wide plate test, SENB, CT, etc., where the test can be designed adequately to represent the loading rate and constraint characteristics of the intended structure. An alternative test method is the Charpy impact test. The method is a high strain rate, blunt notch method and is based on measuring the energy absorbed by the standard specimen given the test specimen is fractured.

The standard for the test is to perform at least three tests at a required temperature determined by the relevant standard. If sets of three tests are available at various temperatures over the ductile to brittle transition region, a transition curve can be constructed using a curve fitting method. The fracture face test specimens may be assessed and the corresponding area of crystallinity which indicated the brittleness of the fracture could be estimated, as well. The Charpy test set up diagram, a test result fracture faces are shown in Figure 5-11 below.

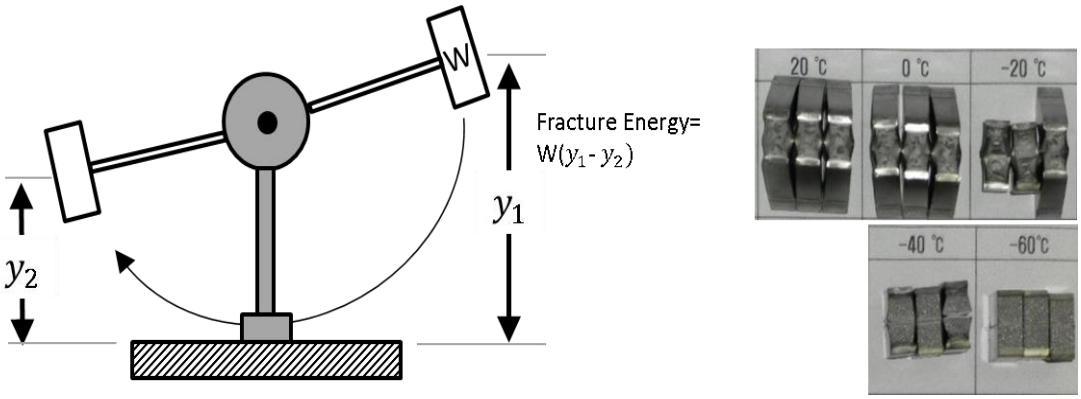

Figure 5-11 The Charpy test set up diagram (Left), fractured specimens (Right)

The Charpy impact test method suffers from a number of limitations such as having a fixed loading rate (impact), and blunt notch versus a sharp notch that may be

present in a real structure. Because of these limitations, this method is generally not preferred for fitness-for-service type assessments. The advantage of the Charpy test is that it is much cheaper and quicker than other toughness testing method. Hence, it is commonly used as a QA/QC tool to check materials fracture quality.

	Normal Steel				32				36				40			
Grade	A	B	D	E	AH	DH	EH	FH	AH	DH	EH	FH	AH	DH	EH	FH
Temperature	Not required	0	-20	-40	0	-20	-40	-60	0	-20	-40	-60	0	-20	-40	-60
Longitudinal	27				31				34				39			
Transverse	20				22				24				26			

Table 5-2 Charpy impact test temperature and acceptance criteria (Lloyd's-Register, 2015)

5.9 Analysis of Charpy data

When CVN (Charpy) data is available over the entire transition region, a sigmoidal function can fit the data. As it is shown by (Wallin, 2011) most of the sigmoidal function show similar fits and choice of sigmoidal function is less important than the fitting algorithm.

The widely used sigmoidal function is the hyperbolic tangent function (tanh), given in equation (5-16) (Wallin, 2011). In this expression, $C_{v\text{-}US}$ is a constant, temperature independent, upper shelf energy and can be estimated from analysis of impact energies corresponding to % 100 ductile fractures. C_{Vmin} is fixed lower shelf energy which can be conservatively fixed, e.g. 5J. Temperature-dependent description of lower and upper shelf can be made, but it normally involves significant uncertainty unless large data in these regions are available.

$$C_V = \frac{C_{V-US} - C_{Vmin}}{2} * \left(1 + tanh\left(\frac{T - T_{50}}{C}\right)\right) + C_{Vmin} \qquad (5\text{-}16)$$

A lower bound estimate of C_{Vmin} may also be estimated using equation (5-17) (Wallin, 2011).

$$C_{Vmin-LB} = 2.5J + \left(\frac{\sigma_Y}{460\ MPa}\right)^2 \qquad (5\text{-}17)$$

There are several different techniques to fit CVN impact energies to tanh function. Least square in relation to CVN (*E*) is the commonly used method. There are two other parameters for which least square analysis can be carried out. Those would be temperature and even distance from the tangent of tanh function. These three

options are visualised in Figure 5-12 below. For well-behaved transition curves, the different fitting procedures produce generally comparative results (Wallin, 2011).

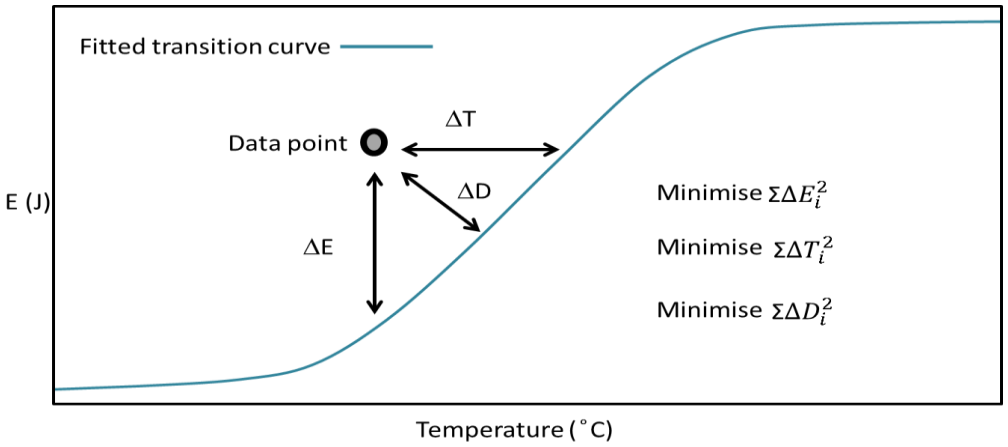

Figure 5-12 Possible fitting algorithms for CVN data (Wallin, 2011)

5.9.1 Indirect estimation of toughness from the Charpy energies

There are several fundamental differences between fracture toughness test and the Charpy-V test. The main differences are listed in Table 5-3 and presented schematically in Figure 5-13.

Difference	K_{IC},K_{JC}	CVN
Event pronounced in test	Fracture initiation	Fracture initiation+ Propagation
Specimen size	Variable	10X10X55
Flaw geometry	Deep crack	Shallow blunt notch
Loading rate	Quasi-static	Dynamic

Table 5-3 Key differences between toughness test and the Charpy test

Any attempt to correlate Charpy energy values with fracture toughness should try to minimise these differences. In Figure 5-13 the effect of these differences is schematised.

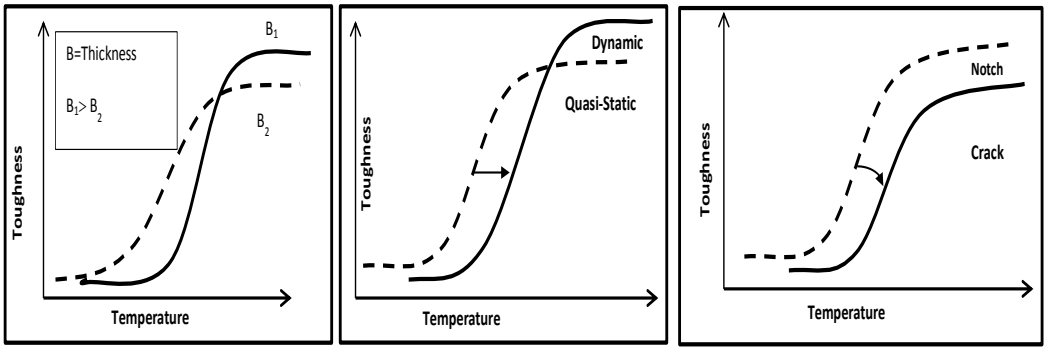

Figure 5-13 The effect of main differences between the Charpy test and fracture toughness

(Wallin, 2011) provides a comprehensive description of the studies that have attempted to correlate Fracture toughness tests results with Charpy test values. Correlation based on the Master Curve approach found to be the most suitable approach and is used in European standardisations and structural integrity methods of SINTAP and FITNET. It is done by correlating a chosen temperature from fracture toughness testing with a chosen temperature from Charpy-V testing. From fracture toughness point of view (see "Fracture toughness" section) it is recommended to choose a temperature corresponding to brittle fracture toughness. This temperature must be sufficiently low that the fracture is not affected by ductile fracture initiation and is significantly higher than lower shelf region, so that variation of absorbed energy by temperature is captured. One commonly used temperature fulfilling these demands is the Master Curve T_0 temperature corresponding to $\overline{K}_{JC} = 100\ MP\sqrt{m}$ for a 25 mm thick specimen. The $T_0$is preferable since it removes the effect of thickness. As the tempreture is chosen as the parameter to correlate in fracture toughness tests, it should also be chosen in Charpy-V tests as well. The selected temperature must, in addition to fulfilling the requirements of the fracture toughness test, correspond to low temperature, so that it is not affected by variations on the applied standards. Also, since ductile crack growth is not allowed, a temperature close to the lower shelf has to be chosen. Additionally, the temperature should correspond to the increasing part of the transition curve. It is also recommended to choose a commonly recognized energy level. One such temperature is T_{27}which is commonly used as a lower limit test requirement for Charpy testing in QA of steel.

5.9.2 Correlation equations

The basis of correlation procedures is estimating K_0in transitional and the lower transitional region from studied correlation equations and then to extrapolate the calculated K_0 to estimate K_{mat} in any given temperature using a valid models such as MC. The validity of these equations depends on the region of the transition curve where the temperature of the interest is located.

5.9.2.1 Transition region

The fracture toughness in the transition curve is described by the master curve as follows (BS7910, 2015 a):

$$K_{mat} = 20 + \{11 + 77e[0.019\,(T - T_0 - 9.5)]\}\left(\frac{25}{B}\right)^{\frac{1}{4}}\left[ln\left(\frac{1}{1-P_f}\right)\right]^{\frac{1}{4}} \quad (5\text{-}18)$$

T: is the temperature at which K_{mat} is to be determined (in °C). B is the thickness of the material for which an estimate of K_{mat} is required (in mm), P_f refers to the relevant percentile of the master curve at the temperature of interest. T_0 may be estimated from equation (5-19) for SENB tests and (5-20) and for CT tests, based on correlation of $T_{27J}$and T_0reported by (Wallin, 2011), which expresses that correlation between $T_{27J}$and T_0depends on σ_Y and upper shelf energy. (Wallin, 2011) analysed 510 different datasets, collected from various both actual fracture toughness and Charpy-V test results. The materials were all kinds of BCC steels including welds. (Wallin, 2011) analysed SENB and CT test data showing the dependency of the correlation on material yield strength and upper shelf energy and concludes that SENB and CT test data sets should not be pooled together.

$$T_{0-SENB} = T_{27J} - 87^oC + \frac{\sigma_Y}{12MP.\,^oC^{-1}} + \frac{1000J.\,^oC^{-1}}{C_{V-US}} \quad (5\text{-}19)$$

$$T_{0-CT} = T_{27J} - 77^oC + \frac{\sigma_Y}{12MP.\,^oC^{-1}} + \frac{1000J.\,^oC^{-1}}{C_{V-US}} \quad (5\text{-}20)$$

T_0 can conservatively be estimated using (5-21) below from annex J of (BS7910, 2015 b), as well:

$$T_0 = T_{27J} - 18℃(standard\ deviation = 15℃) \quad (5\text{-}21)$$

$$T_0 = T_{40J} - 24℃(standard\ deviation = 15℃) \quad (5\text{-}22)$$

5.9.2.2 Lower shelf and lower transition region

When Charpy tests values are available at the temperature of interest, fracture toughness in lower shelf and lower transitions region can be estimated using equation (5-23) below (Wallin, 2011) and (BS7910, 2015 b):

$$K_{mat} = \left[\left(12\sqrt{C_v} - 20\right)\left(\frac{25}{B}\right)^{0.25}\right] + 20 \quad (5\text{-}23)$$

K_{mat} is the estimate of the fracture toughness (in MPa√m), B is the thickness of the material for which an estimate of K_{mat} is required (in mm), C_v is the lower bound Charpy V-notch impact energy at the service temperature (in J) corresponding to 90% confidence and 5 percentile of the master curve at the test temperature. (BS7910, 2015 b) proposes that, when data is available at a single temperature, equation (5-23)

maybe used to calculate an initial K_{mat}, then using equation (5-18) K_{mat}at other temperatures may be evaluated. Similarly, T_{27J} can be calculated using estimated T_0 and one of the equations (5-19), (5-20), or(5-21). T_{40J}may be calculated using equation (5-22).

5.9.2.3 Upper shelf limit (ductile fracture)

In order to avoid overestimating fracture toughness from Charpy test values, correlated fracture toughness values are limited to the upper shelf limit. It is possible to drive a theoretical upper limit for upper shelf fracture toughness based on the total energy that is required to break the CVN test ligament. The total energy is equal to the work done by force P. P is approximately equal to:

$$P = \frac{(W-a)^2.B.K'}{W}\left(\frac{\Delta}{W}\right)^n \quad (5\text{-}24)$$

Where P is the force, W is specimen width, a is instantaneous crack size, B is specimen thickness, K' is a material constant, Δ is displacement, and n is the strain hardening exponent. The J-R follows approximately a power law like equation (5-25) below:

$$J = \frac{\eta \int_0^{\Delta} P.\partial\Delta}{B.(W-a)} = J_{1mm}.\Delta a^m \quad (5\text{-}25)$$

Where η is a constant number, m is J-R curve exponent and J_{1mm} is integral value at 1 mm crack growth. The total energy will be equal to:

$$E_{total} = \frac{J_{1mm}.B.b_0^{m+1}}{(m+1).1mm^m} \quad (5\text{-}26)$$

The above energy estimate will be a theoretical lower bound estimate of upper shelf CVN energy. In the real Charpy test, the blunt test and dynamic loading and friction effects will increase total absorbed energy. Additionally, J-dominance will be lost in fracture of the ligament which increases the required energy, as well. Thus, E_{total}should always be smaller than C_{v-us}. (Wallin, 2011) analysed 162 multi-specimen J-R –curve data sets, tested in room temperature to +100°C, the yield strength were varying between 171-993 MPa and the Charpy energies in the range of 20-300 J, and recommends equation (5-27) as a mean value estimate of J_{1mm} with a lower bound estimate given by equation (5-28). m is given as a function of upper shelf energies and σ_Y by equation (5-29). The materials included pressure vessel steels and their welds, but also some Duplex, stainless and cast steels.

$$J_{1mm} = 269\left(\frac{C_{v-us}}{100}\right)^{1.28} \quad (5\text{-}27)$$

$$J_{1mm-5\%} = 193\left(\frac{C_{v-us}}{100}\right)^{1.28} \quad (5\text{-}28)$$

Where J_{1mm} and $J_{1mm-5\%}$ units are in kJ/m^2.

$$m = 0.432\left(\frac{C_{v-us}}{100}\right)^{0.256} - \frac{\sigma_Y}{4664\,MPa} + 0.03 \quad (5\text{-}29)$$

(BS7910, 2015 b) combines equation(5-26), (5-28), and (5-29) and provides a lower bound estimate of upper shelf fracture toughness value using equation (5-30) below for modern low sulphur low carbon steels, based on estimating fracture toughness for the initiation of ductile tearing, defined as ductile crack extension of 0.2 mm, $K_{J0.2}(MPa\sqrt{m})$.

$$K_{mat} = K_{J0.2} = \sqrt{\frac{E(0.53\,C_{Vus}^{1.28})(0.2^{0.133C_{Vus}^{0.256}})}{1000(1-\nu^2)}} \quad (5\text{-}30)$$

Where, C_{Vus} is the upper shelf energies (J) corresponding to 100% ductile tearing appearance or 0% cleavage. *v* is the Poisson's ratio and E is the material's elastic modulus (MPa). For old high Sulphur steels that have potentially poor tearing resistance (BS7910, 2015 b) recommends equation (5-31) below, where $C_V$is the Charpy test energy (J) at the assessment temperature.

$$K_{mat} = 0.54\,C_V + 55\,(MPa\sqrt{m}) \quad (5\text{-}31)$$

For modern shipbuilding steels equation (5-27) and (5-30) are applicable.

5.9.2.4 Correlation with dynamic K_{ID}

(Rolfe and Barsom, 1977) recommends a method developed by the American Association of State Highway and Transportation (AASHTO) based on correlations from Nil-Ductility-Tests (NDT) and The Charpy tests for pressure vessels which has been adapted for bridges and ship details using experimental results and engineering judgment. The method estimates dynamic fracture toughness $K_{ID}$with a correlation equation given by equation (5-32) below.

$$\frac{(\mathrm{K_{ID}})^2}{\mathrm{E}} = 5\,(\mathrm{CVN}) \quad (5\text{-}32)$$

Where $K_{ID}$is in $psi\sqrt{in}$, and CVN is in $ft - in$. Similar to accounting for effect of dynamic loading rate, which was explained in section "Loading rate", the K_{IC} can be estimated using temperature shift equation (5-33).

$$T_{shift} = 215 - 15\sigma_Y \quad (5\text{-}33)$$

The advantage of this method is that provides a direct correlation of CVN with dynamic fracture toughness and only one variable, i.e. notch acuity, contributes to the uncertainty of correlation, hence when dynamic fracture toughness is required this method is more straightforward and possibly more accurate. In this chapter methods proposed by (Wallin, 2011) are used, instead.

5.10 Fracture toughness data set used in this research

Fracture control in ship construction is mainly done by fracture quality control of steel using Charpy impact testing as this type of data is more available than fracture toughness data. As explained earlier fracture toughness is inherently very scattered hence small size of test samples from one particular steel manufacture and a single batch of steel is not statistically reliable. In this research, as it is listed in Table 5-4 and Table 5-5, about 1500 Charpy impact test results from of seven manufacturers from Europe and the far east was gathered. The variety of the sources and the big sample size was very much in line with the objective of this chapter which is the probabilistic analysis of fracture toughness for ship grade steels. In this approach quantifying measures of scatters for input data are perhaps more important than determining the absolute value as opposed to conventional fracture mechanics for which the main objective is to estimate a conservative lower bound of data from the observed test. This is very much related to the fact that major fracture mechanics procedures are meant to be used in nuclear industry in which consequence of failure is very severe.

Manufacturer ID	1	2	3	4	5	6	7
Country	China	China	Japan	Korea	UK	UK	Belgium
Year	2012	2015	2016	2011	2004	2014	2014

Table 5-4 List of manufacturers codes, origin and the year of steel productions

The analysed data comprises Charpy values for AH36 grade steel, used in the midship area, grade A steel, used in outside midship for passenger ships, and SAW and FCAW weld Charpy tests. The detail of the data set is given in Table 5-5. The Z-quality steel which applies to joints requiring through thickness strength (z-direction), i.e.

Cruciform joints in offshore structures have been excluded, whenever toughnesses were pooled, but was analysed individually on an ad hoc basis.

Steel Type	Normal steel Grades			High strength Steel Grades						Weld (FL)		
Steel grades	A			AH36						SAW, FCAW		
Manufacturer code	#5	#6	#7	#1	#4	#3	#5	#6	#7	#1	#2	#4
Sample size	69	21	767	12	24	12	122	303	131	12	6	12
Sample total	857			604						30		
Data over the whole transition curve	No	No	No	No	Yes	Yes	No	No	No	No	No	No

Table 5-5 Details of the data set

5.11 Analyses of scatter

Fracture toughness data is scattered due to the randomness of locations a crack tip may sample. The randomness may be due to three primary sources: first, the inherent randomness of a carbide inclusion distributed in the structure: Cleavage fracture happens at carbides or non-metallic inclusions that are randomly distributed throughout the component. This randomness causes variability in fracture toughness (ASTM, 2016). As the crack propagates, there is a respective probability of encountering a weak link which leads to cleavage failure. This variability and its corresponding uncertainly is characterised by the master curve approach, explained in "Statistical treatment of fracture toughness data" section. Additionally, there is a possible variability of fracture toughness between two different batches of steel. In ship structures it is very common that a crack grows to more than a metre long before it reaches a critical length, meaning that the crack may initiate in one plate and fail in another. Additionally, the shipbuilder may source its steel from several independent manufactures, and the fracture toughness may differ again due to the variability of the steel supplier. In the coming sections, shipbuilding steel grades from several steel manufacturers are compared, and the variation of fracture toughness across sources is studied. Furthermore, the variation of fracture toughness against the variation in steel batches is studied.

5.11.1 Scatter of toughness among manufacturers

The dataset Charpy (CVN) results at the test temperature were studied. The test temperature was 0(˚C) for AH 36 grade and 20(˚C) for A grade. The data appears to be fitted reasonably well by a normal distribution since it belongs to the upper

transitional region. Mean, standard deviation and coefficient of variation (COV) of CVN test results for each manufacturer were calculated and are given in Table 5-6 below. Additionally, standard errors of the parameters are calculated to give a measure of statistical uncertainty due to the size of the sample.

Steel Grade	Manufacturer	MU		Std		Sample size	Detail	COV	Pf (at 97.5 % confidence)
		mean	St. error	mean	Std. error				
AH36	1	122.9	9.91	34.34	7.49	12		0.28	0.088
	3	113.1	5.12	17.75	3.87	12		0.16	0.007
	4	372.2	4.03	19.74	2.94	24	Removed	0.05	7.822 e-34
	5	133.6	3.056	33.76	2.2	122		0.252	0.006
	6	128	2.45	42.61	1.74	303		0.33	0.024
	7	175.3	3.386	38.75	2.414	131	Average of three tests	0.22	8.9 e-4
A	5	130.5	3.54	29.46	2.53	69		0.23	0.002
	6	124	2.106	9.65	1.56	21		0.08	4.9 e-12
	7	228.8	1.26	34.91	0.89	767	Average of three tests	0.15	2.4 e-8
Weld (weld metal)	2	187.3	6.45	22.35	5	12	SAW	0.12	5.44 e-5
Weld (Fusion Line)	2	224.4	13.4	46.4	10.43	12	SAW	0.2	0.012
	1	175.6	8.3	20.34	7.23	6	FCAW	0.11	0.004
	4	181	0.026	11.7	4.16	6	FCAW	0.06	3.6 e-7
		267	39.27	96.2	34.2	6	SAW	0.36	0.2

Table 5-6 Fracture toughness Statistics from various manufacturers

For AH 36, the COV ranges from 16% to 33% across the manufacturers, and is on average 26%, and is analogous to the constant 28% COV of the master curve. Mean, standard deviation and COV of the mean values are calculated for each steel grade and weld process, and are presented in Table 5-7. The mean COV value for AH 36 is 16% which is significantly lower than the COV of each manufacturer indicating less variability between steel products than the variability that exists within the products of any manufacturer. The mean COV for A steel grade is 30% which is higher than the 16% mean of COVs from Table 5-6 indicating greater variation among manufacturers than the variation within products of any manufacturer. This is mainly due to considerably higher mean values from manufacturer #6. If manufacturer #6 is

removed he mean COV will be reduced to 2% which indicates almost no variation, however removing manufacturer #6 will reduce the data set to only two manufacturers and decreases statistical confidence radically.

Mean COV values for welds are considerably lower in variation compared to variation among test pieces suggesting a possibly small effect of weld quality from different workshops, however it should be noted that the weld tests are for certificate testing and generally of much better quality than a shipyard weld quality and may not be a true representative of a real cases. Also, the sample size may have affected the small variation seen in weld sepecimens toughness. Notice that as given in Table 5-5, the weld data is from 2 manufacturers and in sample sizes of 12, 6 and 12 (30 in total), but the parent material data is from 3 and 6 manufacturers and total of 857 and 604 test specimens for grade A and grade AH36, resepectively.

Material	Mean	Standard deviation	COV
AH36	134.55	21.44	0.16
A	161.13	47.96	0.30
Welds SAW	245.7	21.3	0.08
Welds FCAW	178.3	2.7	0.015

Table 5-7 Statistics of fracture toughness for AH 36, A and Welds (Calculations based on mean values from each manufacturer)

5.11.2 Scatter across steel batches

As discussed in the section “Scatter of toughness among manufacturers”, analysed Charpy test data in the transition region shows a variation ranging from 11% to 36%, regarding COV. Part of this variation is due to variability of steel products from different manufacturers which was studied in “Scatter of toughness among manufacturers” section. The rest of the variation could be due to the variation of toughness among different batches of steel and the variation within one batch of steel due to the randomness of carbide and inclusions fracture initiation site in a component. The latter is theoretically quantified by the MC approach explained in “Master curve” section. The master curve approach uses a Weibull distribution with the shape parameter of 4 (k=4) to represent the above randomness. The Standard deviation (S.D) and Mean values of the Weibull distribution are equal to:

$$S.D_{Weibull} = \sigma = \lambda * \sqrt{\left[\Gamma\left(1+\frac{2}{k}\right) - \left(\Gamma(1+\frac{1}{k})\right)^2\right]} \qquad (5\text{-}34)$$

$$Mean_{Weibull} = \lambda * \Gamma\left(1 + \frac{1}{k}\right) \quad (5\text{-}35)$$

Hence, the coefficient of variation (COV) for the master curve (k=4) will be:

$$CV_{MC} = 0.281 \quad (5\text{-}36)$$

It should be noted that this is a theoretical value under the assumption that Weibull distribution fits perfectly to the data with the shape factor of 4. In reality, only fracture toughness in lower transition and lower shelf region where cleavage dominates the fracture is best described by Weibull distribution. Shape parameter is taken as the constant value of 4 to aid analysis of small sample size data. Overall, calculated $CoV_{MC} = 0.281$ is a good reference point to assess data variability.

5.11.2.1 Scatter at the test temperature

First, the average toughness of each batch was calculated, then, the COV of the averages was calculated. Here, COV represents the variation of toughness among batches. This is given in column six of Table 5-8 below. Then the COV for each batch was calculated using test results, representing COV within each batch. This is given in column 7. The average of COVs was then calculated to estimate a mean value for variations across batches and is given in column seventh of Table 5-8. The total variations can be estimated by vector summation of the two columns. $COV_{total} = \sqrt{COV^2_{All\ batches} + COV^2_{each\ batch}}$.This is shown in Table 5-8. Total COV should be approximately equal to the corresponding values in Table 5-6.

1	2	3	4	5	6	7	8
Manufacturer	Temp.	Batch	Set of three tests	Std. Error	COV of average of each batch	Avg. of COVs between batches	Total COV
1	0	4	4	17.5	0.25	0.11	0.27
3	0	2	4	6.58	0.10	0.11	0.15
4	0	4	8	4.83	0.04	0.03	0.05
4	*-20*	4	8	19.6	0.19	0.28	0.36
5	0	44	44	5.06	0.25	0.04	0.25

Table 5-8 steel batches variation of toughness (average of three tests data)

COV within each manufacturer ranges from 1% to 25% except for manufacturer #4 which has a very low COV of 3% this due to high fracture toughness of this steel type with Z-quality meaning that toughness at 0 °C belong to the upper shelf for this product. This is very clear in Figure 5-14. Thus, it was decided to analyse toughnesses

at -20˚C which is located at upper transition region for this particular product. COV between batches ranges from 0.04 for manufacturer #5 to 28% for manufacturer #4. Manufacturer #4 has a COV of 28% which is comparable to theoretical value based on the master curve. Manufacturer #5 has an average COV of 4% in every batch which may mean either unusual homogeneity for each component or being from the upper-shelf region. The latter is disregarded as the ranges of toughness's are in a range common to the transitional area. All total COVs are consistent with Table 5-6.

5.11.2.2 Scatter of the transition curve

In the previous section, scatter of toughness at a single temperatures were studied. When data over the entire transition region is available, it is advisable to use the transition curve to estimate fracture toughness, particularly when the temperature of the assessment point is different from the test points. Unfortunately, such data is not always available. Charpy impact testing is usually performed as a part of the steel grade certification process and on a QA/QC basis.

Data from only two manufacturers contained test results over the transition curve: Data from manufacturer number 4 for a Z-quality AH 36 grade and manufacturer number 5 for ordinary shipbuilding AH36 steel grade. Transition curves and the data point are shown in Figure 5-14, Figure 5-16 and Figure 5-15. Figure 5-14 shows the best fit distributions, using a Weibull distribution, at test temperatures along the transition curve. At -20˚C material is in upper transition zone where a significant saccert exists due to the fact that some specimens fail in brittle manner and the rest fail in a ductile mode showing charpy energies equal to uppershef values. A more appropriate distribution to model such behaviour would be to use a bimodal distribution (Peterlik and Loidl, 2001), as shown in Figure 5-14 for tests at -20˚C. The bimodal Weibull distribution can be defined using equation (5-37) below:

$$P(J) = 1 - P_{Brittle} * exp\left[\left(-\frac{J}{\lambda_{Brittle}}\right)^{K_{Brittle}}\right] - (1 - P_{Brittle}) * exp\left[\left(-\frac{J}{\lambda_{Ductile}}\right)^{K_{Ductile}}\right] \quad (5\text{-}37)$$

Where, $P_{Brittle}$ is the number of specimens failed in brittle manner to the total number of specimens, $\lambda_{Brittle}$and $K_{Brittle}$ are scale and shape parameters of the brittle part of the distribution and $\lambda_{Ductile}$and $K_{Ductile}$ are scale and shape parameters of theductile part of the distribution.

Primary objective for constructing a transition curve is to estimate T27 temperature, which will then allow us to correlate this temperature with T0 and then combined with the master curve approach estimation of fracture toughness at any point along the transition curve is possible. *T27* is a good measure of cleavage fracture and is the temperature at which charpy enegy is equal to 27 J. Here, in order to investigate the variability of toughness among different batches of steel for specified manufacturers, the variability of *T27* is studied.

Data from manufacturer #3 for AH36 grade is available at -20, 0, and +20˚C. The data set comprises data from two batches. The best fit transition curve was estimated using a least square fit method described in "Analysis of Charpy data" section. Mean transition curve parameters T_{50}, and C and their upper and lower bound values with 95% confidence bounds were calculated. The best fit curves for two batches and for pooled data are shown in Figure 5-15. 90% prediction observations bounds are plotted in dashed lines.

Corresponding *T27* values were then calculated using the estimated parameters and are given in Table 5-9. Similar to the method used in "Scatter at the test temperature" variation of fracture toughness is examined by calculating COV of *T27* for each batch of steel, then calculating the mean value of COVs and *COV* of mean *T27*s. Mean of COV measures the average variation of T27 in each batch and COV between batches shows how much mean T27s vary between batches. The total COV is the vector sum of two values.

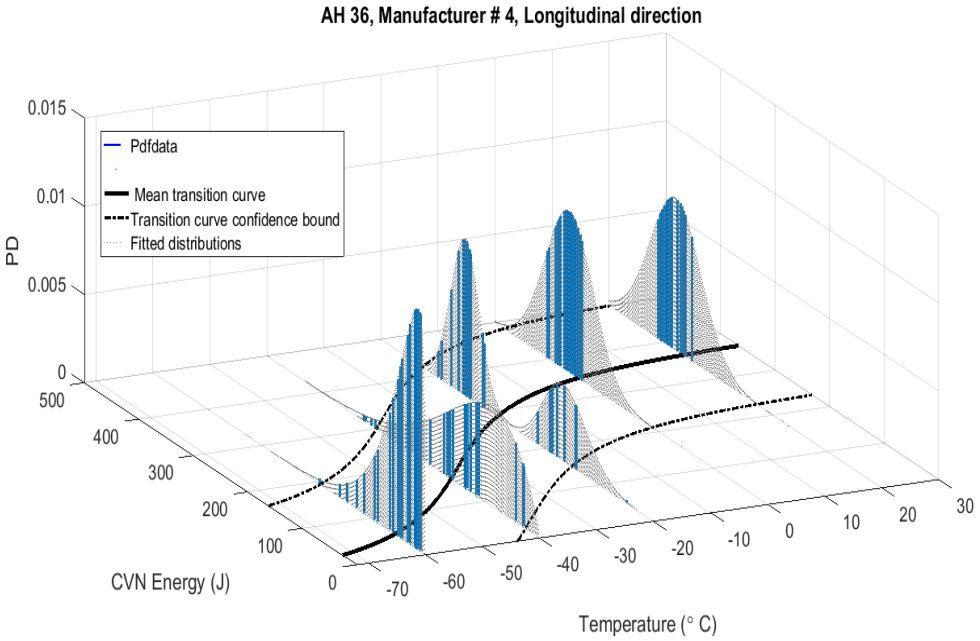

Figure 5-14 Transition curve for z-quality steel

		Sample	T27			Mean of COVs	COV between mean of batches	Total COV
			Mean	LB	COV			
1	Batch 1	6	-43.75	-27.42	0.19	0.22	0.24	0.32
2	Batch 2	6	-71.75	-36	0.25			

Table 5-9 T27 Variation of steel batches for manufacturer #5 (Transition curve analysis)

It can be observed that variation in batches and between the batches are both more than double the COVs calculated in Table 5-8. This is because the method essentially fits the curve in test temperature points and extrapolates the curve to *T27* temperature. Because test temperatures are far from the lower shelf and lower transition region the variation is amplified. Notice that the variation is lower in regions between test temperatures. Another reason for this variation is the small size of the data set used in the calculation of COV; we are essentially comparing two data point (2 batches). The effect of apparent high variation in COV is diminished when *T27*s are used in master curve (equation (5-18)) to estimate fracture toughness as the equation has an exponential form and the variation of calculated fracture toughness will be close across transition region.

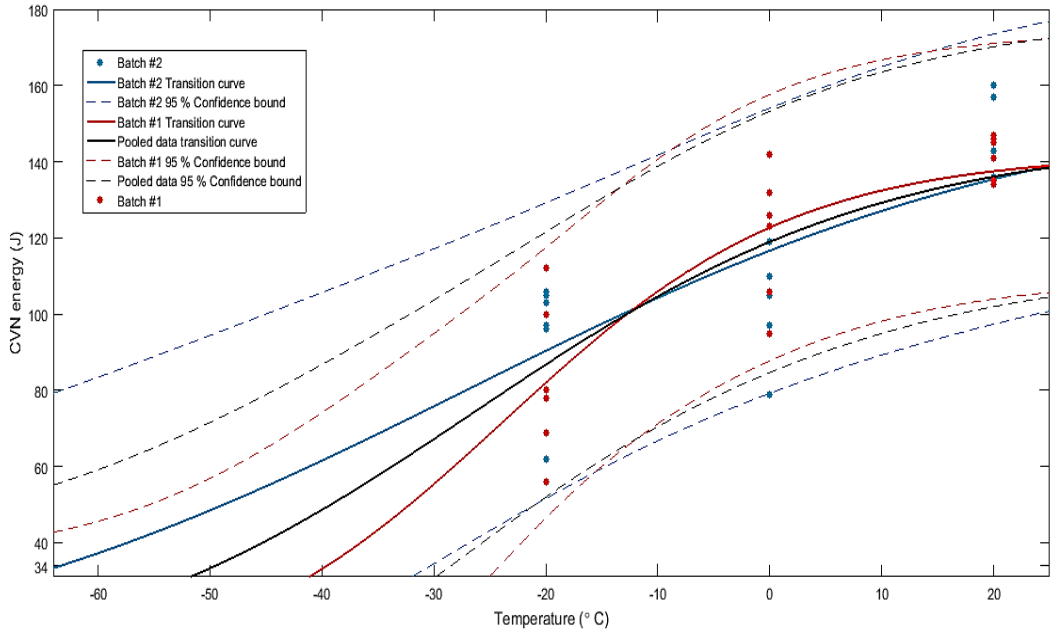

Figure 5-15 transition curve of manufacturer #3 and different batches

Similarly, data from manufacturer #4 were analysed. The results are presented in Table 5-10. Unlike manufacturer #3, the estimated variation of *T27*s is comparable to the variation of Charpy values at -20˚C given in Table 5-8. The reason appears to be larger sample sizes of curves (eight independent batches for manufacturer # 4 compared to 2 batches for manufacturer # 3). Another possible reason is additional test data in lower shelf region at -60 and -40˚C which makes fitted curves closer in

the lower shelf region. The fitted curves are plotted in Figure 5-16. Notice that estimated *T27*s are much closer to data points (lowest being -60˚C) for manufacturer #5 than for manufacturer #3.

	Batch	Thickness of parent plate	Position	T27			Mean of COVs	COV between mean of batches	Total COV
				Mean	LB	COV			
1	Batch 1	12. mm	Top	-60.97	-42.23	0.16	0.19	0.21	0.28
2	Batch 2	12. mm	Top	-53.85	-31.51	0.21			
3	Batch 3	20 mm	Top	-86.27	-29.26	0.34			
4	Batch 4	20 mm	Top	-61.33	-46.73	0.12			
5	Batch 1	12 mm	Bottom	-76.41	-48.46	0.19			
6	Batch 2	12 mm	Bottom	-46.52	-33.54	0.14			
7	Batch 3	20 mm	Bottom	-88.55	-47.86	0.23			
8	Batch 4	20 mm	Bottom	-82.62	-58.28	0.15			

Table 5-10 Variation of T27 across steel batches for manufacturer # 4 (Transition curve analysis)

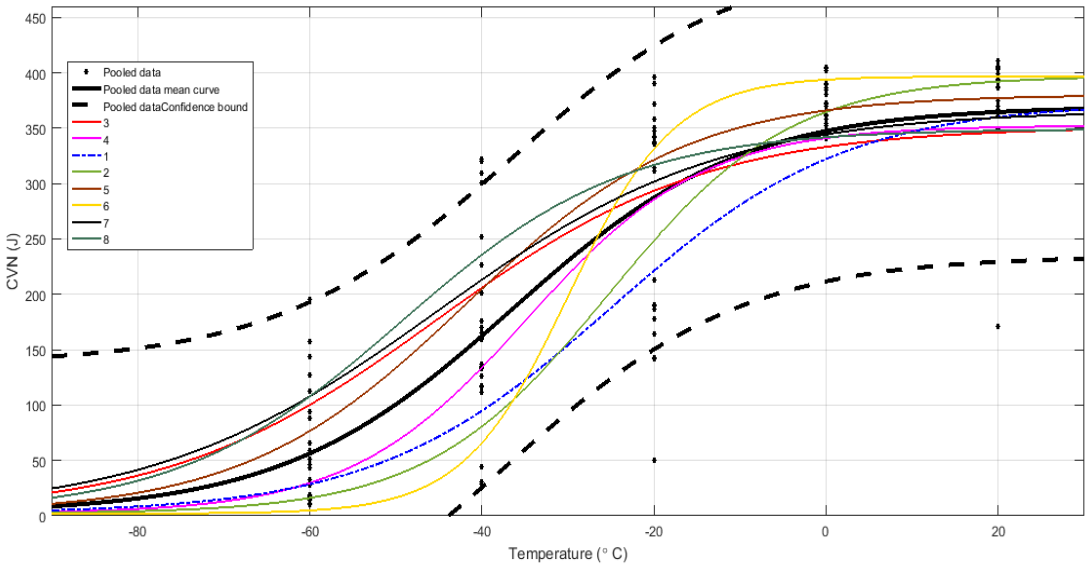

Figure 5-16 Transition curves of manufacturer #4 batches (90% prediction bounds)

5.11.3 The conclusion from analyses of fracture toughness scatter

The master curve approach, a widely adopted approach in modelling scatter of fracture toughness, assumes a constant 28% coefficient of variation. Although scatter due to variation in steel batches is real the combined calculated scatter due to the inherent randomness of carbides and variation in batches were found to be below 28%. Hence, the Master curve COV appears to be a reasonable upper bound value to represent the scatter of toughness in steel products from individual manufacturers.

Mean fracture toughness can vary significantly among manufacturers this was estimated by 16% COV in AH36 and 30% COV in A grade, although the calculated value for A grade is less certain due to small sample size. The variation is very small for the welds tested although the weld test results are not considered to be a good representative of real life weld joints.

5.12 Fracture toughness

Charpy impact energies cannot directly be used in fracture mechanics assessment. Fracture toughness may be calculated from the Charpy energies using the methods explained in "The Charpy impact testing" section. When information over the whole transition curve is available *T27* is calculated from the best fit transition curve. Then *T0* is estimated from *T27* using equation (5-21)or (5-19). Finally, fracture toughness is estimated using equation (5-18). When sufficient data points over the entire transition curve are not available, *T27* cannot be directly calculated from Charpy test results. In this situation (BS7910, 2015 b) recommends an alternative method first to calculate fracture toughness at test temperature using equation (5-23) then calculate *T27* using equation (5-18). Finally, fracture toughness at any temperature can be estimated using the calculated *T27* and equation (5-18). The fracture toughness from the data set was estimated, and the results are given in Table 5-11.

Steel Grade	Manufacturer	K_{mat} $(MPa\sqrt{m})$	Temp. (°C)	T27		T34	T40
				Median	5th percentile	Median	Median
AH36	1	353.0	0	-49.6	-21.1	-46.6	-43.6
	3	330.9	0	-44.0	-16.7	-41	-38
	4 (Z- quality)	539.5	-20	-76.1	-47.5	-73.1	-70.1
	5	367.4	0	-54.6	-25.4	-51.6	-48.6
	6	363.8	0	-50.9	-21.9	-47.9	-44.9
	7	421.8	0	-59.8	-27.9	-56.8	-53.8
A	5	361.2	20	-21.3	0.9	-18.3	-15.3
	6	342.8	20	-15.2	5.9	-12.2	-9.2
	7	479.6	20	-36.9	-9.3	-33.9	-30.9

Table 5-11 Fracture toughness of analysed data

Median fracture toughness of high strength grade AH36 steel ranges from 330.9 to 421.8 $MPa\sqrt{m}$ at 0 °C temperature, excluding the data from manufacturer #4. Normal steel grade grade A steels showed 361-479.6 $MPa\sqrt{m}$ median fracture toughness values. Median values of all tested high strength grade A steel (AH36) meet

toughness criteria for DH36 and EH36 grades. Median values for all normal A grade steels meet toughness criteria for grade B, additionally, those steels from manufacturer #5 and #7 meet the criteria for grade D steel. For the Charpy impact test acceptance criteria see Table 5-2. It should be noted that these are median values (50% cumulative) and does not mean that all the test results will meet the criteria for higher grade steel; however, it gives a good insight about the typical quality of steel productions. For comparison purposes, the 5th percentile values are given, as well. Lower bound 5 percentile values for AH36 data meet DH grade criteria in most cases, apart from manufacturer #3. The shipyard that builds the case study cruise ships uses manufacturer #5 to supply its steel. The corresponding cumulative fracture toughness probability distribution at (0˚C) for AH36, used in the midship area, and A grade steel, used outside midship area are plotted in Figure 5-17 below.

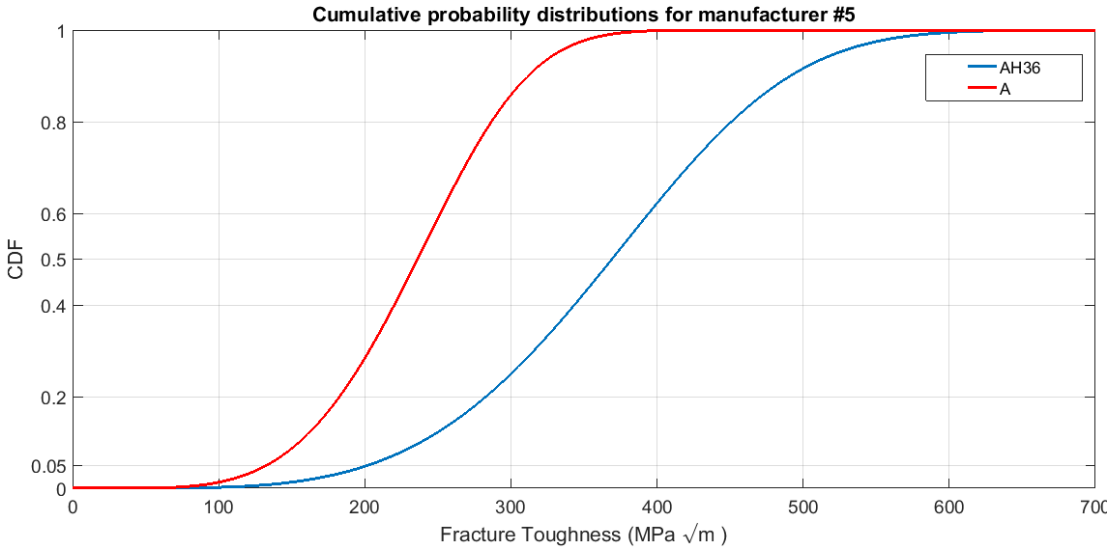

Figure 5-17 Steel toughness distribution for manufacturer # 5 at (0˚C)

5.13 Fracture toughness and steel quality

(Sumpter and Kent, 2004) showed that there is a correlation between steel fracture quality and the probability of brittle fracture. They compared the probability of failure against casualty rate merchant ships. The key input in their study was fracture toughness of shipbuilding steel as a function of year of manufacture. They showed that a reduction in ship casualty rate has an identical gradient as their calculated failure probability given the fracture toughness at any year since 1947. This suggests that ships built recently may have a lower probability of failure provided that the steel quality has improved further. To study this historical fracture toughness data reported by (Sumpter and Kent, 2004) and the fracture toughness estimated in this

work are pooled in one dataset and it is observed that the improvement in fracture toughness follows a similar trend as the data reported by (Sumpter and Kent, 2004) but, has not changed since 2000 . The fracture toughness trend versus year of manufacture is plotted in Figure 5-18 along with a trend line fitted by the least square method. The fracture toughness data from the Liberty ship period has been excluded from the regression as they are significantly lower than the rest of the dataset. It is interesting to note that the range of toughness from Kurdistan tanker lies within the estimated value distribution at the year of construction in Figure 5-18 within one standard deviation of the data above the mean line. The ship was built in 1973 and the *T27* at the time of the incident was estimated 5-20 ˚C ("KurdistanTWI," n.d.), and (Garwood, 2001).

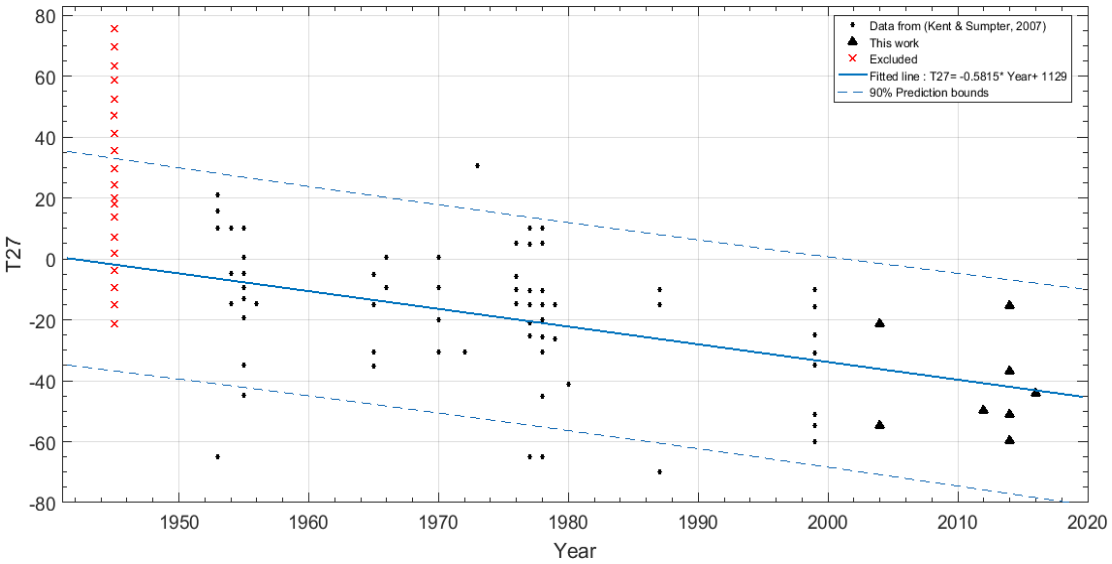

Figure 5-18 Trend of fracture toughness versus year of manufacture

5.14 Chapter summary and conclusion

The presence of a sharp defect combined with low fracture toughness in a ship's hull can cause brittle a fracture. A classic example of this type of failure with a high consequence of failure is the failure of the Kurdistan tanker. The vessel had brittle fracture toughness temperature above ambient temperature and a small weld defect led to the loss of the vessel. Three broad strategies can reduce the probability of brittle fracture, i.e. stresses heat treatment, reducing defects in the structure using NDT or improving the fracture toughness of the steel by manufacturing better quality steels. It was shown by (Sumpter and Kent, 2004) that the fracture toughness of grade A steel has been improving from 1947 to 2000 and resulted in a reduction in ship incidents caused by fracture. Fracture quality of the steel should affect the acceptable

build quality and the extent of NDT during build and through life. For the same through life inspection, a ship that is built with lower fracture toughness than the norm should contain fewer defects to compensate its relative low toughness, and a ship with better steel quality may be tolerant to more or larger defects. This could be quantified using a BS7910, 'Fitness for purpose', approach but historically the steel quality and inspection requirements for ship structures have not been linked.

In this chapter first fracture toughness, parameters affecting fracture toughness relevant to ship structures and different measures of fracture toughness were introduced and methods of testing these measures were reviewed. Then methods of probabilistic assessment of fracture toughness were reviewed.

- Fracture toughness test data can be very narrow banded with a small coefficient of variation and may appear to be best fitted with a normal distribution. However, this should be treated with care as it will result in negative fracture toughness values and consequently incorrect probability of failure in reliability analysis.
- An alternative distribution is a Weibull distribution which has shown to be a good fit with nonnegative values is the Weibull distribution.
- A method developed by Kim Wallin has been widely adopted by standards such as (ASTM, 2016), and (BS7910, 2015 a) and is called Master Curve approach, which describes the scatter of toughness data for a given temperature using a three-parameter Weibull distribution. The shape parameter is fixed to 4 and a location parameter of 20 $MPa\sqrt{m}$ as a minimum toughness value is assumed.
- A bimodal master curve which is a combination of two separate Weibull curves may be used when the data shows two separate peaks. This was observed in this research for a Z-quality AH36 steel at upper transition region (Figure 5-14).

The master curve (MC) is intended to describe the randomness of carbide inclusions in the material which is believed to cause cleavage fracture. The MC has the shape factor of 4 meaning that the coefficient of variation for MC is equal to 28.1%. For reliability analysis, it is necessary to quantify variation of fracture toughness within a vessel as a whole or a fleet of ships. In this research variation in toughness of A and AH36 steel grades were analysed to study the variation of fracture toughness within

individual batches of steel, among several steel batches and across products of several manufacturers from around the globe.

- Charpy impact tests of seven manufacturers from Europe and the Far East were analysed. All steel products were manufactured between 2002-2015.
- The valid average COV within batches ranged between 10%-25%, which is lower than the COV of the MC, indicating the MC is a good conservative model.
- The variation between batches was observed to be as small as 3% up to 28% and generally lower than variation within batches indicating the variation of fracture toughness due to the randomness of carbide inclusions is more dominant.
- Total coefficient of variation ranges between 5%-36%. An expected a value of the total coefficient of variation of 26% is a reasonable estimate. It shows that the master curve approach, with a *COV* of 28%, is a reasonable model to represent the scatter of fracture toughness even throughout the entire structure made of several hundred batches of steel. Where higher variations are expected for example in the upper transition area, a Bi-modal master curve may be used.
- Variation between manufacturers *COV* for AH36 grade was found to be 16%. For grade A the variation is almost twice for AH36 and is 30%. Although the sample size is smaller and only three manufacturer are compared where one of the manufacturers are having unusual mean Charpy values almost 65% higher than two others. The reason is believed to be the fact that steel products are tested for AH grade and by failing the strength criteria are declassed as A grade. Low COV values for weld specimens were observed. 1.5% for the FCAW and 5% for the SAW.
- Data from two manufacturers were available in more than one temperature which allowed estimation of *T27* temperature by fitting a hyperbolic arctan curve using regression analysis. For the well-behaved data from manufacturer number 4, the variations of *T27* were comparable with the variation of test results at the test temperature.

T27 values for the specimens were estimated using the procedure recommended in (BS7910, 2015 a) and median fracture toughness values were calculated using a

modified procedure which uses a more precise correlation equation based on (Wallin, 2011). It was found that:

- Median fracture toughness values from all manufacturer met higher grades than AH36 and A. All tested AH36 grades met criteria for EH and two out of three A grades met criteria for D grades generally indicating very good quality. Lower bound 5 percentile values were compared, as well, and for AH36 data found to be meeting DH grade criteria in most cases.
- The calculated fracture toughness was compared with historical data reported by (Kent and Sumpter, 2007) and it was found that fracture quality has not changed since 2000 and is compatible with the trend predicted by (Kent and Sumpter, 2007).

The fracture toughness calculated in this chapter will be used in reliability assessment. Manufacturer #5 provided steel for the shipyard where the case study ship was built and this data will be used for the reliability assessment.

The fracture toughness data analysed in this chapters are gathered from steel providers and not collected at the shipyard. Such data, in principle, should be available as part of material quality control programs. As the value of such data is highlighted by this research, it is suggested that the shipbuilders keep record of such data and analyse them using the procedures outlined in this chapter for reliability analysis or fracture mechanics analysis which can be utilised for safety case assessments and reliability centred inspection planning.

If no ship-specific data is available for selecting material properties for reliability assessment it is suggested that the data provided here be used. Alternatively, the minimum required values specified by the classification societies can be used as lower bound estimates. But as it is shown in this would be a conservative assumption which is likely to result in over conservative assessments.

Chapter 6

Reliability Calculation

6.1 Chapter Outline

The principles of reliability analysis of the structures containing defects were outlined in chapter 3. Probabilistic analysis of two key inputs in the reliability analysis, namely defect size and frequency, and toughness were discussed in chapters 4 and 5, respectively. In this chapter structural reliability due to the presence of weld defects in ship hull structures is investigated:

- Principles of fatigue analysis using the S-N curve method, its applications and limitations are explained.
- Fracture mechanics analysis of planar defects and the underlying theory is described.
- Two fatigue and fracture mechanics reliability algorithms developed in this research are explained, and their merits, limitations and applications to this work are discussed.
- Different identified modelling uncertainties that may affect the calculated reliabilities are discussed, their impacts on the failure probabilities are investigated, and the appropriate models or values are recommended.
- Study cases of two critical joints are discussed:
    1. The deterministic analysis of a fillet weld, joining the stiffener to the plate.
    2. The probabilistic analysis of a butt weld, joining deck plating of two grand-blocks.
- The effect of NDT methods and defect frequency (rate) on the reliability of the deck structure is studied.

This chapter concludes the work on the reliability assessment and the results will be used in chapter 7 and 8 of this thesis.

6.2 Limit state function

The limit state function of the failure due to cyclic stress is referred to as fatigue limit state. There are two approaches in fatigue assessment of structure; the S-N curve approach and the fracture mechanics approach.

The S-N curve approach is based on results from endurance testing of the structural details. The test specimens are tested under constant amplitude stress levels, S, until a failure occurs after a number of cycles, N. The test is repeated at different stress levels for a specific minimum number of tests. Figure 6-1 shows a schematic example of an S-N curve. The fatigue testing procedures for producing S-N curves and statistical treatment of test data can be found in fatigue textbooks such as (Milella, 2012). Additionally, standards such as (BSI:SO-12107, 2012) provide guidance on statistical planning and analysis of data for fatigue testing of mettalc materials to consider variation of fatigue test data perfomed in laboratories.

The major limitation of the S-N curve approach is that it is not applicable to the structures containing a defect of significant size. Specimens used in generating S-N curves are required to be free from significant defects. In particular, they need to be inspected by surface NDT prior to fatigue testing. The range of crack sizes that are believed to cause fatigue failure in such tests are between 0.05 to 0.2 mm and are mainly toe undercuts (Jonsson et al., 2013)and (BSI7608, 2015). Fabrication defects detected in ship structures are much larger than this size range (mean length around 20 mm) and thus beyond the scope of the S-N curve approach. However, reliability analysis using the S-N curve method can provide information about the intended target reliability of the joint, and is briefly discussed in the next section.

The fracture mechanics approach is specifically applicable to assessing the possible failure of structures containing planar defects.

6.3 Reliability analysis based on S-N curve

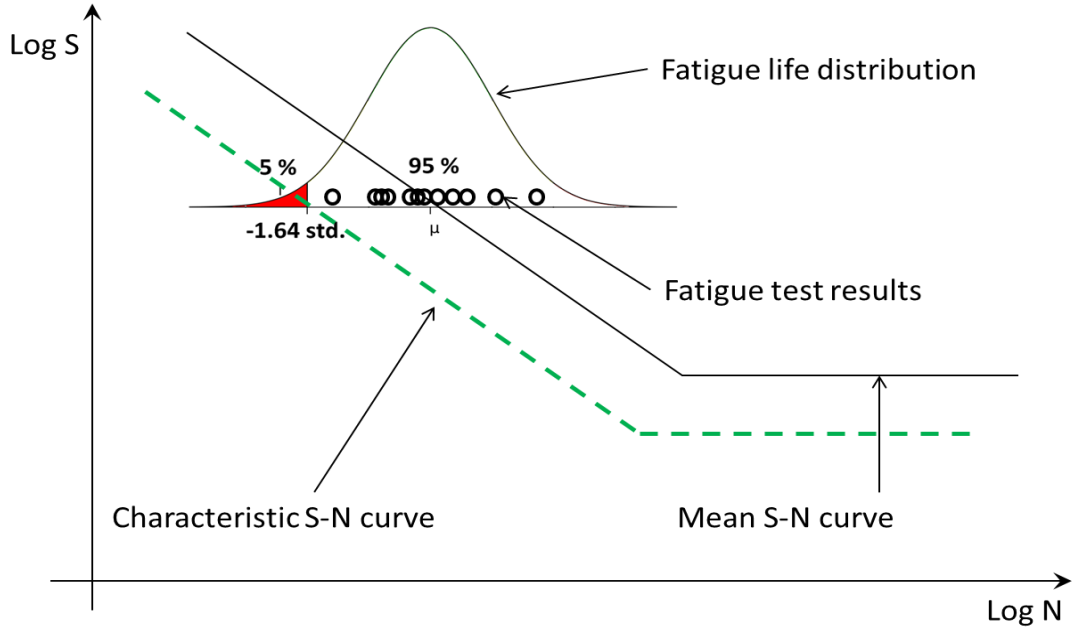

Figure 6-1 Schematic illustration of the S-N curve

The equation for a characteristic S-N curve is given in equation (6-1) below, which relates the number of cycles to failure to the corresponding stress amplitude. Where m and a are properties of the chosen S-N curve (m is the inverse of the negative slope of the curve). The fatigue strength of welded joints is to some extent dependent on plate thickness. This effect is due to the local geometry of the weld toe in relation to the thickness of the adjoining plates. The thickness effect is accounted for by a modification on thickness larger than the reference thickness t_{ref}. (DNV, 2010) recommends t_{ref} equal to 25 mm for welded connections other than tubular joints. The thickness exponent k is considered to account for the different size of the plate through which a crack will most likely grow; k is equal to 0.15, 0.20, and 0.25 depending on the design S-N curve. SD is the standard deviation of the chosen S-N curve and describes the uncertainty in the test results. d is the number of standard deviation from the mean line S-N curve and defines the distance of characteristic S-N curve from the mean line. For example d= 1.64 means that the characteristic curve is 1.64 standard deviation away from mean value μ. This would correspond to 5% probability of failure or 95% survival probability. I.e. if a welded joint is designed with these assumptions, there is 5% chance that it fails during its service life. This is schematised in Figure 6-1, above.

$$Log(N) = Log(a) - k * m * \log\left(\frac{t}{t_{ref}}\right) - m * log(\Delta S) - d * SD, \text{(DNV, 2010)} \quad (6\text{-}1)$$

There is a limit below which the no fatigue limit occurs, in other words, the structure will have an infinite life. This is shown by the plateau line in Figure 6-1.

In practice, and for constant amplitude stress range, the joint is assigned a specific design class, such classifications can be found in fatigue design standards such as (DNV, 2010) or (BSI7608, 2015), then a, m and *SD* values corresponding to that class are extracted from the standards, for example see Table 18 from (BSI7608, 2015), then a d value is chosen depending on criticality of the joint (1.64 or 2 are commonly used), then the maximum stress range the structure can take to survive for its intended life (N) is calculated using equation (6-1) . Alternatively, knowing the stress range, the number of cycles the structure can take to survive is calculated and then the total calculated accumulated damage *D* is n divided by N. D must be less than 1 to indicate that the structure will not fail. (BSI7608, 2015) recommends that the total accumulated damage, *D*, should be limited to 0.5, although the value selected will depend on the criticality of the particular weld.

For variable amplitude, the stress range should be divided into a number of blocks, at least 10 blocks (Naess, 1985). For each block and under the corresponding constant amplitude stress, the cycles (N_i) are calculated using equation (6-1) . The total damage is then found by Palmgren-Miner rule given in equation (6-2):

$$D_{total} = \frac{n_1}{N_1} + \frac{n_2}{N_2} \ldots + \frac{n_i}{N_i} \leq 1 or\ 0.5 \quad (6\text{-}2)$$

Commonly, the uncertainty accounted in fatigue design based on S-N curve approach is through considering the uncertainty in S-N curve itself by choosing an appropriate number of *SD* as described earlier. (Lloyd's-Register, 2009) recommends 2 *SD* corresponding 97.5% survival probabilities. In some practices consequence of failure, to some extent, is taken into account by choosing a different number of *SD* values. Bureau Veritas recommends the use of 1, 2, and 3 *SD* for non-critical, critical, and very critical details respectively (Glenn, 1999). Similarly, (DNV, 2010) recommends design safety factors 1-3 for offshore structures. Design safety factor 3 is intended for "Non-accessible areas, areas not planned to be accessible for inspection and repair during operation". For risers (DNV, 2005) recommends 3, 6 and 10 design safety factors for low, medium and high safety classes. (DNV, 2010) illustrates the effect of the design fatigue factor (DFF) on using an example for a jacket design case. The

relationship between the design safety factor and failure probability for this example is shown in Figure 6-2. This figure shows probability of failure in the last year of service when the structure is designed for 20 years. Accumulated failure probability during service life is also shown in this figure. The uncertainties in fatigue reliability based on S-N curve are loading uncertainty, S-N curve uncertainty, and the uncertainty in Palmgren-Miner damage accumulation rule are considered in probabilistic analysis used to produce this figure. The loading is assumed normally distributed with COV= 0.25, S-N data is assumed to be normally distributed in logarithmic scale with the standard deviation equal to 0.20, and the uncertainty in Palmgren-Miner modelled by a lognormal distribution with a median equal to 1.0 and COV=0.3. This figure is used by (DNV, 2010) to conclude that using DFF values is an efficient mean to reduce probability of fatigue failure.

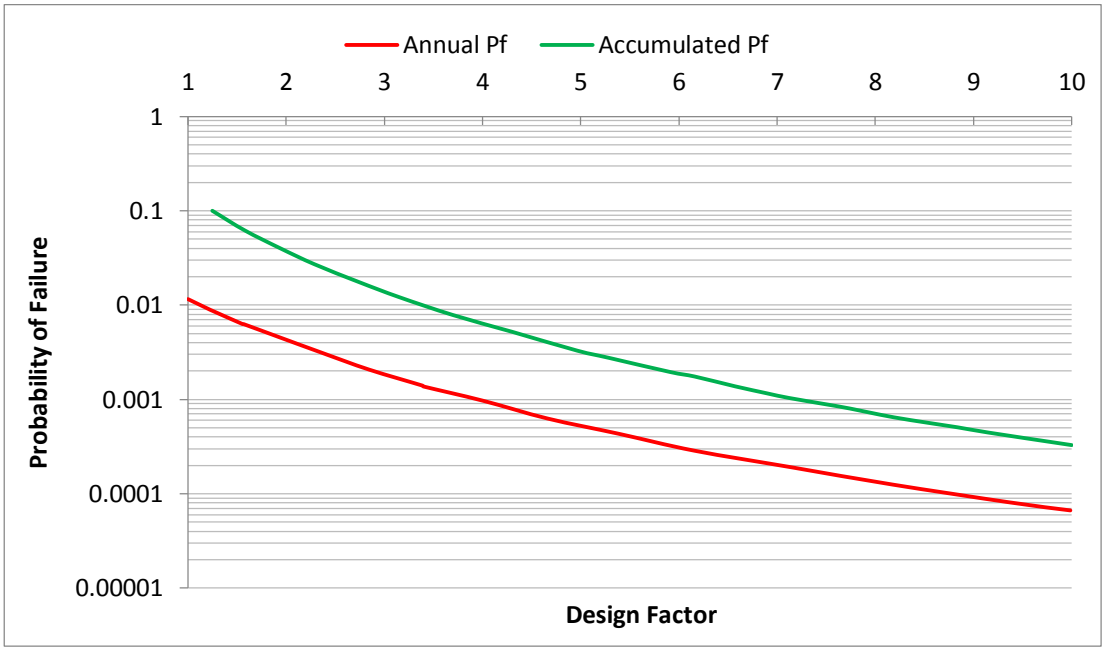

Figure 6-2 Relationship between Fatigue design safety factor and Failure probability (DNV, 2010)

6.4 Fracture Mechanics

The major limitation of the S-N curve approach is that it is only applicable to welds containing very small flaws. Structures containing larger flaws, that may nevertheless be acceptable, are outside the scope of this method. S-N curves are produced by testing specimens that have been found to be defect-free using surface NDT (Hobbacher, 2008).

Fracture mechanics (FM) enables prediction of crack propagation by using the crack growth rate, schematised in Figure 6-3. Region A is where crack growth rate occurs

as soon as $\Delta K \geq \Delta K_{th}$, where ΔK_{th} is the threshold value of ΔK. The threshold value depends on numerous factors such as the stress ratio $= K_{max}/K_{min}$, sequence effect, residual stresses, loading frequency, and environment. Region B is where the crack growth rate increases with ΔK to a constant power. Region C is where the crack growth rate increases rapidly until failure occurs as soon as $K \geq K_{critical}$.

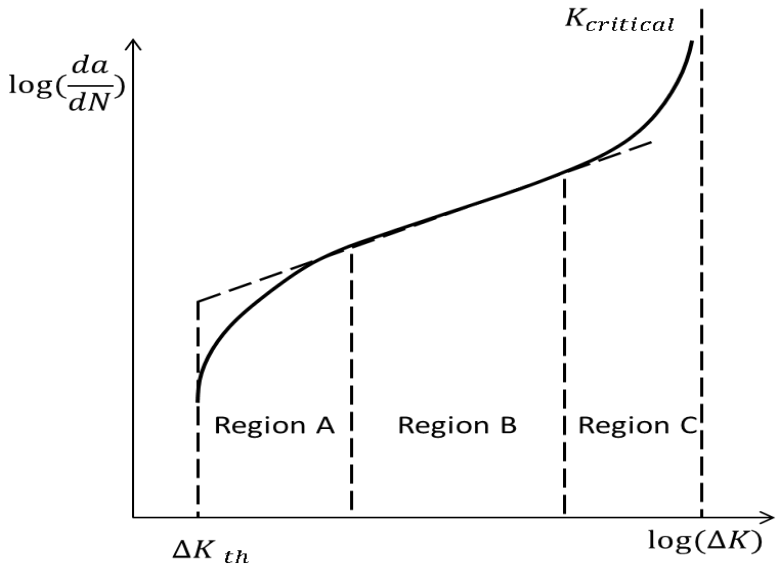

Figure 6-3 Schematic of crack propagation curve according to Paris-Erdogan law

In the FM approach crack growth rate is commonly described by the Paris-Erdogan equation:

$$\frac{da}{dN} = C * \Delta K^m \tag{6-3}$$

where, $\frac{da}{dN}$ is the rate of crack growth with respect to load cycles, ΔK is the change in stress intensity factor, and C and m are material constants. Stress intensity factor is described by:

$$\Delta K = Y\sigma\sqrt{\pi a} \tag{6-4}$$

where, a is flaw size, σ is stress at the flaw, and Y is the geometry function which depends on both the geometry under consideration and the loading mode. There are several ways in which solutions for Y can be obtained. Although it is possible to derive solutions for simple geometries analytically, e.g. using 'weight functions', numerical techniques are more commonly used (finite elements, finite difference or boundary elements methods). Away from other stress concentrating effects, for a centre

through thickness cracks in a plate Y=1, and for an edge crack Y can be taken as 1.12 (Murakami and Keer, 1993).

In practice critical a_f is calculated by substituting K_{mat}, material fracture toughness, in equation (6-4); $K_{mat} = Y\sigma\sqrt{\pi a}$, then (provided Y is a constant for all crack sizes) using equation (6-5) number of cycles to failure can be calculated.

$$N = \int_{a_0}^{a_f} \frac{da}{C(\Delta K)^m} = \frac{1}{A * Y^m * \Delta\sigma^m * \pi^{\frac{m}{2}}} * \frac{a_f^{\left(1-\frac{m}{2}\right)} - a_0^{\left(1-\frac{m}{2}\right)}}{1-\frac{m}{2}} \tag{6-5}$$

Time-dependent crack size can be calculated by rearranging equation (6-5):

$$a = \sqrt[\left(\frac{m-2}{2}\right)]{N * \left(\left(A * Y^m * \Delta\sigma^m * \pi^{\frac{m}{2}}\right) * \left(1-\frac{m}{2}\right)\right) + a_0{}^{\left(1-\frac{m}{2}\right)}} \tag{6-6}$$

The number of cycles a ship is expected to experience in its life can be approximated using equation (6-7) from (IACS, 1999). Where T is life in seconds, L is ship length in meters, and a_0 is a factor taking into account the time needed for loading / unloading operations, repairs, etc. In general, a_0 may be taken equal to 0.85 (IACS, 1999).

$$N = \frac{a_0 * T}{4 * \log(L)}, \text{ (IACS, 1999)} \tag{6-7}$$

Ship and offshore structure are not subjected to constant amplitude stress, but a variable amplitude stress spectrum. If the long-term stress distribution is converted into a step function of *n* blocks generally of equal length in log *N*, the crack size increment for the step i is:

$$\Delta a_i = C(\Delta K_i)^m \Delta N_i \tag{6-8}$$

moreover, the final crack size at the end of the *N* cycles is obtained by summing equation for the *n* stress blocks:

$$a_N = a_0 + \sum_{i=1}^{N} \Delta a_i \tag{6-9}$$

Equation (6-8) is only valid for small values of Δa_i since ΔK_i depends on the crack size, which requires dividing the stress range spectrum into a large number of stress blocks.

The number of cycles to failure may, alternatively, be calculated according to equation (6-10) using an equivalent constant amplitude stress ranges $\Delta\sigma_{eq}$ giving the same amount of damage (Naess, 1985):

$$\Delta\sigma_{eq} = \left[\int_0^{\infty} \Delta\sigma^{\beta}\, p_{\Delta\sigma}(\Delta\sigma) d\Delta\sigma\right]^{1/\beta} \quad (6\text{-}10)$$

where β correspond to the power law in the Paris Law equation. For the central part of the crack growth curve β is often about 3.0. $p_{\Delta\sigma}(\Delta\sigma)$ is the probability density function of stress range $\Delta\sigma$.

6.4.1 FAD

When a crack propagates through a structure, ultimately the crack size reaches a critical size a_f. a_f corresponds to a critical stress intensity factor, usually taken as characteristic of the fracture toughness K_{mat}, at which fracture happens. Alternatively, if the applied load is high and structure tensile strength is low, the structure may reach its tensile strength capacity and fail by plastic collapse. The latter is more favourable as it is usually associated with large deformations prior to failure providing some level of warning. In between brittle fracture and global collapse is an elastoplastic failure mode, where failure occurs before reaching the plastic capacity or toughness limit; this has been best described by failure assessment diagram (FAD) in the R6 procedure in 1976 and improved over time by e.g. by including the options available to model specific materials properties. The body of knowledge encapsulated in R6 affected the development of British Standards documents in various ways over the years, leading to BS7910:1999 (Yates, 2010) and the latest version at the time of writing, (BS7910, 2015 a).

The failure assessment line (FAL) represents the normalised crack driving force:

$$K_r = \frac{K_{elastic}}{K_{elastic\ plastic}} \quad (6\text{-}11)$$

K_r is equal to 1 where applied load is zero and declines as the ratio between applied load and yield load (L_r) increases towards collapse load (see Figure 6-4).

The plastic collapse load is calculated based on yield stress. However, the material has further load carrying capacity as it work-hardens through yield to the ultimate

tensile stress. To take this into account the rightwards limit of the curve is fixed at the ratio of the flow stress to the yield stress:

$$L_r = \frac{\sigma_{flow}}{\sigma_Y} \tag{6-12}$$

The flow stress is the average of the yield and ultimate stresses:

$$\sigma_{flow} = \frac{\sigma_Y + \sigma_U}{2} \tag{6-13}$$

If the assessment point lies inside the envelope (below the FAL), the fracture mechanics driving parameter is lower than the materials resistance parameter and the part should be safe, otherwise there is a risk of failure. The failure assessment diagram can be determined with one of the procedures provided by (BS7910, 2015 a). As it is illustrated in Figure 6-4, FAD may be categorised to three different zones: Zone 1 is the fracture dominant zone, Zone 2 is the elastoplastic region or the knee region, and Zone three is the collapse dominant zone.

(BS7910, 2015 a) has three alternative approaches Option 1, Option 2 and Option 3. These are of increasing complexity in terms of the required material and stress analysis data but provide results of increasing accuracy.

Option 1 (BS7910, 2015 a) is a conservative procedure that is relatively simple to employ and does not require detailed stress/strain data for the materials being analysed. The Failure Assessment Line (FAL) for the Option 1 analysis is given by:

$$K_r = f(L_r) = (1 + 0.5 * L_r^2)^{-0.5} * (0.3 + 0.7 * \exp(-\mu * L_r^6)) \tag{6-14}$$

for $L_r < 1$, where: $\mu = min\left[0.001\frac{E}{\sigma_Y}; 0.6\right]$.

and:

$$K_r = f(L_r) = f(1)L_r^{(N-1)/2N} \tag{6-15}$$

For,$1 < L_r < L_{r,max}$, where N is the estimate of strain hardening exponent given by: $N = 0.3(1 - \frac{\sigma_Y}{\sigma_{UTS}})$. And $L_{r,max} = \frac{\sigma_{flow}}{\sigma_Y}$.

Option 2A/3A of BS 7910:2005 generalised FAD, is similar but not identical to Option 1 (BS7910, 2015 a).

$$K_r = (1 - 0.14 * L_r^2) * (0.3 + 0.7 * \exp(-0.65 * L_r^6)) \quad (6\text{-}16)$$

The (BS7910, 2015 a) Option 2 FAD is based on the use of a material-specific stress-strain curve. The assessment line can be written as:

$$K_r = f(L_r) = \left[\frac{E\varepsilon_{ref}}{L_r\sigma_Y}, \frac{L_r^3\sigma_Y}{2E\varepsilon_{ref}}\right]^{-0.5} \quad (6\text{-}17)$$

ε_{ref} is the true strain obtained from the uniaxial tensile stress-strain curve at a true stress $L_r\sigma_Y$. (BS7910, 2015 a).

The option 3 failure assessment curve is specific to a particular material, geometry and loading type using both elastic and elastic-plastic analyses of the flawed structure It is given by:

$$f(L_r) = \sqrt{\frac{J_e}{J}}, \text{ for } L_r < L_{max} \quad (6\text{-}18)$$

$$f(L_r) = 0, \text{ for } L_r > L_{max} \quad (6\text{-}19)$$

J_e is the value from the J-integral from the elastic analysis at the load corresponding to the value L_r. The Option 3 curve is not suitable for general use. It is useful only for specific cases as an alternative approach to Options 1 and 2 (BS7910, 2015 a).

Options 1&2(BS7910, 2015 a) and Option 2A/3A (BS7910:2005) for typical AH36 steel are illustrated in Figure 6-5. It can be seen that the greatest difference between the three plotted locus is in the collapse region. In this research, the failure cases occur predominantly in Zone 1 where the differences between the options are negligible thus either Option 1 or option 2A/3A may be used.

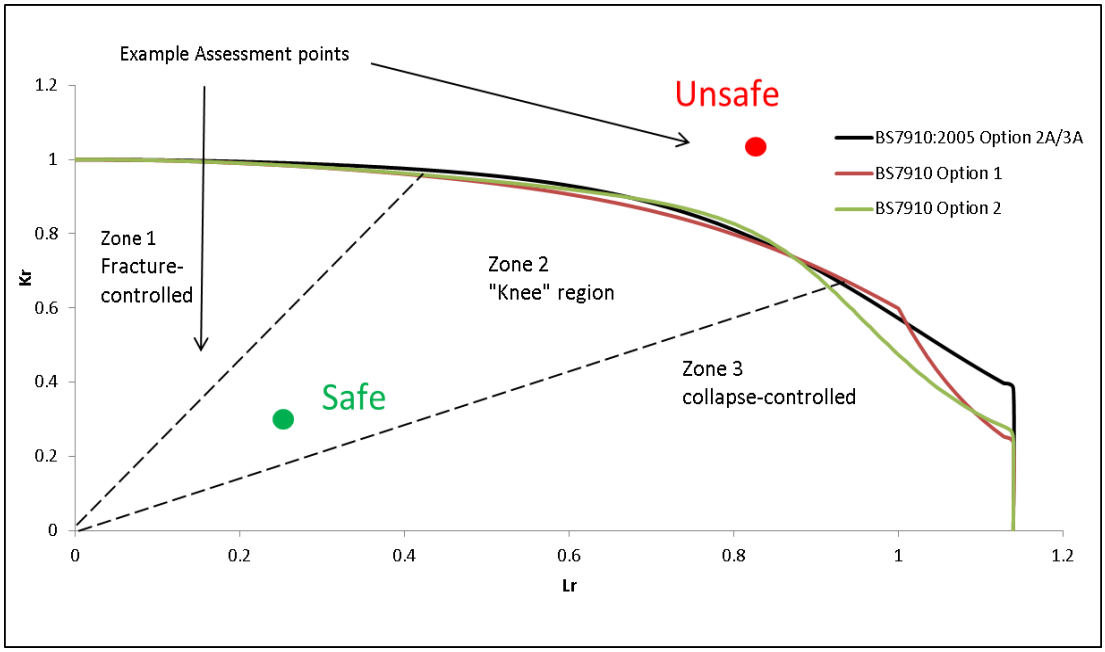

Figure 6-4 Failure Assessment Diagram (FAD)

6.5 Methods of reliability analysis

Principles of the methods of reliability analysis were explained in chapter three. In this research, two independent algorithms and the corresponding computer codes were developed using Mathcad Prime 3.0 programming software. One code is based on Monte Carlo (MC) simulation method, and the other is based on the convolution integral method. The Monte Carlo code can deal with as many stochastic variables as needed but the required number of samples for the results to convergence increases, as the number of random variables increases which in turn raises the computation runtime. The convolution integral code runs much faster than the Monte Carlo code and has the capability to directly include the effect of NDE reliability and inspection interval, but is limited to only three stochastic parameters; Fracture toughness, Defect size and stress, although potentially other stochastic parameters can be included in future version of the code, e.g. variability in Paris Law can be combined with the stress range variability at the beginning of the analysis. Thus the Monte Carlo code was used for studying the effects of each uncertain variable on the failure probability and validating the Convolution Integral code. The convolution integral code is the main programme for the following reliability calculations.

6.5.1 The Monte Carlo simulation code

The Monte Carlo code basis is on generating N series of random numbers for each stochastic variable. This is done using Mathcad built-in random number generating functions. Relevant probability distribution types which best represent the stochastic variable are called to generate the random numbers. For each set of random numbers (samples),i, where $i = 1,2 \dots, N$, an assessment point $(L_{r,i}, K_{r,i})$ and the respective failure assessment line FAL_i are calculated. If the assessment point falls above the assessment line it is considered as a failure otherwise will be treated as no-failure. The process is repeated N times. The code calculates the probability of failure by dividing the number of failure cases to the number of simulations (N). This is shown graphically in Figure 6-5.

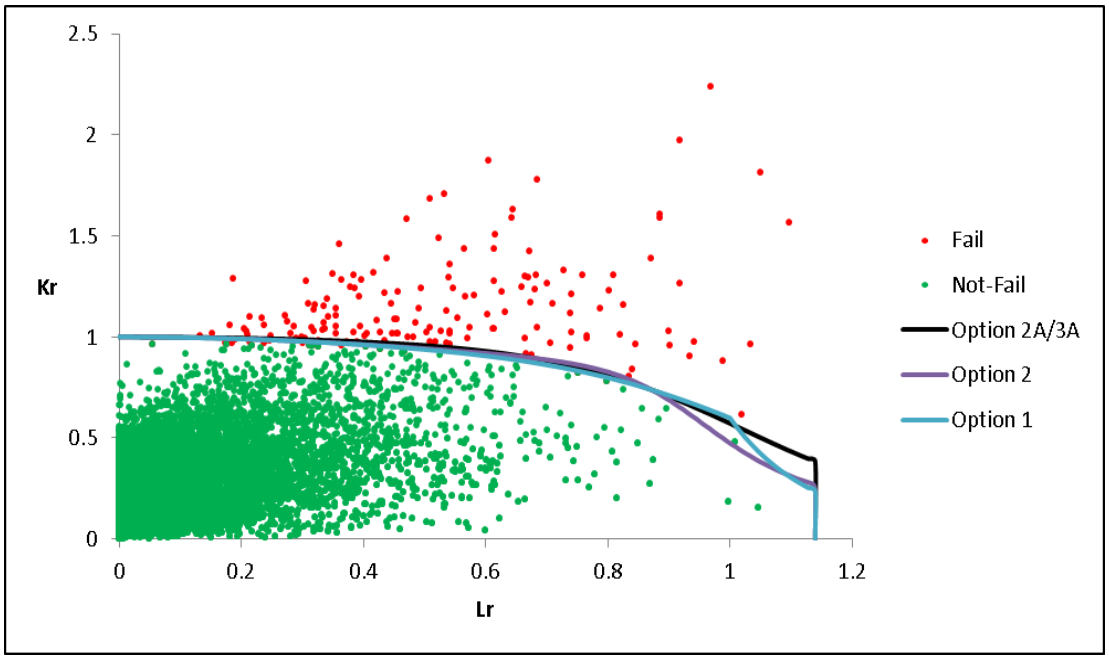

Figure 6-5 Illustration of calculating failure probability using Monte Carlo Simulation for FAD

For time-dependent reliability (Fatigue and Fracture) calculations, random initial defect sizes are generated prior to failure assessment. Then, the generated defect sizes are grown using Paris-Erdogan equation to calculate time variant defect sizes (again allowing for uncertainties). Finally, for any arbitrary point of time in the structure's service life, probabilistic failure assessment is executed to calculate the respective failure probability.The algorithm of time-dependent calculation is shown in Figure 6-6.

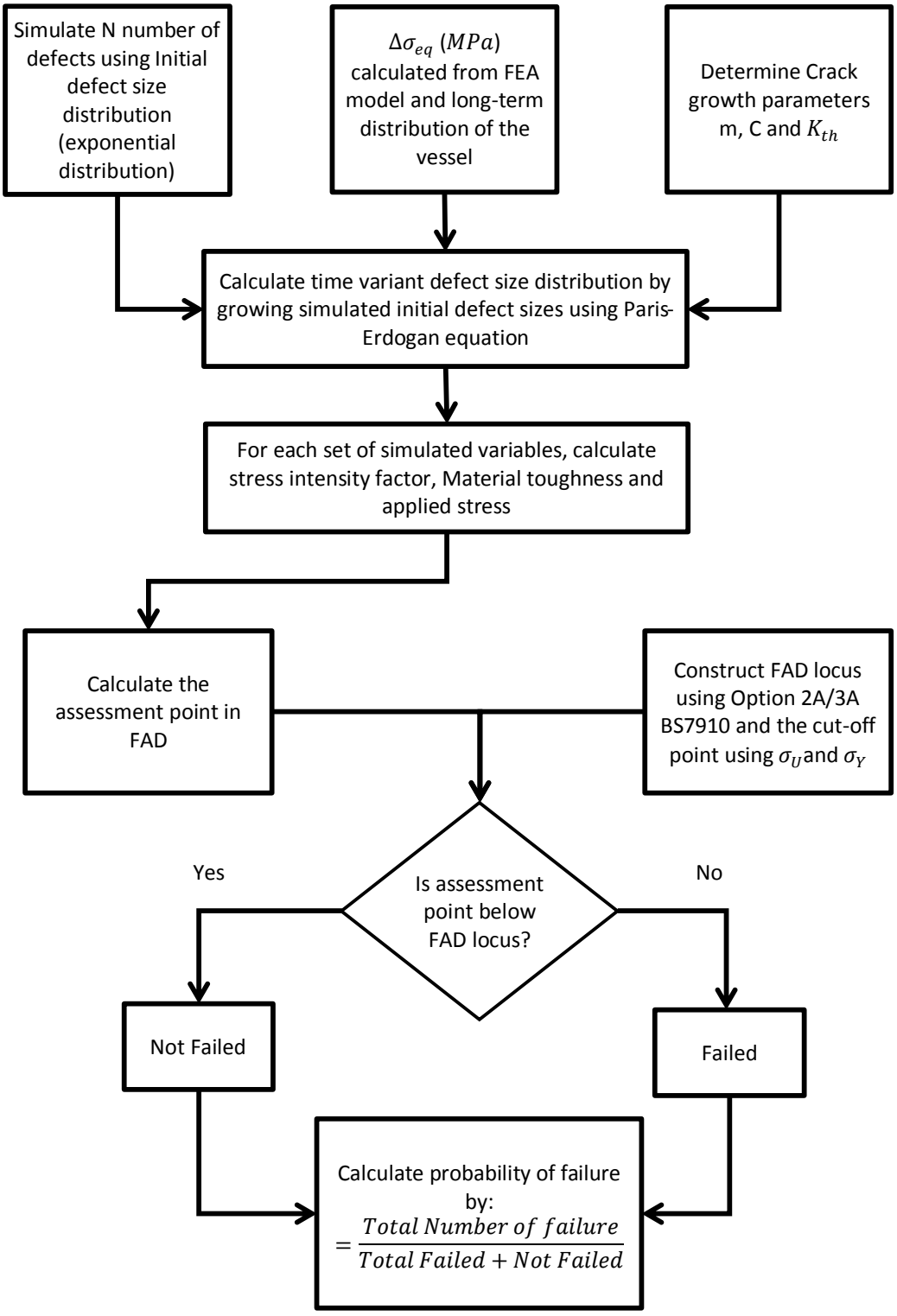

Figure 6-6 Time-dependent (Fatigue and Fracture) reliability calculation algorithm

6.5.2 The Convolution Integral Code

As explained in chapter three the basis of the Convolution Integral method is calculating the probability that the load exceeds a critical value corresponding to a respective value of structural resistance (Figure 6-7).

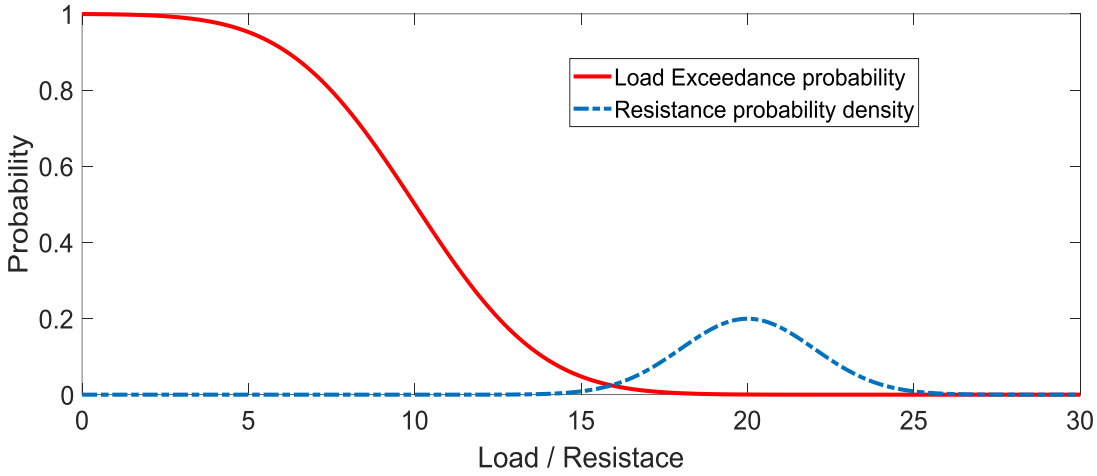

Figure 6-7 schematic principle of the convolution integral method

Here, first, a range of defect size and toughness values are generated, $a_i \; and \; K_j$ for $i = 1,2, \dots, n$ and $j = 1,2, \dots, m$. These values may range from very small values (effectively zero) to very large values to allow for any possible extreme cases. The seed size for the values can be chosen sufficiently low to increase the calculation precision. For each possible combination of defect size and toughness value, the code then calculates the critical stress (σ_{crij}) above which the failure happens. The probability of failure for each pair of toughness and defect size ($a_i \; and \; K_j$) is then, essentially, the long-term stress probability of exceedance of the relevant critical stress. The long-term stress distribution is defined by the Weibull distribution:

$$p(\sigma) = \frac{\zeta}{k}\left(\frac{\sigma}{k}\right)^{\zeta} \exp\left(-\frac{\sigma}{k}\right)^{\zeta} \qquad (6\text{-}20)$$

Where ζ and k are shape and scale parameters of the Weibull distributions. This is explained in the "Long-term response" section of this chapter. The exceedance function is the defined by:

$$P_{exc}(\sigma) = \exp\left(-\frac{\sigma}{k}\right)^{\zeta} \qquad (6\text{-}21)$$

The probability of failure for each pair of defect size and toughness is then, $P_{exc}\left(\sigma_{crij}\right)$.The probability of failure due to the pair needs to be multiplied by the probability of that size times the probability of the toughness value.

$$P_{f_{ij}} = P_{exc}(\sigma_{cri})_{ij} * p(a_i) * p(K_j) \qquad (6\text{-}22)$$

The total probability of failure is the summation of all failure probabilities for all possible combination of defect sizes a_i and toughness values K_i.

$$P_f = \sum_{j=1}^{m} \sum_{i=1}^{n} P_{f\,ij} \tag{6-23}$$

Time-dependent reliability analysis is done by finding the initial defect size and the corresponding number of cycles needed for that initial defect size to reach the critical size. This is achieved by Knowing the cyclic stress and crack growth parameters and through solving Paris-Erdogan equation.

The algorithm is illustrated in Figure 6-8.

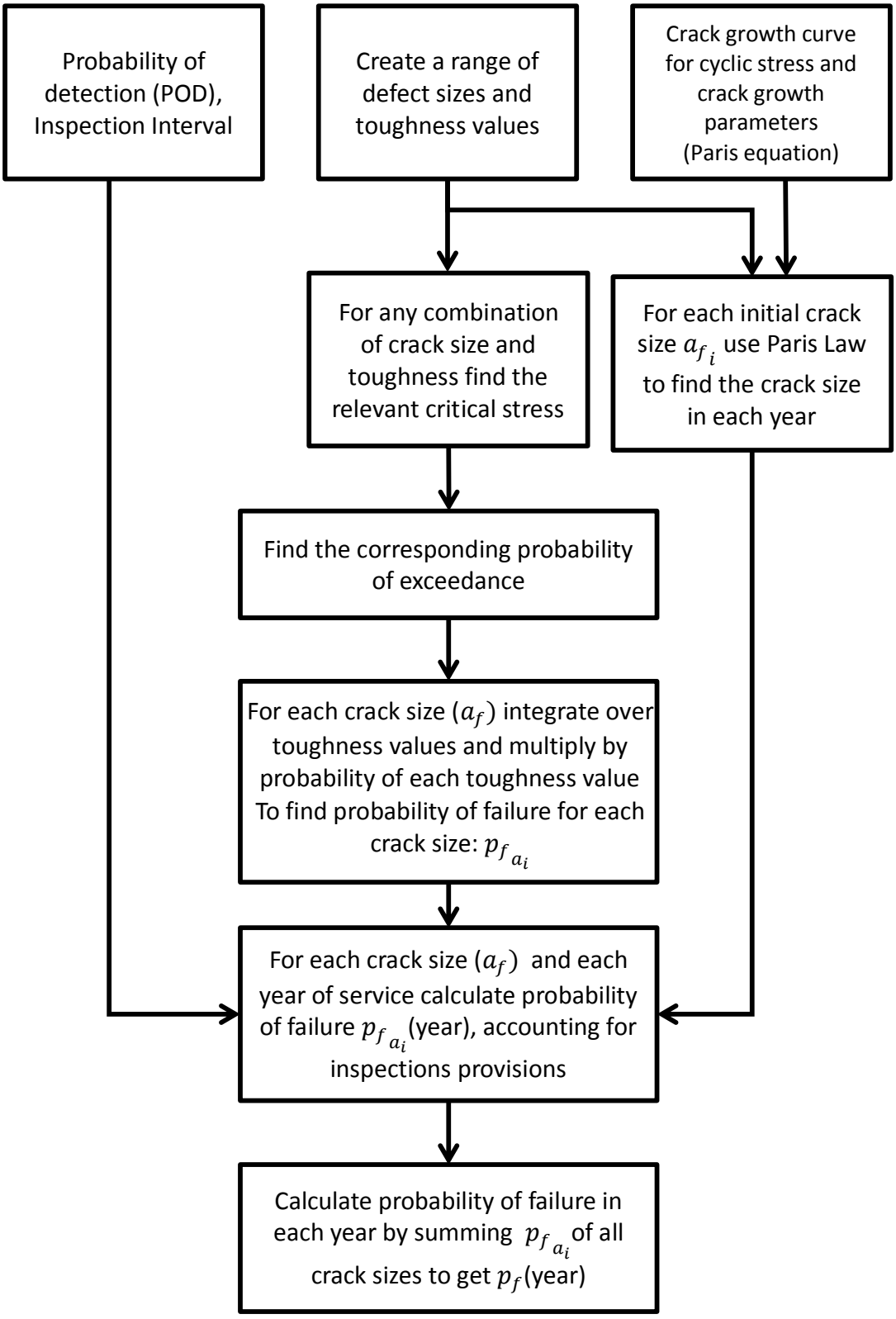

Figure 6-8 Algorithm of time-dependent reliability for Convolution Integral code

6.6 The reliability framework and uncertain variables

Here the emphasis is on uncertain variables that can improve ship reliability by the NDT programme and manufacturing quality such as defect rate and size and material characteristics such as crack growth parameters and toughness. Critical uncertain variables and their relationship with the reliability framework is illustrated in Figure 6-9. The manufacturing quality and NDT programme will have little effects on the stresses that the ship will experience in its lifetime. The approach, here, will be to account for defect-related variables and material toughness fully probabilistically and establish reasonably conservative constant characteristic values for other input variables.

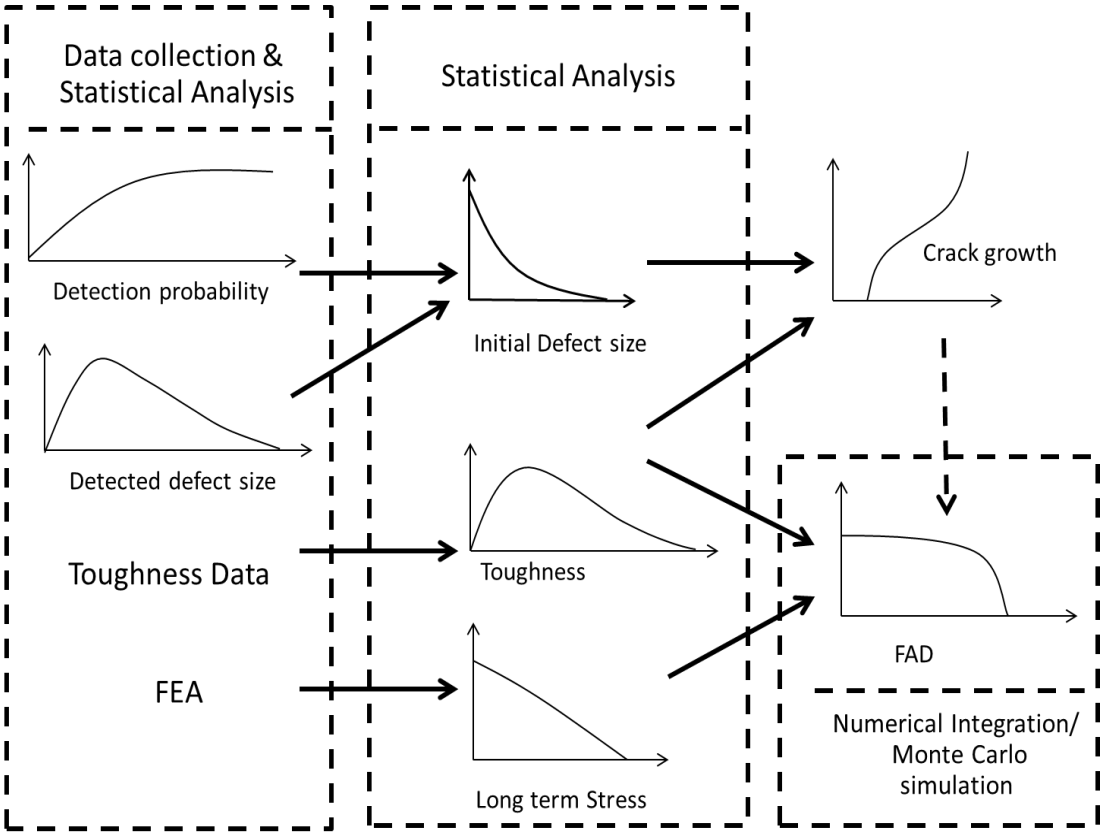

Figure 6-9 Framework for fatigue and fracture reliability analysis

6.6.1 Stress calculation

The stress at the defect is one of three key variables in failure assessment of a planar defect along with the defect size and the material toughness. When using the FAD, the stresses acting on the defect are categorised to primary stress resulting from loads acting on the structure, and secondary stresses, such as weld residual stresses, at the location of the defect. Secondary stresses are short range stresses and do not

cause global ductile failure of the structure, although they can cause a fracture which may ultimately cause the collapse of the whole structure.

6.6.1.1 Load actions on the hull

Loads acting on the ship hull may be categorised into three categories:

1. Loads acting on the longitudinal strength of the ship
2. Loads acting on the transverse strength of the ship
3. Loads acting locally

The longitudinal strength loads are those affecting the global strength of the ship hull girder, in which the structure is assumed to act like a beam or girder. The resulting load actions are global bending moments, torsional moments and shear force. The longitudinal strength loads can be categorised into dynamic wave loads and static loads. Dynamic wave loads are generated as the ship encounters sea waves. As it is illustrated in Figure 6-10, when the ship is positioned at the wave crest it acts similar to a beam under hogging moment, and when the ship is positioned at wave trough, it behaves similar to a beam under the sagging moment. Static longitudinal loads such as still water are generated as a result of the local inequalities between ship weight and buoyancy force acting on the opposite directions. For instance, still water loads cause static bending moment, and shear force along the ship and asymmetrical cargo loads cause static torsional moment. (Okumoto et al., 2009)

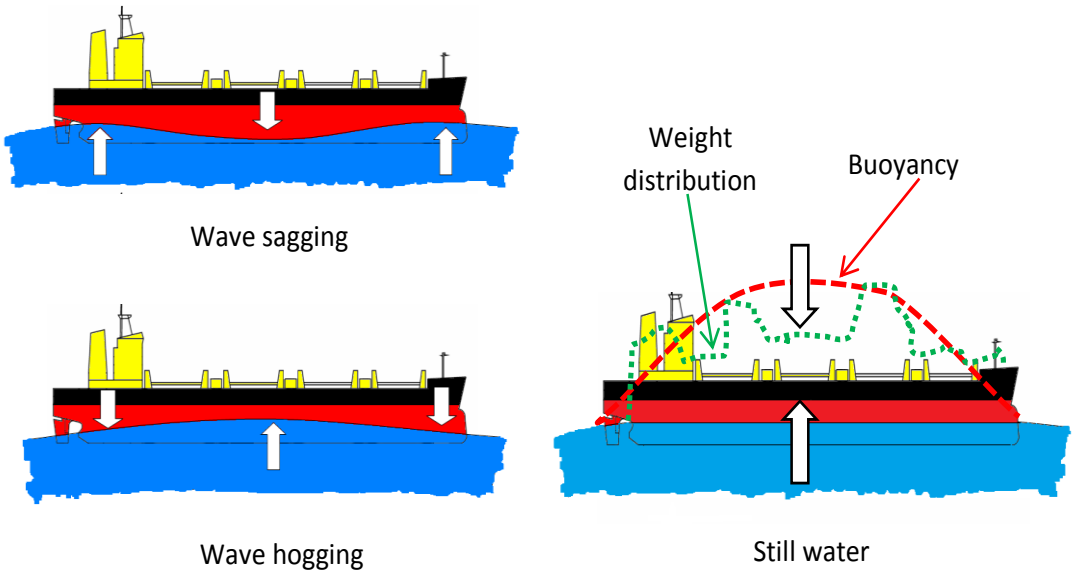

Figure 6-10 Longitudinal strength global loads, adapted from (Wikimedia, 2006 c)

Transverse strength loads are those which cause deformation of transverse structures as a result of inequalities between external and internal loads (Figure 6-11). These loads are assumed to be independent of longitudinal loads which do not cause any transverse deformation. (Okumoto et al., 2009). Hydrostatic and hydrodynamic loads, inertia forces of cargo or ballast due to ship motion, structural weight, ballast water and cargo weight, and impact loads can produce transverse loads.

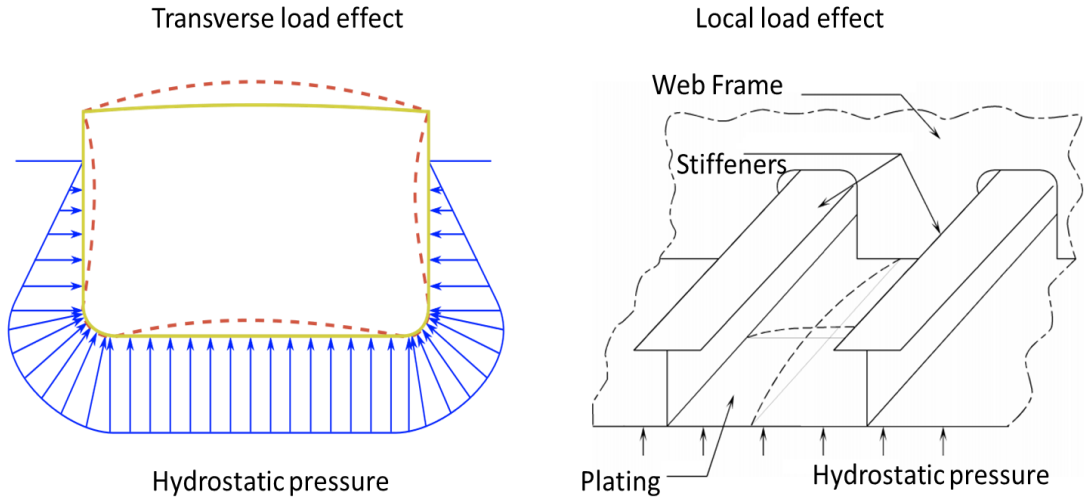

Figure 6-11 Left: Transverse stress during rolling (Wikimedia, 2009), Right: Local load effect (Okumoto et al., 2009)

As it is shown in (Figure 6-11-Right), local loads include those affect the local resisting members such as shell panels, stiffeners, and connections between stiffeners.

6.6.1.2 Finite Element Analysis

The common practice in ship structure design is to perform finite element analysis of the hull using a global coarse mesh to calculate stresses required for scantling of the vessel and use a sub modelling technique to extract refined stresses at stress concentration locations such as openings. In this research, an existing global FEA countor plots provided by the manufacturer's design office was used to calculate long-term stress distribution of the structure at the locations of the interest. Figure 6-12 and Figure 6-13 are contour plots of stress in the deck number 16 of the vessel, which is generally under higher stress levels than other decks due to its relative

vertical distance from ship neutral axis.

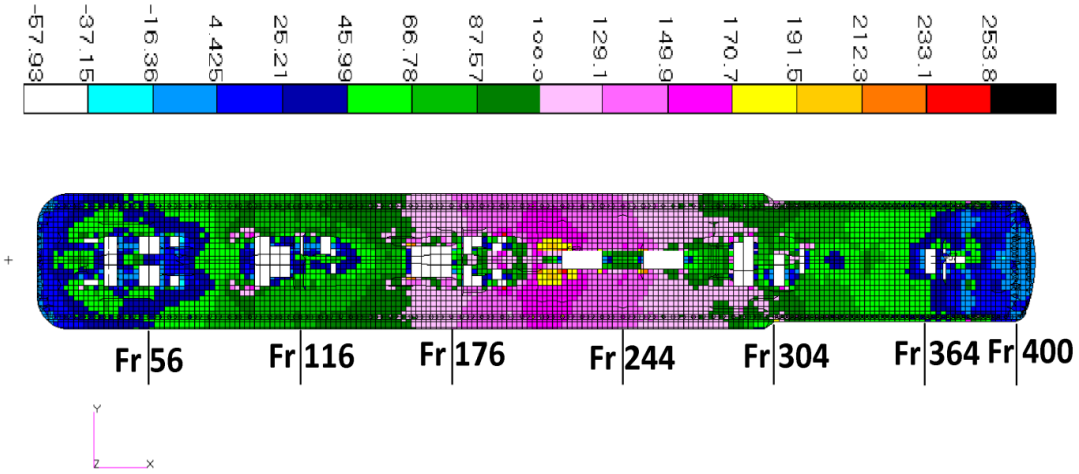

Figure 6-12 Global FEA of case study ship for Deck 16 Still water+ Hogging, σ_{xx} stress (Fr: Frame Number)

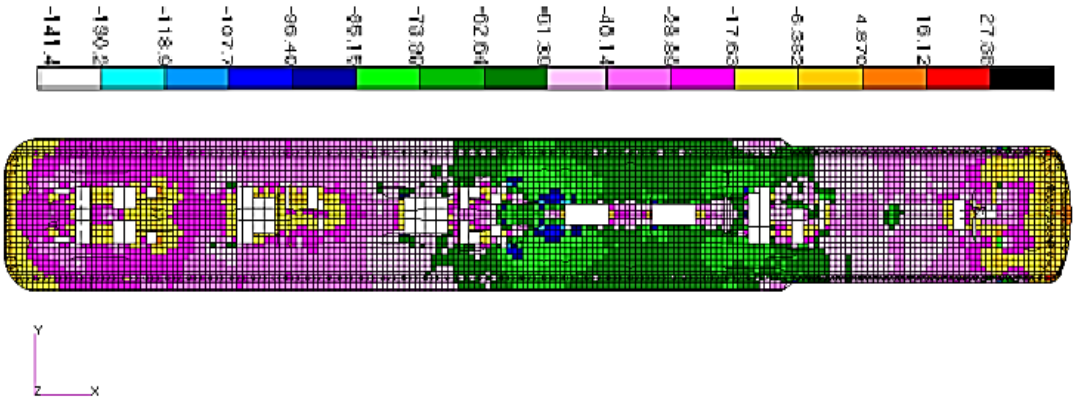

Figure 6-13 Global FEA of case study ship for Deck 16 Still water+ Sagging, σ_{xx} stress

6.6.1.3 Long-term response

Above stresses are design extreme stresses corresponding to exceedance probability of 10^{-8}, i.e. the stresses structure will have to withstand and are likely to occur once in 10^8 cycles, its service life. Stresses applicable to crack propagation of are much less than this level and correspond to 10^{-4} to 10^{-5} probability of exceedance. Long-term stress distribution of ship hull structures can be best described by the Weibull distribution (IACS, 1999):

$$p(\Delta\sigma) = \frac{\zeta}{k}\left(\frac{\Delta\sigma}{k}\right)^{\zeta} \exp\left(-\frac{\Delta\sigma}{k}\right)^{\zeta}, \text{(IACS, 1999)} \qquad (6\text{-}24)$$

where, $\Delta\sigma$ is stress range, k is the characteristic value of the stress range and is equal to $\frac{\Delta\sigma_R}{(\ln N_R)^{1/\zeta}}$, $N_R$is number of cycles corresponding to the probability of exceedance of $1/N_R$, $\Delta\sigma_R$ is stress range with the probability of exceedance of $1/N_R$, ζ is shape parameter. (IACS, 1999) recommends equation (6-25) to estimate the shape parameter, where L is the length of the vessel.

$$\zeta = 1.1 - 0.35 * \frac{L-100}{300}, \text{(IACS, 1999)} \qquad (6\text{-}25)$$

To construct the long-term stress distribution, the shape parameter is calculated using the ship's length, by means of equation (6-25), then using stress from the FEA model ($\Delta\sigma_R$) which corresponds to the probability of exceedance of 10^{-8} ($N_R = 10^8$) the characteristic value(k) is estimated.

The long-term stress distribution $p(\Delta\sigma)$then can be used in equation (6-10) to estimate equivalent constant stress.

Stresses shown in Figure 6-12 and Figure 6-13 are the result of both wave load and still water load and are used superimposed on each other for strength assessment of the structure. In the calculation of long-term stress distribution, it is more accurate to separate two effects. Wave distribution is best represented by Weibull distribution whereas still water loading depends on cargo and ballast arrangement. For this work it is assumed to be a constant value throughout the life of the ship. A separate file containing global bending at each frame was used to calculate the ratio between Stillwater and wave-induced stress, and then corresponding stresses were calculated, subsequently, see Appendix E.

6.6.2 Residual stress

Residual stresses are local stresses and self-balanced over the cross-section of the member. After welding and during the cooling process the interaction between the different fibres results in a locked-in tensile stress in and near the weld that can reach up to approximately the yield stress of the material. This locked-in tension causes compressive residual stress, in the remaining area of the section. This is shown schematically in Figure 6-14. The extent of tensile stresses next to the weld line is equal to $\eta^* * t_p$, where η^* is equal to 3.5–6. Longitudinal residual stresses, σ_l, are generally higher than transverse stresses, σ_t (Milella, 2012). In the case of complete weld shrinkage prevention the resulting residual stresses, σ_l and σ_t, may reach the

yield stress of the weld. The distribution of residual stress in a stiffened panel is more complex than a simple butt welded plate. In fact, the majority of the plate is affected by compressive residual stress which causes the crack propagation to slow down. This is explained in the next section.

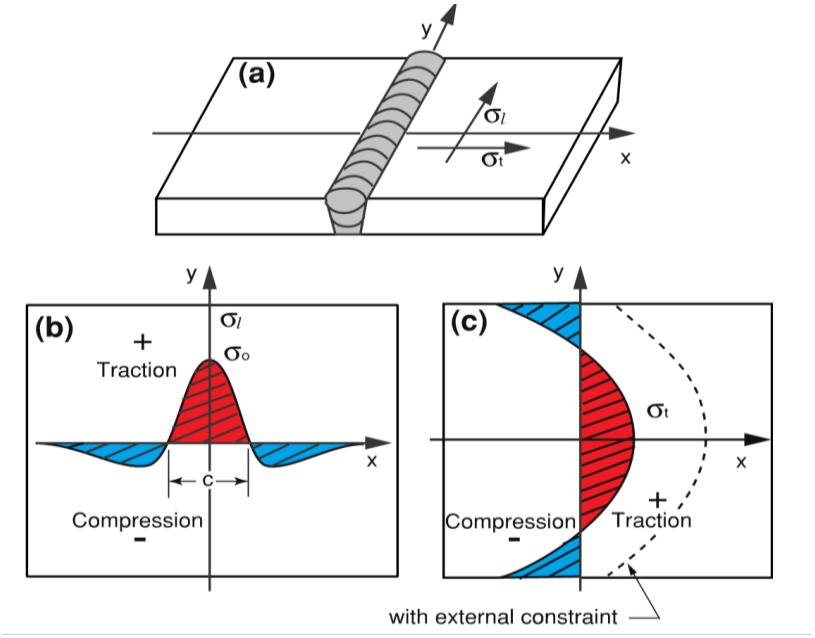

Figure 6-14 Transverse and longitudinal residual stresses in butt welds adapted from (Milella, 2012)

The stress spectrum ('spectrum' as defined here means the distribution of stress ranges) of a structural member in ship hull consists of cycles of both tensile stress followed by compression stress (Figure 6-15, left). Crack propagation in the compression part of the stress cycle is suppressed and the tension part is mainly responsible for crack extension. In the as-welded condition, and in the tensile part of residual stress field, the stress remains tensile even under external compressive stress. In this condition, the stress remains at weld yield stress and fluctuates downwards but always in tension mode. This is shown in Figure 6-15, right. The stress range, in this case, is equal to $\sigma_t + |\sigma_c|$ (Beghin, 2006).

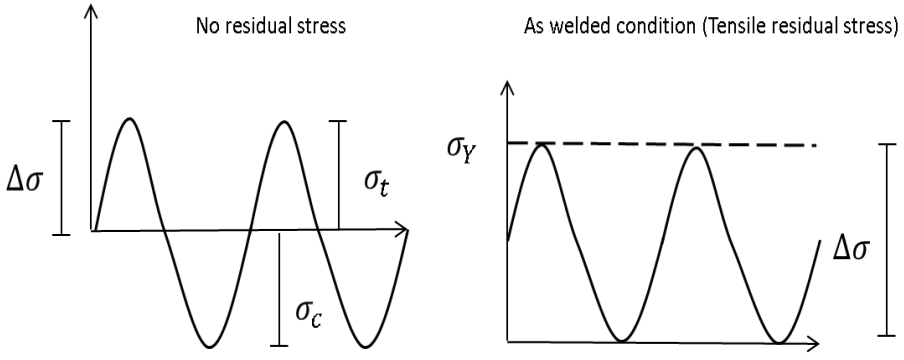

Figure 6-15 Effect of tensile residual stress on cyclic stress range

6.6.2.1 Shakedown

Shakedown is a gradual reduction of the residual stresses in a welded structure under cyclic loading. It occurs when the sum of the applied load stress and residual stress exceeds the yield stress of the material, plastic deformation occurs on loading and the residual stress is reduced when the applied load is removed. (Li et al., 2007).

Accurate prediction of shakedown is very complex and depends on many factors such as the initial residual stress of the detail and service stress history. If advantage is to be taken of shake-down, the Class may require the shake-down effect to be measured and documented (DNV, 2015). The following mean stress reduction factor may be used:

$$f_m = \begin{cases} 1.0 \ ; \frac{\sigma_{mean\ eff}}{\Delta\sigma} \geq 0.5 \\ max\left[0.6\ , 0.9 + 0.2\frac{\sigma_{mean\ eff}}{\Delta\sigma}\right] \ ; \frac{\sigma_{mean\ eff}}{\Delta\sigma} \leq 0.5 \end{cases}, \text{(DNV, 2015)} \qquad \text{(6-26)}$$

$\sigma_{mean\ eff} = \sigma_{mean} = \frac{\sigma_t + |\sigma_c|}{2}$ where shake-down to zero residual stress has been documented, and $\sigma_{mean\ eff} = \sigma_{mean} + \sigma_{Res}$, otherwise. σ_{Res} is residual stress at the hot spot. If the amount of residual stress is not known, it may be assumed equal to the material yield strength as derived from material certificates (DNV, 2015).

It is apparent that the applied stress must be of the order of 50% of the yield strength in order to relieve any residual stress. When the flaw tips are in the base metal and away from the weld (2 to 3 plate thicknesses, See "Effect of residual stress and restraint"), then the tensile weld residual stresses are negligible. However, there are some longer range assembly and construction stresses that still may be present. These may be relieved to some extent with service (shakedown effect) or as the crack grows. However, this effect is difficult to predict and therefore, as a conservative measure, longer range residual stresses equal to 20% of the yield strength are recommended to be included in a fracture analysis. (Dinovitzer and Pussegoda, 2003).

6.6.3 Stress Intensity Factor (SIF) in Stiffened plates

Ship structures particularly in deck and bottom structure, are made from stiffened plates (Figure 6-16); therefore geometry function, Y, used in the stress intensity factor solution changes as the crack propagates towards the location of stiffeners.

Generally, geometry function is around 1 in locations far from stiffeners and reaches to around 0.5 as a crack tip approaches an infinitely stiff stiffener. The behaviour of the crack growth is more complex when residual stresses are taken into account. In this section, these effects are studied.

Two factors cause the reduction in the crack propagation rate in a stiffened panel: the restraint effect and the compressive residual stress between stiffeners arising from the welding process. These two factors are about equally important.

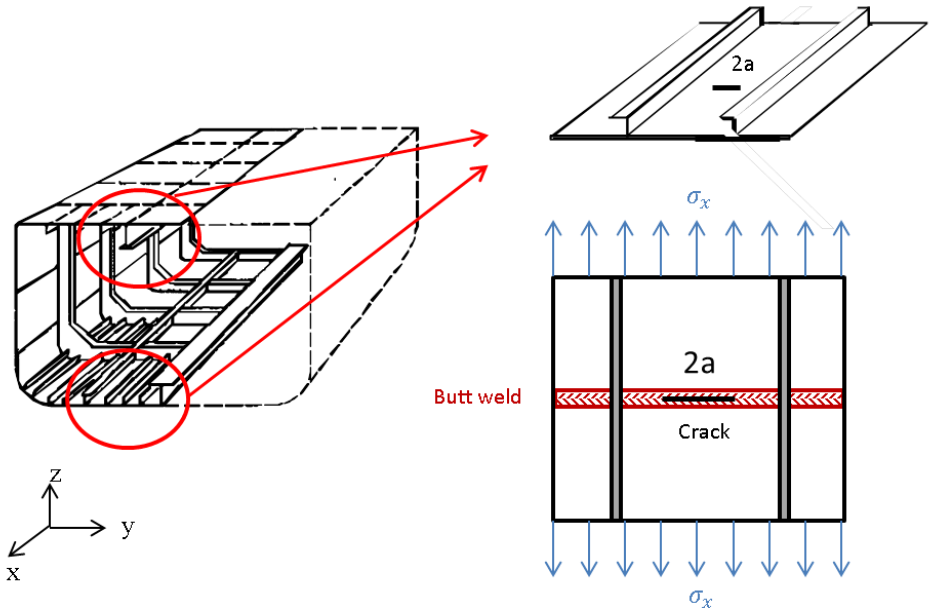

Figure 6-16 Schematic Stiffened plate in ship bottom and deck

6.6.3.1 Effect of restraint

(Poe, 1971) developed a solution for a crack extending in riveted stiffened plate and found that the K solution decreases as the crack approaches a stiffener, suggesting that the stiffener slows down the propagation by restraining the crack. For integral stiffeners such as welded stiffeners, (Poe, 1971) developed a solution that assumed that once a crack reaches a stiffener, the stiffener is severed and the load carried by the stiffener before is shed to the remaining net section. Figure 6-17 demonstrates this solution. Following the sudden reduction in K, it linearly increases until the crack length beyond the stiffener is equal to the stiffener height. (Poe, 1971) also found that the riveted stiffeners continue to limit crack growth after the crack propagates past the stiffener since a crack cannot propagate directly up into the stiffener. In welded stiffeners, on the other hand, the crack may propagate into the stiffener as well as the plate. Since (Poe, 1971)'s study was mainly aimed at riveted structures, it

did not take into account the effect of residual stress. (Poe, 1971)'s K solution became the foundation for analysis of stiffened panels in aerospace engineering.

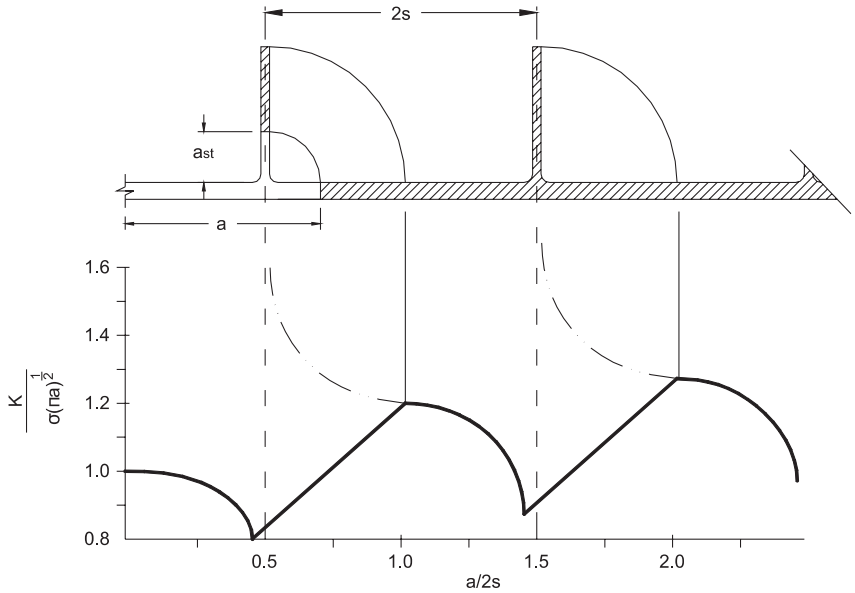

Figure 6-17 K solution for a panel with integral stiffeners proposed by (Poe, 1971)

6.6.3.2 Effect of residual stress and restraint

For stiffened plates, the widely accepted model of residual stress fields is assumed with a triangular form in the tensile part and a constant compressive stress that balances with the tensile part, Faulkner simple model (Faulkner, 1973). In the Faulkner model the width of the tensile region is $W = \eta * t_{plate}$. η is between 3 to 6 of plate thickness, while values between 3 and 3.5 are more typical of ships (Mahmoud and Dexter, 2005). See Figure 6-18.

(Dexter and Pilarski, 2002) carried out fatigue crack propagation tests of through-thickness cracks in the presence of residual stress on multiple of cellular box stiffened plates. One of the key conclusions was that stiffened panels are tolerant to long cracks. The measured residual stresses were correlated well with the Faulkner model. The (Dexter and Pilarski, 2002) work does not study the load shedding effect and redistribution of residual stress due to crack propagation.

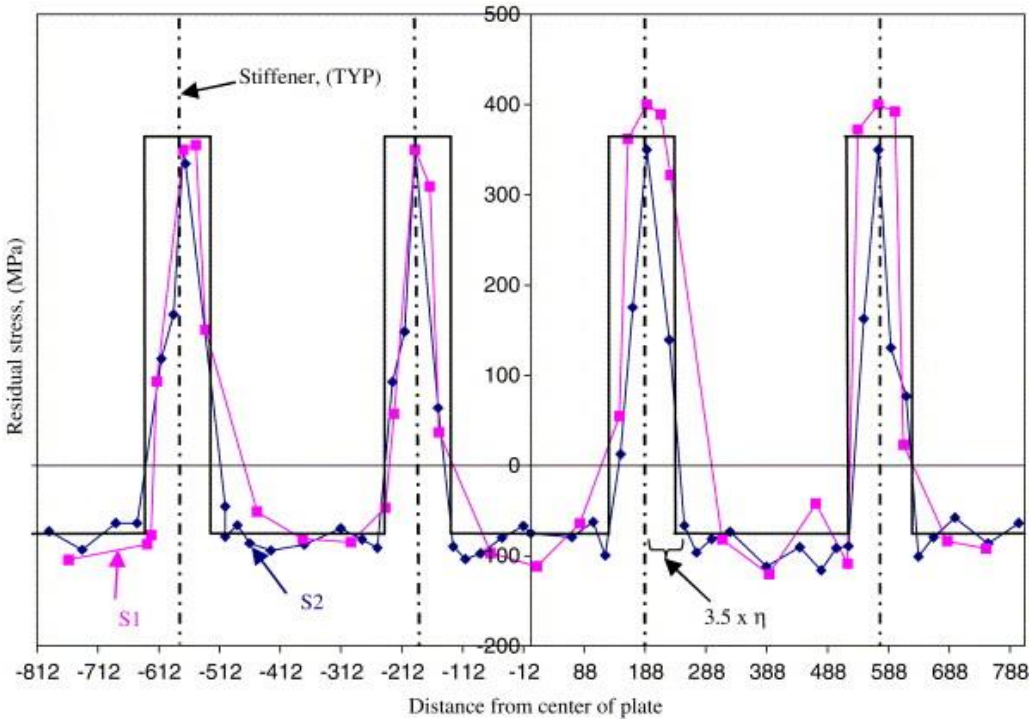

Figure 6-18 Residual stress measurement of the stiffened plate by (Mahmoud and Dexter, 2005).

(Mahmoud and Dexter, 2005) fatigue tested welded stiffened steel plates and showed that the crack propagation rate in stiffened plates is reduced compared to what would be expected in an unstiffened plate. The cycles to grow one stiffener spacing may increase by a factor of 2–4 above what would be estimated in a plate with a centre-crack, as shown in Figure 6-19. The residual stress pattern was similar to what was reported in past studies on the distribution of residual stress in welded stiffened panels.

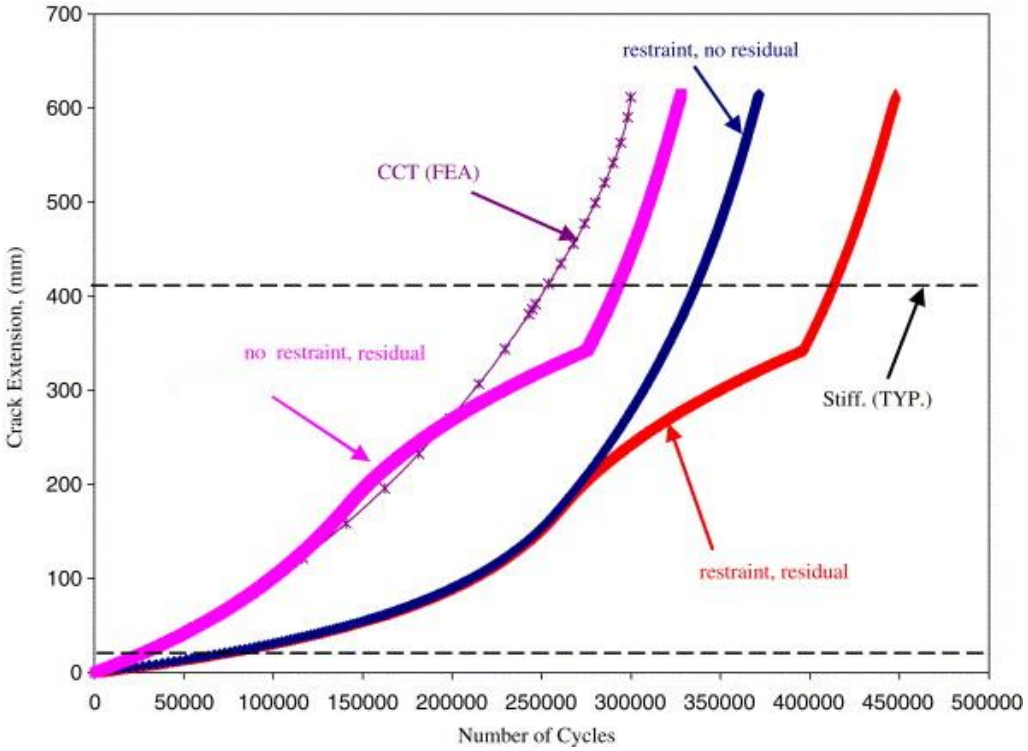

Figure 6-19 Effect of residual stress and constraint on the crack growth rate of stiffened plates (Mahmoud and Dexter, 2005).

It is known that as the long crack propagates the residual stress field redistributes (Ayala-Uraga and Moan, 2007). Additionally, the shakedown effect may remove the peaks of the residual stress fields. These two effects imply that, in principle, a relaxation of the residual stress field could take place during the service life. Account of compressive residual stresses in determining the crack growth would then be none conservative (Ayala-Uraga and Moan, 2007). Thus in this work the positive effects of residual stress is not be considered in favour of conservatism.

6.6.4 Crack growth parameters

Apart from initial crack size and stress intensity factor K, Paris equation (6-3) constants C and m are the most important inputs in crack growth model and subsequently in through life failure probability calculations of a structure containing a flaw. There have been numerous works since the proposal of the Paris-Erdogan law in 1962 to quantify these two parameters, the influencing variables and possible a correlation relationship between them. (Cortie and Garrett, 1988) provides a comprehensive review of these efforts until 1988 and the reader is referred to this paper for further details. The influencing variables on these two parameters are disagreed among the reviewed literature. (Cortie and Garrett, 1988) argues that apart from stress ratio R, the influence of other conditions on the correlation between C

and m is negligible. (Gurney, 1979) suggest that m ranges between 2.5 to 3.6 for real structural steels when a single slope crack growth model is used. There are generally two approaches when dealing with these two parameters. The first approach treats the parameters as two correlated stochastic variables. In the second approach, m is treated as a fixed value and m is taken as the stochastic variable.

6.6.4.1 C and m treated as correlated variables

There are several regression models available among which two below models are commonly used and are recommended by (BS7910, 2015 a) Annex K.

1. From test data in (Gurney, 1979) and derived in (Cortie and Garrett, 1988):

$$\ln(C) = -7.381 - 7.283 * (m) \quad (6\text{-}27)$$

   Units are in N.mm$^{-3/2}$ for ΔK and mm/cycle for $\frac{da}{dN}$. With the 95% confidence interval for the slope, *m* is [7.454, 7.114] and the 95% confidence interval for the intercept is [–7.922, –6.842].

2. From (Tanaka and Matsuoka, 1977):

$$\ln(C) = -8.682 - 6.924 * (m) \quad (6\text{-}28)$$

   Units are in N.mm$^{3/2}$ for ΔK and mm/cycle for $\frac{da}{dN}$.

More recently (Baker and Stanley, 2008) conducted a test programme of 35 welded and non-welded test specimens and suggests below correlation equation which shows comparable results to the equation given by (Cortie and Garrett, 1988).

$$\ln(C) = -8.48 - 6.91 * (m) \quad (6\text{-}29)$$

6.6.4.2 m is deterministic and C is modelled as a random variable

The Paris equation has been traditionally described by a single slope line although recently a bilinear has been widely used. The (BS7910, 2015 a) recommended model is the bilinear model, while the simplified single slope model is cited, as well. Both models are schematised in Figure 6-20.

In most reliability calculations, only C is modelled as a variable. For a simplified (one-slope linear line) relationship between Log(C) and m there are several models in the

literature and are given in Table 6-1. The C and m values in (Snijder et al., 1987) are based on the original work from (Maddox, 1975).

Condition	Source	m	Ln(C)	Std Ln(C)
Weld in Air	DNV(Veritas, 1984)	3.1	-29.84	0.55
	Snider (weld)(Snijder et al., 1987)	3.07	-29.16	0.31
	Snider (Plain Steel) (Snijder et al., 1987)	2.8	-27.76	0.23
Weld in sea water	DNV(Veritas, 1984)	3.5	-31.01	0.77
	DNV(Veritas, 1984) with Cathodic Protection	3.1	-29.84	0.55
In Air	(Johnston, 1983), Based on (Gurney, 1979), weld and steel	3	-29.32	0.24
Weld in Air	BS7910 Upper Bound	3	-28.28	-
Marine	BS7910 Upper Bound	3	-26.80	-

Table 6-1 m and c values for the single slope crack growth model

The only data on probabilistic two stage crack growth model is available from an HSE report by (King, 1998), which has been adopted by (BS7910, 2015 a) as well. Crack growth parameters for welds in Air are given in Table 6-2. It can be observed that stage B also possess less uncertainty. This is because, it applies to larger cracks that their tips sample smaller material cross section and hence is less dependent on the randomness of material microstructure and constraint effects (Baker and Stanley, 2008). A similar observation has been reported in (Baker and Stanley, 2008). Ship cracks are generally very large crack extending in relatively thin plates, and in author's opinion, are governed by stage B regime.

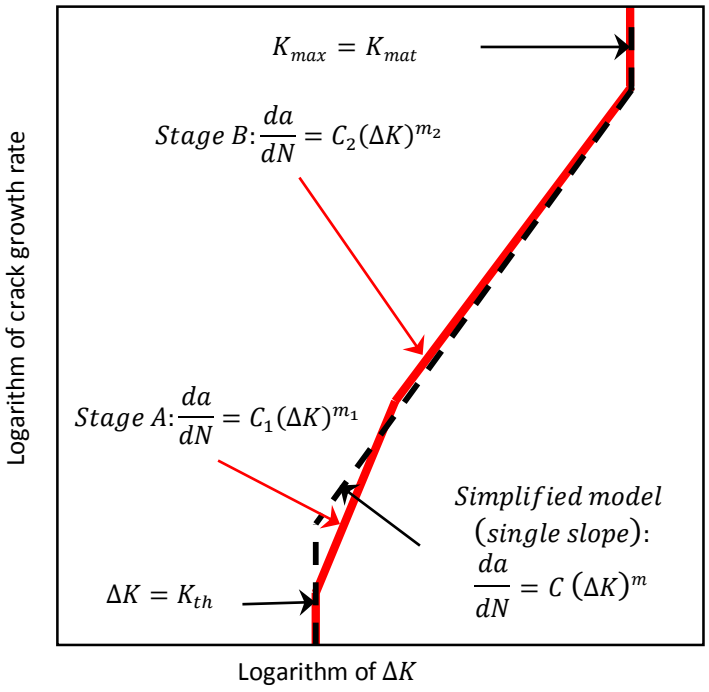

Figure 6-20 Schematic of crack growth models by Paris law

Weld in Air	R	m	Ln(C)	Std Ln(C)
Stage A	<0.5	8.16	-59.88	0.64
	>0.5	5.1	-40.15	0.74
Stage B	<0.5	2.88	-28.59	0.27
	>0.5	2.88	-28.24	0.39

Table 6-2 Two slope crack growth model (King, 1998) and (BS7910, 2015 a) (Annex K)

6.6.4.3 Crack growth in ship construction material

Although the correlation between C and m appears to be independent of steel type, the absolute values are to be studied. The data on crack growth parameters of shipbuilding steel grades are virtually non-existenct. The only published work is a paper by (Chatzidouros et al., 2015). They looked at crack growth parameters of AH36 steel grade and MAG welding process and Hybrid Laser Welding (HLAW) process from FINCANTIERI shipyards. The test performed under 0.1 stress ratio. The results are given in Table 6-3 below along with their threshold stress intensity factor values. It is clear that the reported properties are superior to the values recommended in the literature.

Material	m	Ln(C)	$\Delta K_{th}(N.mm^{3/2})$
LH/MAG	2.5124	-26.405	952
MAG	1.9635	-21.801	974
AH36	3.46	-31.981	395

Table 6-3 (Chatzidouros et al., 2015)

6.6.4.4 Discussion on available models

In order to test goodness of correlation relationships given in "C and m treated as correlated variables" section deterministic m values given in Table 6-1 and Table 6-3 are used to estimate the corresponding C values using the correlation equations, then the estimated values are compared with actual values and presented in Table 6-4 and Figure 6-21. It is apparent that they all appear to be reasonably satisfactory models, although (Cortie and Garrett, 1988) and (Baker and Stanley, 2008) show better estimates.

	m	Actual Values	(Cortie and Garrett, 1988)	(Tanaka and Matsuoka, 1977)	(Baker and Stanley, 2008)
MAG	1.96	-21.80	-21.68	-22.28	-22.05
LH/MAG	2.51	-26.41	-25.68	-26.08	-25.85
Snijder (Plain Steel)	2.8	-27.76	-27.77	-28.07	-27.83
Snijder (weld metal)	3.07	-29.16	-29.74	-29.94	-29.70
DNV	3.1	-29.84	-29.96	-30.15	-29.91
AH36	3.46	-31.98	-32.58	-32.64	-32.39
DNV	3.5	-31.01	-32.87	-32.92	-32.67

Table 6-4 Comparison of correlation relationship equations

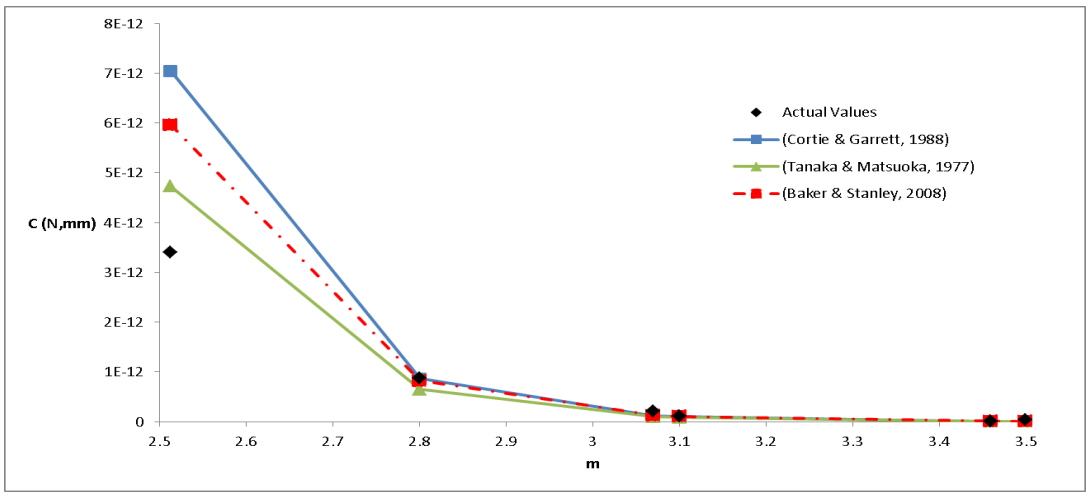

Figure 6-21 Comparison of correlation relationship equations

As it can be seen in Figure 6-22 correlation equations from (Cortie and Garrett, 1988) and (Baker and Stanley, 2008) show very similar results and very close approximation to actual values. As a result, either of these two equations may be used to estimate C from m or vice versa.

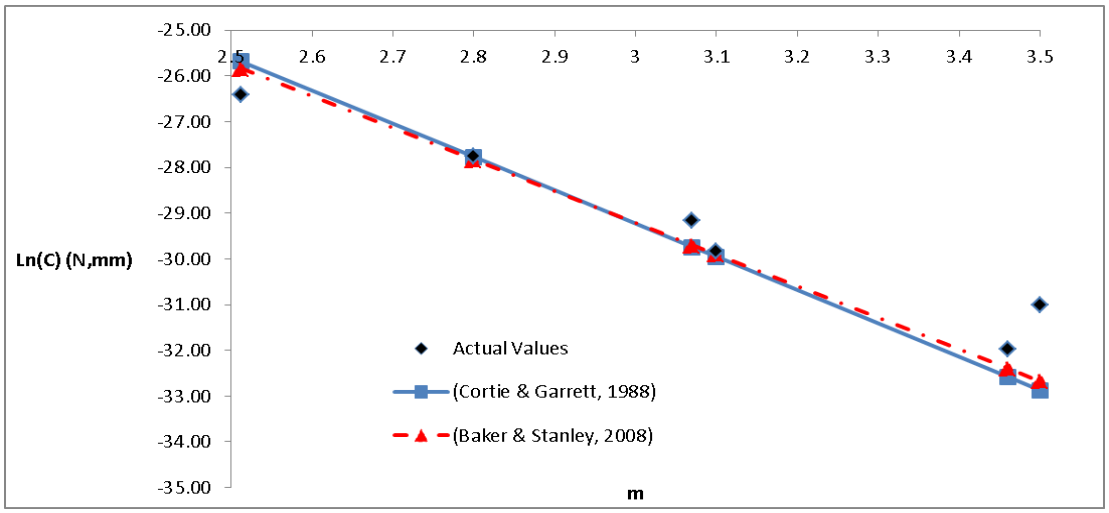

Figure 6-22 Comparison between equation from (Cortie and Garrett, 1988) and (Baker and Stanley, 2008)

Since the case study ship structure is made entirely from AH36 steel in the mid ship area, the C and m value from Table 6-3 may be used for crack growth models when the crack is expected to propagate in the parent material. When a crack is extending in weld material, the corresponding stress ratio is greater than 0.5 hence the values in Table 6-3 could be non-conservative. In this case, values corresponding to stage B from Table 6-2 may be used. A third option would be to model m as a stochastic variable. According to (Gurney, 1979), m ranges between 2.5 to 3.6 for real structural steels thus a good reasonable estimate is to model m with a normal distribution with

a mean value of say 3.05 and standard deviation of 0.275. Then using equation from (Cortie and Garrett, 1988) or (Baker and Stanley, 2008) C can be calculated. Effects of choice of C and m values are shown in Figure 6-23. A through thickness crack of half-length, a, of 10.2 mm under constant amplitude 16 $MPa\sqrt{m}$ cyclic stress, which corresponds to a typical constant amplitude fatigue stress range at a passenger ship deck within the midship area is studied. m parameters and their corresponding mean C parameters are chosen from Table 6-1, Table 6-2 and Table 6-3 for crack growth in Air environment. It is clear that time variant crack size is very sensitive to the choice of the parameters available in the literature. It is interesting to observe that the mean values from (Veritas, 1984) result in smaller crack size than other curves apart from the AH36 data. However, (Veritas, 1984) curve has a very large uncertainty with 0.77 Ln(C) standard deviation and will exhibit a more conservative upper-bound value.

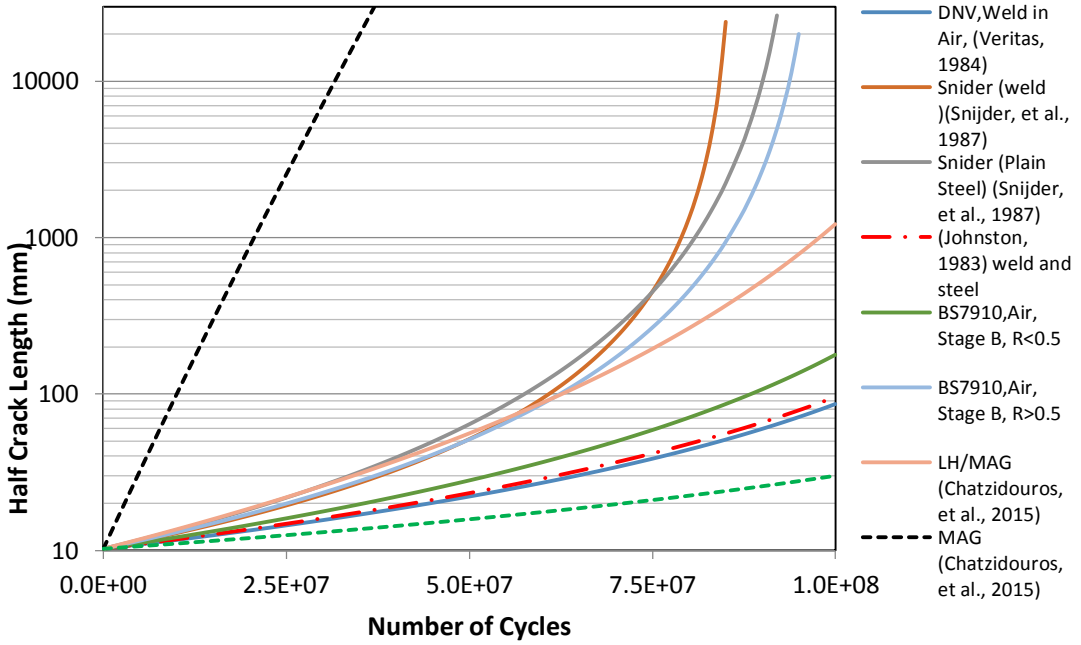

Figure 6-23 Effect of choice of crack propagation parameters

When the structure is made of only one steel type and a known stress rate the standard deviation of Ln(C) is much less than 0.55 from (Veritas, 1984). The Ln(C) equal to 0.24 from (Johnston, 1983), based on (Gurney, 1979) is a more reasonable choice. This issue seems to have been addressed in a recently published document from DNV in which standard deviation of Ln(C) has reduced to 0.33 for weld metal and 0.25 for base metal (DNV, 2015). This is also consistent with the lower uncertainty in stage B crack growth applicable to large cracks extending in the plane stress regime (Baker and Stanley, 2008), (King, 1998), and (BSI7608, 2015) .

(Johnston, 1983) and (Gurney, 1979) models are yet more conservative than AH36 grade steel parameters reported by (Chatzidouros et al., 2015).

6.6.5 Choice of crack growth parameters

As explained in the previous section, crack growth parameters proposed by (DNV, 2015) show the closest but conservative estimate to those reported by (Chatzidouros et al., 2015) for AH36 steel. As a result, the parameters recommended by (DNV, 2015) will be used in reliability calculations of this research. m will be treated as a constant deterministic value equal to 3.0 for weld and parent metal in air environment and weld in the marine environment with cathodic protection. A common practice in fracture mechanics is to take an upper bound value of C, usually corresponding to 90 or 95 percentile on Ln(C). However, Upper bound values of 90 or 95 percentile appear to be over conservative and unrealistic. An alternative approach is to treat C as a stochastic variable. Here, using probabilistic analysis of crack growth a constant C value which gives similar crack growth behaviour as a fully probabilistic model is estimated. The fully probabilistic analysis is performed by the Monte Carlo simulation method. Initial crack size and C are treated as stochastic variables. An exponential initial defect size distribution with a mean value of 15 mm, which corresponds to mean half crack length from ship #2 data, was chosen. m was treated as a constant value and equal to 3.0. C is modelled with the lognormal distribution with mean equal to Ln(1.83E-13), and Standard deviation of Ln(C) equal to 0.25. The simulation results converged after 2000 simulation, but 3000 simulations were performed to give better precision. Then constant C values corresponding to different percentiles of C distribution were tested with the simulated defect length values. Time-dependent mean defect lengths from the fully probabilistic model and models with constant Cs were compared, and as it is shown in Figure 6-2, it was found that C value corresponding to 70 percentile gives a similar crack growth curve to the fully probabilistic model.

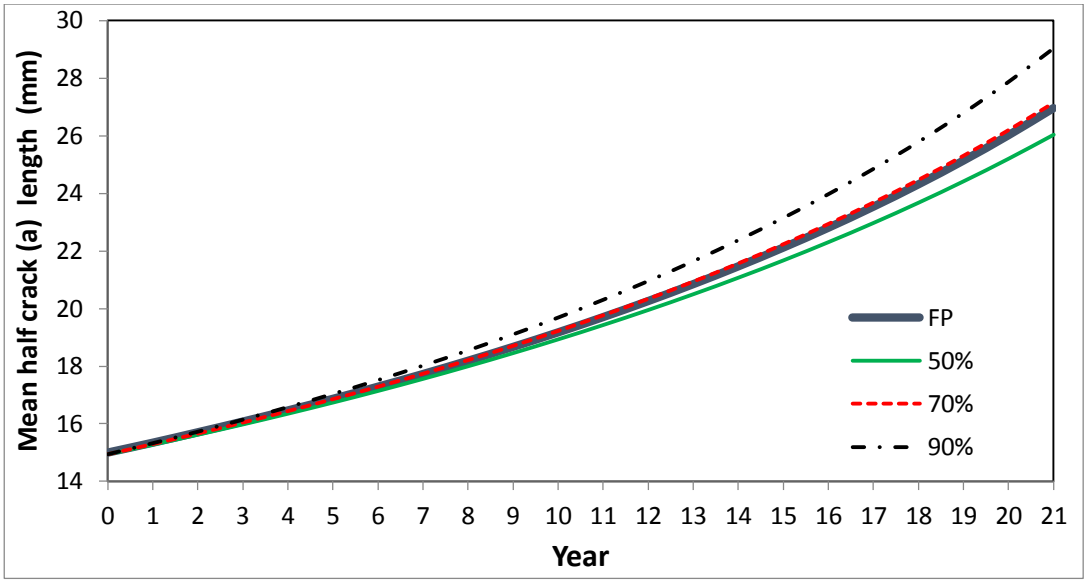

Figure 6-24 Comparison between crack growth curves of various C values

6.6.6 FAD uncertainty

The failure assessment Locus described in section "FAD" is based on the concept of the failure assessment diagram validated by validation studies using mainly wide plate test results covering several materials groups including pressure vessel and pipeline steels and aluminium alloys (Muhammed et al., 2000 a). The data also included some pressure vessel and pipe burst tests. The resulting locus is a lower bound failure function below which probability of failure is very low (Hadley and Pisarski, 2013), (Dowling et al., 2005)and(Muhammed et al., 2000 b). This essentially means that an assessment point may fall in failure region, but there is a chance that the real structure may not fail (Muhammed et al., 2000 a). In other word, probability of failure calculated using FAD is the probability of the assessment points falling in the failure region rather than the actual physical probability of failure.

(Muhammed et al., 2000 a) conducted research to quantify the statistical uncertainty associated with Level 2A/3A BS7910:2005 FAD using the whole dataset that had been employed to derive the original FAD. The failure points in FAD are shown in Figure 6-25 below.

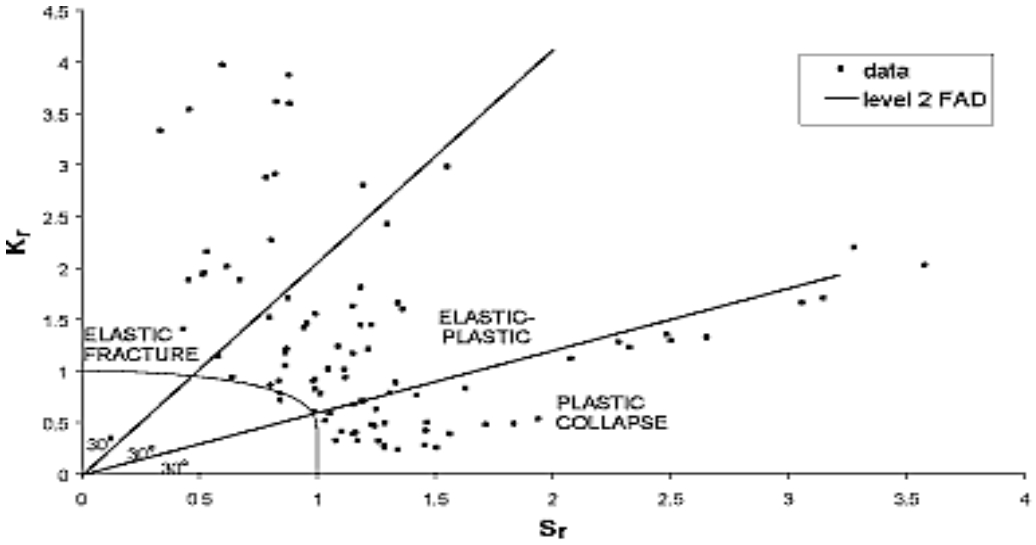

Figure 6-25 Wide plate failure results from (Muhammed et al., 2000 a)

For a failure point F, they described the measure of the uncertainty of the model by comparing the radial distances R and r from the origin to the point and FAD respectively. M_u ,the measure of the uncertainty is obtained from the difference R-r. The concept is illustrated in Figure 6-26.

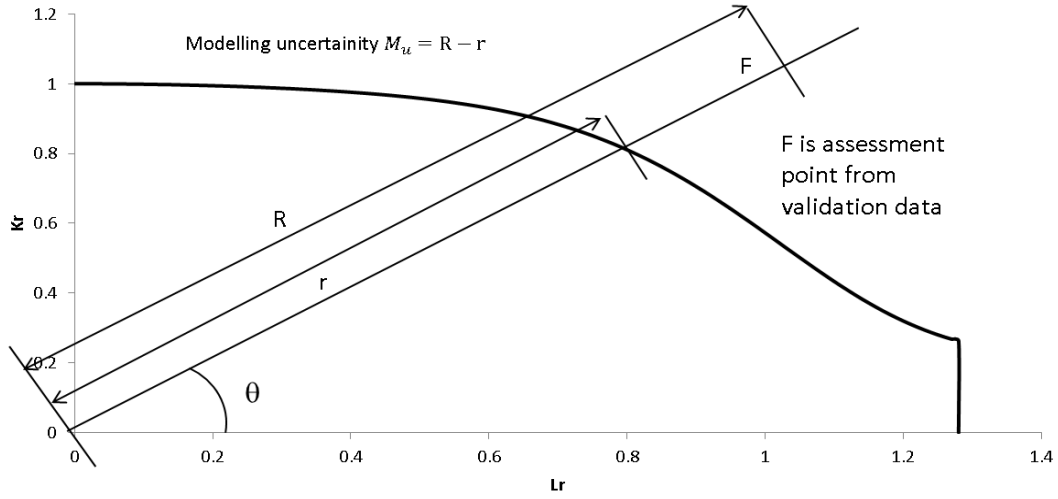

Figure 6-26 Diagram of uncertainty in the (FAD), (Muhammed et al., 2000 a)

The measured uncertainties are quantified in terms of the best fit distribution and also mean and standard deviation values for the three regions of FAD. An overall uncertainty over all three regions was calculated as well. The results are given in Table 6-5. Additionally, the cumulative probability at the FAL line is calculated by the author of the thesis and is given in Table 6-5. This probability is the failure probability for an assessment point that falls exactly on the FAL.

FAD Region	Best-fit dist.	Parameters (Weibull)				Moments	
		Location	Scale	Shape	Cumulative probability at FAL	Mean	Std. dev
Elastic (θ =60-90°)	Weibull	-0.06	1.9	2.13	6.36E-04	1.62	0.83
Elastic-plastic (θ =30-60°)	Weibull	-0.06	0.55	1.08	8.73E-02	0.47	0.49
Collapse (θ =0-30°)	Exponential	-0.06	0.83	1	6.97E-02	0.77	0.83
All (θ =0-90°)	Weibull	-0.06	0.97	1.11	4.45E-02	0.87	0.84

Table 6-5 Results of statistical analysis of model uncertainty in terms of R-r from (Muhammed et al., 2000 a).

To investigate the effect of uncertainty in failure assessment line (FAL) for the structure under study, reliability calculation for a critical grand-block butt weld joint in deck 16 is studied using the developed Monte Carlo code. The same detail will be studied again at the end of this chapter using the developed Convolution Integral code. The Monte Carlo code here will demonstrate the validation of the Convolution Integral code, as well as providing a graphical representation of the FAL uncertainty modelling, as depicted in Figure 6-28. The input variables for this study are listed in Table 6-11. Here the assumption for the reliability calculation is that one defect is present at the structure (one defect per joint) and no inspection is in place. As it is apparent in Figure 6-28 left, assessment points for this study case are located in the fracture dominant zone of the FAD thus only model uncertainties associated with this zone are considered here. As shown in Table 6-5, (Muhammed et al., 2000 a) proposed a three parameter Weibull distribution as the best fit to the data used by (Muhammed et al., 2000 a) accompanied by a set of mean and standard deviation which can be presented by a Normal distribution. Figure 6-27 shows that the significant difference in the choice of the distribution is at the left tail of the distributions. A normal distribution will produce more negative values providing a more conservative estimate of the FAL. This effect is tested in the reliability calculation case study. In the original study, FAD uncertainity was modelled to be input into a reliability study using an inhouse reliability software. The reason that the authors considered Normal distribution in addition to the three-parameter Weibull distribution seems to be the inability of the employed reliability software to model the three-parameter Weibull distribution.

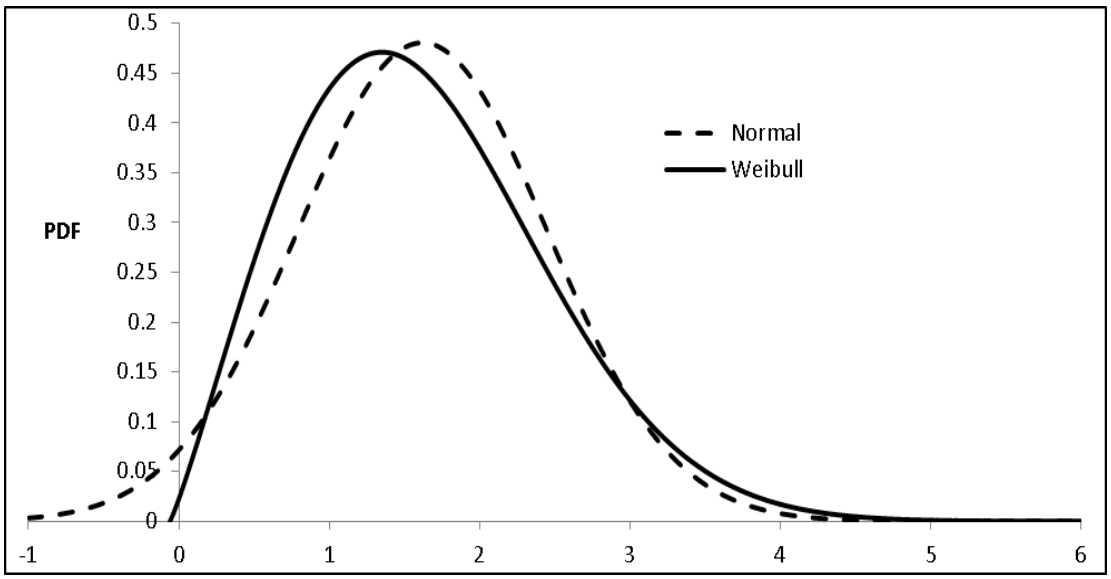

Figure 6-27 Uncertainty modelling in the Fracture dominant zone

Reliability analyses under three different assumptions were carried out: Without including any uncertainty in FAL, modelling the uncertainty using Normal distribution and using best fit Weibull distribution. The results are presented in Table 6-6 and Figure 6-28. In Figure 6-28 the assessment points are shown in the plot on the left. In middle and right side plots simulated uncertainties are plotted modelled by the Normal distribution and Weibull distribution, respectively.

	Without FAL Uncertainty	Uncertainty modelled with Normal distribution	Uncertainty modelled with Weibull distribution
Final Year Probability of failure	2.52E-3	9.42E-4	4.4E-4

Table 6-6 Failure probabilities

Failure probability without any modelling uncertainty gives the highest calculated probability of failure. This result also shows an excellent agreement with the final year reliability calculation using Convolution Integral which is presented in Figure 6-9 (left). Notice that some simulated FAL points using Normal distribution have negative Kr values which are invalid.

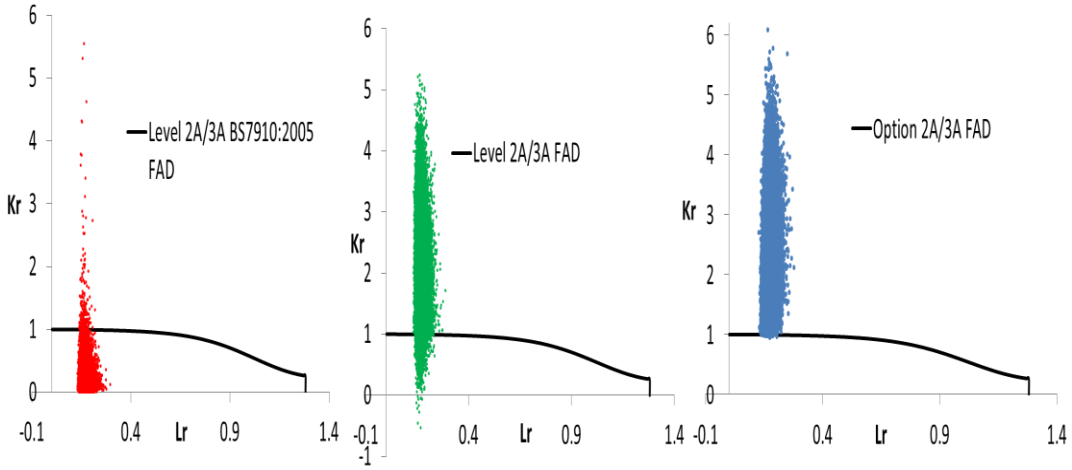

Figure 6-28 FAL uncertainty (Left: Assessment points. Middle: Simulated FADs with Normal dist., Right: Simulated FADs with Weibull distribution)

Additionally, the sensitivity of the Monte Carlo simulation to the number of simulation was investigated, and the results are shown in Figure 6-29. It can be seen that the failure probabilities start to converge after 10^5 samples, a reasonably low number of simulations. The failure probabilities at this number are estimated to be 2.62E-3.

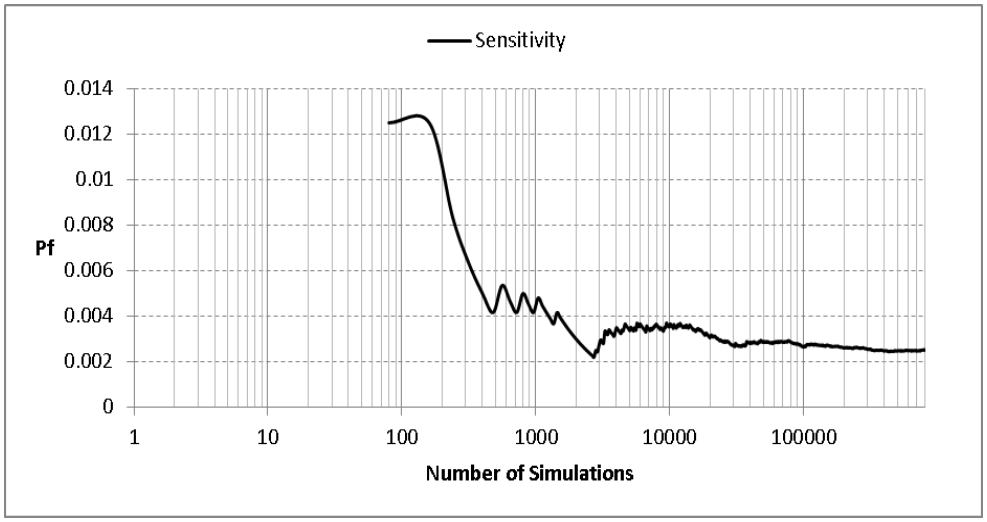

Figure 6-29 Monte Carlo reliability method sensitivity to the number of simulations

The conclusion, here, is that failure probabilities without the FAL uncertainties are noticeably conservative. In this research, the effect of FAL uncertainty will not be considered in favour of better computation time and enhancing the simplicity of the convolution integral code, but may be reflected by the Monte Carlo method if higher precision is required. This limitation in convolution integral code can be potentially addressed by increasing the variability in the extreme stress to allow for the uncertainty in the FAL.

6.7 Fracture Mechanics case studies

In this section two cases are considered:

- A deterministic fracture mechanics analysis of a stiffener fillet weld for the most unfavourable crack orientation
- A probabilistic analysis for the critical grand block butt weld with the most unfavourable crack orientation

Welds joining stiffeners to the plates constitute a substantial amount of total welding performed for ship hull structures, for example, 63% of the total volume of welding performed for ship#2 are fillet welds of the stiffeners.

Transverse butt joints connecting Grand block are considered critical location in the structure as the weld line is perpendicular to the global bending tensile stress of the vessel, and a longitudinal weld crack can grow into a critical length to cause failure under the effect of this stress. Grand block butt welds in the deck area constitute 19% of all the preformed welding of ship#2.

Both cases are selected from deck #16 which is under the highest stress among all the decks (Figure 6-12 and Figure 6-13).

6.7.1 Assessment of the stiffener fillet weld

Stiffened panels in the midship area and the location of the study are made of 8 mm thick plates welded to bulb section with 100X5 mm dimensions (height * thickness), as depicted in Figure 6-30 below. Stiffener pacing is 700 mm, and both the plate and the bulb profile are from AH36 grade shipbuilding steel. The welding process used is hybrid laser arc welding (HLAW).

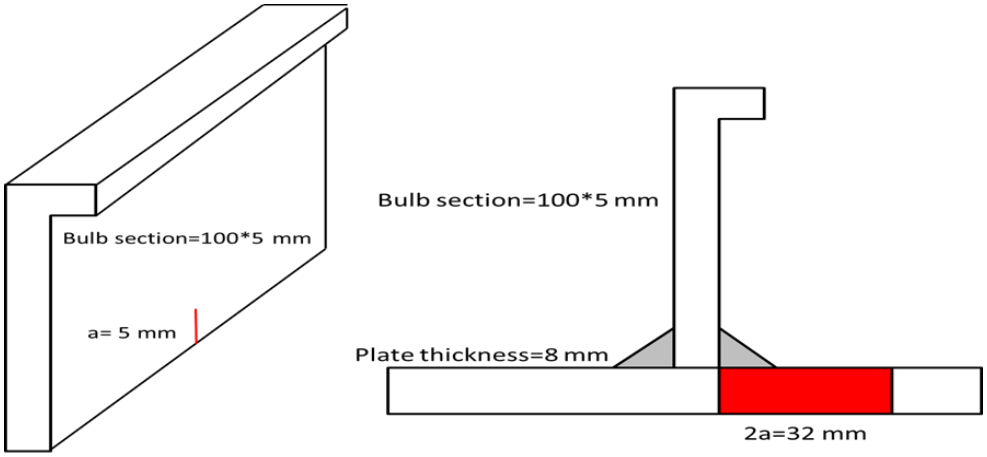

Figure 6-30 Studied stiffened panel detail

In fracture mechanics analysis, when possible, it is best to show acceptability of a defect (Fitness for Purpose) using deterministic procedures. A summary of the chosen parameters is given in Table 6-7.

For a panel stiffener, a conservative hypothetical through-thickness transverse crack was assumed. A crack size equal to the wed throat is a reasonable assumption. Typically fillet weld throat is equal to 0.7 of the stiffener thickness. In this case, stiffener thickness is 5 mm. An additional level of conservatism is also considered by assuming that the tensile residual stress field in the vicinity of the stiffener would increase the crack length to 3.5*t_{plate}, as explained in "Effect of residual stress" section of this chapter. Two cases are considered:

1. The crack growth in the plate with initial 32 mm length
2. Crack growth in the stiffener with initial length of 5 mm

For the case of a crack extending in the plate, 5th percentile fracture toughness, and typical yield and tensile strength for AH36 steel grade was assumed. Upper bound crack growth parameters of single slope crack growth model from BS7910 and zero K_{th}were assumed. Weld residual stress for the crack growth model was assumed negligible but long-range residual stress due to fabrication loads equal to 20% of Yield stress was assumed.

The assessment was conducted using parameters specified in Table 6-7 and using (BS7910, 2015 a)option 1 failure assessment diagram. The analysis results are given in Table 6-8 and Figure 6-31.

Parameter	Value		Description
N	5.32E+07		Total Number of cycles (20 years)
B (mm)	8		Section thickness
W (mm)	30000		Section width
2a (mm)	32 in plate, 5 in stiffener		Crack Length
σ_Y (MPa)	430		Yield Stress
σ_U (MPa)	550		Tensile strength
K_{mat} $(MPa\sqrt{m})$	259.3		Toughness
Pm (MPa)	170		Primary Stress (used in FAD)
$\Delta\sigma_{eq}$ (MPa)	12.2		Equivalent cyclic stress
σ_{res} (MPa)	86 (20% of Yield)	0	Total residual stress
m	3		Crack growth parameter
C	5.21E-13		Crack growth parameter
K_{th}	0		Threshold stress intensity factor

Table 6-7 Assessment inputs for crack growth in the plate

The final crack length was found to be 165.3 mm at the end of design service life. The critical length for fracture is found to be 679 mm, leaving a substantial margin of safety. By back calculating crack growth the initial critical crack was found to be 53 mm. Although, the occurrence of initial defect size as large as 53 mm in this detail is improbable, there is a reasonable chance that sizes beyond the calculated crack size are found with the visual inspection at the yard. As it is shown in chapter 4, a lower bound estimate probability of detection for visual inspection is 80% (good access). As explained in "Effect of residual stress" section at distances beyond 3.5*t_{plate} from the location of the stiffener tensile residual stresses change to compressive residual stress, hence assuming the long range tensile stress applies for longer crack lengths is over conservative and unrealistic. A second analysis was preformed assuming negligible total residual stress at the crack tip. The final critical length and the corresponding initial critical crack size are found to be 1779 mm and 67 mm, respectively. This would result in a higher degree of safety both in terms of greater margin of safety from failure point and increased chance of finding initial critical crack sizes with the visual inspection.

Crack	With tensile residual stress	Zero residual stress	Description
2a	165.3 (mm)	165.3 (mm)	Final Crack Length
$2a_{cr}$	679 (mm)	1779 (mm)	Critical crack size
$2a_{cr}^{inital}$	53 (mm)	67 (mm)	Critical initial crack size

Table 6-8 Fracture Mechanics results for crack growth in the plate

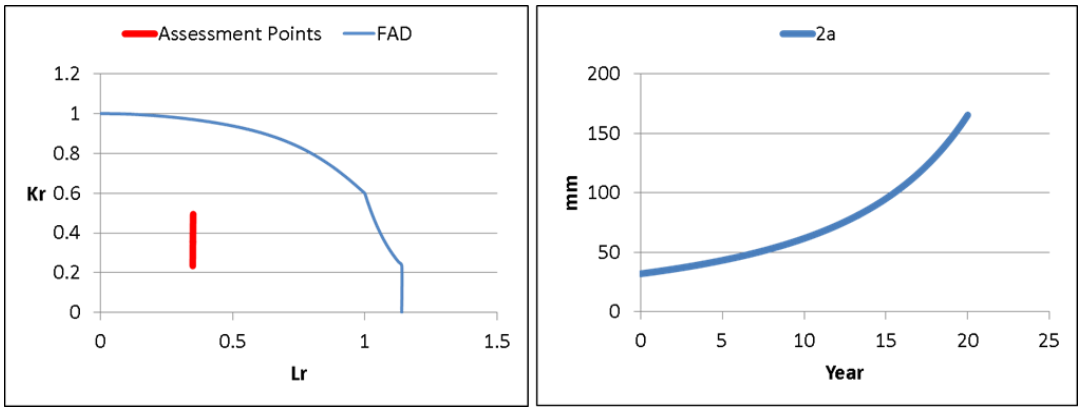

Figure 6-31 Fracture Mechanics results for crack growth in the plate with residual stress

Figure 6-31 right shows crack length growth during time starting from 32 mm at the beginning of the service life reaching to 163.5 mm at end of year 20. Figure 6-31 right shows corresponding assessment points in the Failure Assessment Diagram (FAD). The assessment points start at Kr= 0.21 reaching to Kr=0.52 at the end of year 20. It is evident that the margin of sfaty (distance between assessmt points anf the FAD

locus are substantial.For the case of crack growth in the stiffener, a 5 mm (1.5 mm bigger than weld throat) through thickness edge crack extending towards the stiffener flange is assumed. In this case, tensile residual stress equal to the material yield stress is assumed. All other factors are assumed similar to the case of crack extension in the plate. The input parameters are listed in Table 6-9.

Parameter	Value	Description
N	5.32E+07	Total Number of cycles (20 years)
B (mm)	5	Section thickness
W (mm)	100	Section width
2a (mm)	5	Crack Length
$\sigma_Y\ (MPa)$	430	Yield Stress
$\sigma_U\ (MPa)$	550	Tensile strength
$K_{mat}\ (MPa\sqrt{m})$	290	Toughness
Pm (MPa)	170	Primary Stress (used in FAD)
$\Delta\sigma_{eq}\ (MPa)$	12.2	Equivalent cyclic stress
$\sigma_{res}\ (MPa)$	430 (Equal to Yield Stress)	Total residual stress
m	3	Crack growth parameter
C	5.21E-13	Crack growth parameter
K_{th}	0	Threshold stress intensity factor

Table 6-9 Assessment inputs for crack growth in the Stiffener

As listed in Table 6-10, final crack length at the end of life of the ship life is calculated to be 23.83 mm. Critical crack size and corresponding initial critical crack size are found to be 25.16 (mm) and 5.5 (mm) respectively. This is shown in Figure 6-32.Note that that the section width is only 100 mm, as the crack is propagating along the stiffener height (Figure 6-30). Thus the critical crack size has become much smaller (25.16 mm) than the crack propagating in the plate.

Variable	size	Description
2a	23.83 (mm)	Final Crack Length
$2a_{cr}$	25.16 (mm)	Critical crack size
$2a_{cr}^{inital}$	5.5 (mm)	Critical initial crack size

Table 6-10 Fracture Mechanics results for crack growth in the stiffener

It is apparent that, unlike the previous case of crack growth in the plate, the margin of safety is small and the initial critical crack size has a small chance of being detected by visual inspection (less than 10%). However, the consequence of the failure is low. The deck consists of 42 stiffeners (every 700 mm in a 30 m width deck). Considering that the structure constitutes of 17 decks, a shell structure taking significant portion of global bending stresses, and four longitudinal bulkheads, it is concluded that failure of the stiffener will not cause any service distribution for the ship or danger to

the people on-board. Additionally, even a 5.5 mm crack will not necessarily fail before the end of the ship's lifecycle; the assumptions made were a lower-bound fracture toughness of 5 percentile of toughness distribution, extreme wave load case, and an upper-bound crack growth parameter C (90 to 95 percentile). In reality, the crack growth rate can be slower, and the toughness can be significantly higher. Moreover, the only NDT programme that can ensure detection of critical defect size with a high degree of confidence needs to have 100% coverage, as a transverse crack can happen anywhere along the weld line, and partial inspection is unlikely to be effective unless occurrence of the crack is systematic. Therefore a quality control programme focusing on the welding process would be more meaningful here. HLAW process used in the yard produces a small crack rate of 0.21% (Chapter 4).

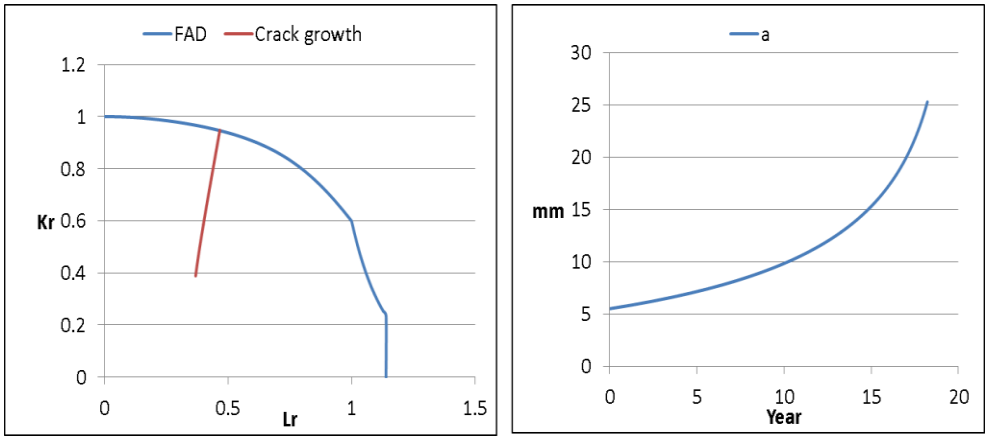

Figure 6-32 Fracture Mechanics results for crack growth in the stiffener

In conclusion, NDT inspection of fillet joints connecting the stiffeners to the plates is not beneficial considering almost zero failure probability of a crack extending in the plate, low failure consequence of a hypothetical crack, extending in the stiffener, and disproportionate cost of an effective NDT programme.

6.7.2 Assessment of the butt weld of a grand block joint

Probabilistic analysis of the butt joint connecting two grand block sections at the deck area in deck 16 is considered here. The input parameters are listed in Table 6-11. The analysis is carried out using the developed Convolution Integral code. Considered probabilistic variables are initial defect size, wave-induced stress, material toughness and NDT probability of detection.

Parameter	Approach	Value
Still Water stress	Constant	71 MPa
Wave-induced stress	Weibull	71 MPa (For Probability of exceedance of 10^{-8})
Weibull shape parameter	Constant	0.85
Residual stress	Constant	$\sigma_Y = 86\ MPa(20\%\ \sigma_Y)$
Crack growth parameters m	Constant	3.0, (DNV, 2015)
Crack growth parameter C	Constant	1.93867E-13 (70 percentile), (DNV, 2015)
Geometry function	Constant	1.0
Initial defect size	probabilistic	Exponential distribution (mean 2a= 72 mm)
Fracture toughness	probabilistic	Weibull distribution (Shape= 4, Scale= 481 MPa)
Yield stress	Constant	430 MPa
Ultimate tensile strength	Constant	550 MPa
FAD modelling uncertainty	probabilistic	Normal distribution (Mean= 0.87,Std.= 0.84)
NDT capability	probabilistic	VT (90 %POD= 121 mm, 50% POD =16mm)
		RT (90 %POD=31.1 mm, 50% POD =9.36mm)
		UT (90 %POD= 21.46 mm, 50% POD =6.46mm)
		MPI/PT (90 %POD= 28.61 mm, 50% POD =8.6mm)
		MPI/PT (90 %POD=5.72 mm, 50% POD =1.72mm) ground crown welds

Table 6-11 parameters used in the reliability analysis of the grand block butt weld

Several through-life reliability cases depending on the choice of the NDT method were considered:

1. No inspection, including visual inspection
2. Visual inspection (VT)
3. Other NDT methods: Radiography (RT), Conventional Ultrasonic (UT), Magnetic particle inspection (MPI), and Dye penetrant (PT)

Time-dependent failure probability without and with visual inspection are shown in Figure 6-33, Figure 6-34 and Figure 6-35. Final year probability of failure without inspection reaches to 2.82E-3. However, the rule agreed among all classification societies is to perform a visual inspection of all the finished welds. Hence, a reliability calculation accounting for the visual inspection was calculated. Final year probability of failure in case of visual inspection is reduced to 2.45E-5. The reduction is consistent

with the results from the previous case of deterministic analysis where minimum initial critical crack length was found to be between 53 to 67 mm with above 80% chance of detection.

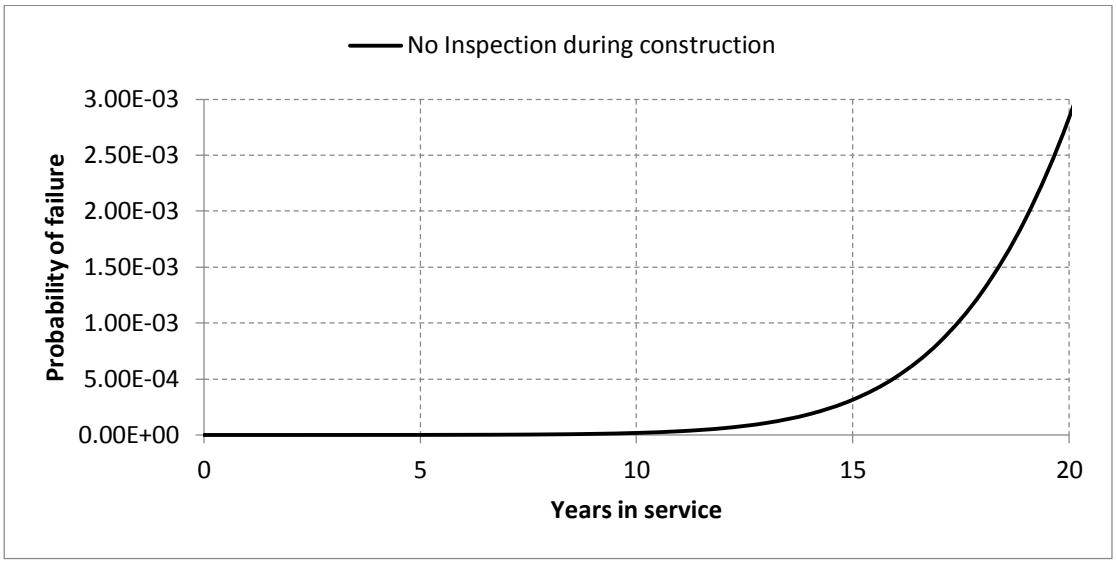

Figure 6-33 Time-dependent probability calculations (No Inspection)

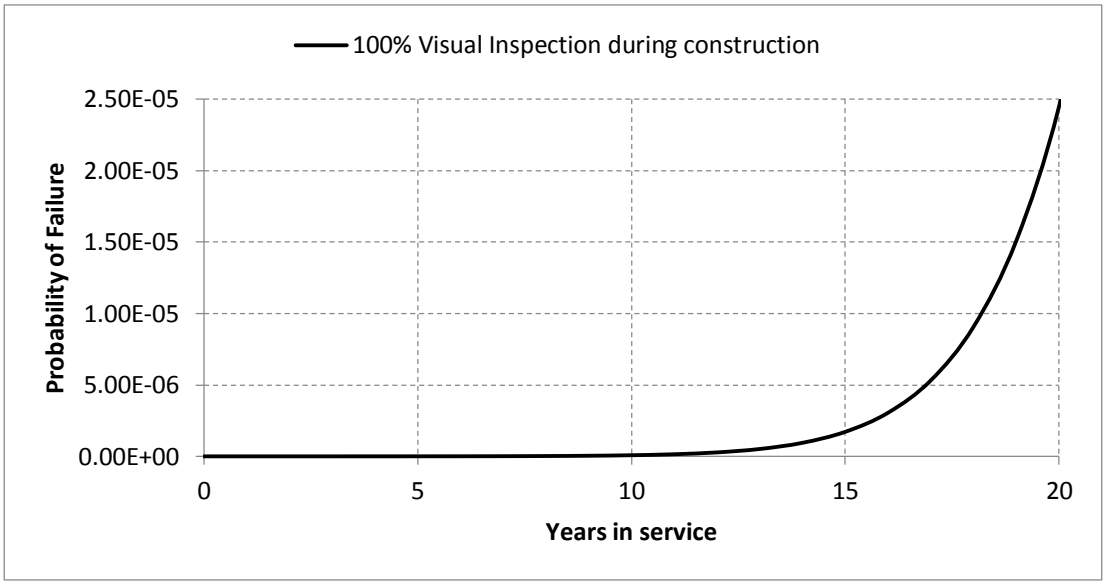

Figure 6-34 Time-dependent probability calculations (Visual Inspection)

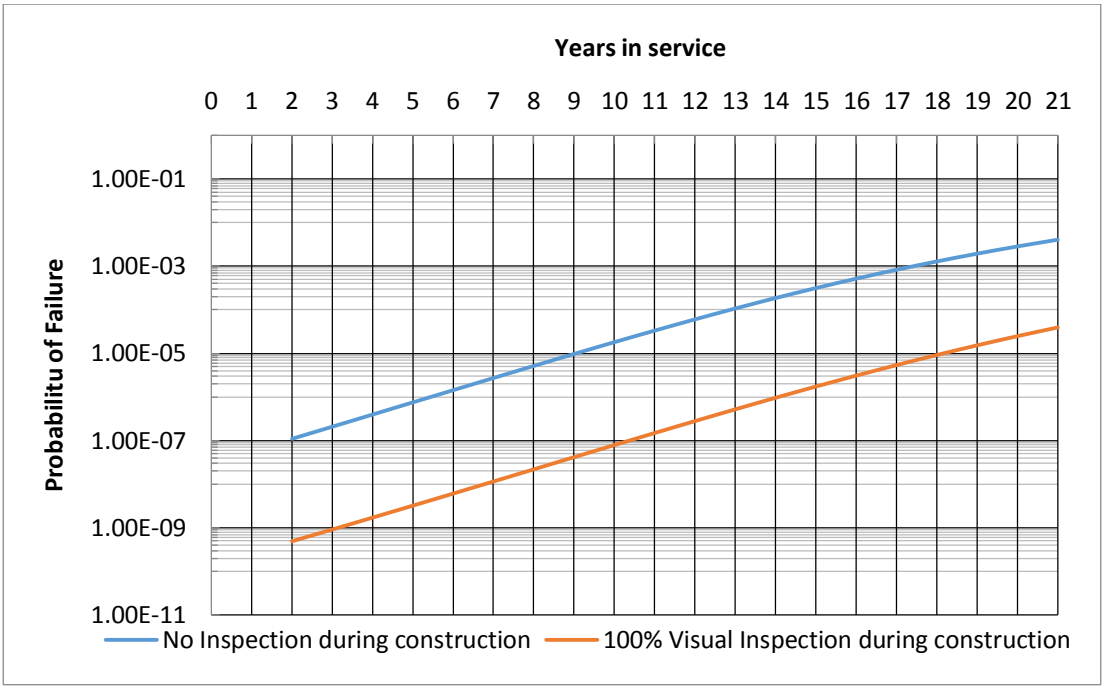

Figure 6-35 Effect of visual inspection on failure probability

The effect of different NDT methods was studied by changing the detection probability function concerning the NDT capabilities (see Table 6-11). The results are shown in Figure 6-36. Final year failure probabilities are 8.8E-12, 1.28E-14,3.11E-12 and 4.23E-23 for Radiography, Ultrasonic, Surface NDT (MPI/PT) as-welded condition, and Surface NDT (with crack extended through-thickness or ground crowns), respectively. Using RT improves reliability more than 6 orders of magnitude, however for this to be effective RT needs to be performed to the similar extent of VT (100%). Using UT instead of RT can improve the reliability by more than 2 orders of magnitude due to the far better capability of UT in detecting planar defects. Surface inspection (MPI/PT) shows a better efficiency than RT and less effectiveness than UT. For through-thickness cracks or good conditions of weld surface, such ground crowns the surface NDT shows drastic increased in efficiency through reducing failure probability by more than 17 orders of magnitude compared to visual inspection. It should be noted that the assumptions here are that the defects are surface breaking- a reasonable assumption for thin plates. In thicker sections, in excess of 15 mm, defects can be internal where surface inspection is ineffective. Additionally, as explained in chapter four, for plates below 6 mm UT cannot be applied, therefore the choices are limited to RT or a surface NDT. RT has the benefit of being highly efficient in detection of nonplanar flaw, as well, but requires health safety restrictions (chapter 4).

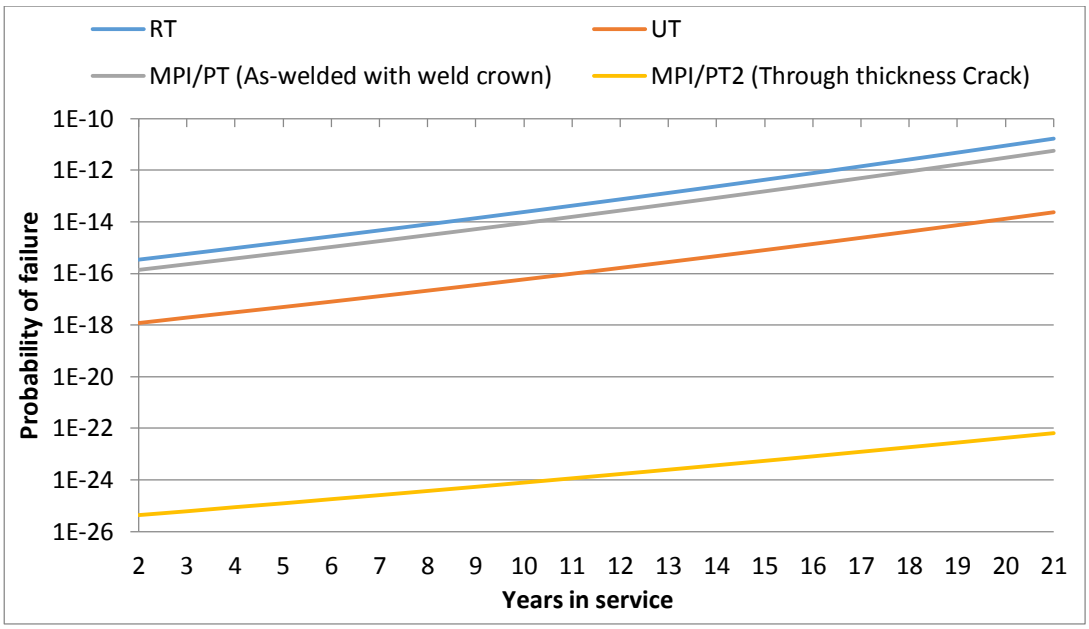

Figure 6-36 Effect of choice of NDT technique

The failure probabilities calculated above are based on the assumption that one defect is present at the weld joint. Strictly speaking, the assumption is that only one defect is present but the size of the defect is uncertain. Therefore the defect size distribution accounts for the uncertainty in size. Therefore, it is necessary to account for failure probability due to various quantities of defects.

Considering the joint as series system and any checkpoint containing a defect as a component failure probability of the joint is:

$$P_{f-Joint} = 1 - (1 - P_{component})^n \tag{6-30}$$

Most likely values of n can be estimated from the Poisson distribution or /binomial distribution which show comparable results (see "7.7 Point estimate of defect rate"). Poisson distribution is defined by equation (6-31) below:

$$P(X = n) = e^{-\lambda} * \lambda^n / n! \tag{6-31}$$

where,λ is the defect rate and n is the number of defects. For high integrity structures ($P_{f-Joint} \ll 1$), the probability of failure the probability of failure be simplified to (Williams and Mudge, 1985):

$$P_{f-Joint} = \sum_{n=1}^{\infty} P(n) * n * P_{fcomponent} \tag{6-32}$$

where, P_f is the individual probability of failure, calculated above. The assumption is that the failure of each defect is independent from each other. Equation (6-32) can be written as:

$$P_{f-Joint} = P_f * \sum_{n=1}^{\infty} P(n) * n = P_{f\ component} * \lambda \qquad (6\text{-}33)$$

In this example λ is the number of defect per welded joint and welded joint is 30m long. From section 4.6 "Defect rates", the defect rate of FCAW process (applicable to the grand block joints) and for planar defects in shipyard #2 is 0.146 per metre length. $\lambda = 0.146 * 30 = 4.38$. The total time-dependent failure probability of the joint is plotted in Figure 6-37. Final year failure probability is 1.07E-04, below the target reliability for a crack extending in the plate of a multi-deck passenger ship which is 2.33E-4 as established in the target reliability section from Chapter 3. The target tolerable failure probability is 2.17 times the calculated probability indicating that higher defects rates or bigger defect size can be tolerated by the structure without exceeding the target failure probability. For instance, provided that the defect size and toughness distributions remain unchanged up to 9 defects per grand block joint or, 0.316 defects per metre, may be allowed.

The time-dependent reliability curves with and without accounting for the defect rate are plotted in Figure 6-37, below. The figure shows the benefit of improving the welding process or using/developing a process which produceces less defects.

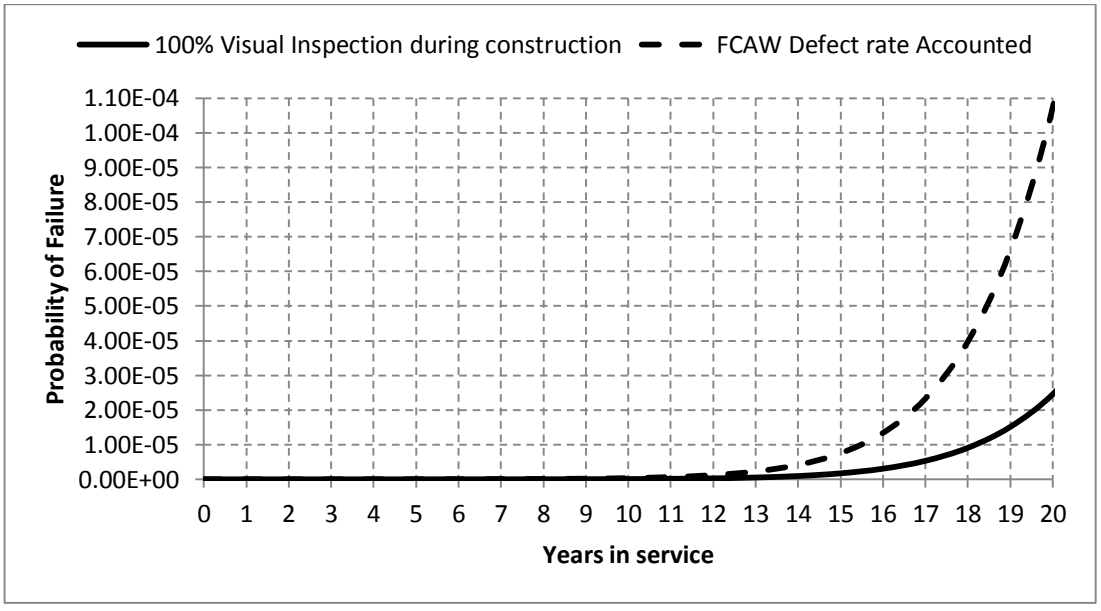

Figure 6-37 Effect of defect rate on failure probability

Passenger ships are not usually subject to in-service inspect of the deck area since the structure is concealed under the outfitting. However, to demonstrate the impact of in-service inspection on the through life reliability two different hypothetical in-service inspections are considered: Full visual inspection at year 5 and year 9 of service. The results are shown in Figure 6-38. The failure probability is reduced as a result of visual inspection, assuming that detected cracks are rapaired afterwards. The code updates the defect distribution after the schadualed inspection to a the distribution of the undetected cracks by considering the Probability of Nondetection (POND). The final year probability of failure in both cases reduces from 1.07E-4 (Figure 6-37) to 2.46E-07 for inspection at year 5 and 6.35E-07 for inspection at year 9 indicating that inspection at year 9 is more effective. This is due to the failure probabilities being more affected by larger crack sizes that only appear in later years of service and since the visual inspection is more effective for large cracks early visual inspection will not benefit the structure as much as a later inspection will do. Notice the difference between failure probability drop in year 5 in the red curve and drop in year 9 of the blue curve in Figure 6-38. An optimal inspection inspection is, hence, an inspection at year 9.

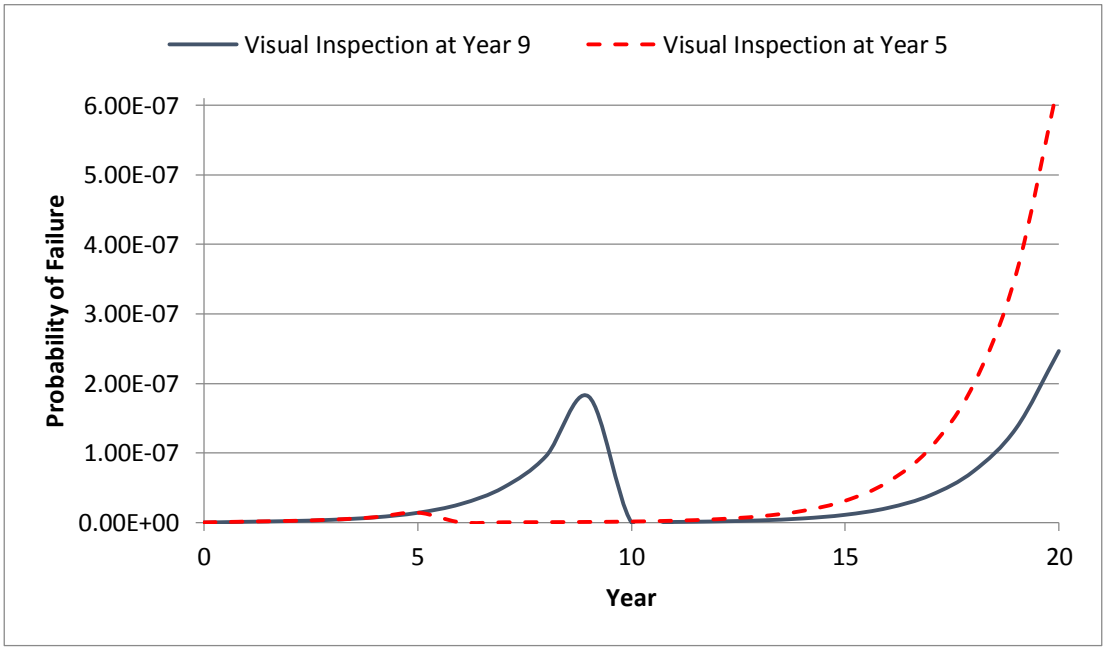

Figure 6-38 Effect of in-service visual inspection on through-life reliability

6.8 Chapter summary

In this chapter the reliability of weld fabrication defects of ship hull structures was investigated:

Principles of fatigue analysis using the S-N curve method, its applications and limitations were explained: S-N curve approach is appropriate for the design and assessment of the joints that are free from significant defects. Moreover, fracture mechanics theory as a tool for assessment of planar defects was explained.

Two fatigue and fracture mechanics reliability algorithms developed in this research were explained, and their merits, limitations and the applications to this work were discussed.

- An algorithm and its respective code based on Monte Carlo simulation method were developed for fully probabilistic analyses (all variable treated stochastically) to study the effect of various random variables on the failure probability and to validate a faster code.
- A faster algorithm and its respective code based on the Convolution Integral method for analysis of the case study structure was developed the method was outlined.

Various identified modelling uncertainties, that affect the calculated reliabilities, were discussed, their impacts on the failure probabilities were investigated, and appropriate models or values were recommended.

- Residual stresses in stiffened panels have favourable effects on crack growth due to compressive stress field in the majority of the plate area along the direction of a critical crack extension.
- Additionally, the stiffeners slow down the crack growth due to their restraining effect which reduces the stress intensity factor in the vicinity of the stiffener.
- Crack growth parameters m and C are treated by two approaches in the literature for probabilistic analysis. The common approach assumes m as a deterministic value and C as a random variable, commonly modelled by lognormal distribution. The second approach treats both variables as random variables using a correlation equation. Various models available in the literature were studied, and the values proposed by (DNV, 2015) were found to be the most appropriate model to the ship structures. For crack in Air environment an m value of 3.0 and Ln(C) value with the mean value of Ln(1.83E-13) and standard deviation of Ln(C) equal to 0.25 is proposed by (DNV, 2015). A probabilistic model of crack growth parameters in a typical deck plate was carried out using the Monte Carlo code, and the analysis showed that Ln(C) equal to 70^{th} percentile of the randomly

modelled Ln(C) would yield similar crack growth results as the probabilistic model.

- FAD uncertainty has been studied using the probabilistic model proposed by (Muhammed et al., 2000 a). Reliability analysis using the Monte Carlo simulation code showed that the calculated final year probability of failure could be substantially reduced by considering the FAD uncertainty particularly, in the fracture dominant region of the FAD.

Study cases of two critical joints were investigated: 1. Deterministic analysis of a fillet weld joining the stiffener to the plate. 2. Probabilistic analysis of a butt weld joining deck plating of two grand-blocks.

- Deterministic fracture mechanics using conservative assumption in accordance to BS7910 showed that NDT for fillet welds of stiffeners is NOT necessary from structural failure point of view.
- Reliability analysis of a butt weld, joining deck plating of two grand-blocks, using the Convolution Integral code found that the final year probability of the structure to be 2.45E-05 considering 100% visual inspection and assuming the defect rate equal to 4.38 defect per joint. The calculated reliability is 2.17 times below the target probability of failure suggesting that the structure may be tolerant of higher defect rates or bigger defect sizes.
- Visual inspection was found to be very effective in reducing the failure probability both during construction and in-service due to the failure being dominated by long cracks that can be effectively detected by visual inspection.
- Choice of NDT method on the reliability of a structure that is inspected 100% was studied, and it was found that the effectiveness of the methods in decreasing order is as follow: MPI/MT of ground welds, UT, MPI/MT of the as-welded joint and RT.

This chapter concludes the work on the reliability assessment and the results will be used in chapter 7 and 8 of this thesis.

Chapter 7

Statistical sampling and process control

7.1 Chapter outline

Safety analysis can benefit from a partial NDE inspection programme by:

- Improving the estimate of the reliability of the structure by reducing epistemic uncertainty (due to lack of knowledge i.e. statistical uncertainty) in defect frequency and size data by increasing the statistical confidence on the data
- Increasing the actual reliability of the structure by, through encouraging quality work and repairing defective work, reducing the number of defects that will be present in the structure
- Monitoring and controlling welding and fabrication process by detecting defects caused by out-of-control processes

The aim of this chapter is to investigate the effect of NDE sample size on statistical confidence about defect data, the reliability estimation of the structure and the quality of the welded joints.

First, different types of causes of errors and their effects on uncertain variables are explained. Then the relationship between sample size and statistical confidence is investigated, and the effect of statistical confidence on the reliability of a welded joint containing defects is studied.

The point estimate of defect rates investigated is explained, and subsequently, a method of determining inspection sample size based on confidence interval is proposed.

Additionally, Bayesian inference theory is outlined, and estimation of defect size distributions, defect rates and material properties based on this theory is studied.

Finally, statistical process control (SPC) method and its application in detection of defects caused by out-of-control processes is described.

7.2 Type of errors and their detection schemes

The errors occurring in products of a process can originate from two types of causes:

- Common causes or natural causes are inherent in the process and are associated with inherent variations in the process.
- Special causes or assignable causes that are unusual and due to real changes in the system which are unexpected. Their effect is unquantifiable.

Common causes normally result in changes in variability (spread/ precision) of the observed errors, whereas special causes can cause change in both variability and absolute level (centring/ accuracy). This is schematised in Figure 7-1 which shows the implication of precision and accuracy in hitting the middle of the circle target.

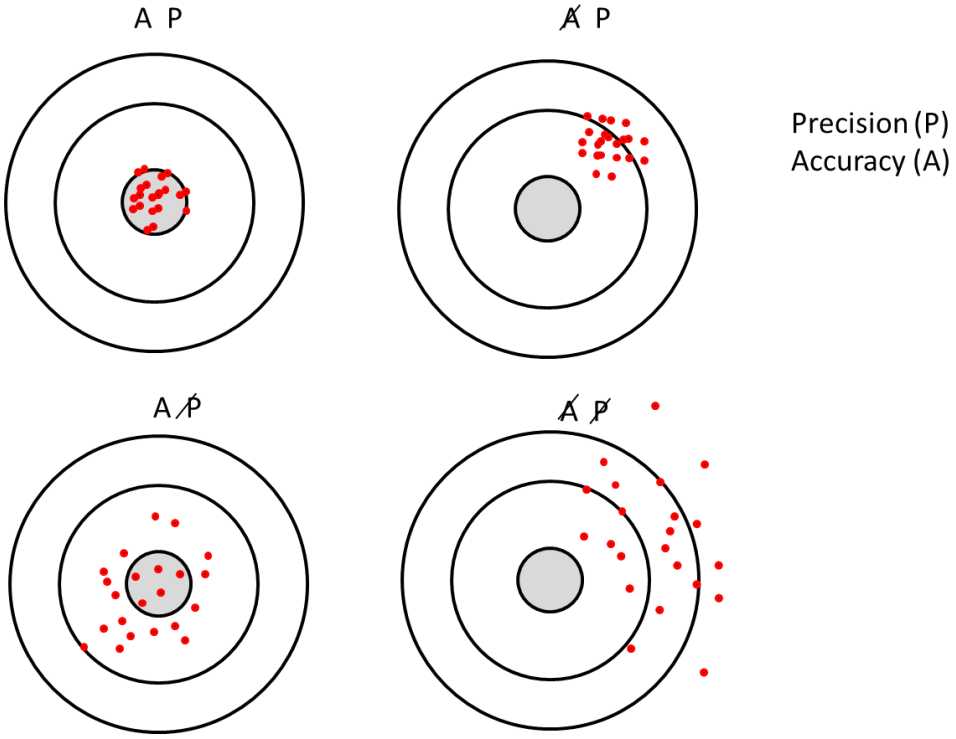

Figure 7-1 Common causes vs assignable causes (Oakland, 2008)

One example of an assignable cause leading to weld defect formation is an abnormal fluctuation in the welding machine power supply which can alter the voltage. A too high voltage will result in poor arc control, inconsistent penetration and a turbulent weld pool that fails to consistently penetrate the base material. Too little voltage results in poor arc starts, control and penetration. It also causes excessive spatter, a convex bead profile and poor tie-in at the toes of the weld. Another example is a case which was witnessed by the author in a shipyard: Caused by poor maintenance of

moulding shoes in an automatic process machine, transverse cracks were produced systematically.

An example of weld defects caused by common causes is cracks occurring due to the welder's skill.

In this research, the assumption is that defects are predominantly caused by common causes. Thus reliability analysis, as a branch of engineering science which deals with safety analysis of the systems with uncertain variables, can provide the tolerable variability of the defect frequency and sizes.

Statistical methods are then used to define the number of samples required to quantify the variability of the data with the required confidence. Collecting too many samples will not just be more expensive, but will not necessarily give more or better information.

The majority of this chapter focuses on the methods of assessing the variability of the data, particularly defect data, using statistical sampling and its connection with statistical confidence.

Defects that are triggered by special causes are considered using another branch of engineering, the statistical process control (SPC). Although these causes are not the prime emphasis of this research, since there is a close relationship between statistical sampling and SPC, the method is outlined in the second part of this chapter, and the generic framework with application to this work is developed with a view of further investigation in future research.

7.3 Sample size and statistical confidence

Increasing the number of NDT checkpoints will increase the statistical confidence in the estimation of defect size and frequency (Visser, 2002). Epistemic uncertainty reduces as the sample size increases. If we were able to perfectly accurately inspect 100% of the welds, the distribution parameters would be the population distribution parameters, or in other words, we would have been 100% confidence on the distribution parameters. By taking samples that do not include the whole population, the sample distributions will inevitably deviate from the population distribution (Holick`y, 2013). This is schematised in Figure 7-2.

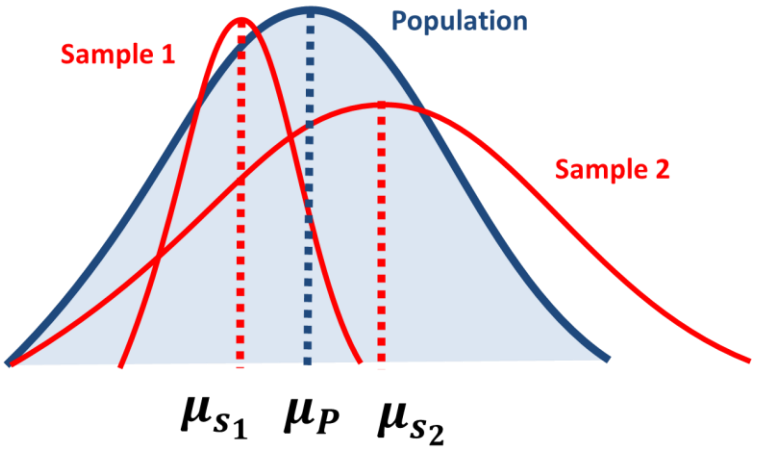

Figure 7-2 Population and sample distributions

7.3.1 Point Estimate of distribution

Point estimate of distribution parameter gives a particular estimated value of the parameters. For data that follows a normal distribution, $N(\mu_m, \sigma_m)$ .The sample mean (m) will follow a normal distribution with a mean value of μ_m and standard deviation of σ_m (Figure 7-3).

The unbiased estimate of the population mean (μ) can be described by the sample mean.

$$\mu_m = \mu \tag{7-1}$$

Standard deviation of the sample mean can be described by:

$$\sigma_m = {}^{\sigma}/_{n} \tag{7-2}$$

where ,σ is the sample standard deviation, and n is the sample size. The sample variance s^2can be described by Chi-squared (X^2) distribution with v=n-1 degree of freedom (Figure 7-3).

$$X^2 = \frac{ns^2}{\sigma^2} \tag{7-3}$$

The unbiased estimate $\hat{s}^2$ of the population variance σ^2 corresponds to the mean μ_{X^2} of the random variableX^2.

$$\mu_{X^2} = \frac{ns^2}{\hat{s}^2} = n - 1 \tag{7-4}$$

The best estimate $\hat{s}^2$ of the population standard deviation σ corresponding to the mean μ_{X^2} of the X^2distribution of the sample variance s^2 follows from equation (7-4) as:

$$\hat{s} = s\sqrt{\frac{n}{n-1}} = \sqrt{\frac{\sum_1^n (x_i - m)^2}{n-1}} \tag{7-5}$$

Thus, the denominator n-1 in the estimate, equation (7-5), is because the best estimate is derived from the mean of the X^2distribution describing the sample variancess^2.

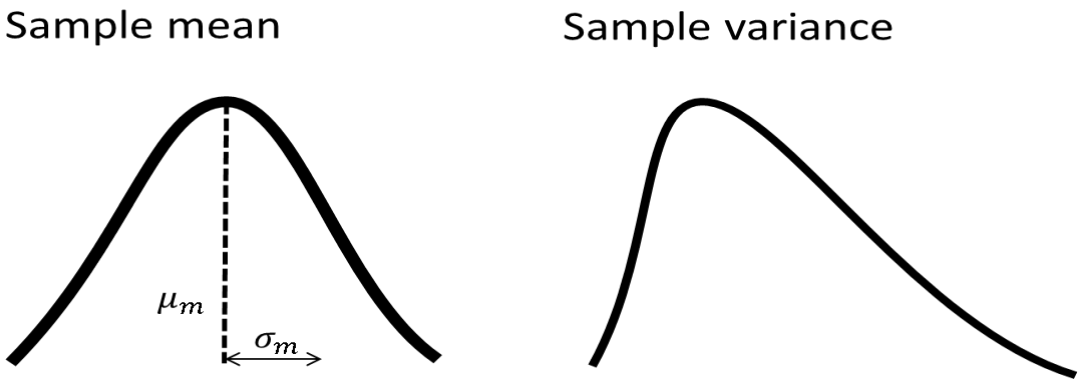

Figure 7-3 Schematics of the sample mean and standard deviation parameter uncertainty distributions

7.3.2 Interval estimate of the distribution parameters

Unlike a point estimate, the interval estimate provides a range of values that are likely to contain the parameter. This range is called the confidence interval. In general, the interval estimates provides better information about the possible range of the population parameters. The interval estimates always correspond to some confidence level. Commonly, the confidence level 1-2p=0.90 or 0.95 is accepted, where the probability p= 0.05 or 0.025 signifies a one-sided probability that the limits will be exceeded. This is shown in Figure 7-4, below. The interval estimates of the population mean depends on whether the population standard deviation σ is known or unknown. If the population standard deviation is unknown then instead of *σ* the sample standard deviation s and appropriate sampling distribution is to be considered.

When standard deviation of the population is known, the interval estimate of mean is estimated by:

$$m - z_p \frac{\sigma}{\sqrt{n}} < \mu < m + z_{1-p} \frac{\sigma}{\sqrt{n}} \tag{7-6}$$

where, $z_p$and $z_{1-p}$are the fractiles of standardised normal variable corresponding to the probabilities *p* and 1-*p*. For relatively big sample sizes the sample standard deviation can be taken as the population standard deviation.

When the standard deviation of the population is unknown (small sample sizes), interval estimate of mean is estimated by:

$$m - t_p\sqrt{\frac{s}{n-1}} < \mu < m + t_{1-p}\sqrt{\frac{s}{n-1}} \tag{7-7}$$

where, $t_p$and $t_{1-p}$are the fractiles of the t-distribution corresponding to the n-1 degree of freedom and probabilities p and 1-p.

The interval estimate of unknown population variance and standard deviation is derived from the X^2-distribution (Holick`y, 2013):

$$\sqrt{\frac{n}{x^2_{1-p2}}}s < \sigma < \sqrt{\frac{n}{x^2_{p2-1}}}s \tag{7-8}$$

where, s is the sample standard deviation. The confidence level is stated as $1 - p_1 - p_2$, where p1 and 1-p2 are the probabilities corresponding to the lower and upper fractiles $X^2_{p1}$and X^2_{1-p2}specified for ν= n-1 degree of freedom.

The interval estimate of population proportion is estimated by:

$$\bar{p} - z_p\sqrt{\frac{p(1-p)}{n}} < p < \bar{p} + z_{1-p}\sqrt{\frac{p(1-p)}{n}} \tag{7-9}$$

where, $\bar{p}$ is the sample proportion.

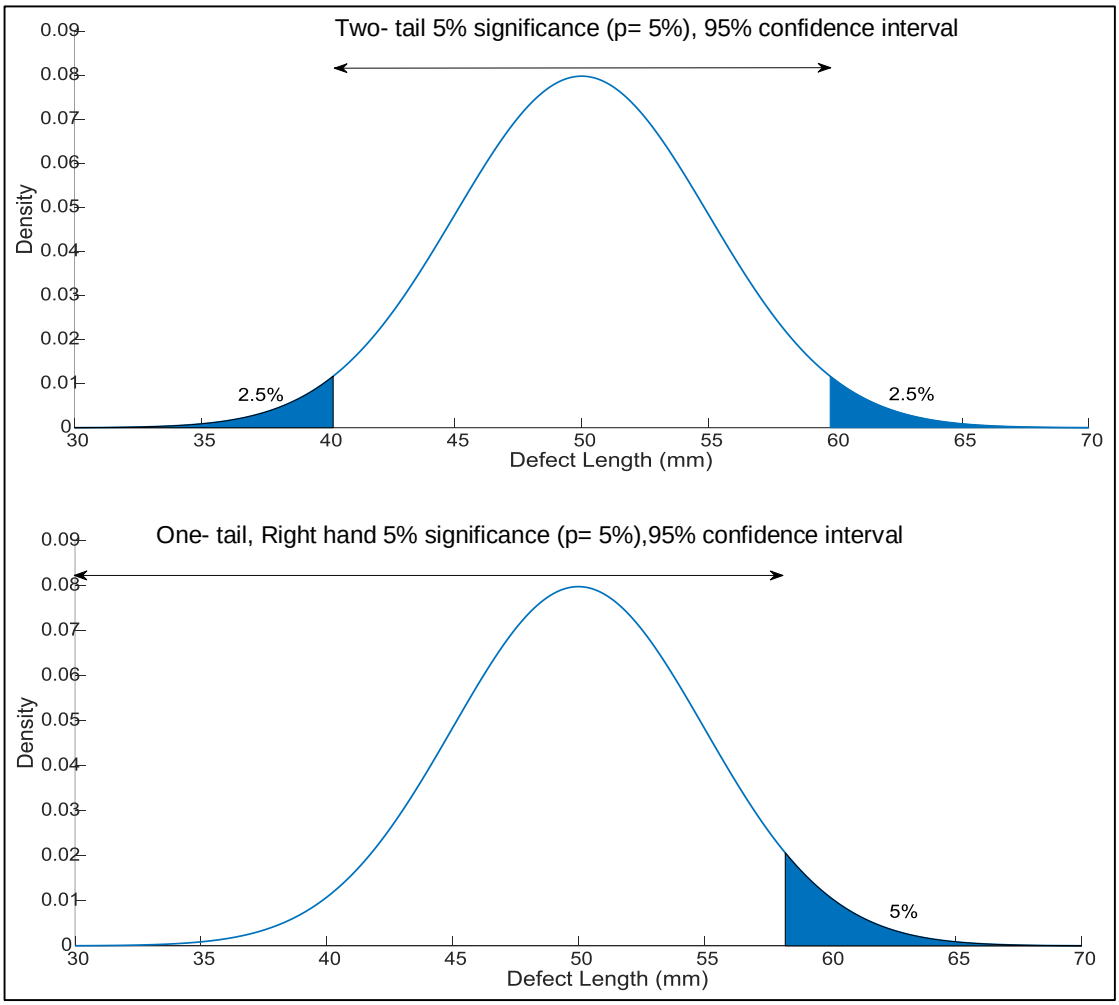

Figure 7-4 Confidence interval and significance level

7.4 Effect of extent of inspection on statistical confidence

In chapter four the defect size and rate data were estimated using the total inspected checkpoints of the vessels (full sample size). These inspections were performed during the construction process and are representative of the randomness of defect size and frequency of the whole structure. The sample sizes were relatively big, resulting in good statistical confidence; this is explained here in more detail.

In chapter six the defect size and frequency distributions were used to calculate the reliability of the case study welded joints. If smaller sample sizes were to be taken, the estimated distribution would have differed from the current estimated distributions. Even if the sample size is not reduced, it may be required to assess the defect statistics before the entire ship is inspected, i.e. at certain time intervals during the construction. Deviation of the defect statistics taken from smaller sample sizes from the full sample size is studied by drawing a series of random samples taken from

the dataset. The sizes of the sample were chosen at different proportions to the full data set. The summary of the samples statistics is given in Table 7-1.

The dataset included defective checkpoints due to cracks and un-defective checkpoints. Checkpoints that included nonplanar defects were excluded. Samples are drawn from defected and undetected checkpoints. Samples sizes of 1.8%, 5%, 10%, 20%, 40%, 60%, 80% and 95% of the full sample were drawn. Sample size is considered very small if it is below seven (n<7), small if it is below 30 (n<30), large if above thirty (n>30) and very large if bigger than hundred (n>100) (Holick`y, 2013). For each sample size, 26 random samples were drawn to achieve reasonable confidence of the sample. The samples were taken with replacement.

	1.8 %	5%	10%	20%	40%	60%	80%	95%	Full Sample
Sample size	60	161	318	637	1276	1915	2552	3030	3189
Average Defective	3.08	6.8	13.27	30	59.5	93	118.3	144	147
Average un-defective	56.92	154.2	304.7	607	681	1822	2433.7	2886	3042
Defect rate	5.12%	4.22%	4.17%	4.71%	4.66%	4.86%	4.64%	4.75%	4.61%

Table 7-1 Summary of the randomly taken samples

Defect length distribution parameters were estimated using the method of moments (MOM) fitting into a lognormal distribution. The confidence bound of the parameters were calculated assuming that the distribution parameters follow a normal distribution. Another way to look at this is that the logarithms of defect lengths follow a normal distribution, then the mean of the logarithms will follow a normal distribution, as well. Mean ln values of all drawn samples are shown in Figure 7-5.

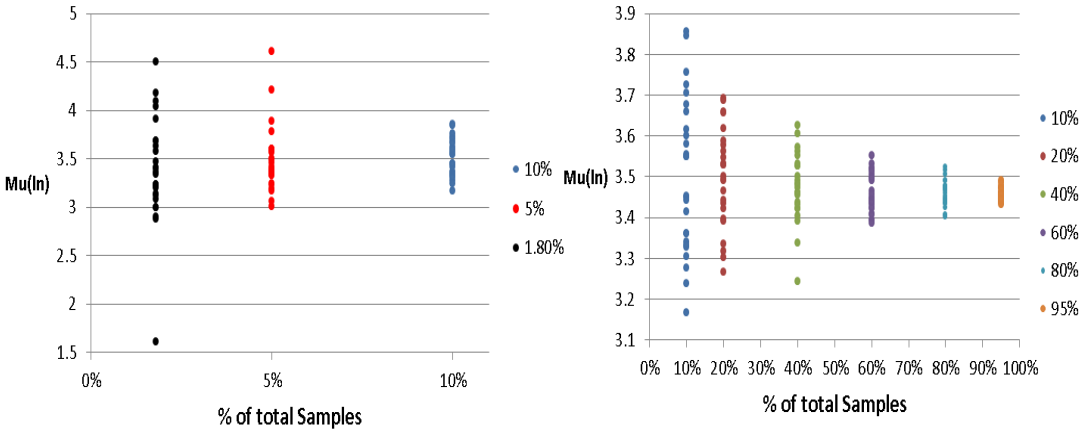

Figure 7-5 Samples mean ln drawn from the dataset

It is clear that the mean values have significant scatter when the sample size is 60. The scatter reduces exponentially as the sample size increases. Using mean and standard deviation of the mean ln lengths (μ) and standard deviation of ln values (σ)

at each sample size proportion, the trends of the reduction in the scatter was calculated and are shown in Table 7-2, Figure 7-6 and Figure 7-7.

Sample size ratio	M		σ	
	Mean	97.5% Upper bound	Mean	97.5% Upper bound
5%	3.5	4.05	0.72	1.21
10%	3.5	3.81	0.74	1.03
20%	3.49	3.69	0.77	1
40%	3.47	3.6	0.77	0.9
60%	3.46	3.53	0.79	0.85
80%	3.46	3.51	0.8	0.85
95%	3.46	3.48	0.8	0.81
100%	3.46		0.79	

Table 7-2 Mean and standard deviation and of ln values and their upper bound limits at each sample size ratio

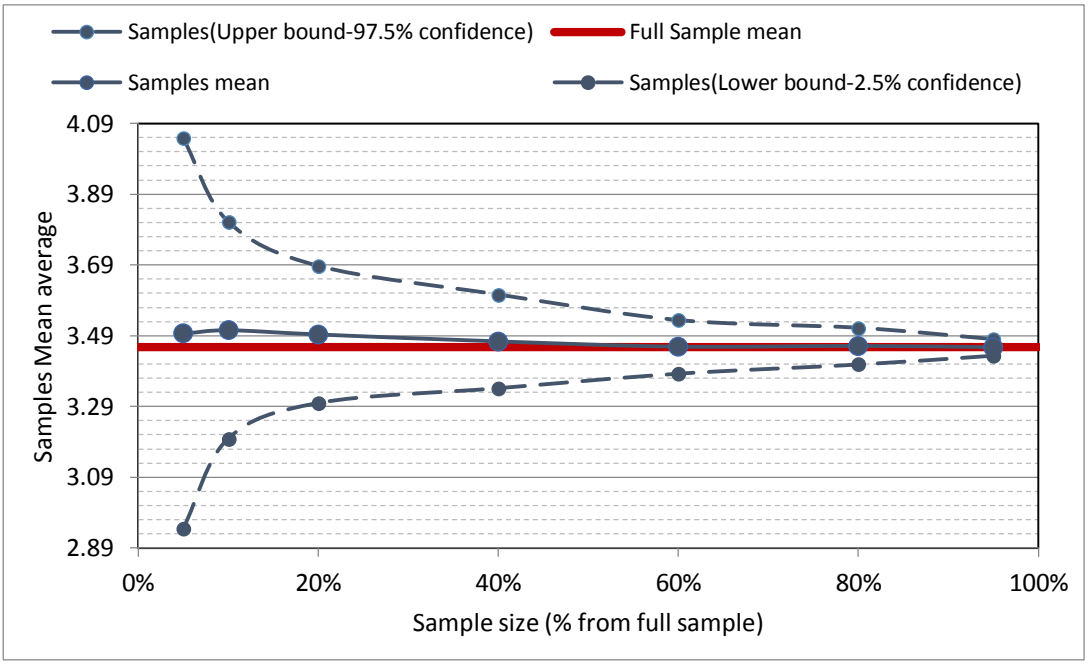

Figure 7-6 Mean of defect length ln values against sample size ratio

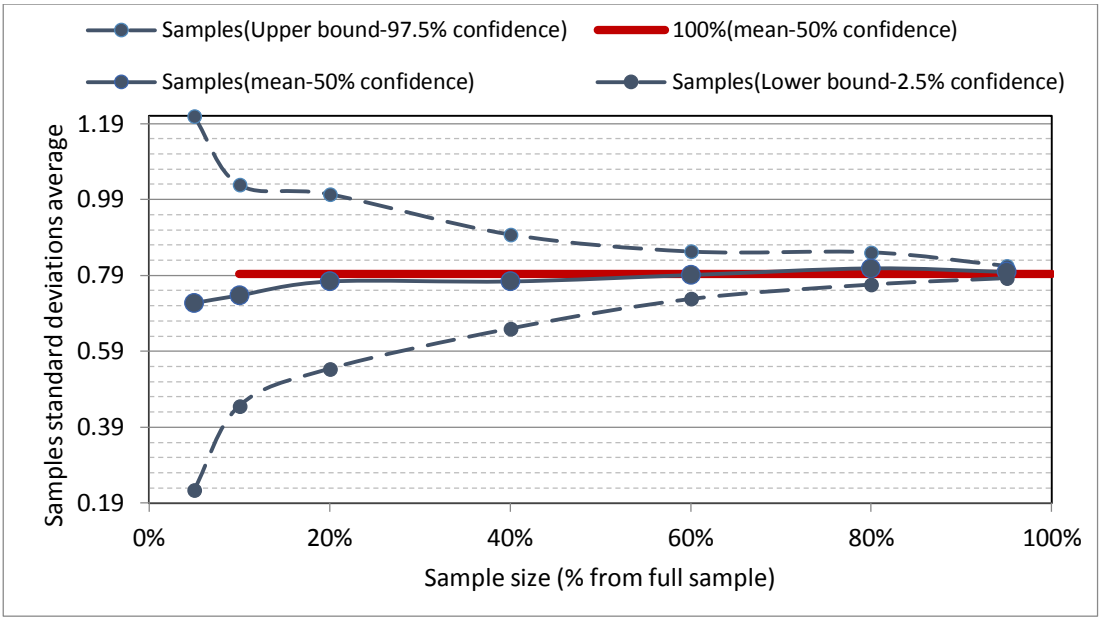

Figure 7-7 Standard deviation of defect length ln values against sample size ratios

The upper bound crack length distributions are also plotted in Figure 7-8. The curves were calculated by treating upper bound μ and σ values as input parameters of the lognormal distribution. As it can be seen: the difference between sample sizes above 40% is small. Notice that the distribution of the 60% sample (1915 checkpoints) and the 80% samples (2552 checkpoints) are almost identical indicating little benefit in increasing the sample size from 60% to 80%.

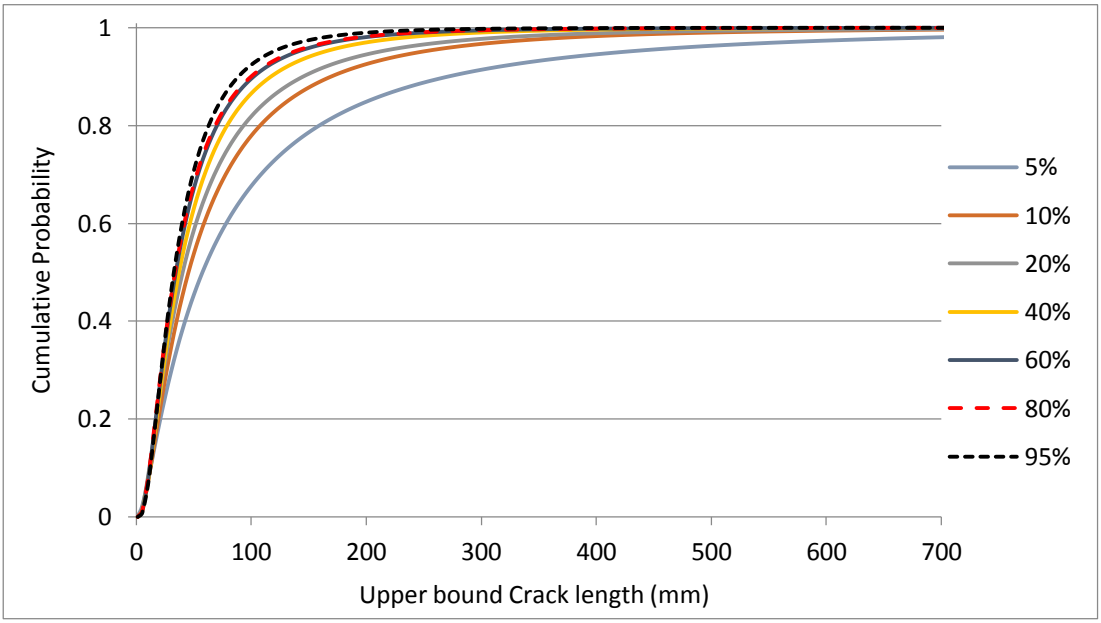

Figure 7-8 Upper bound crack length cumulative lognormal distributions

The reduction in the scatter of μ and σ is caused by the increase in the number of defects rather than the gross number of the checkpoints. I.e. if the defect rate was higher, the same confidence would have been achieved with smaller sample sizes.

As described in the point estimation section, uncertainty in the mean value of the normal distribution is inversely related to the sample size. The general form of above could be applied to any distribution parameter. For a sample of size n, the MLE $\hat{\theta}$ is a consistent estimator of the true parameter θ_0 , assuming its distribution asymptotically Normal, with variance determined by the reciprocal of the Fisher information (Pham, 2006):

$$\sqrt{n}(\hat{\theta} - \theta_0) \rightarrow \mathcal{N}\left(\theta, \frac{1}{I_1(\theta_0)}\right) \tag{7-10}$$

where, $I_1(\theta_0)$ is the Fisher information from a single sample. The observed information at the MLE $I(\hat{\theta})$ tends to the expected information asymptotically, so we can calculate (say 95%) confidence intervals with (Pham, 2006):

$$\hat{\theta} \pm \frac{1.96}{\sqrt{nI_1(\theta_0)}} \tag{7-11}$$

$$I_1(\hat{\theta}) = -\frac{d^2\ell(\hat{\theta})}{(d\hat{\theta})^2} \tag{7-12}$$

The scatter in parameter distribution is the result of the number of defects rather than the sample size. This is examined below:

Statistical uncertainties, due to sample size, were calculated using values in Table 7-1, by treating average detected defects in 26 draws as n values. This is the average number of defects that are fitted to defect size distribution. The statistical uncertainty due to the sample size is then $\frac{1.96}{\sqrt{n}}$ and corresponds to 0.975 upper bound limit. The results are plotted in Figure 7-9 with the blue curve. The absolute observed uncertainty was calculated using values estimated from the sampling listed in Table 7-2 and by subtracting the mean values from the upper bound values. There is an additional uncertainty associated with full sample size (100%). This is equal to $\frac{\sigma_{100\%}}{\sqrt{n_{100\%}}}$, where $\sigma_{100\%}$ is the standard deviation of the full sample and is equal to 0.79 and

$n_{100\%}$ is the number of defects in the full sample and is equal to 147. The full sample uncertainty is then equal to 0.122. This value is subtracted from the absolute observed uncertainties and the relative observed uncertainties are plotted on Figure 7-9 with a red curve. It is clear that both curves show a good agreement. The divergence observed in smaller ratios are due to the fact that we only performed 26 draws from the dataset, if the draws are increased sufficiently the two curves will match perfectly. Method one (the blue curve) is the uncertainty estimated by the theory and the second method (red curve) is empirical observed uncertainty estimated by taking real samples repeatedly.

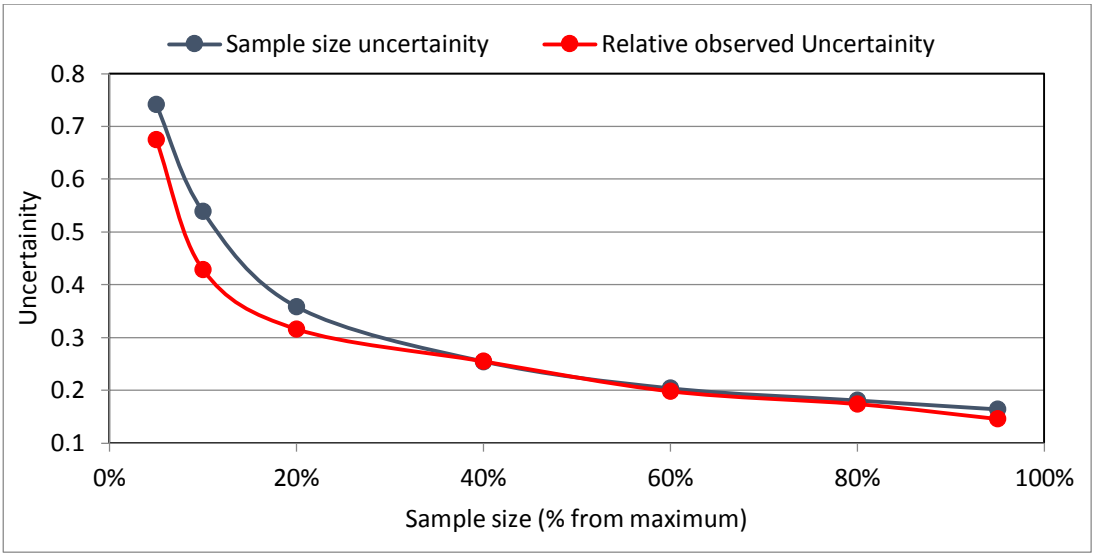

Figure 7-9 Effect of number of the defects on confidence

The real application of the above effect is when a sample is drawn from the data set to asses the true mean values. Since it is not known whether the sampled data is below or above the mean line, a conservative approach would be to assume that the sample is taken from the lower part of the distribution (Figure 7-6). If the sample mean is assumed to correspond to the 5^{th} percentile, the mean value that should only be exceeded 5% of the time can then be estimated. Above analysis indicate that if we make an assessment based on the sample sizes below 60% of the full sample size (90 defect data points) the assessment may be too conservative, but the conservatism can be reduced by collecting more data to reduce the epistemic uncertainty. For sample sizes above 90 defect data points, there will be a little benefit in increasing the checkpoints.

An important conclusion here is that only the numbers of the defects are important in reducing the statistical uncertainty. If the defect rate is very low, there is not much

benefit in increasing inspection size. The drawback here is that the manufacturer may decide to increase the defect rate to achieve better statistical confidence. However, as it was shown in chapter six, failure probability is directly proportional to the number of the defects present in the structure, hence; higher defect rate will directly give rise to failure probability and is unfavourable. This discussed with an example in the next section.

7.5 Effect of confidence on reliability

As explained above, the upper bound estimate of defect size distributions may be used when the data is derived from a sample of the population. This upper bound should result in an over-estimate of calculated failure probabilities. In this section, the effect of the change in statistical confidence on the calculated failure probability is investigated by estimating the reliability of the case study weld joint for a range of sample size proportions. Upper bound defect length distributions, calculated in the previous section, were used to estimate failure probabilities of the structure (as described in chapter 6 the case study section). The Final year failure probabilities of the case study joint for different sample proportions are given in Table 7-3 and Figure 7-10. Through-life failure probabilities are also shown in Figure 7-11.

Sample Ratio	5%	10%	20%	40%	60%	80%	95%	100%
Probability of failure	3.53E-03	1.53E-03	9.55E-04	4.63E-04	2.59E-04	2.31E-04	1.47E-04	1.07E-04

Table 7-3 Final year failure probability of the case study joint for different sample sizes

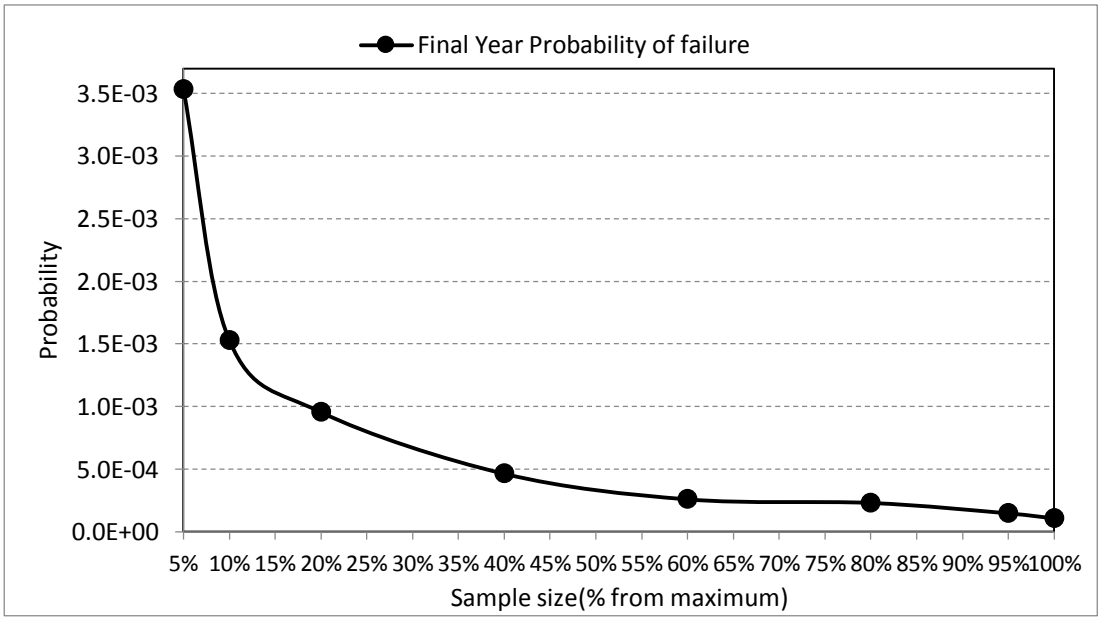

Figure 7-10 Final year failure probability of the case study joint for different sample sizes

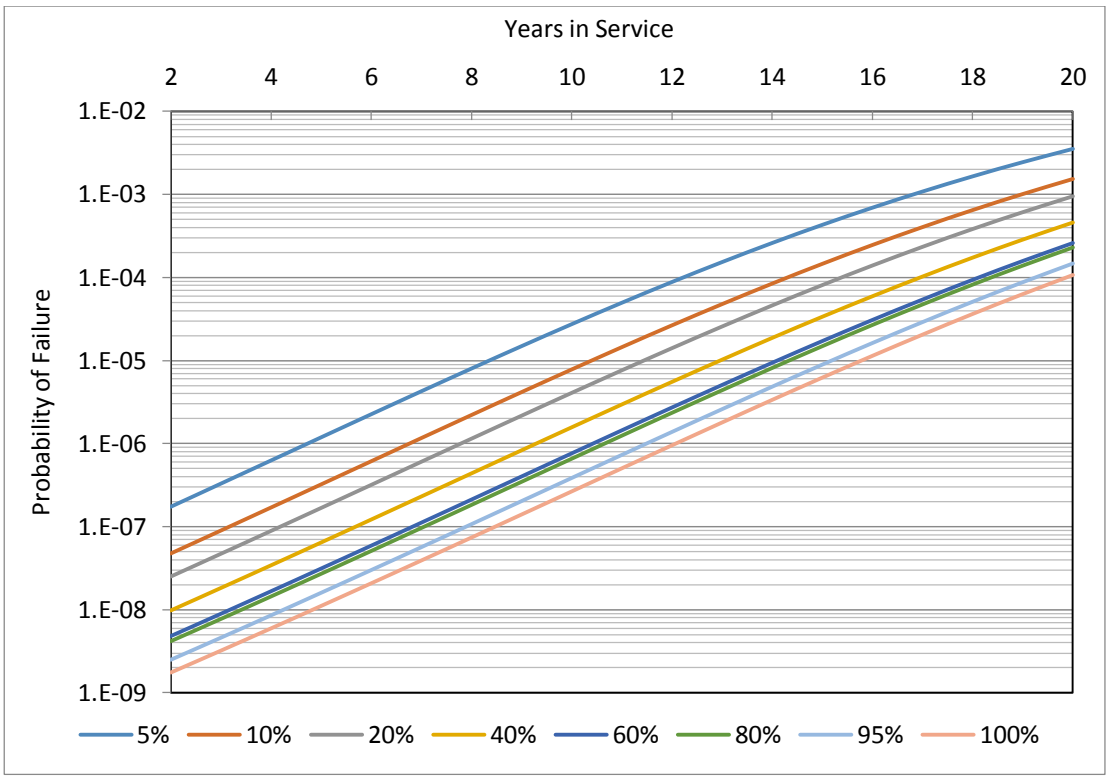

Figure 7-11 Through life failure probability of the case study joint for different sample sizes

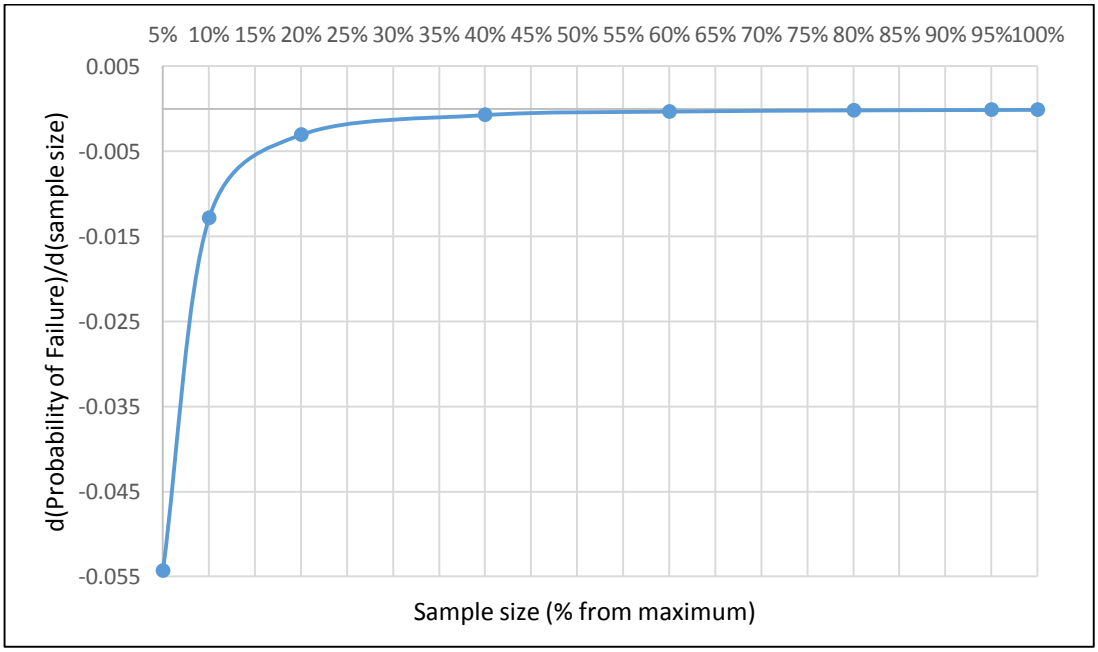

Figure 7-12 Rate of change in final year failure probability of the case study joint with respect to sample size

The change in final year failure probabilities shows a similar trend as the statistical confidence, indicating the direct effect of initial crack size assumptions. The improvements in calculated failure probabilities are significant for increases in the sample size up to a 40% to 60% sample proportion, after which the slope of reduction in failure probabilities plateaus afterwards. The Rate of change in final year failure

probability of the case study joint with respect to sample size is also presented in Figure 7-12. The through-life reliability curves, shown in Figure 7-11, exhibit similar results. It is observed that with the current defect rate of 0.073 per checkpoint sample size corresponding to 40% to 60% of the full possible sample size is a reasonable sample size to achieve good confidence in the defect size distribution. Smaller sample sizes may be used, but for samples containing less than 30 data points (in this case 20% of the full sample size), the upper bound confidence will be too conservative and very unlikely to fulfil target reliability requirements. It is then recommended that estimation of defect distributions be made when the sample size contains 30 to 90 data points. The reliability calculations then can be performed considering upper bound defect size distribution parameters. If the calculated reliability is above the target reliability, it is very likely that adding more data points by doing more inspection increases statistical confidence, reduces the uncertainty in distribution parameters and consequently increases calculated reliability up to the point that the target reliability is achieved. The main limitation of reducing uncertainty by confidence interval approach is that it requires a large sample size, i.e. in this case with a defect rate of 0.073, minimum of 30 data point is only achieved by at least of 410 checkpoints. This may take a long time during the construction of the ship. A possible remedy to this limitation is to use defect size and frequency statistics from the previous construction, shipyard long-term manufacturing data or engineering elicitation. This is best done within the framework of Bayesian theory which combines prior information with collected data to increase statistical confidence. This is studied later in this chapter.

7.6 Effect of extent of inspection on the reliability

As it was shown in chapter six the failure probability for a structure (weld Joint) is:

$$P_{f-Joint} = P_f * \sum_{n=1}^{\infty} P(n) * n = P_f * N \qquad (7\text{-}13)$$

where $P_f$is the probability of failure given the presence of a defect at the structure. N is the number of defects likely to be present in the structure prior to the inspection and is eqaul to the mean defect rate per joint(structure) λ_S . Assuming that the number of defects per metre length of the weld λ_l is constant, the inspection will reduce the estimated number of defects present in the structure λ_S.

$$\lambda_S = \lambda_l * (L_{Joint} - L_{insp.}) \quad (7\text{-}14)$$

where, $L_{insp.}$ is the inspection length. Considering the case of the grand block joint, the joint is 30 (m) long ($L_{Joint} = 30$). From chapter four, the planar defect rate of the FCAW process (applicable le to the grand block joints) in shipyard #2 is 0.146 per metre length ($\lambda_l = 0.146$). The reduction effect as a result of increasing the inspection length is shown in Figure 7-13. In principle, the probability of failure can be reduced to the minimum (depending on the NDE method) by increasing the inspection to the maximum of 100% of the length of the weld, in this case, 30 metre.

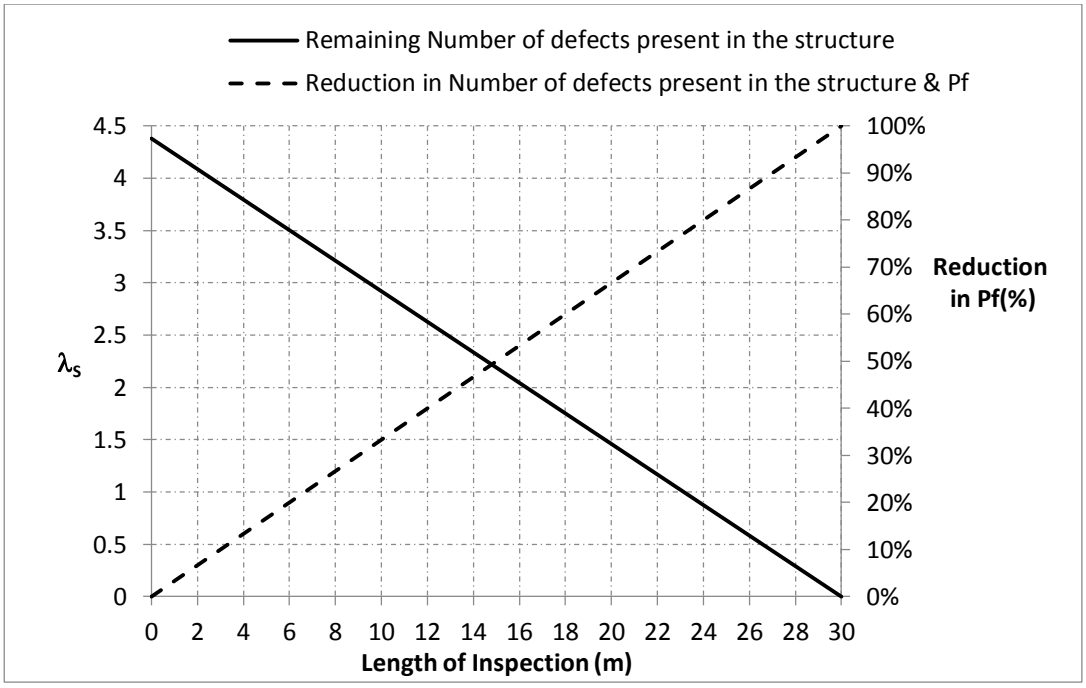

Figure 7-13 Effect of extent of the inspection on the number of remaining defects after the inspection (for inspection with 100% POD)

7.7 Point estimate of defect rate

Two standard models to describe aleatory (random) uncertainty in defect rate are Poisson distribution (Zhao and Stacey, 2002) and (Williams and Mudge, 1985) and binomial distribution (Kelly and Smith, 2011). In the binomial distribution, the probability for obtaining x failures in k demands is given by the binomial:

$$\Pr(X = x) = f(x \mid p) = \binom{n}{k} p^x (1-p)^{n-x} \quad (7\text{-}15)$$

The unknown parameter in this model is p, and the observed data are the number of failures, denoted by x, in a specified (i.e., known) number of demands, denoted by n. Where $0 \leq x \leq n$ and $\binom{n}{k}$ is the binomial coefficient. The binomial coefficient gives

the number of ways that x failures can occur in n demands (i.e., the number of combinations of n demands selected x at a time).

Note that the binomial distribution describes the aleatory uncertainty in the observed number of failures, x. The binomial distribution for p=4.38/60 in 60 inspections (N=60) is shown in Figure 7-14.

In the Poisson model, the probability of x failure is given by:

$$P(X = x) = e^{-\lambda} * \lambda^{x}/x! \qquad (7\text{-}16)$$

where, λ is the defect rate. For the defect rate, λ = 4.38 per structure (60 checkpoints), the Poisson distribution is shown in Figure 7-14. Notice that the Poisson and the binomial distributions result in similar models.

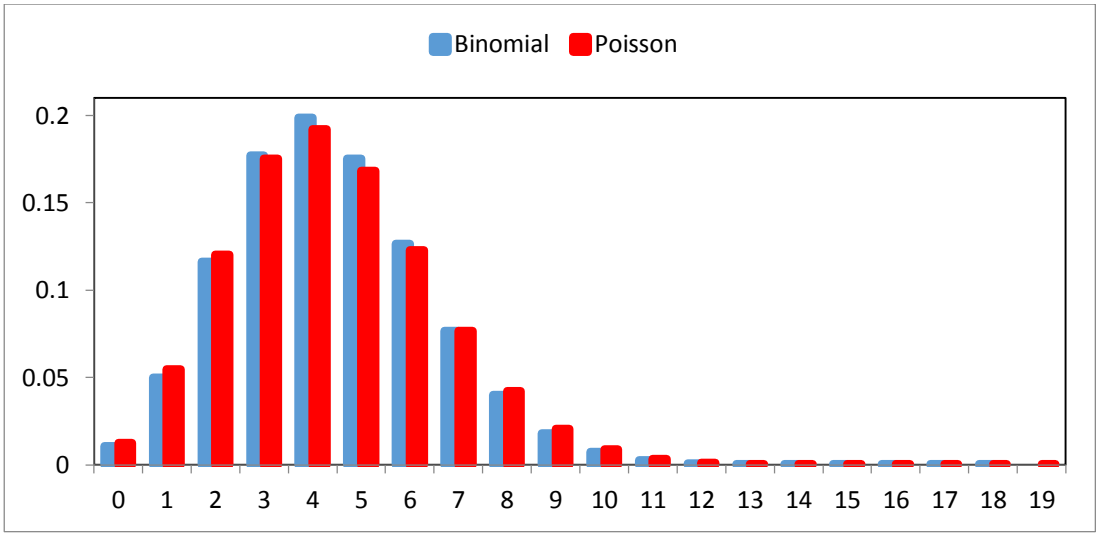

Figure 7-14 Poisson and binomial distribution of defect rate in a structure comprising 60 checkpoints

Although Poisson and binomial models exhibit comparable results, the binomial distribution has the benefit that the number of checkpoints can be inputted directly as the n parameter. This will allow plotting density functions for different sample sizes more conveniently.

Figure 7-15 shows binomial distributions for p=0.073(4.38/60) and various numbers of checkpoints, n, (5, 10, 15, 20 and 60).

These distributions have one important implication: the number of defects we expect from a particular number of checkpoints, given a known defect rate. Up to 12

checkpoints the highest probability is associated with the zero defects: It is expected that no defects are found. Then even for 20 checkpoints, the highest probability is associated with one defect: It is expected that one defect is found. If 5 checkpoints are inspected, there is almost 70% probability that no defect is found. Conversely, finding 2 defects has the low probability of 4.2% indicating that if two defects are found, the defect rate is probably higher than assumed value. If the checkpoints are increased to 15, and the total number of detected checkpoints remains one, we may conclude that the defect rate of 4.38 per joint is still valid given that the highest probability of detection is associated with one defect for the 15 checkpoints curve.

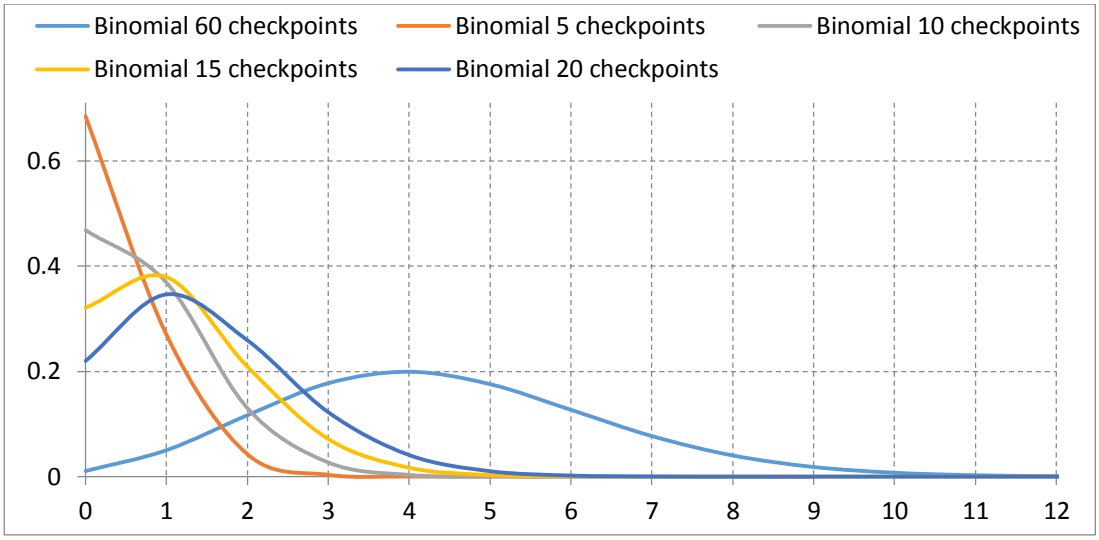

Figure 7-15 Binomial distributions of different sample sizes for a joint comprising 60 possible checkpoints

This may be the basis for deciding about the tolerable number of detected defects for a particular number of checkpoints.

The concept is also illustrated in Figure 7-16 which shows the probability of exceeding the number of defects (1- cumulative probability). Notice that the probability of finding more than two defects in the case of 5 checkpoints and 10 checkpoints are almost zero. If we find three defects, there is a high chance the defect rates at that joint is more than the assumed rate of 0.073.

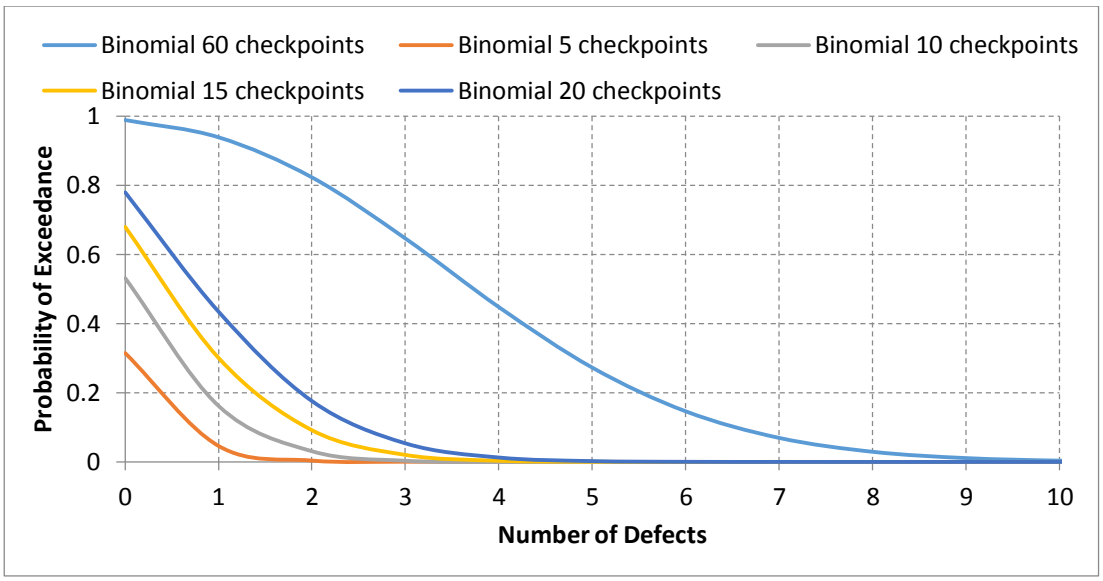

Figure 7-16 Probability of exceedance

More practical use of these curves in the context of defect rate acceptance limits will be by using the tolerable defect rates determined by reliability analysis. If the tolerable defect rate was 8.74/60, as determined in chapter six, the probability of exceedance would be as it is shown in Figure 7-17. Notice that the probability of finding the defects has increased. For example, now the probability of finding any defect with the inspection of 10 checkpoints is almost 80%. If no defects were found, we could be 80% confident that the real defect rate in the structure is below the tolerable defect rate.

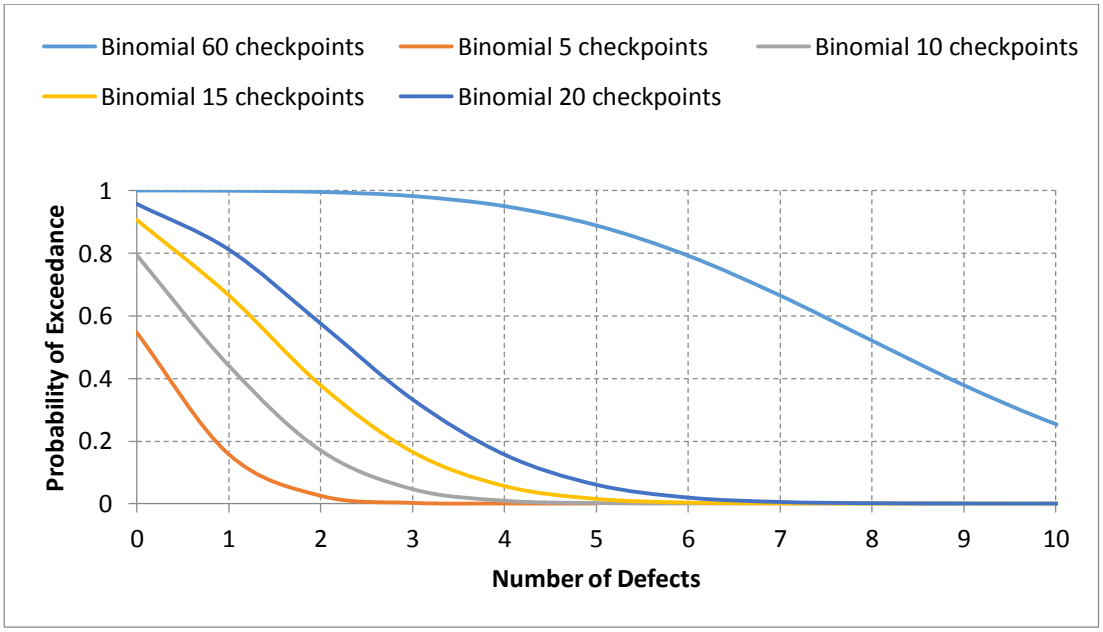

Figure 7-17 Probability of exceedance for 8.74/60 defect rate (p)

The principle outlined above is analogous to the concept of Probability of Inclusion (PoI) without replacement developed by (Georgiou, 2006). The probability of Inclusion is defined as the probability of including a defect in a specific sample size given a specific defect rate.

$$POI = \begin{cases} 1 - \frac{\binom{k}{0} * \binom{N-D_d}{k}}{\binom{N}{k}}, (k \leq N - D_d) \\ 1, (k > N - D_d) \end{cases} \quad (7\text{-}17)$$

Where, *N* is the total number of possible samples (population size) and is set to 100 (100%), D_d is the estimated number of defects corresponding to a certain damage mechanism, and k is the extent of inspection, and in (Georgiou, 2006) denotes the percentage of the required inspection area.

The defect rate corresponds to a particular damage mechanism. (Georgiou, 2006) proposes that given a certain damage mechanism is active (i.e. corrosion), PoI can be used to estimate the required extent of the inspection to find the corresponding defects, as shown in Figure 7-18. For example, if the critical corrosive mechanism produces the corrosion rate (corrosion area / total area) of 10% we need to inspect 25% of the area to be close to 100% confident (e.g. 99.9%)that the damage mechanism is not active. i.e. if 25% of the area is inspected no corrosion defects were found the damage mechanism is not active. For higher defect rates this is achieved with lower coverage, for example, if the critical defect rate was 30% after inspection of only 11% of the area, we achieve the 100% confidence (Figure 7-18).

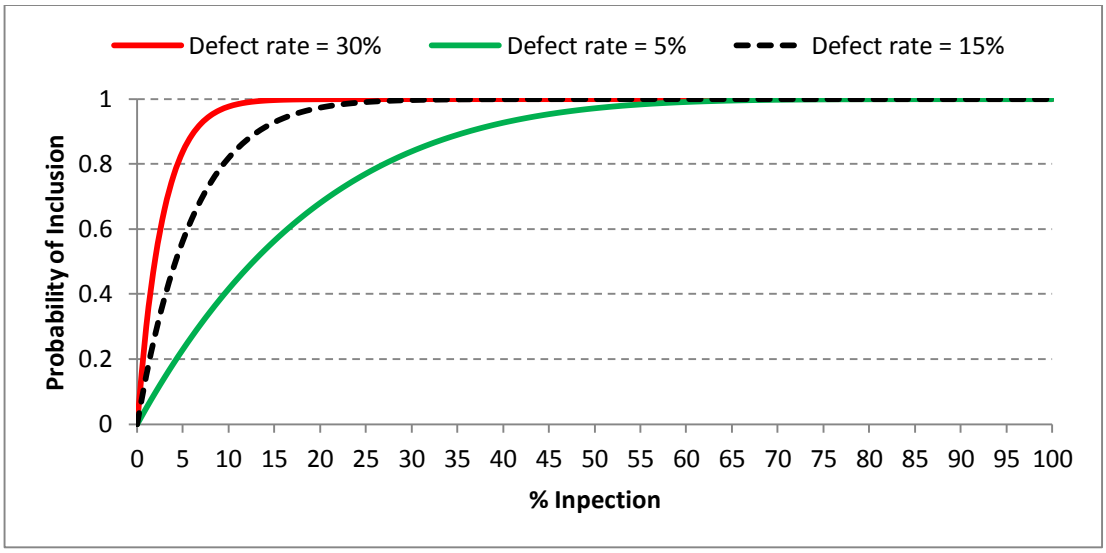

Figure 7-18 Illustration of Probability of Inclusion (POI) for three different defect rates

7.7.1 The epistemic uncertainty of defect rate model

The aleatory uncertainty of the defect rate is modelled by binomial distribution. This is the natural randomness of the defect frequency given that the defect rate is certain. Epistemic uncertainty in the defect rate model can be modelled by quantifying the uncertainty in the distribution parameter (p) in binomial distribution. This is commonly described by the Beta distribution (Kelly and Smith, 2011).

$$P(X = p) = p^{(\alpha-1)} * (1-p)^{(\beta-1)} * \frac{\Gamma(\alpha+\beta)}{\Gamma(\alpha)\Gamma(\beta)} \qquad (7\text{-}18)$$

α can be thought of as the number of failures contained in the prior distribution, and the sum of α and β is equivalent to the number of demands over which these failures occurred (n in binomial distribution).

For a joint comprising 60 possible checkpoints which are expected to contain 4.38 defects, $\alpha = 4.38$ and $\beta = 60 - \alpha = 55.62$, the Beta distribution which models the epistemic uncertainty of p is shown in Figure 7-19.

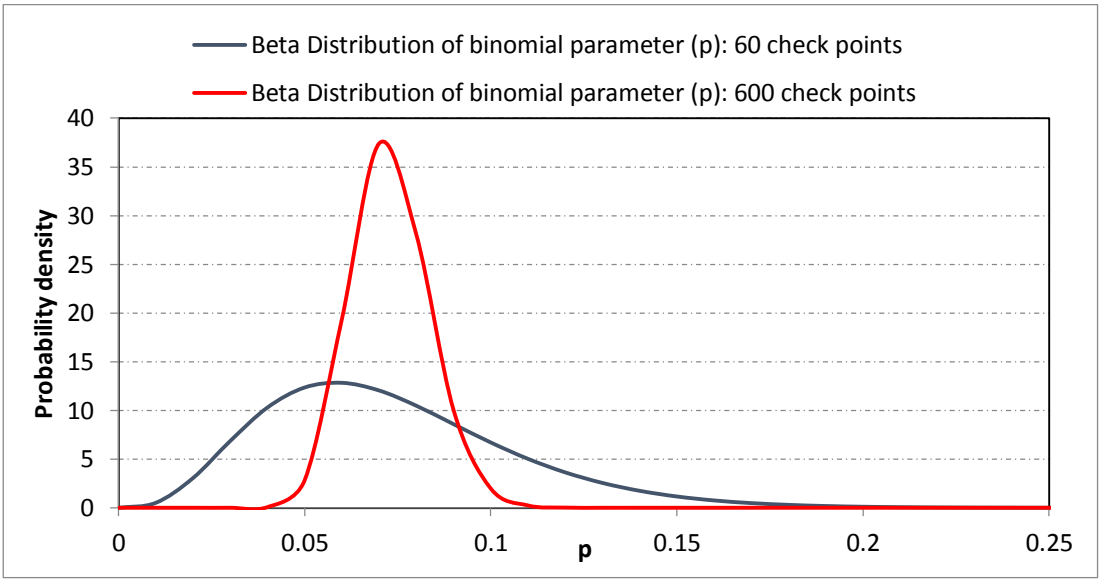

Figure 7-19 Beta density function for the binomial distribution Parameter

In the Beta distribution the expected value is equal to: $\frac{\alpha}{\alpha+\beta}$, that is the expected value for p. The 95% upper bound value of p is then found from the inverse cumulative distribution corresponding to the probability of 0.95. And for the above case is 0.1347 per checkpoint or 8.08 per joint (60 checkpoints).

If the data was recorded from a bigger sample size, say 600 instead of 60, and 43.8 defects (4.38 times 10) defects were found the confidence on the expected p value would have been higher. Here, the expected value of p, $\frac{\alpha}{\alpha+\beta}$,remains the same (0.073) but, as it can be seen in Figure 7-19, the uncertainty in the defect rate parameter has been reduced by increasing the sample size and the distribution became less scattered (more narrow banded). The 95% upper bound value of p in this case is 0.0912 per checkpoint or 5.47 per joint (60 checkpoints).

When the Poisson distribution is used instead of the binomial distribution to describe defect frequency, the Gamma distribution may be used to model epistemic uncertainty in defect rate parameter,λ, using a similar approach, and the results will yield an analogous outcome.

7.8 Determining sample size from the confidence interval

As explained earlier in this chapter the statistical confidence in the data is related to the sample size of the collected data. This can be used to determine a minimum number of samples required to achieve a certain confidence level, which is described by:

$$n = \left(\frac{z * \sigma_x}{e}\right)^2 \tag{7-19}$$

where, *e* is the sample error, equal to the difference between the sample mean and the population mean. *z* is the fractile of standardised normal variable corresponding to the chosen probabilities representing required confidence level on sample mean (Figure 7-20). σ_x is the sample standard deviation.

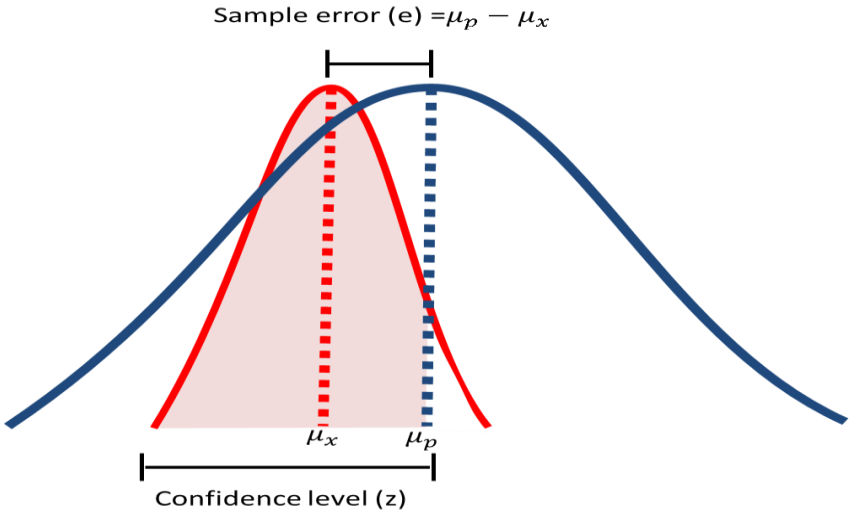

Figure 7-20 Sample error and confidence level diagram

For estimation of proportions in large population minimum sample size can be calculated using equation (7-20)

$$n = z^2 * p * (\frac{1-p}{e^2}) \quad (7\text{-}20)$$

When the size of the population is small , $\frac{n}{N} > 5\%$ (Waller, 2008), where, N is the size of the population, the minimum sample size can be calculated using the equation below:

$$n = \frac{z^2 * p * (1-p) * N}{z^2 * p * (1-p) + e^2 (N-1)}, \text{ (Noble et al., 2006)} \quad (7\text{-}21)$$

Assuming *N*=60, *p*=0.073, *e*=0.167 and for various confidence levels (z) the minimum sample size (n) is calculated and is presented in Table 7-4. As explained in "Effect of extent of inspection on the reliability" section, inspection of the weld will reduce the probability of the failure depending on the number of inspected checkpoints at a particular joint. This effect is taken into account by considering the effect of the calculated sample size on the (p) value and calculating a new updated n. The process is iterated until a converged value for n is achieved. The adjusted n values accounting for the reduction in defect frequency is given in Table 7-4, as well.

One-sided Confidence level	z	n	Adjusted n
80%	0.842	6	5
90%	1.282	13	9
95%	1.645	18	12
99%	2.326	28	18

Table 7-4 Minimum Sample size for the grand block joint in deck 16 midship area

If nine checkpoints are inspected, and no defects are found, we can be 90% confident that the defect rate is below 4.38 per joint (60 checkpoints). If 12 checkpoints are inspected, and one defect is found we can be 95% confident that the defect rate is not above 4.38.

The required confidence level may be chosen based on the criticality (consequence of failure) of the joint. i.e. 80% for low risk, 90% for medium risk and 95% for high risk are recommended, but higher confidence levels may be selected if required by the stakeholders.

7.9 Bayesian Inference

One limitation of point estimate inference is that it only considers the collected data. In many real-life cases, there exists some prior information about the population. For example, in the case of defect, unless caused by special causes, the defect length is between very small sizes close to zero and large lengths of maximum 500 mm and expected to follow an exponential or lognormal distribution. This assumption is too crude to be a basis for fracture mechanics type analysis. It would be useful to somehow refine this assumption with the aid of more data to increase confidence. The issue becomes more apparent considering that in order to make a confident estimate purely based on collected data it would be necessary to collect large samples. It has already been shown that at least 30 data points are required to achieve reasonable confidence. With the defect rate of 0.073 per inspection, at least 411 checkpoints are needed. An alternative approach is the Bayesian inference which uses both prior information and collected data simultaneously.

The confidence interval (frequentistic) approach and the Bayesian approach have fundamentally different views on the uncertainty and the interpretation of the probability.

For the frequentist, the *true* mean of the parameter is within the confidence intervals. In safety analysis, the conservative interval bound is then chosen for the demonstration of the claim in question. The decision problem is whether to accept or reject a hypothesis and on what confidence the decision can be made.

Bayes' Theorem combines information and data, in the context of a probabilistic model, in order to update a prior state of knowledge (Kelly and Smith, 2011) and (Hamada et al., 2008). This theorem modifies a prior probability, yielding a posterior probability, via the expression:

$$\pi(\theta \mid x) = \frac{f(x \mid \theta)\,\pi(\theta)}{\int f(x \mid \theta)\,\pi(\theta)dx} \tag{7-22}$$

Where, $\pi(\theta)$denotes the prior distribution from knowledge of the hypothesis θ that is independent of data, $\pi(\theta \mid x)$ is the posterior probability (the distribution given the data x), which is conditional upon the data x that is known be related to the hypothesis θ . And $f(x \mid \theta)$ is the sampling, Likelihood or aleatory model, representing the process or mechanism that provides data. $\int f(x \mid \theta)\,\pi(\theta)dx$ is the marginal distribution, which serves as a normalisation constant.

If the posterior and the prior distribution are from the same family (distributions which have similar equattion forms but one or more disimilar parameters), they are called conjugate distributions, and the prior is called conjugate prior of the likelihood distribution (Raiffa, 1974)

If the posterior distribution has a closed-form solution the conjugate prior may be obtained analytically; otherwise, numerical integration may be necessary. Some likelihood distributions relevant to this work and their corresponding conjugate prior and posterior predictive distributions are given in Table 7-5. Hyperparameter is a parameter of a prior distribution.

Sampling Distribution (Likelihood)	Conjugate prior	Prior Hyperparam-eters	Posterior Hyperparameters	Posterior predictive,(Murphy, 2007)
Binomial(p)	Beta	α, β	$\alpha + \sum_{i=1}^{n} x_i$, $\beta + n - \sum_{i=1}^{n} x_i$	$p' = \frac{\alpha'}{\alpha' + \beta'}$,(Kelly and Smith, 2011)
Exponential (λ)	Gamma	α, β	$\alpha + n, \beta + \sum_{i=1}^{n} x_i$	$Logmax(\hat{x} \mid \beta', \alpha')$
Normal (μ, σ^2 known)	Normal	μ_0 , ${\sigma_0}^2$	$\frac{1}{\frac{1}{\sigma_0^2}+\frac{n}{\sigma^2}}\left(\frac{\mu_0}{\sigma_0^2}+\frac{\sum_{i=1}^{n} x_i}{\sigma^2}\right)$, $\left(\frac{1}{\sigma_0^2}+\frac{n}{\sigma^2}\right)^{-1}$	$N(\hat{x} \mid {\mu_0}', {\sigma_0}^{2'} + \sigma^2)$ (Normal distribution)
Normal(σ^2, μ known)	Inverse Gamma	α, β	$\alpha + \frac{n}{2}$, $\beta + \frac{\sum_{i=1}^{n}(x_i-\mu)^2}{2}$	$t_{2\acute{\alpha}}(\hat{x} \mid \mu, \sigma^2 = \beta'/\alpha')$
Poisson(λ)	Gamma	α, β	$\alpha + \sum_{i=1}^{n} x_i$, β	$NB(\hat{x} \mid \alpha', \frac{1}{1+\beta'})$ (Negative Binomial)

Table 7-5 Common conjugate priors (Hamada et al., 2008)

For example, the Yield strength of AH36 steel grade can be estimated to be at around 380 MPa with a broad uncertainty represented by standard deviation of 60 MPa. At the yard, three tensile tests were performed as part of the material quality control programme, and the results of the test were as follows: 400.332, 409.522, and 428.085 MPa. The prior, Likelihood and Posterior distributions are shown in Figure 7-21. Standard deviation of the likelihood function is assumed known and equal to 20 MPa.

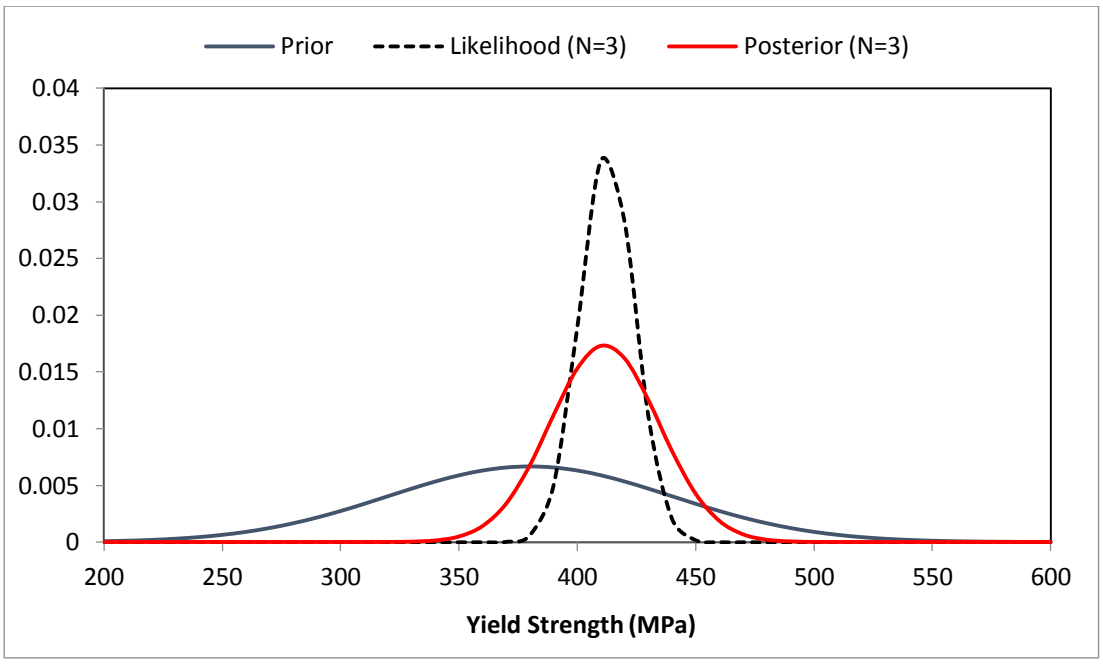

Figure 7-21 Example of Bayesian inference model: material Yield strength, N=3

If the sample sizes increase, eventually, posterior distribution will approach the likelihood distribution and become similar to a point estimate, i.e., MLE of the variable. In the above example, the sample size was increased to *N*=30, and the resulting distributions are shown in Figure 7-22.

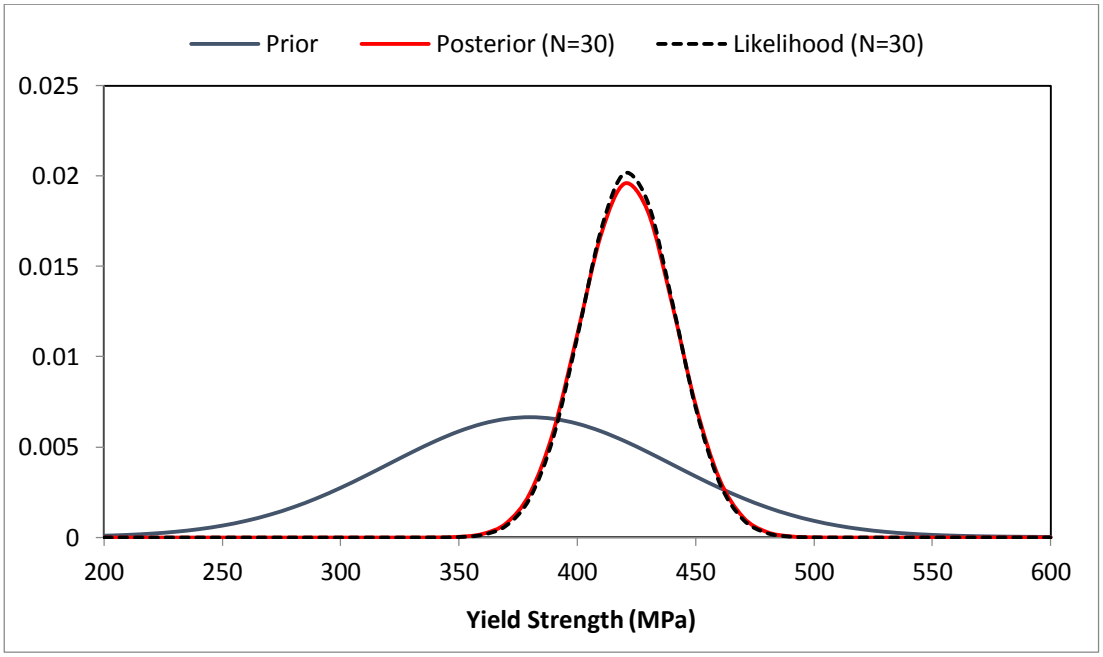

Figure 7-22 Example of Bayesian inference model: material Yield strength (N=30)

The benefit of the Bayesian estimate is that for small sample sizes the prior distribution affects the inference about the population characteristics and with enough data points converges with the collected the data distribution.

7.9.1 Bayesian estimate of defect size

As explained in Chapter four, a suitable distribution choice for modelling detected defect size is the lognormal distribution. The lognormal distribution is essentially the Normal distribution of the logarithm of the data. This allows us to perform the Bayesian operation of the defect size data using a Normal distribution. First, the data is transformed to a logarithm scale (equation (7-23)), then the Bayesian inference is conducted by treating the transformed data as a variable which is normally distributed. Finally, the Posterior distribution is transformed back to the normal scale.

$$Z_i = \ln(x_i) \tag{7-23}$$

From Table 7-5, Normal mean Hyper-parameter of posterior distribution with known standard deviation is:

$$\mu_0{}' = \frac{1}{\frac{1}{\sigma_0^2} + \frac{n}{\sigma^2}} \left(\frac{\mu_0}{\sigma_0^2} + \frac{\sum_{i=1}^{n} z_i}{\sigma^2} \right) \tag{7-24}$$

Normal standard deviation Hyper-parameter of posterior distribution with known deviation is:

$$\sigma_0{}' = \sqrt{\left(\frac{1}{\sigma_0^2} + \frac{n}{\sigma^2} \right)^{-1}} \tag{7-25}$$

Posterior predictive is:

$$Posterior = LN(\hat{z} \mid \mu_0, {\sigma_0}^{2\prime} + \sigma^2) \tag{7-26}$$

Here, detected crack length distribution from previous construction (shipyard #3 from chapter four) that follows a lognormal distribution with parameters (3.12, 0.8) is assumed. Two defects were randomly selected from shipyard #2 dataset with 46.5 and 18 mm length. The standard deviation logarithm values of cracks lengths, σ is assumed known and equal to 0.8. The Prior, Likelihood and the resulting Posterior parameter derived from Bayesian inference are given in Table 7-6. Actual distribution parameters of shipyard #2 data analysed by MLE of 154 samples provided as well, for comparison purposes. The normal and lognormal distributions of defect length given by the Bayesian theory are shown in Figure 7-23 and Figure 7-24, respectively.

	Prior	Likelihood	Posterior	Actual distribution (MLE: 154 sample)
μ_{ln}	3.12	3.367	3.285	3.49
σ_{ln}	0.8	0.8	0.924	0.81
Mean defect length (mm)	31.2	40	41	33

Table 7-6 Prior, Likelihood and the resulting Posterior parameter derived from Bayesian inference, N=2

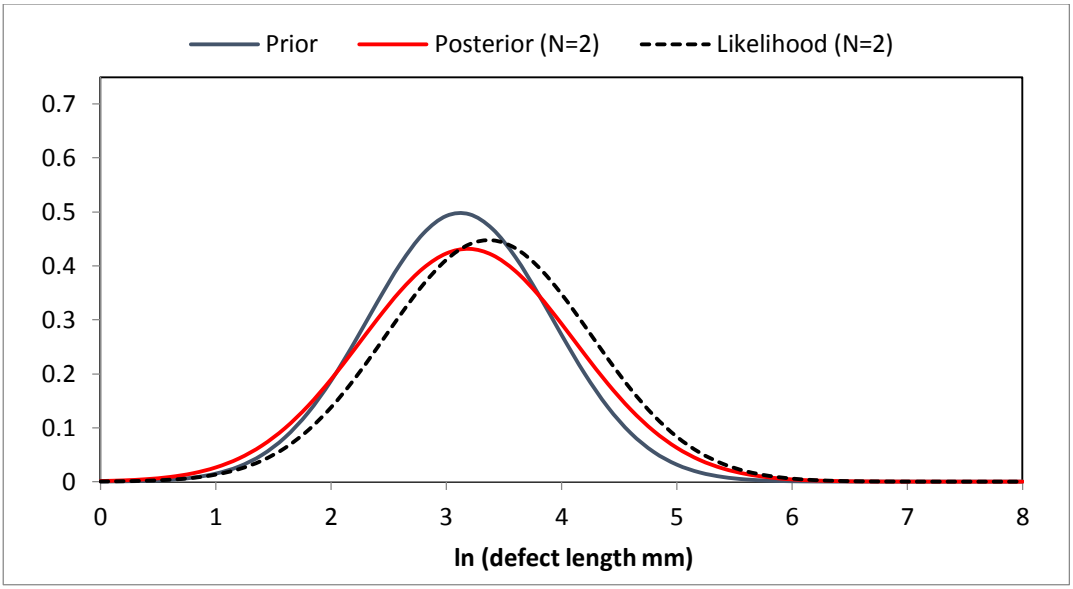

Figure 7-23 Bayesian inference Normal distributions of defect length with N=2

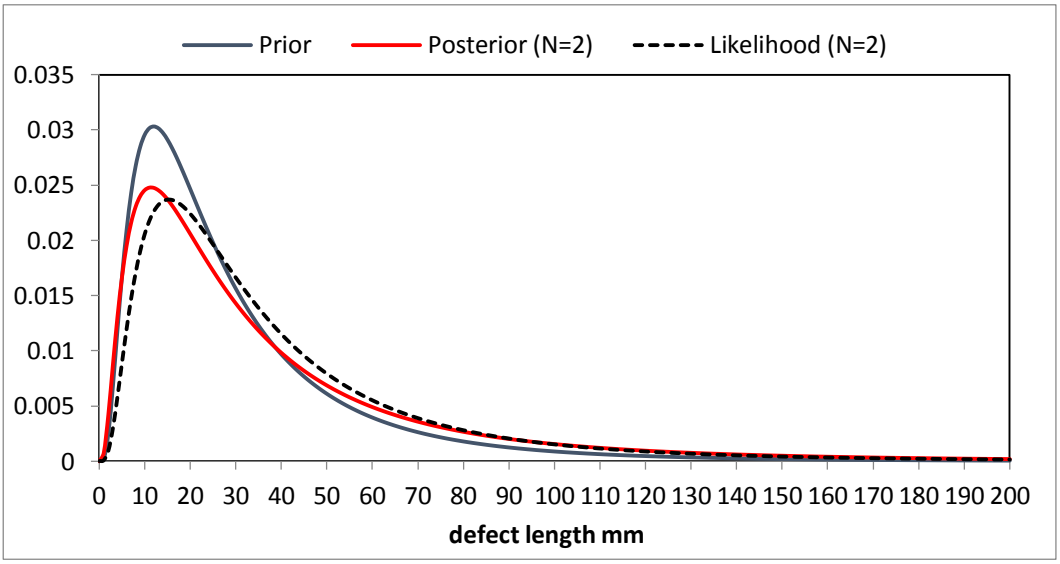

Figure 7-24 Bayesian inference lognormal distributions of defect length with N=2

Increasing the sample size from *N*=2 to *N*=10 will result in less scatter of the posterior distribution as the σ'reduces to 0.836. The Posterior distribution becomes much closer to the likelihood distribution. This is shown in Table 7-7, Figure 7-25 and Figure 7-26.

	Prior	Likelihood	Posterior	Actual distribution (MLE: 154 sample)
μ_{ln}	3.12	3.776	3.717	3.49
σ_{ln}	0.8	0.8	0.836	0.81
Mean defect length (mm)	31.2	60.1	58.3	33

Table 7-7 Prior, Likelihood and the resulting Posterior parameter derived from Bayesian inference, N=10

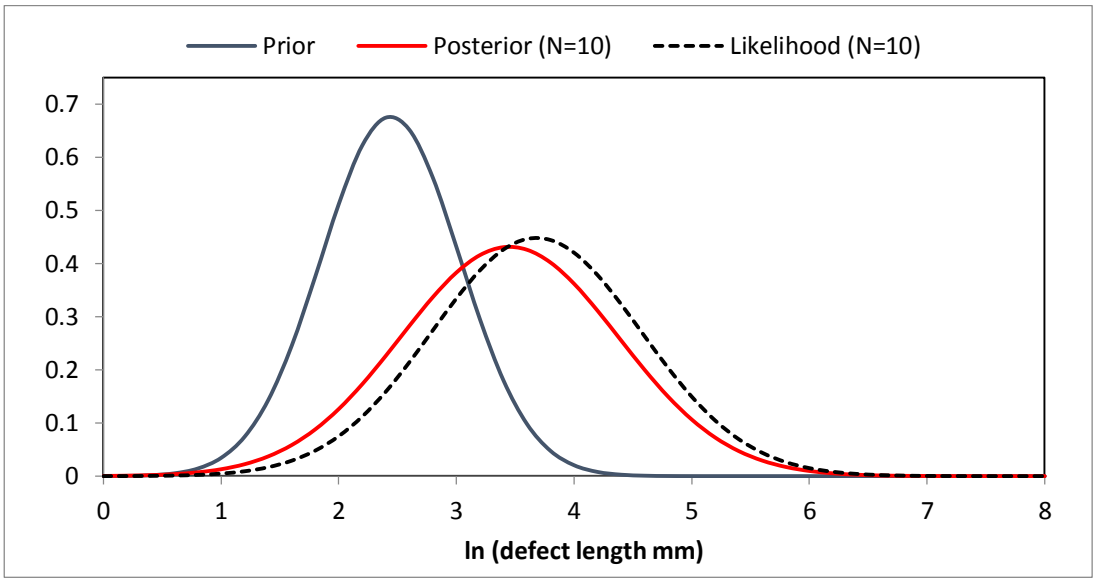

Figure 7-25 Bayesian inference Normal distributions of defect length with N=10

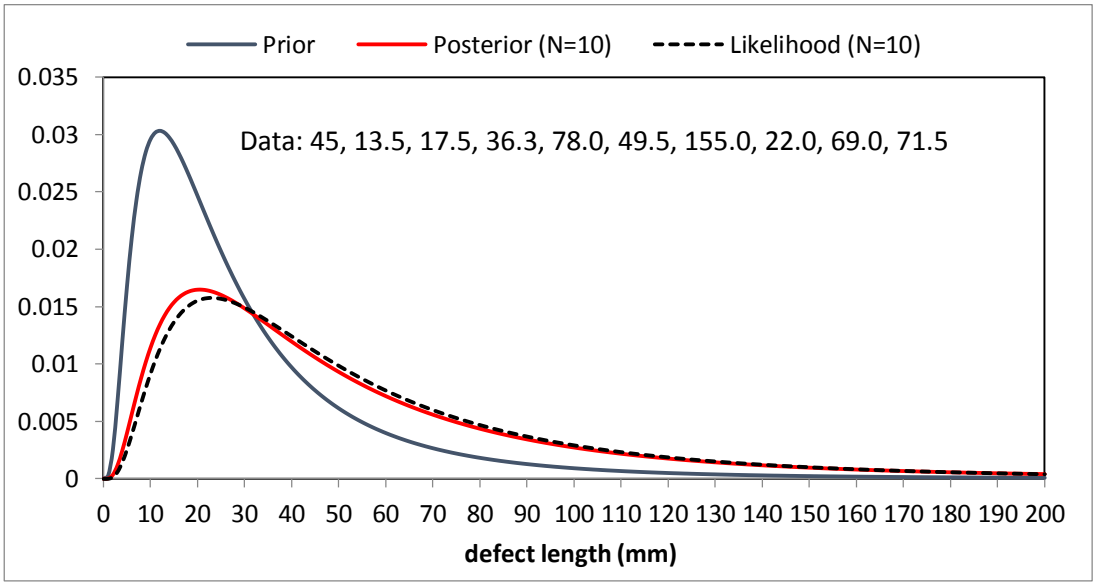

Figure 7-26 Bayesian inference lognormal distributions of defect length with N=10

7.9.1.1 Bayesian updating

Another method of the Bayesian method is the recursive Bayesian updating method which updates the prior distribution at each time step using new data. In this method, the posterior distribution obtained at each time step is treated as the prior

distribution for the next step. This is equivalent to a Kalman filter estimate of the current state, in which the probability distribution of interest is related to the current states conditioned on the measurements up to the current time step.

Using this method μ_{ln} of defect length distribution sample size of 5 was calculated for 100 time steps. The initial prior distribution was chosen from shipyard #3 crack data. The samples were taken from shipyard #2 dataset. Summary of the input assumptions are given in Table 7-8.

Parameter	Prior	Likelihood
μ_{ln}	3.12	3.49
σ_{ln}	0.8	0.81

Table 7-8 Summary of the input assumption in Recursive Bayesian example

The estimated $\mu_{ln}(Mu)$ are shown in Figure 7-27. The prior $\mu_{ln}(Mu)$, point estimate mean value from analysis of whole data set and confidence bound of $\mu_{ln}(Mu)$ assuming sample size equal to 5 are also shown for comparison. It can be seen that initial prior distribution has shifted the estimated points downwards towards the prior (the red line). The estimates will not converge owing to the randomness of the likelihood data which shows that using this method will result in a more prominent influence of individual samples as opposed to, for example, pooling all the samples up to the current state. An assessment based on this method will show a better estimate of the local structure (the structure that the current sample is taken from), but be less representative of the whole structure.

As mentioned before after about 30 samples of the measured data sufficient statistical confidence is achieved, and we may replace the initial prior distribution, which was based on the previous shipyard, with a distribution fitted to the data collected up to the 30th sample.

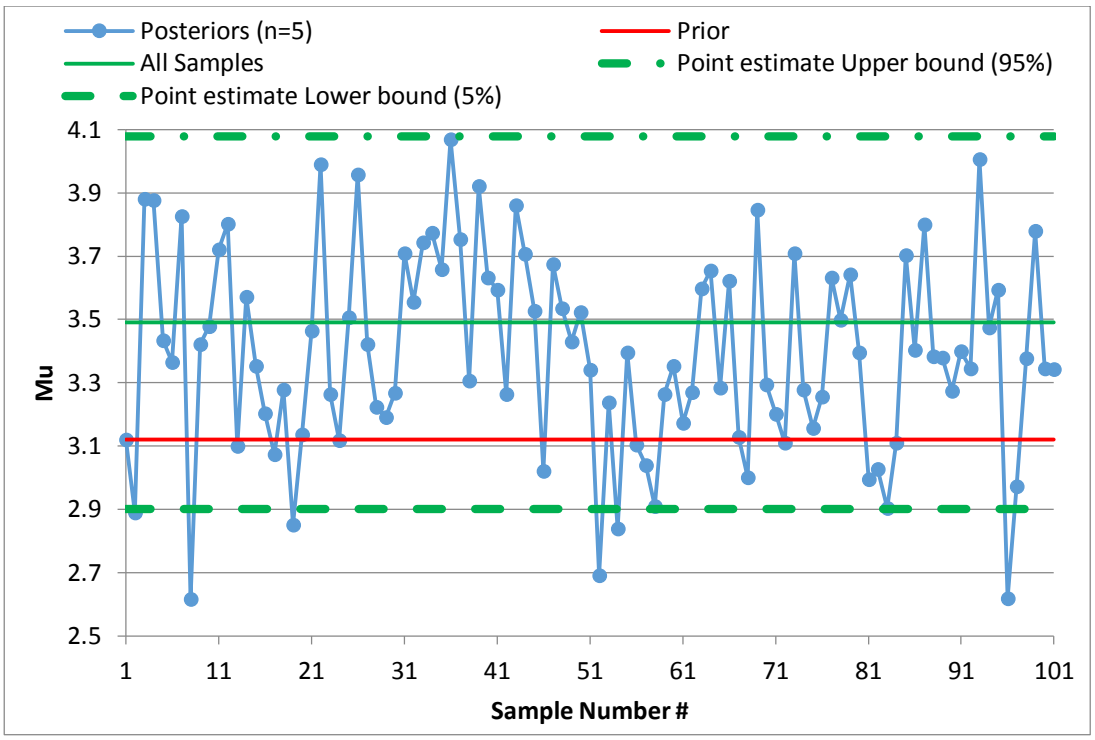

Figure 7-27 Recursive Bayesian updating

To investigate the difference between the recursive Bayesian updating approach and the confidence interval point estimate method 100 sets of samples each comprising 5 samples were randomly taken with mean value of (3.49) and sample standard deviation of $^{0.8}/_{\sqrt{5}}$. The samples are shown in Figure 7-28. These two processes are compared graphically: Although if the process is repeated, some sample sets with lower scatter will be observed, but Figure 7-28 is generally reasonable representative of samples created by the point estimate random sample simulation. The Bayesian process shows relatively narrower scatter by creating fewer extreme cases. Also, the sudden immediate shifts between two extreme estimates are observed less frequently in the Bayesian process, and neighbouring points seem to be generally more connected than the point estimate method resulting from the influence of measured data up to the current time step.

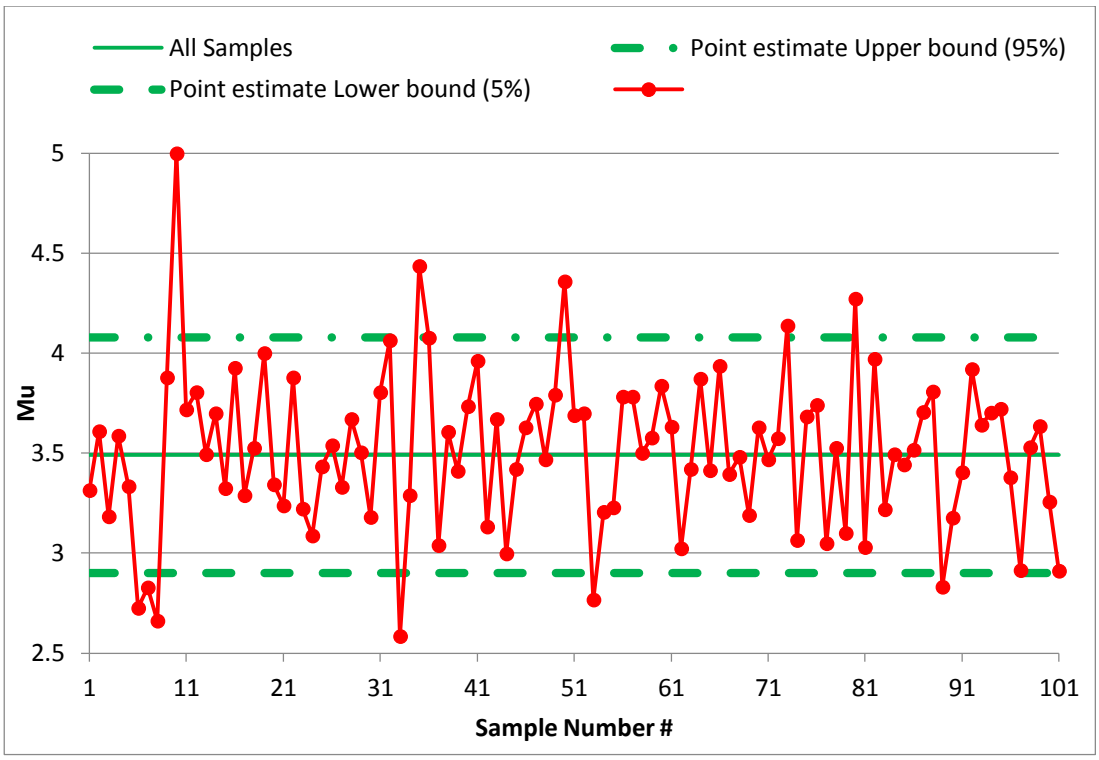

Figure 7-28 Non-Bayesian randomly drawn samples

7.9.2 Bayesian estimate of defect rate

Using a similar procedure outlined before, epistemic uncertainty in the defect rate data can be estimated using the Bayesian theorem. The aleatory uncertainty is modelled by a binomial distribution, and from Table 7-5 the conjugate prior distribution for binomial distribution is the Beta distribution.

As an example, we consider a case where the long-term defect rate of the yard is 4.38 per 60 checkpoints. From a grand block joint in the deck structure in midship area, 8 checkpoints were randomly selected. Two checkpoints contained planar defects. The updated defect rate using Bayesian inference is:

$$p' = \frac{\alpha'}{\alpha' + \beta'} \tag{7-27}$$

Where, $\alpha' = \alpha + \sum_{i=1}^{n} x_i$, $\beta' = \beta + n - \sum_{i=1}^{n} x_i$, n is the size of sampled data, and x_i are sampled data. Here, $= 4.38$, and $\beta = 60 - \alpha = 55.62, p = 0.073$, $\alpha' = 6.38$, $\beta' = 61.62$ and $p' = 0.094$.

Prior and posterior distributions of p (mean defect rate), describing epistemic uncertainty in defect rate, are shown in Figure 7-29. Corresponding Prior, likelihood

and posterior binomial distributions describing aleatory uncertainty in defect rate for 60 checkpoints (entire joint) are shown in Figure 7-30.

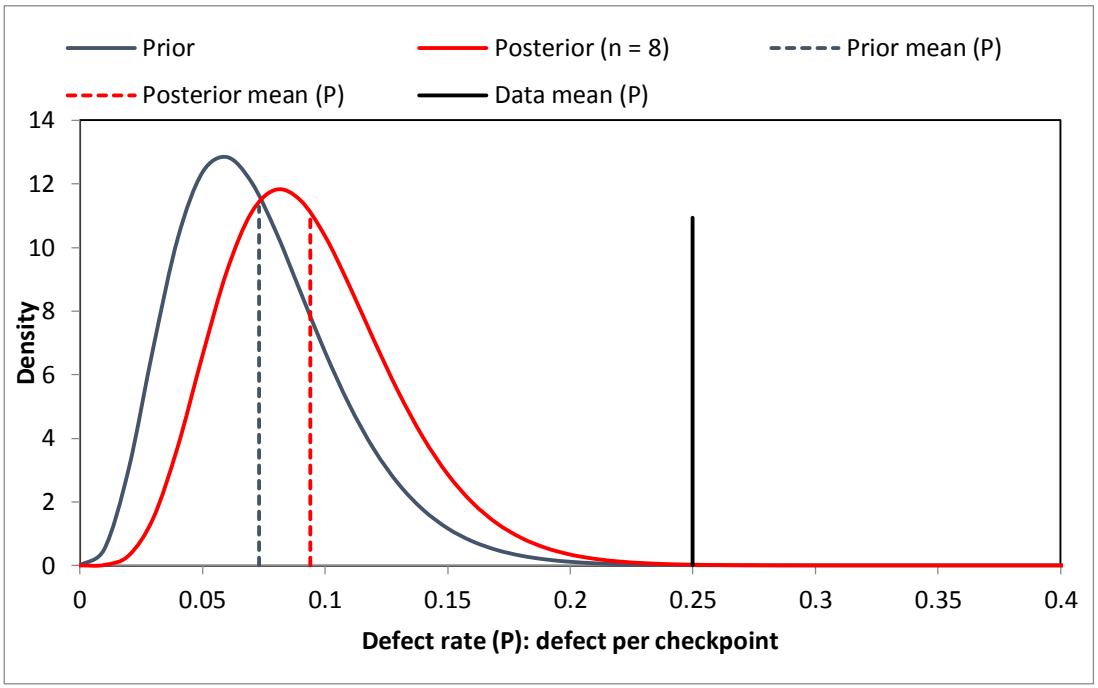

Figure 7-29 Mean defect rate (p) estimation using Bayesian method

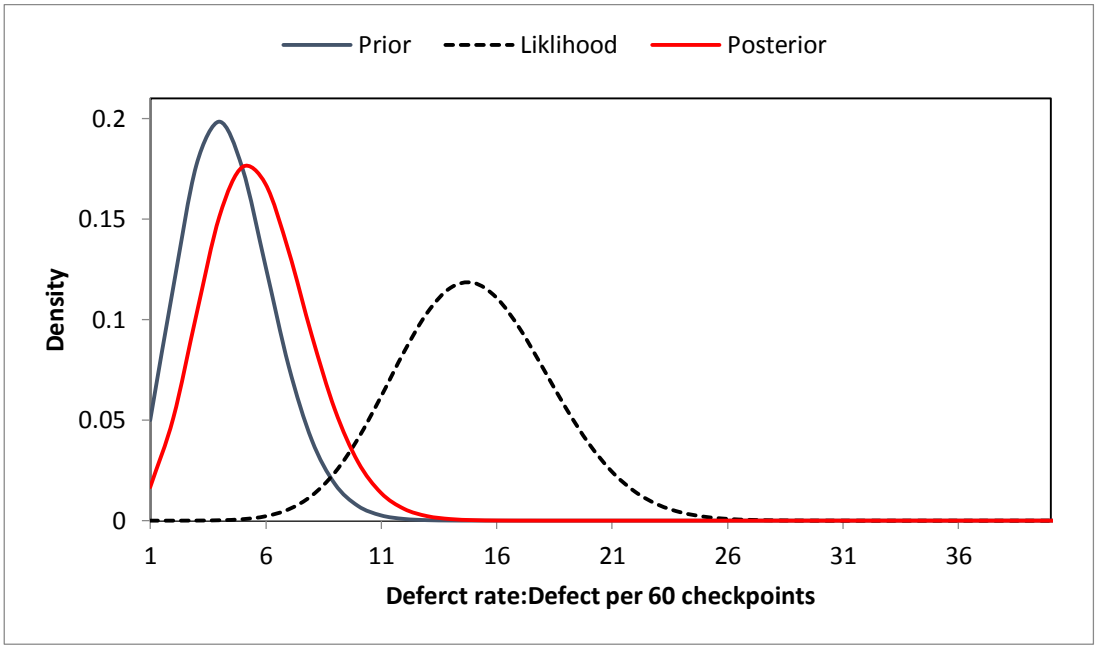

Figure 7-30 Defect rate (defect per 60 checkpoints) estimation using the Bayesian method

7.9.3 Bayesian estimate of Fracture toughness

The focus of this chapter is on defect frequency and size, but since fracture toughness is another key probabilistic input of reliability analysis and because the toughness testing using Charpy impact testing is a relatively cheap testing method, which is

commonly performed at the shipyard as part of material quality control programme, the application of Bayesian estimation of toughness is studied here, as well.

As described in chapter 5, the mean value of Charpy tests for manufacturer #5 is 133.36 Joules with standard deviation of 33.76. Toughness may be modelled by a lognormal distribution with ($\mu_{ln} = 4.86, \sigma_{ln} = 0.25$). Here, we assume that Charpy test data from three tests sampling one batch of steel were examined providing the likelihood data of 141.7, 150, 142 Joules. Assuming that the data's standard deviation is equal to the manufacturer's standard deviation, the prior, likelihood and posterior distributions can be estimated using the same procedure described for defect length data. Summary of the calculations are given in Table 7-9 and the distributions are shown in Figure 7-31.

	Prior	Likelihood	Posterior
μ_{ln}	4.86	4.973	4.945
σ_{ln}	0.25	0.25	0.28
Median	129	144.46	140.47

Table 7-9 Summary of Bayesian estimation for the toughness example

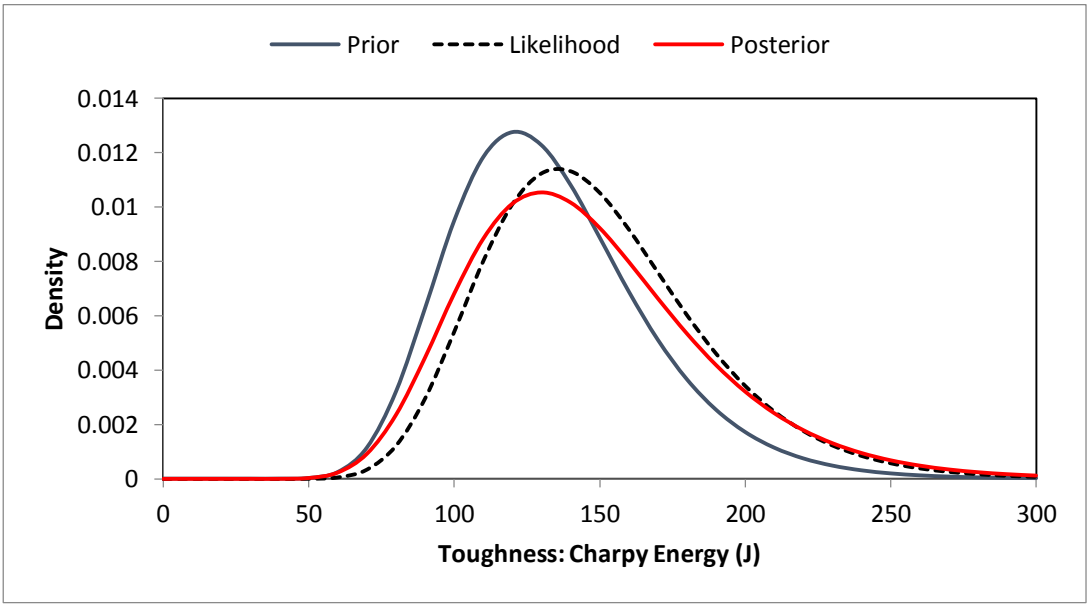

Figure 7-31 Bayesian estimation distributions for the toughness example

7.10 Statistical Process control

Statistical Process Control (SPC) or Statistical Quality Control (SQC) is a quality control/assurance approach based on statistical methods to monitor and control a process. The focus of the SPC is the special (assignable) causes. Tools such as control

charts are employed to detect the assignable causes by distinguishing them from common (natural) causes. In this chapter, so far, we treated the defects regardless of this classification. The explained approaches ensure that the defect rates are in a range that is tolerable by the structure and for an uncertain, but known, defect size distribution. SPC emphasises on early detection and prevention of problems, rather than the correction of problems after they have occurred. If for example, a welding process is creating an abnormal defect rate (or type of defect) as a result of a special cause, it is beneficial to detect the abnormality, find the source of the cause and possibly rectify it to prevent future excessive NDE inspections. If the process is producing fewer defects than the normal limits, the cause of this special reduction may be investigated, and the process should be ideally kept at the reduced defect rate level.

The basis of the method is illustrated in Figure 7-32. The process is in control, and quality characteristic has the mean value of μ_0 and the standard deviation of σ_0 until the time t_1 that assignable cause 1 occurs. The standard deviation is unchanged but the mean is increased and the process is out of control.

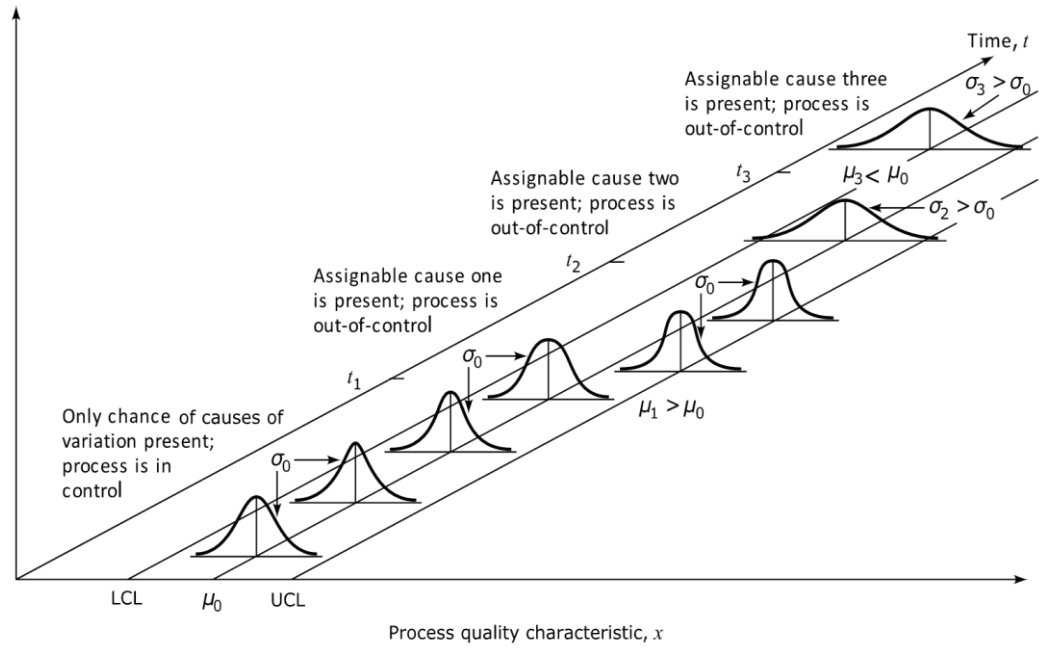

Figure 7-32 Illustration of Statistical Process Control (Montgomery, 2009).

At the time t_2 assignable cause 2 brings the mean back to the target mean μ_0 but also increases the standard deviation. The process is out of control. At the time $t_3$the assignable cause 3 reduces the mean to a new mean μ_0 and a standard deviation higher than the initial standard deviation. The process is again out of control.

One challenge in statistical process control is to establish a reference point beyond which the process is considered as out-of-control which itself depends on specific welding processes and their variables. Another perhaps more critical challenge is that the fabrication process which is a crucial parameter in SPC is shipyard specific. For example, one shipyard may work 24 hours a day and another only 8 hours, this means that the automatic welding machines will have different run times, different maintenance schedule, and etc.. Or one ship may happen to be built during summer when a little wind blows at the dry dock, and another may be built during the winter when the harsher weather is known to affect the weld quality significantly. All these considerations will affect an SPC system considerably and could be investigated in separate research work.

In principle, the same inspection plan determined based on risk and reliability can be used by an SPC programme which considers the schedule of the construction to find the special causes as early as possible during the construction.

The SPC framework developed in this research can be used as a connection point between two approaches.

7.11 Control Charts

Control charts or *Shewhart* charts are used to detect changes in the quality, q, of the manufactured product. It was introduced by Walter Shewhart in 1920. If the desired quality is the target line then the measured quality, q, is plotted against sample numbers on a graph as shown in Figure 7-33, where the limit lines are centred around the target line and indicate that the quality is deviating from the desired level. Note that in some cases we may consider deviations in one direction only. For example, in the case of defect size or frequency, we will be more interested in the cases above the target line.

Traditional control charts are all drawn on the basis of normal distributions, and the upper control limit (UCL) and lower control limit (LCL) are commonly specified as the mean plus and minus three times the standard deviation:

$$UCL=\mu+3\sigma, \quad LCL=\mu-3\sigma$$

For example, if the mean and standard deviation of ln(defect length)s is 3.49 and 0.81, respectively the control chart is as illustrated in Figure 7-33. Here, UCL is equal to 5.89 and LCL is equal to 1.09. Sample number 12 is considered as out-of-control.

The probability that a point is beyond the control limits but the process has not actually changed is called the probability of false alarm or α. For a process that follows a normal distribution and with control limits three standard deviations away from the mean line α is equal to 0.0027.

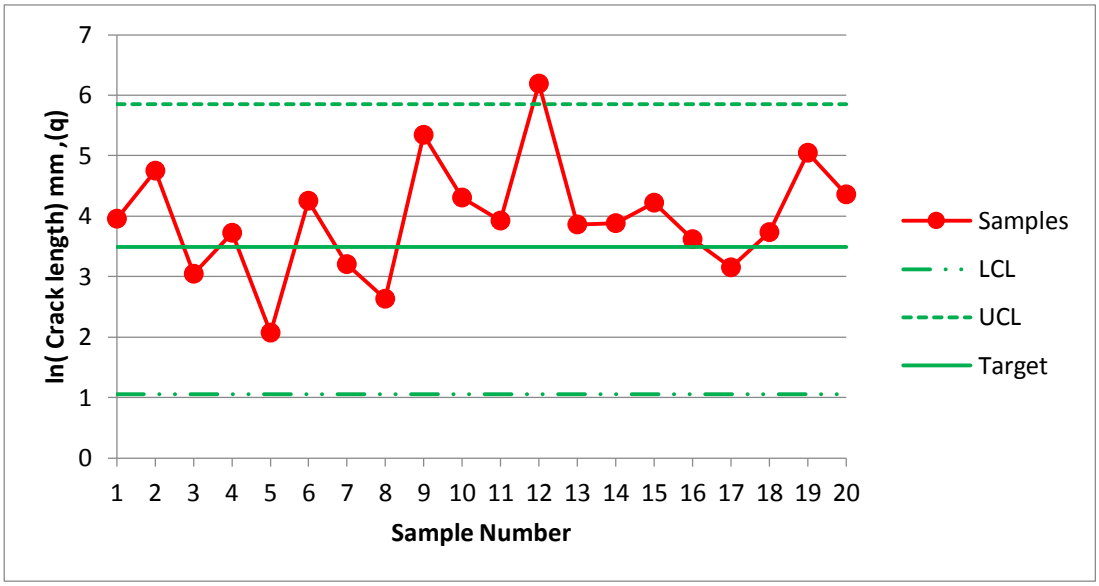

Figure 7-33 Illustration of a traditional control chart

So far all the defect sizes from the dataset, including the extreme values, have been considered in the probabilistic modelling of the defect length. This is a valid assumption for reliability analysis as the occurrence of extreme values is a possibility that affects the reliability of the structure. In SPC however, the extreme values need to be excluded so that the defect size distribution only models values generated by common causes. It is believed that decision on the sizes that are considered normal or abnormal require detailed study of various welding processes and procedure and the influencing variables which is beyond the scope of this work. Alternatively, statistical methods may be used to estimate an upper bound limit. Three methods are commonly used:

- Trimming the data visually,
- Removing values above or below chosen percentiles of the data.
- The Winsorizing method which is replacing values higher than a chosen percentile by that percentile value. The 90^{th} and 95^{th} percentile are commonly used.

Here, the Winsorizing method is used which also showed a good agreement with the visual trimming method. For the above data, the 95^{th} percentile is equal to 181.9

mm. The Winsorized mean and standard deviation of ln(length) are 3.47 and 0.73, respectively. The UCL and LCL are then equal to 5.66 and 1.28, respectively. Lower UCL and higher LCL may be chosen in order to increase conservatism.

There are several types of control charts that are commonly used in quality monitoring field. They are all developed based on exact probability limits. In the following section, first, control charts based on exact probability limits are explained then c-chart, and p-chart control charts are described.

7.11.1 Control charts based on exact probability limits

When the distribution of the process is skewed, i.e. binomial and Poisson distributions, the false alarm probability is different from the three standard deviation rule in normal distribution.

For high-quality processes, it is essential to use probability limits instead of traditional 3σ limits. For any plotted quality characteristic *Y*, the probability limits LCL_Y and UCL_Y can be derived as:

$$\mathrm{P}(X < LCL_Y) = \mathrm{P}(X > UCL_Y) = {}^{\alpha}/_{2} \tag{7-28}$$

For control-chart monitoring the number of nonconforming items in samples of size n, if the process's nonconforming rate is p, the probability that there are exactly k nonconforming items in the sample is described by the binomial distribution:

$$\mathrm{P}(X = k) = \binom{n}{k} p^k (1-p)^{n-k}\,, k = 0{,}1 \ldots n \tag{7-29}$$

moreover, the probability limits can be calculated as:

$$\mathrm{P}(X \le LCL) = \sum_{i}^{LCL} \binom{n}{i} p^i (1-p)^{n-i} = {}^{\alpha}/_{2} \tag{7-30}$$

$$\mathrm{P}(X \le UCL) = \sum_{i}^{UCL} \binom{n}{i} p^i (1-p)^{n-i} = 1 - {}^{\alpha}/_{2} \tag{7-31}$$

For the case of grand block joint the block comprises 60 total possible samples. Using reliability analysis for case study joint the maximum tolerable defect is calculated to be 9 defects. This corresponds to the probability of exceedance of 0.011 for 60

checkpoints. Setting $\frac{a}{2} = 0.011$ and using equation (7-30) the number defects that should trigger alarm can be computed. This is calculated for various sample sizes (n) and is given in Table 7-10. Furthermore, values based on $\frac{a}{2} = 0.00135$, corresponding to the 3σ rule in normal distribution, were computed. This is also shown graphically in Figure 7-34. UCL values computed based on the reliability limit are very similar to what was concluded in "Point estimate of defect rate". This is no surprise since both methods are using the same models and limits. There the interpretation was that if defects beyond a certain number are found it is not possible to conclude with a certain confidence that the defect rate is within acceptable limits. Here, the interpretation is that if the number of the defects are beyond a limit, there is a possibility that the process is creating abnormal defect rates caused by special causes and beyond tolerable limits. The UCL calculated based on $\frac{a}{2} = 0.00135$ are higher than those obtained based on a reliability limit showing more tolerance. A proposed approach could be to treat defect rates beyond the limits defined by reliability analysis as caused by common causes and increase the sample size to improve confidence on the gathered data which at the same time reduces failure probability; this may be viewed as an alarm limit. If the defect rates were beyond the UCL limits specified, based on $\frac{a}{2} = 0.00135$, they be treated as caused by possible special causes: this may be viewed as an action limit. For example, assume that the sampling starts with 8 checkpoints and 2 defects are found. We may increase the sample size to 13. If no additional defects are found no further inspection is required. But if we find two more defects, we may investigate the possibility of a special cause. If we had found 3 defects in 8 checkpoints, this could have been an action point for special causes, as well.

Sample size (n)	UCL ($\frac{a}{2} = 0.011$)	UCL ($\frac{a}{2} = 0.00135$)
5	1	2
8	2	3
10	2	3
12	2	3
13	3	4
15	3	4

Table 7-10 UCL limits for various samples size of the case study joint

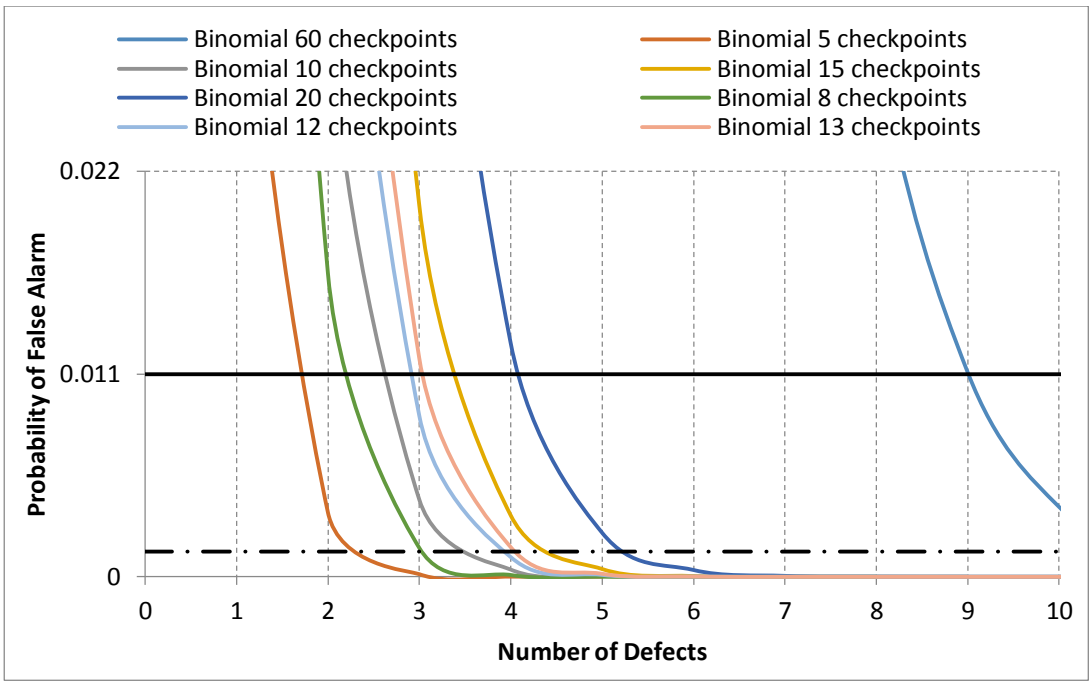

Figure 7-34 UCL limits for various samples sizes of the case study joint

7.11.2 c-chart:

The *c*-chart is based on observing the number of defects in a sample. This method assumes that the number of defects in a sample follow a Poisson distribution. The control limits are obtained by:

$$LCL = \bar{c} - 3 * \sqrt{\bar{c}}\,, \qquad UCL = \bar{c} + 3 * \sqrt{\bar{c}} \tag{7-32}$$

where *c* is the process long-term average number of defects in the sample, and the LCL is set to be zero when the value is negative. The UCL values for the grand block case study joint were calculated using equation (7-32), and the results are presented in Figure 7-35 showing similar results to those given in Table 7-10 and for $\frac{a}{2} = 0.00135$. The advantage of this method is its simpler equation which is easier to use on-site.

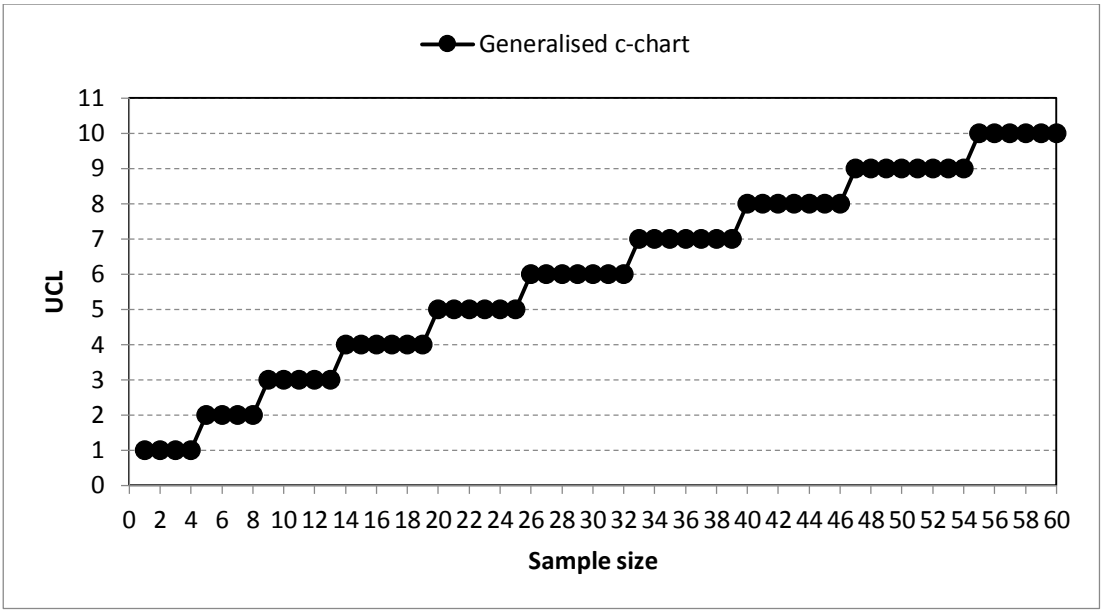

Figure 7-35 c-chat UCL values for different sample sizes

7.11.3 p-chart

p-chart is similar to the c-chart but is based on binomial distribution and used to monitor the proportion of nonconforming products in a sample, where the sample proportion nonconforming is defined as the ratio of the number of nonconforming products to the sample size, *n*. The control limits are:

$$UCL, LCL = \tilde{p} \pm 3 * \sqrt{\frac{\tilde{p} * (1 - \tilde{p})}{n}} \quad (7\text{-}33)$$

Using equation (7-33) , assuming $\tilde{p} = 0.073$ and for the case study grand block joint the calculated UCL values yield the same results as obtained by c-chart and exact probability method given in Table 7-10.

7.12 Chapter summary and conclusions

Defects may be caused by common causes as a result of inherent variations in the process. This variation is quantifiable. Otherwise, they are caused by assignable causes that are unusual, due to real changes in the welding process and their variations are unquantifiable. Statistical inference methods were used to quantify epistemic uncertainty in defect size and frequency of weld defects.

Partial NDE inspection of welds can be beneficial through:

- Reducing epistemic uncertainty in defect frequency and size data by increasing the statistical confidence on the data which in turn improves estimated reliability.

- Assuming removing the defects after detection, it will increase the actual reliability of the structure by reducing the number of defects that will be present in the structure.

- Improves the reliability through monitoring and controlling the welding and fabrication process by detecting defects caused by assignable causes, assuming that the remdial actions will be taken after detection.

There is a close connection between the calculated reliability and statistical confidence in uncertain variables. Statistical confidence is strongly dependent on the sample size of the collected data. In this chapter the main methods of estimating statistical confidence namely: point estimation, interval estimation and Bayesian inference and their relation with NDE sample size were studied.

The point estimate and interval estimate are in effect analogous approaches with interval estimate providing better information about the possible range of the population parameters. This range is called the confidence interval. The confidence interval is proportional to the scatter of the data and inversely related to the square root of the sample size.

Effect of the defect data confidence level on the reliability of a welded joint was studied, and it was found that:

- At least 30 defect data points are needed to make a reasonably confident estimate of defect size distribution and as a result structural reliability.
- Increasing the data points will reduce epistemic uncertainty in the defect size and consecutively the estimated reliability.
- There is little benefit in increasing the data points beyond 90.
- Reduction in the epistemic uncertainty of the defect size is the function of number of samples containing defects and not the gross quantity of checkpoints. The case study ship has the defect rate of 0.073 meaning that at least 411 checkpoints are required to achieve 30 data point. A process with worse (higher) defect rate will provide better statistical confidence, but, as investigated, the benefit from higher confidence is mitigated by the rise in the total number defects

that are present in the structure which is directly proportional to the estimated probability of failure.

An equation, based confidence interval approach, is proposed to specify a minimum number of NDE samples per joint.

Binomial and Poisson distributions are commonly used to describe aleatory uncertainty in the defect rate. Both models show comparable results with binomial distribution being the preferred method in this research due to its capability to model the number of checkpoints directly. The epistemic uncertainty of binomial distribution parameters is modelled by beta distribution.

The binomial distribution was used to study the effect of sample size on the probability of finding defects for a known defect rate. Then Binomial distribution in conjunction with tolerable defect rate and required confidence were used to calculate an acceptable number of defects for various sample sizes.

The major limitation of the confidence interval method is its ineffectiveness when dealing with small sample sizes. Bayesian inference theory is an effective method to deal with this problem and combines prior knowledge with collected data. The method is outlined, and estimation of defect size distributions, defect rates and material properties were studied.

- When the sample size is small, the results from the Bayesian inference method are amid the prior assumptions and collected data. As the sample size increases the Bayesian estimate converges towards the collected data.

Statistical process control (SPC) method and its application in detection of defects caused by out-of-control processes were described.
Control charts based on binomial distribution and Poisson distribution were used to calculate false alarm limits for defect rate and size.
A two stage defect rate limit is proposed:

- The first stage is based on reliability limit and indicates the possibility that the variability of the natural variation causing unacceptable reliability
- The second limit is based on false alarm probability and indicates the possibility of the process being out of control.

Chapter 8

The proposed method for improved inspection

8.1 Chapter outline

The aim of this research was to optimise NDE inspection of newbuilding ship hull structure by developing a risk and reliability framework. In chapter three the risk and reliability framework was outlined, various aspects that needed investigation and the tools requiring development were introduced. In chapters four to seven the areas required investigation were discussed in detail, and the necessary tools were developed.

In this chapter, a framework is proposed based on the studies discussed in preceding chapters. The method can be seen as a flow diagram comprised of six stages from initial data input to final quality control stage.

First, the overview of the method and its stages are introduced. The overview section is then followed by more detail descriptions of each stage. Finally, an example of a quality improvement scheme using Pareto charts and an Ishikawa diagram is provided.

The method proposed here is the final output of this research.

8.2 Overview of the method

The method proposed in this chapter has two key objectives:

1. To ensure the intended reliability of the structure containing weld fabrication defects
2. And, to control and improve weld fabrication quality by monitoring defect frequency and size.

These two objectives are achieved by combining risk and reliability assessment with a quality control programme through statistical sampling. The schema of the method is shown in Figure 8-1.

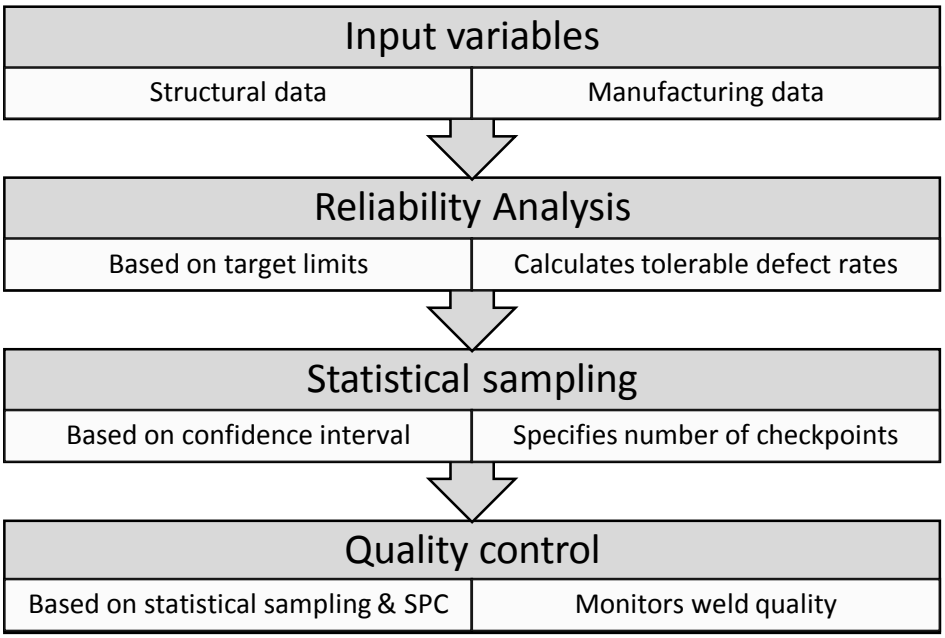

Figure 8-1 Big picture of the proposed inspection scheme

Structural components are assigned with target reliabilities considering possible consequences of their failure and the in-service inspection measures. The developed reliability model predicts time-dependent reliability which is dependent on defect frequency and size inferred from inspected NDE checkpoints. The intended reliability of the structure is achieved by keeping the predicted reliability above the target reliability. Predictive reliability of the structure can be assessed using the data collected from NDE inspection. The predictive reliability inferred from partial NDE inspection is related to the full NDE inspection using statistical confidence. Here, statistical confidence is used to calculate a required number of checkpoints. For quality control purposes, tolerable defect rates are calculated by risk and reliability calculations.

Additionally, statistical process control (SPC) tools are used to monitor weld fabrication process. This is achieved by limiting detected defect rate and sizes to false-alarm limits. SPC can be supplemented by taking improvement actions to enhance the welding quality which may allow reduced NDE checkpoints of welds performed with improved processes.

The framework is illustrated in Figure 8-2. The brief picture of each of the six stages are as follows and the more detail descriptions are explained in the following sections.

In stage 1, the input data is collected, which could be the manufacturer's long-term data or the data from previous construction. In the absence of such data, a conservative assumption of external data may be used by selecting a dataset or processed data which is believed to be relevant to the structure under study. In stage 2, chosen data is processed by utilisation of an appropriate fitting model and technique or selecting a suitable external model (i.e. from literature). In stage 3, the predictive reliability model utilises processed data to estimate time variant reliability of the structure which is then used in conjunction with target reliability levels to calculate tolerable defect frequencies. In stage 4, the tolerable defect frequencies are used to calculate the required NDE checkpoints (sample size) based on statistical sampling principles.

Stage 5 is the inspection stage. Here, the defect size and frequency data are recorded and used in stage 6 for quality control purposes. The recorded data may be used to update assumptions made in stage 2, the data processing in Figure 8-2, stage using a Bayesian updating method. Finally, in stage 6 the quality of the weld is assessed based on the limits on the number of defects defined by reliability analysis. In this stage, the welding process may also be controlled by monitoring the defect size and rate.

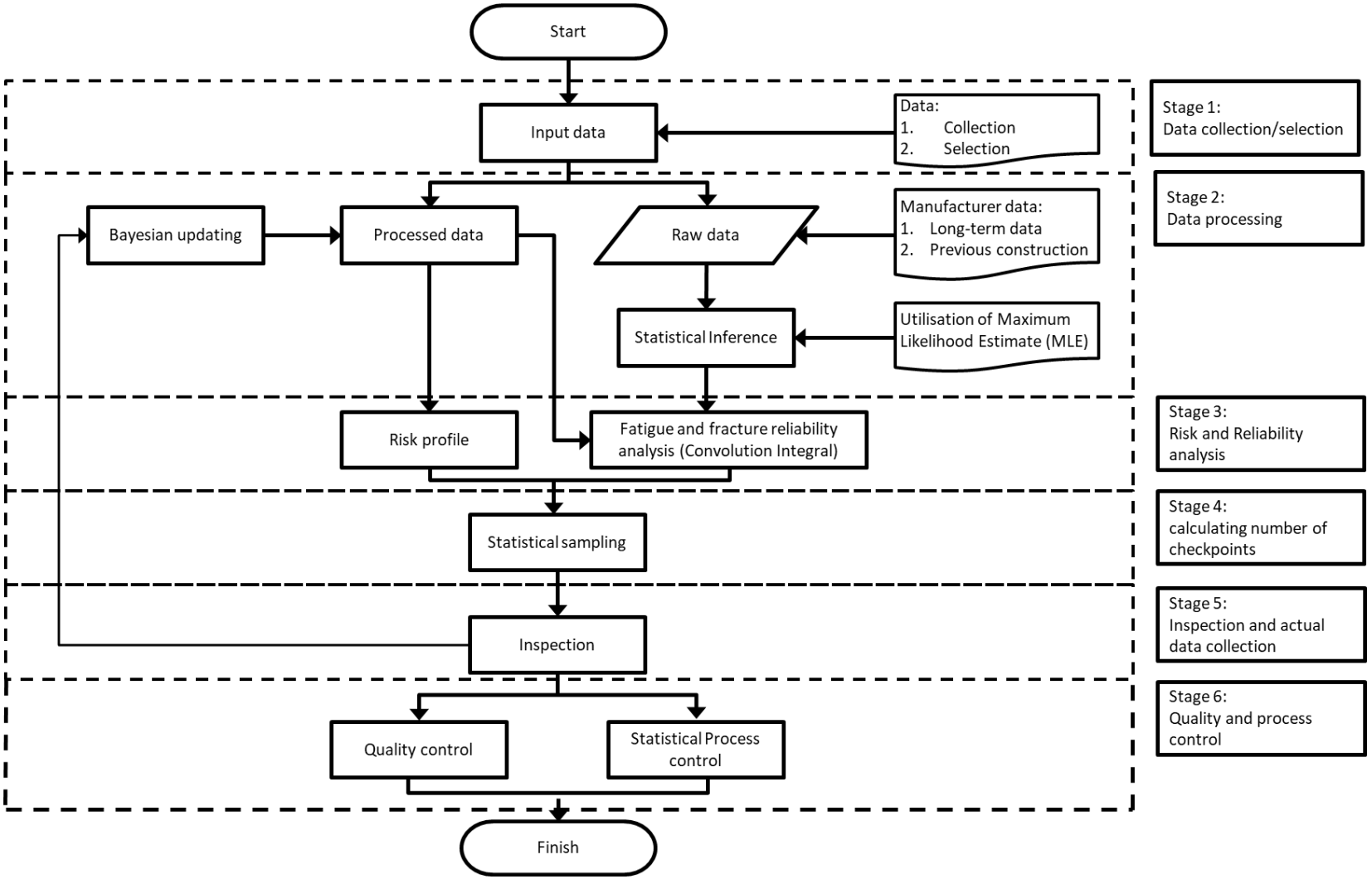

Figure 8-2 Overview of the inspection framework

8.3 Data acquisition and data statistical inference

Data acquisition and statistical inference play a central role in the proposed method. The input data may be categorised into four categories:

1. The manufacturer defect data
2. Material toughness data
3. Structural data
4. NDE capabilities

The first three categories affect actual structural reliability as well as predicted reliability. NDE capabilities will have a significant impact on actual reliabilities only if the structure is subjected to nearly 100% NDE, but it also affects predicted reliabilities, i.e. better NDE methods detect more and smaller defects, even when partial NDE is performed.

When possible, a data set which is believed to be similar to the data of the ship under investigation should be used. This could be data from a previously built ship or manufacturers' long-term data. For example, if the same welding contractor or steel provider is used, the natural choice would be such data. Otherwise, the long-term data can be used. In the absence of manufacturer data, generic data from the literature or this thesis may be used. This is a starting point for the preliminary inspection plan; as the inspection is progressed, new data is recorded, and initial assumptions are updated. If the updated data are significantly different from the initial assumption, the programme will suggest an updated inspection plan.

Structural data is specific to the ship under inspection and should be available prior to planning. Particularly, the ship stress model is required to construct long-term stress distribution of the structure.

Once the data are gathered or selected they should be transformed into statistical functions so that they can be used in reliability analyses. Appropriate methods of such transformations are discussed in relevant chapters of this thesis.

The data acquisition and statistical inference flow diagram is shown in Figure 8-3.

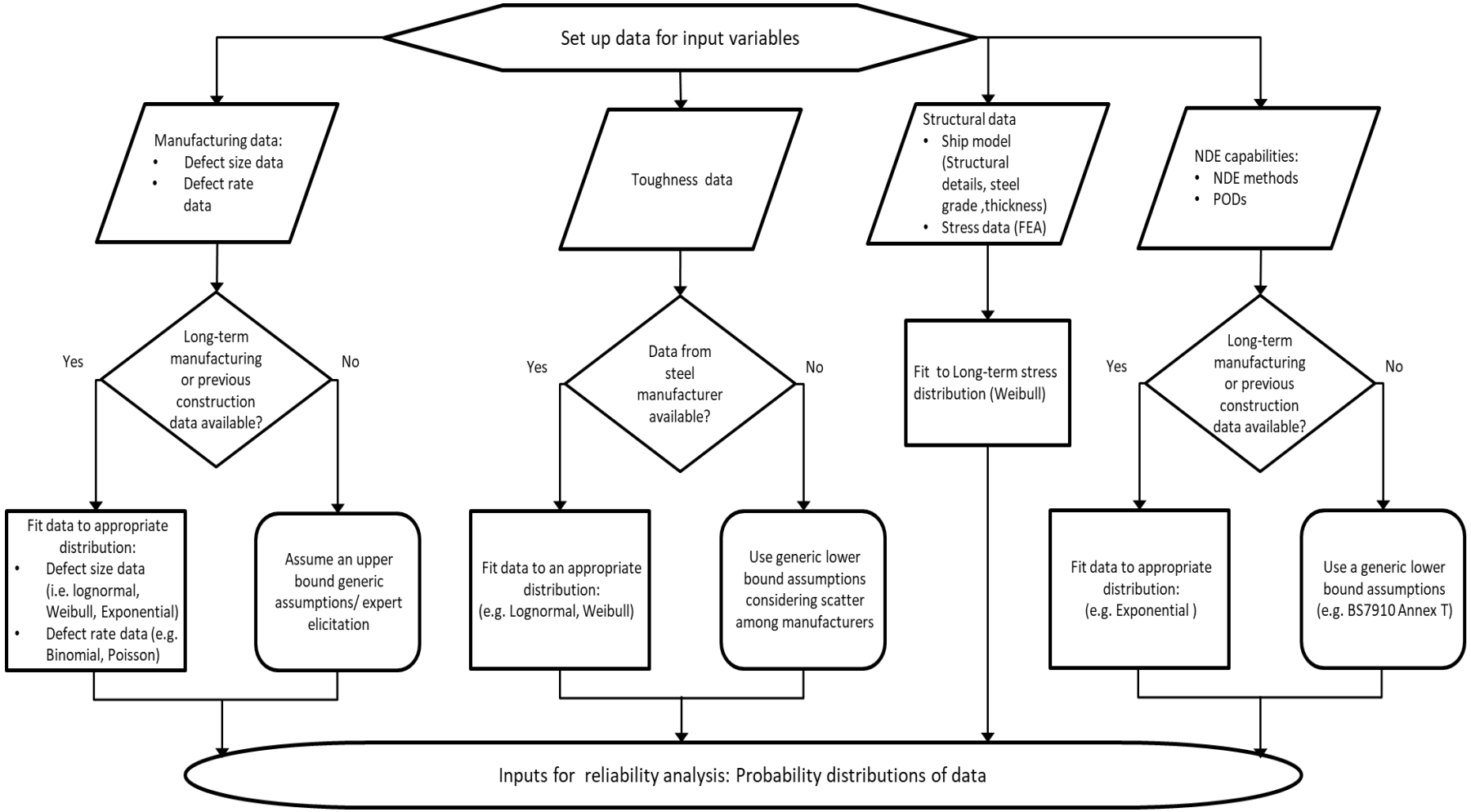

Figure 8-3 Data acquisition and statistical inference flow diagram

8.4 Risk and Reliability

The risk and reliability module is the core of the proposed framework. The predictive reliabilities are a function of input data and are discussed, in detail, in chapter three and six of this thesis. These reliabilities should be kept above the target reliabilities. The target reliabilities are specified based on the risk model developed in chapter three which is dependent on the consequence of failure, type of the ship and inspection programmes of the structure during service life. When the predicted reliability is above target reliability the extent of the inspection is defined using a statistical sampling approach. Otherwise, the manufacturer should ensure that the selected welding processes produce superior defects rates or sizes. Alternatively, significantly high coverage of NDE may be used to increase actual reliabilities. This coverage can reach up to 100% which as shown in chapter six can reduce the probability of failure to almost zero. The risk and reliability flow diagram is presented in Figure 8-4.

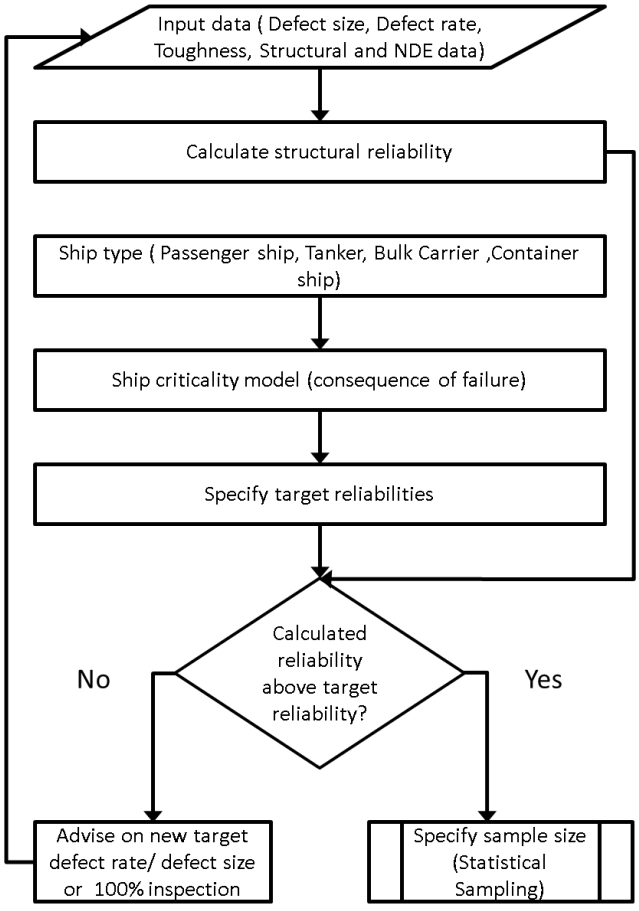

Figure 8-4 Risk and reliability flow diagram

8.5 Statistical Sampling

The extent of inspection (number of checkpoints) is calculated based on the assumption that using initial inputs the structure is capable of tolerating a range of defect occurrences. If the defect rates are within the range, the target reliability is achieved. NDE inspection informs us about the true defect rate. Since samples of the welds are inspected, the gathered information will inevitably be associated with a level of uncertainty. This uncertainty is quantified by statistical confidence. Higher sample size results in higher confidence and less uncertainty. Here, the required number of checkpoints to achieve target defect rates with specified confidence is calculated using the relationship between confidence level and sample size. The flow diagram for determining the required number of NDE checkpoints is shown in Figure 8-5.

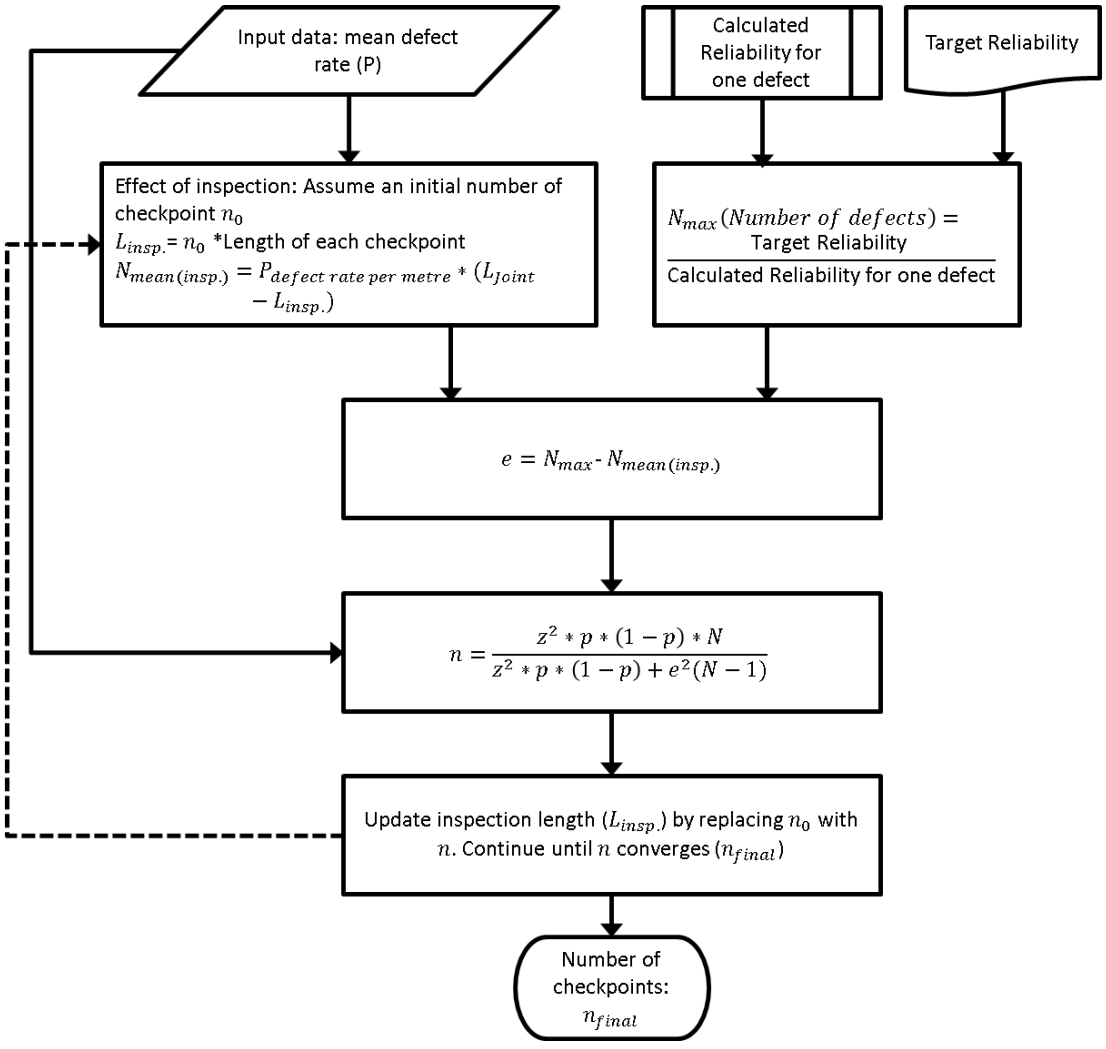

Figure 8-5 Flow diagram for calculating the required number of checkpoints

The reliability programme calculates the failure probability due to the presence of one defect. The total probability of failure is the product of this failure probability and the estimated number of defects. Provided that the failure probabilities are small otherwise, $P_{joint} = 1 - (1 - P_f)^n$ needs to be used, see section 6.7.2, equation (6-31).The maximum number of defects (N_{max}) can be calculated by reversing the above procedure. This maximum number (N_{max}) and mean number of defects remaining in the structure after inspection ($N_{mean(insp)}$) in conjunction with a statistical confidence level measure (z) are used to compute the required number of checkpoints and N is the number of the items in the population.

8.6 Quality control

The number of defects found during NDE inspection should be compared against the tolerable limits defined by risk and reliability analysis. The reliability model gives an allowable number of defects per joint. As only a fraction of the joint is sampled for inspection, the number of tolerable defects per inspection length will differ from those found by 100% inspection. This is discussed in chapter seven in detail. If the number of detected defects is higher than the allowable number, the length of inspection should be increased to increase statistical confidence. This also improves the reliability by reducing the total number of defects that remain in the joint (uninspected part) after inspection. The assumption here is that detected defects are repaired after inspection, as it is the current requirement of ship classification societies. Unacceptable defect rates should also be checked by process control requirement to ensure that they are not caused by an out-of-control process. The flow diagram for the quality control stage is shown in Figure 8-6.

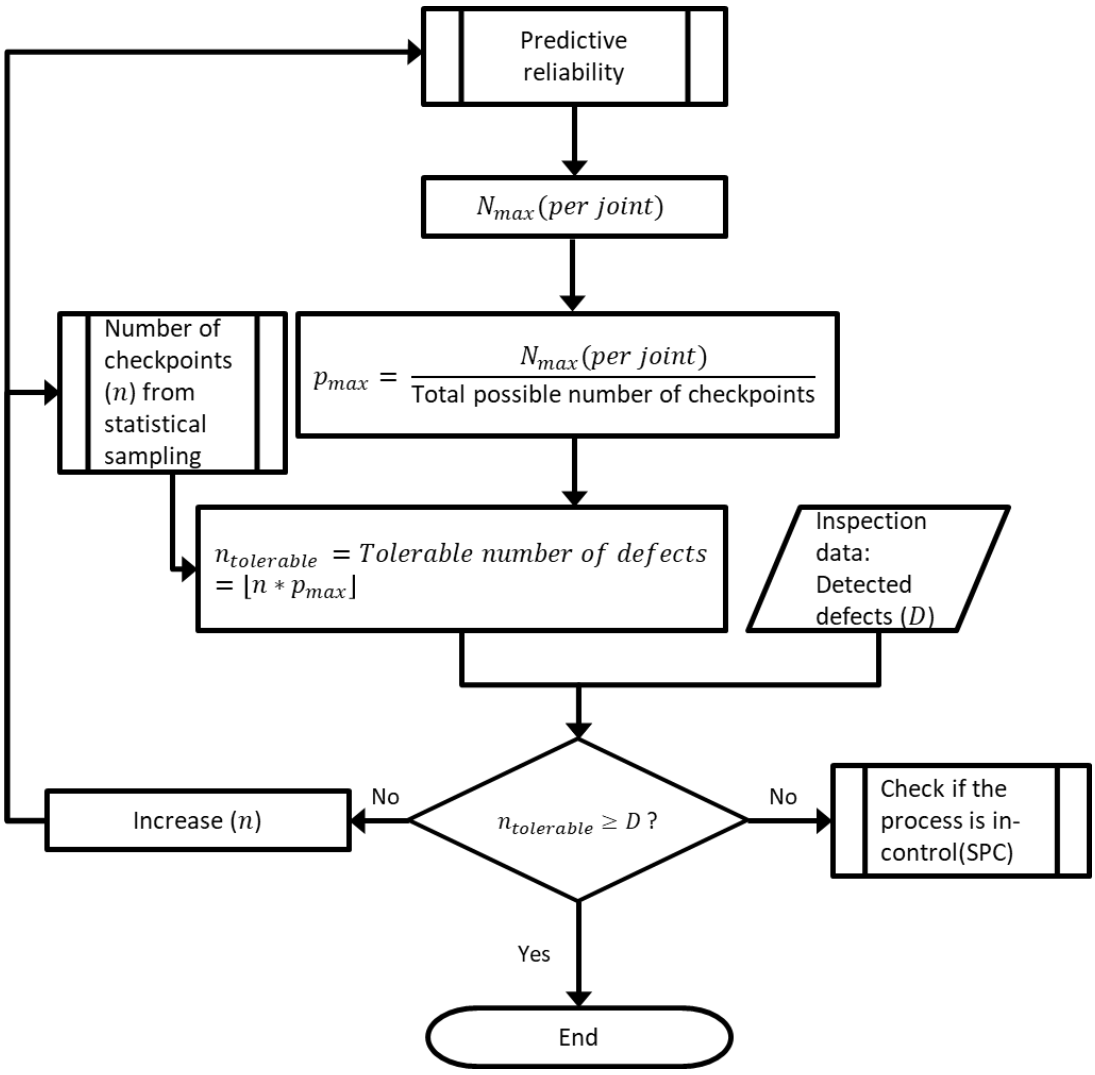

Figure 8-6 Quality control flow diagram

8.7 Process control

When defect frequencies and sizes are caused by normal causes the quality control scheme described in the previous section is adequately efficient, particularly for inspection of the finished welds. Defects can also be caused by a special cause resulting in abnormal defect rates or sizes. In this case, it is more efficient to determine the special cause and improve the process. This will reduce the defect rate and sizes which in turn may allow avoiding extra NDE of welds that have not been executed. It is also possible that special causes yield lower defect rates or sizes. It would be beneficial to find the causes and possibly maintain the defect production rate at the improved state. The improved defect statistics then may allow us to

perform less NDE on the welds that are going to be performed in future. The process control flow diagram is shown in Figure 8-7.

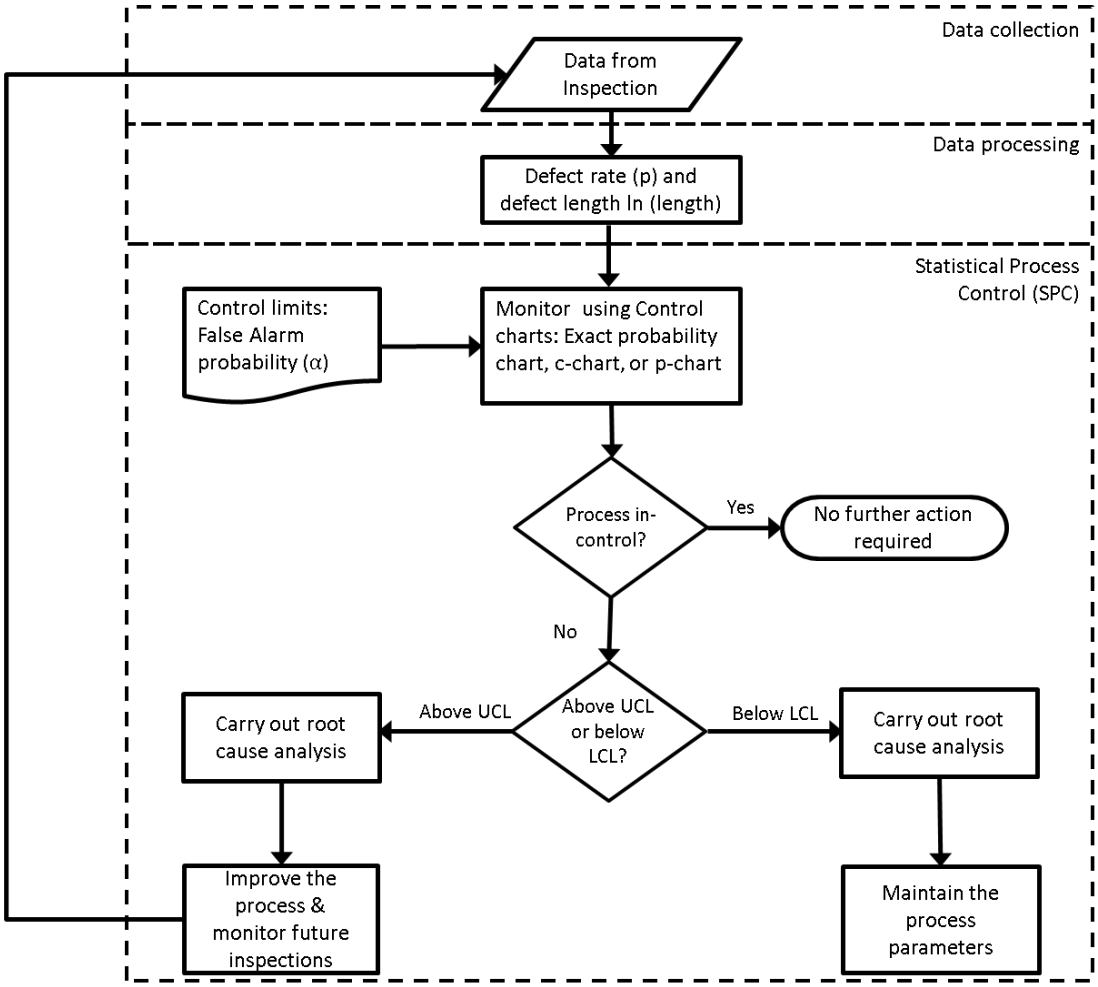

Figure 8-7 Process control flow diagram

8.8 Quality Improvement

As explained in the previous section the mean defect rates and sizes may require improvement. Application of control charts is proposed in chapter seven as a tool to detect the presence of special causes which produce abnormal defect rates or sizes. However, in order to determine the nature of special causes other process control tools should be used. Two commonly tools are Pareto chart and Ishikawa (fishbone) diagram.

Pareto charts are used to determine the types of error which have the highest impact on total error. The values are represented by bars in descending order, and corresponding cumulative values are shown by lines. For instance, the Pareto diagram for planar defects in ship #3 is presented in Figure 8-8. It is clear that the

Lack of Fusion defects and longitudinal cracks are responsible for a large majority of planar defects. If we were to reduce the defect rates, provided that all defects have the same criticality, it would be best to focus on one or both of these two defect types.

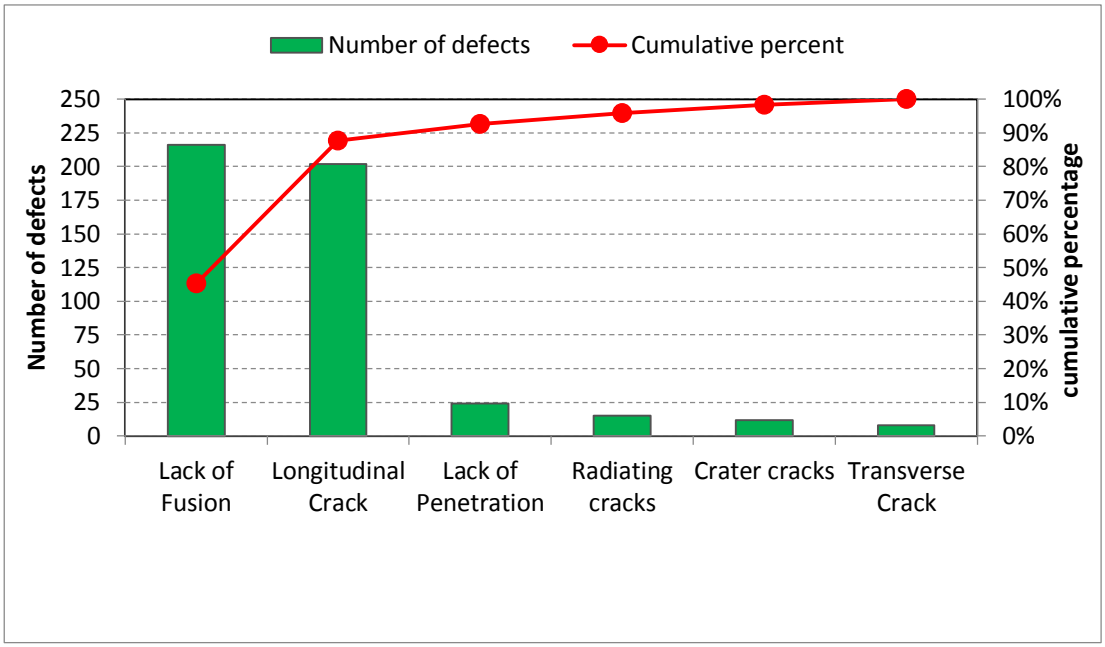

Figure 8-8 Pareto diagram of planar defects in ship #3

Once the defect types that contribute most to the defect production are identified the causes of those defects can be investigated using a root-cause-analysis tool such as Ishikawa cause-and-effect diagram. The diagram structures the root cause analysis by categorising the main causes of the defect into several (normally 5 to 6) potential main causes. Each main cause may be categorised into several subcategories or causes. The diagram helps to perform the root-cause analysis in a more structured and convenient way.

An Ishikawa diagram of weld cracking is developed and is illustrated in Figure 8-9. This diagram can help the quality control team at the shipyard to investigate the cause(s) of weld cracking.

As explained in chapter two the primary cause of lack of fusion/ lack of penetration defects are the welder's skill thus the Ishikawa diagram for these defect types are not developed here. To reduce lack of fusion/ lack of penetration defects the quality control team may focus on improving welder's skill by retraining them or revaluation of their certificates or reviewing their working hours and shifts.

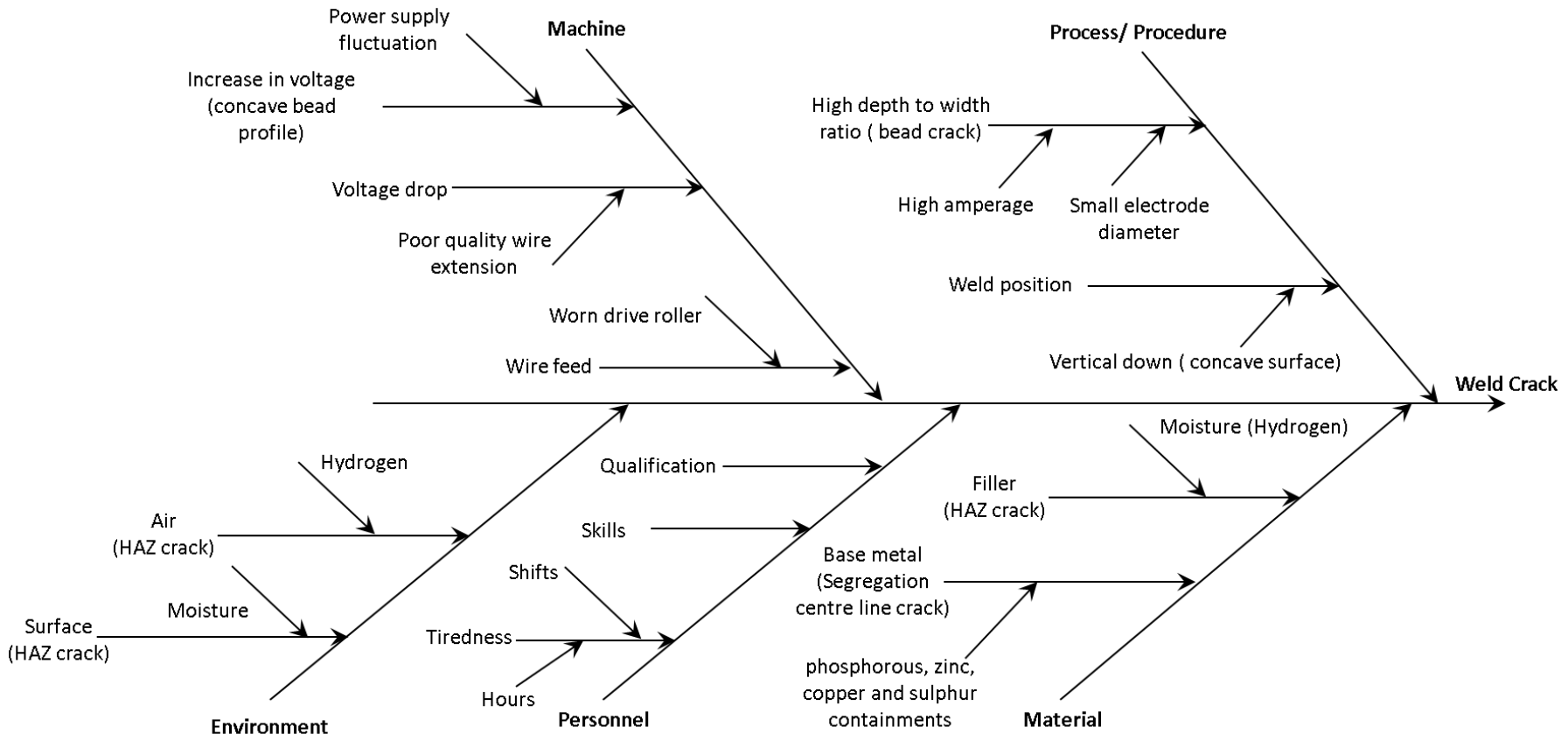

Figure 8-9 Root cause analysis of weld cracking using the Ishikawa diagram

8.9 Application to the case study structure

As outlined in chapter 1, one of the decks of a cruise ship was selected as the case study structure. This is based on two primarily reasons:

1. The majority of welding is performed in the deck area. For a similar ship about 85% of the welding work conducted in deck structures.
2. Unlike the shell structures, the decks are covered with outfitting and are practically uninspected during service, and growing cracks are likely to remain unnoticed until fracture failure (local or propagating).

The ship decks are numbered in ascending order from the deck immediately above the bottom to the deck at the utmost top. Deck number 16 which has the furthest vertical distance from ship neutral axis and thus is subjected to the highest global bending stress was selected as the case study deck. There are two additional small decks above deck 16 with limited contribution to global strength of the structure and hence experience lower stresses.

In chapters six and seven, where predictive reliability and sampling schemes are developed, characteristics of mid area of deck 16 were used wherever the developed approaches were studied.

Here, the proposed framework for optimised NDE inspection is examined for all block joints across the entire deck 16.

8.9.1 Description of the case study deck

Deck 16 is comprised of 21 block joints running along the width of the deck and connecting deck components of ship blocks. The deck overall length is 278 m and the average width is 30 m. A diagram of the deck is shown in Figure 8-10.

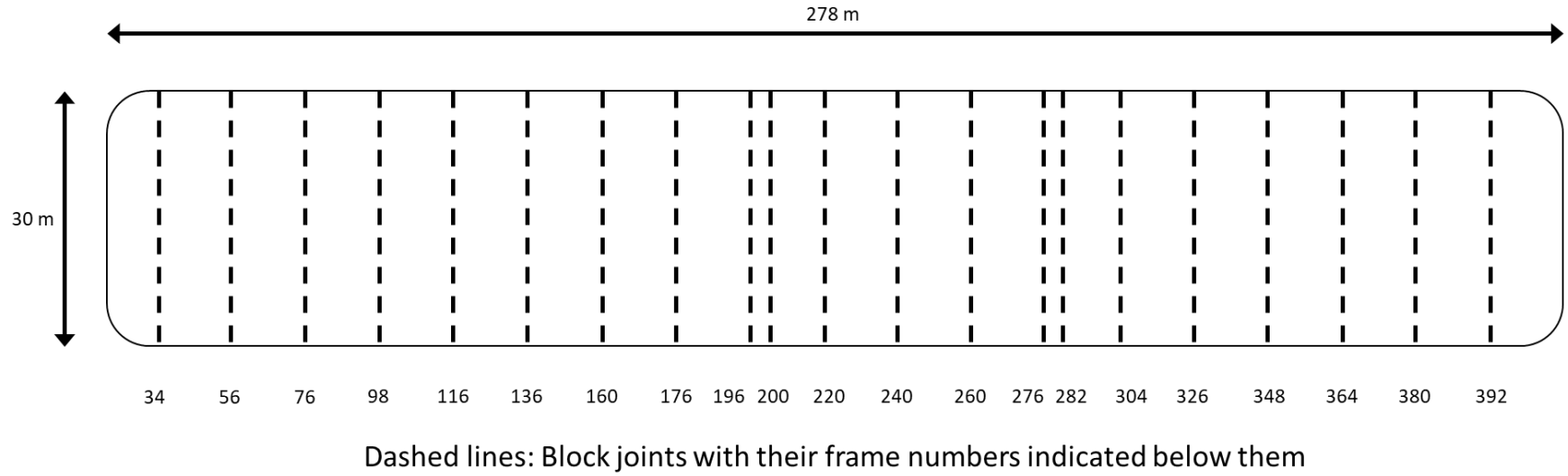

Figure 8-10 Diagram of deck 16

8.9.2 Stage 1 and 2: Data collection and data processing

8.9.2.1 Material properties

The deck plating is made from high strength A grade shipbuilding steel (AH36), and the thickness is generally between 5 mm to 8mm, starting at 5 mm at the aft and forward area to 8 mm in midship. At locations around the openings where higher stress levels due to stress concentration are expected, thickness ranges between 10 mm to 14 mm.

The material supplier is the manufacturer # 5 in chapter 5 providing AH36 steel with characteristics given in below Table 8-1.

	Fracture toughness $(MPa\sqrt{m})$	Ultimate tensile strength (MPa)	Yield stress (MPa)
Mean value	367.4	560	445
Coefficient of variation	0.25	0.035	0.06
Distribution	Lognormal/ Weibull	Normal	Normal

Table 8-1 Material properties of the case study structure

8.9.2.2 Structural data

Structural data includes stresses due to global bending of the structure calculated using Finite Element Analysis (FEA). FEA of the structure was performed by the manufacturer and validated by the class design approval office. The results were provided to the author in terms of FEA counterplots and tables containing applied bending moment and shear forces at the location of transverse frames. These are shown in the Appendix E. The FEA results are then used to calculate long-term stress distribution of structure using the procedure described in section 6.6.1.

8.9.2.3 Defect data

Defect data includes planar defect size and frequency data of ship #2 collected from NDE inspection of the case study ship. The data analysis was discussed in detail in chapter four. The defect size and defect rate data are given in Table 8-2 and Table 8-3, respectively.

	Defect type	Distribution	Parameters	
Detected defects size	Crack	Lognormal	Mu=3.49	Sigma=0.81
	Crack+LOP+LOF	Lognormal	Mu=3.98	Sigma=1.21
Initial defect size	Crack	Exponential	$\lambda_0 = 30$	
	Crack+LOP+LOF	Exponential	$\lambda_0 = 72.4$	

Table 8-2 Defect size data for case study ship based on table 4-13

Sample size	Planar Defect	Defect rate	
		Defect number vs. number of inspections(n/N)	Number of defects per meter (n/m)
7099 checkpoints; 3444.9 (m)	Crack	0.033	0.069
	LOP/LOF	0.038	0.079
	Cracks+ LOP/LOF	0.073	0.148

Table 8-3 Defect rate data for case study ship based on table 4-15

8.9.2.4 NDE capabilities

NDE capabilities comprise of probability detection functions for the various NDE techniques as discussed in detail in chapter four and are given here in Table 8-4. The POD values are fitted to a cumulative exponential distribution and then used in predictive reliability calculations.

NDT	PODs
VT	(90 %POD= 121 mm, 50% POD =16mm)
RT	(90 %POD=31.1 mm, 50% POD =9.36mm)
UT	(90 %POD= 21.46 mm, 50% POD =6.46mm)
MPI/PT	(90 %POD= 28.61 mm, 50% POD =8.6mm)
MPI/PT	(90 %POD=5.72 mm, 50% POD =1.72mm) ground crown welds

Table 8-4 NDT reliability characteristics assumptions based on section 4.5

8.9.3 Stage 3: Risk and reliability analysis

Using the data defined above through-life reliability of the structure at various block joints were calculated using the developed software described in section 6.5.2. The final year failure probabilities at any location along the weld line assuming the presence of a planar defect are shown in Table 8-5. As described in section 3.10, target reliability of $2.3 * 10^{-4}$ is chosen for joints at deck area.

Frame	Pf
34	5.04E-14
56	5.04E-14
76	5.04E-14
98	5.04E-14
116	5.04E-14
136	4.89E-12
156	4.12E-09
176	4.55E-09
196	4.55E-09
200	2.68E-05
220 Portside	2.68E-05
220 Centre	0.00774
220 Starboard	2.68E-05
240	3.06E-07
260	4.55E-09
272	4.55E-09
276	4.55E-09
282	4.55E-09
304	4.12E-09
326	5.04E-14
348	5.04E-14
364	5.04E-14
380	2.58E-16
392	2.58E-16

Table 8-5 Final year failure probabilities at any location along the joint due to the presence of a planar defect

8.9.4 Stage 4: Calculation of checkpoints

Using equation (6-31), the target reliability, the predictive reliability and the maximum acceptable defect rate were then calculated and are shown in Table 8-6. The existing inspection plan is also given in this table for comparison purposes. Employing statistical sampling methods outlined in section 7.8, and by using equation (7-21), the required number of inspection checkpoints to achieve a certain statistical confidence about the required reliability of the joint was calculated. The results are given in Table 8-6 below. Notice that at the joints located at the centre area of frame 220 the predictive probability of failure is so high that the corresponding allowable defect rate is so low that in order to achieve such defect rate the entire area needs to be inspected. This is due to high hogging stress at this location. This is shown in Figure 8-11, where locations in yellow, orange and red colour are the highly stressed area. The length of the joint in this area is around 8.3 metre and assuming that the length of each checkpoint is 0.5 meter, 17 checkpoints are required. At other parts of the joint 220 and centre of the joint 200, the stress is lower and partial inspection can be used. The probabilities of failure in the rest of the joints are so low that the

structure can sustain very high defect rates, assuming that the cracks are not interacting.

Frame	Pf	Target Pf	Allowable defect rate per checkpoint (maximum 1)	Checkpoints Based on Reliability				Existing Inspection plan
				Statistical confidence				
				80%	90%	95%	99%	
34	5.04E-14	0.00023	1	0	0	0	0	7
56	5.04E-14	0.00023	1	0	0	0	0	5
76	5.04E-14	0.00023	1	0	0	0	0	7
98	5.04E-14	0.00023	1	0	0	0	0	6
116	5.04E-14	0.00023	1	0	0	0	0	5
136	4.89E-12	0.00023	1	0	0	0	0	7
156	4.12E-09	0.00023	1	0	0	0	0	13
176	4.55E-09	0.00023	1	0	0	0	0	9
196 (Port & Stb)	4.55E-09	0.00023	1	0	0	0	0	5
200 (Centre)	2.68E-05	0.00023	0.14479	7	11	15	20	9
220 (Port)	2.68E-05	0.00023	0.14479	5	7	8	9	3
220 (Centre)	0.00774	0.00023	0.0005	17	17	17	17	5
220 (Starboard)	2.68E-05	0.00023	0.14479	5	7	8	9	3
240	3.06E-07	0.00023	1	0	0	0	0	9
260	4.55E-09	0.00023	1	0	0	0	0	8
272	4.55E-09	0.00023	1	0	0	0	0	5
276	4.55E-09	0.00023	1	0	0	0	0	4
282	4.55E-09	0.00023	1	0	0	0	0	8
304	4.12E-09	0.00023	1	0	0	0	0	5
326	5.04E-14	0.00023	1	0	0	0	0	8
348	5.04E-14	0.00023	1	0	0	0	0	7
364	5.04E-14	0.00023	1	0	0	0	0	7
380	2.58E-16	0.00023	1	0	0	0	0	5
392	2.58E-16	0.00023	1	0	0	0	0	6
Total				34	42	48	55	156

Table 8-6 Calculation of required number of checkpoints based on reliability analysis

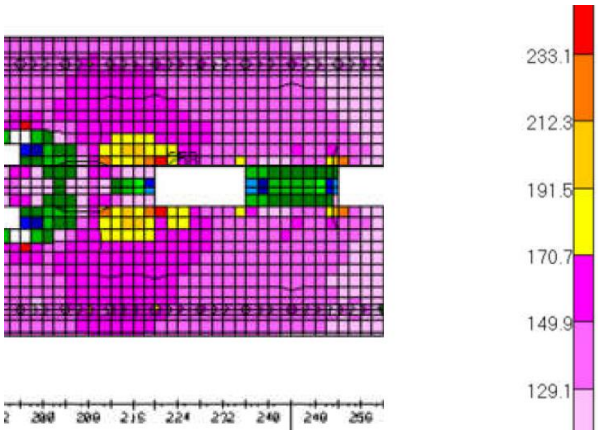

Figure 8-11 Stress due to global bending (Hogging) at around frame 200

Similarly, the required numbers of checkpoints are calculated based on statistical process control (SPC) limits. The upper control limit (UCL) control 99 percentile is chosen, which corresponds to 0.167 defect rate. The calculated number of checkpoints based on SPC and for various confidence levels are given in Table 8-7.

Frame	Pf	Target Pf	UCL defect rate (per checkpoint)	Checkpoints based on SPC					Existing plan
				Statistical confidence					
				75%	80%	90%	95%	99%	
34	5.04E-14	0.00023	0.167	4	5	11	16	25	7
56	5.04E-14	0.00023	0.167	4	5	11	16	25	5
76	5.04E-14	0.00023	0.167	4	5	11	16	25	7
98	5.04E-14	0.00023	0.167	4	5	11	16	25	6
116	5.04E-14	0.00023	0.167	4	5	10	14	21	5
136	4.89E-12	0.00023	0.167	4	5	11	16	25	7
156	4.12E-09	0.00023	0.167	4	5	11	16	25	13
176	4.55E-09	0.00023	0.167	4	5	11	16	25	9
196 (Port & Stb)	4.55E-09	0.00023	0.167	3	4	8	11	17	5
200 (Centre)	2.68E-05	0.00023	0.167	2	2	4	6	9	9
220 (Port)	2.68E-05	0.00023	0.167	2	2	4	6	9	3
220 (Centre)	0.00774	0.00023	0.167	2	2	4	6	9	5
220 (Starboard)	2.68E-05	0.00023	0.167	2	2	4	6	9	3
240	3.06E-07	0.00023	0.167	4	5	11	16	25	9
260	4.55E-09	0.00023	0.167	4	5	11	16	25	8
272	4.55E-09	0.00023	0.167	4	5	11	16	25	5
276	4.55E-09	0.00023	0.167	4	5	11	16	25	4
282	4.55E-09	0.00023	0.167	4	5	11	16	25	8
304	4.12E-09	0.00023	0.167	4	5	11	16	25	5
326	5.04E-14	0.00023	0.167	4	5	11	16	25	8
348	5.04E-14	0.00023	0.167	4	5	11	16	25	7
364	5.04E-14	0.00023	0.167	4	5	11	16	25	7
380	2.58E-16	0.00023	0.167	4	5	11	16	25	5
392	2.58E-16	0.00023	0.167	4	5	11	16	25	6
Total				87	107	232	337	524	156

Table 8-7 Calculation of required number of checkpoints based on statistical process control limits

The proposed strategy is to combine both methods to a unified approach. At each joint, the number of the checkpoints is defined based on the approach which gives the higher number. A level of confidence needs to be chosen by the user. This can be agreed between the stakeholders prior to planning or based on a cost-benefit analysis. Here, for the reliability approach, a 90% confidence level as a common engineering assumption is used. For process control, a lower confidence level is assumed to be sufficient since the reliability calculations have shown the capacity of the structure to deal with high defect rates. Here, 75% confidence was chosen. This

seems to be an appropriate confidence level as the method will use the collected data for the entire deck to update the defect rate and size statistics, thus, may require a further inspection if deemed necessary. The results are presented in Table 8-8.

Frame	90% confidence in reliability and 75% confidence in process control	Existing plan
34	4	7
56	4	5
76	4	7
98	4	6
116	4	5
136	4	7
156	4	13
176	4	9
196 (Port & Stb)	3	5
200 (Centre)	11	9
220 (Port)	7	3
220 (Centre)	17	5
220 (Starboard)	7	3
240	4	9
260	4	8
272	4	5
276	4	4
282	4	8
304	4	5
326	4	8
348	4	7
364	4	7
380	4	5
392	4	6
Total	121	156

Table 8-8 Proposed inspection plan based on the unified approach

The existing inspection plan which is based Lloyds Register rules generally provides higher number of NDT checkpoints. The noticeable difference is at joint number 200 and 220 where the existing plan is unconservative compared to the proposed plan.

8.9.5 Stage 5: Inspection

Having defined the number of checkpoints per joint, the next step is to perform the inspection and gather the results. Here, the inspection results of the existing plan (156 checkpoints) are used. The inspection was performed using Radiography testing (RT). The results of defective checkpoints containing planar defects are given in Table 8-9.

Frame	Position	ID No	NDE	Defect Length (mm)	Crack	Lack of fusion /penetration
34	Port	16-003	RT		Longitudinal	
34	Stbd	16-009	RT	50		Lack of Fusion
56	Port	16-015	RT			Lack of Fusion
76	Port	16-022	RT		Longitudinal	
116	Stbd	16-043	RT	40		Lack of Fusion
156	Port	16-059	RT			Lack of Fusion
156	Port	16-063	RT	50		Lack of Penetration
200	Stbd	16-107	RT		Longitudinal	
220	Port	16-112	RT		Longitudinal	
220	Port	16-116	RT	30		Lack of Fusion
240	Port	16-129	RT	45	Longitudinal	
240	Stbd	16-135	RT		Longitudinal	
260	Port	16-142	RT	50	Longitudinal	
260	Port	16-143	RT	70		Lack of Fusion
260	Port	16-144	RT		Longitudinal	
260	Port	16-144	RT	40		Lack of Fusion
276	Port	16-158	RT		Longitudinal	
276	Port	16-158	RT		Longitudinal	
276	Port	16-158	RT	25		Lack of Penetration
348	Port	16-196	RT	5	Transverse	
348	Port	16-196	RT		Transverse	
348	Port	16-196	RT		Longitudinal	
56	Port	PL-175	RT			Lack of Fusion
304	Port	PL-433	RT	350		Lack of Fusion

Table 8-9 The results of defected checkpoints containing planer defects

8.9.6 Stage 6: Quality control and process control

In this stage, the inspection results are analysed to examine whether the inspection findings comply with the reliability and process control requirements. For each joint, the defect rate is checked to be below the target rate. This is done by utilising the Binomial distribution as outlined in section 7.7. In this case, the defect rates derived from reliability and process control are close (0.1447 for reliability and 0.167). For simplicity 0.1447 is used to devise limits on detected defect rates from binomial distribution as shown in Figure 8-12 and Table 8-10. As discussed in chapter seven, defect size distribution is dependent on the number of detected cracks, and for the expected defect rate in this ship such data per joint will be too small to have a

significant effect on the prior information, instead the significance of defect size is checked based on the data collected from the entire deck using the Bayesian updating approach.

Table 8-10 is then used to identify the joints that require further inspection, and the results are presented in Table 8-11.

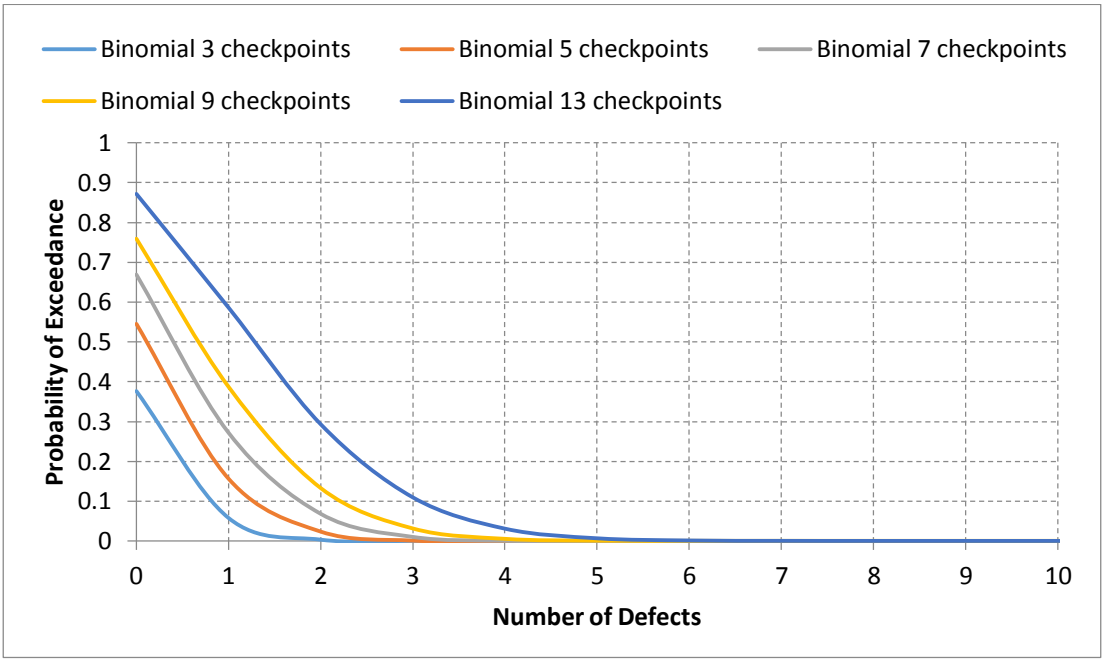

Figure 8-12 Probability of exceedance for various samples assuming the defect rate of 0.1447 (per checkpoint)

Number of checkpoints	Number of defects requiring further inspection
4 and below	1
5 and above	2
9 and above	3
13	4

Table 8-10 limits for unacceptable checkpoints per joint

Frame	Existing plan	limit	Defects found	Require further inspection
34	7	1	3	Yes
56	5	1	1	No
76	7	1	1	No
98	6	1	0	No
116	5	1	1	No
136	7	1	0	No
156	13	3	2	No
176	9	2	0	No
196 (Port & Stb)	5	1	0	No
200 (Centre)	9	0	1	Yes
220 (Port)	3	0	1	Yes
220 (Centre)	5	1	0	No
220 (Starboard)	3	0	1	Yes
240	9	1	2	Yes
260	8	1	4	Yes
272	5	1	0	No
276	4	0	3	Yes
282	8	1	0	No
304	5	1	1	No
326	8	1	0	No
348	7	1	3	Yes
364	7	1	0	No
380	5	1	0	No
392	6	1	0	No

Table 8-11 Identifying joints which require further inspection

8.9.7 Bayesian updating

The defect size and rate statistics are updated using the Bayesian method, as described in section 7.9. The results for detected defect lengths are given in Table 8-12, and the resulting distributions are plotted in Figure 8-13. Then using the method outlined in section 4.5.2, initial defect length distributions and probability of detections were estimated and are presented in Table 8-13 and Figure 8-14. It is observed that the updated distribution shows more favourable defect sizes indicating possible lower failure probabilities than those predicted based on prior defect sizes. However, the effect of the updated defect rate needs to be examined as well.

Similarly, the updated defect rate distributions were estimated and are given in Table 8-14 and Figure 8-15. The updated defect rates are significantly higher than the prior suggesting that the predictive reliabilities could be higher than those estimated earlier. To examine the combined effect of increased defect rates and reduced defect sizes updated reliability of the joint at frame 200 was studied. The resulting through-life reliabilities are shown in Figure 8-16. It is observed that, overall, the failure probabilities are reduced indicting higher influence of initial defect sizes on reliabilities than the defect rates.

Parameter	Prior (Table 8-2)	Likelihood (Table 8-9)	Posterior
$Mean_{ln}$	3.98	3.751	3.763
$Std._{ln}$	1.21	0.942	0.982

Table 8-12 Parameter estimate using Bayesian updating of detected defects for deck 16

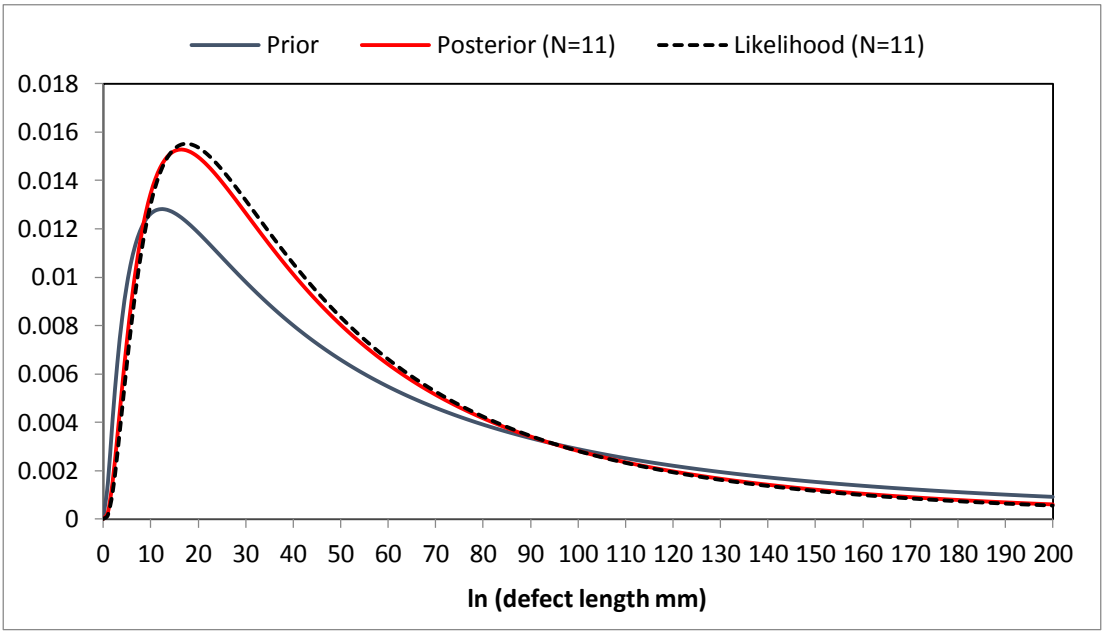

Figure 8-13 Defect length distribution Bayesian updating of detected defects for deck 16

	Distribution	Prior (Table 4.11)	Posterior
Initial defect size distribution	Exponential	72.4	49.37
RT POD	Cumulative Exponential	4.6	7.32

Table 8-13 Parameter estimate using Bayesian updating of initial defects length and POD for RT in deck 16

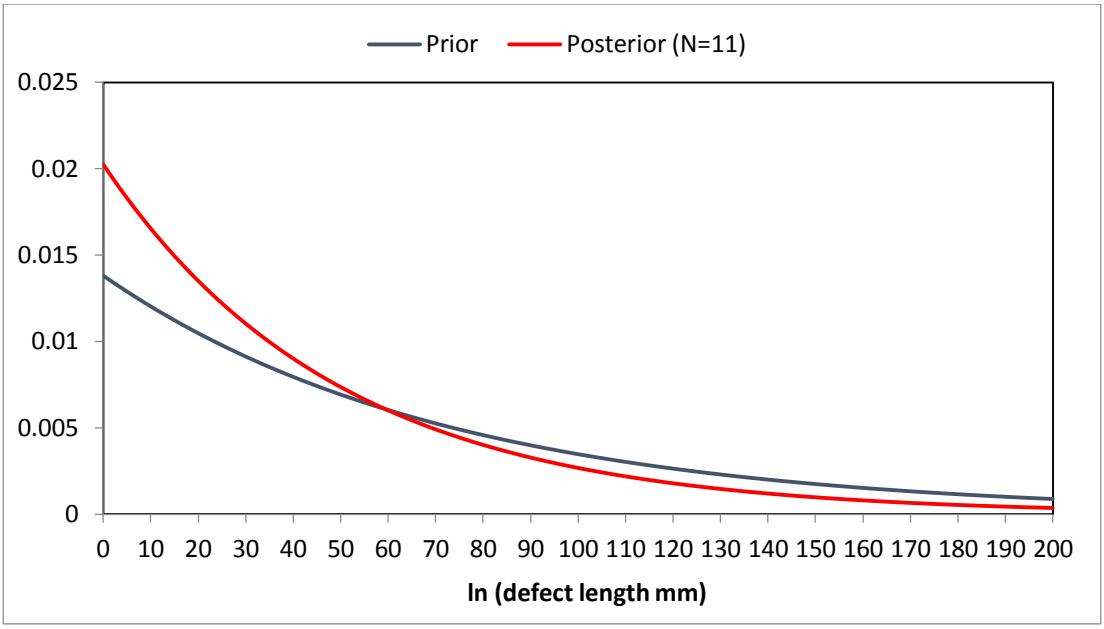

Figure 8-14 Probability distribution of initial defects length using Bayesian updating for deck 16

Prior				Likelihood		Posterior		
m	α	β	λ	n	d	α'	β'	λ'
All possible checkpoints per joint	Prior beta distribution parameters		Prior defect rate	Number of inspected checkpoints	Number of defects	Posterior beta distribution parameters		Posterior defect rate
60	$\lambda * m$	$m - \alpha$				$\alpha + d$	$\beta + n - d$	$\frac{\alpha'}{\alpha' + \beta'}$
60	96.36	1223.64	0.073	156	24	28.3	187.62	0.13

Table 8-14 Parameter estimate of defect rate distribution using Bayesian updating in deck 16

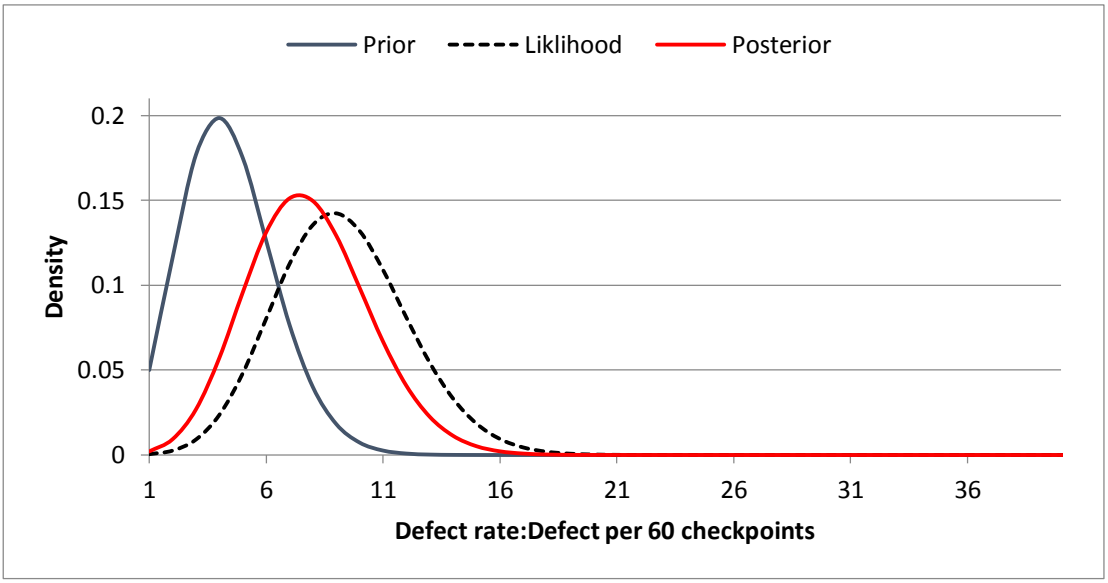

Figure 8-15 Probability distribution of defect rate using Bayesian updating for deck 16

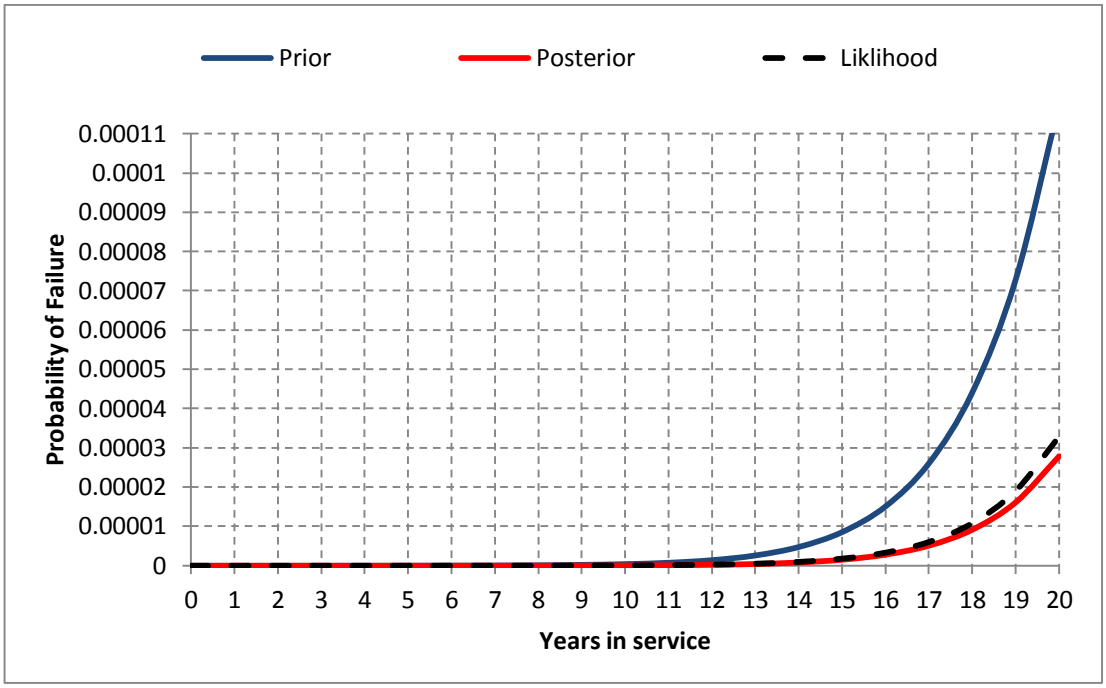

Figure 8-16 Updated probability of failure for joint No 200

8.9.8 Remarks on the application of the proposed framework to the case study structure

The framework identified locations of a critical joint (joint 220) that require 100% inspection, which if implemented will improve the structural reliability. Such improvements are not possible based on current classification rules. The framework also defined the required level of partial inspection to achieve a certain confidence in the reliability, which also improves reliability by reducing the number of defects that are likely to remain in the structure. Furthermore, the joints requiring no NDT from the reliability perspective are identified. The framework identified the extent of the inspection for these joints from the process control point of view.

The limiting numbers of unacceptable checkpoints per joints were defined, and the joints requiring further inspection were identified.

The inspection results are fed into a Bayesian updating scheme to update the prior knowledge about the defect rate and size data which were used to update predictive reliability calculations confirming superior reliabilities of the structure than predicted. The updated statistics can be used to increase/ decrease the extent of inspection in other parts of the ship.

The proposed framework has improved the reliability of the structure compared to the existing plan by establishing the critical areas requiring 100% NDT, while reducing the total number of the checkpoint by at least 22% (Table 8-8).

8.10 Chapter summary

In this chapter, a framework was proposed based on the work in preceding chapters. The aim of this research was to optimise NDE inspection of newbuilding ship hull structure by developing a risk and reliability framework.

The proposed framework is the final output of this research and is comprised of six stages:

1. Data collection/selection which depends on the availability of data
5. Data processing based on statistical data analysis methods
6. Risk and reliability analysis to assess the failure probability of the structure and corresponding possible consequences of failure
7. Calculation of number of checkpoints based on statistical sampling
8. NDE inspection, new data collection and updating initial data assumptions
9. Quality control and process control

First, the overview of the method and its stages were introduced. Then each stage was explained independently.

The chapter was concluded by demonstrating the application of the framework to a case-study deck structure in which the reliability of the structure was improved compared to the existing plan by establishing the critical areas requiring a rigours NDE plan (up to 100%) while reducing the total number of the checkpoint by at least 22% (Table 8-8).

Chapter 9

Concluding remarks

9.1 Novelty of present research

9.1.1 Gaps

The gaps in the status quo and state-of-the-art were identified through a critical review of rules for NDE inspection of newbuilding ship hull structures undergoing classification society survey by studying relevant sections of the rules of mainstream International Classification Societies (IACS) members. Moreover, a series of discussions with various experts, including new construction ship surveyors, in-service surveyors, welding engineers, NDT specialist and structural designers, and shipyard quality control teams highlighted limitations of current practices. One key limitation is that the rules favour a "one-size-fits-all" approach. In addition to that, a significant discrepancy exists between rules of different classification societies. Inspection regimes need to be adjusted taking cognisance of the perspectives of key stakeholders involved in shipbuilding—specifically, ship owners, manufacturers, and classification societies. Factors that interest these stakeholders include assurance of intended safety and structural reliability of the vessel, saving time and the costs associated with NDE and subsequent remedial action, and incorporating manufacturing quality.

9.1.2 Approach

The research presented provides a novel way of addressing these challenges: The developed approach optimises inspection in such a way that inspection can be reduced to a level which provides a certain confidence level about the quality of the welding while ensuring intended reliability of the structure. The method links weld manufacturing to NDE capabilities and structural reliability using statistical inference concepts and probabilistic fracture mechanics.

9.1.3 Contribution to knowledge

Reliability of ship hull structures due to the presence of significant fabrication defects has been studied. To the best of the authors' knowledge, no published work has assessed such a scenario. Instead, the attempts have been to focus on cracks initiating from small fabrication defects at locations with stress concentrations. In this research, the assessment had to be performed for large fabrication defects which may grow and cause failure. This approach gives information about early life reliability of the ship hulls, which also governs through life reliability. One of the possible reasons that such a study was not conducted before is lack fabrication defect data in the literature specific to ship hulls. In this research, such data was collected, analysed, and will be available in the public domain for future studies. Similar to defect data, material fracture toughness of shipbuilding steels was collected from a diverse population of manufacturers in Europe and the Far East, which allowed estimation of scatter in material toughness available in the market. Additionally, scatter of fracture toughness with respect to steel batches were quantified, which provides a better estimate of the toughness scatters in a real-life hull structure.

The key findings for each of these are discussed in the following.

9.1.4 Key findings and review of the thesis

Key stochastic variables were studied in chapter 4 and 5. In chapter 4, statistical analyses of defect type, frequency and size data collected from a shipyard and those from literature showed superior weld quality properties of HLAW compared to FCAW and SAW. The choice of NDT method was found to have a significant impact on the recorded defect rates. Recommendations about gaps in current practices were made with respect to the choice of volumetric examination, defect type, defect rates, joint type, and welding process. In chapter 5, statistical analyses of A and AH36 steels showed that, the variation between batches are generally lower than variation within batches. The calculated fracture toughness was compared with historical data since 2000 (Kent and Sumpter, 2007) showing similar steel qualities to those reported in 2000. In chapter 6, reliability analysis of a butt weld, joining deck plating of two grand-blocks, showed that the structure may be tolerable to higher defect rates or bigger defect sizes. Visual inspection is found to be very effective in reducing the failure probability both during construction and in-service due to the failure being dominated by long cracks that can be effectively detected by visual inspection. The calculated reliabilities were compared against target levels of reliabilities, established

in chapter 3 based on the developed model for consequence of failure due to presence of weld defects for cruise ship.

It was shown in chapter 7 that, there is a close connection between the calculated reliability and statistical confidence in uncertain variables. Statistical confidence is strongly dependent on the sample size of the collected data. Reduction in the epistemic uncertainty of the defect size is a function of the number of samples containing defects and not the gross quantity of checkpoints. A process with worse (higher) defect rate will provide better statistical confidence, but, as investigated, the benefit from higher confidence is mitigated by the rise in the total number defects that are present in the structure.

In chapter 8, application of the proposed framework to a case study deck structure was compared to the existing practice and showed improvement of structural reliability by establishing the critical areas requiring a 100% NDE, while reducing the total number of the checkpoint by at least 22%.

9.2 Recommendations for future works

9.2.1 Methodology

Further refinement of the methodology is possible, for example by:

- Treating the deck structure as a system comprising stiffened panels components rather than the deck being one component which may result in a more realistic predication of failure.
- Interaction of multiple cracks growing in the structure can also be added by considering the correlation effects building into a system reliability model.
- Further refinement of uncertain inputs, particularly long term loading, and uncertainties in the estimation of long-term stress distribution shape parameter of the structure can reduce conservatism assumed in the developed model.
- It would be beneficial to calibrate the developed predictive reliability model using in-service inspection data to further refine the model.
- The process control module can be further extended to a method which integrates weld parameter, such as parameters likely to cause certain defect types (weld current, parent material composition, thickness, welding positions, etc.). Recently, new welding machines have been equipped with IT

tools capable of recording the majority of these parameters which can be used to achieve the above implementation. It is expected that such employment would reduce the inspection efforts considerably since it was observed in chapter 8 that the majority of the NDT checkpoints were specified based on process control limits.

9.2.2 Case study

Application of the framework to cracks in other parts of the structure such as shell structure or connections between stiffeners can extend the applicability to any component in the structure. This is expected to be straightforward as the developed reliability framework can easily be adapted. The challenge, however, is to gather defect height data, which is more relevant to thick sections and parts of the structure were water or cargo leakage is considered as a significant consequence.

9.2.3 Transferability

Application of the approach to other ship types has been discussed. Transferability to similar structures, such as offshore oil platforms, wind turbines, bridges and leisure equipment, will be beneficial. It was shown in chapter 2 that existing practices in these industries are not based on risk and reliability or process control.

Offshore wind turbines (OWT), in particular, can benefit from a number of findings of this research about weld quality, NDT capabilities and reliability, deterministic and probabilistic fracture mechanics and risk based inspection. A Fracture mechanics based design framework can help to design wind turbine structures accounting for the in-service inspections (Design for Inspection) or structural health monitoring (SHM) capabilities. Such frameworks would help to design, commission and operate safer and more economical turbines which in turn reduces harvested electricity costs.

Furthermore, design of OWT structures are evolving to become bigger structures and capable of operating in deeper water to harvest more wind energy, which results in development of novel designs. Design and construction of novel structures are always challenging owing to various epistemic uncertainties due to lack of previous experiences. The most robust way of analysis and design of such structures is a reliability based design.

The tools developed in chapter 3 and 6 can be adapted to develop fracture mechanics based frameworks or to conduct reliability analyses and designs for OWT.

The statistical tools developed in chapter 7 can be employed to inspect systems such as Overhead Transmission Lines (OHL) which consist of large number of similar line components exposed to degrading environment. The approach can be used in determining a suitable inspection sampling of line components and to provide an overall condition status report on the line with a certain degree of confidence.

9.3 Contribution

This research propose a framework that optimises NDT inspection by reducing overall extent of the inspection while focusing on more susceptible components, by accounting for various parameters such as NDT capabilities. This is achieved through linking weld quality and structural reliability under the light of statistical inference, which to the best of author's knowledge has not been done before. Various parts of the framework have been examined from different angles and their relationships with other theoretical and practical viewpoints have been studied, and cross validated.

The proposed framework will improve current prescriptive practices to a more reliable and cost-effective risk based approach. The impact of this research on the funding bodies, stakeholders in ship manufacturing and academia is as follows:

9.3.1 Lloyds Register sponsoring

The Lloyd's Register Foundation was established in 2012 to protect life and property at sea, on land, and in the air through supporting education, research, public engagement, and promoting scientific excellence.

In this research, as showed in chapter 6 and 8, the application of the developed framework will enhance the safety of ships by improving their structural reliability.

Lloyds Register Group as a member of International members Association of Classification Societies (IACS) strives to rationalise their rules and achieve a more robust philosophy for their NDE checkpoint regimes. IACS members try to establish, review, promote, and develop minimum satisfactory technical requirements concerning design, construction, and survey of ships, and other marine units as part of their commitments to IACS directions.

In this research, the differences between Lloyds Register rules and other classification societies were identified in detail through a comprehensive review of the literature. The application of the developed framework showed various areas within existing

rules, which can be further improved. For instance, the choice of NDE technique, the required number of checkpoints, limits on nonconforming checkpoints, and better interpretation of defect rates with respect to PODs were addressed from a risk and reliability perspective.

The industrial impact for Lloyds Register was expressed on Lloyds Register Foundation monthly news bulletin issue 12/2017 on 22 December 2017 (LRF, 2017):

"A great example of Foundation funded research leading towards impact is the NSIRC PhD of Peyman Amirafshari. Peyman has been researching the application of risk based inspection methods, usually applied to existing systems, in the context of the ship building process. Peyman has been mentored by Martyn Wright, Principal NDE Specialist at Lloyd's Register Group in Southampton GTC, UK, providing a real world focus to the research. An important part of mentoring is the translation of research into the community and in this case the knowledge from Peyman's research has been applied in the Rule proposal No. 2017/MAT07 to the Rules and Regulations for the Classification of Special Service Craft, July 2017"

9.3.2 TWI sponsoring

TWI is a world leading organisation in structural integrity assessment and fracture mechanics and has been carrying extensive research in this field which has been built into British standard's "Guide to methods for assessing the acceptability of flaws in metallic structures" (BS7910). There has been increasing demand for considering probabilistic fracture mechanics, in which engineering risk can be evaluated from an understanding of both the probability of failure and the consequences of failure (Hadley, 2019). One of these has been answered by the work conducted in chapter 3 about the methods of establishing target levels of reliabilities which will be implemented in 2019 version of the standard in Annex K. Additionally, clauses on probabilistic modelling of parameters in Paris equation will be updated, as well.

9.3.3 Ship manufacturing stakeholders

The impacts for classification societies have already been discussed. Furthermore, manufacturers will be benefited through the feature of the approach in relating the weld quality to the extent of inspections required. Welds with lower defect rates or sizes will be required less inspection. The approach also accounts for capabilities of NDT method in detecting defects, thus, using techniques with a higher probability of detection will not necessarily lead to higher actual defects rates, which has made

those methods less welcomed by the shipbuilders. The manufacturers are expected to be encouraged to invest in improving welding quality and their NDT capabilities, and their quality control programs.

Ship owners will benefit from this framework by receiving a more reliable asset at the end of the construction. The lifecycle maintenance costs are expected to be reduced due to the implementation of a more targeted inspection during construction.

9.3.4 Academic impact

In addition to the publication of a peer-reviewed paper, the framework and its application were also presented at several conferences (see Appendix G). It was acknowledged that the application of the framework helps to move from current prescriptive approaches to a more data-driven reliability centred assessment and maintenance. In this way, it has already received attentions from researchers in related fields such as offshore wind turbine (OWT) and overhaul towers.

9.3.5 Final thoughts

To conclude, there is a paradigm shift towards reliability centred design, manufacturing and maintenance. The developed framework shows how such approaches can reduce manufacturing and maintenance costs and delivery time while enhancing through life safety of the vessel including people on-board by ensuring intended reliability of the structure and optimising the resources used to achieve these benefits. The approach and the developed tool can be adopted by other industries to achieve similar goals.

REFERENCES

ABS, 2012: Review Of Current Practices Of Fracture Repair Procedures For Ship Structures. Ship Structure Committee.

ABS, 2014: Guide for non-destructive inspection of hull welds. American Bureau of Shipping, Houston.

ACI, 1999: Building code requirements for structural concrete:(ACI 318-99); and commentary (ACI 318R-99).

Amirafshari, P., 2017: Application Of Probabilistic Fracture Mechanics In Risk Based Non Destructive Examination Of New Building Ships. 3rd NSIRC Conference.

Amirafshari, P.; Barltrop, N.; Bharadwaj, U.; Wright, M.; Oterkus, S., 2018: A Review of Nondestructive Examination Methods for New-building Ships Undergoing Classification Society Survey. *Journal of Ship Production and Design*., **33**, 1–11.

Anderson, T. L., 2005: Fracture Mechanics: Fundamentals and Applications.

ANSI/AISC, 1999: Specification for structural steel buildings. *AISC, December*., **27**.

API, 1998: *API 650, The standard for Oil steel tanks and Oil storage*. API.

API, 1999: *Standard API Std-1104-1999: Welding of Pipelines and Related Facilities*. API.

API, 2008: API RP 581 Risk Based Inspection Technology. API, USA.

API, 2009: *API Recommended Practice 580 Risk Based Inspection*. API Publications, USA.

API, R., 1993: 2A-LRFD: API Recommended Practices for Planning, Designing and Constructing Fixed Offshore Platforms-Load and Resistance Factor Design.

Asariotis, R.; Benamara, H.; Hoffmann, J.; Jaimurzina, A.; Premti, A.; Rubiato, J. M.; Valentine, V.; Youssef, F., 2018: *UNCTAD Review of Maritime Transport, 2018*.

ASTM, E., 2016: *Standard Test Method for Determination of Reference Temperature, T0, for Ferritic Steels in the Transition Range. 2016*. ASTM International.

AWS, 1999: *AWS D1.1.2000, Structural Welding Code Steel* 17th edn. American Welding Society.

AWS, 2015: *AWS D.15 Bridge Weding Code*. American Welding Society.

Ayala-Uraga, E.; Moan, T., 2007: Time-variant reliability assessment of FPSO hull girder with long cracks. *Journal of offshore mechanics and Arctic engineering.*, **129**, 81–89.

Ayala-Uraga, E., 2009: *Reliability-based Assessment of Deteriorating Ship-shaped Offshore Structures*.

Ayyub, B.; Akpan, U.; Rushton, P.; Koko, T.; Ross, J.; Lua, J., 2002: *Risk-informed inspection of marine vessels*. *SSC-421, Ship Structures Committee, Washington DC*.

Bäckström, M.; Kivimaa, S., 2009: Estimation of crack propagation in a passenger ship's door corner. *Ships and Offshore Structures.*, **4**, 241–251.

Baker; Kountouris; Ohmart, 1988: Weld Defects in An Offshore Structure, A Detailed Study. *Int. Conf. On Behavior of Offshore Structures*.

Baker, M.; Stanley, I., 2008: Assessing and modelling the uncertainty in fatigue crack growth in structural steels. *Health and Safety Executive Research Report RR643, Norwich*.

Barltrop, N., 2011a: *RISPECT Component Reliability*.

Barltrop, N., 2011b: *Reliability-Based Marine Structural Design Course Hand-out*.

Becher, P.; Hansen, B., 1974: *Statistical evaluation of defects in welds and design implications*. Riso Danish Atomic energy commission research establishment.

Beghin, D., 2006: *FATIGUE OF SHIP STRUCTURAL DETAILS*. The Society of Naval Architects and Marine Engineers.

Béghin, D.; Hughes, O. F.; Paik, J. K., 2010: *Ship structural analysis and design*. Society of Naval Architects and Marine Engineers.

Bertsche, B., 2008: *Reliability in automotive and mechanical engineering: determination of component and system reliability*. Springer Science \& Business Media.

Bharadwaj, U.; Wintle, J., 2011: Risk-Based Optimization of Inspection Planning in Ships. *Journal of Ship Production and Design.*, **27**, 111–117.

Bhattacharya, B.; Basu, R.; Ma, K. tung, 2001: Developing target reliability for novel structures: the case of the Mobile Offshore Base. *Marine structures.*, **14**, 37–58.

Boekholt, R., 1996: *Welding Mechanisation and Automation in Shipbuilding Worldwide: Production Methods and Trends Based on Yard Capacity*. Abington Publishing.

Bokalrud, T.; Karlsen, A., 1982: *Probabilistic fracture mechanics evaluation of fatigue failure from weld defects in butt welded joints. Proc. Conf. on fitness for purpose validation of welded constructions*.

BRSBrokers, 2018: Shipbuilding-Some breathing space. https://www.brsbrokers.com/assets/review_splits/BRS-Review2018-01-Shipbuilding.pdf.

BS-31010, 2010: 31010 2010. *Risk management: Risk assessment techniques. London: BSI Standards Publication*.

BS7910, B. S., 2015a: BS 7910:2013+A1:2015. *British Standards Institutions, London.*, **2015**.

BS7910, B. S., 2015b: BS 7910:2013+A1:2015 AnnexJ. British Standards Institutions, London.

BSI, 2005: BS EN 1990: 2002+ A1: 2005-Basis of Structural Design.

BSI, 2011a: Non-destructive testing of welds — Ultrasonic testing — Acceptance levels (ISO 11666:2010). The British Standards Institution, Brussels.

BSI, 2011b: *Execution of steel structures and aluminium structures-Part 2: Technical requirements for steel structures*. BSI.

BSI, 2013: Non-destructive testing of welds — Acceptance levels for radiographic testing Part 1: Steel, nickel, titanium and their alloys. The British Standards Institution.

BSI, 2015a: Non-destructive testing of welds — Magnetic particle testing — Acceptance levels(ISO 23278:2015). The British Standards Institution, Brussels.

BSI, 2015b: Non-destructive testing of welds — Penetrant testing — Acceptance levels (ISO 23277:2015). BSI Standards Limited, Brussels.

BSI, 2015c: *BS ISO 17842-1:2015 Safety of amusement rides and amusement devices Part 1: Design and manufacture*. BSI.

BSI, 2017: *PD ISO/TS 20273:2017 Guidelines on weld quality in relationship to fatigue strength*. 2017.

BSI:SO-12107, 2012: Metallic materials-Fatigue testing-Statistical planning and analysis of data. *International Organization for Standardization*.

BSI7608, 2015: Guide to fatigue design and assessment of steel products. *London: BSI Standards Publication*.

Burdekin, F.; Towned, P., 1981: Reliability Aspects of Fracture on Stress Concentration Regions in Offshore Structures, Integrity of Offshore Structures, 2nd Int. *Symp., Glasgow.*

Chaturvedi, M. C., 2011: *Welding and joining of aerospace materials*. Elsevier.

Chatzidouros, E.; Tsiourva, T.; Pantelis, D.; Lopez, A., 2015: Fatigue crack growth performance of laser hybrid and arc welds of AH36 naval steels. *Analysis and Design of Marine Structures V.*, 225.

Clarkson, 2017: Container Intelligence Monthly . *Clarkson Research.*, **19**.

Cornell, C. A., 1969: A probability-based structural code. *Journal Proceedings.*, Vol. 66pp. 974–985.

Cortie, M.; Garrett, G., 1988: On the correlation between the C and m in the Paris equation for fatigue crack propagation. *Engineering fracture mechanics.*, **30**, 49–58.

Cruise-Industry-News, 2018: Cruise Industry News Annual Report 2019.

Cruise-Market-Watch, 2018: Cruise Market Watch.

De Florio, F., 2016: *Airworthiness: An introduction to aircraft certification and operations*. Butterworth-Heinemann.

Dexter, R.; Pilarski, P., 2002: Crack propagation in welded stiffened panels. *Journal of Constructional Steel Research.*, **58**, 1081–1102.

Dinovitzer, A.; Pussegoda, N., 2003: Fracture toughness of a ship structure. *SSC-430, Ship Structure Committee (SSC), Washington DC.*

DNV, 1992: *Structural reliability analysis of marine structures*. Det Norske Veritas.

DNV, 1996: *Guidelines for Offshore Structural Reliability Analysis-Application to Jacket Platforms*.

DNV, 2000: Fatigue reliability of old semi-submersibles. *OTO report.*, **52**.

DNV, 2005: Riser fatigue. *Recommended Practice, DNV-RP-F204*.

DNV, 2010: Fatigue design of offshore steel structures. *DNV Recommended Practice DNV-RP-C203*.

DNV, 2015: *DNVGL-RP-C210-Probabilistic methods for planning of inspection for fatigue cracks in offshore structures*.

DNV-GL, 2017: *Design of Offshore Steel Structures, General (LRFD Method)*.

DNV.GL, 2015: Rules for classification Ships Part 2 Materials and welding Chapter 4 Fabrication and testing, pp. 80–85.

Dowling, A.; Hadley, I.; WINTLE, J., 2005: The future of fracture assessment. *Developments in Pressure Equipment: Where to Next*., **1020**, 81.

Du, X., 2005: First order and second reliability methods. *Probabilistic engineering design*., 1–33.

Dufresne, J., 1981: *Probabilistic application of fracture mechanics*.

E-bookshelf.de, 2000: Tanker Castor deck crack.

EMSA, 2018: Annual overview of marine casualties and incidents-2018.

Eurocode-3, 2006: *Eurocode 3 — Design of steel structures — Part 2: Steel bridges*. BSI.

f-cca.com, 2019: Cruise Industry Overview.

Faulkner, D., 1973: *A review of effective plating to be used in the analysis of stiffened plating in bending and compression*.

Freudenthal, A. M.; Garrelts, J. M.; Shinozuka, M., 1964: *The analysis of structural safety*.

Garwood, S., 2001: Investigation of the MV KURDISTAN Casualty. *Failure Analysis Case Studies II*. Elsevier, pp. 117–138.

Georgiou, G. A., 2006: Probability of Detection (POD) curves: derivation, applications and limitations. *Jacobi Consulting Limited Health and Safety Executive Research Report*., **454**.

Gerritsen, C. H.; Howarth, D. J., 2005: A review of the development and application of laser and laser-arc hybrid welding in European shipbuilding. *11th CF/DRDC International Meeting on Naval Applications of Materials Technology*., pp. 7–9.

Glenn, I., 1999: *Fatigue Resistant Detail Design Guide for Ship Structures*. Ship Structure Committee.

Guide to Weld Inspection for Structural Steelwork, (n.d.). The British Constructional Steelwork Association Ltd.

Gurney, T. R., 1979: *Fatigue of welded structures*. CUP Archive.

Hadley, I.; Pisarski, H., 2013: Overview of BS 7910: 2013. *FESI ESIA12-12th International Conference on Engineering Structural Integrity Assessment*., pp. 28–29.

Hadley, I., 2019: Improving Safety with Advanced Fracture Mechanics.

Hamada, M. S.; Wilson, A.; Reese, C. S.; Martz, H., 2008: *Bayesian reliability*. Springer Science \& Business Media.

Harris, D., 1995: Probabilistic fracture mechanics. *Probabilistic structural mechanics handbook*. Springer, pp. 106–145.

Hasofer, A. M.; Lind, N. C., 1974: Exact and invariant second-moment code format. *Journal of the Engineering Mechanics division*., **100**, 111–121.

Hellier, C.; Shakinovsky, M., 2001: *Handbook of nondestructive evaluation*. Mcgraw-hill New York, Vol. 10.

Hobbacher, A., 2008: RECOMMENDATIONS FOR FATIGUE DESIGN OF WELDED JOINTS AND COMPONENTS.

Hodgson, J.; Boyd, G., 1958: Brittle fracture in welded ships. *The Institution of Naval Architects, Quarterly Transaction*., **100**.

Holick`y, M., 2013: *Introduction to probability and statistics for engineers*. Springer Science \& Business Media.

HSE, 2001a: Probabilistic Methods: uses and abuses in structural integrity. *contract research report*., **398**, 2001.

HSE, 2001b: *HSE's decision-making process. The Tolerability of Risk*. HSE.

i.Stack, 2018: Eddy Current Figure .

IACS, 1999: *No.56 FATIGUE ASSESSMENT OF SHIP STRUCTURES*. International Assosiation of Classification Societies.

IACS, 2003: *Surveyor's Glossary Hull Terms & Hull Survey Terms - Recommendation 82*.

IACS, 2006: *IACS Common Structural Rules for Double Hull Oil Tankers, Background Document-SECTION 2 – RULE PRINCIPLES*.

IACS, 2012: *Common Structural Rules for Double Hull Oil Tankers*. IACS.

ISO, 2014: *Welding-Fusion-welded joints in steel, nickel, titanium and their alloys (beam welding excluded)—Quality levels for imperfections*.

ISO, 2016: *Non-destructive testing of welds - General rules for metallic materials (ISO 17635:2016)*. ISO.

ISO 2394, I., 2015: General principles on reliability for structures. *Zurich: ISO*.

ISO, B., 2007: *6520-1 (2007)"Welding and allied processes: Classification of geometric imperfections in metallic materials." Part 1: Fusion Welding*. Brussels, pp. 6520–6521.

ISO-14971, 2012: BS EN ISO 14971: 2012—Application of risk management to medical devices.

ISO-28590, 2017: *Sampling procedures for inspection by attributes. Introduction to the ISO 28590 series of standards for sampling for inspection by attributes*. ISO.

ISO-31000, B., 2018: 31000,(2018) Risk management-Principles and guidelines. *International Organization for Standardization, Geneva, Switzerland*.

IUMI, G. M. P. G. M. F., 2018: The Global Maritime Issues Monitor 2018. https://www.globalmaritimeforum.org/content/2018/10/Global-Maritime-Issues-Monitor-2018.pdf.

Jenkinson, L. R.; Simpkin, P.; Rhodes, D.; Jenkison, L. R.; Royce, R., 1999: *Civil jet aircraft design*. Arnold London, Vol. 338.

Johnston, G., 1983: Statistical scatter in fracture toughness and fatigue crack growth rate data. *Probabilistic fracture Mechanics and Fatigue Methods: Applications for structural design and maintenance*. ASTM International.

Jonsson, B.; Dobmann, G.; Hobbacher, A.; Kassner, M.; Marquis, G., 2013: IIW guidelines on weld quality in relationship to fatigue strength. *IIW document.*, **13**, 2510–2513.

Jordan, A. E., 2018: Curise Ship Market .

Journal, S., 2009: FCAWProcces.

Kelly, D.; Smith, C., 2011: *Bayesian inference for probabilistic risk assessment: a practitioner's guidebook*. Springer Science \& Business Media.

Kent, J.; Sumpter, J., 2007: *Probability of brittle fracture for a cracked ship*.

Kihara, H.; Oba, H.; Susei, S., 1971: Precautions for avoidance of fracture of pressure vessels. *International Conference on Practical Application of Fracture Mechanics to Pressure Vessel Technology, Institute of Mechanical Engineering, London*.

King, R., 1998: *A review of fatigue crack growth rates in air and seawater*. Health and Safety Executive London, UK-HSE Report OTH 511.

Kobelco, 2011: State-of-the-art automatic arc welding processes meet the latest shipbuilding requirements. *Kobelco welding today.*, **14**.

Kolmogorov, A. N.; others, 1950: Foundations of the theory of probability.

Kountouris, I.; Baker, M., 1989a: *Defect assessment: analysis of the dimensions of defects detected by ultrasonic inspection in an offshore structure*. Imperial College of Science and Technology Engineering Structures Laboratories.

Kountouris, I.; Baker, M., 1989b: *Reliability of Non-destructive Examination of Welded Joints*. Imperial College of Science and Technology Engineering Structures Laboratories.

Kountouris, I.; Baker, M., 1989c: *Defect assessment: analysis of the dimensions of defects detected by magnetic particle inspection in an offshore structure*. Imperial College of Science and Technology Engineering Structures Laboratories.

KR, 2015: Part 2 Materials and welding. KR, Busan, Korea, pp. 81–94.

KurdistanTWI, (n.d.).

Lassen, T.; Recho, N., 2013: *Fatigue life analyses of welded structures: flaws*. John Wiley \& Sons.

Li, L.; Moan, T.; Zhang, B., 2007: Residual stress shakedown in typical weld joints and its effect on fatigue of FPSOs. *ASME 2007 26th International Conference on Offshore Mechanics and Arctic Engineering.*, pp. 193–201.

Lincoln, 2015: An Excerpt from Fabricators' and Erectors' Guide to Welded Steel Construction. *The James F. Lincoln Arc Welding Foundation*.

Lloyd's-Register, 2009: *ShipRight Design and Construction Fatigue Design Assessment Level 3 Procedure*. Lloyd's Register.

Lotsberg, I.; Sigurdsson, G.; Fjeldstad, A.; Moan, T., 2016: Probabilistic methods for planning of inspection for fatigue cracks in offshore structures. *Marine Structures.*,

46, 167–192.

LR, 2015: *Rules and Regulations for the Classification of Ships*. Lloyd's Register Group Limited, pp. 352–354.

LR, 2017: *Guidance notes for the risk based inspection of hull structures* Version 2.0.

LRF, 2017: Lloyds Register Foundation monthly news bulletin.

Maddox, S., 1975: An analysis of fatigue cracks in fillet welded joints. *International Journal of Fracture*., **11**, 221–243.

Mahmoud, H. N.; Dexter, R. J., 2005: Propagation rate of large cracks in stiffened panels under tension loading. *Marine Structures*., **18**, 265–288.

Mandal, N. R., 2017: *Ship Construction and Welding*. Springer.

Mansour, A., 1994: *Probability-based ship design procedures: loads and load combinations*. Ship Structure Committee.

Mansour, A.; Hovem, L., 1994: Probability-based ship structural safety analysis. *Journal of Ship Research*., **38**, 329–339.

Mansour, A., 1996: *Probability Based Ship Design: Implementation of Design Guidelines: a Demonstration*. Ship Structure Committee.

Marcello Consonni, C. F. W., 2012: Repair rates in welded construction - an analysis of industry trends. *Welding & Cutting*., 33–35.

Marshall, W., 1982: An assessment of the integrity of PWR pressure vessels.

Matzkanin, G. A.; Yolken, H., 2001: *Probability of detection (POD) for Nondestructive Evaluation (NDE)*.

Melchers, R. E., 1999: *Structural reliability analysis and prediction*. John Wiley \& Sons.

Milella, P. P., 2012: *Fatigue and corrosion in metals*. Springer Science \& Business Media.

Moan, T.; Vårdal, O.; Hellevig, N. C.; Skjoldli, K., 1997: In-service observations of cracks in north sea jackets. A study on initial crack depth and POD values. *PROCEEDINGS OF THE INTERNATIONAL CONFERENCE ON OFFSHORE MECHANICS AND ARCTIC ENGINEERING*., pp. 189–198.

Moan, T.; Wei, Z.; Vardal, O., 2001: Initial crack depth and POD data based on underwater inspection of fixed steel platforms. *Structural Safety and Reliability:*

ICOSSAR'01., 2001.

Moan, T., 2005: Reliability-based management of inspection, maintenance and repair of offshore structures. *Structure and Infrastructure Engineering*., **1**, 33–62.

Moan, T.; Ayala-Uraga, E., 2008: Reliability-based assessment of deteriorating ship structures operating in multiple sea loading climates. *Reliability Engineering \& System Safety*., **93**, 433–446.

Montgomery, D. C., 2009: *Introduction to statistical quality control*. John Wiley \& Sons (New York).

Moon, D.; Park, J.; Kim, M., 2017: Effects of the Crack Tip Constraint on the Fracture Assessment of an Al 5083-O Weldment for Low Temperature Applications. *Materials*., **10**, 815.

Muhammed, A.; Pisarski, H.; Stacey, A., 2000a: Using wide plate test results to improve predictions from probabilistic fracture mechanics. *13 th European Conference on Fracture, ECF*., Vol. 13pp. 6–9.

Muhammed, A.; Pisarski, H.; Sanderson, R., 2000b: Calibration of probability of failure estimates made from probabilistic fracture mechanics analysis. *Offshore technology report*., **21**.

Murakami, Y.; Keer, L., 1993: Stress intensity factors handbook, vol. 3. *Journal of Applied Mechanics*., **60**, 1063.

Murphy, K. P., 2007: Conjugate Bayesian analysis of the Gaussian distribution. *def*., **1**, 16.

Naess, A., 1985: Fatigue handbook: offshore steel structures.

NK, 2015: Rules for the survey and construction of steel ships, pp. 24–31.

Noble, R. B.; Bailer, A. J.; Kunkel, S. R.; Straker, J. K., 2006: Sample size requirements for studying small populations in gerontology research. *Health Services and Outcomes Research Methodology*., **6**, 59–67.

Oakland, J. S., 2008: *Statistical Process Control*. Routledge.

Okumoto, Y.; Takeda, Y.; Mano, M.; Okada, T., 2009: *Design of ship hull structures: a practical guide for engineers*. Springer Science \& Business Media.

Olsen, F. O., 2009: *Hybrid laser-arc welding*. Elsevier.

Papanikolaou, A., 2009: *Risk-based ship design: Methods, tools and applications*. Springer Science \& Business Media.

Partner, A. O., 1999: *Review of probabilistic inspection analysis methods*. Health and Safety Executive.

Peterlik, H.; Loidl, D., 2001: Bimodal strength distributions and flaw populations of ceramics and fibres. *Engineering Fracture Mechanics.*, **68**, 253–261.

Pham, H., 2006: *Springer handbook of engineering statistics*. Springer Science \& Business Media.

Pires, J. N.; Loureiro, A.; Bölmsjo, G., 2006: *Welding robots: technology, system issues and application*. Springer Science \& Business Media.

Poe, C., 1971: Fatigue crack propagation in stiffened panels. *Damage Tolerance in Aircraft Structures*. ASTM International.

Raiffa, H., 1974: Applied statistical decision theory.

RINA, 2007: *Rules for carrying out non-destructive examinations of welding*. RINA S.p.A.

Rogerson, J.; Wong, W., 1982: Weld defect distributions in offshore structures and their influence on structural reliability. *Soc. Pet. Eng. AIME, Pap.;(United States).*, **2**.

Rolfe, S. T.; Barsom, J. M., 1977: *Fracture and fatigue control in structures: Applications of fracture mechanics*. ASTM International.

Shi, G. jie; Gao, D. wei, 2018: Analysis of hull girder ultimate strength for cruise ship with multi-layer superstructures. *Ships and Offshore Structures.*, 1–11.

Shinozuka, M., 1990: *Relation of inspection findings to fatigue reliability*.

Ship-Order-Book, 2019: Ship-Order-Book.

SINTAP, 1999: Structural integrity assessment procedures for European industry. *British Steel Report, Rotherham*.

Smith, R. A., 2017: *Report from the Workshop on NDT Requirements for Automotive Composites*.

Snijder, H.; Gijsbers, F.; Dijkstra, O.; Avest, F., 1987: Probabilistic fracture mechanics approach of fatigue and brittle fracture in tubular joints. *Elsevier Science Publishers,.*, 927–939.

Sumpter, J.; Caudrey, A., 1995: Recommended fracture toughness for ship hull steel and weld. *Marine structures.*, **8**, 345–357.

Sumpter, J.; Kent, J., 2004: Prediction of ship brittle fracture casualty rates by a probabilistic method. *Marine structures.*, **17**, 575–589.

Tanaka, K.; Matsuoka, S., 1977: A tentative explanation for two parameters, C and m, in Paris equation of fatigue crack growth. *International Journal of Fracture*., **13**, 563–583.

Timings, R., 2008: *Fabrication and welding engineering*. Routledge.

Tobe, Y.; Lawrence Jr, F., 1977: Effect of inadequate joint penetration on fatigue resistance of high-strength structural steel welds. *Weld. J.(Miami);(United States)*., **56**.

Townend, P., 1980: *Distribution of Lack of Fusion and Lack of Penetration Defects in Tube to Tube 90° and 45° Joints Produced by Manual Metal Arc Welding of BS 4360 Grade 50D Steel*. University of Manchester Institute of Science and Technology.

Tracy, N. A.; Moore, P. O., 2003: *Nondestructive Testing Handbook: Liquid Penetrant Testing/Technical Editor, Noel A. Tracy; Editor, Patrick O. Moore*. American Society for Nondestructive Testing.

TWI, 2013: PAUT Countor TWI.

TWI, 2015a: *Intruduction to Welding and Non Destructive Testing*.

TWI, 2015b: *Structural Integrity Assessment and Practical Application of BS 7910 Procedures for the Assessment of Flaws in Metallic Structures*.

TWI, 2016a: Solidification Crack.

TWI, 2016b: RISKWISE software for Risk Based Inspection (RBI) / Risk Based Maintenance (RBM) software for Oil, Gas & Chemical Plant and Power Plant.

TWI, 2018a: SAW figure TWI.

TWI, 2018b: HLAW Figure TWI.

TWI, 2018c: *TWI Image Library*.

TWI, 2018d: MPI Figure TWI.

UNCTAD, 2015: *Review of maritime transport*. United Nations Pubns.

UNCTAD, 2017: *United Nations Conference on Trade and Development (UNCTAD) Handbook of Statistics*. United Nations Publications.

Veritas, D. N., 1984: Fatigue strength analysis for mobile offshore units. *Classification Note No. 30.2*.

Visser, W., 2002: *POD/POS curves for non-destructive examination*. HSE Books.

Waller, D. L., 2008: Statistics for business. Routledge.

Wallin, K., 1984: The scatter in KIC-results. *Engineering Fracture Mechanics.*, **19**, 1085–1093.

Wallin, K.; Nevasmaa, P.; Laukkanen, A.; Planman, T., 2004: Master Curve analysis of inhomogeneous ferritic steels. *Engineering Fracture Mechanics.*, **71**, 2329–2346.

Wallin, K., 2011: *Fracture toughness of engineering materials: Estimation and application*. EMAS publishing.

Webster, S.; Kristensen, J.; Petring, D., 2008: Joining of thick section steels using hybrid laser welding. *Ironmaking \& Steelmaking.*, **35**, 496–504.

Wiesner, C.; MacGillivray, H., 1999: Loading rate effects on tensile properties and fracture toughness of steel. *7 th Symposium on Fracture, Plastic Flow and Structural Integrity.*, pp. 149–173.

Wikimedia, 1993: SMAW figure.

Wikimedia, 2006a: Conventional UT Principle.

Wikimedia, 2006b: PAUT Principle.

Wikimedia, 2006c: Longitudinal strength Loads.

Wikimedia, 2011: TOFD diagram.

Wikimedia, 2012: GMAW weld procces diagram.

Williams, S.; Mudge, P., 1985: Statistical aspects of defect evaluation using ultrasonics. *NDT international.*, **18**, 123–131.

Wintle, J., 2002: *A review of methods for determining the frequency and size distribution of welding flaws in steel fabrications*.

Yates, J., 2010: *Failure Assessment Diagram*. University of Manchester.

Zerbst, U.; Heerens, J.; Pfuff, M.; Wittkowsky, B.; Schwalbe, K. H., 1998: Engineering estimation of the lower bound toughness in the transition regime of ferritic steels. *Fatigue and Fracture of Engineering Materials and Structures(UK).*, **21**, 1273–1278.

Zerbst, U.; Klinger, C.; Clegg, R., 2015: Fracture mechanics as a tool in failure analysis—Prospects and limitations. *Engineering Failure Analysis*., **55**, 376–410.

Zhao, W.; Stacey, A., 2002: Review of Defect Distributions for Probabilistic Structural Integrity Assessment. *ASME 2002 21st International Conference on Offshore Mechanics and Arctic Engineering*., pp. 607–619.

Appendices

Appendix A

This section contains the data gathered from experts. A questioner were asked from two panels of surveyors with experiences ranging 5 to 15 years of ship structural survey. The panels included seven new construction marine surveyors in total. Four surveyors were experienced in cruise ship construction and three surveys were experienced in cargo ships (Oil Tankers, Bulk Carriers and Container ships). The questions were asked from the panels and answers agreed between panel members. The questioners were ask by the author himself in physical meetings with panels. The panels were provided with a paper copy of the question, as well. The intention was to clarify aspects of current practices which are down to surveyors to decide, identify the areas and items where defects are more commonly found, and other characteristics of the defects (size, type, etc.) based on their experiences.

Question	Answers
Checkpoint length? For UT,RT,DP and MPI?	UT: 500-600(If Cross joint) mm continuation: 1 meter, RT:440-450 mm if extended another 450mm, MPI: 200 mm+ 200 mm(fillet welds: 200 mm each side of the stiffener). 300 mm for brackets (see notes).
Typical process for section welds?	FCAW and 500EGW SAW, SAW+CW
Timing of inspection? Each stage of building process	As it's progressed
Defects? Surface breaking, embedded or through thickness? How much	Thick sections (18mm and above): Surface breaking defects. Thin section (10 mm and below): through thickness
Measuring defect size? How precise?	UT precision.
How do you measure defect size? Per checkpoints: sum or longest	Sum. If the whole check point is affected by porosity the whole length is considered as the length.
Measuring defect size: How do you measure porosity and transverse cracks?	If the whole check point is affected by porosity the whole length is considered as the length.
How big crack length you see and detect with NDE? how small?(biggest/ Smallest)	Max: 30 mm LOF length- longitudinal 5 mm max- Transvers through thickness- Parent material average 19- 22 mm.
Fillet or butt welds?	Butt welds as the rules focus on volumetric examination of butt welds.

Question	Answers
How do you focus on highly stressed areas? By judgment of looking and FEA model	Using the construction monitoring (CM) plan
Section welds: welding position: do you do overhead position	Only repair
Section welds: how many start stop location	Every 5-7 meter
Do you record which weld was done by who and when?	No
Posts weld treatment?	Only the Cast
Which factors affects occurrence of defects more? Welder's skill, poor incorrect fit up, welding condition(accessibility, position) and etc.	In this particular project: Welder's Skill, lack of maintenance for the Machin for three wire saw, proper fit up of ceramic backing.
Specific run: Root, fill or cap	Root: more than 50% needs repair (three wire machine).In this shipyard most problems on final pass- in Korea root.
Specific location within component	Between mega blocks. Ambient: wind: shielded gas is blown away. It's in dry dock.
Joint type: Butt or fillet	Butt welds. The thicker materials the more the pass, the more the slag.
Production stage	More in Dry dock.
Type of Crack? Solidification, Hydrogen crack	Varies
Additional inspections?	If closer to ends of checkpoint extend half a length in each direction. If the defect is continued beyond the checkpoint extend until defected area disappears.

Appendix B

Risk profiles for ship types

Tanker Ship

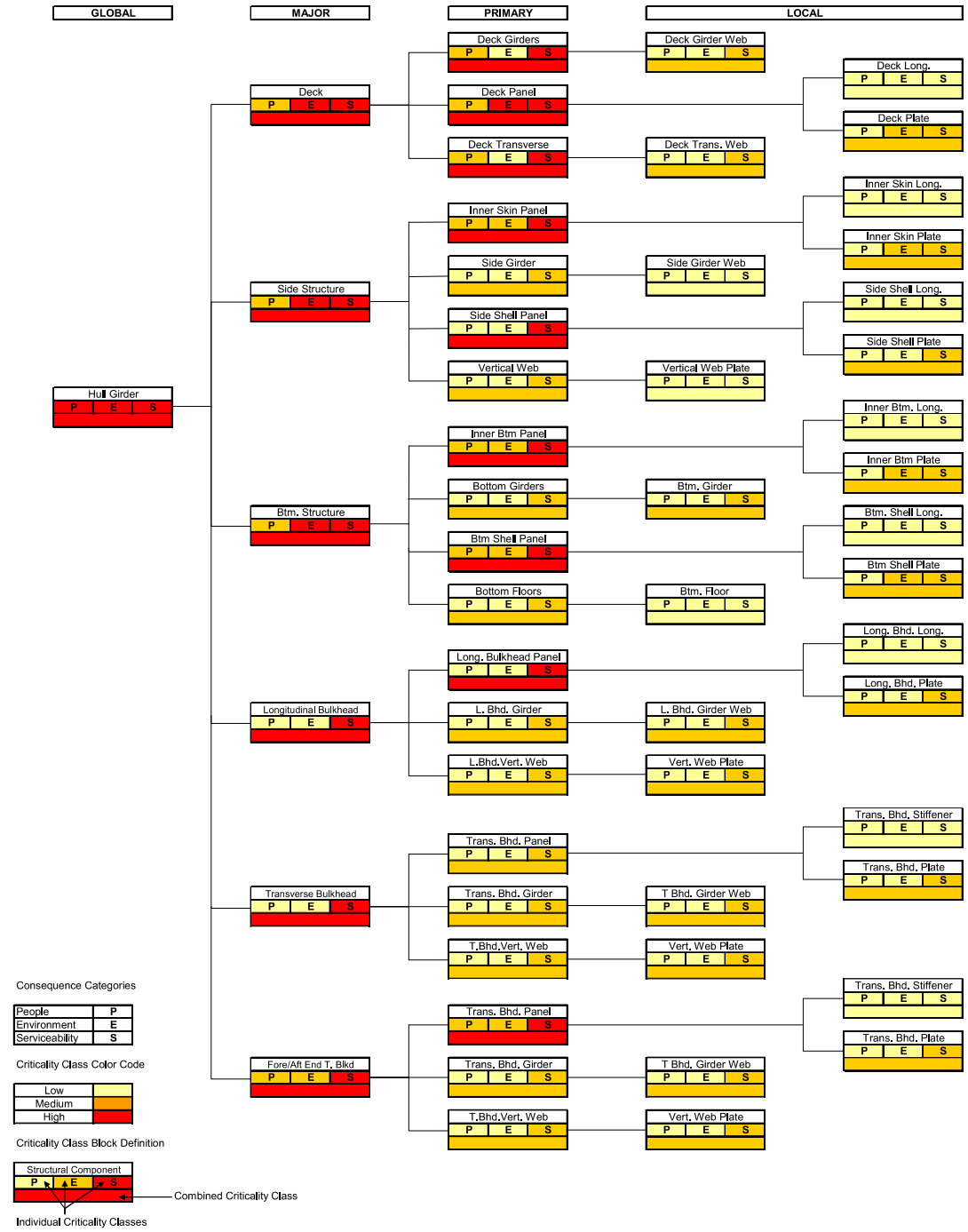

Figure B-1 Criticality Class model for Tanker ships proposed by (ABS, 2012)

Bulk Carrier

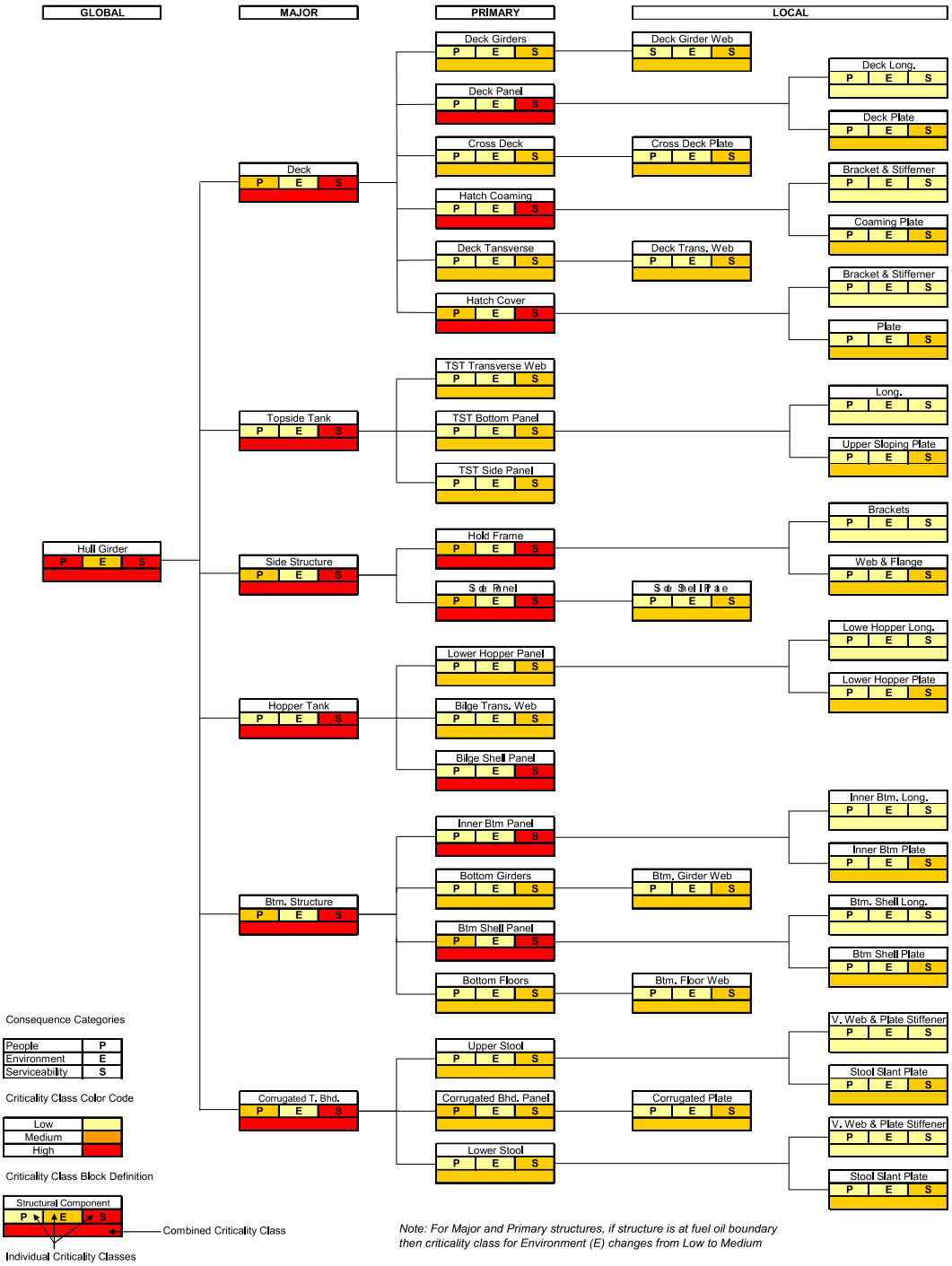

Figure B-2 Criticality Class model for Bulk Carrier ships proposed by (ABS, 2012)

Container ship

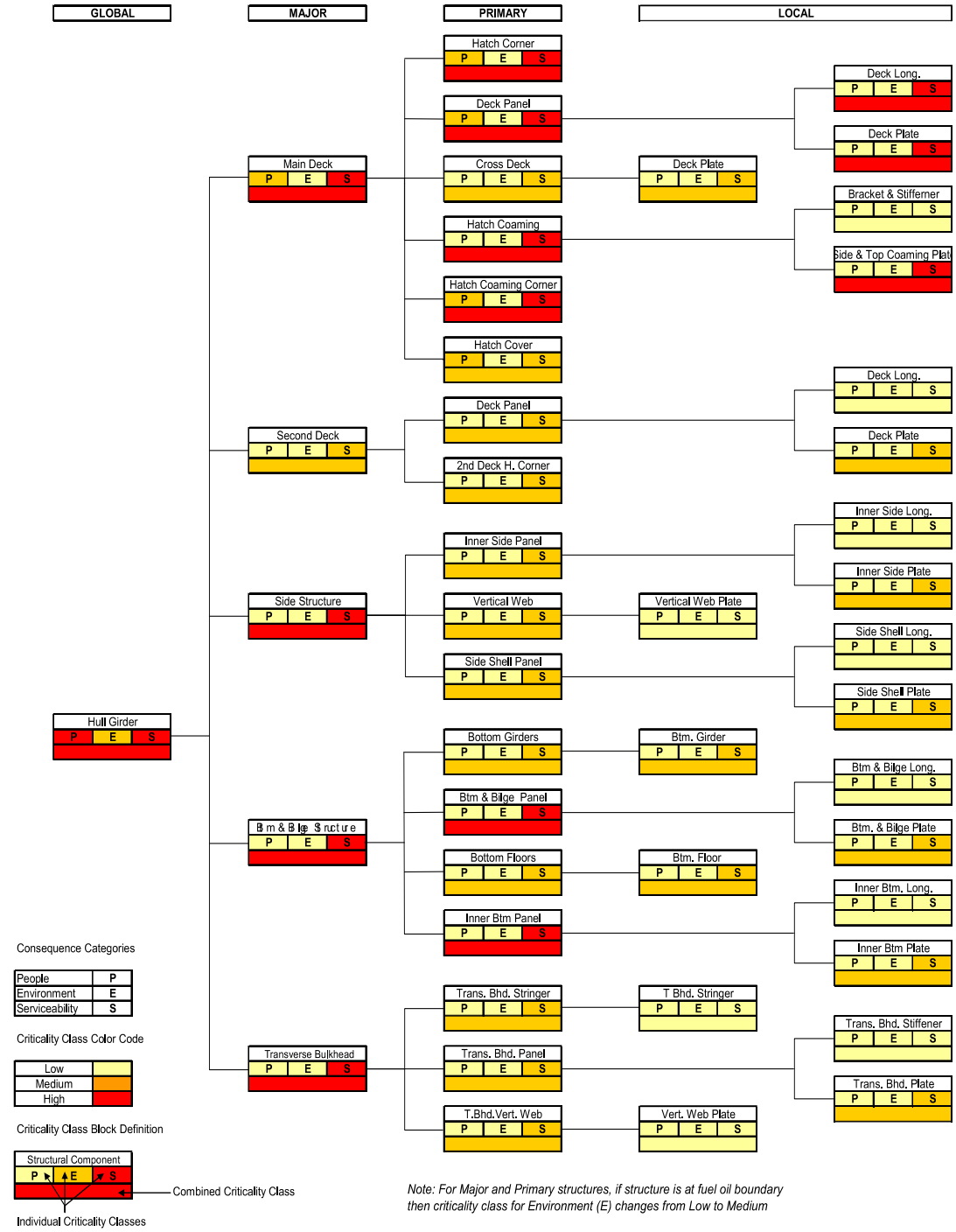

Figure B-3 Criticality Class model for Container ships proposed by (ABS, 2012)

Appendix C

Maximum likelihood estimate

Maximum likelihood estimation is based on the likelihood function, $l(\theta; x)$. For a given statistical model, i.e. a family of distributions $\{f(.;\theta)|\ \theta \in \Theta\}$, where θ, is the parameter (possibly multidimensional) for the model. Θ , is the bounds of the parameter. The method finds, θ, that maximises the likelihood function , $l(\theta; x)$.

$$\hat{\theta} \in \{\arg\max l(\theta; x)\}$$

Maximum likelihood estimator for models without a closed form solution is found through numerical global optimisation.

Statistical distributions

Normal distribution

Probability Density Function (PDF)

$$PDF(x) = \frac{1}{\sqrt{2\pi\sigma^2}} e^{-\frac{(x-\mu)^2}{2\sigma^2}}$$

where, erf is the error function, μ is the location parameter and, σ is the scale parameter.

Cumulative Density Function (CDF)

$$CDF = \frac{1}{2}\left[1 + \text{erf}(\frac{x-\mu}{\sigma\sqrt{2}})\right]$$

Parameter estimation

μ and σ are estimated using the method moment (MOM) in which μ, is equal to the expected value of the data, $\bar{x}$, and σ is equal to standard deviation of the data.

Lognormal distribution

Probability Density Function (PDF)

$$PDF(x) = \frac{1}{x\sqrt{2\pi\sigma^2}} e^{-\frac{(\ln(x)-\mu)^2}{2\sigma^2}}$$

where, erf is the error function, μ is the location parameter and, σ is the scale parameter.

Cumulative Density Function (CDF)

$$CDF(x) = \frac{1}{2}\left[1 + \text{erf}(\frac{\ln(x) - \mu}{\sigma\sqrt{2}})\right]$$

Parameter estimation

μ and σ are estimated using the method moment (MOM) in which μ, is equal to the expected value of the logarithm of the data , $\overline{\ln(x)}$,and σ is equal to standard deviation of logarithm of the data.

Exponential distribution

Probability Density Function (PDF)

$$PDF(x) = \lambda e^{-\lambda x}$$

Cumulative Density Function (CDF)

$$CDF(x) = 1 - e^{-\lambda x}$$

Parameter estimation

Parameter, λ is either method of moments (MOM) or maximum likelihood estimation (MLE) is equal to the expected value of the data $\bar{x}$.

Weibull distribution

Probability Density Function (PDF)

$$PDF(x) = \begin{cases} \frac{k}{\lambda}\left(\frac{x}{\lambda}\right)^{k-1} e^{-(x/\lambda)^k}, & x \geq 0 \\ 0 & , x < 0 \end{cases}$$

where, k is the shape parameter and λ, is the scale parameter.

Cumulative Density Function (CDF)

$$PDF(x) = \begin{cases} 1 - e^{-(x/\lambda)^k} & , x \geq 0 \\ 0 & , x < 0 \end{cases}$$

Parameter estimation

The MLE of the shape and scale parameters are the simultaneous solution of below equation for the shape and scale estimators $\hat{k}$, $\hat{\lambda}$,:

$$\hat{k} = \left[\left(\frac{1}{n}\right)\sum_{i=1}^{1} {x_i}^{\hat{\lambda}}\right]^{1/\hat{\lambda}}$$

$$\hat{\lambda} = \frac{n}{(1/\hat{\eta})\sum_{i=1}^{n} {x_i}^{\hat{\lambda}} \log(x_i) - \sum_{i=1}^{n} \log(x_i)}$$

Appendix D

Material Properties

Fracture toughness

LR Specification			Data					
Grade	Temperature	Longitudinal	Mean	Std.	Max	Min	Sample size	Number of Manufacturers
A	20	27	110.8	42.14	185	41	99	1
B	0	34	155.5	54.66	259	84	7	2
D	-20	41	181	97	352	57	46	3
AH32	0	31	182	98.6	370	91	18	3
AH36	0	34	118.817	66.21	406.33	55	169	4
DH36	-20	34	183	90.73	370	46	36	3

Table D-1 Descriptive statistics of the raw data

Normal Grade steels

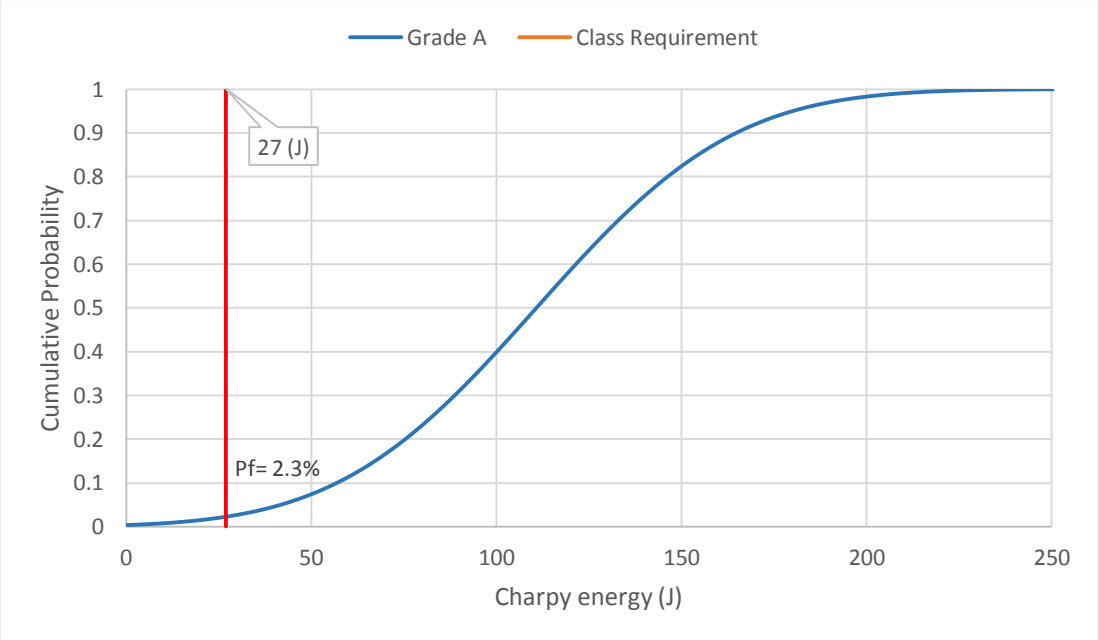

Figure D-1 Normal Cumulative density function of grade A steel

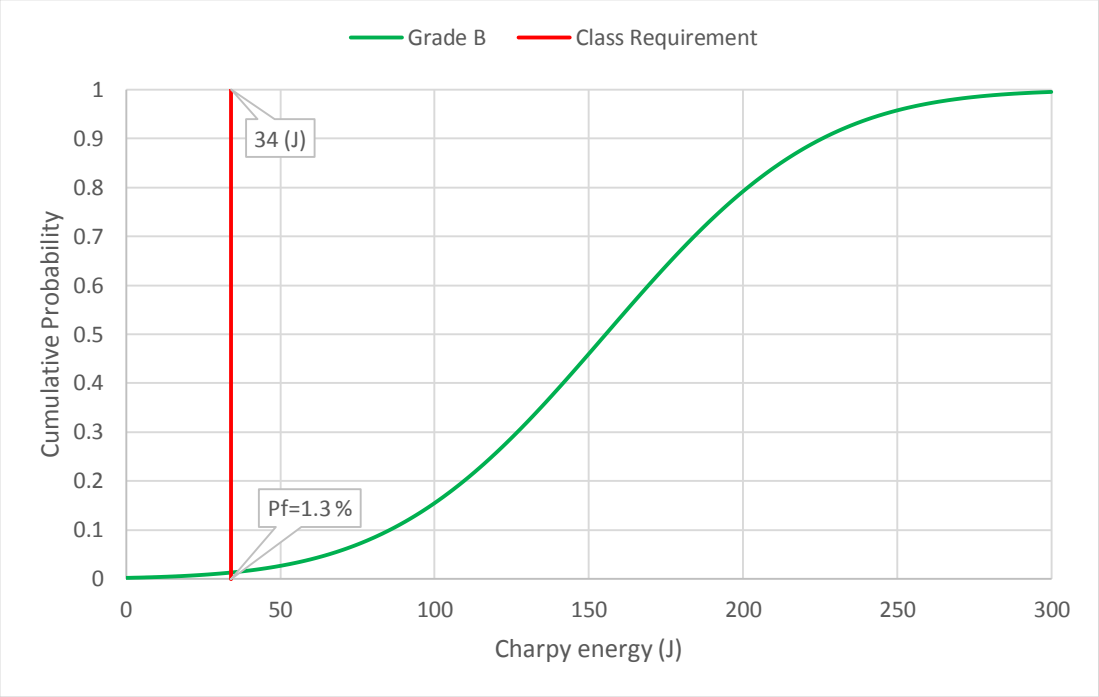

Figure D-2 Normal Cumulative density function of grade D steel

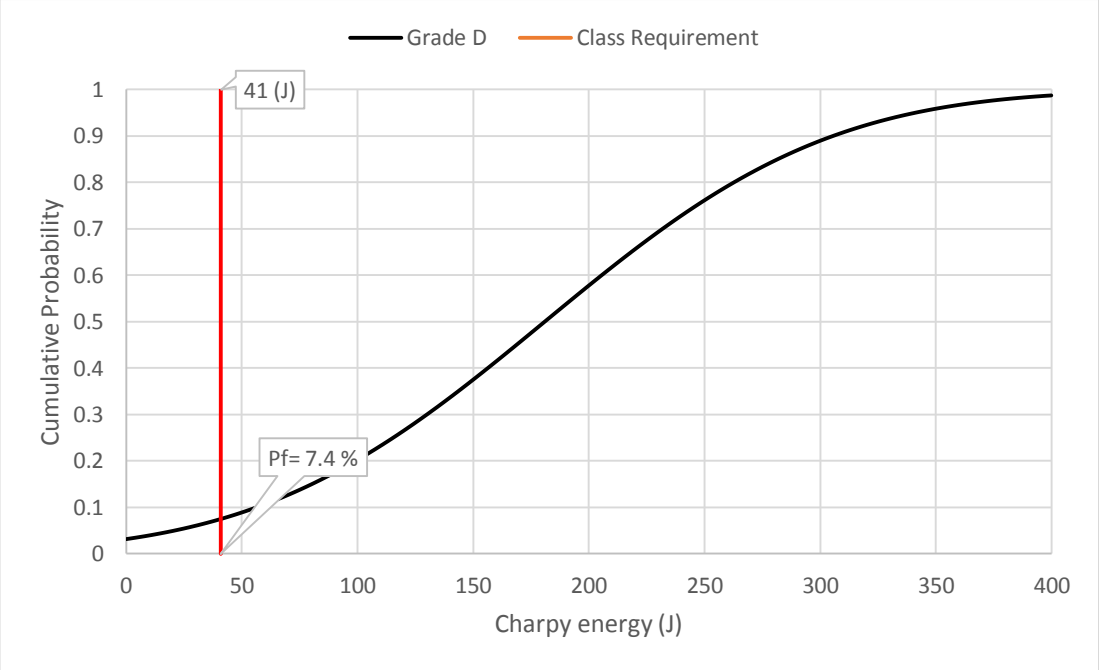

Figure D-3 Normal Cumulative density function of grade D steel

High strength steel grades

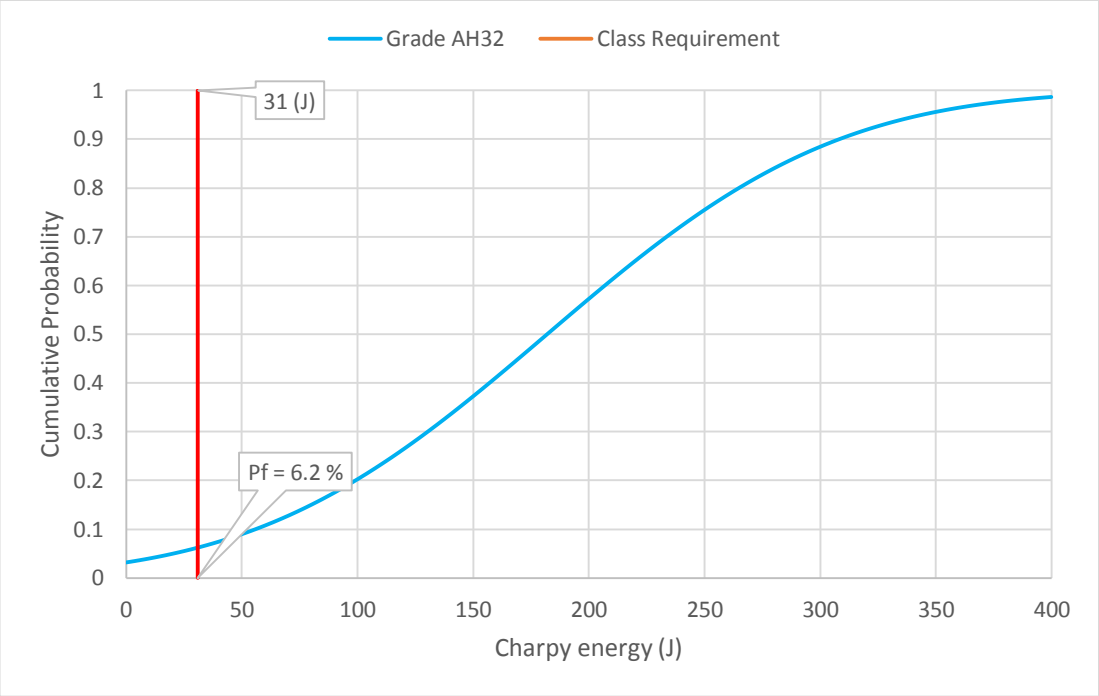

Figure D-4 Normal Cumulative density function of grade AH32 steel

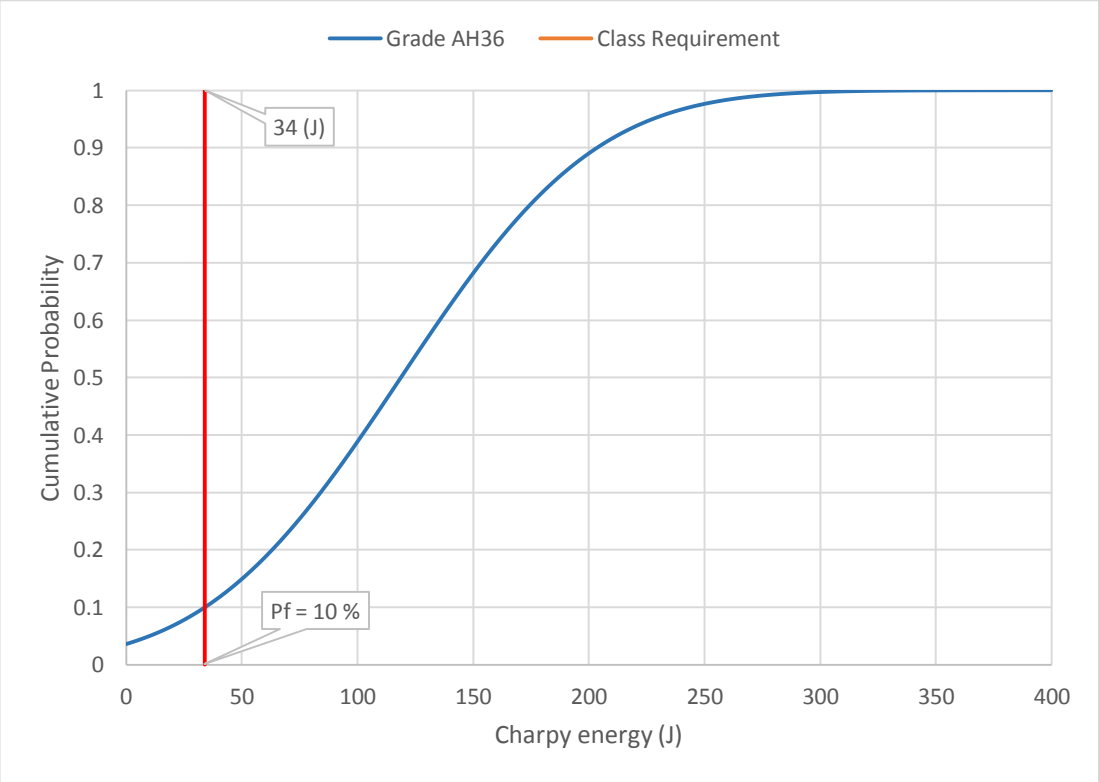

Figure D-5 Normal Cumulative density function of grade A36 steel

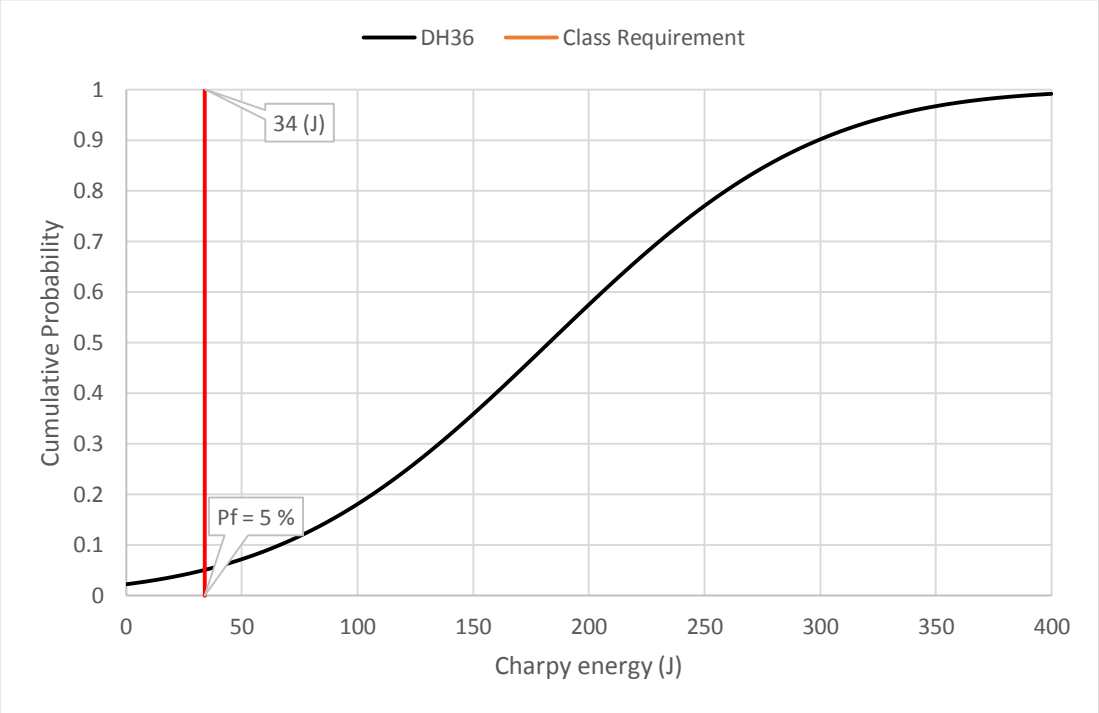

Figure D-6 Normal Cumulative density function of grade DH36 steel

Appendix E

Case study data

NDE inspection plan

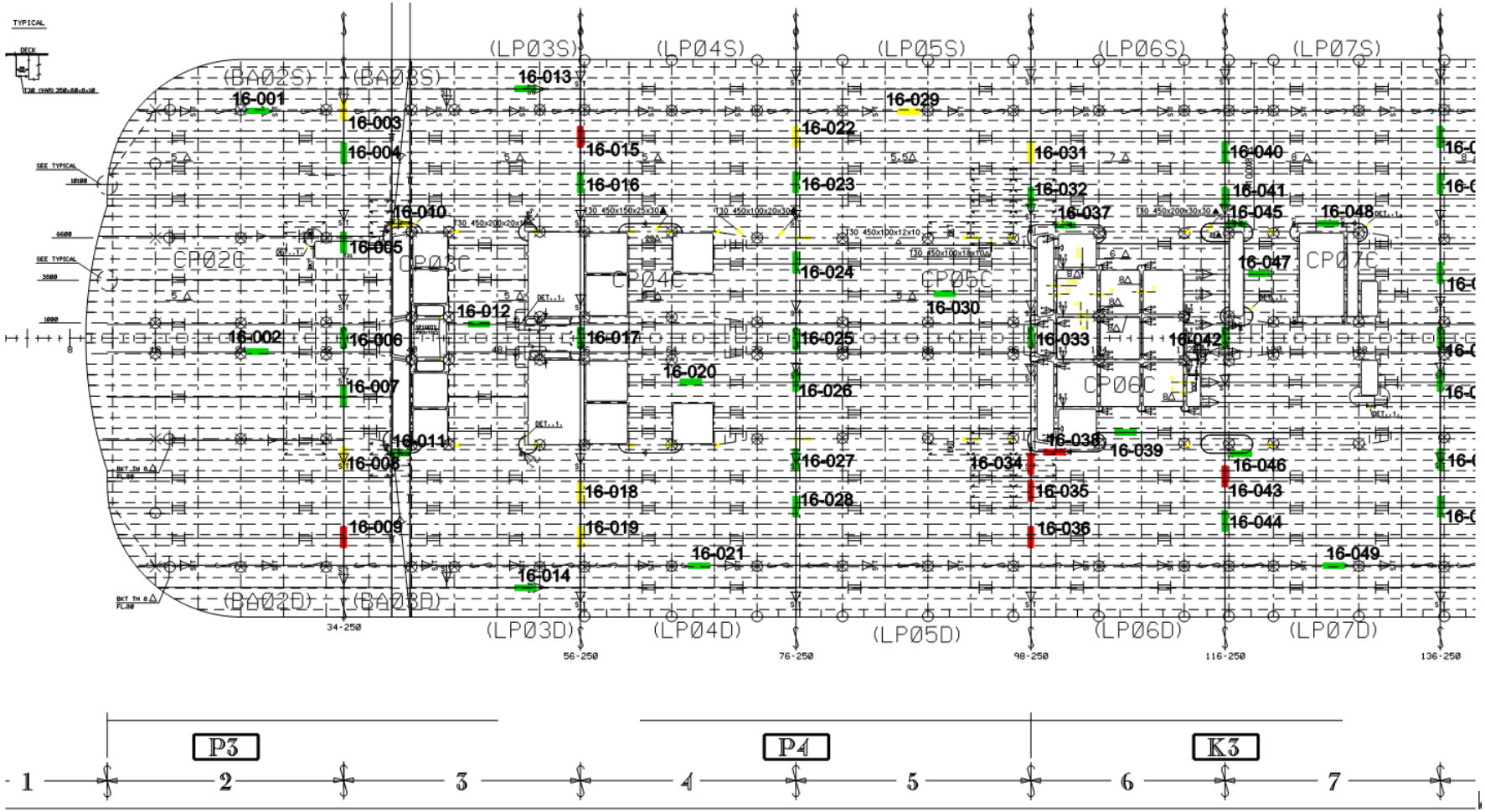

Figure E-1 Existing inspection plan for deck 16 (Stern)

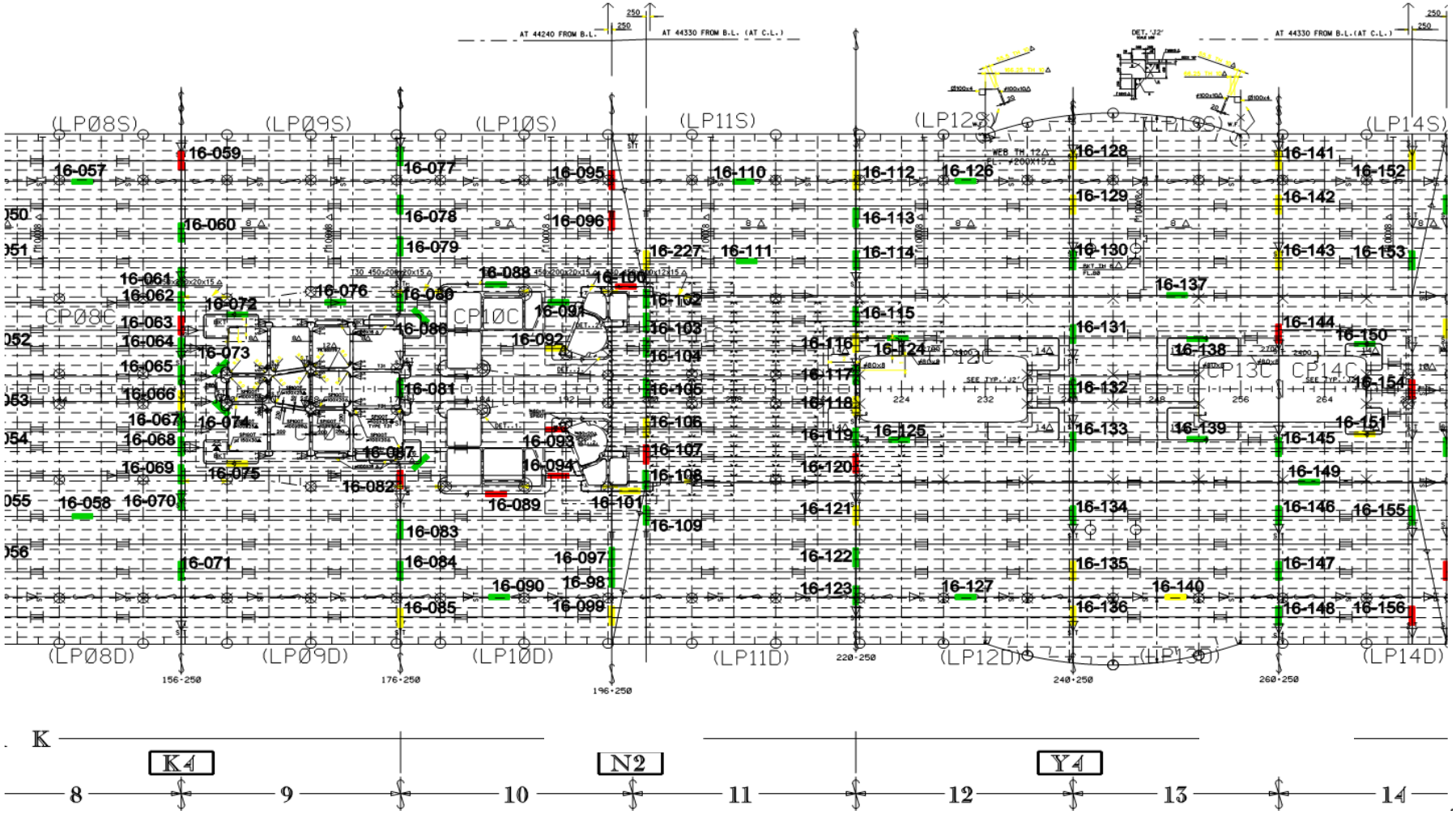

Figure E-2 Existing inspection plan for deck 16 (mid ship)

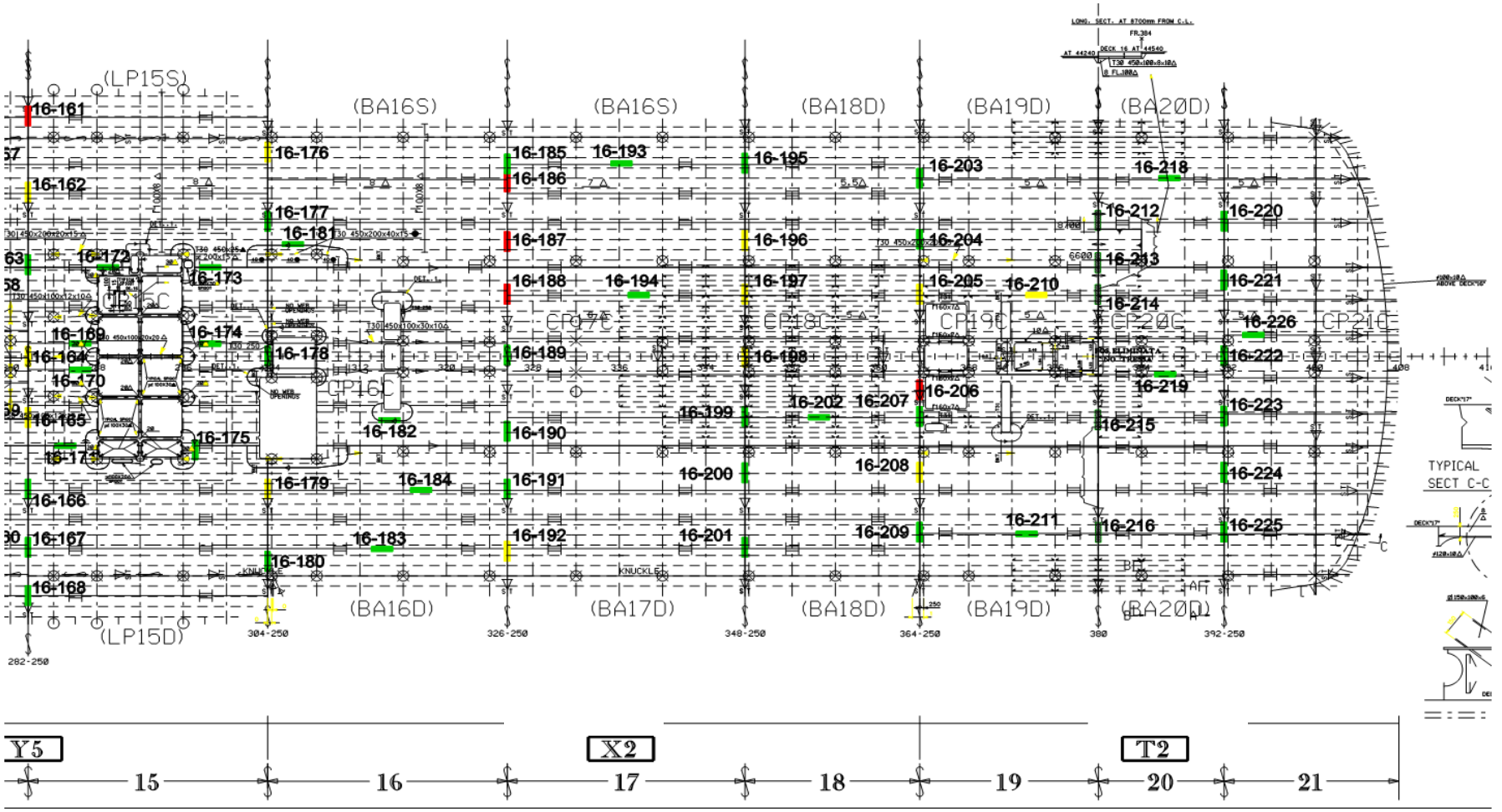

Figure E-3 Existing inspection plan for deck 16 (Bow)

Structural data

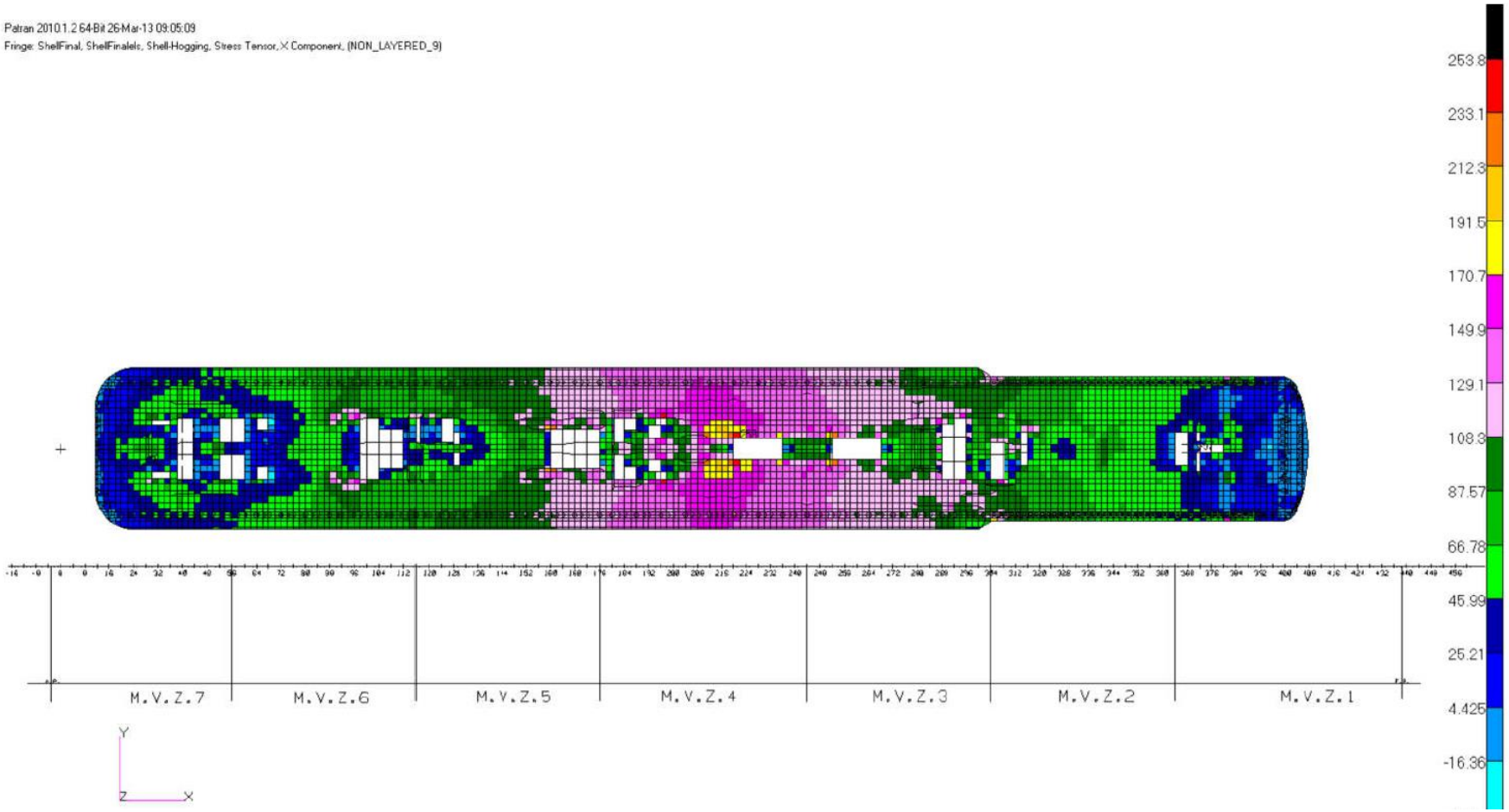

Figure E-4 FEA counter plot for deck 16 (Still water +Wave Hogging)

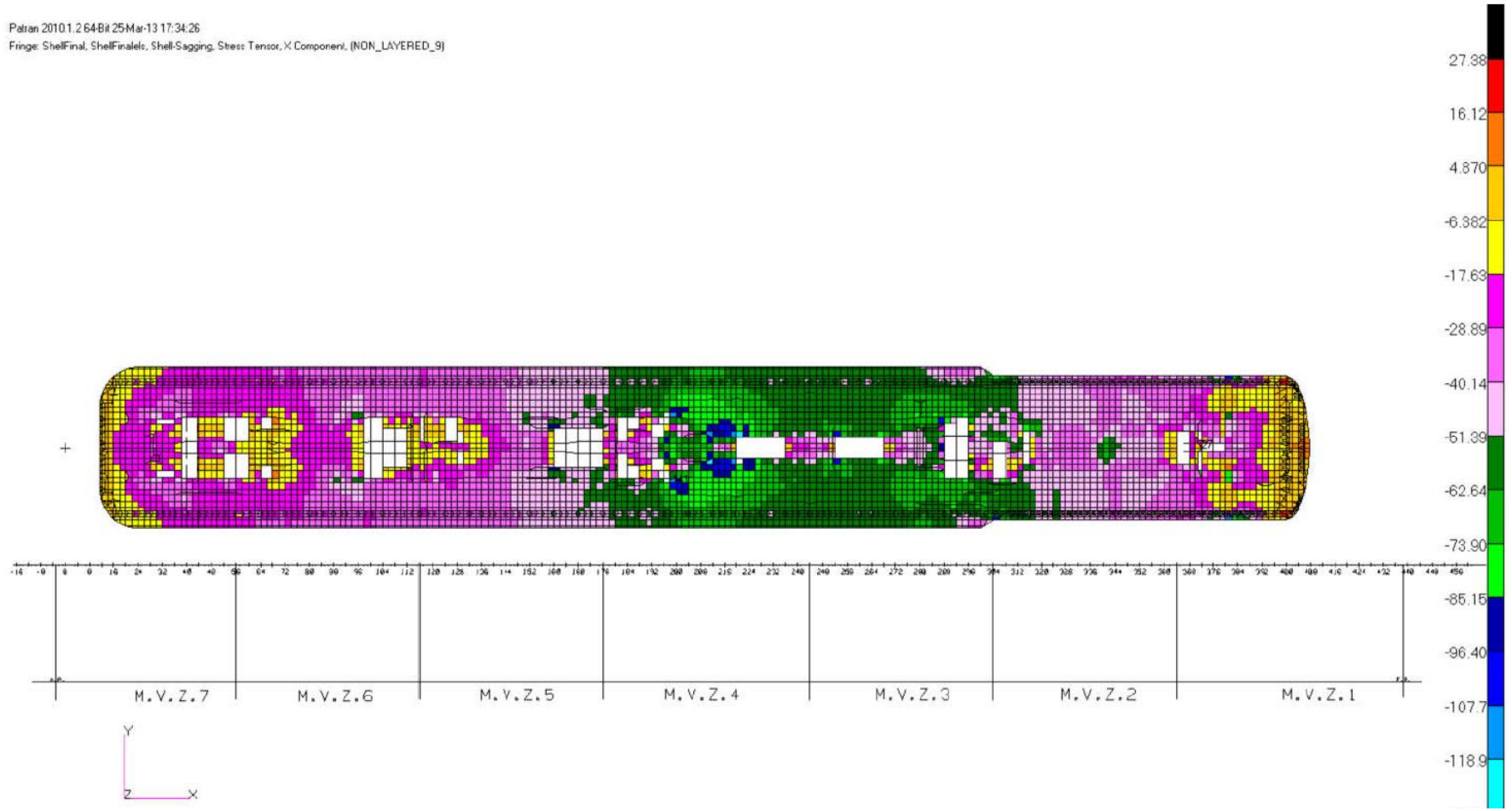

Figure E-5 FEA counter plot for deck 16 (Still water +Wave Sagging)

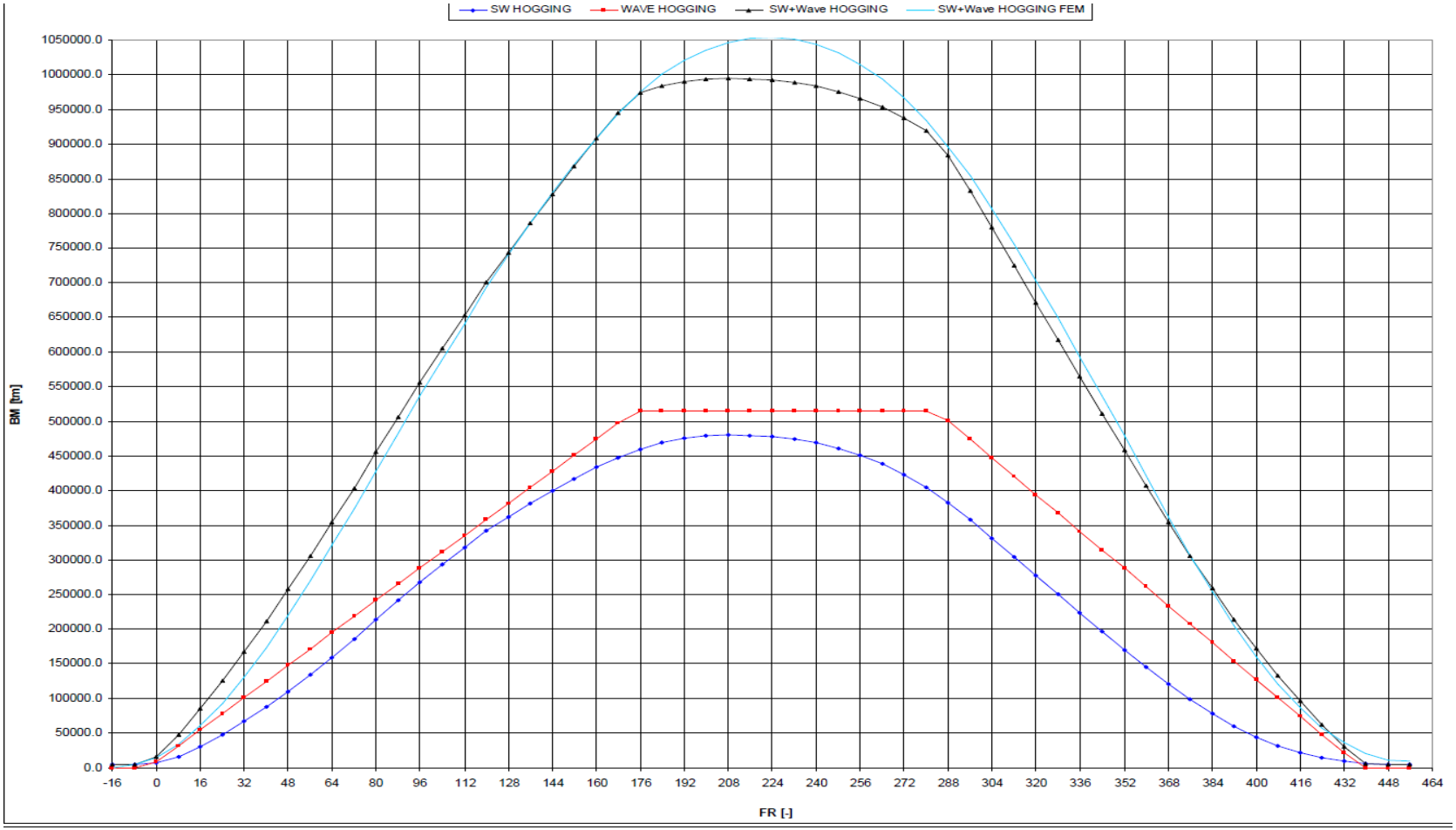

Figure E-6 Global bending moment diagrams for ship (Wave hogging)

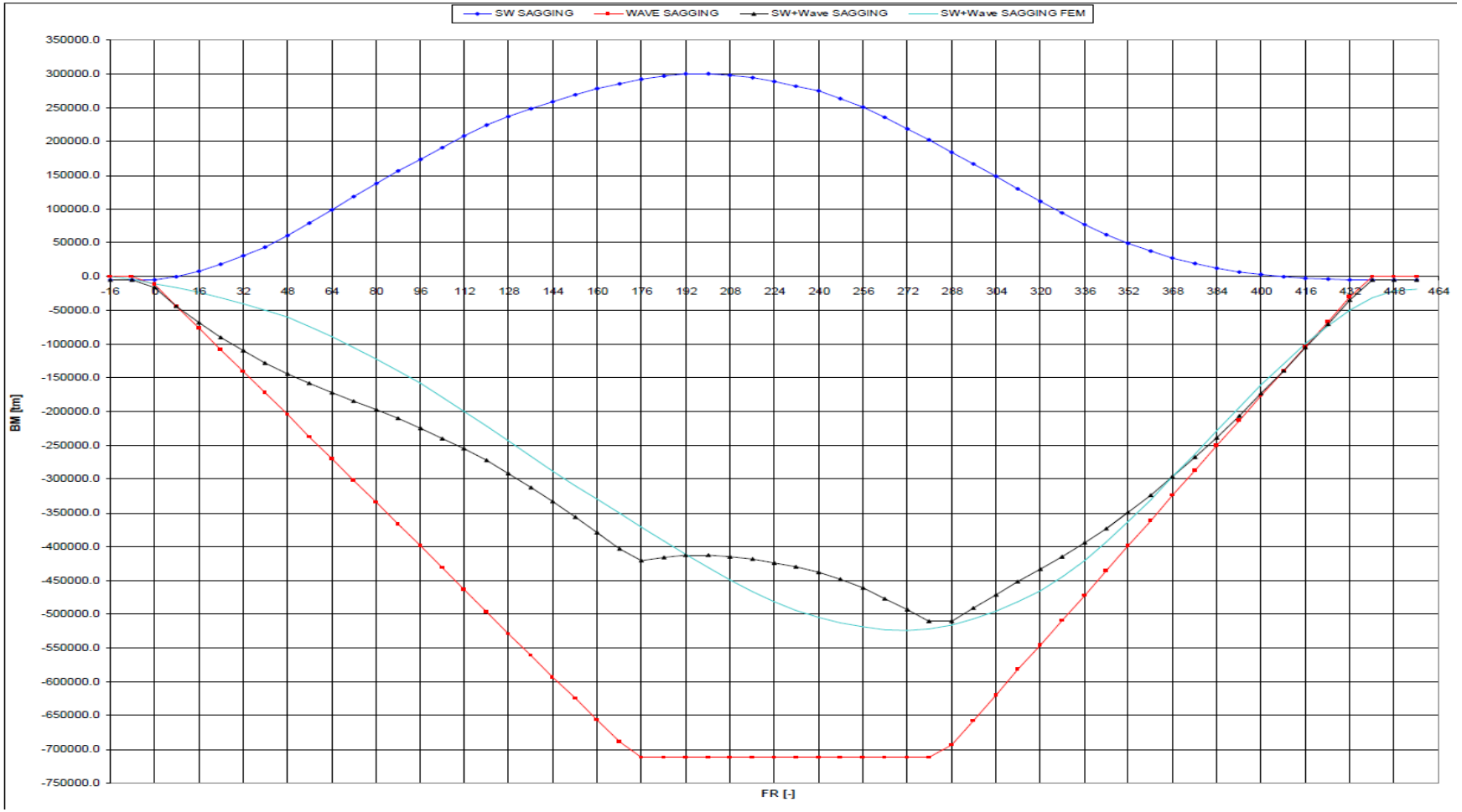

Figure E-7 Global bending moment diagrams for ship (Wave sagging)

		SW HOGGING		WAVE HOGGING		SW+ Hogging		
		ALLOWABLE		RULE Wave		FEM		
X [m]	FR [-]	BM [tm]	SF [t]	BM [tm]	SF [t]	FR [-]	BM [tm]	SF [t]
-11.040	-16	5000.0	148.0	0.0	0.0	-16	275.8	395.7
-5.520	-8	5400.0	426.0	0.0	0.0	-8	4287.3	1405.5
0.000	0	7000.0	1250.0	8408.9	137.8	0	14789.1	2936.6
5.520	8	16200.0	2290.0	31617.6	518.3	8	33932.4	4451.8
11.040	16	30200.0	3090.0	54826.3	898.7	16	60725.0	5528.3
16.560	24	47440.0	3710.0	78035.0	1279.2	24	93175.9	6490.4
22.080	32	66780.0	4160.0	101243.7	1659.6	32	130723.6	7438.7
27.600	40	87500.0	4400.0	124452.4	2040.0	40	173298.4	8201.8
33.120	48	109900.0	4640.0	147661.1	2420.5	48	219713.1	8762.5
38.760	56	133995.8	4879.0	171374.3	2809.2	56	269775.3	9175.3
44.400	64	159300.0	5100.0	195087.6	3197.9	64	321792.5	9463.0
49.920	72	185600.0	5240.0	218296.3	3578.3	72	374433.3	9785.6
55.440	80	214000.0	5200.0	241505.0	3958.8	80	428324.3	9861.5
60.960	88	241600.0	5120.0	264713.7	4217.9	88	482348.1	9891.1
66.480	96	268300.0	4980.0	287922.4	4217.9	96	536383.4	9774.8
72.000	104	293900.0	4800.0	311131.0	4217.9	104	589335.6	9457.6
77.520	112	318201.7	4601.7	334339.7	4217.9	112	640680.6	9188.8
83.280	120	342000.0	4400.0	358557.5	4217.9	120	692900.8	8913.2
88.800	128	362000.0	4160.0	381766.2	4217.9	128	740971.9	8452.2
94.320	136	381100.0	3890.0	404974.9	4149.2	136	786490.9	7985.8
99.840	144	399300.0	3590.0	428183.6	4065.3	144	829476.0	7557.0
105.360	152	416700.0	3280.0	451392.3	3981.4	152	870128.3	7207.3
110.880	160	433500.0	3000.0	474601.0	3897.5	160	908425.5	6646.3
116.400	168	447500.0	2640.0	497809.7	3813.6	168	943570.8	5993.3
122.040	176	459651.3	2221.8	514627.6	3752.8	176	975080.8	5019.1
127.680	184	469300.0	1800.0	514627.6	3752.8	184	1001166.7	4025.9
133.200	192	475800.0	1500.0	514627.6	3752.8	192	1021217.4	2984.6
138.720	200	479000.0	1500.0	514627.6	3752.8	200	1035788.2	2157.2
144.240	208	479800.0	-1500.0	514627.6	-3752.8	208	1046042.3	1351.6
149.760	216	479400.0	-1800.0	514627.6	-3752.8	216	1052061.6	714.1
155.280	224	477400.0	-2300.0	514627.6	-3752.8	224	1053773.0	-220.3
160.800	232	473800.0	-2890.0	514627.6	-3752.8	232	1050908.9	-997.7
166.320	240	469000.0	-3450.0	514627.6	-3752.8	240	1043839.8	-1749.4
172.080	248	460932.8	-3934.0	514627.6	-3752.8	248	1031653.2	-2725.1
177.600	256	450900.0	-4440.0	514627.6	-3752.8	256	1014746.6	-3517.2
183.120	264	438500.0	-4820.0	514627.6	-3794.5	264	993303.0	-4479.1
188.640	272	423300.0	-5050.0	514627.6	-3945.7	272	966394.9	-5519.7
194.160	280	404500.0	-5250.0	514627.6	-4097.0	280	933924.1	-6450.8
199.680	288	382100.0	-5410.0	501269.4	-4248.2	288	896515.2	-7244.7
205.200	296	357900.0	-5510.0	474745.1	-4399.5	296	854490.0	-8118.1
210.840	304	331785.7	-5550.0	447644.3	-4554.0	304	806786.8	-8897.0
216.480	312	304700.0	-5530.0	420543.5	-4591.3	312	755462.4	-9341.6
222.000	320	277500.0	-5450.0	394019.2	-4591.3	320	703073.1	-9746.9
227.520	328	250300.0	-5370.0	367495.0	-4591.3	328	648826.5	-9985.8
233.040	336	223400.0	-5230.0	340970.8	-4591.3	336	593239.6	-10208.9
238.560	344	196600.0	-5090.0	314446.6	-4591.3	344	536498.6	-10367.9
244.080	352	170300.0	-4930.0	287922.4	-4591.3	352	479123.9	-10434.4
249.600	360	145500.0	-4650.0	261398.1	-4591.3	360	421364.6	-10461.2
255.360	368	120895.0	-4367.6	233720.7	-4591.3	368	361733.9	-10128.9
260.880	376	98800.0	-4000.0	207196.5	-4313.2	376	306586.0	-9683.5
266.400	384	78400.0	-3620.0	180672.2	-3761.1	384	254261.6	-9060.6
271.920	392	60100.0	-3240.0	154148.0	-3208.9	392	205439.0	-8404.0
277.440	400	44500.0	-2800.0	127623.8	-2656.7	400	160699.7	-7541.1
282.960	408	32100.0	-2320.0	101099.6	-2104.6	408	120958.5	-6643.3
288.480	416	21800.0	-1870.0	74575.3	-1552.4	416	86436.5	-5652.2
294.000	424	14400.0	-1410.0	48051.1	-1000.3	424	57906.5	-4385.4
299.520	432	9600.0	-956.0	21526.9	-448.1	432	36116.3	-3272.4
305.040	440	6000.0	-580.0	0.0	0.0	440	20509.2	-2074.0
310.560	448	5200.0	-356.0	0.0	0.0	448	11535.1	-867.2
316.080	456	5000.0	-150.0	0.0	0.0	456	9345.1	101.2

Figure E-8 Ship Global bending moment and shear force table (Wave Hogging)

		SW SAGGING		WAVE SAGGING		SW+ Sagging		
		ALLOWABLE		RULE Wave		FEM		
X [m]	FR [-]	BM [tm]	SF [t]	BM [tm]	SF [t]	FR [-]	BM [tm]	SF [t]
-11.040	-16	-5000.0	-100.0	0.0	0.0	-16	-295.4	-425.2
-5.520	-8	-4900.0	-100.0	0.0	0.0	-8	-4126.0	-1016.8
0.000	0	-4500.0	250.0	-11643.1	-254.5	0	-10314.9	-1090.5
5.520	8	-100.0	890.0	-43778.0	-956.8	8	-16687.7	-1115.6
11.040	16	7600.0	1350.0	-75912.9	-1659.2	16	-23357.1	-1319.6
16.560	24	18000.0	1730.0	-108047.9	-2361.5	24	-31151.6	-1505.9
22.080	32	30400.0	2080.0	-140182.8	-3063.9	32	-39936.1	-1604.4
27.600	40	44000.0	2400.0	-172317.7	-3766.2	40	-49394.7	-1831.8
33.120	48	60800.0	2720.0	-204452.6	-4468.6	48	-60257.5	-2141.4
38.760	56	79319.3	2919.3	-237286.1	-5186.2	56	-73459.2	-2505.3
44.400	64	98800.0	3060.0	-270119.6	-5840.2	64	-88623.3	-2808.4
49.920	72	118300.0	3140.0	-302254.5	-5840.2	72	-104834.0	-2978.5
55.440	80	137500.0	3100.0	-334389.5	-5840.2	80	-121985.5	-3145.0
60.960	88	156300.0	3060.0	-366524.4	-5840.2	88	-140019.3	-3234.0
66.480	96	174200.0	2960.0	-398659.3	-5840.2	96	-158524.5	-3381.3
72.000	104	191400.0	2820.0	-430794.2	-5840.2	104	-178159.6	-3662.7
77.520	112	207865.5	2632.4	-462929.2	-5840.2	112	-199056.2	-3821.9
83.280	120	224000.0	2350.0	-496461.2	-5840.2	120	-221417.6	-3900.3
88.800	128	237200.0	2070.0	-528596.2	-5840.2	128	-243521.0	-4072.8
94.320	136	248900.0	1820.0	-560731.1	-5648.2	136	-266197.0	-4013.9
99.840	144	259500.0	1660.0	-592866.0	-5413.8	144	-288132.6	-3874.7
105.360	152	269300.0	1540.0	-625000.9	-5179.4	152	-309521.7	-3688.8
110.880	160	278500.0	1300.0	-657135.9	-4945.1	160	-330084.6	-3607.3
116.400	168	285700.0	900.0	-689270.8	-4710.7	168	-350058.0	-3527.8
122.040	176	291974.8	561.3	-712556.9	-4540.8	176	-370606.4	-3707.9
127.680	184	297000.0	0.0	-712556.9	-4540.8	184	-391515.0	-3633.7
133.200	192	300000.0	0.0	-712556.9	-4540.8	192	-411542.6	-3607.2
138.720	200	300000.0	0.0	-712556.9	4540.8	200	-431153.1	-3415.4
144.240	208	298000.0	0.0	-712556.9	4540.8	208	-449580.4	-3210.3
149.760	216	294500.0	0.0	-712556.9	4540.8	216	-466656.8	-2819.0
155.280	224	289100.0	0.0	-712556.9	4540.8	224	-481931.9	-2516.7
160.800	232	282200.0	0.0	-712556.9	4540.8	232	-494834.6	-2015.1
166.320	240	275000.0	-350.0	-712556.9	4540.8	240	-504831.1	-1449.0
172.080	248	264109.2	-713.0	-712556.9	4540.8	248	-512300.1	-1151.5
177.600	256	251300.0	-1070.0	-712556.9	4540.8	256	-518216.7	-840.4
183.120	264	236100.0	-1490.0	-712556.9	4631.0	264	-522580.6	-458.4
188.640	272	219200.0	-1950.0	-712556.9	4958.7	272	-523888.6	124.1
194.160	280	202000.0	-2350.0	-712556.9	5286.3	280	-522014.3	742.4
199.680	288	184000.0	-2550.0	-694061.1	5614.0	288	-516380.3	1546.8
205.200	296	166300.0	-2600.0	-657335.4	5941.6	296	-507329.9	1903.3
210.840	304	148424.4	-2600.0	-619811.4	6276.4	304	-495979.2	2314.1
216.480	312	130400.0	-2600.0	-582287.4	6357.1	312	-481983.4	2854.9
222.000	320	112000.0	-2600.0	-545561.8	6357.1	320	-465049.3	3378.5
227.520	328	94000.0	-2480.0	-508836.2	6357.1	328	-444834.7	4123.6
233.040	336	77500.0	-2240.0	-472110.6	6357.1	336	-420619.8	4796.2
238.560	344	62500.0	-1980.0	-435384.9	6357.1	344	-393062.0	5314.5
244.080	352	49200.0	-1770.0	-398659.3	6357.1	352	-362603.0	5719.5
249.600	360	38000.0	-1650.0	-361933.7	6357.1	360	-330735.4	5886.0
255.360	368	27512.6	-1408.0	-323611.3	6357.1	368	-296292.2	6099.6
260.880	376	19000.0	-1110.0	-286885.7	5972.1	376	-262462.6	6204.1
266.400	384	12000.0	-870.0	-250160.0	5207.6	384	-228138.6	6240.5
271.920	392	6700.0	-730.0	-213434.4	4443.1	392	-194005.8	6112.6
277.440	400	3500.0	-650.0	-176708.8	3678.5	400	-160749.7	5898.7
282.960	408	-100.0	-450.0	-139983.2	2914.0	408	-128900.4	5634.3
288.480	416	-1900.0	-100.0	-103257.6	2149.5	416	-99168.0	5097.1
294.000	424	-3500.0	100.0	-66531.9	1385.0	424	-72502.0	4581.1
299.520	432	-5000.0	100.0	-29806.3	620.5	432	-49267.5	3620.2
305.040	440	-5000.0	100.0	0.0	0.0	440	-31564.2	2471.9
310.560	448	-5000.0	100.0	0.0	0.0	448	-20776.0	1041.5
316.080	456	-5000.0	100.0	0.0	0.0	456	-18114.2	-169.8

Figure E-9 Ship Global bending moment and shear force table (Wave sagging)

		WAVE HOGGING		WAVE SAGGING	
		RULE Wave		RULE Wave	
X [m]	FR [-]	BM [tm]	SF [t]	BM [tm]	SF [t]
-11.040	-16	0.0	0.0	0.0	0.0
-5.520	-8	0.0	0.0	0.0	0.0
0.000	0	8408.9	137.8	-11643.1	-254.5
5.520	8	31617.6	518.3	-43778.0	-956.8
11.040	16	54826.3	898.7	-75912.9	-1659.2
16.560	24	78035.0	1279.2	-108047.9	-2361.5
22.080	32	101243.7	1659.6	-140182.8	-3063.9
27.600	40	124452.4	2040.0	-172317.7	-3766.2
33.120	48	147661.1	2420.5	-204452.6	-4468.6
38.760	56	171374.3	2809.2	-237286.1	-5186.2
44.400	64	195087.6	3197.9	-270119.6	-5840.2
49.920	72	218296.3	3578.3	-302254.5	-5840.2
55.440	80	241505.0	3958.8	-334389.5	-5840.2
60.960	88	264713.7	4217.9	-366524.4	-5840.2
66.480	96	287922.4	4217.9	-398659.3	-5840.2
72.000	104	311131.0	4217.9	-430794.2	-5840.2
77.520	112	334339.7	4217.9	-462929.2	-5840.2
83.280	120	358557.5	4217.9	-496461.2	-5840.2
88.800	128	381766.2	4217.9	-528596.2	-5840.2
94.320	136	404974.9	4149.2	-560731.1	-5648.2
99.840	144	428183.6	4065.3	-592866.0	-5413.8
105.360	152	451392.3	3981.4	-625000.9	-5179.4
110.880	160	474601.0	3897.5	-657135.9	-4945.1
116.400	168	497809.7	3813.6	-689270.8	-4710.7
122.040	176	514627.6	3752.8	-712556.9	-4540.8
127.680	184	514627.6	3752.8	-712556.9	-4540.8
133.200	192	514627.6	3752.8	-712556.9	-4540.8
138.720	200	514627.6	3752.8	-712556.9	-4540.8
144.240	208	514627.6	3752.8	-712556.9	-4540.8
149.760	216	514627.6	3752.8	-712556.9	-4540.8
155.280	224	514627.6	-3752.8	-712556.9	4540.8
160.800	232	514627.6	-3752.8	-712556.9	4540.8
166.320	240	514627.6	-3752.8	-712556.9	4540.8
172.080	248	514627.6	-3752.8	-712556.9	4540.8
177.600	256	514627.6	-3752.8	-712556.9	4540.8
183.120	264	514627.6	-3794.5	-712556.9	4631.0
188.640	272	514627.6	-3945.7	-712556.9	4958.7
194.160	280	514627.6	-4097.0	-712556.9	5286.3
199.680	288	501269.4	-4248.2	-694061.1	5614.0
205.200	296	474745.1	-4399.5	-657335.4	5941.6
210.840	304	447644.3	-4554.0	-619811.4	6276.4
216.480	312	420543.5	-4591.3	-582287.4	6357.1
222.000	320	394019.2	-4591.3	-545561.8	6357.1
227.520	328	367495.0	-4591.3	-508836.2	6357.1
233.040	336	340970.8	-4591.3	-472110.6	6357.1
238.560	344	314446.6	-4591.3	-435384.9	6357.1
244.080	352	287922.4	-4591.3	-398659.3	6357.1
249.600	360	261398.1	-4591.3	-361933.7	6357.1
255.360	368	233720.7	-4591.3	-323611.3	6357.1
260.880	376	207196.5	-4313.2	-286885.7	5972.1
266.400	384	180672.2	-3761.1	-250160.0	5207.6
271.920	392	154148.0	-3208.9	-213434.4	4443.1
277.440	400	127623.8	-2656.7	-176708.8	3678.5
282.960	408	101099.6	-2104.6	-139983.2	2914.0
288.480	416	74575.3	-1552.4	-103257.6	2149.5
294.000	424	48051.1	-1000.3	-66531.9	1385.0
299.520	432	21526.9	-448.1	-29806.3	620.5
305.040	440	0.0	0.0	0.0	0.0
310.560	448	0.0	0.0	0.0	0.0
316.080	456	0.0	0.0	0.0	0.0

Figure E-10 Ship Global bending moment and shear force table

NDE inspection raw data

Frame	Position	ID No	NDE Type	NDE Result	Confined/ Extended	Length (mm)	Crack	Cavity	Solid inclusion	Lack of fusion /penetration	Imperfection of shape and dimensions	Miscellaneous imperfections	Thickness (mm)	Welding Process	Block	Section
24	Port	16-001	RT	Acceptable									5	FCAW		P3
24	Stbd	16-002	RT	Acceptable									5	H.LASER	CP02Cn	P3
34	Port	16-003	RT	Not Acceptable			Longitudinal						5	FCAW		P3
34	Port	16-003	RT	Acceptable									5	FCAW		P3
34	Port	16-003	RT	Not Acceptable	C	50		Worm hole					5	FCAW		P3
34	Port	16-004	RT	Acceptable									5	FCAW		P3
34	Port	16-005	RT	Acceptable									5	FCAW		P3
34	Cnt	16-006	RT	Acceptable				Porosity					5	FCAW		P3
34	Stbd	16-007	RT	Acceptable				Uniformly distributed porosity					5	FCAW		P3
34	Stbd	16-008	RT	Acceptable									5	FCAW		P3
34	Stbd	16-008	RT	Not Acceptable	C	60		Clustered porosity					5	FCAW		P3
34	Stbd	16-009	RT	Acceptable									5	FCAW		P3
34	Stbd	16-009	RT	Acceptable									5	FCAW		P3
34	Stbd	16-009	RT	Not Acceptable	C	50				Lack of Fusion			5	FCAW		P3
34	Port	16-010	RT	Acceptable				Porosity					5-12	FCAW		P3
34	Port	16-010	RT	Not Acceptable	C	50		Worm hole					5-12	FCAW		P3
34	Stbd	16-011	RT	Acceptable				Elongated porosity					5-12	FCAW		P3
48	Port	16-012	RT	Acceptable									5	H.LASER	CP03Cn	P3
52	Port	16-013	RT	Acceptable								Spatter	5	H.LASER	LP03Sn	P3
52	Stbd	16-014	RT	Acceptable				Porosity					5	FCAW	LP03Dn	P3
52	Stbd	16-014	RT	Not Acceptable	C	40		Linear porosity					5	H.LASER	LP03Dn	P3

Frame	Position	ID No	NDE Type	NDE Result	Confined/ Extended	Length (mm)	Crack	Cavity	Solid inclusion	Lack of fusion /penetration	Imperfection of shape and dimensions	Miscellaneous imperfections	Thickness (mm)	Welding Process	Block	Section
56	Port	16-015	RT	Acceptable									5	FCAW		P4+P3
56	Port	16-015	RT	Acceptable									5	FCAW		P4+P3
56	Port	16-015	RT	Not Acceptable						Lack of Fusion			5	FCAW		P4+P3
56	Port	16-016	RT	Acceptable									5	FCAW		P4+P3
56	Cnt	16-017	RT	Acceptable				Gas pore					5	FCAW		P4+P3
56	Stbd	16-018	RT	Acceptable									5	FCAW		P4+P3
56	Stbd	16-018	RT	Not Acceptable	C	30		Worm hole					5	FCAW		P4+P3
56	Stbd	16-019	RT	Acceptable									5	FCAW		P4+P3
56	Stbd	16-019	RT	Not Acceptable	C	50		Worm hole					5	FCAW		P4+P3
64	Stbd	16-020	RT	Acceptable							Undercut		5	H.LASER	CP04Cn	P4
68	Stbd	16-021	RT	Acceptable									5	FCAW		P4
76	Port	16-022	RT	Acceptable									5-5.5	FCAW		P4
76	Port	16-022	RT	Not Acceptable			Longitudinal						5-5.5	FCAW		P4
76	Port	16-023	RT	Acceptable				Porosity					5-5.5	FCAW		P4
76	Port	16-024	RT	Acceptable				Porosity	Solid Inclusion				5	FCAW		P4
76	Cnt	16-025	RT	Acceptable									5	FCAW		P4
76	Stbd	16-026	RT	Acceptable				Porosity					5	FCAW		P4
76	Stbd	16-026	RT	Not Acceptable	C	40		Worm hole					5	FCAW		P4
76	Stbd	16-027	RT	Acceptable					Solid Inclusion				5-5.5	FCAW		P4
76	Stbd	16-028	RT	Acceptable									5-5.5	FCAW		P4
88	Port	16-029	RT	Not Acceptable				Worm hole					5.5	FCAW		P4
88	Port	16-029	RT	Acceptable				Porosity					5.5	FCAW		P4
88	Port	16-029	RT	Not Acceptable	C	110		Worm hole					5.5	FCAW		P4

Frame	Position	ID No	NDE Type	NDE Result	Confined/ Extended	Length (mm)	Crack	Cavity	Solid inclusion	Lack of fusion /penetration	Imperfection of shape and dimensions	Miscellaneous imperfections	Thickness (mm)	Welding Process	Block	Section
88	Port	16-030	RT	Acceptable									5	H.LASER	CP05Cn	P4
98	Port	16-031	RT	Acceptable							Imperfect shape		5.5-7	FCAW		K3+P4
98	Port	16-031	RT	Not Acceptable	C	40		Worm hole					5.5-7	FCAW		K3+P4
98	Port	16-032	RT	Acceptable									5.5-7	FCAW		K3+P4
98	Cnt	16-033	RT	Acceptable									6	FCAW		K3+P4
98	Stbd	16-034	RT	Acceptable									5.5-7	FCAW		K3+P4
98	Stbd	16-034	RT	Acceptable				Gas pore					5.5-7	FCAW		K3+P4
98	Stbd	16-034	RT	Acceptable				Porosity					5.5-7	FCAW		K3+P4
98	Stbd	16-034	RT	Not Acceptable	E	480			Solid Inclusion				5.5-7	FCAW		K3+P4
98	Stbd	16-035	RT	Acceptable									5.5-7	FCAW		K3+P4
98	Stbd	16-035	RT	Acceptable									5.5-7	FCAW		K3+P4
98	Stbd	16-035	RT	Acceptable									5.5-7	FCAW		K3+P4
98	Stbd	16-035	RT	Not Acceptable	E	400			Solid Inclusion				5.5-7	FCAW		K3+P4
98	Stbd	16-036	RT	Acceptable									5.5-7	FCAW		K3+P4
98	Stbd	16-036	RT	Acceptable				Porosity					5.5-7	FCAW		K3+P4
98	Stbd	16-036	RT	Acceptable									5.5-7	FCAW		K3+P4
98	Stbd	16-036	RT	Not Acceptable	E	480			Solid Inclusion				5.5-7	FCAW		K3+P4
100	Port	16-037	RT	Acceptable									7-14	FCAW		K3
100	Stbd	16-038	RT	Not Acceptable	C	50		Worm hole					7-14	FCAW		K3
100	Stbd	16-038	RT	Acceptable									7-14	FCAW	CP06Cn	K3
100	Stbd	16-038	RT	Acceptable									7-14	FCAW	CP06Cn	K3
108	Stbd	16-039	RT	Acceptable									6-14	H.LASER	CP06Cn	K3
116	Port	16-040	RT	Acceptable									7-8	FCAW		K3
116	Port	16-041	RT	Acceptable									7-8	FCAW		K3
116	Cnt	16-042	RT	Acceptable									7	FCAW		K3

Frame	Position	ID No	NDE Type	NDE Result	Confined/ Extended	Length (mm)	Crack	Cavity	Solid inclusion	Lack of fusion /penetration	Imperfection of shape and dimensions	Miscellaneous imperfections	Thickness (mm)	Welding Process	Block	Section
116	Stbd	16-043	RT	Acceptable									7-8	FCAW		K3
116	Stbd	16-043	RT	Acceptable				Porosity					7-8	FCAW		K3
116	Stbd	16-043	RT	Not Acceptable	C	40				Lack of Fusion			7-8	FCAW		K3
116	Stbd	16-044	RT	Acceptable									7-8	FCAW		K3
117	Port	16-045	RT	Acceptable									7-25	FCAW	CP07Cn	K3
117	Stbd	16-046	RT	Acceptable									7-25	FCAW	CP07Cn	K3
120	Port	16-047	RT	Acceptable									7	H.LASER	CP07Cn	K3
124	Port	16-048	RT	Acceptable									7-16	FCAW	CP07Cn	K3
128	Stbd	16-049	RT	Acceptable									8	FCAW		K3
136	Port	16-050	RT	Acceptable									8	FCAW		K4+K3
136	Port	16-051	RT	Acceptable									8	FCAW		K4+K3
136	Port	16-052	RT	Acceptable									7-8	FCAW		K4+K3
136	Cnt	16-053	RT	Acceptable									7-8	FCAW		K4+K3
136	Stbd	16-054	RT	Acceptable									7-8	FCAW		K4+K3
136	Stbd	16-055	RT	Acceptable									8	FCAW		K4+K3
136	Stbd	16-056	RT	Acceptable									8	FCAW		K4+K3
148	Port	16-057	RT	Acceptable									8	FCAW		K4
148	Stbd	16-058	RT	Acceptable									8	H.LASER	CP08Cn	K4
156	Port	16-059	RT	Not Acceptable					Solid Inclusion				8	FCAW	MP08Sn+	K4
156	Port	16-059	RT	Not Acceptable					Solid Inclusion				8	FCAW	MP08Sn+	K4
156	Port	16-059	RT	Not Acceptable					Solid Inclusion				8	FCAW	MP08Sn+	K4
156	Port	16-059	RT	Acceptable									8	FCAW	MP08Sn+	K4
156	Port	16-059	RT	Acceptable					Solid Inclusion				8	FCAW		
156	Port	16-059	RT	Not Acceptable				Porosity	Solid Inclusion	Lack of Fusion			8	FCAW	MP08Sn+	K4
156	Port	16-060	RT	Acceptable									8	FCAW		K4

Frame	Position	ID No	NDE Type	NDE Result	Confined/ Extended	Length (mm)	Crack	Cavity	Solid inclusion	Lack of fusion /penetration	Imperfection of shape and dimensions	Miscellaneous imperfections	Thickness (mm)	Welding Process	Block	Section
156	Port	16-061	RT	Acceptable									8	FCAW		K4
156	Port	16-062	RT	Acceptable				Shrinkage cavity			Undercut		7-8	FCAW		K4
156	Port	16-063	RT	Acceptable					Solid Inclusion				7	FCAW		K4
156	Port	16-063	RT	Acceptable					Solid Inclusion				7	FCAW		K4
156	Port	16-063	RT	Not Acceptable	C	50		Porosity		Lack of Penetration			7	FCAW		K4
156	Port	16-064	RT	Acceptable									7	FCAW		K4
156	Port	16-065	RT	Acceptable									7	FCAW		K4
156	Stbd	16-066	RT	Acceptable									7	FCAW		K4
156	Stbd	16-066	RT	Not Acceptable	C	30		Worm hole					7	FCAW		K4
156	Stbd	16-067	RT	Acceptable									7	FCAW		K4
156	Stbd	16-068	RT	Acceptable									7	FCAW		K4
156	Stbd	16-069	RT	Acceptable									7-8	FCAW		K4
156	Stbd	16-070	RT	Acceptable				Elongated porosity	Solid Inclusion				8	FCAW		K4
156	Stbd	16-071	RT	Acceptable									8	FCAW		K4
160	Port	16-072	RT	Acceptable					Solid Inclusion				7-25	FCAW	CP09Cn	K4
158	Port	16-073	RT	Acceptable				Porosity					7-8	FCAW	CP09Cn	K4
158	Stbd	16-074	RT	Acceptable									7-8	FCAW	CP09Cn	K4
160	Stbd	16-075	RT	Acceptable									7-25	FCAW	CP09Cn	K4
160	Stbd	16-075	RT	Not Acceptable	C	50			Solid Inclusion				7-25	FCAW	CP09Cn	K4
172	Port	16-076	RT	Acceptable									7-8	H.LASER	CP09Cn	K4
176	Port	16-077	RT	Acceptable				Porosity					8	FCAW		N2+K4
176	Port	16-078	RT	Acceptable				Porosity					8	FCAW		N2+K4
176	Port	16-079	RT	Acceptable									8	FCAW		N2+K4
176	Port	16-080	RT	Acceptable				Porosity					7-8	FCAW		N2+K4

Frame	Position	ID No	NDE Type	NDE Result	Confined/ Extended	Length (mm)	Crack	Cavity	Solid inclusion	Lack of fusion /penetration	Imperfection of shape and dimensions	Miscellaneous imperfections	Thickness (mm)	Welding Process	Block	Section
176	Cnt	16-081	RT	Acceptable				Porosity					7	FCAW		N2+K4
176	Stbd	16-082	RT	Acceptable									7-8	FCAW		N2+K4
176	Stbd	16-082	RT	Not Acceptable				Worm hole	Solid Inclusion				7-8	FCAW		N2+K4
176	Stbd	16-082	RT	Not Acceptable									7-8	FCAW		N2+K4
176	Stbd	16-082	RT	Not Acceptable									7-8	FCAW		N2+K4
176	Stbd	16-082	RT	Acceptable				Porosity	Solid Inclusion		Imperfect shape		7-8	FCAW		N2+K4
176	Stbd	16-082	RT	Not Acceptable	E	400		Worm hole					7-8	FCAW		N2+K4
176	Stbd	16-083	RT	Acceptable				Porosity					8	FCAW		N2+K4
176	Stbd	16-084	RT	Acceptable				Porosity					8	FCAW		N2+K4
176	Stbd	16-085	RT	Acceptable									8	FCAW		N2+K4
176	Stbd	16-085	RT	Not Acceptable	C	130			Solid Inclusion				8	FCAW		N2+K4
178	Port	16-086	RT	Acceptable									7-16	FCAW	CP10Cn	N2
178	Stbd	16-087	RT	Acceptable				Gas pore	Solid Inclusion		Undercut		7-16	FCAW	CP10Cn	N2
184	Port	16-088	RT	Acceptable					Solid Inclusion				7-16	FCAW	CP10Cn	N2
184	Stbd	16-089	RT	Acceptable									7-16	FCAW	CP10Cn	N2
184	Stbd	16-089	RT	Acceptable				Elongated porosity					7-16	FCAW	CP10Cn	N2
184	Stbd	16-089	RT	Acceptable									7-16	FCAW	CP10Cn	N2
184	Stbd	16-089	RT	Not Acceptable	E	300		Uniformly distributed porosity					7-16	FCAW	CP10Cn	N2
184	Stbd	16-090	RT	Acceptable									8	FCAW		N2
192	Port	16-091	RT	Acceptable									7	SAW	CP10Cn	N2
192	Port	16-092	RT	Acceptable									7	FCAW	CP10Cn	N2

Frame	Position	ID No	NDE Type	NDE Result	Confined/ Extended	Length (mm)	Crack	Cavity	Solid inclusion	Lack of fusion /penetration	Imperfection of shape and dimensions	Miscellaneous imperfections	Thickness (mm)	Welding Process	Block	Section
192	Port	16-092	RT	Not Acceptable	C	80		Worm hole					7	SAW	CP10Cn	N2
192	Stbd	16-093	RT	Acceptable									7	FCAW	CP10Cn	N2
192	Stbd	16-093	RT	Acceptable									7	FCAW	CP10Cn	N2
192	Stbd	16-093	RT	Not Acceptable	C	60		Linear porosity	Solid Inclusion				7	SAW	CP10Cn	N2
192	Stbd	16-094	RT	Acceptable					Solid Inclusion		Imperfect shape		7	FCAW	CP10Cn	N2
192	Stbd	16-094	RT	Not Acceptable				Worm hole					7	FCAW	CP10Cn	N2
192	Stbd	16-094	RT	Acceptable									7	FCAW	CP10Cn	N2
192	Stbd	16-094	RT	Not Acceptable	C	80				Lack of Penetration			7	SAW	CP10Cn	N2
196	Port	16-095	RT	Acceptable									8	FCAW		N2
196	Port	16-095	RT	Acceptable					Solid Inclusion				8	FCAW		N2
196	Port	16-095	RT	Not Acceptable	E	250			Solid Inclusion				8	FCAW		N2
196	Port	16-096	RT	Acceptable									8	FCAW	CP10Cn	N2
196	Port	16-096	RT	Acceptable									8	FCAW	CP10Cn	N2
196	Port	16-096	RT	Not Acceptable	E	200		Gas pore					8	FCAW	CP10Cn	N2
196	Stbd	16-097	RT	Acceptable									8	FCAW	CP10Cn	N2
196	Stbd	16-098	RT	Acceptable					Solid Inclusion				8	FCAW	CP10Cn	N2
196	Stbd	16-099	RT	Acceptable									8	FCAW	MP10Dn+	N2
196	Stbd	16-099	RT	Not Acceptable	C	110		Worm hole	Solid Inclusion				8	FCAW	MP10Dn+	N2
198	Port	16-100	RT	Not Acceptable	C	80			Solid Inclusion				8-30	FCAW	CP11Cn	N2
198	Port	16-100	RT	Acceptable									8-30	FCAW	CP11Cn	N2
198	Port	16-100	RT	Not Acceptable					Solid Inclusion				8-30	FCAW	CP11Cn	N2
198	Port	16-100	RT	Acceptable									8-30	FCAW	CP11Cn	N2

Frame	Position	ID No	NDE Type	NDE Result	Confined/ Extended	Length (mm)	Crack	Cavity	Solid inclusion	Lack of fusion /penetration	Imperfection of shape and dimensions	Miscellaneous imperfections	Thickness (mm)	Welding Process	Block	Section
198	Port	16-100	RT	Acceptable									8-30	FCAW	CP11Cn	N2
198	Stbd	16-101	RT	Not Acceptable	C	70		Worm hole	Solid Inclusion				8-30	FCAW	CP11Cn	N2
198	Stbd	16-101	RT	Not Acceptable					Solid Inclusion				8-30	FCAW	CP11Cn	N2
198	Stbd	16-101	RT	Acceptable									8-30	FCAW	CP11Cn	N2
200	Port	16-102	RT	Acceptable									7-8	FCAW	CP11Cn	N2
200	Port	16-103	RT	Acceptable									7	FCAW	CP11Cn	N2
200	Port	16-104	RT	Acceptable									7	FCAW	CP11Cn	N2
200	Cnt	16-105	RT	Acceptable									7	FCAW	CP11Cn	N2
200	Stbd	16-106	RT	Not Acceptable	C	10		Worm hole					7	FCAW	CP11Cn	N2
200	Stbd	16-106	RT	Acceptable									7	FCAW	CP11Cn	N2
200	Stbd	16-107	RT	Not Acceptable	C	30		Gas pore	Solid Inclusion				7	FCAW	CP11Cn	N2
200	Stbd	16-107	RT	Not Acceptable									7	FCAW	CP11Cn	N2
200	Stbd	16-107	RT	Not Acceptable			Longitudinal						7	FCAW	CP11Cn	N2
200	Stbd	16-107	RT	Acceptable									7	FCAW	CP11Cn	N2
200	Stbd	16-108	RT	Acceptable				Gas pore					7-8	FCAW	CP11Cn	N2
200	Stbd	16-109	RT	Acceptable					Solid Inclusion				8	FCAW	CP11Cn	N2
208	Port	16-110	RT	Acceptable				Porosity					8	FCAW		N2
208	Port	16-111	RT	Acceptable							Undercut		8	SAW	CP11Cn	N2
220	Port	16-112	RT	Acceptable									8	FCAW		Y4+N2
220	Port	16-112	RT	Not Acceptable			Longitudinal						8	FCAW		Y4+N2
220	Port	16-113	RT	Acceptable									8	FCAW		Y4+N2
220	Port	16-114	RT	Acceptable									8	FCAW		Y4+N2
220	Port	16-115	RT	Acceptable				Porosity					7	FCAW		Y4+N2

Frame	Position	ID No	NDE Type	NDE Result	Confined/ Extended	Length (mm)	Crack	Cavity	Solid inclusion	Lack of fusion /penetration	Imperfection of shape and dimensions	Miscellaneous imperfections	Thickness (mm)	Welding Process	Block	Section
220	Port	16-116	RT	Acceptable					Solid Inclusion				7-14	FCAW		Y4+N2
220	Port	16-116	RT	Not Acceptable	C	30				Lack of Fusion	Continuous undercut		7-14	FCAW		Y4+N2
220	Port	16-117	RT	Acceptable									7-14	FCAW		Y4+N2
220	Stbd	16-118	RT	Acceptable									7-14	FCAW		Y4+N2
220	Stbd	16-118	RT	Not Acceptable	C	15		Worm hole					7-14	FCAW		Y4+N2
220	Stbd	16-119	RT	Acceptable					Solid Inclusion		Undercut		7-14	FCAW		Y4+N2
220	Stbd	16-120	RT	Acceptable				Porosity					7	FCAW		Y4+N2
220	Stbd	16-120	RT	Acceptable				Porosity					7	FCAW		Y4+N2
220	Stbd	16-120	RT	Acceptable									7	FCAW		Y4+N2
220	Stbd	16-120	RT	Not Acceptable	C	110		Worm hole	Solid Inclusion				7	FCAW		Y4+N2
220	Stbd	16-121	RT	Acceptable				Porosity					8	FCAW		Y4+N2
220	Stbd	16-121	RT	Not Acceptable				Worm hole					8	FCAW		Y4+N2
220	Stbd	16-122	RT	Acceptable									8	FCAW		Y4+N2
220	Stbd	16-123	RT	Acceptable				Porosity					8	FCAW		Y4+N2
224	Port	16-124	RT	Acceptable									7-14	FCAW	CP12Cn	Y4
224	Stbd	16-125	RT	Acceptable									7-14	FCAW	CP12Cn	Y4
228	Port	16-126	RT	Acceptable				Porosity					8	FCAW		Y4
228	Stbd	16-127	RT	Acceptable							Imperfect shape		8	FCAW		Y4
240	Port	16-128	RT	Not Acceptable					Solid Inclusion				8	FCAW	MP12Sn+	Y4
240	Port	16-128	RT	Acceptable									8	FCAW	MP12Sn+	Y4
240	Port	16-128	RT	Not Acceptable	C	50		Elongated porosity	Solid Inclusion				8	FCAW	MP12Sn+	Y4
240	Port	16-129	RT	Not Acceptable					Solid Inclusion				8	FCAW		Y4

Frame	Position	ID No	NDE Type	NDE Result	Confined/ Extended	Length (mm)	Crack	Cavity	Solid inclusion	Lack of fusion /penetration	Imperfection of shape and dimensions	Miscellaneous imperfections	Thickness (mm)	Welding Process	Block	Section
240	Port	16-129	RT	Acceptable					Solid Inclusion				8	FCAW		Y4
240	Port	16-129	RT	Not Acceptable	C	45	Longitudinal						8	FCAW		Y4
240	Port	16-130	RT	Acceptable									8	FCAW		Y4
240	Port	16-131	RT	Acceptable				Porosity					7	FCAW		Y4
240	Cnt	16-132	RT	Acceptable									7	FCAW		Y4
240	Stbd	16-133	RT	Acceptable				Elongated porosity					7	FCAW		Y4
240	Stbd	16-134	RT	Acceptable				Porosity					8	FCAW		Y4
240	Stbd	16-135	RT	Not Acceptable			Longitudinal						8	FCAW		Y4
240	Stbd	16-135	RT	Acceptable					Solid Inclusion				8	FCAW		Y4
240	Stbd	16-135	RT	Not Acceptable	C	20			Solid Inclusion				8	FCAW		Y4
240	Stbd	16-136	RT	Acceptable				Gas pore					8	FCAW	MP12Dn+	Y4
240	Stbd	16-136	RT	Not Acceptable	E	480					Imperfect shape		8	FCAW	MP12Dn+	Y4
248	Port	16-137	RT	Acceptable									7	H.LASER	CP13Cn	Y4
252	Port	16-138	RT	Acceptable									7-14	FCAW	CP13Cn	Y4
252	Stbd	16-139	RT	Acceptable				Porosity					7-14	FCAW	CP13Cn	Y4
248	Stbd	16-140	RT	Acceptable									8	FCAW		Y4
248	Stbd	16-140	RT	Not Acceptable	E	480					Imperfect shape		8	FCAW		Y4
260	Port	16-141	RT	Acceptable				Porosity					8	FCAW		Y5+Y4
260	Port	16-142	RT	Acceptable					Solid Inclusion				8	FCAW		Y5+Y4
260	Port	16-142	RT	Not Acceptable	C	50	Longitudinal						8	FCAW		Y5+Y4
260	Port	16-143	RT	Acceptable									8	FCAW		Y5+Y4
260	Port	16-143	RT	Not Acceptable	C	70		Worm hole		Lack of Fusion			8	FCAW		Y5+Y4

Frame	Position	ID No	NDE Type	NDE Result	Confined/ Extended	Length (mm)	Crack	Cavity	Solid inclusion	Lack of fusion /penetration	Imperfection of shape and dimensions	Miscellaneous imperfections	Thickness (mm)	Welding Process	Block	Section
260	Port	16-144	RT	Not Acceptable			Longitudinal						7	FCAW		Y5+Y4
260	Port	16-144	RT	Acceptable									7	FCAW		Y5+Y4
260	Port	16-144	RT	Acceptable									7	FCAW		Y5+Y4
260	Port	16-144	RT	Not Acceptable	C	40				Lack of Fusion			7	FCAW		Y5+Y4
260	Stbd	16-145	RT	Acceptable									7	FCAW		Y5+Y4
260	Stbd	16-146	RT	Acceptable									8	FCAW		Y5+Y4
260	Stbd	16-147	RT	Acceptable									8	FCAW		Y5+Y4
260	Stbd	16-148	RT	Acceptable									8	FCAW		Y5+Y4
264	Stbd	16-149	RT	Acceptable									8	H.LASER	CP14Cn	Y5
268	Port	16-150	RT	Acceptable									7-14	FCAW	CP14Cn	Y5
268	Stbd	16-151	RT	Acceptable									7-14	FCAW	CP14Cn	Y5
268	Stbd	16-151	RT	Not Acceptable	C	15	Longitudinal						7-14	FCAW	CP14Cn	Y5
272	Port	16-152	RT	Acceptable				Porosity					8	FCAW	LP14Sn	Y5
272	Port	16-152	RT	Not Acceptable	E	400			Solid Inclusion				8	FCAW	LP14Sn	Y5
272	Port	16-153	RT	Acceptable				Elongated porosity					8	FCAW	CP14Cn	Y5
272	Cnt	16-154	RT	Not Acceptable				Gas pore					7	FCAW	CP14Cn	Y5
272	Cnt	16-154	RT	Not Acceptable					Solid Inclusion				7	FCAW	CP14Cn	Y5
272	Cnt	16-154	RT	Acceptable				Gas pore					7	FCAW	CP14Cn	Y5
272	Cnt	16-154	RT	Acceptable				Porosity	Solid Inclusion				7	FCAW	CP14Cn	Y5
272	Cnt	16-154	RT	Acceptable				Gas pore					7	FCAW	CP14Cn	Y5
272	Cnt	16-154	RT	Not Acceptable					Solid Inclusion				7	FCAW	CP14Cn	Y5
272	Cnt	16-154	RT	Acceptable									7	FCAW	CP14Cn	Y5
272	Cnt	16-154	RT	Not Acceptable					Solid Inclusion				7	FCAW	CP14Cn	Y5

Frame	Position	ID No	NDE Type	NDE Result	Confined/ Extended	Length (mm)	Crack	Cavity	Solid inclusion	Lack of fusion /penetration	Imperfection of shape and dimensions	Miscellaneous imperfections	Thickness (mm)	Welding Process	Block	Section
272	Cnt	16-154	RT	Acceptable							Imperfect shape		7	FCAW	CP14Cn	Y5
272	Cnt	16-154	RT	Not Acceptable	E	280			Solid Inclusion				7	FCAW	CP14Cn	Y5
272	Stbd	16-155	RT	Acceptable									8	FCAW	CP14Cn	Y5
272	Stbd	16-156	RT	Acceptable				Porosity					8	FCAW	LP14Dn	Y5
272	Stbd	16-156	RT	Acceptable				Porosity					8	FCAW	LP14Dn	Y5
272	Stbd	16-156	RT	Not Acceptable	E	250			Solid Inclusion				8	FCAW	LP14Dn	Y5
276	Port	16-157	RT	Acceptable				Gas pore					8	FCAW	CP14Cn	Y5
276	Port	16-158	RT	Not Acceptable			Longitudinal						7-8	FCAW	CP14Cn	Y5
276	Port	16-158	RT	Not Acceptable			Longitudinal						7-8	FCAW	CP14Cn	Y5
276	Port	16-158	RT	Acceptable									7-8	FCAW	CP14Cn	Y5
276	Port	16-158	RT	Not Acceptable	C	25	Transverse			Lack of Penetration			7-8	FCAW	CP14Cn	Y5
276	Stbd	16-159	RT	Acceptable				Gas pore					7-8	FCAW	CP14Cn	Y5
276	Stbd	16-160	RT	Acceptable				Linear porosity				Spatter	8	FCAW	CP14Cn	Y5
282	Port	16-161	RT	Acceptable									8	FCAW	MP14Sn+	Y5
282	Port	16-161	RT	Acceptable									8	FCAW	MP14Sn+	Y5
282	Port	16-161	RT	Not Acceptable	E	400		Worm hole	Solid Inclusion				8	FCAW	MP14Sn+	Y5
282	Port	16-162	RT	Acceptable							Imperfect shape		8	FCAW		Y5
282	Port	16-162	RT	Not Acceptable	C	30		Worm hole					8	FCAW		Y5
282	Port	16-163	RT	Acceptable									8	FCAW		Y5
282	Cnt	16-164	RT	Acceptable							Imperfect shape		7	FCAW		Y5
282	Cnt	16-164	RT	Not Acceptable	C	50		Worm hole					7	FCAW		Y5

Frame	Position	ID No	NDE Type	NDE Result	Confined/ Extended	Length (mm)	Crack	Cavity	Solid inclusion	Lack of fusion /penetration	Imperfection of shape and dimensions	Miscellaneous imperfections	Thickness (mm)	Welding Process	Block	Section
282	Stbd	16-165	RT	Acceptable					Solid Inclusion		Undercut		7	FCAW		Y5
282	Stbd	16-165	RT	Not Acceptable	C	30			Solid Inclusion				7	FCAW		Y5
282	Stbd	16-166	RT	Acceptable							Undercut		8	FCAW		Y5
282	Stbd	16-167	RT	Acceptable									8	FCAW		Y5
282	Stbd	16-168	RT	Acceptable					Solid Inclusion		Imperfect shape		8	FCAW	MP14Dn+	Y5
284	Port	16-169	RT	Acceptable									7	H.LASER	CP15Cn	Y5
284	Stbd	16-170	RT	Acceptable									7	H.LASER	CP15Cn	Y5
284	Stbd	16-171	RT	Acceptable									7	H.LASER	CP15Cn	Y5
288	Port	16-172	RT	Acceptable									7-30	FCAW	CP15Cn	Y5
300	Port	16-173	RT	Acceptable									7-30	FCAW	CP15Cn	Y5
300	Port	16-174	RT	Acceptable								Spatter	7	FCAW	CP15Cn	Y5
298	Stbd	16-175	RT	Acceptable									7-30	FCAW	CP15Cn	Y5
304	Port	16-176	RT	Acceptable					Solid Inclusion				8	FCAW		X2+Y5
304	Port	16-176	RT	Not Acceptable	C	40		Uniformly distributed porosity	Solid Inclusion				8	FCAW		X2+Y5
304	Port	16-177	RT	Acceptable									8	FCAW		X2+Y5
304	Cnt	16-178	RT	Acceptable									7	FCAW		X2+Y5
304	Stbd	16-179	RT	Acceptable									8	FCAW		X2+Y5
304	Stbd	16-179	RT	Not Acceptable	C	40		Worm hole					8	FCAW		X2+Y5
304	Stbd	16-180	RT	Acceptable								Miscellaneous imperfections	8	FCAW		X2+Y5
306	Port	16-181	RT	Acceptable									8-30	FCAW	CP16Cn	X2
314	Stbd	16-182	RT	Acceptable									7-16	FCAW	CP16Cn	X2
312	Stbd	16-183	RT	Acceptable									8	H.LASER	CP16Cn	X2
316	Stbd	16-184	RT	Acceptable									8	H.LASER	CP16Cn	X2

Frame	Position	ID No	NDE Type	NDE Result	Confined/ Extended	Length (mm)	Crack	Cavity	Solid inclusion	Lack of fusion /penetration	Imperfection of shape and dimensions	Miscellaneous imperfections	Thickness (mm)	Welding Process	Block	Section
326	Port	16-185	RT	Acceptable									7-8	FCAW		X2
326	Port	16-186	RT	Not Acceptable					Solid Inclusion				7-8	FCAW		X2
326	Port	16-186	RT	Not Acceptable					Solid Inclusion				7-8	FCAW		X2
326	Port	16-186	RT	Not Acceptable					Solid Inclusion				7-8	FCAW		X2
326	Port	16-186	RT	Acceptable									7-8	FCAW		X2
326	Port	16-186	RT	Acceptable					Solid Inclusion				7-8	FCAW		X2
326	Port	16-186	RT	Acceptable					Solid Inclusion				7-8	FCAW		X2
326	Port	16-186	RT	Not Acceptable	E	480			Solid Inclusion				7-8	FCAW		X2
326	Port	16-187	RT	Acceptable									7-8	FCAW		X2
326	Port	16-187	RT	Not Acceptable				Porosity					7-8	FCAW		X2
326	Port	16-187	RT	Not Acceptable				Porosity					7-8	FCAW		X2
326	Port	16-187	RT	Acceptable									7-8	FCAW		X2
326	Port	16-187	RT	Acceptable									7-8	FCAW		X2
326	Port	16-187	RT	Not Acceptable	E	480			Solid Inclusion				7-8	FCAW		X2
326	Port	16-188	RT	Acceptable				Porosity					7	FCAW		X2
326	Port	16-188	RT	Acceptable				Porosity					7	FCAW		X2
326	Port	16-188	RT	Not Acceptable				Porosity	Solid Inclusion				7	FCAW		X2
326	Port	16-188	RT	Acceptable				Porosity					7	FCAW		X2
326	Port	16-188	RT	Not Acceptable	E	480			Solid Inclusion				7	FCAW		X2
326	Cnt	16-189	RT	Acceptable									7	FCAW		X2
326	Stbd	16-190	RT	Acceptable									7	FCAW		X2
326	Stbd	16-191	RT	Acceptable									7-8	FCAW		X2

Frame	Position	ID No	NDE Type	NDE Result	Confined/ Extended	Length (mm)	Crack	Cavity	Solid inclusion	Lack of fusion /penetration	Imperfection of shape and dimensions	Miscellaneous imperfections	Thickness (mm)	Welding Process	Block	Section
326	Stbd	16-192	RT	Acceptable									7-8	FCAW		X2
326	Stbd	16-192	RT	Not Acceptable	E	200			Solid Inclusion				7-8	FCAW		X2
336	Port	16-193	RT	Acceptable									7	H.LASER	CP17Cn	X2
336	Port	16-194	RT	Acceptable									6-7	H.LASER	CP17Cn	X2
348	Port	16-195	RT	Acceptable									5.5-7	FCAW		X2
348	Port	16-196	RT	Not Acceptable	C	5	Transverse						5-5.5-7	FCAW		X2
348	Port	16-196	RT	Not Acceptable			Transverse						5-5.5-7	FCAW		X2
348	Port	16-196	RT	Not Acceptable			Longitudinal						5-5.5-7	FCAW		X2
348	Port	16-196	RT	Acceptable									5-5.5-7	FCAW		X2
348	Port	16-197	RT	Acceptable									5-5.5-7	FCAW		X2
348	Port	16-197	RT	Not Acceptable	C	35		Worm hole	Solid Inclusion				5-5.5-7	FCAW		X2
348	Cnt	16-198	RT	Acceptable									5-7	FCAW		X2
348	Cnt	16-198	RT	Not Acceptable	C	40			Solid Inclusion				5-7	FCAW		X2
348	Stbd	16-199	RT	Acceptable							Continuous undercut		5-5.5-7	FCAW		X2
348	Stbd	16-200	RT	Acceptable									5.5-7	FCAW		X2
348	Stbd	16-201	RT	Acceptable					Solid Inclusion				5.5-7	FCAW		X2
356	Stbd	16-202	RT	Acceptable									5-5.5	H.LASER	CP18Cn	X2
364	Port	16-203	RT	Acceptable				Porosity					5-5.5	FCAW		T2+X2
364	Port	16-204	RT	Acceptable									5-5.5	FCAW		T2+X2
364	Port	16-205	RT	Acceptable							Undercut		5-5.5	FCAW		T2+X2
364	Port	16-205	RT	Not Acceptable	E	200		Worm hole	Solid Inclusion				5-5.5	FCAW		T2+X2
364	Cnt	16-206	RT	Acceptable				Porosity					5	FCAW		T2+X2
364	Cnt	16-206	RT	Acceptable									5	FCAW		T2+X2

Frame	Position	ID No	NDE Type	NDE Result	Confined/ Extended	Length (mm)	Crack	Cavity	Solid inclusion	Lack of fusion /penetration	Imperfection of shape and dimensions	Miscellaneous imperfections	Thickness (mm)	Welding Process	Block	Section
364	Cnt	16-206	RT	Not Acceptable	C	120		Worm hole	Solid Inclusion				5	FCAW		T2+X2
364	Stbd	16-207	RT	Acceptable				Gas pore	Solid Inclusion				5-5.5	FCAW		T2+X2
364	Stbd	16-208	RT	Acceptable									5-5.5	FCAW		T2+X2
364	Stbd	16-208	RT	Not Acceptable	C	30		Worm hole					5-5.5	FCAW		T2+X2
364	Stbd	16-209	RT	Acceptable					Solid Inclusion				5-5.5	FCAW		T2+X2
376	Port	16-210	RT	Acceptable									5	FCAW	CP19Cn	T2
376	Port	16-210	RT	Not Acceptable	C	60		Linear porosity					5	H.LASER	CP19Cn	T2
372	Stbd	16-211	RT	Acceptable									5	H.LASER	CP19Cn	T2
380	Port	16-212	MT	Acceptable									5	FCAW		T2
380	Port	16-213	MT	Acceptable									5	FCAW		T2
380	Port	16-214	MT	Acceptable									5	FCAW		T2
380	Stbd	16-215	MT	Acceptable									5	FCAW		T2
380	Stbd	16-216	MT	Acceptable									5	FCAW		T2
388	Port	16-218	RT	Acceptable							Undercut		5	H.LASER	CP20Cn	T2
384	Stbd	16-219	RT	Acceptable				Clustered porosity					5	H.LASER	CP20Cn	T2
392	Port	16-220	RT	Acceptable									5	FCAW		T3+T2
392	Port	16-221	RT	Acceptable									5	FCAW		T3+T2
392	Cnt	16-222	RT	Acceptable									5	FCAW		T3+T2
392	Stbd	16-223	RT	Acceptable									5	FCAW		T3+T2
392	Stbd	16-224	RT	Acceptable									5	FCAW		T3+T2
392	Stbd	16-225	RT	Acceptable							Imperfect shape		5	FCAW		T3+T2
396	Port	16-226	RT	Acceptable									5	FCAW	CP21Cn	T3
200	Port	16-227	RT	Not Acceptable	C	20			Solid Inclusion				8	FCAW	CP11Cn	N2
200	Port	16-227	RT	Acceptable									8	FCAW	CP11Cn	N2

Frame	Position	ID No	NDE Type	NDE Result	Confined/ Extended	Length (mm)	Crack	Cavity	Solid inclusion	Lack of fusion /penetration	Imperfection of shape and dimensions	Miscellaneous imperfections	Thickness (mm)	Welding Process	Block	Section
200	Stbd	INS16-107	RT	Acceptable			Longitudinal						7	FCAW	CP11Cn	N2
318	Stbd	PL-102	MT	Acceptable									8-12	FCAW		CQ16Cn+X2
56	Port	PL-175	RT	Acceptable									6-8	FCAW		I2+I1
56	Port	PL-175	RT	Not Acceptable						Lack of Fusion			6-8	FCAW		I2+I1
56	Stbd	PL-180	RT	Acceptable									6-8	FCAW		I2+I1
56	Stbd	PL-180	RT	Not Acceptable	C	10		Gas pore	Solid Inclusion				6-8	FCAW		I2+I1
58	Port	PL-199	MT	Acceptable									5	FCAW		I2+P4
58	Stbd	PL-204	MT	Acceptable									5	FCAW		I2+P4
96	Stbd	PL-242	RT	Acceptable									5	FCAW		I3+I2
96	Stbd	PL-242	RT	Not Acceptable	C	90			Solid Inclusion				5	FCAW		I3+I2
96	Port	PL-249	RT	Acceptable				Porosity					5	FCAW		I3+I2
100	Stbd	PL-264	MT	Acceptable									5	FCAW		I3+K3
108	Port	PL-271	MT	Acceptable									5	FCAW		I3+K3
118	Stbd	PL-274	MT	Acceptable									5	FCAW		I3+K3
118	Port	PL-287	MT	Acceptable									5	FCAW		I3+K3
158	Port	PL-317	MT	Acceptable									5	FCAW		I3+K4
177	Stbd	PL-338	MT	Acceptable									5	FCAW		I4+N2
177	Port	PL-339	MT	Acceptable									5	FCAW		I4+N2
290	Stbd	PL-390	MT	Acceptable									5	FCAW		L1+Y5
298	Port	PL-421	MT	Acceptable									5	FCAW		Y5+Y3
304	Port	PL-433	RT	Acceptable									6	FCAW	CQ16Cn	L1
304	Port	PL-433	RT	Acceptable				Gas pore					6	FCAW	CQ16Cn	L1
304	Port	PL-433	RT	Acceptable									6	FCAW	CQ16Cn	L1
304	Port	PL-433	RT	Not Acceptable	E	350				Lack of Fusion			6	FCAW	CQ16Cn	L1
366	Stbd	PL-474	MT	Acceptable									5	FCAW		L2+T2

Frame	Position	ID No	NDE Type	NDE Result	Confined/ Extended	Length (mm)	Crack	Cavity	Solid inclusion	Lack of fusion /penetration	Imperfection of shape and dimensions	Miscellaneous imperfections	Thickness (mm)	Welding Process	Block	Section
366	Port	PL-489	MT	Acceptable									5	FCAW		L2+T2

Appendix F

Failure probabilities of case study structure (deck 16)

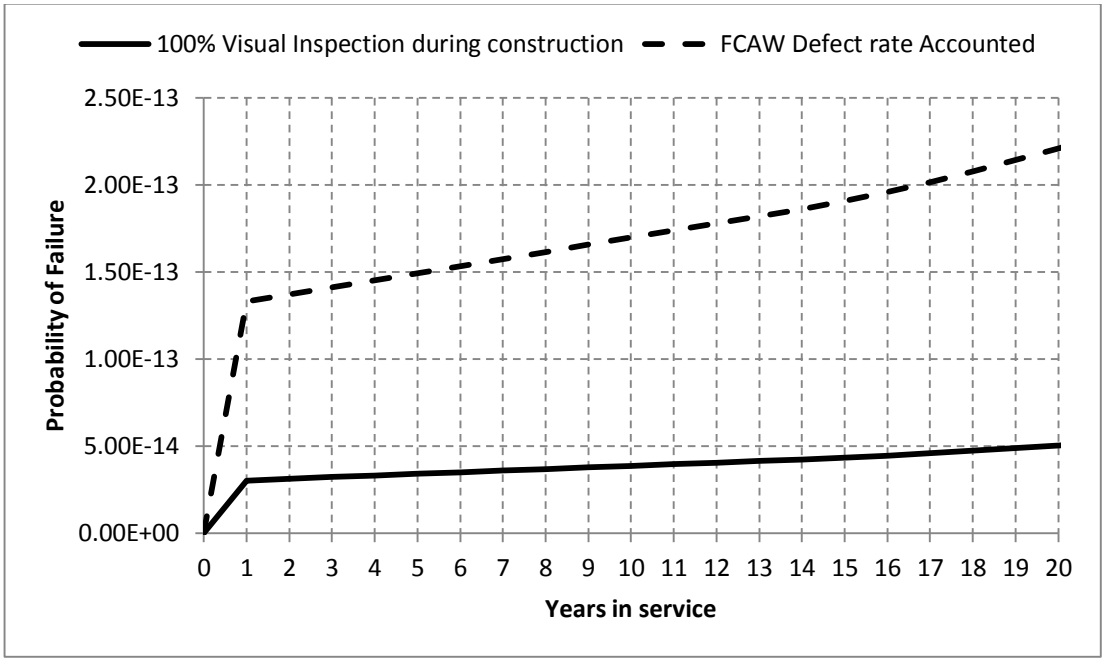

Figure F-1 Time variant probabilities of failure for frame 34, 56, 76, 98, 348, and 364 in deck 16

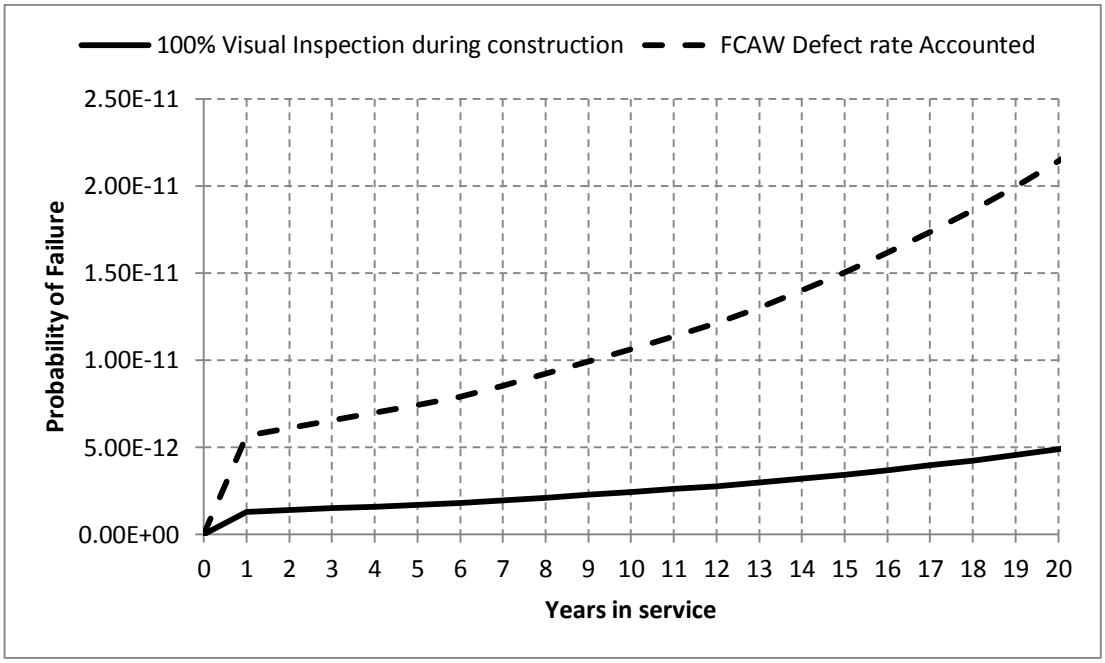

Figure F-2 Time variant probabilities of failure for frame 116, 136, and 326 in deck 16

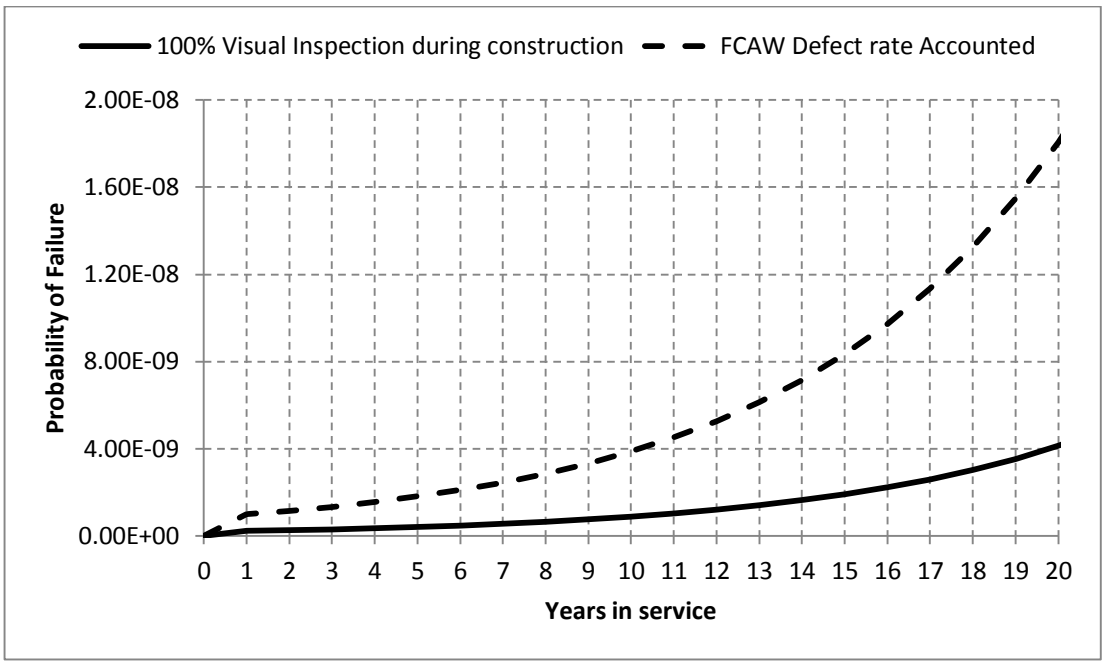

Figure F-3 Time variant probabilities of failure for frame 156, and 304 in deck 16

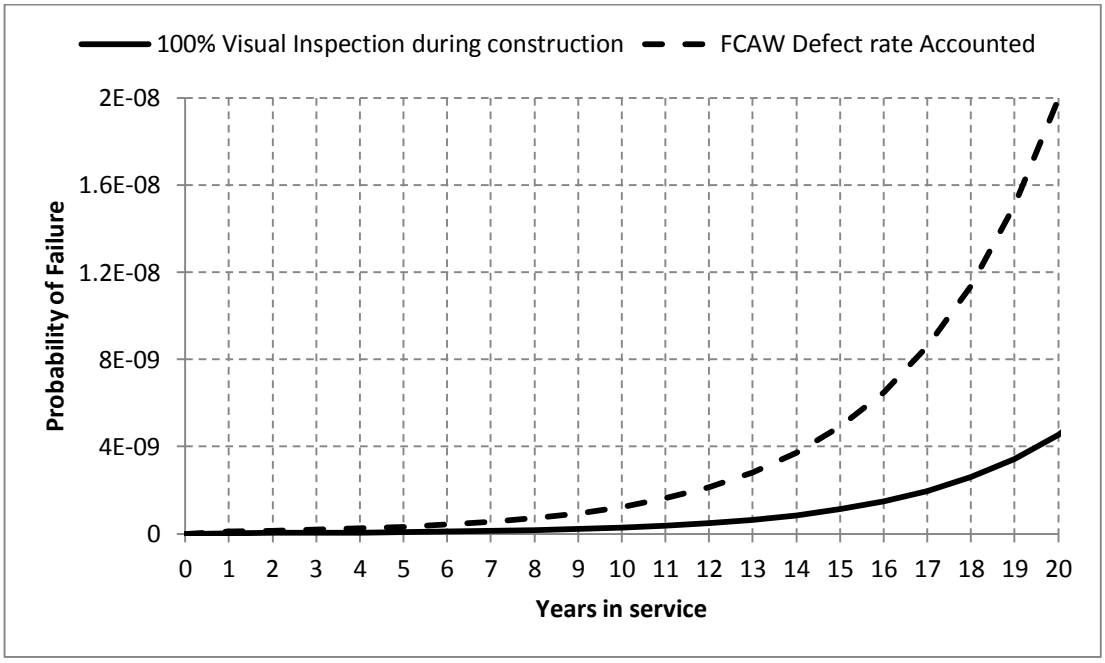

Figure F-4 Time variant probabilities of failure for frame 176, 196, 260, 272, 276, and 282 in deck 16

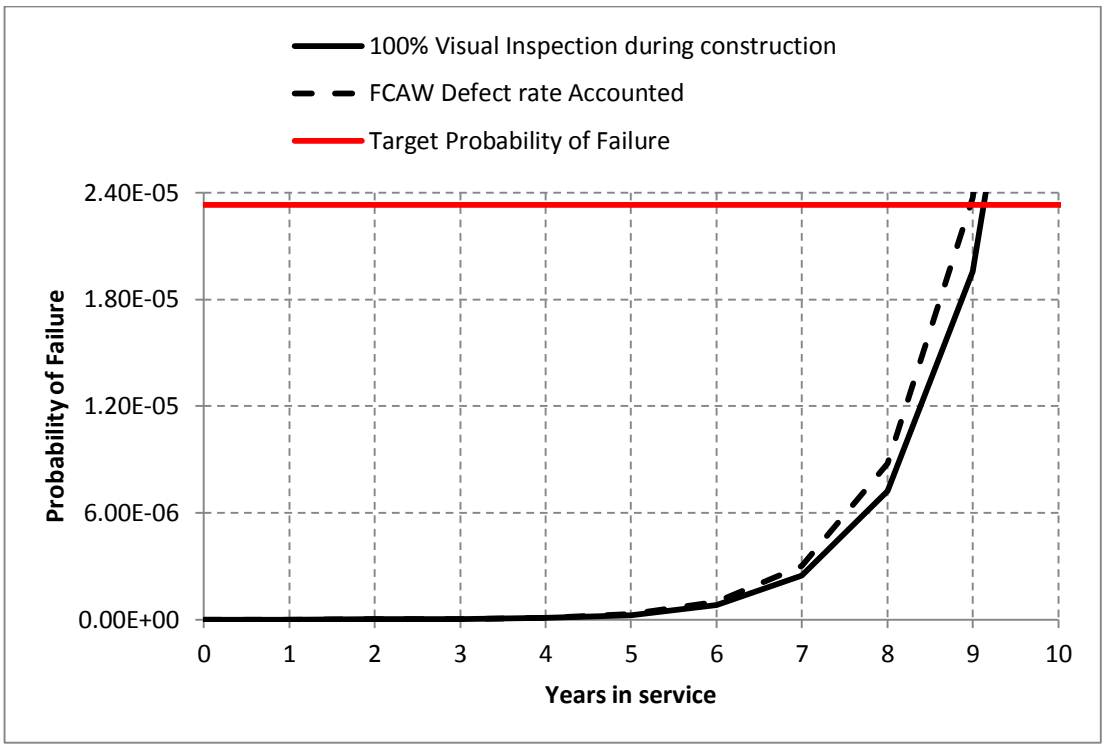

Figure F-5 Time variant probabilities of failure for centre part of frame 220 in deck 16

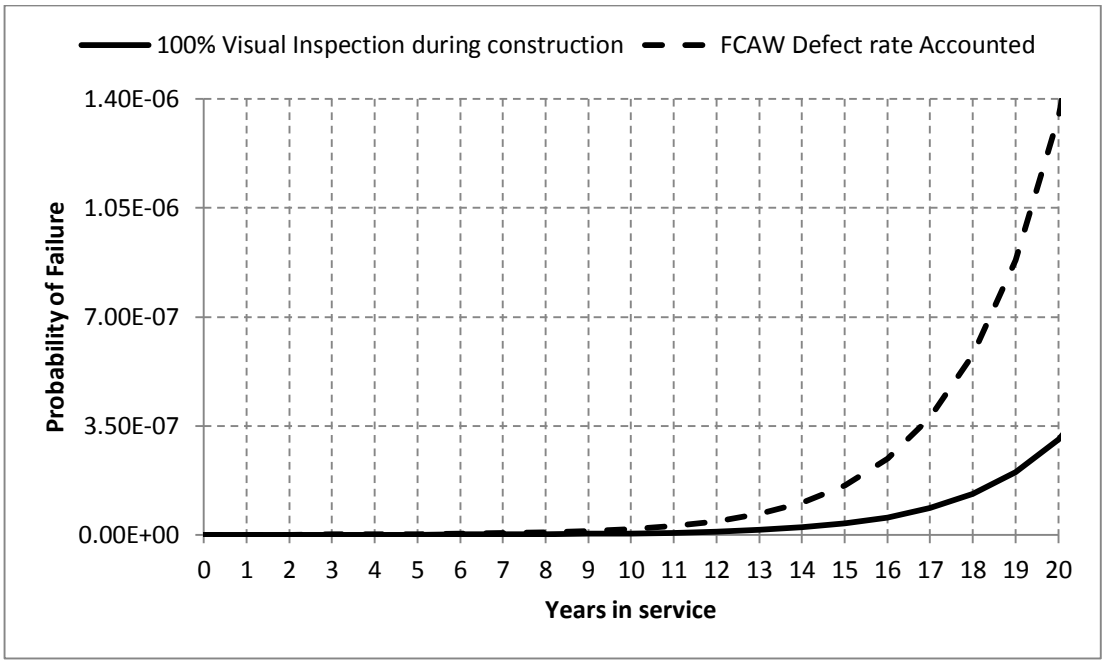

Figure F-6 Time variant probabilities of failure for frame 240 in deck 16

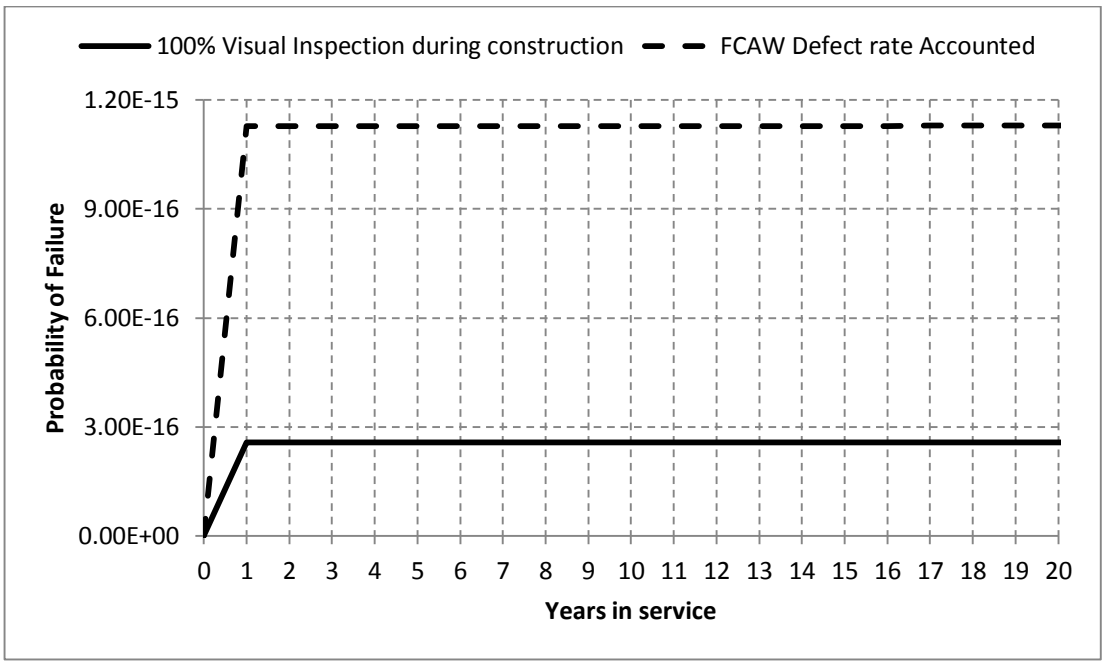

Figure F-7 Time variant probabilities of failure for frame 380, and 392 in deck 16

Appendix G

Conferences and Publications

Peer reviewed publications

Amirafshari, P., and Stacey, P. REVIEW OF AVAILABLE PROBABILISTIC MODELS OF THE CRACK GROWTH PARAMETERS IN PARIS EQUATION. OMAE 2019, Glasgow.

Amirafshari, P.; Barltrop, N.; Bharadwaj, U.; Wright, M.; Oterkus, S., 2018: A Review of Nondestructive Examination Methods for New-building Ships Undergoing Classification Society Survey. *Journal of Ship Production and Design*, **33**, 1–11, https://doi.org/10.5957/JSPD.33.2.160039

MICHALA, AL., BARLTROP, N., AMIRAFSHARI, P., LAZAKIS, I. And THEOTOKATOS, G. An Intelligent System For Vessel Structural Reliability Evaluation. In: International Conference On Maritime Safety And Operations. 2016. P. 14th. http://strathprints.strath.ac.uk/58434/

Conferences and oral presentations

AMIRAFSHARI, P., Non-Destructive Examination of New-Building Ships – Current State, Gaps, Needs, and Recommendations. **Oral presentation** at Maritime & Naval Test Development Symposium, Amsterdam. 2017.

AMIRAFSHARI, P., Application Of Probabilistic Fracture Mechanics In Risk-Based Non-Destructive Examination Of New Building Ships. **Extended abstract and oral presentation** at 3rd NSIRC Conference, Cambridge, 2017.

AMIRAFSHARI, P., Development Of A Risk-Based Approach To Optimise NDE Inspection Regime For New Built Ships. **Extended Abstract and oral presentation** at: 2nd NSIRC Conference. 2016. On Maritime Safety And Operations. 2016. P. 14th.

AMIRAFSHARI, P. “Optimising NDE Inspection plans of Ship Hull structures by Developing a Risk-based Framework”. **Oral presentation** at YMC Seminar Series of The Welding Institute ,Cambridge. November 2017.

AMIRAFSHARI, P., “Engineering critical assessment with application to NDE inspection of newbuilding ship hull structures”, **Oral presentation** at Lloyd’s Register Marine, Cadiz, Spain. July 2017.

AMIRAFSHARI, P., “Risk-based inspection of new-building ship hull structures”, **Oral presentation** at Lloyd’s Register Foundation, London, September 2015.